DELAYED INJURY MECHANISMS AFTER ISCHEMIC AND HEMORRHAGIC STROKE

EDITED BY: Devin William McBride, Budbazar Enkhjargal, Prativa Sherchan and Qin Hu

PUBLISHED IN: Frontiers in Neurology

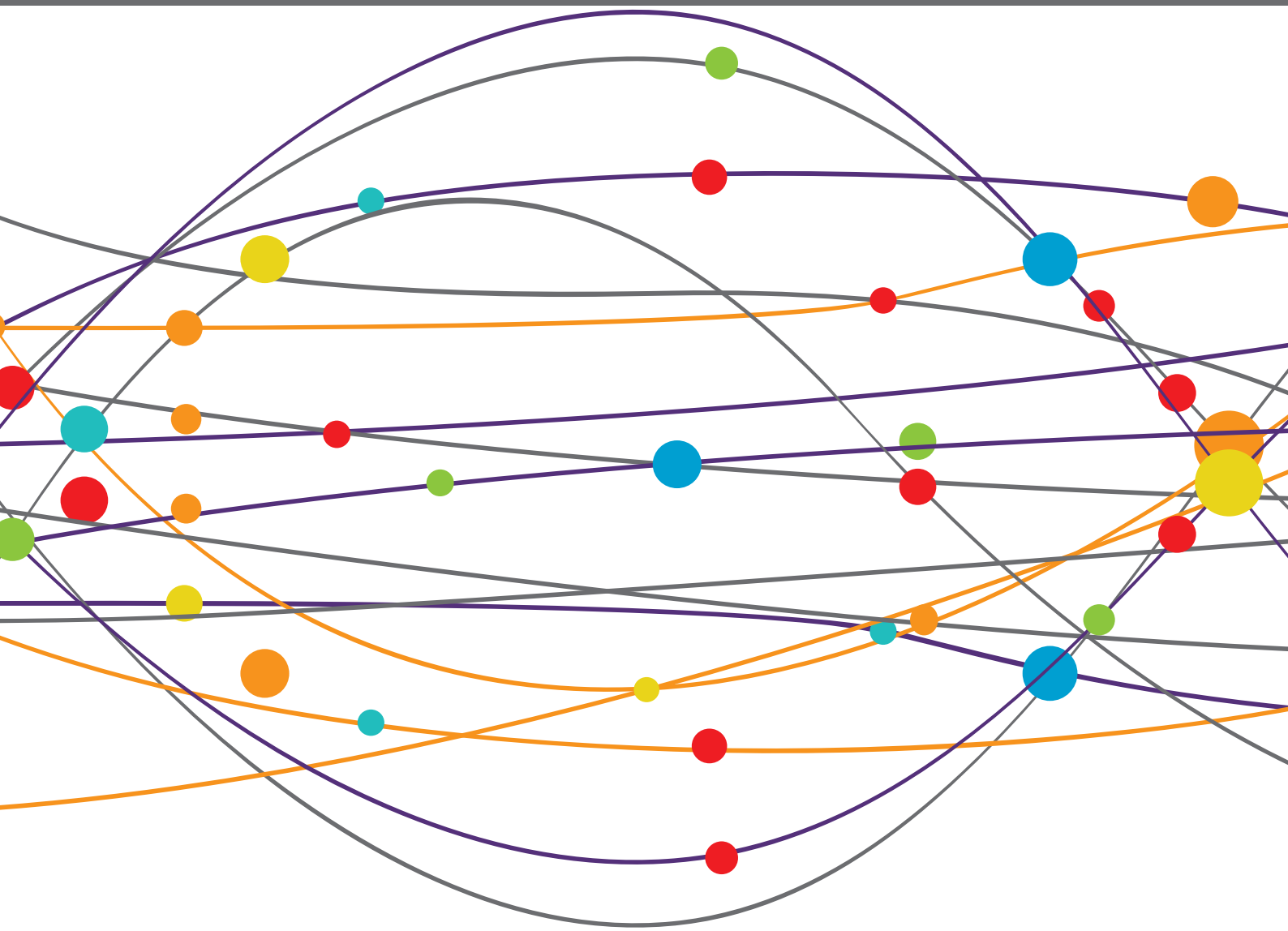

frontiers Research Topics

frontiers

ISSN 1664-8714
ISBN 978-2-88976-808-0
DOI 10.3389/978-2-88976-808-0

About Frontiers

Frontiers is more than just an open-access publisher of scholarly articles: it is a pioneering approach to the world of academia, radically improving the way scholarly research is managed. The grand vision of Frontiers is a world where all people have an equal opportunity to seek, share and generate knowledge. Frontiers provides immediate and permanent online open access to all its publications, but this alone is not enough to realize our grand goals.

Frontiers Journal Series

The Frontiers Journal Series is a multi-tier and interdisciplinary set of open-access, online journals, promising a paradigm shift from the current review, selection and dissemination processes in academic publishing. All Frontiers journals are driven by researchers for researchers; therefore, they constitute a service to the scholarly community. At the same time, the Frontiers Journal Series operates on a revolutionary invention, the tiered publishing system, initially addressing specific communities of scholars, and gradually climbing up to broader public understanding, thus serving the interests of the lay society, too.

Dedication to Quality

Each Frontiers article is a landmark of the highest quality, thanks to genuinely collaborative interactions between authors and review editors, who include some of the world's best academicians. Research must be certified by peers before entering a stream of knowledge that may eventually reach the public - and shape society; therefore, Frontiers only applies the most rigorous and unbiased reviews.
Frontiers revolutionizes research publishing by freely delivering the most outstanding research, evaluated with no bias from both the academic and social point of view. By applying the most advanced information technologies, Frontiers is catapulting scholarly publishing into a new generation.

What are Frontiers Research Topics?

Frontiers Research Topics are very popular trademarks of the Frontiers Journals Series: they are collections of at least ten articles, all centered on a particular subject. With their unique mix of varied contributions from Original Research to Review Articles, Frontiers Research Topics unify the most influential researchers, the latest key findings and historical advances in a hot research area! Find out more on how to host your own Frontiers Research Topic or contribute to one as an author by contacting the Frontiers Editorial Office: frontiersin.org/about/contact

DELAYED INJURY MECHANISMS AFTER ISCHEMIC AND HEMORRHAGIC STROKE

Topic Editors:
Devin William McBride, University of Texas Health Science Center at Houston, United States
Budbazar Enkhjargal, Boston University, United States
Prativa Sherchan, Loma Linda University, United States
Qin Hu, Shanghai Jiao Tong University, China

Topic Editor, Dr. Devin McBride, received financial support from Celense. The other Topic Editors declare no competing interests with regard to the Research Topic subject.

Citation: McBride, D. W., Enkhjargal, B., Sherchan, P., Hu, Q., eds. (2022). Delayed Injury Mechanisms After Ischemic and Hemorrhagic Stroke.
Lausanne: Frontiers Media SA. doi: 10.3389/978-2-88976-808-0

Table of Contents

frontiers in Neurology

EDITORIAL
published: 18 March 2022
doi: 10.3389/fneur.2022.881629

Editorial: Delayed Injury Mechanisms After Ischemic and Hemorrhagic Stroke

Devin W. McBride[1†], Prativa Sherchan[2†], Qin Hu[3†] and Budbazar Enkhjargal[4†]*

[1] The Vivian L. Smith Department of Neurosurgery, The University of Texas Health Science Center at Houston, Houston, TX, United States, [2] Department of Basic Sciences, Loma Linda University, Loma Linda, CA, United States, [3] School of Medicine, Shanghai Jiao Tong University, Shanghai, China, [4] School of Medicine, Whitaker Cardiovascular Institute, Boston University, Boston, MA, United States

Keywords: delayed injury, stroke, hemorrhage–cerebral, cerebral ischemia, biomarkers

Editorial on the Research Topic

Delayed Injury Mechanisms After Ischemic and Hemorrhagic Stroke

Stroke is a leading cause of death worldwide with about 12 million new cases per year. To date, no one is able to predict when a stroke will occur. Although "time is brain" has been the slogan for stroke care, many patients still arrive for care outside of the desired time window. Thus, research endeavors have focused on developing treatments to restore injured brain tissue. With the exception of a few treatments, many drug candidates fail in clinical trials. To better understand the pathological events following stroke, as well as to identify novel therapeutic targets, research focused on delayed injury mechanisms is ongoing.

Inflammation, edema, and vascular dysfunction are crucial pathophysiological events involved in delayed injury after stroke. While considerable research has been undertaken to understand these damaging processes in the acute phase, less is known about their respective contributions to delayed injury occurring 4–14 days after stroke. Furthermore, different stroke subtypes (i.e., ischemic vs. hemorrhagic) have similar, yet slightly differing delayed injury mechanisms.

The goal of this Research Topic is to provide a collection of papers investigating delayed injury mechanisms after stroke. Numerous experimental papers focus on the acute injury phase following stroke, usually <3 days. However, research looking at the role of these pathological events causing and during the delayed phase (typically 3–10 days in animals, 5–14 days in humans) is limited, especially with respect to experimental studies. This collection will promote the importance of delayed injury as an injury phase of stroke which can be prevented, thereby promoting recovery from the initial stroke (ischemic or hemorrhagic) injury. Naturally, research regarding delayed injury continues to examine potential biomarkers and predictors which can be used to identify patients at-risk for delayed injury.

DELAYED INJURY IN ISCHEMIC STROKE

Shen et al. investigate the utility of various hyperglycemia ratios in predicting poor outcome after ischemic stroke. The prospective study observed that using the ratio of fasting glucose to glycated hemoglobin (assessed by 48 h post-injury) is independently associated with worse outcomes at 3 and 6 months.

OPEN ACCESS

Edited and reviewed by:
Jean-Claude Baron, University of Cambridge, United Kingdom

***Correspondence:**
Devin W. McBride
devin.w.mcbride@uth.tmc.edu

†These authors have contributed equally to this work

Specialty section:
This article was submitted to Stroke, a section of the journal Frontiers in Neurology

Received: *22 February 2022*
Accepted: *25 February 2022*
Published: *18 March 2022*

Citation:
McBride DW, Sherchan P, Hu Q and Enkhjargal B (2022) Editorial: Delayed Injury Mechanisms After Ischemic and Hemorrhagic Stroke. Front. Neurol. 13:881629. doi: 10.3389/fneur.2022.881629

DELAYED INJURY IN INTRACEREBRAL HEMORRHAGE

In patients with intracerebral hemorrhage, peri-hematoma cerebral blood flow assessed 6 h post-hemorrhage was reported to be an independent risk factor for hematoma expansion in a delayed fashion. The results of the study by Wang et al. suggest closely monitoring cerebral blood flow in the peri-hematoma tissue. At a more delayed time point, Haque et al. performed a longitudinal imaging study to determine the volumes of the peri-hematoma tissue and hematoma, and microstructural integrity. The findings suggest that imaging at 1 month post-intracerebral hemorrhage can predict patients that are at-risk for poor outcomes at 3 and 6 months.

DELAYED INJURY IN SUBARACHNOID HEMORRHAGE

Delayed injury following subarachnoid hemorrhage manifests as delayed cerebral ischemia and neurological decline. To date there exists many studies which have investigated various factors for their use as predictors of delayed cerebral ischemia. While not an exhaustive list, hematoma volume, inflammation, vasospasm, and other serum cytokines/chemokines/factors have been reported. Some of the factors reported can easily be obtained (e.g., clinical data/characteristics, routine labs), while others (e.g., cytokines, serum proteins) require special methods. The study by Csók et al. in this topic develops a risk prediction model using easily obtained/available clinical data. The authors observed that their model, which combines hematoma volume, level of consciousness, and sonographic mean flow velocity of the intracranial arteries from admission to post-bleed day 5, is a simple and precise method for identifying subarachnoid hemorrhage patients which are at-risk for delayed cerebral ischemia. Another study in this topic also investigated readily available clinical data for predicting delayed cerebral ischemia. In their retrospective study, Lin et al. examined clinical characteristics and laboratory data to identify factors which can predict development of cerebral infarction in elderly subarachnoid hemorrhage patients. Of the factors assessed, admission body temperature was found to be independently associated with cerebral infarction. The findings from the study suggest that patients who have an admission body temperature lower than 36.6°C are at increased risk for developing cerebral infarction than patients who have an admission body temperature <36.6°C. The final manuscript investigating biomarkers/factors which can predict development of delayed cerebral ischemia examines inflammatory data. In a prospective study, Gusdon et al. observed that male subarachnoid hemorrhage patients had a higher number of monocytes than females. Furthermore, in males, early elevation of monocytes can predict delayed cerebral ischemia and poor outcomes.

Microthrombi and microvessel dysfunction have been receiving more attention as evidence of their contributions to delayed cerebral ischemia increase. In this topic, Pang et al. perform a mechanistic experimental study investigating microthrombi and pericytes. In agreement with others, microthrombi and microvessel dysfunction are factors contributing to poor outcome after subarachnoid hemorrhage. The work presented by Pang et al. shows that microvessels containing microthrombi have reduced pericyte coverage which may contribute to vasculature dysfunction. This study suggests that there may be a direct connection between microthrombi and microvessel dysfunction *via* pericytes and P-selectin. Additionally, the authors provide evidence that ApoE deficiency may contribute to more extensive damage *via* pericyte loss and microthrombi formation. Future studies need to be performed to investigate if reduced pericyte coverage has any effect on delayed injury.

In the future, understanding precise molecular and pathophysiological mechanism of delayed brain injury after stroke is crucial as a key of diagnostic and therapeutic strategy. Perspective studies require to fill this gap in stroke study as well as to discover successful drug candidates for the patients.

AUTHOR CONTRIBUTIONS

All authors listed have made a substantial, direct, and intellectual contribution to the work and approved it for publication.

FUNDING

DWM was funded by grants from the NIH and the Brain Aneurysm Foundation.

Conflict of Interest: The authors declare that the research was conducted in the absence of any commercial or financial relationships that could be construed as a potential conflict of interest.

Publisher's Note: All claims expressed in this article are solely those of the authors and do not necessarily represent those of their affiliated organizations, or those of the publisher, the editors and the reviewers. Any product that may be evaluated in this article, or claim that may be made by its manufacturer, is not guaranteed or endorsed by the publisher.

frontiers in Neurology

ORIGINAL RESEARCH
published: 28 June 2021
doi: 10.3389/fneur.2021.666311

Music Therapy Alleviates Motor Dysfunction in Rats With Focal Cerebral Ischemia–Reperfusion Injury by Regulating BDNF Expression

Weiguan Chen[1†], *Jiaxuan Zheng*[1,2†], *Guangyu Shen*[1], *Xin Ji*[3], *Linlin Sun*[3], *Xia Li*[1], *Feng Xu*[4*] and *Jin-hua Gu*[3*]

[1] Department of Rehabilitation Medicine, Affiliated Hospital of Nantong University, Nantong, China, [2] Department of Rehabilitation Medicine, The First Affiliated Hospital, Sun Yat-sen University, Guangzhou, China, [3] Department of Clinical Pharmacy, Affiliated Maternity & Child Healthcare Hospital of Nantong University, Nantong, China, [4] Department of Neurosurgery, Huashan Hospital, Shanghai Medical College, Fudan University, Shanghai, China

OPEN ACCESS

Edited by:
Prativa Sherchan,
Loma Linda University, United States

Reviewed by:
Julian Nicolas Acosta,
Yale University, United States
Andleeb Khan,
Jazan University, Saudi Arabia

***Correspondence:**
Jin-hua Gu
jhgu@ntu.edu.cn
Feng Xu
fengxu.dr@gmail.com

[†]These authors have contributed equally to this work

Specialty section:
This article was submitted to Stroke, a section of the journal Frontiers in Neurology

Received: 10 February 2021
Accepted: 27 May 2021
Published: 28 June 2021

Citation:
Chen W, Zheng J, Shen G, Ji X, Sun L, Li X, Xu F and Gu J-h (2021) Music Therapy Alleviates Motor Dysfunction in Rats With Focal Cerebral Ischemia–Reperfusion Injury by Regulating BDNF Expression. Front. Neurol. 12:666311. doi: 10.3389/fneur.2021.666311

Background/Aim: Music-based therapy plays a role in central nervous system diseases. We aimed to explore the effect of different doses and durations of music therapy on motor function recovery after stroke and the underlying molecular mechanisms.

Methods: Adult male Sprague–Dawley rats were subjected to middle cerebral artery occlusion (MCAO) for 1 h, which was followed by reperfusion. In experiment 1, the rats that survived 1 week after MCAO surgery were randomly allocated into four groups (n = 10 per group): MCAO group, 1 h music group (Mozart K.448 music therapy 1 h per day for 2 weeks), 12 h music group (Mozart K.448 music therapy 12 h/day for 2 weeks), and accelerated music group (reversely accelerated music therapy 12 h for 2 weeks, AM group). In experiment 2, the survived rats were randomly divied into three groups: MCAO group, 12 h music group (music therapy 12 h/day for 3 weeks), and 12 h music-R group (music therapy 12 h/day for 2 weeks and rest for 1 week). Three neuroscores were evaluated daily, starting on the first day after surgery until the end of the experiment. The rats were killed 3 weeks after MCAO surgery in experiment 1 or 4 weeks after surgery in experiment 2. Nissl staining of infart core, peri-infarct zone, and motor cortex was performed to assess neuronal survival and regeneration. Western blot and immunofluorescence were used to detect the expression and distribution of brain-derived neurotrophic factor (BDNF) and glial fibrillary acidic protein (GFAP) in ipsilateral hemispheres.

Results: In the experiment of different music therapy doses, the motor function in the 12-h music group but not in the 1-h music group and AM group was significantly improved compared with that of the MCAO group. The BDNF protein level of the ipsilateral hemisphere motor cortex in the 12-h music group and the 1-h music group was higher than that of the MCAO group. The neurons and Nissl bodies were more in the 12-h music group than in the MCAO group. Immunofluorescence assay showed that a

12 h music therapy induces BDNF and GFAP accumulation at the damage boundary. In the experiment of different music therapy durations, 3 weeks music therapy (12 h music group) induced more longer cell synapses and more clearer cell-to-cell connections than 2 weeks music intervention (12 h music-R group). Moreover, the GFAP morphology in the 12-h music group was more similar to mature activated astrocytes than that in the 12-h music-R group.

Conclusions: Music therapy may improve poststroke motor function and promote neuronal repair in the long term. The mechanism may be through stimulating BDNF and GFAP secretion in the injured motor cortex.

Keywords: music, middle cerebral artery occlusion, motor dysfunction, brain derived neurotrophic factor, glial fibrillary acidic protein

HIGHLIGHTS

- Music therapy can improve motor function after stroke.
- Music therapy induces BDNF accumulation in the motor cortex after stroke.
- Music therapy promotes neuronal repair and improves brain plasticity.

INTRODUCTION

Stroke is a common and serious global health problem, and ischemic stroke accounts for ∼75–85% of the total number of strokes (1). Stroke has become the second leading cause of death worldwide (2) and the first cause of mortality among Chinese urban and rural residents (3). Motor dysfunction due to stroke is one of the most common dysfunctions after stroke, accounting for about 70% of all cases, and seriously affects patients' activities (4). Currently, effective drugs for poststroke dysfunction are lacking (5–7). Although existing rehabilitation treatments based on exercise and occupational and physical therapies have greatly contributed to alleviating dysfunctions, they have extremely limited effects when the patient's disease course exceeds 1 year. Moreover, further improving patients' functional capacity is challenging, and the fatigue it brings to the patient also makes it difficult for the patient to persist in training.

Based on a practical function, music therapy is used to treat diseases or promote physical and mental health in accordance with systematic therapeutic procedures. As an emerging rehabilitation intervention, music therapy has achieved certain effects in various neurological disorders (8). Music therapy, including rhythmic auditory stimulation, can effectively improve poststroke motor function, such as upper limb function (9), gait, and stride length (10) and reduce reliance on compensatory movements (11). A previous study has shown that music therapy has different effects in regulating human blood pressure, heart rate, and hormones (12). In addition, music therapy can activate the auditory area, motor area, and hippocampus and plays a positive role in various neurological diseases (13, 14). Furthermore, music therapy has a positive effect on speech disorders, motor dysfunction, cognitive disorders, and mood disorders after stroke (8, 15).

Currently, Mozart's music is recognized as one of the most effective and therapeutic music to listen to. Studies have confirmed that it has beneficial effects in relaxing the body and mind and in regulating blood pressure, heart rate, and endocrine and cerebral blood flow (16, 17). In a rat model of epilepsy, brain-derived neurotrophic factor (BDNF) levels were increased after playing Mozart's music (16, 17). However, studies on the molecular mechanism of music therapy on stroke are few, and the optimal dose and duration of music therapy remains unclear.

Therefore, we aimed to explore the effect of music therapy on motor function recovery after stroke and to determine the influence of different doses and durations of music therapy on neuronal repair.

MATERIALS AND METHODS

Animals

Adult male Sprague–Dawley rats weighing 220–250 g were kindly provided by Nantong University (Nantong, China). This study was approved by the Animal Care and Use Committee (IACUC) of the Affiliated Maternity and Child Health Care Hospital of Nantong University. All procedures were performed according to the guidelines issued by the IACUC (No. S20170422-112).

Reagents and Antibodies

Primary antibodies BDNF (1:500), GFAP (1:2,500), and β-actin (1:10,000) used in this study were obtained from Millipore company (Billerica, MA, USA). Alexa Fluor®488- and Alexa Fluor®647-conjugated donkey anti-rabbit IgG were obtained from Jackson ImmunoResearch Laboratories (West Grove, PA, USA). The enhanced chemiluminescence (ECL) kit was from Thermo Scientifc (Rockford, IL, USA). Other chemicals were from Sigma (St. Louis, MO, USA).

Middle Cerebral Artery Occlusion

All rats were raised for 1 week to acclimate to a temperature of 25°C and humidity of 55–75% and were exposed to a 12-h photoperiod (2,800 Lux). Rats were fed on water *ad libitum* and standard chow. In preparation for the middle cerebral artery occlusion (MCAO), 80 rats were continually anesthetized with

3% isoflurane, which was followed by intubation and ventilation with 2.0–2.5% isoflurane in a mixture of 30% oxygen and 70% air. They were inverted and fixed; subsequently, an area of the skin over the right carotid artery was exposed. After clipping the hair, the skin was scrubbed with betadine, rinsed in alcohol, and painted with iodine. A skin incision was made over the right common carotid artery. The internal and external carotid arteries were isolated and exposed. A 5–0 monofilament Nylon (Doccol Corporation; Sharon, MA, USA) was threaded into the internal carotid artery through a small incision on the external carotid artery. The suture was advanced toward the middle cerebral artery region to induce focal ischemia and was retained for 1 h; thereafter, it was removed for reperfusion. Sham rats underwent the same protocol without MCAO. Rats' body temperature was maintained with the heating pad and a warming blanket. Rats were weaned off the respirator until recumbent and alert. Ten sham-operated rats underwent identical surgery, but the suture was not inserted.

Postoperative Care

Subcutaneous fluids were administered acutely (5 ms/kg sterile saline) following surgery to prevent dehydration. Rats were kept in a warm environment (e.g., 28°C) until fully conscious and were checked 2–3 h after surgery and at least once daily for 1 week. Postoperative pain was managed by intraperitoneal injection of 5 mg/kg ketoprofen. After 1 week, 10 of 80 MCAO rats died (the mortality rate is 12.5%).

Music Intervention

Experiment 1

To study the effects of different doses of music therapy, the survived rats suffered from MCAO surgery and sham-operated

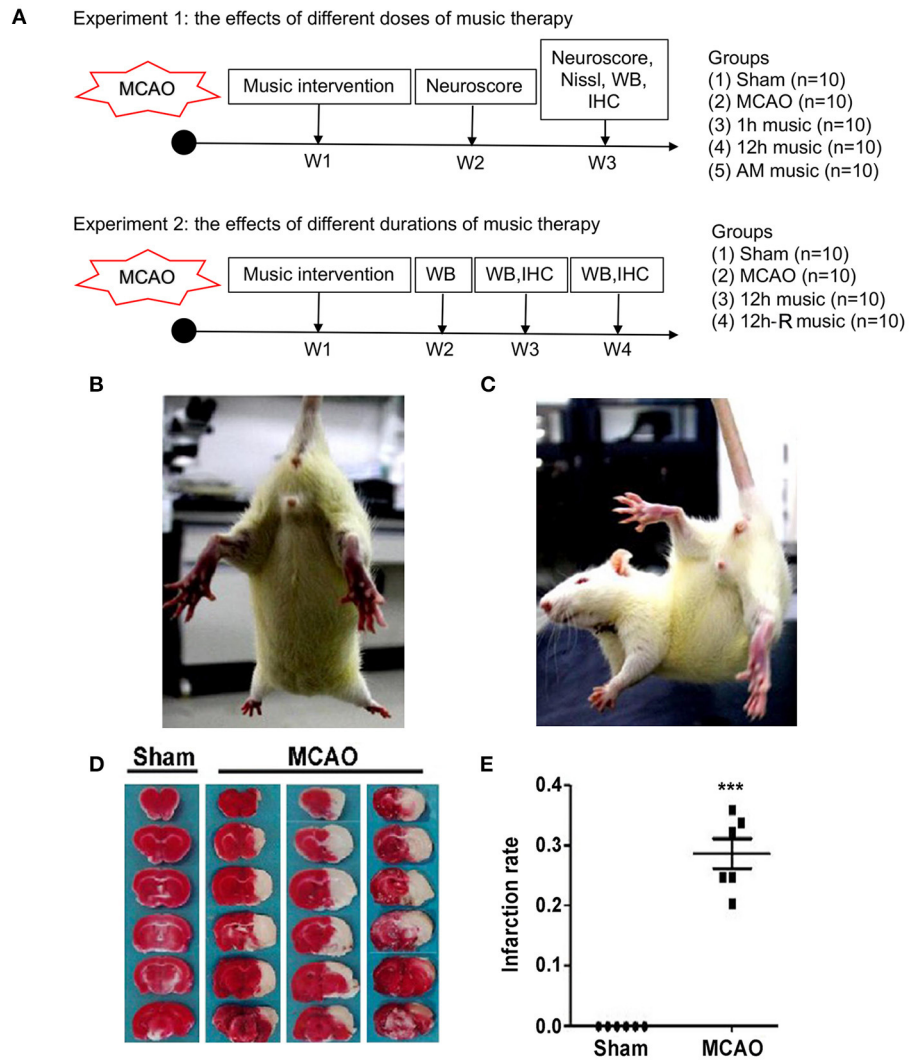

FIGURE 1 | Experimental design and verification of cerebral MCAO surgery in rats. **(A)** Experimental design and animal groups. **(B,C)** The postural reflex test for sham rat and MCAO rat. **(D,E)** Coronal sections of the sham and MCAO rats were stained with TTC. AM, accelerated music; IHC, immunohistochemistry; MCAO, middle cerebral artery occlusion; W, week; WB, western blot. ***$p < 0.001$. The asterisks represent significant difference compared with the sham group.

rats were divided into five groups ($n = 10$ per group): sham, MCAO, 1 h music, 12 h music, and accelerated music group (AM group). Music intervention started at 1 week after surgery. The rats in the 1-h music group were exposed to Mozart K.448 (65–75 dB) from 8 to 9 p.m. every day (17), those in the 12-h music group continually received the music therapy from 8 p. m. to 8 a.m., and those in the AM group were exposed to reversely accelerated music (8 × speedup). The music therapy continued for 2 weeks. The sham and MCAO groups were left undisturbed (∼25 dB). The rats in both groups were housed at a density of one rat per cage (**Figure 1A**, upper panel).

Experiment 2

To study the effects of different durations of music therapy, the survived rats and sham-operated rats were randomly assigned to four groups ($n = 10$ per group): sham, MCAO, 12 h music (music without rest), and 12 h music-R (music with rest) group. At 1 week after operation, the rats in the 12-h music group continually received the music therapy for 3 weeks. Music intervention in the 12-h music-R group lasts for 2 weeks and then rest for 1 week (**Figure 1A**, lower panel).

Neurobehavioral Evaluation

Modified neurological severity score (mNSS), general deficits, focal deficits, and beam walking tests were performed daily, starting on the first day after the surgery and were continued until the end of the experiment. The examiners were blinded to the procedures that the rat underwent. To evaluate the neuroprotective effects of music therapy, the original neurological severity score was modified (18). mNSS, which is a composite of motor, sense, beam balance, and reflection tests, was evaluated according to the scoring scheme presented in **Table 1**. The scoring of general deficits and focal deficits is presented in **Tables 2**, **3**. To evaluate the motor function of the rats, postural reflex test was performed; the rats were gently lifted by the tail (1 m above the ground) and observed for body rotation and limbs flexing.

TABLE 1 | The scoring scheme of the modified neurological severity score (mNSS) based on motor, sensor, beam balance and reflection tests.

Test types	Points
Motor test	
Raising by the tail	
Forelimb flexion	1
Hindlimb flexion	1
Head deflection more than 10 degrees on the vertical axis in 30 s	1
Placing on the floor	
Normal walk	1
Inability to walk	1
Turning to the sick side	2
Falling down to the sick side	3
Sensor test	
Placing test	
Vision and tactility	1
Proprioceptive neuromuscular test	
Push the rat paws to the edge of the table to stimulate limb muscles	1
Beam balance test	
Maintaining balance and stable posture	0
Holding on to the balance beam	1
Hugging the beam while one limb falling down from the beam	2
Hugging the beam while two limbs falling down, or spinning on the beam	3
Trying to maintain balance but falling down after 40 s	4
Trying to maintain balance but falling down after 20 s	5
Falling down without trying to stay steady within 20 s	6
Reflection test	
Head shaking when stimulating the external ear canal	1
Blinking when gently stimulating the cornea with cotton	1
Motor reflection to a brief noise from clapping	1
Seizures, myoclonus, or myospasm	1

Triphenyl Tetrazolium Chloride Staining

The rats were decapitated under anesthesia at the end of the 24-h period after MCAO. Brain tissues were carefully obtained and washed in precold phosphate-buffered saline (PBS). The fresh brain tissues were immediately frozen at −20°C for 20 min and subsequently cut into 2-mm-thick coronary sections. The coronal sections were incubated in 2% triphenyl tetrazolium chloride (TTC) (Sigma-Aldrich, St. Louis, MO, USA) prepared in PBS at 37°C in the dark for 20 min. The coronal sections were then fixed in 4% paraformaldehyde overnight. The infarction rate was examined using Image J software (NIH, Bethesda, MD, USA).

Nissl Staining

Tissue sections on coated slides were washed for 10 min three times in PBS. Thereafter, the slides were immersed in chloroform for 30 min and subsequently in acetone for 15 min. The tissues were rehydrated in graded ethyl alcohol (100, 95, and 70%; 30 s each). The slides were rinsed in distilled water twice and stained using cresyl violet (Beyotime, Shanghai, China) for 15–30 min at room temperature. Moreover, the slides were washed in distilled water, differentiated in ethyl alcohol (70, 95, and 100%; 30 s each), immersed in chloroform for 5 min, and incubated with 95% ethyl alcohol (the pH was adjusted to 4.1 using acetic acid). Thereafter, the slides were treated with ethyl alcohol (95, 100, and 100%; 30 s each), which was followed by deparaffinization with xylene (three times for 2–3 min each treatment). Lastly, the slides were mounted in neutral balsam.

Western Blot Analysis

The tissues were collected from the right motor cortex and lysed in radio-immunoprecipitation assay lysis buffer (Beyotime) supplemented with phenylmethanesulfonyl fluoride (Beyotime) and protease inhibitor cocktail (Roche, Mannheim, Germany). After homogenate extraction, the extract was maintained on ice for 30 min. The supernatant was collected by centrifugation (4°C, 12,000 rpm, 15 min), which was performed twice. Protein concentration was examined using

TABLE 2 | The scoring scheme of the general deficits in fur, ears, eyes, body position, spontaneous activity, and epilepsy.

Test types	Points
Hair	
Shiny, clean, and tidy	0
Vertical or dirty hair in 1–2 places usually around the nose and eyes	1
Vertical or dirty hair in more than 2 places	2
Ears test	
The ears are stretched to the side and back, and respond quickly to noise from the vertical direction	0
One or both ears are loose and weak, in a horizontal extension state, unable to extend back, and can respond to noise	1
One or both ears are loose and weak, in a state of lateral extension, unable to stretch back, and unable to respond to noise	2
Eyes test	
Eyes are open, clean and can react quickly	0
Eyes secrete watery or mucus-like discharge, and the eyes react slowly	1
Eyes are dark and dull	2
The cracks in the eyes are not round but oval and accompanied by discharge	3
Eyes are closed	4
Posture	
The rat can stand upright, its back is parallel to the ground, and when it is gently rocking, it can quickly maintain stability with its limbs	0
When the rat rests and walks, the back is bulged; the body is lowered when it is shaking instead of keeping the limbs stable	1
Head or part of the torso is resting on the ground	2
The rat's body is tilted to one side, but it can transform itself into an upright state	3
Inability to turn into upright and prone positions	4
Spontaneous activity	
Being alert, agile, and actively exploring	0
Being calm and quiet, start and stop exploring slowly and repeatedly	1
Listless, moving slowly, but no exploratory behaviors	2
Drowsy, unconscious, and hardly moving	3
No spontaneous movement, except for occasional responses to stimuli	4
Epileptic behavior	
Present with epilepsy symptoms	0
Suddenly rush out, repeatedly climb the cage wall or swing aimlessly	1
Be aggressive and nervous, look sluggish, or over-excited	3
Excessive excitement, galloping after being stimulated, showing localized seizures or generalized convulsions	9
Severe seizures with changes in breathing or consciousness	12

TABLE 3 | The scoring scheme of the focal deficits in symmetry, gait, climbing, circling, and sensory response.

Test types	Points
Symmetry test	
Limbs are placed symmetrically under the body, with the tail straight back	0
The body is slight asymmetry and tilts to the affected side, the tail always deviates from the midline, and the limbs are not significantly asymmetry	1
The body is moderately asymmetry, the body is inclined to the affected side, the paralyzed limbs are stretched out, and the tail is off the midline	2
The body is significantly asymmetry, the body is bent into an arc, and the affected side is leaning on the table	3
The body is extremely asymmetrical, the body and tail are tightly bent, and the affected side is always on the table	4
Gait test	
Normal gait: flexible, symmetrical, fast	0
Mechanical gait: stiff, inflexible walking, moving in a hunched posture, or slowing down	1
Slight limp, asymmetry during grasping or movement	2
Severe limping, drifting, falling, obvious defects in gait	3
No spontaneous walking, no more than 3 steps after stimulation	4
Climbing test	
Quickly climb to the top edge of the slope	0
Climbing slowly, obviously tightening	1
Stay on the slope and do not slide down or climb up	2
Gradually decline, make efforts to stop the decline, but fail	3
Slid immediately and made no effort to stop it	4
Circling test	
Turn left or right equally	0
Spin mainly to one side	1
Turn sideways without continuity	2
Keep turning to one side	3
Rotating, swaying, moving slowly in circles, or maintaining motionless	4
Sensory response test	
Turn the head to the irritated area and stay away from the irritation	0
The affected side's reaction is delayed and weakened, while the contralateral reaction is normal	1
Absent response on the affected side, normal response on the contralateral side	2
Absent response on the affected side, weakened response on the contralateral side	3
Lack of bilateral proprioceptive response	4

bicinchoninic acid kit (Thermo Science Fisher, Waltham, MA, USA) according to the user's manual. Approximately 20 μg of proteins were loaded and electrophoresed on 10% sodium dodecyl sulfate-polyacrylamide gel electrophoresis. The proteins were electronically transferred onto a polyvinylidene fluoride membrane (Millipore, Bedford, MA, USA). The membrane carrying the proteins was blocked with 5% skim milk for 90 min at room temperature. After washing in Tris-buffered saline–Tween (TBST), the membrane was incubated with primary antibodies against BDNF, GFAP, and β-actin (Millipore, Billerica, MA, USA) overnight at 4°C. The membrane was rinsed in TBST for 15 min three times; subsequently, it was incubated with horseradish peroxidase-conjugated goat-anti-mouse or goat-anti-rabbit IgG (Bioworld, Minneapolis, MN, USA) at 37°C for 1 h. Protein bands were determined using a chemiluminescent

substrate kit (Thermo Science Fisher) before visualization using Image J software.

Immunohistofluorescence

The frozen brain tissue section was washed in PBS for 15 min three times and inubated with 1% Triton in PBS for 15 min. Slides were inucbated with 5% normal donkey serum for 90 min. Thereafter, the slides were incubated with primary antibodies against BDNF and GFAP at 4°C overnight and were subsequently washed in PBS for 20 min three times. Alexa Fluor®488- and Alexa Fluor®647-conjugated donkey-anti-rabbit IgG were used to amplify the protein signaling (Jackson ImmunoResearch, West Grove, PA, USA), and the incuabtion was performed at room temperature for 60 min. To detect nuclei, 2-(4-amidinophenyl)-6-indolecarbamidine dihydrochloride (Beyotime) was incubated with the slides for 15 min. The slides were photographed with a confocal scanning microscope (Leica, Wetzlar, Germany) installed with Image J software.

Statistical Analysis

Statistical analysis was conducted with IBM SPSS Statistics 21 software (IBM Corporation, Armonk, NY, USA). Data are presented as menas ± standard error mean of at least three independent experiments. One- or two-way analysis of variance was used to compare the difference between multiple groups. Least significant difference was used for pairwise comparison; *U*-test, for non-parametric comparision. A difference with $p < 0.05$ was considered to be statistically significant.

RESULTS

Effects of Music on Neurobehavioral Outcomes of MCAO Rats

Postural reflex test was performed after MCAO. Sham rats showed no obvious neurological deficit during limb extension (**Figure 1B**), while the MCAO rats flexed to the affected side, retracted and internally rotated the left limb, and tilted the trunk to the affected side (**Figure 1C**). Moreover, TTC staining showed considerable infarct changes in the MCAO group compared with the sham group ($p < 0.001$) (**Figures 1D,E**). These results indicated that MCAO model in rats was effectively established.

Music intervention was initiated on day 8 post-MCAO and was provided for 2 weeks. We assessed the effects of music therapy on neurological function. The mNSS of the sham group was significantly lower than that of the MCAO, 1 h music, 12 h music, and AM groups on days 2, 7, 14, and 21 post-MCAO ($p < 0.001$) (**Figure 2A**). Before music intervention, mNSS showed no significant difference between MCAO and 1 h music, 12 h music, or AM groups ($p > 0.05$) (days 2 and 7 post-MCAO). The 12-h music group showed a significantly decreased mNSS compared with the MCAO group on days 14 and 21 post-MCAO ($p < 0.05$) (**Figure 2A**). The mNSS of the 12-h music group was lower than that of the 1-h music group on days 14 and 21 ($p < 0.05$) (**Figure 2A**). Moreover, MCAO significantly caused general deficits addressing the hair, ears, eyes, posture, spontaneous activity, and epileptic behavior on the second day after MCAO ($p < 0.01$ or $p < 0.001$) (**Figure 2B**). MCAO resulted in focal

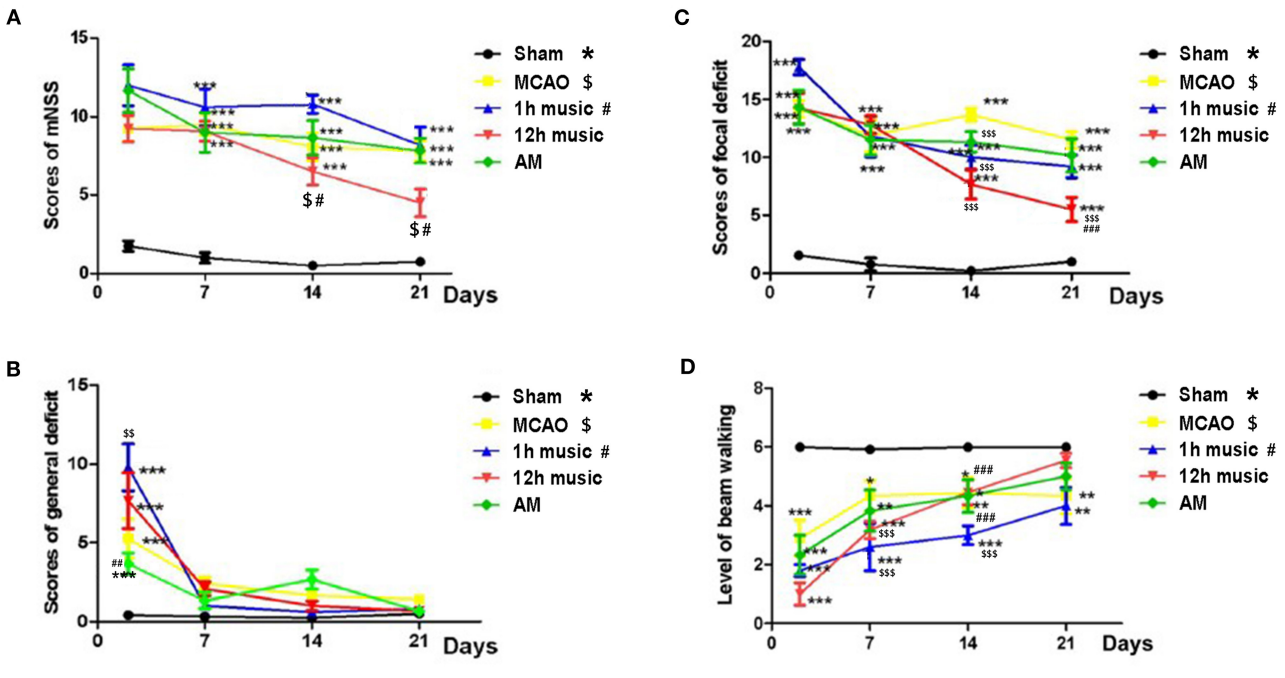

FIGURE 2 | Effects of music on neurobehavioral outcomes of MCAO rats. **(A)** mNSS, **(B)** general deficit scores, **(C)** focal deficit scores, and **(D)** beam walking level of the sham, MCAO, 1 h music, 12 h music, and AM rats. Music therapy was initiated on the eighth day after MCAO. $^{*,\$,\#}p < 0.05$; $^{**,\$\$,\#\#}p < 0.01$; $^{***,\$\$\$,\#\#\#}p < 0.001$. The asterisk, dollar sign, and number symbol represent a significant difference compared with the sham, MCAO, and 1 h music groups, respectively.

deficits affecting symmetry, gait, climbing, circling, and sensory response ($p < 0.05$). Music therapy significantly ameliorated the focal neurological deficits in the 12-h music group on days 14 and 21 post-MCAO ($p < 0.001$) (**Figure 2C**). In addition, the beam walking ability, which was impaired by MCAO, improved in the 12-h music group ($p < 0.001$) (**Figure 2D**).

Effect of Music Therapy on Brain Tissue Loss and Neuronal Repair in MCAO Rats

The MCAO rats exhibited brain atrophy and liquefied changes. In the 12-h music group, brain atrophy was improved (**Figure 3A**). Furthermore, we performed Nissl staining of the infarct area, boundary, and motor cortex in the sham, MCAO, 1 h music, 12 h music, and AM groups. After 2 weeks of music intervention, the number of nerve cells was increased, the intercellular space reduced, and the neurons and Nissl bodies in infarction, boundary, and motor cortex increased in the 1-h music and 12-h music groups compared with the MCAO group. Particularly, the 12-h music therapy increased nerve cell generation and induced network structure formation between nerve cells (**Figure 3B**). The normal neurons and Nissl bodies around the injured area was higher in the 12-h music group than in the AM group; the AM group was dominated by vacuole-like cells instead of Nissl bodies (**Figure 3C**). Thus, in MCAO, which could result in significant damages to the brain structures, a 12-h music therapy has a therapeutic value.

Effects of Music Therapy on BDNF and GFAP Expression

To explore the molecular mechanisms in the amelioration of cerebral ischemia–reperfusion injury by music therapy, the BDNF level in the motor cortex was examined. After 2 weeks of music intervention, the BDNF content in the right motor area was significantly higher in the 12-h music group than that in the sham ($p = 0.0001$), MCAO ($p = 0.0001$), or AM ($p < 0.0001$) groups (**Figure 4A**). No significant difference in BDNF content between the MCAO group and AM group was found ($p > 0.05$). Similarly, the BDNF content was significantly higher in the 1-h music group than that in the sham ($p = 0.003$) or MCAO groups ($p = 0.007$). However, no significant difference in BDNF content between the 1-h music and 12-h music groups was observed ($p > 0.05$).

To better understand the repair of the infarct area, we performed immunofluorescence analysis to detect the expression and distribution of BDNF and GFAP after 2 weeks of music intervention. BDNF and GFAP in the sham, MCAO, 1 h music, 12 h music, and AM groups were evaluated; the 12-h music group showed the highest content and the widest distribution of BDNF in new undifferentiated cells and astrocytes (**Figure 4B**). The BDNF fluorescence intensity in the 1-h music group was slightly lower than that in the 12-h music group, although the GFAP content was relatively high and the connection was formed in the liquefaction zone in the 1-h music group. Relatively few newly born and undifferentiated cells were observed in the 1-h music group. In the MCAO group, BDNF distribution was scattered and BDNF was detected in newly born and undifferentiated cells.

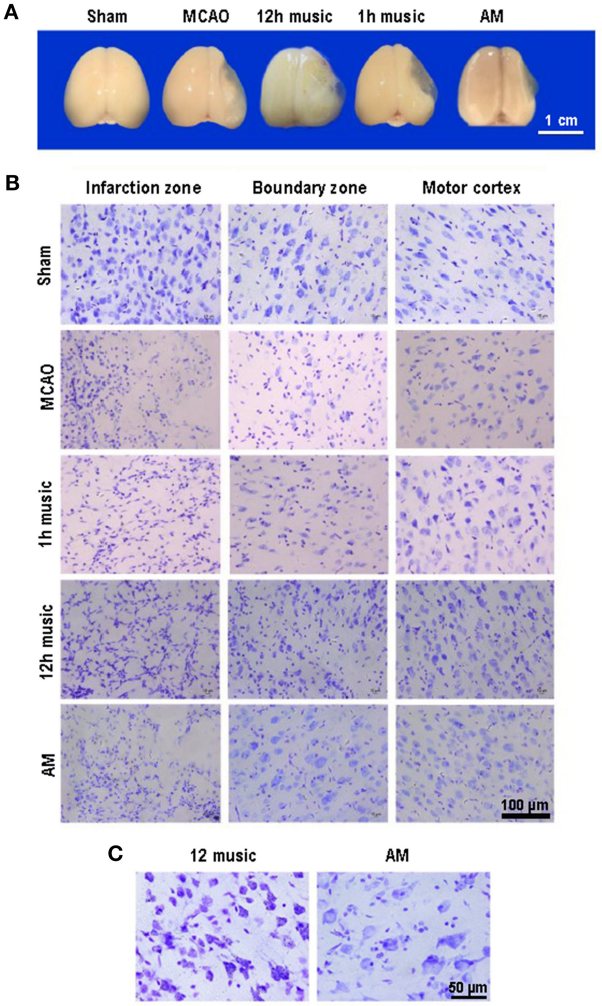

FIGURE 3 | Music therapy induced changes in brain morphology and neuronal repair. **(A)** Brains of sham, MCAO, 1 h music, 12 h music, and AM rats 21 days after MCAO operation. **(B)** Comparison of the effects of forward music and those of 8 × speedup reverse music on neuron repair. Music therapy was started on the eighth day after MCAO, and the treatment continued for 2 weeks. **(C)** Enlarged morphology comparison between 12 h music group and AM group.

GFAP fluorescence intensity was weak and GFAP was distributed in dots. In the AM group, BDNF was distributed in dots, and the BDNF fluorescence intensity was not significantly different from that in the MCAO group; the nuclei were evenly distributed in the liquefaction zone, and low GFAP expression was observed.

Persistent Effects of 12 h Music Therapy on BDNF and GFAP Expression

To determine the duration of the effects of one course of 12 h music therapy, we examined the expression and distribution of BDNF and GFAP at 1, 2, and 3 weeks after the music intervention, which corresponded to the second, third, and fourth week after MCAO. As shown in **Figure 5A**, the brains of the MCAO group gradually liquefied and collapsed and were not

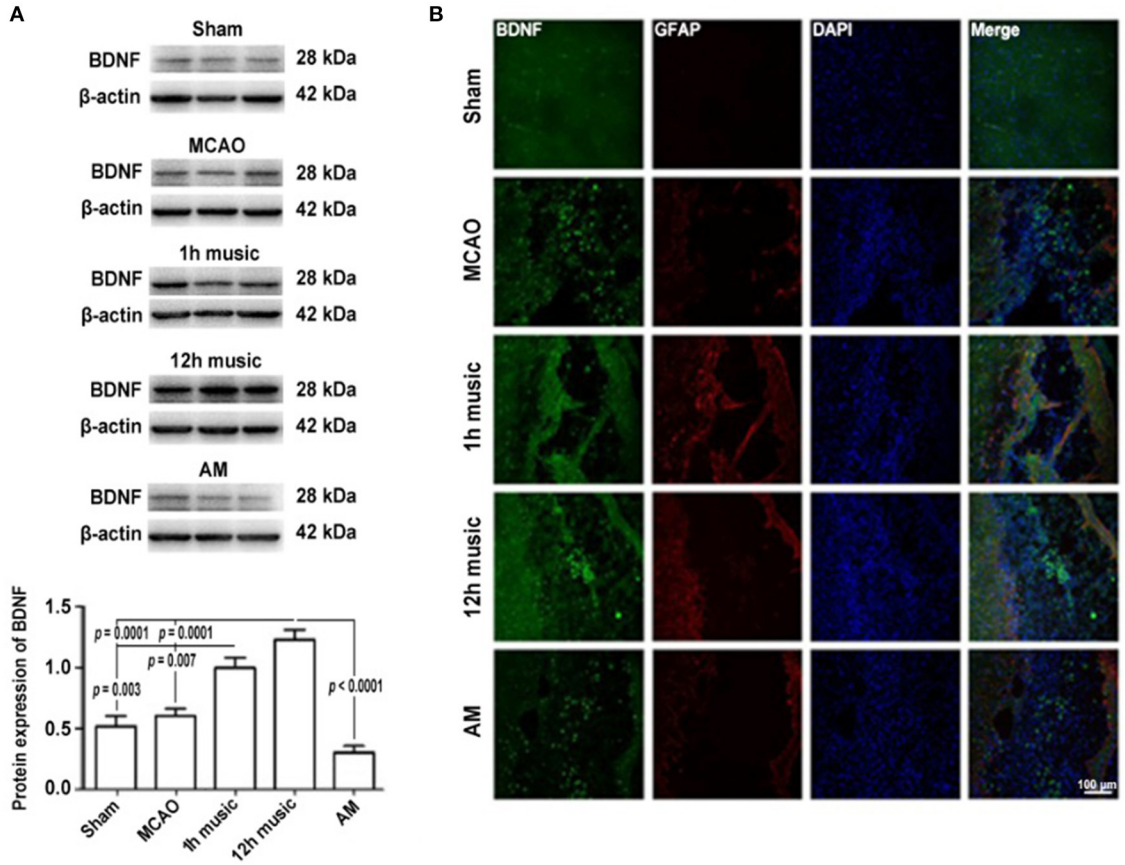

FIGURE 4 | Music therapy after MCAO increased the BDNF expression. **(A)** Western blot analysis of BDNF in the lesioned area. **(B)** Relative fluorescence intensity of BDNF and GFAP in the motor cortex. Music therapy was started on the eighth day after MCAO, and the treatment continued for 2 weeks.

filled with new jelly until the fourth week after the operation. One week after the music intervention, the brains of the 12-h music group were intact and full, and the infarct core area was semipermeable; 2 weeks after the intervention, the non-infarcted area was filled with transparent jelly, and filiform connections were visible; and 3 weeks after the intervention, the brain shape remained full and brain volume was similar to that of the sham group.

No significant difference in BDNF content among the sham, MCAO, and 12 h music groups was found after 1 week of music intervention. The BDNF content in the 12-h music group was significantly higher than that of the MCAO and sham groups after 2 weeks of intervention ($p = 0.014$). However, no significant difference was observed among the three groups after 3 weeks of intervention ($p > 0.05$) (**Figures 5B,C**). The GFAP content in the 12-h music group was significantly higher after 3 weeks of intervention than that after 1 week of intervention. However, no significant difference in GFAP content in the 12-h music group was found between 3 and 2 week interventions ($p > 0.05$) (**Figures 5B,D**). Moreover, the BDNF content in the 12-h music-R group (in which music intervention was performed for 2 weeks followed by 1 week of rest) was not significantly different from that in the sham, MCAO, and 12 h music groups ($p > 0.05$) (**Figures 6A,B**). Similarly, no statistically significant difference in the GFAP content was noted between the 12-h music and the 12-h music-R groups (**Figures 6A,C**). Additionally, immunofluorescence assay showed BDNF accumulation in newborn cells and astrocyte cell morphology in the music group, and the GFAP fluorescence intensity was stronger in the music group than that in the MCAO group (**Figure 6D**).

The different courses of music intervention resulted in increased BDNF content in the motor area, which subsequently decreased. Music intervention lasts for 2 weeks and then rest for 1 week; the BDNF level was significantly lower in the 12-h music-R group than that of the music group with 2-week intervention ($p = 0.032$) (**Figures 7A,B**). Although the GFAP levels in the 12-h music and 12-h music-R groups were significantly different after 2 weeks of intervention, the difference was not statistically significantly after 3 weeks of intervention ($p > 0.05$) (**Figures 7A,C**). No significant difference in BDNF fluorescence intensity was found between the 12-h music and the 12-h music-R groups (**Figure 7D**). Moreover, the cells in the 12-h music and 12-h music-R groups gradually differentiated into mature astrocytes; both groups showed better cell differentiation than the

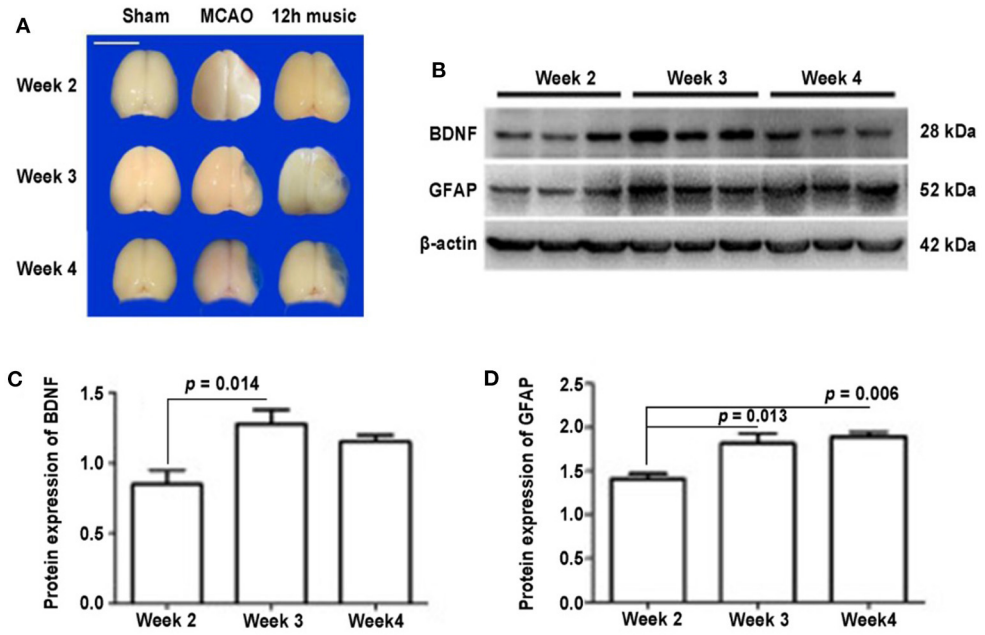

FIGURE 5 | Effects of 12 h music therapy on brain morphology and the expression of BDNF and GFAP at 2, 3, and 4 weeks after MCAO. **(A)** Brains of sham, MCAO, and 12 h music groups at 2, 3, and 4 weeks after MCAO. Bar, 1 cm. **(B)** Western blot analysis of BDNF and GFAP in the lesioned area of the 12-h music group. Quantification of **(C)** BDNF and **(D)** GFAP examined by Western blot.

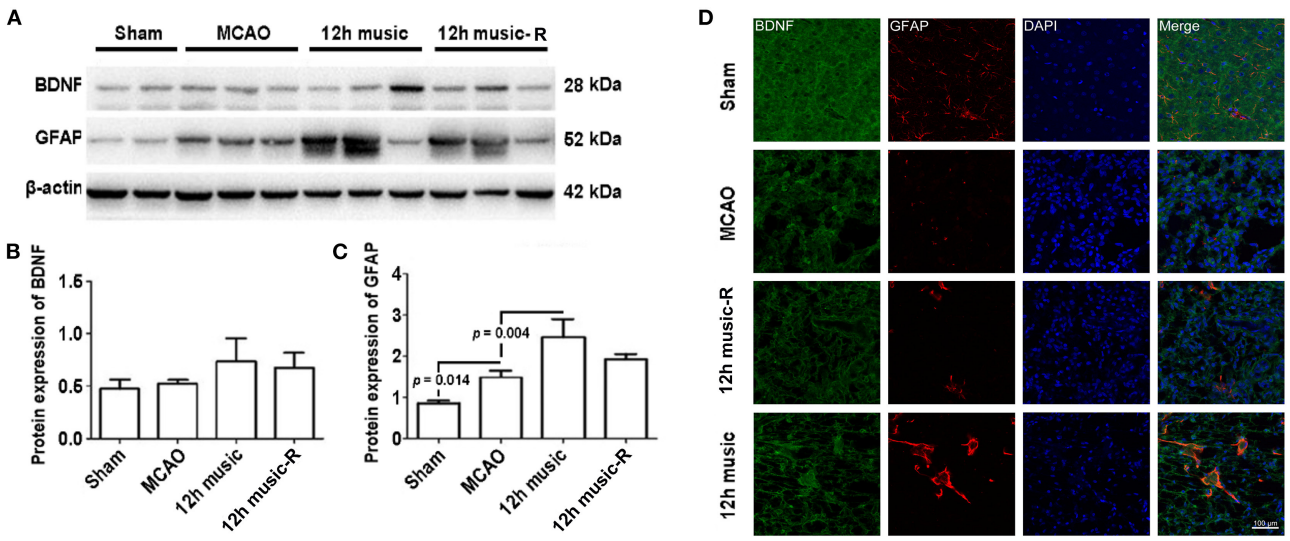

FIGURE 6 | Effects of 12 h music therapy on BDNF and GFAP expressions at 4 weeks after MCAO. **(A)** Western blot analysis of BDNF in the lesioned area. Quantification of **(B)** BDNF and **(C)** GFAP examined by Western blot. **(D)** Relative fluorescence intensity of BDNF and GFAP in motor cortex. The BDNF and GFAP expressions were examined after 3 weeks of intervention in the 12-h music group and after 2 weeks of intervention plus 1-week rest in the 12-h music-R group.

MCAO group. In the MCAO group, the BDNF in the newborn cells of the infarct core area formed a network structure; however, the cell boundaries were unclear, clear synaptic connections are lacking, and GFAP was mostly distributed in dots. In the 12-h music-R group, the newborn cells had short synaptic connections, which form an astrocyte morphology. In the 12-h music group, the continuous intervention resulted in longer synapses and clearer cell-to-cell connections, and the GFAP morphology was closer to that of mature activated astrocytes, and the cells differentiated well.

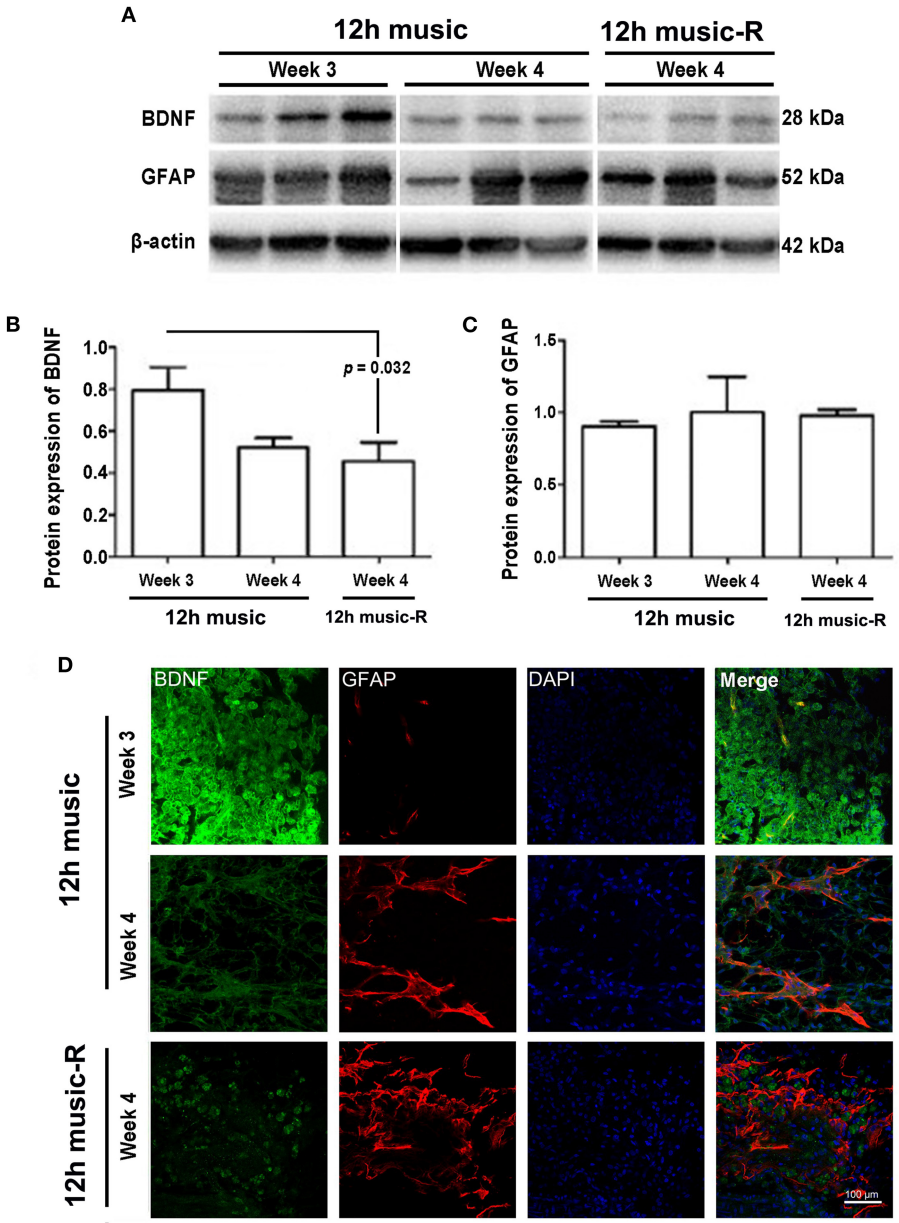

FIGURE 7 | Persistent effects of 12 h music therapy on BDNF and GFAP expression. **(A)** Western blot analysis of BDNF in the lesioned area. Quantification of **(B)** BDNF and **(C)** GFAP examined by Western blot. **(D)** Relative fluorescence intensity of BDNF and GFAP in the motor cortex. Rats in the 12-h music group continually received the intervention for 3 weeks; those in the 12-h music-R group, for 2 weeks plus 1-week rest. BDNF and GFAP levels were examined at 3 and 4 weeks after MCAO.

DISCUSSION

Motor dysfunction, which directly affects a patient's activities of daily living, is the most common dysfunction after stroke and is related to patient's quality of life (19). A number of clinical studies have confirmed that the use of music rehabilitation measures can significantly improve poststroke dysfunction, including motor dysfunction (20) and speech disorder (21). Thus, this study aimed to focus on the effect of music on poststroke movement disorders. Here, an MCAO rat model was used to simulate the pathological state of human stroke, and music therapy was used as the intervention.

Music can regulate various human body activities. A previous study has shown that hypertensive rats that listen to Mozart's music for 2 h a day under light conditions showed reduced heart rate without blood pressure changes and that Ligeti's music can increase blood pressure (22). Studies have also shown that music can regulate breathing and cardiovascular contraction

and relaxation and has a role in the inflammatory response regulation (23). For example, Mozart's piano sonatas has been proven to reduce the expression of inflammation markers and improve the activation of the immune system natural killer cells (23).

Our study focused on the influence of music on the MCAO and did not involve a discussion on specific musical elements. Given that the therapeutic effects of different musical elements vary, our study used Mozart K.448, which has been frequently studied. However, our study adopted the form of three movements, which was played in a loop; more musical elements were incorporated to make the rhythm, melody, and chord more diverse, which may be helpful to achieve a more comprehensive stimulation effect.

In our study, a 12-h music therapy ameliorated focal neurological deficits due to MCAO, suggesting that the music therapy can effectively improve poststroke motor dysfunction. A previous clinical research focused on active music therapy, that is, active training based on musical elements (24). In our study, passive music therapy was used as the intervention; however, the activities of the rats were not restricted during the intervention period to simulate clinical completion of corresponding training based on music. Thus, our results are more reliable. Previous studies proposed that different musical elements including rhythm, melody, pitch, and musical cycle, play a role in the improvement of physiological dysfunctions (25–27). Rhythm-based music therapy, such as auditory rhythmic stimulation, has a significant effect on improving the patient's walking function (28), and participatory music therapy has a significant effect on improving upper limb function (29). Additionally, it has been shown that music therapy activates the limbic system, induces the production of neuropeptides associated with happiness and reward mechanisms, and continually regulates mood (30).

BDNF, which is an essential neurotrophic factor, plays an important role in promoting neuron growth by binding to the high-affinity tyrosine kinase receptor β (31). Music can stimulate pathological or healthy mice to release BDNF in different areas of their brains, especially in the hippocampus CA3, dentate gyrus, prefrontal cortex, amygdala, and hypothalamus (32, 33). A previous study confirmed that exogenous BDNF effectively repairs the ischemic penumbra and protects the residual neurons against MCAO *in vivo* (34). Our results suggested that music therapy promotes BDNF accumulation and influences neuron repairing and synapse regeneration, whereas noise has an adverse effect on brain repair after stroke. In addition, our results showed that music therapy induces GFAP distribution in the brain. GFAP, which is an astrocyte-specific intermediate filament component, plays a role in the improvement of ischemic brain damage due to focal cerebral ischemia with partial reperfusion (35). Moreover, music therapy promotes cell regeneration in the early stage and subsequently induces the differentiation and growth of synapses.

Music therapy may have a persistent effect on brain plasticity. Studies demonstrated that combined music exercise can continually reduce the loss of white matter and gray matter in the brain of the elderly individuals (36). Another study showed that the volume of gray matter and white matter is increased in people who received music training for a long time (37, 38). The use of musical instruments expands the connection fibers between the auditory and motor zones, thereby further enhancing the connection between the remote areas and such connection will not disappear with time (8). However, previous studies reported that the long-term effects of music therapy on some degenerative neuropathy are unsatisfactory. A study showed that with the cessation of music therapy, the motor function of Parkinson's patients cannot be maintained (39). In our study, although the BDNF content decreased in the fourth week, the cells in the injured area were well-differentiated and no significant difference between the 12-h music and 12-h music-R groups were found. Hence, music therapy has a long-term effect on brain plasticity.

CONCLUSIONS

In summary, an appropriate dose of music therapy can effectively alleviate poststroke motor dysfunction, stimulate BDNF and GFAP secretion in the injured motor cortex, promote cell regeneration in the core area of the infarction, and induce the repair of residual neurons in the peripheral area. The mechanism may be through stimulating the absorption and resecretion of BDNF and GFAP by astrocytes, which in turn regulate the redistribution of BDNF and GFAP in time and space.

DATA AVAILABILITY STATEMENT

The raw data supporting the conclusions of this article will be made available by the authors, without undue reservation.

ETHICS STATEMENT

The animal study was reviewed and approved by Animal Care and Use Committee (IACUC) of Affiliated Maternity and Child Health Care Hospital of Nantong University.

AUTHOR CONTRIBUTIONS

All authors listed have made a substantial, direct and intellectual contribution to the work, and approved it for publication.

FUNDING

This study was funded by the National Natural Science Foundation of China (grant No. 81870941) and Nantong Science and Technology Planning Project (No. MS12020018).

REFERENCES

1. Langhorne P, Bernhardt J, Kwakkel G. Stroke rehabilitation. *Lancet.* (2011) 377:1693–702. doi: 10.1016/S0140-6736(11)60325-5
2. Avan A, Digaleh H, Napoli MD, Stranges S, Behrouz R, Shojaeianbabaei G, et al. Socioeconomic status and stroke incidence, prevalence, mortality, and worldwide burden: an ecological analysis from the Global Burden of Disease Study 2017. *BMC Med.* (2019) 17:191. doi: 10.1186/s12916-019-1397-3
3. Wu S, Wu B, Liu M, Chen Z, Wang W, Anderson CS, et al. Stroke in China: advances and challenges in epidemiology, prevention, and management. *Lancet Neurol.* (2019) 18:394–405. doi: 10.1016/S1474-4422(18)30500-3
4. Rathore SS, Hinn AR, Cooper LS, Tyroler HA, Rosamond WD. Characterization of incident stroke signs and symptoms: findings from the atherosclerosis risk in communities study. *Stroke.* (2002) 33:2718–21. doi: 10.1161/01.STR.0000035286.87503.31
5. Tang H, Gamdzyh M, Huang L, Gao L, Lenahan C, Kang R, et al. Delayed recanalization after MCAO ameliorates ischemic stroke by inhibiting apoptosis via HGF/cMet/STAT3/Bcl02 pathway in rats. *Exp Neurol.* (2020) 330:113359. doi: 10.1016/j.expneurol.2020.113359
6. Yu J, Wang WN, Matei N, Li X, Pang JW, Mo J, et al. Ezetimibe attenuates oxidative stress and neuroinflammation via AMPK/Nrf2/TXNIP pathway after MCAO in rats. *Oxi Med Cell Longev.* (2020) 2020:4717258. doi: 10.1155/2020/4717258
7. Ashafaq M, Intakhab Alam M, Khan A, Islam F, Khuwaja G, Hussain S, et al. Nanoparticle of resveratrol attenuates oxidative stress and inflammation after ischemic stroke in rats. *Int Immunopharmacol.* (2021) 94:107494. doi: 10.1016/j.intimp.2021.107494
8. Francois C, Grau-Sánchez J, Duarte E, Rodriguez-Fornells A. Music training as an alternative and effective method for neuro-education and neuro-rehabilitation. *Front Psychol.* (2015) 6:475. doi: 10.3389/fpsyg.2015.00475
9. Raghavan P, Geller D, Guerrero N, Aluru V, Eimicke JP, Teresi JA, et al. Music upper limb therapy-integrated: an enriched collaborative approach for stroke rehabilitation. *Front Hum Neurosci.* (2016) 10:498. doi: 10.3389/fnhum.2016.00498
10. Ghai S, Ghai I. Effects of (music-based) rhythmic auditory cueing training on gait and posture post-stroke: a systematic review and dose-response meta-analysis. *Sci Rep.* (2019) 9:2183. doi: 10.1038/s41598-019-38723-3
11. Malcolm MP, Massie C, Thaut M. Rhythmic auditory-motor entrainment improves hemiparetic arm kinematics during reaching movements: a pilot study. *Top Stroke Rehabil.* (2009) 16:69–79. doi: 10.1310/tsr1601-69
12. Knight WE, Rickard NS. Relaxing music prevents stress-induced increases in subjective anxiety, systolic blood pressure, and heart rate in healthy males and females. *J. Music Ther.* (2001) 38:254–72. doi: 10.1093/jmt/38.4.254
13. Li J, Luo C, Peng Y, Xie Q, Gong J, Dong L, et al. Probabilistic diffusion tractography reveals improvement of structural network in musicians. *PLoS ONE.* (2014) 9:e105508. doi: 10.1371/journal.pone.0105508
14. Stoessl AJ, Lehericy S, Strafella AP. Imaging insights into basal ganglia function, Parkinson's disease, and dystonia. *Lancet.* (2014) 384:532–44. doi: 10.1016/S0140-6736(14)60041-6
15. Tomaino CM. Effective music therapy techniques in the treatment of nonfluent aphasia. *Ann N Y Acad Sci.* (2012) 1252:312–7. doi: 10.1111/j.1749-6632.2012.06451.x
16. Dastgheib SS, Layegh P, Sadeghi R, Foroughipur M, Shoeibi A, Gorji A. The effects of Mozart's music on interictal activity in epileptic patients: systematic review and meta-analysis of the literature. *Curr Neurol Neurosci Rep.* (2014) 14:420. doi: 10.1007/s11910-013-0420-x
17. Xing Y, Xia Y, Kendrick K, Liu X, Wang M, Wu D, et al. Mozart, Mozart rhythm and retrograde Mozart effects: evidences from behaviours and neurobiology bases. *Sci Rep.* (2016) 6:18744. doi: 10.1038/srep18744
18. Chen J, Li Y, Wang L, Zhang Z, Lu D, Lu M, et al. Therapeutic benefits of intravenous administration of bone marrow stromal cells after cerebral ischemia in rats. *Stroke.* (2001) 32:1005–11. doi: 10.1161/01.STR.32.4.1005
19. Raghavan P. Upper limb motor impairment after stroke. *Phys Med Rehabil Clin N Am.* (2015) 26:599–610. doi: 10.1016/j.pmr.2015.06.008
20. Fotakopoulos G, Kotlia P. The value of exercise rehabilitation program accompanied by experiential music for recovery of cognitive and motor skills in stroke patients. *J Stroke Cerebrovasc Dis.* (2018) 27:2932–9. doi: 10.1016/j.jstrokecerebrovasdis.2018.06.025
21. Leonardi S, Cacciola A, De Luca R, Aragona B, Andronaco V, Milardi D, et al. The role of music therapy in rehabilitation: improving aphasia and beyond. *Int J Neurosci.* (2018) 128:90–9. doi: 10.1080/00207454.2017.1353981
22. Lemmer B. Effects of music composed by Mozart and Ligeti on blood pressure and heart rate circadian rhythms in normotensive and hypertensive rats. *Chronobiol Int.* (2008) 25:971–86. doi: 10.1080/07420520802539415
23. Cervellin G, Lippi G. From music-beat to heart-beat: a journey in the complex interactions between music, brain and heart. *Eur J Intern Med.* (2011) 22:371–4. doi: 10.1016/j.ejim.2011.02.019
24. Raglio A, Zaliani A, Baiardi P, Bossi D, Sguazzin C, Capodaglio E, et al. Active music therapy approach for stroke patients in the post-acute rehabilitation. *Neruol Sci.* (2017) 38:893–7. doi: 10.1007/s10072-017-2827-7
25. Cha Y, Kim Y, Chung Y. Immediate effects of rhythmic auditory stimulation with tempo changes on gait in stroke patients. *J Phys Ther Sci.* (2014) 26:479–82. doi: 10.1589/jpts.26.479
26. Leo V, Sihvonen AJ, Linnavalli T, Tervaniemi M, Laine M, Soinila S, et al. Sung melody enhances verbal learning and recall after stroke. *Ann N Y Acad Sci.* (2018) 1423:296–307. doi: 10.1111/nyas.13624
27. Thaut MH. The discovery of human auditory-motor entrainment and its role in the development of neurologic music therapy. *Prog Brain Res.* (2015) 217:253–66. doi: 10.1016/bs.pbr.2014.11.030
28. Mainka S, Wissel J, Völler H, Evers S. The use of rhythmic auditory stimulation to optimize treadmill training for stroke patients: a randomized controlled trial. *Front Neurol.* (2018) 9:755. doi: 10.3389/fneur.2018.00755
29. Altenmüller E, Marco-Pallares J, Münte TF, Schneider S. Neural reorganization underlies improvement in stroke-induced motor dysfunction by music-supported therapy. *Ann N Y Acad Sci.* (2009) 1169:395–405. doi: 10.1111/j.1749-6632.2009.04580.x
30. Ferreri L, Mas-Herrero E, Zatorre RJ, Ripollés P, Gomez-Andres A, Alicart H, et al. Dopamine modulates the reward experiences elicited by music. *Proc Natl Acad Sci USA.* (2019) 116:3793–8. doi: 10.1073/pnas.1811878116
31. Ferreri I, Ballabriga J, Martí E, Pérez E, Alberch J, Arenas E. BDNF up-regulates TrkB protein and prevents the death of CA1 neurons following transient forebrain ischemia. *Brain Pathol.* (1998) 8:253–61. doi: 10.1111/j.1750-3639.1998.tb00151.x
32. Angelucci F, Ricci E, Padua L, Sabino A, Tonali PA. Music exposure differentially alters the levels of brain-derived neurotrophic factor and nerve growth factor in the mouse hypothalamus. *Neurosci Lett.* (2007) 429:152–5. doi: 10.1016/j.neulet.2007.10.005
33. Li WJ, Yu H, Yang JM, Gao J, Jiang H, Feng M, et al. Anxiolytic effect of music exposure on BNDFMet/Met transgenic mice. *Brain Res.* (2010) 1347:71–9. doi: 10.1016/j.brainres.2010.05.080
34. Guan J, Tong W, Ding W, Du S, Xiao Z, Han Q, et al. Neuronal regeneration and protection by collagen-binding BDNF in the rat middle cerebral artery occlusion model. *Biomaterials.* (2012) 33:1386–95. doi: 10.1016/j.biomaterials.2011.10.073
35. Nawashiro H, Brenner M, Fukui S, Shima K, Hallenbeck JM. High susceptibility to cerebral ischemia in GFAP-null mice. *J Cereb Blood Flow Metab.* (2000) 20:1040–4. doi: 10.1097/00004647-200007000-00003
36. Tabei KI, Satoh M, Ogawa JI, Tokita T, Nakaguchi N, Nakao K, et al. Physical exercise with music reduces gray and white matter loss in the front cortex of elderly people: the mihama-kiho scan project. *Front Aging Neurosci.* (2017) 9:174. doi: 10.3389/fnagi.2017.00174

37. Halwani GF, Loui P, Rüber T, Schluag G. Effects of practice and experience on the arcuate fasciculus: comparing singers, instrumentalists, and non-musicians. *Front Psychol*. (2011) 2:156. doi: 10.3389/fpsyg.2011.00156
38. James CE, Oechslin MS, Van De Ville D, Hauert CA, Descloux C, Lazeyras F. Musical training intensity yields opposite effects on grey matter density in cognitive versus sensorimotor networks. *Brain Struct Funct*. (2014) 219:353–66. doi: 10.1007/s00429-013-0504-z
39. Thaut MH, Rice RR, Braun Janzen T, Hurt-Thaut CP, McIntosh GC. Rhythmic auditory stimulation for reduction of falls in Parkinson's disease: a randomized controlled study. *Clin Rehabil*. (2019) 33:34–43. doi: 10.1177/0269215518788615

Conflict of Interest: The authors declare that the research was conducted in the absence of any commercial or financial relationships that could be construed as a potential conflict of interest.

frontiers in Neurology

REVIEW
published: 15 July 2021
doi: 10.3389/fneur.2021.659740

Secondary White Matter Injury and Therapeutic Targets After Subarachnoid Hemorrhage

Xufang Ru [1,2†], Ling Gao [3†], Jiru Zhou [4], Qiang Li [1,2], Shilun Zuo [5], Yujie Chen [1,2], Zhi Liu [1,2*] and Hua Feng [1,2]*

[1] State Key Laboratory of Trauma, Burn and Combined Injury, Department of Neurosurgery, Southwest Hospital, Third Military Medical University (Army Medical University), Chongqing, China, [2] Chongqing Key Laboratory of Precision Neuromedicine and Neuroregenaration, Southwest Hospital, Third Military Medical University (Army Medical University), Chongqing, China, [3] Department of General Practice, Audio-Visual Education Center, Third Military Medical University (Army Medical University), Chongqing, China, [4] Department of Neurosurgery, The First Affiliated Hospital of Chongqing Medical University, Chongqing, China, [5] Department of Neurology, Xinqiao Hospital, Third Military Medical University (Army Medical University), Chongqing, China

Aneurysmal subarachnoid hemorrhage (SAH) is one of the special stroke subtypes with high mortality and mobility. Although the mortality of SAH has decreased by 50% over the past two decades due to advances in neurosurgery and management of neurocritical care, more than 70% of survivors suffer from varying degrees of neurological deficits and cognitive impairments, leaving a heavy burden on individuals, families, and the society. Recent studies have shown that white matter is vulnerable to SAH, and white matter injuries may be one of the causes of long-term neurological deficits caused by SAH. Attention has recently focused on the pivotal role of white matter injury in the pathophysiological processes after SAH, mainly related to mechanical damage caused by increased intracerebral pressure and the metabolic damage induced by blood degradation and hypoxia. In the present review, we sought to summarize the pathophysiology processes and mechanisms of white matter injury after SAH, with a view to providing new strategies for the prevention and treatment of long-term cognitive dysfunction after SAH.

Keywords: subarachnoid hemorrhage, white matter injury, oligodendrocyte, diffusion tensor imaging, therapeutic targets

OPEN ACCESS

Edited by:
Devin William McBride, University of Texas Health Science Center at Houston, United States

Reviewed by:
Sabina Medukhanova, National Center for Neurosurgery, Kazakhstan
Gang Chen, The First Affiliated Hospital of Soochow University, China
Zhong Wang, Soochow University, China

***Correspondence:**
Yujie Chen
yujiechen6886@foxmail.com
orcid.org/0000-0002-9905-9138
Zhi Liu
516043248@qq.com

† These authors have contributed equally to this work

Specialty section:
This article was submitted to Stroke, a section of the journal Frontiers in Neurology

Received: *28 January 2021*
Accepted: *11 June 2021*
Published: *15 July 2021*

Citation:
Ru X, Gao L, Zhou J, Li Q, Zuo S, Chen Y, Liu Z and Feng H (2021) Secondary White Matter Injury and Therapeutic Targets After Subarachnoid Hemorrhage. Front. Neurol. 12:659740. doi: 10.3389/fneur.2021.659740

INTRODUCTION

Aneurysmal subarachnoid hemorrhage (SAH) is one of the special stroke subtypes with high mortality and mobility. Neurosurgical clipping or endovascular coiling is highly recommended for the early repair of ruptured aneurysms (1), focusing the medical management of SAH patients on early brain injury and delayed cerebral ischemia (2). However, more than 70% of survivors suffer from varying degrees of neurological deficits and cognitive impairments, leaving a heavy burden on individuals, families, and the society (3). Compared with cohorts with unruptured intracranial aneurysm, patients with aneurysmal SAH have higher mean diffusivity in white matter, leading to cognitive impartment 3 months after SAH onset (4). Apparently, the mammillothalamic tract is more vulnerable than the corticospinal tract in SAH patients with a good Glasgow Outcome Scale at 3 months after ictus (5), which demonstrates a correlation between early brain injury and long-term cognitive dysfunction after SAH.

White matter contains most of the volume of human brain and is made up of neural axons and myelin sheath. As early as 1989, the autopsy of six SAH cases had reported the remarkable hyperemia and edema in the deep frontal white matter, with microscopic axonal degeneration (6). Despite that enormous progresses have been made in the pathophysiology of early brain injury after SAH, the mechanisms of white matter injury are still a blur (7). Unlike intracerebral hemorrhage and traumatic brain injury, most SAH patients, especially those without obvious hematoma volume, do not usually fracture the nervous tract due to primary mechanical stress but suffer with remarkable secondary brain injury and neurological deficits. Mechanical pressure due to increased intracerebral pressure, glial response, and ischemia is considered as the pivotal mechanism of white matter injury after SAH but lacks high-quality clinical and basic research evidence (7).

In the present review, we sought to summarize the pathophysiology processes and mechanisms of white matter injury after SAH, with a view to providing new strategies for the prevention and treatment of long-term cognitive dysfunction after SAH.

WHITE MATTER INJURY AFTER SAH

Previous clinical studies have not significantly improved neurological outcomes in patients with SAH. Recent studies have shown that there is a significant white matter injury after SAH, which plays an important role in the early brain injury secondary to SAH. The development of stroke imaging techniques suggests that the protection of white matter injury is very important for the recovery of neurological function and prognosis in patients with SAH. However, the relationship between white matter injury and SAH remains unclear. It has been reported that common cognitive dysfunction after SAH may be caused by white matter injury (8). Studies have shown that white matter injuries such as demyelination and axial rupture are reversible to a certain extent (9), while gray matter injuries such as neuronal apoptosis are difficult to recover. Therefore, the study of white matter injury after SAH may be of more importance than we currently know. Lee et al. found extensive white matter abnormalities in SAH patients through tract-based spatial statistical analysis, but not in retrolenticular parts of the internal capsule, right superior longitudinal fasciculus, or right superior corona radiata (10), providing important data support for the accurate diagnosis of the presence and severity of nerve injury in patients with subarachnoid hemorrhage. Clinical studies did find different types of white matter lesions in SAH patients. For example, the white matter lesions around the ventricle are mostly moon-shaped, thin-shaped, or cap-shaped, and these small spots or caps are asymptomatic and progress slowly (11); the white matter lesions in the deep brain are mostly patchy, macular, or fused large masses which progress rapidly and lead to long-term disease (11). In addition, autopsy observations of death cases with SAH showed white matter edema and demyelination (12). Brain tissue from a patient who died in the acute phase of SAH showed multiple subcortical white matter abnormalities in the brain, cerebellum, and brainstem (13). Distinct kinds of white matter injuries lead to cognitive dysfunction, memory loss, emotional apathy, movement disorders, and many other related clinical manifestations in SAH patients (11).

Retrospective quantitative MRI studies have also shown diffuse vasogenic edema and white matter injury after SAH (14). In recent years, diffusion tensor imaging (DTI) has been used to evaluate the neural tracts and structures in SAH patients (15). Jang et al. found 62.5% of SAH patients had at least one hemisphere of mammillothalamic tract abnormal 6 weeks after SAH onset (16). Some other SAH patients may have severe memory impairment and provoked confabulation in clear consciousness since SAH onset, with Papez circuit injury even 3 months later (17). In addition, Schweizer et al. also reported a reduction in hippocampal white matter integrity and long-term memory loss of SAH patients (18). In 2007, Liu et al. suggested that SAH may cause whole brain edema in the deep gray and white matter (19). Subsequently, Rejmer et al. reported that the mean white matter diffusion rate 2 weeks after onset in 49 patients with aneurysmal SAH was higher than that in 22 patients with unruptured aneurysms (4). Moreover, the gray matter/white matter ratio has been proved to be a good predictor for long-term cognitive function and quality of life in SAH patients (20). These studies suggest that it is essential to pay attention to white matter injury for the recovery of neurological function after SAH.

POTENTIAL PATHOPHYSIOLOGY MEDIATED SECONDARY WHITE MATTER INJURY AFTER SAH

Acute white matter injury in ICH and TBI is similar in principle and is caused by barotrauma and physical expansion of hematoma masses (21, 22). The difference is that barotrauma in TBI is caused by a blow to the outside of the head, whereas ICH is caused by the impact of a large amount of blood rushing out of the arteries in the brain cavity (21). In addition, neuroinflammation, oxidative stress, and excitatory toxicity induced by hematoma effect played major roles in the injury of secondary white matter (23). White matter, especially deep white matter, receives less collateral circulation than gray matter and is more sensitive to ischemia (24). Thus, ischemic stroke damages white matter rapidly and profoundly. In addition, oliodendrocytes are highly susceptible to cerebral ischemia-induced oxidative stress (25), excitotoxicity (26), and neuroinflammation, leading to oliodendrocyte apoptosis and consequent white matter damage.

Since most blood spread into the subarachnoid space without direct nervous tract disruption, white matter injury after SAH is initially considered to be the consequence of blood–brain barrier disruption (27, 28) and neurotoxicity of blood disintegration (29). Physical factors such as biological stress, mainly caused by elevated intracranial pressure, attack the whole brain in the acute phase, while biochemical factors including thrombin, excitatory amino acids, and inflammatory cytokines lead to subsequent white matter injury after SAH (**Figure 1**).

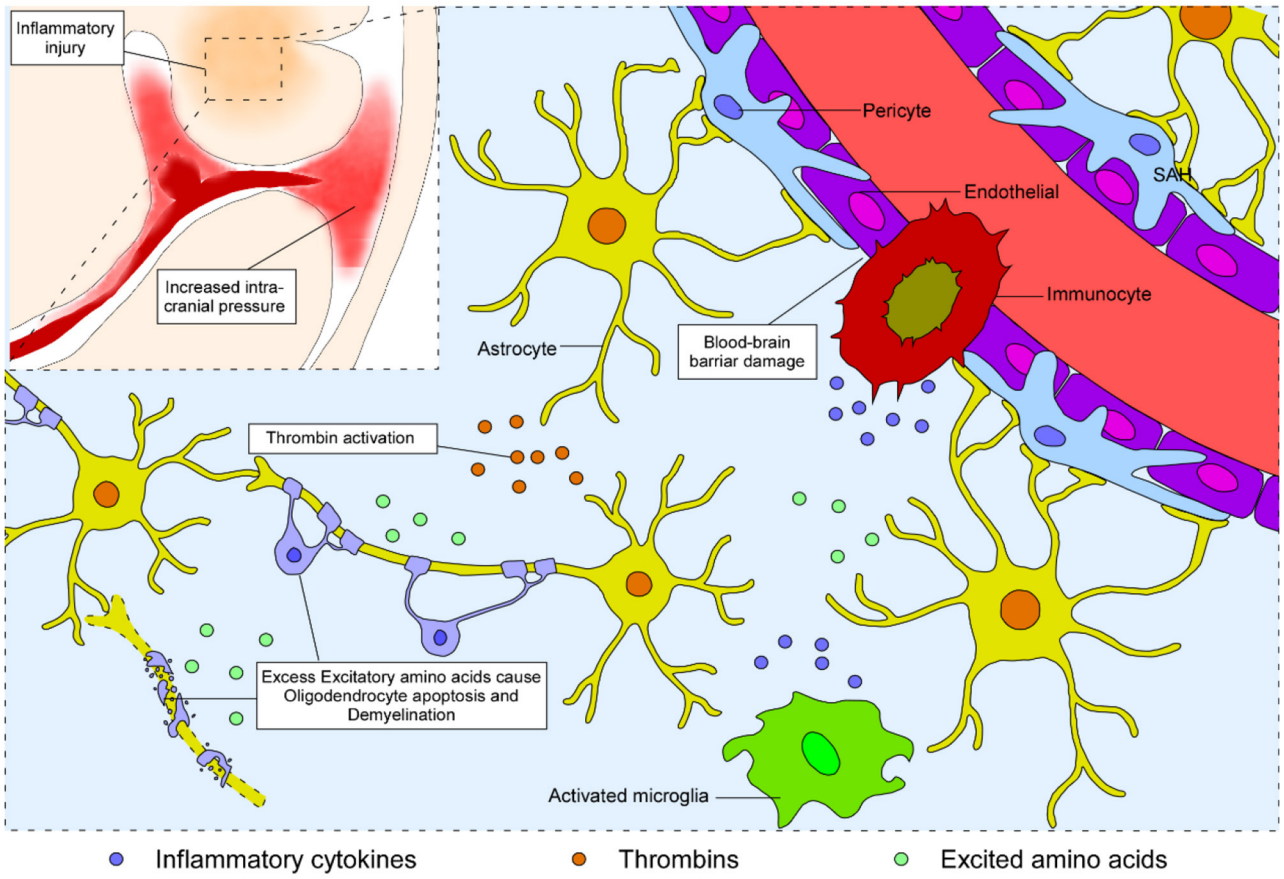

FIGURE 1 | Schematic representation of the process of white matter injury in the brain after SAH. Blood from the ruptured vessel enters the subarachnoid space and increases the intracranial pressure. Subsequently, biochemical factors, including thrombin, excitatory amino acids, and inflammatory cytokines, lead to disruption of the blood–brain barrier, neural apoptosis, and demyelination, eventually causing white matter injury after SAH.

Elevated Intracranial Pressure

Changes occurring within 1 min after aneurysmal SAH cause early brain injury, and the degree of early brain injury affects the final prognosis of patients (30). There is evidence that acute intracranial hypertension after SAH is often accompanied by sudden loss of consciousness and worse prognosis (31). Therefore, control of intracranial pressure in the acute phase of SAH is helpful to improve patient prognosis. Blood breaks into the enclosed cranial cavity after SAH, causing a sharp increase in intracranial pressure (ICP). Cerebral white matter midline displacement directly caused by uneven pressure causes the brain tissue to bulge into the tentorium cerebellum and foramen magnum, inducing the herniation of the supraoptic temporal lobe or cerebellar tonsillar hernia, and then squeezes the brain stem and respiratory center, resulting in acute crisis, loss of consciousness, respiratory depression, and cardiac arrest (32). Therefore, almost one-third of patients suffering from SAH consequently die of cerebral hernia due to high intracranial pressure. The indirect effects of high intracranial pressure on white matter after SAH seem clear as well. First, elevated intracranial pressure leads to neurovascular coupling disorders, reducing the focal cerebral blood flow and blood supply to the white matter (33). Second, high intracranial pressure disrupts the blood–brain barrier (BBB) at a very early phase after SAH. Excessive water (H[[sb]]2[[/s]]O) and Na+ diffuse into the brain parenchyma *via* the impaired BBB, resulting in vasogenic white matter edema. Edema also aggravates intracranial pressure again after SAH (34). Third, increased intracranial pressure causes the extrusion of H[[sb]]2[[/s]]O into the extracellular mesenchyme along the white matter fiber bundles, enhancing interstitial cerebral edema following SAH (33, 35). Since cerebrospinal fluid penetrates the ventricle wall and infiltrates the white matter surrounding the ventricle, it increases hydrostatic pressure and results in myelin disintegrating and disappearing rapidly (34). Finally, increased intracranial pressure suppresses the venous and lymphatic systems, leading to obstruction of venous and lymphatic influx, further increasing cerebral edema and intracranial pressure (36).

It is of great importance to develop intervention strategies that target pathogens to improve ICP-induced white matter injury after SAH. The primary cause is the occupancy effect of excess blood in the subarachnoid space. Hence, early intracranial

hematoma evacuation and cerebrospinal fluid drainage can alleviate white matter damage after SAH. Another cause of increased ICP after SAH is hydrocephalus. Both traffic hydrocephalus and non-traffic hydrocephalus aggravate the increase in ICP (34) and further compress the central aqueducts, impeding the absorption and circulation of cerebrospinal fluid (37). Therefore, a lumbar puncture and drainage procedure or application of diuretics is urgently needed to reduce white matter injury after SAH. As mentioned above, mitigation of brain edema is beneficial to reduce the damage of intracranial pressure on the white matter. However, at present, hormone drugs based on improvement of the BBB are not recommended because of their disadvantages, such as poor specificity and side effects (38).

Thrombin

Thrombin plays inclusive roles in the human brain, including coagulation cascades and non-clotting processes. Under physiological conditions, thrombin exists in the form of prothrombin participating in the endogenous and exogenous coagulation cascade (39). Thrombin is also involved in non-clotting processes, such as maintenance of the blood–brain barrier, aggregation and activation of platelets, formation of cerebral edema, inflammatory cell infiltration, physiological proliferation, and repair of brain tissue (40). Cerebrovascular spasm is highly correlated with the prognosis of SAH patients (41), and thrombin plays an important role in it (42). The stimulative effect of thrombin on vasospasm after SAH is irreversible (43). Therefore, how to reduce the enhancing effect of thrombin on vasospasm after SAH so as to reduce the subsequent toxic effect and improve the prognosis of SAH patients remains to be further studied.

Excessive activation of thrombin during pathological scenarios shows neurotoxic effects. First, thrombin activates its membrane receptors and accumulates intracellular calcium (Ca^{2+}), which activates the calcium-dependent apoptosis signaling pathway, killing the neurons and glial cells (44). Second, thrombin activates matrix metalloproteinases (MMPs), which may degrade various extracellular matrix proteins (such as tight junction proteins), increasing blood–brain barrier permeability and aggravating posterior cerebral edema after SAH (45). Third, activation of microglia in the brain and peripheral blood immune cells, which enter the central nervous system through an impaired blood–brain barrier, may cause serious neuroinflammatory injury (46). Fourth, studies regarding ischemia–reperfusion injury in mouse models have reported that astrocytes originally activated by thrombin may aid in the production of MMP-2 and reduce myelin cells (47). The MMP-2 inhibitor reduced the proliferation of astrocytes and the damage of myelin cells but failed to reduce the damage to oligodendrocytes caused by thrombin (47), which suggests that the damage of thrombin to oligodendrocytes may occur through apoptotic or inflammatory pathways rather than through the MMP pathway.

Although thrombin receptor inhibitors should work against white matter injury after SAH, very few antagonists of thrombin receptors have been applied to SAH patients because of the risk of secondary hemorrhage (48). Furthermore, most small molecular inhibitors of thrombin have been found to be effective in animal experiments, yet failed in clinical trials (49). Recent research in our laboratory found that the direct use of antagonist peptides of the thrombin receptor in a mouse model of SAH promoted remyelination and neurological recovery (50). However, in consideration of the substantial differences among species, there is still a long way to go to achieve a clinical transformation.

Blood–Brain Barrier Damage

Approximately 10% of SAH patients suffer from severe edema in many cerebral regions, including the white matter, cortical cortex, and corpus callosum (51). Vasogenic edema caused by disruption of the blood–brain barrier is an independent risk factor for death and disability in SAH patients (52). The blood–brain barrier maintains the homeostasis of the internal environment of the human brain with its particular structure: a basal membrane, pericytes, an endothelium, and astrocytic endfeet (53). An ultrastructural observation showed changes in the blood–brain barrier after SAH, including a decrease in the number of pericytes, a lack of connection between the pericytes and the endothelium, disintegration of the astrocytic endfeet, destruction of the tight junctions of the endothelium, degradation of the basal membrane, vacuole-like changes in the endothelial cells, and plasma leakage (54). Furthermore, some phenomena, such as myelin edema, axonal energizing and information transmission disorders, and disintegration of white matter fibers, have also been observed after SAH (55). Interestingly, the MMPs that cause destruction of the endothelial tight junctions and disruption of the BBB have shown promotion of remyelination in the peripheral nervous system (56, 57), suggesting that the potential mechanism of correlation between BBB damage and white matter injury remains elusive in SAH scenarios.

Two mechanisms have been involved in BBB maintenance: tight junction and transcytosis (58). The MMPs, as tissue scissors, regulate the integrity of tight junctions, while docosahexaenoic acid (DHA) suppresses endothelial transcytosis (58). Our previous works found that both mechanisms were apparent in the regulation of the BBB in white matter (where it is adjacent to the blood clot directly) after SAH (58). Moreover, capillary pericytes are involved in the two mechanisms by secreting matrix metalloproteinase-9 (MMP-9) and DHA, revealing an interesting role of pericytes in white matter injury after SAH.

Excitatory Amino Acids

Glutamate is the main excitatory amino acid (EAA) of the human brain. Glutamatergic neurons participate in mediating motor conduction in the spinal cord, red nucleus giant cells, and Deiters' nucleus giant cells (59). The concentration of glutamate is abundant (up to 10 μmol/g brain tissue) in the human central nervous system (60). Its receptors (glutamate receptor, GluR) include the metabotropic (mGluR) and ionic (iGluR) receptors (60). The former, mGluR, is a G protein-coupled receptor that activates protein modification and regulates the process of learning, memory, anxiety, and pain transmission. The latter, iGluR, is a ligand-gated ion channel that is further subdivided into three subtypes: the N-methyl-D-aspartate receptor (NMDAR), aminohydroxymethyl oxazole

propionate receptor (AMPAR), and kainate receptor (KAR). Studies have found that both mGluR and iGluR are widely distributed in white matter (61). In pathological scenarios, excess glutamate is released from damaged glutamatergic neurons, causing demyelination, axonal injury, and glial cell death (62). Furthermore, the blocking of reuptake and physiological elimination of glutamate also lead to its excessive accumulation (62). This reuptake failure is mainly because of the functional inhibition of the presynaptic membrane of neurons or the transporter of glutamic acids (GluTs, which consume ATP) on the glial cell membrane (62). In the ischemic and hypoxic environment caused by stroke, ATP supply is disturbed, and glutamate reuptake is weakened (62). However, the antiport of the sodium-dependent glutamate transporter further aggravates the accumulation of glutamate and causes cell excitotoxicity (62). Excessive glutamate leads to intracellular calcium overload, oxidative stress, and endoplasmic reticulum stress, resulting in oligodendrocyte apoptosis, and demyelination (62).

Excess glutamate is found in cerebrospinal fluid and brain tissues of SAH patients. A correlation study analyzed the level of excitatory amino acids in the intercellular substance of SAH patients using microdialysis and found that the elevation of aspartic acid and glutamate levels was negatively correlated with the prognosis of SAH patients (63). Another animal experiment showed that the expression of mGluR and the glutamate transporter decreased significantly in the early stage of SAH (64). In their report, upregulation of the glutamate receptor and its transporter by using magnesium sulfate or nimodipine significantly improved neurological functions (64). These studies suggest that glutamate levels in the brain may be an important indicator of white matter injury after SAH.

Inflammatory Injury

Neuroinflammation has been shown to be an important pathogenic factor for white matter injury after SAH (65). A case comparison study by Leviton and colleagues classified neonatal intracerebral hemorrhage into three types according to whether there was white matter injury: cerebral hemorrhage with white matter injury (68 cases), cerebral hemorrhage without white matter injury (123 cases), and no cerebral hemorrhage or white matter injury (1,677 cases). This study found that the inflammatory response was more significant and lasting in patients who had white matter injury (66). After SAH, the majority of inflammation was induced by the polarization of microglia from the resting state (M0 type) to the immune damage state (M1 type) or neuroprotection state (M2 type) (67). Therefore, it was a promising direction of inflammatory therapy by converting the polarization of microglia after SAH (68). Peng et al. recently reported that low-density lipoprotein receptor-related protein-1 activation could modulate M2 microglial polarization and attenuate white matter injury after SAH (69), and apolipoprotein E and its mimetic peptide COG1410 could reduce M1 microglia activation for the protection of white matter injury after SAH (70). In addition, peripheral lymphocytes, such as T lymphocytes and macrophages, penetrated into the brain through the damaged blood–brain barrier after SAH (71). These immune cells either killed or phagocytosed neurons and glia, causing white matter inflammatory injury (71). Microglia secrete proinflammatory factors such as TNFα, NIL1, and IL13, leading to oligodendrocyte and periventricular white matter injury in ischemic circumstances (72). Activation of microglia also transformed inactive MMPs into active MMP-3 and MMP-9, thereby destroying the BBB and degrading myelin (73). In addition, intervention of inflammatory injury after SAH should be undertaken as early as possible since inflammation can interfere with the videographic diagnosis of SAH (74).

REPAIR FACTORS OF WHITE MATTER AFTER SAH

Oligodendrocyte Precursor Cells

Oligodendrocytes are responsible for the myelination of axons. During the development of the brain, oligodendrocytes usually originate from the neuroepithelial area where neural stem cells differentiate into oligodendrocyte precursor cells (OPCs) before developing into early oligodendrocytes (75). Recent studies have shown that OPCs develop in stages and form potentially diverse populations (76). OPCs from different sources have different susceptibilities and transcriptional profiles (76). If some OPCs are more sensitive than others, there may be a promising therapeutic strategy to target the vulnerable OPC subpopulation. OPCs, which still exist in the adult brain, are crucial for myelin maintenance and can be recruited for remyelination in the case of myelin damage (77). Moreover, in adult mice, OPCs account for ∼8–9% of the white matter cell population and 2–3% of the gray matter cell population, suggesting that OPCs are the most important cells mobilized in remyelination after brain injury (77).

After proliferation, most OPCs are integrated into neural circuits, and excessive ones are removed by microglia (78). In addition, it has been shown that myelination is a dynamic and plastic process (79). For example, studies in animals and humans have shown that neural activity facilitates the differentiation and myelination of OPCs during exercise and learning (79). OPCs have a gross cone-like structure and can reach damaged areas under the guidance of multiple chemokines (80). For example, the concentration gradients of bone morphogenetic protein (BMP), Sonic hedgehog (Shh), and Wnt protein determine the direction of migration of OPCs (80). Other factors, such as growth factors, extracellular matrix proteins, axon-inducing molecules, and neural activity, can also influence the migration of OPCs (77). In addition, it has been shown that the migration of OPCs is also stimulated by extracellular matrix components such as laminin, fibronectin, vitronectin, anosmin-1, and tenascin-C (81). Interestingly, glutamate can promote the migration of OPCs by stimulating the expression of polysialic acid–neuronal cell adhesion molecules and activating the Tiam1/Rac1/ERK signaling transduction pathway (82). A recent study by Tsai and colleagues showed that correct cerebral vascularization was essential for the migration of OPCs (83). More specifically, OPCs migrated by "crawling" along the blood vessels and could also "jump" from one blood vessel to another (83). This behavior of OPCs may aim to ensure an adequate oxygen

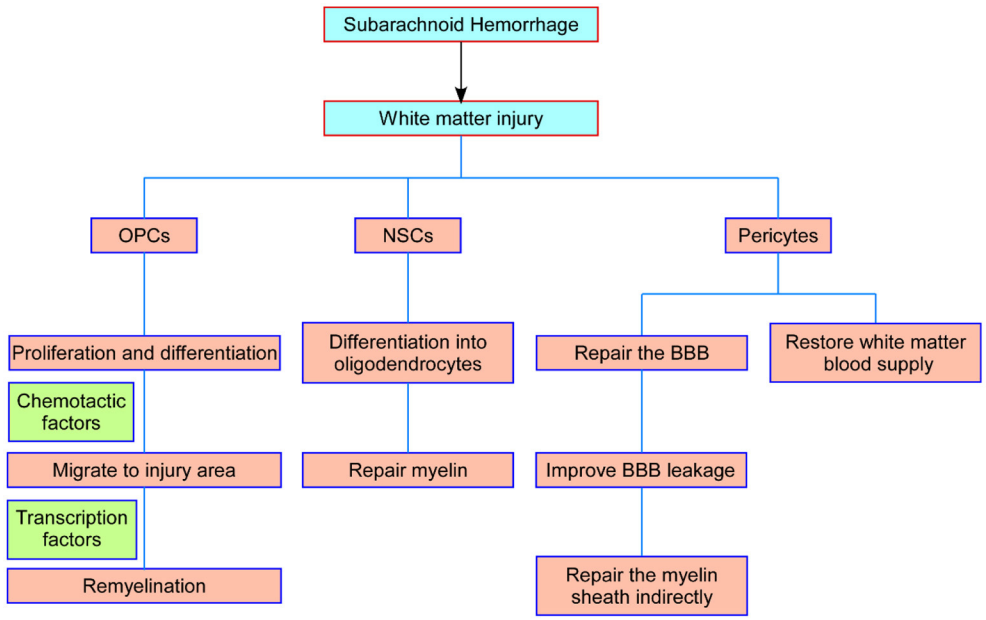

FIGURE 2 | Schematic representation of the main processes of NSCs, OPCs, and pericytes in white matter repair after SAH. OPCs proliferate and migrate to the injured foci and differentiate into oligodendrocytes to repair damaged myelin. NSCs differentiate into white matter neurons and oligodendrocytes to repair axons and myelin. Pericytes restore the blood supply to the white matter by modulating capillary constriction; moreover, pericytes enhance BBB integrity and alleviate white matter injury after SAH. NSCs, neural stem cells; OPCs, oligodendrocyte precursor cells; SAH, subarachnoid hemorrhage; BBB, blood–brain barrier.

supply during the myelination process, which requires a high oxygen consumption. Xu and colleagues recently reported that perioxisomal dysfunction exacerbated white matter injury after SAH, at least partly through thioredoxin-interacting protein and glycerone phosphate acyl transferase signals (84).

OPCs will not stop proliferating after reaching their destination until the number of OPCs reaches homeostasis (75). OPCs are in a state of moderate proliferation and differentiation inhibition. PDGF signaling is the main inducer of OPC proliferation, while Notch and Wnt signaling and downstream transcription factors are inhibitors of OPC differentiation (85, 86). The inhibition of OPC differentiation is relieved after white matter injury, and OPCs differentiate into immature oligodendrocytes and eventually form myelin sheaths under the promotion of transcription factors such as myelin regulators (Myrf) (87). Mature oligodendrocytes ultimately achieve myelin assembly of axons by expressing a large number of myelin genes after contact with neuronal axons, including myelin-associated glycoprotein (MAG), myelin oligodendrocyte glycoprotein (MOG), myelin basic protein (MBP), and myelin protein lipoprotein (PLP) (88). Therefore, the proliferation, migration, differentiation, and maturation of OPCs, as well as the internal regulatory mechanism, could provide new strategies for plastic myelin regeneration after SAH (**Figure 2**).

Neural Stem Cells

Neural stem cells (NSCs) are located in the stem pool (subventricular zone and hippocampus) of the brain and are considered to be the center of cerebral regeneration (89). Surprisingly, NSCs are the source of myelin repair by differentiating into oligodendrocytes (90). Stem cell therapy has been confirmed in rescue organs and tissues in a variety of animal models (90). However, most of these therapies are still experimental, and only small-scale and experimental stem cell therapy trials have been conducted in clinical practice (90). Furthermore, some issues that are not negligible, including directional differentiation, side effects, and risk of immune rejection, have not been resolved at present.

Compared with other described therapeutic cells, including embryonic stem cells, mesenchymal stem cells, umbilical cord stem cells, and induced pluripotent stem cells, human NSCs have shown the advantage of stable proliferation, mainly differentiating into neurons and oligodendrocytes. Studies have shown that nasal administration of mesenchymal stem cells (MSCs) after 6 days of SAH in rats significantly reduced brain injury and neuroinflammation and improved neurofunctional outcomes after 21 days of SAH (91). The first case of venous stem cell treatment of a high-grade aneurysmal SAH patient indicated that the patient recovered rapidly and well after intravenous infusion of bone marrow-derived allogeneic MSCs on day 3 after hemorrhage and achieved a modified Rankin Scale score of 3 at 6 months (92). The immunological rejection of neural stem cell transplantation may be improved by gene editing in the future, and we may quickly obtain a large number of neurons by using iPSC technology, reducing costs and shortening the transplantation time (93). These clinical trials suggest that neural stem cells have great clinical application value and

should be used as one of the treatment options for white matter injury.

In recent years, some achievements have been made in basic and clinical studies of stem cell therapy, but there are still some limitations. The safety and reliability of stem cell therapy, especially the safety of long-term treatment, need to be verified by more experiments. Stem cell type, delivery location and route, and optimal time of intervention of stem cell therapy need to be further explored. There are great challenges and still has a long way to go from animal experiments to clinical applications, but we believe that these findings provide a certain basis and guidance for stem cell therapy in the treatment of white matter injury after SAH (**Figure 2**).

Pericytes

The pericytes surrounding capillaries are essential for maintaining the structure and function of the blood–brain barrier. Pericytes have been found to be involved in white matter injury in cerebral arterial disease with subcortical infarcts and leukoencephalopathy, cerebral ischemia, and primary brain calcification (94). Deletion of beta-type platelet-derived growth factor receptor (PDGFRb) causes pericyte loss and affects white matter functions in two ways: one is that the loss or dysfunction of pericytes leads to blood–brain barrier leakage, causing further toxic injury and white matter edema (95); the other is that pericyte contraction causes microcirculatory disturbance, blocking the white matter blood supply and causing white matter ischemia and hypoxia damage (96). Under pathological conditions, pericytes can be transformed into α-smooth muscle actin (a-SMA)-positive phenotype, showing the regulation of contractile function and leading to neurological impairment (97). Our previous studies have shown that regulating eNOS/NO signal can inhibit the conversion of pericytes to a-SMA-positive phenotype, thereby increasing the diameter of capillaries and regulating the neurological dysfunction caused by microcirculation disturbance after SAH (98). Moreover, increased expression and secretion of MMP-9 in pericytes after SAH degrades endothelial tight junction protein and basement membrane (99), while cyclosporine A (CsA) can improve nerve injury caused by vasogenic edema by inhibiting this process (58). The activation of oxidative stress induced by SAH leads to increased apoptosis of pericytes, and edaravone can inhibit this change and improve the early brain injury after SAH (100). In addition, pericytes also show stem cell properties and differentiate into neurons under certain conditions and further repair nerve damage (101). Therefore, pericytes have great potential in the treatment and intervention of white matter injury (**Figure 2**).

POTENTIAL THERAPEUTIC STRATEGIES TARGETING WHITE MATTER INJURY AFTER SAH

Currently, clinical trials on SAH mainly focus on alleviating vascular spasm, and there are few studies related to white matter injury. The study on the neuroprotective effect of ketamine infusion after aneurysmal SAH is in phase 3 clinical trial now, which will provide an effective treatment for the protection of neurocognitive function in patients with SAH after completion (ClinicalTrials.gov identifier: NCT02636218). Moreover, the effect of Xenon treatment on brain injury in the acute phase after aneurysmal SAH is in the initial phase of a phase 2 clinical trial and is expected to be a new approach for treating white matter injury after SAH (ClinicalTrials.gov identifier: NCT04696523).

In addition, there are a variety of drugs that promote remyelination or impedance demyelination in preclinical and clinical application stages. For example, bazedoxifene (BZA) is one of the third-generation selective estrogen receptor modulators that has been shown in preclinical studies to promote myelin regeneration (102) and is currently undergoing phase II clinical trials in MS patients (ClinicalTrials.gov identifier: NCT04002934). In an animal model of cuprizone-induced demyelination, testosterone promotes the proliferation and differentiation of OPCs into mature oligodendrocytes through targeting neuroandrogen receptors (103). Due to the potential side effects and risk of overdose of hormone therapy, the phase II clinical study of testosterone is currently being conducted only in patients with testosterone deficiency, with the primary objective of determining the efficacy of testosterone in MS (ClinicalTrials.gov identifier: NCT03910738). Experiments have shown that metformin can promote the expansion, migration, and differentiation of endogenous neural progenitor cells in injured rodent brains, so as to carry out self-repair and functional recovery (104). The research on the effect of metformin on endogenous neural progenitor cells in patients with multiple sclerosis is undergoing phase II clinical trial (ClinicalTrials.gov identifier: NCT04121468). Canavan disease is a congenital white matter disorder characterized by severe motor abnormalities and low myelination, and a phase II clinical trial of RAAV-Oligo001-ASPA in the treatment of Canavan disease has just initiated (ClinicalTrials.gov identifier: NCT04833907). RAAV-Olig001-ASPA is the first gene therapy targeting oligodendrocytes, which are critical for myelination and brain development (105). A phase II clinical trial of nanocrystalline gold for multiple sclerosis has initiated (ClinicalTrials.gov identifier: NCT03536559). If these clinical trials are successful, the high specificity of gene therapy and strong targeting of nanomaterials will provide new therapeutic strategies for remyelination after SAH. Besides, clomastine, solinacine, and benzotropine have been tested in preclinical studies and approved for clinical use. Other promising drugs, such as VX15/2503, BIIB033, and GSK239512, promoted the differentiation of oligodendrocyte precursor cells by inhibiting Wnt, Notch, and other signaling pathways *in vitro*/animal experiments, thus promoting myelin regeneration. However, no relevant clinical studies have been conducted so far. Several drugs and their targets are summarized in **Table 1**.

PERSPECTIVE AND CONCLUSION

Previous studies have focused on early brain injury (EBI) and delayed cerebral ischemia (DCI) in patients with SAH. Most of

TABLE 1 | Advances in drug research for myelin repair.

Medicines	Targets	Mechanism	Current state	Correlational research
Fingolimod	S1P1 receptor	Promotion of the maturity of oligodendrocytes	FDA approved for RRMS	(106)
Benzatropine	Notch signal; muscarinic receptor	Reduction in cholinergic demyelination; promotion of the differentiation of OPC	Approved for Parkinson's, dystonia, and EAE	(107)
Quetiapine hemifumarate	D2, 5-HT2A antagonist, H1, α1, and 5-HT1A receptor	Promotion of the proliferation and maturation of oligodendrocytes; increased antioxidative stress	Approved for schizophrenia, bipolar disorder; MS patient phase I clinical trial (ClinicalTrials.gov: NCT02087631)	(108)
Simvastatin	3-Hydroxy-3-methylglutaryl-CoA (HMG-CoA) reductase inhibitor	Reduction in brain atrophy SPMS; reduction in recurrent frequency or lesion load	Approved for hypercholesterolemia; phase III clinical trials of SPMS (NCT00647348)	(109)
Clobetasol	Corticosteroid receptors	Promotion of the differentiation of OPC cells	Local antimicrobials; no clinical studies have been conducted	(110)
Indomethacin	Nonsteroidal anti-inflammatory drugs; drug (NSAID) inhibits cyclic oxidase	Increase the phosphorylation of β-catenin and induce its degradation; promotion of differentiation of OPC cells	Approved as an OTC pain reliever. No clinical studies have been conducted	(111)
BIIB033	LINO-1; RhoA signal	Enhancement of oligodendrocyte maturation, myelin formation, and reduction in severity of EAE	MS phase II clinical trial (NCT01864148); phase I of optic neuritis (NCT01721161)	(112)
Clemastine	Antihistamine/anticholinergic compounds; blocks histamine H1 receptor	Enhancement of OPC cell differentiation	RRMS patient II clinical trial (NCT02040298)	(113)
Solifenacin	Blocks CHRM3, an M3R muscarine acetylcholine receptor	Enhancement of OPC cell differentiation	FDA approval for contractive bladder contraction; no clinical studies have been conducted	(114)
BQ788	Endothelin (ET) receptor antagonist	Blocking of astrocytes and oligodendrocyte demyelination	*In vitro*/animal experimental evidence, no clinical application or related test	(115)
IRX4204	Retinoic acid receptor g (RXR-g)	Enhancement of oligodendrocyte differentiation	Clinical trials of MS patients are in the planning stage	(116)
VX15/2503	SEMA4D/plexinB1 signal	Promotion of OPC differentiation; repair of the BBB	MS patient phase I clinical trial (NCT01764737)	(117)
rHigM22	Hypoprotein/fibronectin receptor	Reduction in glial cell apoptosis; promotion of the regeneration of myelin	MS patient phase I clinical trial (NCT01803867)	(118)
GSK239512	Histamine H3 receptor agonist	Promotion of OPC differentiation	Patients with MS were given an additional therapy trial for the glatiramer acetate or interferon b-1a, which was completed in phase II (NCT01772199)	(119)

these studies focus on the cortical gray matter neurovascular units or white matter neurons and ignore the myelin sheath regeneration and the structure and function of white matter fiber tracts. While <20% of the volume of white matter is present in commonly used laboratory rodents, white matter makes up more than 50% of the human brain. From the perspective of clinical treatment, even if damage of gray matter can be restored, the treatment of patients is difficult to achieve ideal results without repair of white matter fiber bundle and myelin sheath. These studies suggest that it is important to pay attention to white matter injury for neurological rehabilitation after subarachnoid hemorrhage.

The therapeutic strategies for white matter injury are mainly limited to maintaining the balance of damage and reconstruction of white matter components after SAH ictus. The present review discusses the pathogenic factors and repair mechanisms of white matter injury after SAH, as well as the anti-inflammatory mechanisms to mitigate existing damage by reducing blood–brain barrier destruction, decreasing intracranial pressure, blocking thrombin-activating molecular cascades, and other means. On the other hand, regeneration of the myelin sheath and the repair of neurovascular can be promoted through the repair and functional stability of OPC cells, neural stem cells, and pericytes. The combination of these two strategies can reduce white matter injury after SAH and accelerate the recovery of neurological function. Potential drugs have been approved for clinical use and are expected to be used in the treatment of white matter injury after SAH. Given these exciting works, especially in preclinical studies, new breakthroughs in the treatment of neurological deficits caused by white matter injury in SAH patients may be possible in the near future.

AUTHOR CONTRIBUTIONS

XR, LG, JZ, QL, SZ, YC, and ZL draft the manuscript and figures. HF, ZL, and YC proof read and revise the manuscript. YC and ZL give the final prove for this submission. All authors contributed to the article and approved the submitted version.

FUNDING

This work was supported by the National Natural Science Foundation of China (82030036 and 81901216); Natural Science Foundation of Chongqing (cstc2019jcyj-msxmX0535); State Key Laboratory of Trauma, Burn, and Combined Injury (SKLYQ202002); and Southwest Hospital (SWH2018BJKJ-05).

REFERENCES

1. Dong Y, Guo ZN, Li Q, Ni W, Gu H, Gu YX, et al. Chinese stroke association guidelines for clinical management of cerebrovascular disorders: executive summary and 2019 update of clinical management of spontaneous subarachnoid haemorrhage. *Stroke Vasc Neurol.* (2019) 4:176–81. doi: 10.1136/svn-2019-000296
2. Neifert SN, Chapman EK, Martini ML, Shuman WH, Schupper AJ, Oermann EK, et al. Aneurysmal subarachnoid hemorrhage: the last decade. *Transl Stroke Res.* (2020) 12:428–46. doi: 10.1007/s12975-020-00867-0
3. Macdonald RL, Schweizer TA. Spontaneous subarachnoid haemorrhage. *Lancet.* (2017) 389:655–66. doi: 10.1016/S0140-6736(16)30668-7
4. Reijmer YD, Van Den Heerik MS, Heinen R, Leemans A, Hendrikse J, De Vis JB, et al. Microstructural white matter abnormalities and cognitive impairment after aneurysmal subarachnoid hemorrhage. *Stroke.* (2018) 49:2040–5. doi: 10.1161/STROKEAHA.118.021622
5. Darwazeh R, Wei M, Zhong J, Zhang Z, Lv F, Darwazeh M, et al. Significant injury of the mammillothalamic tract without injury of the corticospinal tract after aneurysmal subarachnoid hemorrhage: a retrospective diffusion tensor imaging study. *World Neurosurg.* (2018) 114:e624–30. doi: 10.1016/j.wneu.2018.03.042
6. Nakazawa S, Kobayashi S, Yokota H, Shimura T. [A clinical and pathological study of diffuse axonal injury]. *No Shinkei Geka.* (1989) 17:247–53.
7. Wu Y, Peng J, Pang J, Sun X, Jiang Y. Potential mechanisms of white matter injury in the acute phase of experimental subarachnoid haemorrhage. *Brain.* (2017) 140:e36. doi: 10.1093/brain/awx084
8. Wong GK, Lam SW, Wong A, Mok V, Siu D, Ngai K, et al. Early MoCA-assessed cognitive impairment after aneurysmal subarachnoid hemorrhage and relationship to 1-year functional outcome. *Transl Stroke Res.* (2014) 5:286–91. doi: 10.1007/s12975-013-0284-z
9. Adina M, Patricia R, Peter S. *Chapter 11-Stroke and Head Injury*. *The Nervous System*. 2nd ed. Edinburgh: Churchill Livingstone (2010) 199–226p. doi: 10.1016/B978-0-7020-3373-5.00011-3
10. Lee SJ, Kim MS, Jang SH. White matter abnormalities in spontaneous subarachnoid hemorrhage: a tract-based spatial statistics study. *Stroke.* (2020) 51:e246–9. doi: 10.1161/STROKEAHA.120.029996
11. Guo D, Wilkinson DA, Thompson BG, Pandey AS, Keep RF, Xi G, et al. MRI characterization in the acute phase of experimental subarachnoid hemorrhage. *Transl Stroke Res.* (2017) 8:234–43. doi: 10.1007/s12975-016-0511-5
12. Neil-Dwyer G, Lang DA, Doshi B, Gerber CJ, Smith PW. Delayed cerebral ischaemia: the pathological substrate. *Acta Neurochir.* (1994) 131:137–45. doi: 10.1007/BF01401464
13. Satomi J, Hadeishi H, Yoshida Y, Suzuki A, Nagahiro S. Histopathological findings in brains of patients who died in the acute stage of poor-grade subarachnoid hemorrhage. *Neurol Med Chir.* (2016) 56:766–70. doi: 10.2176/nmc.oa.2016-0061
14. Weimer JM, Jones SE, Frontera JA. Acute cytotoxic and vasogenic edema after subarachnoid hemorrhage: a quantitative MRI study. *AJNR Am J Neuroradiol.* (2017) 38:928–34. doi: 10.3174/ajnr.A5181
15. Cho MK, Jang SH. Diffusion tensor imaging studies on spontaneous subarachnoid hemorrhage-related brain injury: a mini-review. *Front Neurol.* (2020) 11:283. doi: 10.3389/fneur.2020.00283
16. Jang SH, Choi BY, Kim SH, Chang CH, Jung YJ, Kwon HG. Injury of the mammillothalamic tract in patients with subarachnoid haemorrhage: a retrospective diffusion tensor imaging study. *BMJ Open.* (2014) 4:e005613. doi: 10.1136/bmjopen-2014-005613
17. Jang SH, Yeo SS. Injury of the papez circuit in a patient with provoked confabulation following subarachnoid hemorrhage: a diffusion tensor tractography study. *Acta Neurol Belg.* (2016) 116:655–8. doi: 10.1007/s13760-016-0602-9
18. Schweizer TA, Al-Khindi T, Loch Macdonald R. Diffusion tensor imaging as a surrogate marker for outcome after perimesencephalic subarachnoid hemorrhage. *Clin Neurol Neurosurg.* (2012) 114:798–800. doi: 10.1016/j.clineuro.2011.12.045
19. Liu Y, Soppi V, Mustonen T, Kononen M, Koivisto T, Koskela A, et al. Subarachnoid hemorrhage in the subacute stage: elevated apparent diffusion coefficient in normal-appearing brain tissue after treatment. *Radiology.* (2007) 242:518–25. doi: 10.1148/radiol.2422051698
20. Ali A, Bitir B, Abdullah T, Sabanci PA, Aras Y, Aydoseli A, et al. Gray-to-white matter ratio predicts long-term recovery potential of patients with aneurysmal subarachnoid hemorrhage. *Neurosurg Rev.* (2020) 43:195–202. doi: 10.1007/s10143-018-1029-y
21. Powers WJ. Intracerebral hemorrhage and head trauma: common effects and common mechanisms of injury. *Stroke.* (2010) 41:S107–10. doi: 10.1161/STROKEAHA.110.595058
22. Kummer TT, Magnoni S, Macdonald CL, Dikranian K, Milner E, Sorrell J, et al. Experimental subarachnoid haemorrhage results in multifocal axonal injury. *Brain.* (2015) 138:2608–18. doi: 10.1093/brain/awv180
23. Tao C, Hu X, Li H, You C. White matter injury after intracerebral hemorrhage: pathophysiology and therapeutic strategies. *Front Hum Neurosci.* (2017) 11:422. doi: 10.3389/fnhum.2017.00422
24. Iadecola C, Park L, Capone C. Threats to the mind: aging, amyloid, and hypertension. *Stroke.* (2009) 40:S40–4. doi: 10.1161/STROKEAHA.108.533638
25. Husain J, Juurlink BH. Oligodendroglial precursor cell susceptibility to hypoxia is related to poor ability to cope with reactive oxygen species. *Brain Res.* (1995) 698:86–94. doi: 10.1016/0006-8993(95)00832-B
26. Domercq M, Sanchez-Gomez MV, Sherwin C, Etxebarria E, Fern R, Matute C. System xc- and glutamate transporter inhibition mediates microglial toxicity to oligodendrocytes. *J Immunol.* (2007) 178:6549–56. doi: 10.4049/jimmunol.178.10.6549
27. Egashira Y, Zhao H, Hua Y, Keep RF, Xi G. White matter injury after subarachnoid hemorrhage: role of blood-brain barrier disruption and matrix metalloproteinase-9. *Stroke.* (2015) 46:2909–15. doi: 10.1161/STROKEAHA.115.010351
28. Toyota Y, Wei J, Xi G, Keep RF, Hua Y. White matter T2 hyperintensities and blood-brain barrier disruption in the hyperacute stage of subarachnoid hemorrhage in male mice: the role of lipocalin-2. *CNS Neurosci Ther.* (2019) 25:1207–14. doi: 10.1111/cns.13221
29. Egashira Y, Hua Y, Keep RF, Xi G. Acute white matter injury after experimental subarachnoid hemorrhage: potential role of lipocalin 2. *Stroke.* (2014) 45:2141–3. doi: 10.1161/STROKEAHA.114.005307
30. Chen S, Feng H, Sherchan P, Klebe D, Zhao G, Sun X, et al. Controversies and evolving new mechanisms in subarachnoid hemorrhage. *Prog Neurobiol.* (2014) 115:64–91. doi: 10.1016/j.pneurobio.2013.09.002
31. Suwatcharangkoon S, Meyers E, Falo C, Schmidt JM, Agarwal S, Claassen J, et al. Loss of consciousness at onset of subarachnoid hemorrhage as an important marker of early brain injury. *JAMA Neurol.* (2016) 73:28–35. doi: 10.1001/jamaneurol.2015.3188
32. Lee VH, Temes RE, John S, Conners JJ, Bleck T, Prabhakaran S. Posterior reversible leukoencephalopathy syndrome presenting with global cerebral edema and herniation. *Neurocrit Care.* (2013) 18:81–3. doi: 10.1007/s12028-012-9798-6

33. Hartwell RC, Sutton LN. Mannitol, intracranial pressure, and vasogenic edema. *Neurosurgery*. (1993) 32:444–450; discussion 450. doi: 10.1097/00006123-199303000-00017
34. Leinonen V, Vanninen R, Rauramaa T. Raised intracranial pressure and brain edema. *Handb Clin Neurol.* (2017) 145:25–37. doi: 10.1016/B978-0-12-802395-2.00004-3
35. Rabinstein AA, Lanzino G. Aneurysmal subarachnoid hemorrhage: unanswered questions. *Neurosurg Clin N Am.* (2018) 29:255–62. doi: 10.1016/j.nec.2018.01.001
36. Nemoto EM. Dynamics of cerebral venous and intracranial pressures. *Acta Neurochir Suppl.* (2006) 96:435–7. doi: 10.1007/3-211-30714-1_89
37. Owler BK, Pitham T, Wang D. Aquaporins: relevance to cerebrospinal fluid physiology and therapeutic potential in hydrocephalus. *Cerebrospinal Fluid Res.* (2010) 7:15. doi: 10.1186/1743-8454-7-15
38. Hampl R, Bicikova M, Sosvorova L. Hormones and the blood-brain barrier. *Horm Mol Biol Clin Investig.* (2015) 21:159–64. doi: 10.1515/hmbci-2014-0042
39. Coughlin SR. Protease-activated receptors in hemostasis, thrombosis and vascular biology. *J Thromb Haemost.* (2005) 3:1800–14. doi: 10.1111/j.1538-7836.2005.01377.x
40. Alberelli MA, De Candia E. Functional role of protease activated receptors in vascular biology. *Vascul Pharmacol.* (2014) 62:72–81. doi: 10.1016/j.vph.2014.06.001
41. Kassell NF, Sasaki T, Colohan AR, Nazar G. Cerebral vasospasm following aneurysmal subarachnoid hemorrhage. *Stroke.* (1985) 16:562–72. doi: 10.1161/01.STR.16.4.562
42. White RP, Robertson JT. Role of plasmin, thrombin, and antithrombin III as etiological factors in delayed cerebral vasospasm. *Neurosurgery*. (1985) 16:27–35. doi: 10.1227/00006123-198501000-00007
43. Kikkawa Y, Kameda K, Hirano M, Sasaki T, Hirano K. Impaired feedback regulation of the receptor activity and the myofilament Ca2+ sensitivity contributes to increased vascular reactiveness after subarachnoid hemorrhage. *J Cereb Blood Flow Metab.* (2010) 30:1637–50. doi: 10.1038/jcbfm.2010.35
44. Babu R, Bagley JH, Di C, Friedman AH, Adamson C. Thrombin and hemin as central factors in the mechanisms of intracerebral hemorrhage-induced secondary brain injury and as potential targets for intervention. *Neurosurg Focus.* (2012) 32:E8. doi: 10.3171/2012.1.FOCUS11366
45. Yang CC, Hsiao LD, Yang CM, Lin CC. Thrombin enhanced matrix metalloproteinase-9 expression and migration of SK-N-SH cells via PAR-1, c-Src, PYK2, EGFR, Erk1/2 and AP-1. *Mol Neurobiol.* (2017) 54:3476–91. doi: 10.1007/s12035-016-9916-0
46. Li L, Tao Y, Tang J, Chen Q, Yang Y, Feng Z, et al. A cannabinoid receptor 2 agonist prevents thrombin-induced blood-brain barrier damage via the inhibition of microglial activation and matrix metalloproteinase expression in rats. *Transl Stroke Res.* (2015) 6:467–77. doi: 10.1007/s12975-015-0425-7
47. Walker EJ, Rosenberg GA. Divergent role for MMP-2 in myelin breakdown and oligodendrocyte death following transient global ischemia. *J Neurosci Res.* (2010) 88:764–73. doi: 10.1002/jnr.22257
48. Gulati D, Dua D, Torbey MT. Hemostasis in intracranial hemorrhage. *Front Neurol.* (2017) 8:80. doi: 10.3389/fneur.2017.00080
49. Esteve-Pastor MA, Hernandez-Romero D, Valdes M, Marin F. New approaches to the role of thrombin in acute coronary syndromes: quo vadis bivalirudin, a direct thrombin inhibitor? *Molecules.* (2016) 21:284. doi: 10.3390/molecules21030284
50. Li Q, Zhao HL, Pan PY, Ru XF, Zuo SL, Qu J, et al. Nexilin regulates oligodendrocyte progenitor cell migration and remyelination and is negatively regulated by protease-activated receptor 1/Ras-proximate-1 signaling following subarachnoid hemorrhage. *Front Neurol.* (2018) 9:282. doi: 10.3389/fneur.2018.00282
51. Hayman EG, Patel AP, James RF, Simard JM. Heparin and heparin-derivatives in post-subarachnoid hemorrhage brain injury: a multimodal therapy for a multimodal disease. *Molecules.* (2017) 22:724. doi: 10.3390/molecules22050724
52. Mocco J, Prickett CS, Komotar RJ, Connolly ES, Mayer SA. Potential mechanisms and clinical significance of global cerebral edema following aneurysmal subarachnoid hemorrhage. *Neurosurg Focus.* (2007) 22:E7. doi: 10.3171/foc.2007.22.5.8
53. Sweeney MD, Sagare AP, Zlokovic BV. Blood-brain barrier breakdown in alzheimer disease and other neurodegenerative disorders. *Nat Rev Neurol.* (2018) 14:133–50. doi: 10.1038/nrneurol.2017.188
54. Zhao Z, Nelson AR, Betsholtz C, Zlokovic BV. Establishment and dysfunction of the blood-brain barrier. *Cell.* (2015) 163:1064–78. doi: 10.1016/j.cell.2015.10.067
55. Hase Y, Horsburgh K, Ihara M, Kalaria RN. White matter degeneration in vascular and other ageing-related dementias. *J Neurochem.* (2018) 144:617–33. doi: 10.1111/jnc.14271
56. Lehmann HC, Kohne A, Bernal F, Jangouk P, Meyer Zu Horste G, Dehmel T, et al. Matrix metalloproteinase-2 is involved in myelination of dorsal root ganglia neurons. *Glia.* (2009) 57:479–89. doi: 10.1002/glia.20774
57. Skuljec J, Gudi V, Ulrich R, Frichert K, Yildiz O, Pul R, et al. Matrix metalloproteinases and their tissue inhibitors in cuprizone-induced demyelination and remyelination of brain white and gray matter. *J Neuropathol Exp Neurol.* (2011) 70:758–69. doi: 10.1097/NEN.0b013e3182294fad
58. Pan P, Zhang X, Li Q, Zhao H, Qu J, Zhang JH, et al. Cyclosporine A alleviated matrix metalloproteinase 9 associated blood-brain barrier disruption after subarachnoid hemorrhage in mice. *Neurosci Lett.* (2017) 649:7–13. doi: 10.1016/j.neulet.2017.03.050
59. Tremblay R, Lee S, Rudy B. GABAergic interneurons in the neocortex: from cellular properties to circuits. *Neuron.* (2016) 91:260–92. doi: 10.1016/j.neuron.2016.06.033
60. Macrez R, Stys PK, Vivien D, Lipton SA, Docagne F. Mechanisms of glutamate toxicity in multiple sclerosis: biomarker and therapeutic opportunities. *Lancet Neurol.* (2016) 15:1089–102. doi: 10.1016/S1474-4422(16)30165-X
61. Bakiri Y, Burzomato V, Frugier G, Hamilton NB, Karadottir R, Attwell D. Glutamatergic signaling in the brain's white matter. *Neuroscience.* (2009) 158:266–74. doi: 10.1016/j.neuroscience.2008.01.015
62. Spitzer S, Volbracht K, Lundgaard I, Karadottir RT. Glutamate signalling: a multifaceted modulator of oligodendrocyte lineage cells in health and disease. *Neuropharmacology.* (2016) 110:574–85. doi: 10.1016/j.neuropharm.2016.06.014
63. Davalos A, Shuaib A, Wahlgren NG. Neurotransmitters and pathophysiology of stroke: evidence for the release of glutamate and other transmitters/mediators in animals and humans. *J Stroke Cerebrovasc Dis.* (2000) 9:2–8. doi: 10.1053/jscd.2000.18908
64. Feng D, Wang W, Dong Y, Wu L, Huang J, Ma Y, et al. Ceftriaxone alleviates early brain injury after subarachnoid hemorrhage by increasing excitatory amino acid transporter 2 expression via the PI3K/Akt/NF-kappaB signaling pathway. *Neuroscience.* (2014) 268:21–32. doi: 10.1016/j.neuroscience.2014.02.053
65. Zhao H, Qu J, Li Q, Cui M, Wang J, Zhang K, et al. Taurine supplementation reduces neuroinflammation and protects against white matter injury after intracerebral hemorrhage in rats. *Amino Acids.* (2018) 50:439–51. doi: 10.1007/s00726-017-2529-8
66. Leviton A, Allred EN, Dammann O, Engelke S, Fichorova RN, Hirtz D, et al. Systemic inflammation, intraventricular hemorrhage, and white matter injury. *J Child Neurol.* (2013) 28:1637–45. doi: 10.1177/0883073812463068
67. Miyanohara J, Kakae M, Nagayasu K, Nakagawa T, Mori Y, Arai K, et al. TRPM2 channel aggravates CNS inflammation and cognitive impairment via activation of microglia in chronic cerebral hypoperfusion. *J Neurosci.* (2018) 38:3520–33. doi: 10.1523/JNEUROSCI.2451-17.2018
68. Dambska M, Maslinska D, Laure-Kamionowska M, Toborowicz J. Inflammatory and reparative tissue reaction in developing human central nervous system. *Acta Neurobiol Exp.* (2004) 64:475–80.
69. Peng J, Pang J, Huang L, Enkhjargal B, Zhang T, Mo J, et al. LRP1 activation attenuates white matter injury by modulating microglial polarization through Shc1/PI3K/Akt pathway after subarachnoid hemorrhage in rats. *Redox Biol.* (2019) 21:101121. doi: 10.1016/j.redox.2019.101121
70. Pang J, Peng J, Matei N, Yang P, Kuai L, Wu Y, et al. Apolipoprotein E exerts a whole-brain protective property by promoting M1? Microglia quiescence after experimental subarachnoid hemorrhage in mice. *Transl Stroke Res.* (2018) 9:654–68. doi: 10.1007/s12975-018-0665-4
71. Wang X, Mallard C. Editorial: white blood cells matter in neonatal white-matter injury. *J Leukoc Biol.* (2016) 99:4–6. doi: 10.1189/jlb.3CE0615-242R

72. Qin C, Fan WH, Liu Q, Shang K, Murugan M, Wu LJ, et al. Fingolimod protects against ischemic white matter damage by modulating microglia toward M2 polarization via STAT3 pathway. *Stroke.* (2017) 48:3336–46. doi: 10.1161/STROKEAHA.117.018505
73. Narantuya D, Nagai A, Sheikh AM, Wakabayashi K, Shiota Y, Watanabe T, et al. Microglia transplantation attenuates white matter injury in rat chronic ischemia model via matrix metalloproteinase-2 inhibition. *Brain Res.* (2010) 1316:145–52. doi: 10.1016/j.brainres.2009.12.043
74. Marder CP, Narla V, Fink JR, Tozer Fink KR. Subarachnoid hemorrhage: beyond aneurysms. *AJR Am J Roentgenol.* (2014) 202:25–37. doi: 10.2214/AJR.12.9749
75. Hughes EG, Kang SH, Fukaya M, Bergles DE. Oligodendrocyte progenitors balance growth with self-repulsion to achieve homeostasis in the adult brain. *Nat Neurosci.* (2013) 16:668–76. doi: 10.1038/nn.3390
76. Crawford AH, Tripathi RB, Richardson WD, Franklin RJM. Developmental origin of oligodendrocyte lineage cells determines response to demyelination and susceptibility to age-associated functional decline. *Cell Rep.* (2016) 15:761–73. doi: 10.1016/j.celrep.2016.03.069
77. De Castro F, Bribian A. The molecular orchestra of the migration of oligodendrocyte precursors during development. *Brain Res Brain Res Rev.* (2005) 49:227–41. doi: 10.1016/j.brainresrev.2004.12.034
78. Taylor DL, Pirianov G, Holland S, Mcginnity CJ, Norman AL, Reali C, et al. Attenuation of proliferation in oligodendrocyte precursor cells by activated microglia. *J Neurosci Res.* (2010) 88:1632–44. doi: 10.1002/jnr.22335
79. Svatkova A, Mandl RC, Scheewe TW, Cahn W, Kahn RS, Hulshoff Pol HE. Physical exercise keeps the brain connected: biking increases white matter integrity in patients with schizophrenia and healthy controls. *Schizophr Bull.* (2015) 41:869–78. doi: 10.1093/schbul/sbv033
80. Simpson PB, Armstrong RC. Intracellular signals and cytoskeletal elements involved in oligodendrocyte progenitor migration. *Glia.* (1999) 26:22–35.
81. Bribian A, Esteban PF, Clemente D, Soussi-Yanicostas N, Thomas JL, Zalc B, et al. A novel role for anosmin-1 in the adhesion and migration of oligodendrocyte precursors. *Dev Neurobiol.* (2008) 68:1503–16. doi: 10.1002/dneu.20678
82. Gudz TI, Komuro H, Macklin WB. Glutamate stimulates oligodendrocyte progenitor migration mediated via an alphav integrin/myelin proteolipid protein complex. *J Neurosci.* (2006) 26:2458–66. doi: 10.1523/JNEUROSCI.4054-05.2006
83. Tsai HH, Niu J, Munji R, Davalos D, Chang J, Zhang H, et al. Oligodendrocyte precursors migrate along vasculature in the developing nervous system. *Science.* (2016) 351:379–84. doi: 10.1126/science.aad3839
84. Xu W, Yan J, Chen S, Ocak U, Shao A, Zhang J. Peroxisomal dysfunction contributes to white matter injury following subarachnoid hemorrhage in rats via thioredoxin-interacting protein-dependent manner. *Front Cell Dev Biol.* (2020) 8:576482. doi: 10.3389/fcell.2020.576482
85. Calver AR, Hall AC, Yu WP, Walsh FS, Heath JK, Betsholtz C, et al. Oligodendrocyte population dynamics and the role of PDGF *in vivo*. *Neuron.* (1998) 20:869–82. doi: 10.1016/S0896-6273(00)80469-9
86. Guo F, Lang J, Sohn J, Hammond E, Chang M, Pleasure D. Canonical Wnt signaling in the oligodendroglial lineage–puzzles remain. *Glia.* (2015) 63:1671–93. doi: 10.1002/glia.22813
87. Bujalka H, Koenning M, Jackson S, Perreau VM, Pope B, Hay CM, et al. MYRF is a membrane-associated transcription factor that autoproteolytically cleaves to directly activate myelin genes. *PLoS Biol.* (2013) 11:e1001625. doi: 10.1371/journal.pbio.1001625
88. Nawaz S, Sanchez P, Schmitt S, Snaidero N, Mitkovski M, Velte C, et al. Actin filament turnover drives leading edge growth during myelin sheath formation in the central nervous system. *Dev Cell.* (2015) 34:139–51. doi: 10.1016/j.devcel.2015.05.013
89. Corsini NS, Knoblich JA. Tracing stem cell division in adult neurogenesis. *Cell Stem Cell.* (2018) 22:143–5. doi: 10.1016/j.stem.2018.01.012
90. Bond AM, Ming GL, Song H. Adult mammalian neural stem cells and neurogenesis: five decades later. *Cell Stem Cell.* (2015) 17:385–95. doi: 10.1016/j.stem.2015.09.003
91. Nijboer CH, Kooijman E, Van Velthoven CT, Van Tilborg E, Tiebosch IA, Eijkelkamp N, et al. Intranasal stem cell treatment as a novel therapy for subarachnoid hemorrhage. *Stem Cells Dev.* (2018) 27:313–25. doi: 10.1089/scd.2017.0148
92. Brunet MC, Chen SH, Khandelwal P, Hare JM, Starke RM, Peterson EC, et al. Intravenous stem cell therapy for high-grade aneurysmal subarachnoid hemorrhage: case report and literature review. *World Neurosurg.* (2019) 128:573–5. doi: 10.1016/j.wneu.2019.04.055
93. Takahashi J. Stem cells and regenerative medicine for neural repair. *Curr Opin Biotechnol.* (2018) 52:102–8. doi: 10.1016/j.copbio.2018.03.006
94. Ghosh M, Balbi M, Hellal F, Dichgans M, Lindauer U, Plesnila N. Pericytes are involved in the pathogenesis of cerebral autosomal dominant arteriopathy with subcortical infarcts and leukoencephalopathy. *Ann Neurol.* (2015) 78:887–900. doi: 10.1002/ana.24512
95. Keller A, Westenberger A, Sobrido MJ, Garcia-Murias M, Domingo A, Sears RL, et al. Mutations in the gene encoding PDGF-B cause brain calcifications in humans and mice. *Nat Genet.* (2013) 45:1077–82. doi: 10.1038/ng.2723
96. Li Q, Liu X, Ruan H, Chen Y, Feng H. Pericyte: potential target for hemorrhagic stroke prevention and treatment. *Curr Drug Deliv.* (2017) 14:773–84. doi: 10.2174/1567201813666160829103222
97. Thanabalasundaram G, Schneidewind J, Pieper C, Galla HJ. The impact of pericytes on the blood-brain barrier integrity depends critically on the pericyte differentiation stage. *Int J Biochem Cell Biol.* (2011) 43:1284–93. doi: 10.1016/j.biocel.2011.05.002
98. Li Q, Chen Y, Li B, Luo C, Zuo S, Liu X, et al. Hemoglobin induced NO/cGMP suppression deteriorate microcirculation via pericyte phenotype transformation after subarachnoid hemorrhage in rats. *Sci Rep.* (2016) 6:22070. doi: 10.1038/srep22070
99. Pan P, Zhao H, Zhang X, Li Q, Qu J, Zuo S, et al. Cyclophilin a signaling induces pericyte-associated blood-brain barrier disruption after subarachnoid hemorrhage. *J Neuroinflammation.* (2020) 17:16. doi: 10.1186/s12974-020-1699-6
100. Fumoto T, Naraoka M, Katagai T, Li Y, Shimamura N, Ohkuma H. The role of oxidative stress in microvascular disturbances after experimental subarachnoid hemorrhage. *Transl Stroke Res.* (2019) 10:684–94. doi: 10.1007/s12975-018-0685-0
101. Dore-Duffy P, Katychev A, Wang X, Van Buren E. CNS microvascular pericytes exhibit multipotential stem cell activity. *J Cereb Blood Flow Metab.* (2006) 26:613–24. doi: 10.1038/sj.jcbfm.9600272
102. Green AJ, Gelfand JM, Cree BA, Bevan C, Boscardin WJ, Mei F, et al. Clemastine fumarate as a remyelinating therapy for multiple sclerosis (ReBUILD): a randomised, controlled, double-blind, crossover trial. *Lancet.* (2017) 390:2481–9. doi: 10.1016/S0140-6736(17)32346-2
103. Ghoumari AM, Abi Ghanem C, Asbelaoui N, Schumacher M, Hussain R. Roles of progesterone, testosterone and their nuclear receptors in central nervous system myelination and remyelination. *Int J Mol Sci.* (2020) 21:3163. doi: 10.3390/ijms21093163
104. Dadwal P, Mahmud N, Sinai L, Azimi A, Fatt M, Wondisford FE, et al. Activating endogenous neural precursor cells using metformin leads to neural repair and functional recovery in a model of childhood brain injury. *Stem Cell Reports.* (2015) 5:166–73. doi: 10.1016/j.stemcr.2015.06.011
105. Francis JS, Markov V, Wojtas ID, Gray S, Mccown T, Samulski RJ, et al. Preclinical biodistribution, tropism, and efficacy of oligotropic AAV/Olig001 in a mouse model of congenital white matter disease. *Mol Ther Methods Clin Dev.* (2021) 20:520–34. doi: 10.1016/j.omtm.2021.01.009
106. Choi JW, Gardell SE, Herr DR, Rivera R, Lee CW, Noguchi K, et al. FTY720 (fingolimod) efficacy in an animal model of multiple sclerosis requires astrocyte sphingosine 1-phosphate receptor 1 (S1P1) modulation. *Proc Natl Acad Sci USA.* (2011) 108:751–6. doi: 10.1073/pnas.1014154108
107. Deshmukh VA, Tardif V, Lyssiotis CA, Green CC, Kerman B, Kim HJ, et al. A regenerative approach to the treatment of multiple sclerosis. *Nature.* (2013) 502:327–32. doi: 10.1038/nature12647
108. Liu J, Dupree JL, Gacias M, Frawley R, Sikder T, Naik P, et al. Clemastine enhances myelination in the prefrontal cortex and rescues behavioral changes in socially isolated mice. *J Neurosci.* (2016) 36:957–62. doi: 10.1523/JNEUROSCI.3608-15.2016
109. Miron VE, Zehntner SP, Kuhlmann T, Ludwin SK, Owens T, Kennedy TE, et al. Statin therapy inhibits remyelination in the central nervous system. *Am J Pathol.* (2009) 174:1880–90. doi: 10.2353/ajpath.2009.080947
110. Najm FJ, Madhavan M, Zaremba A, Shick E, Karl RT, Factor DC, et al. Drug-based modulation of endogenous stem cells promotes functional remyelination *in vivo*. *Nature.* (2015) 522:216–20. doi: 10.1038/nature14335

111. Preisner A, Albrecht S, Cui QL, Hucke S, Ghelman J, Hartmann C, et al. Non-steroidal anti-inflammatory drug indometacin enhances endogenous remyelination. *Acta Neuropathol.* (2015) 130:247–61. doi: 10.1007/s00401-015-1426-z
112. Mi S, Pepinsky RB, Cadavid D. Blocking LINGO-1 as a therapy to promote CNS repair: from concept to the clinic. *CNS Drugs.* (2013) 27:493–503. doi: 10.1007/s40263-013-0068-8
113. Mei F, Fancy SPJ, Shen YA, Niu J, Zhao C, Presley B, et al. Micropillar arrays as a high-throughput screening platform for therapeutics in multiple sclerosis. *Nat Med.* (2014) 20:954–60. doi: 10.1038/nm.3618
114. Abiraman K, Pol SU, O'bara MA, Chen GD, Khaku ZM, Wang J, et al. Anti-muscarinic adjunct therapy accelerates functional human oligodendrocyte repair. *J Neurosci.* (2015) 35:3676–88. doi: 10.1523/JNEUROSCI.3510-14.2015
115. Hammond TR, Mcellin B, Morton PD, Raymond M, Dupree J, Gallo V. Endothelin-B receptor activation in astrocytes regulates the rate of oligodendrocyte regeneration during remyelination. *Cell Rep.* (2015) 13:2090–7. doi: 10.1016/j.celrep.2015.11.002
116. Huang JK, Jarjour AA, Oumesmar BN, Kerninon C, Williams A, Krezel W, et al. Retinoid X receptor gamma signaling accelerates CNS remyelination. *Nat Neurosci.* (2011) 14:45–53. doi: 10.1038/nn.2702
117. Yamaguchi W, Tamai R, Kageura M, Furuyama T, Inagaki S. Sema4D as an inhibitory regulator in oligodendrocyte development. *Mol Cell Neurosci.* (2012) 49:290–9. doi: 10.1016/j.mcn.2011.12.004
118. Watzlawik JO, Warrington AE, Rodriguez M. PDGF is required for remyelination-promoting IgM stimulation of oligodendrocyte progenitor cell proliferation. *PLoS ONE.* (2013) 8:e55149. doi: 10.1371/journal.pone.0055149
119. Saligrama N, Case LK, Del Rio R, Noubade R, Teuscher C. Systemic lack of canonical histamine receptor signaling results in increased resistance to autoimmune encephalomyelitis. *J Immunol.* (2013) 191:614–22. doi: 10.4049/jimmunol.1203137

Conflict of Interest: The authors declare that the research was conducted in the absence of any commercial or financial relationships that could be construed as a potential conflict of interest.

frontiers in Neurology

ORIGINAL RESEARCH
published: 20 July 2021
doi: 10.3389/fneur.2021.691631

Hippocampal Transcriptome Changes After Subarachnoid Hemorrhage in Mice

Angelique S. Regnier-Golanov[1], Friederike Dündar[2], Paul Zumbo[2], Doron Betel[3,4,5], Magda S. Hernandez[1], Leif E. Peterson[6], Eng H. Lo[7], Eugene V. Golanov[1†] and Gavin W. Britz[1†]*

[1] Laboratory of Cerebrovascular Research, Department of Neurosurgery, Houston Methodist Hospital, Houston, TX, United States, [2] Applied Bioinformatics Core, Department of Physiology and Biophysics, Weill Cornell Medicine, New York, NY, United States, [3] Applied Bioinformatics Core, Weill Cornell Medicine, New York, NY, United States, [4] Division of Hematology and Medical Oncology, Department of Medicine, Weill Cornell Medicine, New York, NY, United States, [5] Institute for Computational Biomedicine, Weill Cornell Medicine, New York, NY, United States, [6] Center for Biostatistics, Houston Methodist Research Institute, Houston, TX, United States, [7] Laboratory of Neuroprotection Research, Harvard Medical School, Massachusetts General Hospital, Charlestown, MA, United States

After subarachnoid hemorrhage (SAH), up to 95% of surviving patients suffer from post-SAH syndrome, which includes cognitive deficits with impaired memory, executive functions, and emotional disturbances. **Although these long-term cognitive deficits are thought to result from damage to temporomesial–hippocampal areas, the underlying mechanisms remain unknown**. To fill this gap in knowledge, we performed a systematic RNA sequencing screen of the hippocampus in a mouse model of SAH. SAH was induced by perforation of the circle of Willis in mice. Four days later, hippocampal RNA was obtained from SAH and control (sham perforation) mice. Next-generation RNA sequencing was used to determine differentially expressed genes in the whole bilateral hippocampi remote from the SAH bleeding site. Functional analyses and clustering tools were used to define molecular pathways. Differential gene expression analysis detected 642 upregulated and 398 downregulated genes (false discovery rate <0.10) in SAH compared to Control group. Functional analyses using IPA suite, Gene Ontology terms, REACTOME pathways, and MsigDB Hallmark gene set collections revealed suppression of oligodendrocytes/myelin related genes, and overexpression of genes related to complement system along with genes associated with innate and adaptive immunity, and extracellular matrix reorganization. Interferon regulatory factors, TGF-β1, and BMP were identified as major orchestrating elements in the hippocampal tissue response. The MEME-Suite identified binding motifs of Krüppel-like factors, zinc finger transcription factors, and interferon regulatory factors as overrepresented DNA promoter motifs. This study provides the first systematic gene and pathway database of the hippocampal response after SAH. Our findings suggest that damage of the entorhinal cortex by subarachnoid blood may remotely trigger specific hippocampal responses, which include suppression of oligodendrocyte function. Identification of these novel pathways may allow for development of new therapeutic approaches for post-SAH cognitive deficits.

Keywords: subarachnoid hemorrhage, cognitive deficits, post-SAH syndrome, hippocampus, transcriptome, complement, oligodendrocyte

OPEN ACCESS

Edited by:
Budbazar Enkhjargal, Boston University, United States

Reviewed by:
Nicolas K. Khattar, University of Louisville, United States
Fei Liu, Central South University, China

***Correspondence:**
Gavin W. Britz
gbritz@houstonmethodist.org

† These authors have contributed equally to this work and share last authorship

Specialty section:
This article was submitted to Stroke, a section of the journal Frontiers in Neurology

Received: *06 April 2021*
Accepted: *11 June 2021*
Published: *20 July 2021*

Citation:
Regnier-Golanov AS, Dündar F, Zumbo P, Betel D, Hernandez MS, Peterson LE, Lo EH, Golanov EV and Britz GW (2021) Hippocampal Transcriptome Changes After Subarachnoid Hemorrhage in Mice. Front. Neurol. 12:691631. doi: 10.3389/fneur.2021.691631

INTRODUCTION

Subarachnoid hemorrhage (SAH), blood accumulation in the subarachnoid space (1), in 85% of the cases results from aneurysmal rupture (2, 3). While SAH is the least frequent stroke disorder, accounting for 3–4% of all strokes (4), it has the most catastrophic outcome with 40% fatality (5). Fifty percent of cases occur in population under the age of 55, which otherwise has a good life expectancy (2, 6, 7). Ninety-five percent of survivors experience permanent disabilities and post-SAH syndrome, which includes depression, anxiety, impaired memory and executive functions, trouble of attention, and emotional and cognitive disturbances (5). Subsequently, a significant number, up to 45%, of SAH patients are unable to continue with their professional activities (7, 8).

Morphological brain damage following SAH includes atrophy of the temporomesial/hippocampal area (9, 10), which is associated with the long-term cognitive deficit and correlates with decreased neurocognitive scores (8). The role of hippocampal formation in cognitive processes and memory formation has been extensively documented (11). Following an aneurysmal rupture, most often localized at the base of the skull (12, 13), blood extravasates into the subarachnoid space damaging basal brain surface, including entorhinal cortices, which issue the main afferents to the hippocampus (14, 15). Lesions of entorhinal cortex lead to the damage of the perforant pathway and its hippocampal termination fields (16–18). We hypothesize that bleeding in the subarachnoid space triggers remote hippocampal damage, possibly by direct blood contact with the entorhinal cortex. Blood toxicity to the brain parenchyma has been well-established (19, 20). This would cause global changes in the gene expression resulting in the persistent disturbance of the hippocampal function.

We therefore used next generation RNA sequencing (RNA-seq) to explore specific changes in hippocampal transcriptome 4 days following SAH. Cellular and molecular perturbations accompanying early brain injury (within 72 h post-ictus) after sub-arachnoid have been well documented in the literature and reported non-specific response to brain insult (21, 22). However, mechanisms and respective pathways, underlying secondary brain injury, attributed to neurological and neurocognitive complications, taken place after 72 h have not been well characterized (23, 24). In the present study, we aim to explore biological processes and secondary mechanisms at the cusp between degeneration and regeneration happening at 4 days (25, 26) following SAH, closely mimicking delayed cerebral ischemia observed in humans (23) to explore processes at the origin of long-term consequences of SAH. Considering immense diversity of the various cells and their continuous interaction in the hippocampus, e.g., Iyer and Tole (27), this study was designed to gain an insight into leading biological processes occurring in hippocampus as a whole and to avoid changes in gene expression related to tissue processing for single-cell transcriptome analysis (28). Here, we aim to identify new therapeutic targets for the treatment of post-SAH syndrome.

MATERIALS AND METHODS

Data Availability

The authors declare that all supporting data are available within this article and its Data Supplement. The RNA-seq data and the list of differentially expressed genes (DEGs) can be viewed at the Gene Expression Omnibus (GEO) under accession number GSE167110 (29). Scripts and code are uploaded to [Regnier-Golanov AS, (29)]. Other datasets generated for this study are available upon request to the corresponding author.

Animal Procedures

Animal experimental procedures were conducted in accord with the U.S. National Institutes of Health "Guide for the care and use of laboratory animals" and in compliance with the ARRIVE guidelines. All experimental procedures were approved by the Institutional Animal Care and Use Committee of Houston Methodist Research Institute, Houston, TX (Protocol #: AUP-0220-0009). Animals were housed in the institutional animal facilities on a 12 h day/night cycle with *ad libitum* access to food and water.

Unilateral SAH Induction

Studies were performed in 11 male C56BL/6J mice, 10–14 weeks old (Jackson Labs). To minimize the variability of the RNA-seq experiments, the present study was limited to the male animals. Animals from the same batch were randomly assigned to one of three groups: SAH ($n = 4$), Sham ($n = 3$), and Naïve ($n = 3$). Experimental SAH was induced by the unilateral perforation of the Circle of Willis as previously described (30). Anesthesia was induced with 3% isoflurane in air and maintained at 1.5–1.75% isoflurane in 80% N_2/20% O_2. For regional cerebral blood flow (rCBF) measurement, needle probe (1.5 mm diameter, Moor Instruments, Wilmington, DE) fixed to the stereotaxic holder was placed over the intact skull over the parietal cortex through the appropriately prepped (alcohol and chlorhexidine 2%) skin cut on the side of perforation, after animal anesthetization and placement in stereotaxic frame. Drop of mineral oil was applied to the skull for optical contact between the probe and the skull. Animal placed on a homeothermic blanket with the body temperature maintained at 37°C by the rectal probe feedback (Harvard apparatus) was rotated in a supine position. The heart rate was continuously monitored (LabChart, AD Instruments). Neck skin was shaved and prepped with alcohol and chlorhexidine (2%). In aseptic conditions through the midline neck incision, common, external, and internal carotid arteries were exposed. All three arteries were mobilized using silk thread (7–0). The external carotid artery was cut between two ligatures, and a stump was formed. To minimize the bleeding and avoid mortality, 6-0 prolene filament (length 12 mm) was advanced through the stump into the internal carotid and moved forward for ∼0.5 mm beyond the point of slight resistance. The filament was withdrawn and stump ligated, and the wound was closed. In sham-operated mice, the filament was advanced to the resistance point and withdrawn without puncture (30). Wounds were closed, and animals were allowed to recover before returning to the home cage. Following the surgery, mice were

monitored daily for 96 h. We experienced no procedural or post-surgery mortality when performing experiments in this study.

SAH Severity and Neurological Assessment

Only SAH mice showing a rCBF drop by ≥50% (average 80 ± 15%, $P < 0.001$) immediately after perforation were selected for the study. A representative photograph of an SAH experimental animal done for the study is shown (**Supplementary Figure 5**).

Neurological assessment was done with the Garcia scale as previously reported (31) daily. No significant difference was observed in the baseline scores for the animals randomly assigned to either group [$H_{(3)} = 3.6133$, $P = 0.1581$, $n = 3$–4/group] at 24–96 h after surgery (**Supplementary Table 2**). Due to the limited number of animals, Garcia scale, initially developed for stroke neurological consequences evaluation (31), was not sufficiently sensitive to detect differences of neurological outcomes between Sham and SAH in our experiments, but to rather detect effects of surgery. Further neurobehavioral studies ($N = 18$ with $n = 10$ for SAH and $n = 8$ for Sham) in our laboratory detected no neurological impairments with the Garcia scale but instead showed significant neurocognitive deficits at 4 days after SAH with Y-maze, Social interaction, and Open-field test (in preparation).

RNA Extraction and RNA Sequencing

Four days following surgery, mice were euthanized with CO_2 followed by thoracotomy and decapitation. Immediately after bilateral whole hippocampus of SAH ($n = 4$), Sham ($n = 3$), and Naïve ($n = 3$) group was manually collected by an experimenter blinded to the specific group and total RNA was extracted immediately after using QIAzol reagent (RNeasy Mini Kit, Qiagen Inc., Hilden, Germany). RNA was quantified using the Nanodrop 1000 spectrophotometer (Thermo Fisher Scientific, Waltham, MA). RNA-seq was performed by RNA core of Weill Cornell Medicine (New York, NY). Total RNA integrity was evaluated with the Agilent Bioanalyzer 2100 (Agilent Biotechnologies, Santa Clara, CA), and only samples with an RNA integrity number (RIN) >9.0 were further processed for RNA-seq. All RNA-seq libraries were prepared using 100 ng of total RNA with the TruSeq Stranded Total RNA sample preparation kit (ribosomal RNA depletion and stranded RNA-Seq) with Ribo-Zero according to the manufacturer's specified protocol (Illumina, San Diego, CA). Samples were multiplexed and sequenced across multiple lanes of a HiSeq 4000 Sequencing System (Illumina) using 50-base paired-end reads to achieve a minimum depth of 30 million aligned read-pairs, which is sufficient to evaluate the similarity between transcriptional profiles according to ENCODE guidelines (32).

RNA Sequencing Analysis

Before differential gene expression analysis, the quality of the sequences was assessed based on several metrics using FastQC and QoRTs (33, 34). All our samples passed the quality control (**Supplementary Figures 1A–F**). We aligned, with default parameters, the RNA-seq reads to the mouse reference genome (mm9) using STAR (35). Gene coverage estimates were obtained with featureCounts using composite gene models (union of the exons of all transcript isoforms per gene) from UCSC mm9 annotation from Illumina's iGenomes (36, 37). Uniquely mapped reads that unambiguously overlapped with no more than one Gencode composite gene model were counted for that gene model; the remaining reads were discarded. The counts for each gene model were used for the subsequent analyses.

Differentially Expressed Genes

DEGs were determined with DESeq2 (38), a statistical software package tailored to the gene-wise testing of expression differences using read count data. In brief, DESeq2 assumes an underlying negative binomial distribution of the read counts per sample and gene; it accounts for heteroskedasticity, differences in sequencing depth, and RNA repertoire, as well as for low sample numbers when estimating the expression differences between contrasts of interest.

Functional Analysis to Identify Gene Sets of Interest

Functional analysis to identify gene sets of interest was done using the compareCluster function of the clusterProfiler R package. The overrepresentation analyses (ORA) based on hypergeometric distribution with additional multiple hypothesis-testing correction (39, 40) were run with the gene sets of the Gene Ontology (GO) consortium (41) and REACTOME pathways (42). ORA was done for each group of significantly up- or downregulated DEGs. The results were represented as dotplots representing the *gene ratio* calculated *as the genes related to a given GO term/total number of DEGs*. This allowed us to visualize the most significantly overrepresented gene sets in our study. The top 20 enriched GO terms for each group were plotted. We also generated network-based representations of the most overrepresented gene sets using the cnetplot function of the clusterProfiler package, plotting the top five enriched gene sets. This allowed us to visualize which individual genes are shared or unique to individual gene sets.

Gene Set Enrichment Analysis

Gene set enrichment analysis (GSEA) was performed using the *fgsea* package against MSigDB Hallmark (Broad Institute) pathways (43). Genes were ranked by the DESeq2 Wald test statistic. Hallmark gene sets represent biological processes as defined by publicly available data sets such as microarrays and RNA-seq (44). A normalized enrichment score (NES) was calculated for each pathway, and the top pathways with FDR < 0.05 were displayed.

To identify putative master regulators orchestrating the expression of our DEGs expression, we used the Ingenuity Pathway Analysis suite (IPA; QIAGEN, Hilden, Germany). We used the upstream regulator analysis (URA) tool to identify the molecules whose activity may explain the observed gene expression changes (45). We mined for putative upstream regulators by filtering for genes with the highest activation *z*-score.

To test for the enrichment of DNA motifs in the promoters of DEGs, we used several tools. We used HOMER (v4.9.1) (46) with

the flags-start −1,000 -end 50 to look only for motifs enriched within the promoters of genes (47) relative to all other promoters defined as −1,000 to +50 bp relative to each gene's transcription start site (TSS).

In the MEME suite (48), which offers several tools for DNA motif analyses, we extracted the DNA sequences representing 500 bp upstream of each TSS of both up- and downregulated DEGs. We first ran DREME, which discovers short, ungapped motifs that are relatively enriched in the sequences of interest compared to control sequences (47). DREME was run with default settings, using 500 randomly sampled promoter regions of genes that showed no significant change as control regions.

We then ran CentriMo (49), which identifies known or user-provided motifs that show a significant preference for particular locations. CentriMo takes a set of motifs and a set of equal-length sequences and plots the positional distribution of the best match of each motif (50). We used 500 randomly sampled promoter regions of genes that showed no significant change as control regions.

Finally, we used AME (51), which identifies user-provided motifs that are relatively enriched in the sequences of interest compared with control sequences (51, 52). In contrast to CentriMo, the location of the motif within the supplied set of promoter sequences is not considered. We ran AME *via* the web server using the promoter regions of the upregulated DEGs and to determine if known motifs were found to be enriched compared to promoter regions of genes without changes.

Rt-qPCR for RNA-Seq Validation

Hippocampal tissue and RNA extraction were obtained identically to RNA-seq experiments. Male C56BL/6J mice, 10–14 weeks old ($N = 18$ with $n = 9$ for SAH, $n = 9$ for Sham), were used for this set of experiments. A preamplification step was simultaneously done with the reversed transcription (RT) step using the iScript Explore One-step kit (Biorad, Hercules, CA). Briefly, 1 μg of DNase-treated total RNA was reverse transcribed for 60 min at 45°C, RT was inactivated by increasing temperature to 95°C for 3 min, and 14 preamplification steps were done with the following thermocycler protocol: 95°C for 15 s and 58°C for 4 min, hold at 4°C. Primers (**Supplementary Table 1**) (Sigma-Aldrich, St. Louis, MO), designed with NCBI tool (53), and 2.5 μl of a custom preamplification assay pool of the reverse and forward primers, diluted at 200 μM, were added to the reaction. The preamplification samples were diluted 10-fold in TE buffer (Invitrogen, Carlsbad, CA). Quantitative PCR was run using 5 μl of diluted cDNA and SYBR green chemistry with the SsoAdvanced Universal SYBR green supermix on a CFX Connect thermocycler (Biorad, Hercules, CA) and a cycling program of 30 s at 95°C, and 40 cycles of 95°C for 15 s and 60°C for 30 s. Primers were used at a 300 nM final concentration in a 20 μl total volume. After completion of qPCR, a melting curve of amplified products was determined. Pgk1 was selected as our reference gene after comparing several common housekeeping genes (54) and our RNA-seq list of genes showing no difference in expression between the control and SAH group. In short, the mean of the threshold cycle (Ct) of three technical replicates was used as the Ct for the target of a given animal $\Delta Ct(Animal) = Ct(Target) - Ct(\text{Pgk1})$, and fold changes were calculated using the following equation: $2^{-\Delta\Delta Ct} = 2^{-[Mean\Delta Ct(SAH) - Mean\Delta Ct(Sham)]}$ (55).

Western Blot

Male C56BL/6J mice, 10–14 weeks old ($N = 7$ with $n = 3$ for SAH, $n = 4$ for Sham), were used for this set of experiments. Mouse bilateral whole hippocampus was homogenized in ice-cold RIPA buffer [25 mM Tris-HCl pH 7.6, 150 mM NaCl, 1% NP-40, 0.5% sodium deoxycholate, 0.1% SDS, 1X HALT Protease and Phosphatase Inhibitor Cocktail Solutions (ThermoFisher Scientific)], centrifuged, and stored at −80°C until use. Proteins were quantified by Pierce BCA Protein Assay Kit (ThermoFisher Scientific) and resolved by high resolution Nupage 4–12% Bis-Tris Gel (Thermo Fisher Scientific-Invitrogen). Anti-rabbit MOG (1:1,000; #12690-1-AP, Proteintech) was incubated overnight and diluted in blocking buffer (5% dried milk in Tris-buffered saline, pH 7.4, and 0.2% Tween-20, TBST). After no-stripping of the membrane, anti-rabbit GAPDH linked to HRP (1:2,000; #8884, Cell Signaling Technology) was incubated on the same membrane following MOG labeling overnight and diluted in blocking buffer. Detection was done with Pierce ECL detection reagent (ThermoFisher Scientific). Protein bands were detected with X-ray film (GenHunter.com), and densitometry was calculated after scanning the films at 600 dpi using ImageJ software and the Miller's tutorial (56). Results were expressed as percentage of change from Sham.

Statistical Analysis

Graphs were plotted and statistical analysis was done with GraphPad Prism 9 (GraphPad Software, San Diego, CA). Shapiro–Wilk test was used for test of normality, and *F*-test for heterogeneity of the variance. Parametric data are represented as mean ± SD, and nonparametric as median with interquartile range. Statistical significance was set at $P < 0.05$. Pairwise comparisons were analyzed using a two-tailed *t*-test. For the Garcia scale, a Kruskal–Wallis test was done. Statistics are reported in the text and figure legend.

RESULTS

Changes in Differentially Expressed Genes

Validation of RNAseq findings was performed with mRNA expression analysis using RtqPCR. We found 10 overexpressed DEGs genes statistically significant in a different cohort of animals (**Figure 1**). To explore active ongoing processes in the hippocampus, we analyzed DEGs using REACTOME pathways and GO-biological processes (GO-BP) analyses and searched for clusters of interrelated processes. The five top interacting clusters identified, using both approaches, revealed overexpression of groups of genes related to immune and inflammatory processes and extracellular matrix reorganization (**Figures 2**, **3**). Additional exploration using Ingenuity Pathway Analysis canonical pathways (IPA, QIAGEN, 2020) and GSEA Hallmark collection confirmed the prevalence of these processes (**Supplementary Figure 3**). Five top upregulated genes included

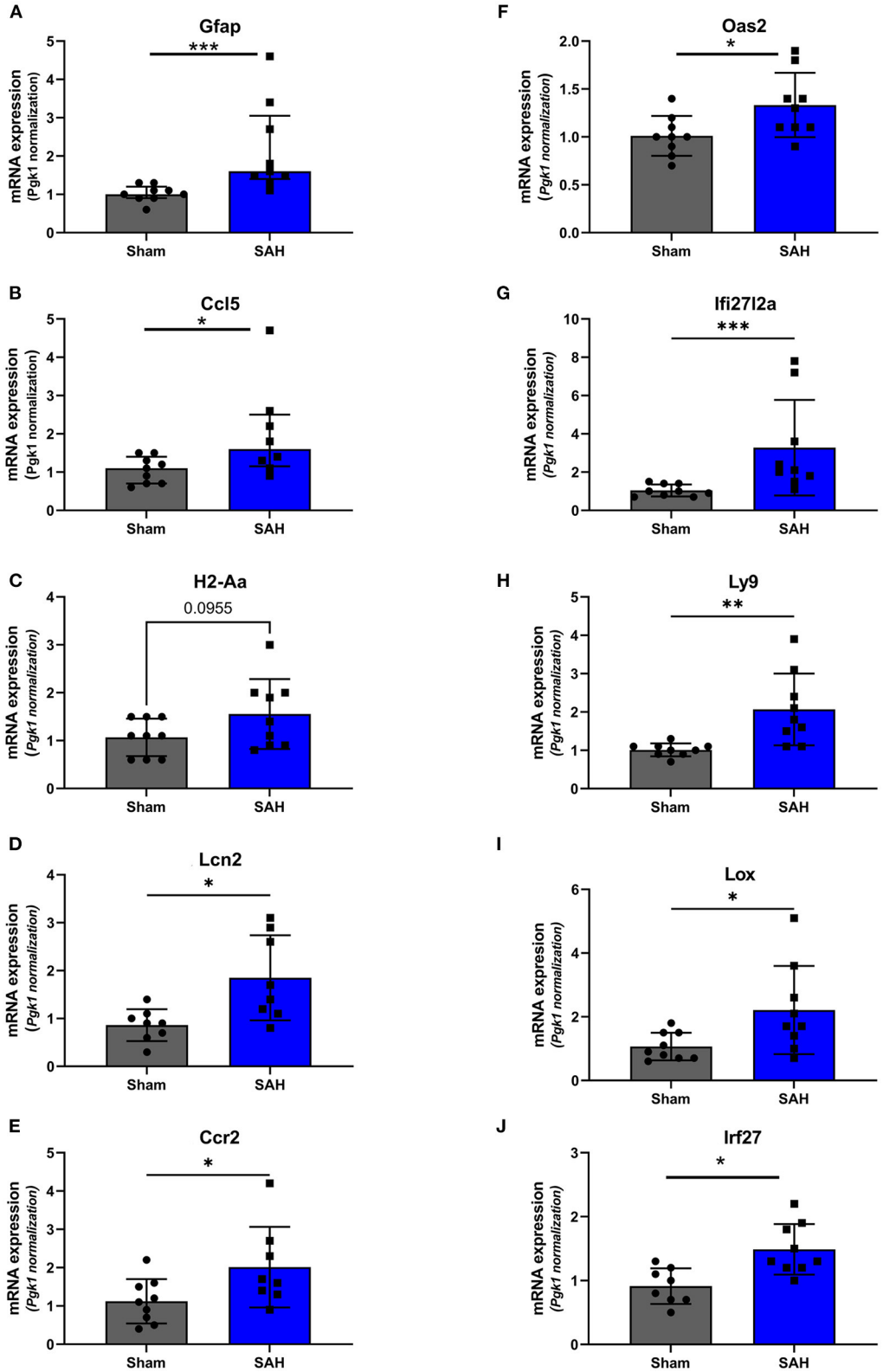

FIGURE 1 | Validation of the RNAseq findings by expression analysis of 10 overexpressed DEGs using Rt-qPCR at 4 days after SAH. Fold change, calculated by $2^{-\Delta\Delta Ct}V$, of mRNA expression of **(A)** GFAP: $U = 4$, $P = 0.0006$; **(B)** Ccl5: $U = 14.50$, $P = 0.0379$ **(C)**. H2-Aa: $t_{(16)} = 1.772$, $P = 0.0955$; **(D)** Lcn2: $t_{(14)} = 2.940$, $P = 0.0108$; **(E)** Ccr2: $t_{(15)} = 2.20$, $P = 0.0439$; **(F)** Oas2: $t_{(16)} = 2.247$, $P = 0.0264$; **(G)** Ifi27l2a: $U = 3.500$, $P = 0.0004$; **(H)** Ly9: $t_{(8.521)} = 3.327$, $P = 0.0095$; **(I)** Lox: $t_{(9.547)} = 2.364$, $P = 0.0408$; **(J)** Irf27: $t_{(15)} = 3.247$, $P = 0.0037$. $^*P < 0.05$; $^{**}P < 0.01$; $^{***}P < 0.0001$. $N = 18$, with $n = 9$ for SAH, $n = 9$ for Sham.

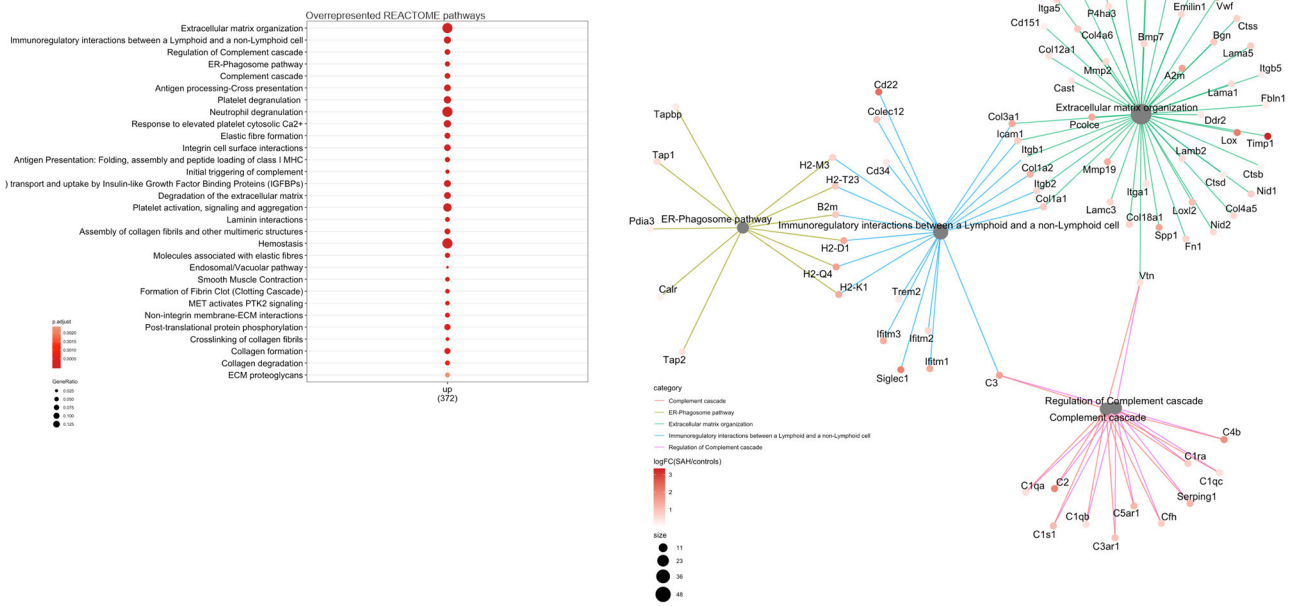

FIGURE 2 | Overrepresented REACTOME pathways 4 days after SAH. **(A)** Dot plot (gene ratio = genes related to a given GO term/total number of DEGs) of the overrepresented REACTOME pathways of all upregulated genes. Note the overrepresentation of immune response-related processes such as "*Extracellular matrix organization*," "*Immunoregulatory interactions between a Lymphoid and a non-Lymphoid cell*," and "*ER phagosome pathway.*" **(B)** Interconnected clusters of the five top overexpressed REACTOME pathways. Nodes represent individual genes belonging to a given gene set (or central node), and edges indicate which gene set it belongs to.

Ccl5, *Lcn2*, *Plin4*, *Timp1*, and *Gpr65* related to inflammation (**Figure 4**; **Table 1**).

The top five downregulated interacting clusters of GO-BP related to myelin ensheathment and oligodendrocyte activity (**Figure 3C**). Significantly decreased was the expression of genes specific to the myelin structure: *Pllp*, *Mbp*, *Mal*, *Mag*, *Cntnap1*, *Plp1*, *Mog*, and *Mobp* as well as the oligodendrocytes signature genes: *Olig1*, *Sox8*, *Sox10*, and *Nkx6.2* (**Supplementary Table 3**). Decreased levels of the mRNA of *Mog*, *Mag*, and *Rnf122*, oligodendrocytes-related genes by Rt-qPCR and decrease in MOG protein expression by Western blot (**Figures 5A,B**) confirmed the decrease of oligodendrocyte activity.

Immune Response

Over-expression of DEGs of GO-BP suggested activation of genes related to innate and adaptive immunity (**Figure 3A**). In addition, IPA and GSEA (**Supplementary Figures 3A,B**) processes demonstrated significant activation of the complement system with activation of the genes coding for the key elements of the complement system *C1*, *C2*, *C3*, *C4*, and *Cfb* and complement system regulators *Cfh* and *C1-inh* (*Serping1*) (**Supplementary Table 4**). Components of complement receptors CR3 (Cd11b+CD18) and CR4 (Cd11c+CD18), integrins alpha *Itga1*, *5* and integrins beta *Itgb1*, *2* (CD18), and *5* were also overexpressed. Expression of the gene comprising "membrane attack complex" (*C5-C9*) did not change significantly.

Increased expression of genes belonging to IPA canonical pathways "*Dendritic cell maturation*" and "*Th2 pathway*" suggested activation of adaptive immunity processes (**Supplementary Figure 3A**). These pathways share class I major histocompatibility complex (MHCI)-related genes, *H2-D1*, *H2-K1*, and *β2m* (**Supplementary Table 5**) with the "*Immunoregulatory interactions between a Lymphoid and a non-Lymphoid cell*" REACTOME (**Figures 2A,B**) along with "A*ntigen presentation*: *folding*, *assembly*, and *peptide loading of class I MHC*" pathways (**Figure 2A**). Genes associated with major histocompatibility II (MHCII) *Cd74*, *H2-Aa*, *H2-Ab1*, and *H2-Eb1* were also upregulated as well as the costimulatory molecule gene *CD86* (**Supplementary Table 6**). Chemokine genes involved in macrophage/monocyte recruitment *Ccl5* (4-$\log_2$-fold increase; **Figure 4**; **Table 1**), *Ccr2* (2.5-$\log_2$-fold increase; **Figure 4**; **Table 1**), and its murine ligand *Ccl12* as well as *Cxcl10* (**Supplementary Table 7**) were also increased. Toll-like receptors (*TLR*) *2* (0.91-$\log_2$-fold increase, $P < 0.01$), *8* (1.67-$\log_2$-fold increase, $P < 0.06$), and 13 (0.83-$\log_2$-fold increase, $P < 0.003$) did significantly increase 4 days after SAH.

Our data showed upregulation of microglial markers of M1-like pro-inflammatory phenotype, particularly microglial signature genes of phagocytotic processes *Calr*, *Itgb2*, *Cd68*,

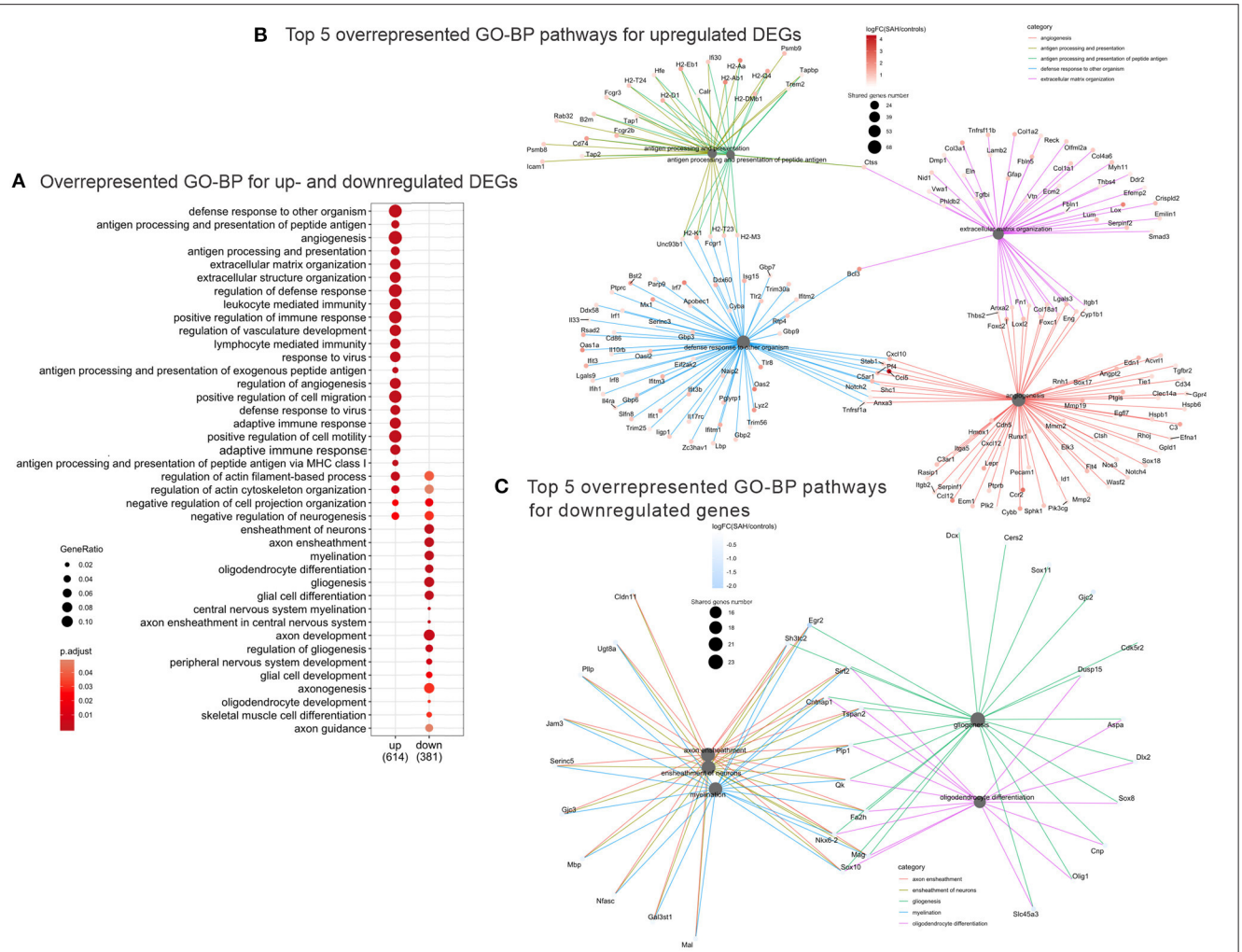

FIGURE 3 | Overrepresented GO Biological Processes 4 days after SAH. **(A)** Dotplot of the most enriched GO biological processes terms for up- and downregulated gene plot. Note that majority of overrepresented biological processes relate to immune response genes ("*immune response*," "*regulation of vasculature development*," "*response to virus*," "*adaptive immune response*," and "*lymphocyte mediated immunity*"), while the downregulated GO Biological Processes are myelin/axon/oligodendrocytes-related ("*axon ensheathment*," "*ensheathment of neurons*," "*myelination*," "*oligodendrocyte differentiation*," and "*gliogenesis*"). Color represents adjusted *p*-value or FDR, gene ratio = genes related to a given GO term/total number of DEGs. **(B)** Interconnected clusters of the five top overrepresented GO Biological Processes terms for upregulated genes. Nodes represent individual genes belonging to a given gene set (or central node), and edges indicate which gene set it belongs to. Gene number reflects number of downregulated genes in the central node. **(C)** Interconnected clusters of the five top overrepresented GO Biological Processes terms for downregulated genes. Nodes represent individual genes belonging to a given gene set (or central node), and edges indicate which gene set it belongs to. Color represents adjusted *p*-value or FDR. Gene number reflects number of downregulated genes in the central node.

Cxcl16, *Scara5*, and scavenging receptor gene *Scarf1*, along with IgG Fc receptors *Fcgr2b (CD32)*, *Fcgr4 (CD16)*, lectin *Lgals3*, and *Trem2* and its ligand *Tyrobp* (**Supplementary Table 8**). M2-like anti-inflammatory phenotype *Il14ra*, *Il13ra1*, and *Il10rb* and M0-resting-state microglia along with upregulation of the growth factors supporting damage repairment and tissue remodeling *Cxcl10*, *Igf1*, *Tgfbr2*, *Tgfbr3*, *Pdgfd*, and *Mmp2* (**Supplementary Table 8**) were also increased.

Upstream Regulators

IPA upstream regulator analysis (URA) showed activation of five top gene sets regulated by IFNG, IRF7, IRF3, STAT1, and CHUK (**Supplementary Table 9A**). Also, among significantly activated sets of genes were genes under upstream regulators TNF-α, IL1-β, TLR4, and IFNAR1. Supporting the involvement of type I and II interferons' pathways at 4 days after SAH were the overexpression of interferon-related DEGs *Irf7*, *Irf1*, and *Irf8* as well as upregulation of *Ifit1*, *Usp18*, *Isg15*, *Ifih1*, and *Unc93b1*(**Supplementary Table 10**) downstream of interferon regulatory genes.

The URA also identified TGFβ1 as a potential activated upstream regulator (**Supplementary Table 9A**). Supporting TGFβ pathway engagement 4 days after SAH are the overexpression of bone morphogenetic proteins *Bmp5*, *Bmp6*, and *Bmp7* in DEGs (**Supplementary Table 11**), *Smad6* and *Smad7*, inhibitory Smads in the TGFβ intracellular pathway, as

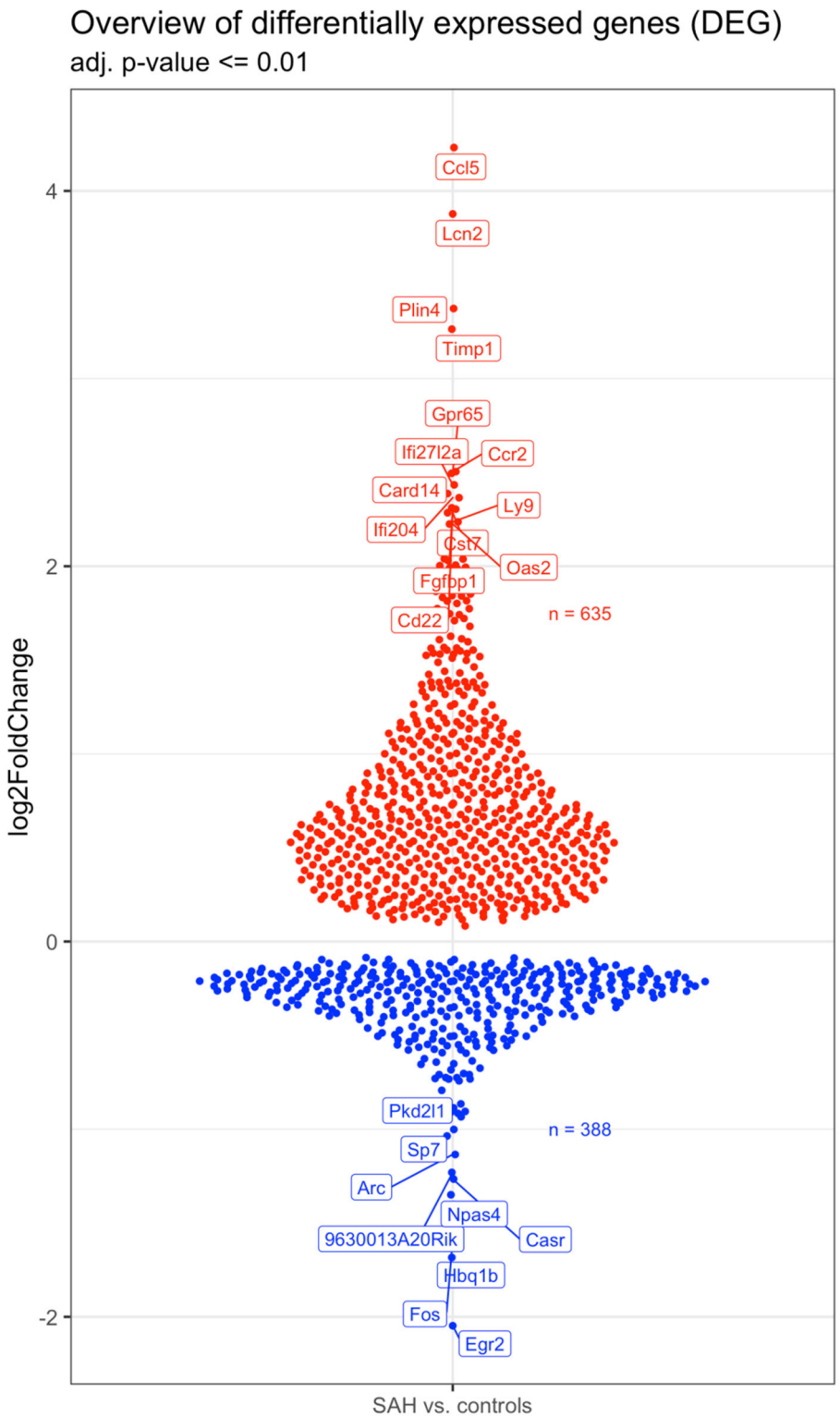

FIGURE 4 | Overview of the 642 upregulated (in red) and 398 downregulated (in blue) genes in the SAH vs. the control samples. The names of the topmost up- and downregulated genes are indicated. $N = 10$ with $n = 4$ for SAH, $n = 3$ for Sham, $n = 3$ for Naïve.

TABLE 1 | Top 10 upregulated genes potentially associated with different cellular types from single-cell transcriptomics studies.

Gene symbol	Gene name	Log_2-fold change	*padj* value	Cell origin (57)	Cell origin (58)
Ccl5	C-C motif chemokine 5	4.23	3.2×10^{-7}	Microglia	T cells, NK/NK T cells
Lcn2	Neutrophil gelatinase-associated lipocalin	3.87	0.004	Endothelial	Neutrophils
Plin4	Perilipin-4	3.37	0.005	NA	NA
Timp1	Metalloproteinase inhibitor 1	3.26	0.0003	Endothelial	NA
Ccr2	C-C Chemokine receptor type 2	2.50	0.002	Microglia, OPC	BAM, cDC, Monocytes, Tcells, and NK/NK T cells
Gpr65	Psychosine receptor	2.49	0.0003	Microglia	BAM, NK/NK T cells
Ifi27l2a	Interferon alpha-inducible protein 27-like protein2	2.43	5.5×10^{-9}	Microglia	BAM, cDC, B cells, Monocytes, and T cells
Card14	Caspase recruitment domain containing protein 14	2.38	0.007	NA	NA
Ifi204	Myeloid cell nuclear differentiation antigen	2.36	6.2×10^{-9}	Microglia	BAM, monocytes
Cd22	B-cell receptor	2.31	0.002	Microglia	T cells, NK/NK T cells

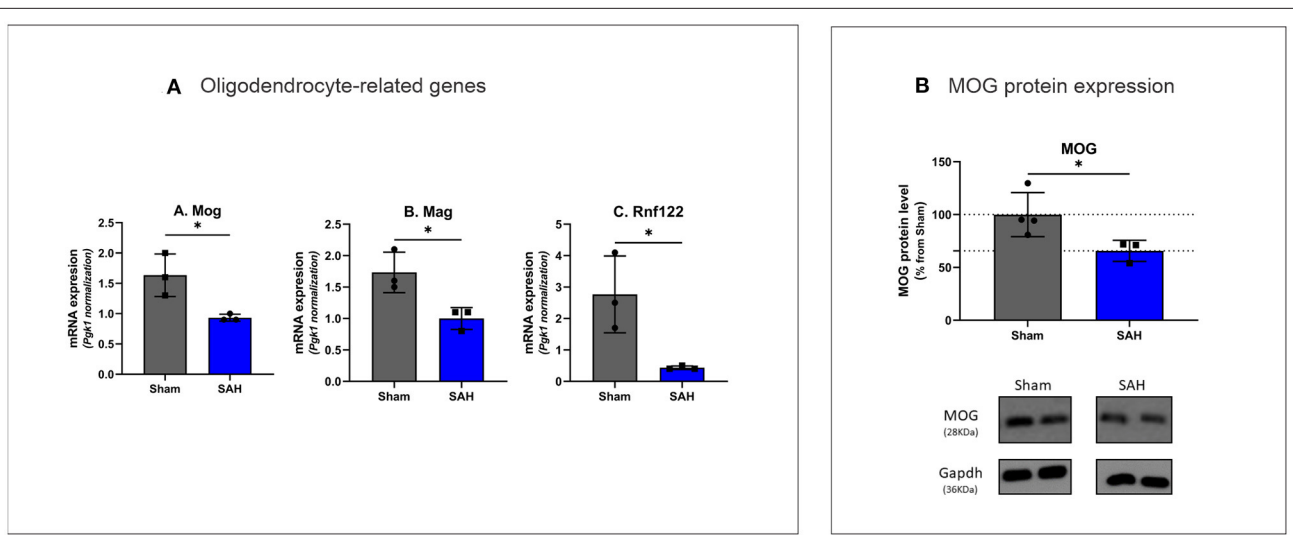

FIGURE 5 | (A) Rt-qPCR analysis of oligodendrocyte specific gene expression 4 days after SAH Mog: $t_{(4)} = 3.407$, $P = 0.0271$, Mag: $t_{(4)} = 3.479$, $P = 0.0254$, Rnf122: $t_{(4)} = 3.304$, $P = 0.0298$. *$P < 0.05$. $N = 18$, with $n = 9$ for SAH, $n = 9$ for Sham. **(B)** Western blot analysis of myelin oligodendrocyte glycoprotein with MOG protein expression decreased by 34.31% in SAH group $t_{(5)} = 2.590$, $P = 0.0488$. $N = 7$, with $n = 3$ for SAH, $n = 4$ for Sham.

well as *Smad3*. Also increased in DEGs were the TGFβ receptors *Tgfbr3* and *Tgfbr2* (**Supplementary Table 11**).

Motif Enrichment Analyses

Transcription factor binding motif prediction and enrichment analyses (AME, MEME-suite) confirmed URA identification of interferons as upstream regulators, showing enrichment of IRF7 binding motifs and enrichment of STAT1/STAT2 along with binding motif of SPIB (Spi-B Transcription Factor) (**Supplementary Figure 4A**).

Analysis of enriched motifs independently of their location within the promoter (CENTRIMO, MEME-suite) suggested enrichment of binding sites for the moderately expressed Krüppel-like factor 3 (KLF3) and SP1 transcription factors (**Supplementary Figures 3B,C**).

DISCUSSION

In the present study, we observed overexpression of genes related to an immune/neuroinflammatory response in the mouse hippocampus 4 days after SAH. Functional and master regulator's analysis evidenced for an overexpression of genes related to *an innate and adaptive immune response* with possible involvement of blood-resident cells as well as parenchymal reorganization in the hippocampus at 4 days.

These observations are in line with what has been described in the pathophysiology of stroke as a biphasic mechanism, which has become clear over the years of research (9, 59), with the damaged brain exhibiting an initial detrimental response following the acute injury, and regenerative processes during the recovery phase. However, the present study shed light on the

leading pathways and specific gene expression occurring in the hippocampus remotely from the site of the infarct, the entorhinal cortex. We discuss further potential use of this newly found druggable targets and potential drug repurposing.

There are some limitations of the study. First is the limited number of animals, which may affect to some degree the significance of the gene expression changes. We used cutoff for DEGs of 0.1, which left out a large number of genes demonstrating sizable increase in expression. Second, the only time point, 4 days, chosen because this is the point when SAH-induced delayed cerebral ischemia (DCI) starts to occur (23, 24). These events have not been well characterized and need further investigations. Additional time points, e.g., 24 h and 30 days, would be useful to understand the dynamics of ongoing processes.

Specifically, we unveiled involvement of the complement in SAH 4 days after the infarct. Genes related to the classical and alternative pathways of the complement system (60) were significantly overexpressed (**Supplementary Table 4**). These observations are in line with a growing body of evidence demonstrating the importance of the complement activation in neuroinflammation, synaptic pruning, crucial for the establishment of healthy neuronal connections, in neural development and aging (60). Opsonized elements undergo phagocytosis, as reflected in the increased expression of endoplasmic reticulum phagosome pathway and overexpression of signature genes of phagocytosis *Calr*, *Itgb2*, *Cd68*, *Cxcl16*, and *Scara5* (61), currently found in this study. C1 binding initiates classic pathway of complement system activation leading to generation of complement-related opsonins. However, we did not observe increase in lectin pathway genes, nor did we find significant change in the "membrane attack complex," excluding the complement role in the cell death at least 4 days post-injury. Complement-targeted drugs benefit from intense investigation for neurological diseases and could be potentially used for SAH patients' survivors (62, 63).

We detected overexpression of genes related to monocytes-derived macrophages infiltrating the brain parenchyma following CNS injury and acquiring macrophages phenotype (64). *CCL5* was the highest upregulated gene in this study. CSF levels of its coded protein, chemokine C-C motif ligand 5, was identified as possible predictor of SAH outcome severity (65). CCL5 can be synthesized by astrocytes, microglia, and oligodendrocytes and often associated with major fiber tracts (66). CCL5 attracts T-cells and monocytes/macrophages (67). *CCR2* was also among the top upregulated genes (**Table 1**; **Figure 4**). Monocytes with a high expression of CCR2 are reported to enter the brain after transection of the perforant pathway, while lack of CCR2 prevented the entry of macrophages and T cells into the brain parenchyma (68). We also showed an increase in MHCII related genes, which is known to be involved in the crosstalk between microglia/macrophages and T cells (69). Invasion of the brain parenchyma of blood-resident cells has been extensively shown in stroke (70), but little to no evidence was shown after SAH. Our results indicate that immuno-therapy targeting myeloid cells could be employed in the treatment of SAH (71).

We observed a decrease of genes expression related to axons, myelin, and myelin formation as well as decrease in oligodendrocytes-related genes, which suggest a demyelinating process (**Figure 3C**; **Supplementary Table 3**). This process could be mediated by increased expression of *Bmp* and semaphorin genes, which are known to suppress myelination and oligodendrocyte differentiation (72). It was also reported that *Lcn2*, our second top overexpressed gene preferentially localized to the white matter, is activated after SAH and plays an important role in damaging oligodendrocytes (73). Silencing or blocking *Lcn2* could protect oligodendrocytes viability and engage in a faster remyelination process (74).

The gene expression profile of microglia-related genes presented here is comparable to demyelination/remyelination processes at the end of 6 weeks in cuprizone multiple sclerosis model (61) with M1, M2, and M0 signature genes (**Supplementary Table 8**). Myelin clearance following axonal damage is crucial as the presence of myelin debris inhibits the processes of regeneration and repair (75). Expression of *TREM2* and its ligand *Tyrobp* were significantly increased in the present study. TREM2 has been shown to play a significant role in Alzheimer's disease (76). TREM2 microglial receptor is critical for efficient removal of myelin debris after cuprizone-triggered demyelination (77), and other genes related to phagocytosis, such as *Fcγ R3*, *CD68*, and *Lamp2*, were also significantly overexpressed (**Supplementary Table 12**) (78). Modulation of TREM-2 could accelerate myelin debris clearance and promotes repair (79, 80).

Mutually promoting relations between vessels and axon growth are known (81): blood vessels guide developing axons by secretory factors (82) and form a migratory scaffold for neuroblast in post-stroke area (83). Pleiotropic TGFβ/BMP pathways, identified by URA, can exert a dual pro- and anti-inflammatory action on the CNS (84) and may participate in the regenerative processes such as scar formation and angiogenesis (85). Our functional analysis detected an overrepresentation of the GSEA pathways "*Epithelial_Mesenchymal_Transition*" and "*Angiogenesis*" pathways (**Supplementary Figure 3B**), as well as GO-BP terms "*angiogenesis*" and "*extracellular matrix and structure organization*" (**Figure 3A**). These data suggest that the relation between EC-OPCs and role of TGFβ superfamily deserves more investigation after SAH.

IPA URA and findings of the enrichment of DNA binding motif suggested activation of interferon-pathway related genes (**Supplementary Table 9A**). These results were supported by the GSEA analysis that detected an enrichment in the "*interferon-γ response*" and "*interferon-α response*" gene-sets (**Supplementary Figure 3B**). It is known that activation of TLRs regulates immune response through MyD88 or TRIF pathways and leads to activation of interferon regulated transcription factors (IRF) (86). *TLR* 2, 8, and 13 were among overexpressed DEGs, which serve as a pattern recognition receptor and co-regulate antigen processing and presentation (87). TLR 2, located on the cell surface, preferentially binds lipid-containing damage associated molecular patterns (DAMP) and shares intracellular pathways with TLR4. TLR8 and TLR13 are intracellular receptors located in the endosomes and are specific for double-stranded

and single-stranded nucleic acid detection (87). In our study, *Irf7*, *Irf1*, and *Irf8* were significantly overexpressed along with activation of 35 out of 36 genes comprising IRF3 regulated group, including overexpression of interferon-α inducible protein 27 gene (*Ifi27l2a*) (**Figure 1**). *Irf7* increased by 2.1-$\log_2$-fold in our DEGs, and our common motif analysis demonstrated its significant presence among our set of DEGs. Irf7 is regulated in a cell-type-dependent manner and is required for a maximal type I IFN-α gene response (88). Irf8 was shown to be an important factor during the recovery phase following spinal cord injury (89). Type I IFN-α and II (IFN-γ) gene responses have been repeatedly shown to be important for brain repair and maintenance (90). IFN-γ is a critical regulator of blood cell entry in the brain at the choroid plexus entry point (90).

Our motif enrichment analysis supported the involvement of adaptive immunity cells and the regeneration process with SPIB (Spi-B Transcription Factor), which plays a critical role in regulation of dendritic cell and B cell development and antigenic stimulation (91). Also enriched was binding motif of FOXO3, which participates in controlling of expression of autophagy related genes (92). KLF3 is a known regulator of B cells (93), and SP1 plays a role in regeneration gene expression (40).

The present transcriptome analysis of the processes in the hippocampal tissue 4 days after SAH suggests the development of an inflammation in the hippocampus remote from the entorhinal cortex. Data suggest that direct application of blood to the brain surface damages neurons of the entorhinal cortex, leading to the damage of the perforant pathway, main projections to the hippocampus (14, 15), and to the hippocampus itself (16–18). This initial event would lead to the gene expression we described and expression of the specific genes involved. Further experimental explorations of the results highlighted here will allow identification of new therapeutic targets to alleviate long-term consequences of SAH.

DATA AVAILABILITY STATEMENT

The datasets presented in this study can be found in online repositories. The names of the repository/repositories and accession number(s) can be found at: https://www.ncbi.nlm.nih.gov/geo/ (GSE167110); https://github.com/abcwcm/Regnier-Golanov2021 (Regnier-Golanov2021).

ETHICS STATEMENT

The animal study was reviewed and approved by Institutional Animal Care and Use Committee of Houston Methodist Research Institute, Houston, TX.

AUTHOR CONTRIBUTIONS

AR-G and EG conceived and designed experiments, acquired, analyzed, interpreted data, and wrote the manuscript. MH, FD, PZ, DB, and LP analyzed and interpreted data and edited the manuscript. EL interpreted data and drafted and critically revised the manuscript. GB conceived the experiments, analyzed data, and drafted and critically revised the manuscript. All authors contributed to the article and approved the submitted version.

FUNDING

This research was funded by the HMH Neurosurgery department and a grant from the Houston Methodist Foundation. The authors also declare that this study received funding from MLN Company. The funder was not involved in the study design, collection, analysis, interpretation of data, the writing of this article or the decision to submit it for publication.

ACKNOWLEDGMENTS

This paper has been published as a pre-print on Research Gate [Regnier-Golanov AS, (94)].

SUPPLEMENTARY MATERIAL

The Supplementary Material for this article can be found online at: https://www.frontiersin.org/articles/10.3389/fneur.2021.691631/full#supplementary-material

REFERENCES

1. Sacco RL, Kasner SE, Broderick JP, Caplan LR, Connors JJ, Culebras A, et al. An updated definition of stroke for the 21st century: a statement for healthcare professionals from the American Heart Association/American Stroke Association. *Stroke.* (2013) 44:2064–89. doi: 10.1161/STR.0b013e318296aeca
2. van Gijn J, Kerr RS, Rinkel GJ. Subarachnoid haemorrhage. *Lancet.* (2007) 369:306–18. doi: 10.1016/S0140-6736(07)60153-6
3. Macdonald RL, Schweizer TA. Spontaneous subarachnoid haemorrhage. *Lancet.* (2017) 389:655–66. doi: 10.1016/S0140-6736(16)30668-7
4. Terpolilli NA, Brem C, Buhler D, Plesnila N. Are we barking up the wrong vessels? Cerebral microcirculation after subarachnoid hemorrhage. *Stroke.* (2015) 46:3014–9. doi: 10.1161/STROKEAHA.115.006353
5. Haug Nordenmark T, Karic T, Roe C, Sorteberg W, Sorteberg A. The post-aSAH syndrome: a self-reported cluster of symptoms in patients with aneurysmal subarachnoid hemorrhage. *J Neurosurg.* (2019) 132:1556–65. doi: 10.3171/2019.1.JNS183168
6. Leon-Carrion J, Dominguez-Morales Mdel R, Barroso y Martin JM, Murillo-Cabezas F. Epidemiology of traumatic brain injury and subarachnoid hemorrhage. *Pituitary.* (2005) 8:197–202. doi: 10.1007/s11102-006-6041-5
7. Rinkel GJ, Algra A. Long-term outcomes of patients with aneurysmal subarachnoid haemorrhage. *Lancet Neurol.* (2011) 10:349–56. doi: 10.1016/S1474-4422(11)70017-5
8. Connolly, E. S. Jr., Rabinstein AA, Carhuapoma JR, Derdeyn CP, Dion J, et al. Guidelines for the management of aneurysmal subarachnoid hemorrhage: a guideline for healthcare professionals from the American Heart Association/american Stroke Association. *Stroke.* (2012) 43:1711–37. doi: 10.1161/STR.0b013e3182587839
9. Al-Khindi T, Macdonald RL, Schweizer TA. Cognitive and functional outcome after aneurysmal subarachnoid hemorrhage. *Stroke.* (2010) 41:e519–36. doi: 10.1161/STROKEAHA.110.581975
10. Bendel P, Koivisto T, Aikia M, Niskanen E, Kononen M, Hanninen T, et al. Atrophic enlargement of CSF volume after subarachnoid hemorrhage: correlation with neuropsychological outcome. *AJNR Am J Neuroradiol.* (2010) 31:370–6. doi: 10.3174/ajnr.A1804

11. Moscovitch M, Cabeza R, Winocur G, Nadel L. Episodic memory and beyond: the hippocampus and neocortex in transformation. *Annu Rev Psychol.* (2016) 67:105–34. doi: 10.1146/annurev-psych-113011-143733
12. Yoshimoto T, Kayama T, Kodama N, Suzuki J. Distribution of intracranial aneurysm. *Tohoku J Exp Med.* (1978) 126:125–32. doi: 10.1620/tjem.126.125
13. Aarhus M, Helland CA, Wester K. Differences in anatomical distribution, gender, and sidedness between ruptured and unruptured intracranial aneurysms in a defined patient population. *Acta Neurochir (Wien).* (2009) 151:1569–74. doi: 10.1007/s00701-009-0316-3
14. Amaral, D, and Lavenex, P. Hippocampal neuroanatomy. In: Andersen P. Morris R, Amaral D, Bliss T, O'Keefe J, editors. *The Hippocampus Book*. New York, NY: Oxford University Press. (2007). p. 37–131.
15. van Strien NM, Cappaert NL, Witter MP. The anatomy of memory: an interactive overview of the parahippocampal-hippocampal network. *Nat Rev Neurosci.* (2009) 10:272–82. doi: 10.1038/nrn2614
16. Kovac AD, Kwidzinski E, Heimrich B, Bittigau P, Deller T, Nitsch R, et al. Entorhinal cortex lesion in the mouse induces transsynaptic death of perforant path target neurons. *Brain Pathol.* (2004) 14:249–57. doi: 10.1111/j.1750-3639.2004.tb00061.x
17. Vuksic M, Del Turco D, Vlachos A, Schuldt G, Muller CM, Schneider G, et al. Unilateral entorhinal denervation leads to long-lasting dendritic alterations of mouse hippocampal granule cells. *Exp Neurol.* (2011) 230:176–85. doi: 10.1016/j.expneurol.2011.04.011
18. Simard JM, Tosun C, Ivanova S, Kurland DB, Hong C, Radecki L, et al. Heparin reduces neuroinflammation and transsynaptic neuronal apoptosis in a model of subarachnoid hemorrhage. *Transl Stroke Res.* (2012) 3(Suppl 1):155–65. doi: 10.1007/s12975-012-0166-9
19. Matz PG, Fujimura M, Chan PH. Subarachnoid hemolysate produces DNA fragmentation in a pattern similar to apoptosis in mouse brain. *Brain Res.* (2000) 858:312–9. doi: 10.1016/S0006-8993(99)02454-3
20. Wang X, Mori T, Sumii T, Lo EH. Hemoglobin-induced cytotoxicity in rat cerebral cortical neurons: caspase activation and oxidative stress. *Stroke.* (2002) 33:1882–8. doi: 10.1161/01.STR.0000020121.41527.5D
21. Fujii M, Yan JH, Rolland WB, Soejima Y, Caner B, Zhang JH. Early brain injury, an evolving frontier in subarachnoid hemorrhage research. *Transl Stroke Res.* (2013) 4:432–46. doi: 10.1007/s12975-013-0257-2
22. Sabri M, Lass E, Macdonald RL. Early brain injury: a common mechanism in subarachnoid hemorrhage and global cerebral ischemia. *Stroke Res Treat.* (2013) 2013:394036. doi: 10.1155/2013/394036
23. Anzabi M, Ardalan M, Iversen NK, Rafati AH, Hansen B, Østergaard L. Hippocampal atrophy following subarachnoid hemorrhage correlates with disruption of astrocyte morphology and capillary coverage by AQP4. *Front Cell Neurosci.* (2018) 12:19. doi: 10.3389/fncel.2018.00019
24. van Lieshout JH, Marbacher S, Muhammad S, Boogaarts HD, Bartels RHMA, Dibué M, et al. Proposed definition of experimental secondary ischemia for mouse subarachnoid hemorrhage. *Transl Stroke Res.* (2020) 11:1165–70. doi: 10.1007/s12975-020-00796-y
25. Lo EH. A new penumbra: transitioning from injury into repair after stroke. *Nat Med.* (2008) 14:497–500. doi: 10.1038/nm1735
26. Lo EH. Degeneration and repair in central nervous system disease. *Nat Med.* (2010) 16:1205–9. doi: 10.1038/nm.2226
27. Iyer A, Tole S. Neuronal diversity and reciprocal connectivity between the vertebrate hippocampus and septum. *Wiley Interdiscip Rev Dev Biol.* (2020) 9:e370. doi: 10.1002/wdev.370
28. van den Brink SC, Sage F, Vertesy A, Spanjaard B, Peterson-Maduro J, Baron CS, et al. Single-cell sequencing reveals dissociation-induced gene expression in tissue subpopulations. *Nat Methods.* (2017) 14:935–6. doi: 10.1038/nmeth.4437
29. Regnier-Golanov AS, Dündar F, Zumbo P, Betel D, Hernandez MS, Peterson LE, et al. *Hippocampal Transcriptome Changes after Subarachnoid Hemorrhage in Mice.* (2021).
30. Golanov EV, Bovshik EI, Wong KK, Pautler RG, Foster CH, Federley RG, et al. Subarachnoid hemorrhage - Induced block of cerebrospinal fluid flow: role of brain coagulation factor III (tissue factor). *J Cereb Blood Flow Metab.* (2018) 38:793–808. doi: 10.1177/0271678X17701157
31. Garcia JH, Wagner S, Liu KF, Hu XJ. Neurological deficit and extent of neuronal necrosis attributable to middle cerebral artery occlusion in rats. Statistical validation. *Stroke.* (1995) 26:627–34; discussion 635. doi: 10.1161/01.STR.26.4.627
32. ENCODE Consortium. *Standards, Guidelines and Best Practices for RNA-Seq.* (2011). Available online at: https://genome.ucsc.edu/ENCODE/protocols/dataStandards/ENCODE_RNAseq_Standards_V1.0.pdf (accessed October 17, 2017).
33. Andrews S. *FastQC: A Quality Control Tool for High Throughput Sequence Data.* (2010). Available online at: http://www.bioinformatics.babraham.ac.uk/projects/fastqc (accessed January 04, 2019).
34. Hartley SW, Mullikin JC. QoRTs: a comprehensive toolset for quality control and data processing of RNA-Seq experiments. *BMC Bioinform.* (2015) 16:224. doi: 10.1186/s12859-015-0670-5
35. Dobin A, Davis CA, Schlesinger F, Drenkow J, Zaleski C, Jha S, et al. STAR: ultrafast universal RNA-seq aligner. *Bioinformatics.* (2013) 29:15–21. doi: 10.1093/bioinformatics/bts635
36. Harrow J, Frankish A, Gonzalez JM, Tapanari E, Diekhans M, Kokocinski F, et al. GENCODE: the reference human genome annotation for The ENCODE Project. *Genome Res.* (2012) 22:1760–74. doi: 10.1101/gr.135350.111
37. Liao Y, Smyth GK, Shi W. featureCounts: an efficient general purpose program for assigning sequence reads to genomic features. *Bioinformatics.* (2014) 30:923–30. doi: 10.1093/bioinformatics/btt656
38. Anders S, Huber W. Differential expression analysis for sequence count data. *Genome Biol.* (2010) 11:R106. doi: 10.1186/gb-2010-11-10-r106
39. Yu G, Wang LG, Han Y, He QY. clusterProfiler: an R package for comparing biological themes among gene clusters. *OMICS.* (2012) 16:284–7. doi: 10.1089/omi.2011.0118
40. Miras-Portugal MT, Gomez-Villafuertes R, Gualix J, Diaz-Hernandez JI, Artalejo AR, Ortega F, et al. Nucleotides in neuroregeneration and neuroprotection. *Neuropharmacology.* (2016) 104:243–54. doi: 10.1016/j.neuropharm.2015.09.002
41. Gene Ontology Consortium. *The Gene Ontology Resource.* (1999). Available online at: http://geneontology.org (accessed April 1, 2019).
42. Reactome. *Reactions, Proteins and Pathways.* (2003). Available online at: https://reactome.org (accessed April 1, 2019).
43. Subramanian A, Tamayo P, Mootha VK, Mukherjee S, Ebert BL, Gillette MA, et al. Gene set enrichment analysis: a knowledge-based approach for interpreting genome-wide expression profiles. *Proc Natl Acad Sci U S A.* (2005) 102:15545–50. doi: 10.1073/pnas.0506580102
44. Liberzon A, Birger C, Thorvaldsdottir H, Ghandi M, Mesirov JP, Tamayo P. The Molecular Signatures Database (MSigDB) hallmark gene set collection. *Cell Syst.* (2015) 1:417–25. doi: 10.1016/j.cels.2015.12.004
45. Kramer A, Green J, Pollard JJr, Tugendreich S. Causal analysis approaches in Ingenuity Pathway Analysis. *Bioinformatics.* (2014) 30:523–30. doi: 10.1093/bioinformatics/btt703
46. Heinz S, Benner C, Spann N, Bertolino E, Lin YC, Laslo P, et al. Simple combinations of lineage-determining transcription factors prime cis-regulatory elements required for macrophage and B cell identities. *Mol Cell.* (2010) 38:576–89. doi: 10.1016/j.molcel.2010.05.004
47. Bailey TL. DREME: motif discovery in transcription factor ChIP-seq data. *Bioinformatics.* (2011) 27:1653–9. doi: 10.1093/bioinformatics/btr261
48. Bailey TL, Boden M, Buske FA, Frith M, Grant CE, Clementi L, et al. MEME Suite: tools for motif discovery and searching. *Nucleic Acids Res.* (2009) 37:W202–W8. doi: 10.1093/nar/gkp335
49. Bailey TL, Machanick P. Inferring direct DNA binding from ChIP-seq. *Nucleic Acids Res.* (2012) 40:e128. doi: 10.1093/nar/gks433
50. Lesluyes T, Johnson J, Machanick P, Bailey TL. Differential motif enrichment analysis of paired ChIP-seq experiments. *BMC Genomics.* (2014) 15:752. doi: 10.1186/1471-2164-15-752
51. McLeay RC, Bailey TL. Motif Enrichment Analysis: a unified framework and an evaluation on ChIP data. *BMC Bioinform.* (2010) 11:165. doi: 10.1186/1471-2105-11-165
52. Machanick P, Bailey TL. MEME-ChIP: motif analysis of large DNA datasets. *Bioinformatics.* (2011) 27:1696–7. doi: 10.1093/bioinformatics/btr189
53. NCBI. *Primer-BLAST.* (1988). Available online at: https://www.ncbi.nlm.nih.gov/tools/primer-blast/index.cgi (accessed June 19, 21019).
54. Panina Y, Germond A, Masui S, Watanabe TM. Validation of common housekeeping genes as reference for qPCR gene expression analysis during iPS reprogramming process. *Sci Rep.* (2018) 8:8716. doi: 10.1038/s41598-018-26707-8
55. Yuan JS, Reed A, Chen F, Stewart CNJr. Statistical analysis of real-time PCR data. *BMC Bioinform.* (2006) 7:85. doi: 10.1186/1471-2105-7-85

56. Miller L. *Analyzing Gels and Western Blots With ImageJ*. (2010). Available online at: http://lukemiller.org/index.php/2010/11/analyzing-gels-and-western-blots-with-image-j/ (accessed October 15, 2020).
57. Zhang Y, Chen K, Sloan SA, Bennett ML, Scholze AR, O'Keeffe S, et al. An RNA-sequencing transcriptome and splicing database of glia, neurons, and vascular cells of the cerebral cortex. *J Neurosci.* (2014) 34:11929–47. doi: 10.1523/JNEUROSCI.1860-14.2014
58. Van Hove H, Martens L, Scheyltjens I, De Vlaminck K, Pombo Antunes AR, De Prijck S, et al. A single-cell atlas of mouse brain macrophages reveals unique transcriptional identities shaped by ontogeny and tissue environment. *Nat Neurosci.* (2019) 22:1021–35. doi: 10.1038/s41593-019-0393-4
59. Guo X, Wang XF. Signaling cross-talk between TGF-beta/BMP and other pathways. *Cell Res.* (2009) 19:71–88. doi: 10.1038/cr.2008.302
60. Coulthard LG, Hawksworth OA, Woodruff TM. Complement: the emerging architect of the developing brain. *Trends Neurosci.* (2018) 41:373–84. doi: 10.1016/j.tins.2018.03.009
61. Olah M, Amor S, Brouwer N, Vinet J, Eggen B, Biber K, et al. Identification of a microglia phenotype supportive of remyelination. *Glia.* (2012) 60:306–21. doi: 10.1002/glia.21266
62. Ricklin D, Hajishengallis G, Yang K, Lambris JD. Complement: a key system for immune surveillance and homeostasis. *Nat Immunol.* (2010) 11:785–97. doi: 10.1038/ni.1923
63. Kim BJ, Mastellos DC, Li Y, Dunaief JL, Lambris JD. Targeting complement components C3 and C5 for the retina: Key concepts and lingering questions. *Prog Retin Eye Res*. (2020) 100936. doi: 10.1016/j.preteyeres.2020.100936. [Epub ahead of print].
64. Shechter R, London A, Varol C, Raposo C, Cusimano M, Yovel G, et al. Infiltrating blood-derived macrophages are vital cells playing an anti-inflammatory role in recovery from spinal cord injury in mice. *PLoS Med.* (2009) 6:e1000113. doi: 10.1371/journal.pmed.1000113
65. Chaudhry SR, Kinfe TM, Lamprecht A, Niemela M, Dobreva G, Hanggi D, et al. Elevated level of cerebrospinal fluid and systemic chemokine CCL5 is a predictive biomarker of clinical outcome after aneurysmal subarachnoid hemorrhage (aSAH). *Cytokine.* (2020) 133:155142. doi: 10.1016/j.cyto.2020.155142
66. Farina C, Aloisi F, Meinl E. Astrocytes are active players in cerebral innate immunity. *Trends Immunol.* (2007) 28:138–45. doi: 10.1016/j.it.2007.01.005
67. Mack M, Cihak J, Simonis C, Luckow B, Proudfoot AE, Plachy J, et al. Expression and characterization of the chemokine receptors CCR2 and CCR5 in mice. *J Immunol.* (2001) 166:4697–704. doi: 10.4049/jimmunol.166.7.4697
68. Babcock AA, Kuziel WA, Rivest S, Owens T. Chemokine expression by glial cells directs leukocytes to sites of axonal injury in the CNS. *J Neurosci.* (2003) 23:7922–30. doi: 10.1523/JNEUROSCI.23-21-07922.2003
69. Carson MJ. Microglia as liaisons between the immune and central nervous systems: functional implications for multiple sclerosis. *Glia.* (2002) 40:218–31. doi: 10.1002/glia.10145
70. Garcia-Culebras A, Duran-Laforet V, Pena-Martinez C, Ballesteros I, Pradillo JM, Diaz-Guzman J, et al. Myeloid cells as therapeutic targets in neuroinflammation after stroke: Specific roles of neutrophils and neutrophil-platelet interactions. *J Cereb Blood Flow Metab.* (2018) 38:2150–64. doi: 10.1177/0271678X18795789
71. Schwartz M, Arad M, Ben-Yehuda H. Potential immunotherapy for Alzheimer disease and age-related dementia. *Dialogues Clin Neurosci.* (2019) 21:21–5. doi: 10.31887/DNC.2019.21.1/mschwartz
72. Grinspan JB. Bone Morphogenetic Proteins: Inhibitors of myelination in development and disease. *Vitam Horm.* (2015) 99:195–222. doi: 10.1016/bs.vh.2015.05.005
73. Egashira Y, Hua Y, Keep RF, Iwama T, Xi G. Lipocalin 2 and blood-brain barrier disruption in white matter after experimental subarachnoid hemorrhage. *Acta Neurochir Suppl.* (2016) 121:131–4. doi: 10.1007/978-3-319-18497-5_23
74. Kumfu S, Siri-Angkul N, Chattipakorn SC, Chattipakorn N. Silencing of lipocalin-2 improves cardiomyocyte viability under iron overload conditions *via* decreasing mitochondrial dysfunction and apoptosis. *J Cell Physiol.* (2020) 236:5108–20. doi: 10.1002/jcp.30219
75. Egawa N, Lok J, Washida K, Arai K. Mechanisms of axonal damage and repair after central nervous system injury. *Transl Stroke Res.* (2017) 8:14–21. doi: 10.1007/s,12975-016-0495-1
76. Krasemann S, Madore C, Cialic R, Baufeld C, Calcagno N, El Fatimy R, et al. The TREM2-APOE pathway drives the transcriptional phenotype of dysfunctional microglia in neurodegenerative diseases. *Immunity.* (2017) 47:566–81.e569. doi: 10.1016/j.immuni.2017.08.008
77. Poliani PL, Wang Y, Fontana E, Robinette ML, Yamanishi Y, Gilfillan S, et al. TREM2 sustains microglial expansion during aging and response to demyelination. *J Clin Invest.* (2015) 125:2161–70. doi: 10.1172/JCI77983
78. Kocur M, Schneider R, Pulm AK, Bauer J, Kropp S, Gliem M, et al. IFNbeta secreted by microglia mediates clearance of myelin debris in CNS autoimmunity. *Acta Neuropathol Commun.* (2015) 3:20. doi: 10.1186/s40478-015-0192-4
79. Cignarella F, Filipello F, Bollman B, Cantoni C, Locca A, Mikesell R, et al. TREM2 activation on microglia promotes myelin debris clearance and remyelination in a model of multiple sclerosis. *Acta Neuropathol.* (2020) 140:513–34. doi: 10.1007/s00401-020-02193-z
80. Griciuc A, Tanzi RE. The role of innate immune genes in Alzheimer's disease. *Curr Opin Neurol.* (2021) 34:228–36. doi: 10.1097/WCO.0000000000000911
81. Carmeliet P, Tessier-Lavigne M. Common mechanisms of nerve and blood vessel wiring. *Nature.* (2005) 436:193–200. doi: 10.1038/nature03875
82. Makita T, Sucov HM, Gariepy CE, Yanagisawa M, Ginty DD. Endothelins are vascular-derived axonal guidance cues for developing sympathetic neurons. *Nature.* (2008) 452:759–63. doi: 10.1038/nature06859
83. Grade S, Weng YC, Snapyan M, Kriz J, Malva JO, Saghatelyan A. Brain-derived neurotrophic factor promotes vasculature-associated migration of neuronal precursors toward the ischemic striatum. *PLoS One.* (2013) 8:e55039. doi: 10.1371/journal.pone.0055039
84. Kim BH, Levison SW. TGFbeta1: Friend or foe during recovery in encephalopathy. *Neuroscientist.* (2019) 25:192–198. doi: 10.1177/1073858418793131
85. Diniz LP, Matias I, Siqueira M, Stipursky J, Gomes FCA. Astrocytes and the TGF-beta1 pathway in the healthy and diseased brain: a double-edged sword. *Mol Neurobiol.* (2019) 56:4653–79. doi: 10.1007/s12035-018-1396-y
86. Kumar V. Toll-like receptors in the pathogenesis of neuroinflammation. *J Neuroimmunol.* (2019) 332:16–30. doi: 10.1016/j.jneuroim.2019.03.012
87. Vijay K. Toll-like receptors in immunity and inflammatory diseases: past, present, and future. *Int Immunopharmacol.* (2018) 59:391–412. doi: 10.1016/j.intimp.2018.03.002
88. Marie I, Durbin JE, Levy DE. Differential viral induction of distinct interferon-alpha genes by positive feedback through interferon regulatory factor-7. *EMBO J.* (1998) 17:6660–9. doi: 10.1093/emboj/17.22.6660
89. Kobayakawa K, Ohkawa Y, Yoshizaki S, Tamaru T, Saito T, Kijima K, et al. Macrophage centripetal migration drives spontaneous healing process after spinal cord injury. *Sci Adv*. (2019) *5:* eaav5086. doi: 10.1126/sciadv.aav5086
90. Deczkowska A, Baruch K, Schwartz M. Type I/II interferon balance in the regulation of brain physiology and pathology. *Trends Immunol.* (2016) 37:181–92. doi: 10.1016/j.it.2016.01.006
91. Sasaki I, Kaisho T. Transcriptional control of dendritic cell differentiation. *Curr Top Microbiol Immunol.* (2014) 381:257–78. doi: 10.1007/82_2014_378
92. Li L, Tan J, Miao Y, Lei P, Zhang Q. ROS and autophagy: interactions and molecular regulatory mechanisms. *Cell Mol Neurobiol.* (2015) 35:615–21. doi: 10.1007/s10571-015-0166-x
93. Vu TT, Gatto D, Turner V, Funnell AP, Mak KS, Norton LJ, et al. Impaired B cell development in the absence of Kruppel-like factor 3. *J Immunol.* (2011) 187:5032–42. doi: 10.4049/jimmunol.1101450
94. Regnier-Golanov AS, Dündar F, Zumbo P, Betel D, Hernandez MS, Peterson LE, et al. *Hippocampal Transcriptome Changes After Subarachnoid Hemorrhage in Mice.* (2021). Available online at: https://www.ncbi.nlm.nih.gov/geo/query/acc.cgi?acc=GSE167110 (accessed February 16, 2021).

Conflict of Interest: The authors declare that the research was conducted in the absence of any commercial or financial relationships that could be construed as a potential conflict of interest.

frontiers in Neurology

ORIGINAL RESEARCH
published: 26 July 2021
doi: 10.3389/fneur.2021.694996

Time Course of Peripheral Leukocytosis and Clinical Outcomes After Aneurysmal Subarachnoid Hemorrhage

*Aaron M. Gusdon[1], Jude P. J. Savarraj[1], Eyad Shihabeddin[1], Atzhiry Paz[1], Andres Assing[1], Sang-Bae Ko[2], Louise D. McCullough[3] and Huimahn Alex Choi[1]**

[1] Department of Neurosurgery, McGovern Medical School, University of Texas Health Science Center, Houston, TX, United States, [2] Department of Neurology, Seoul National University College of Medicine, Seoul, South Korea, [3] Department of Neurology, McGovern Medical School, University of Texas Health Science Center, Houston, TX, United States

Objective: Systemic inflammation after subarachnoid hemorrhage (SAH) is implicated in delayed cerebral ischemia (DCI) and adverse clinical outcomes. We hypothesize that early changes in peripheral leukocytes will be associated with outcomes after SAH.

Methods: SAH patients admitted between January 2009 and December 2016 were enrolled into a prospective observational study and were assessed for Hunt Hess Scale (HHS) at admission, DCI, and modified Ranked Scale (mRS) at discharge. Total white blood cell (WBC) counts and each component of the differential cell count were determined on the day of admission (day 0) to 8 days after bleed (day 8). Global cerebral edema (GCE) was assessed on admission CT, and presence of any infection was determined. Statistical tests included student's *t*-test, Chi-square test, and multivariate logistic regression (MLR) models.

Results: A total of 451 subjects were analyzed. Total WBCs and neutrophils decreased initially reaching a minimum at day 4–5 after SAH. Monocyte count increased gradually after SAH and peaked between day 6–8, while basophils and lymphocytes decreased initially from day 0 to 1 and steadily increased thereafter. Neutrophil to lymphocyte ratio (NLR) reached a peak on day 1 and decreased thereafter. WBCs, neutrophils, monocytes, and NLR were higher in patients with DCI and poor functional outcomes. WBCs, neutrophils, and NLR were higher in subjects who developed infections. In MLR models, neutrophils and monocytes were associated with DCI and worse functional outcomes, while NLR was only associated with worse functional outcomes. Occurrence of infection was associated with poor outcome. Neutrophils and NLR were associated with infection, while monocytes were not. Monocytes were higher in males, and ROC curve analysis revealed improved ability of monocytes to predict DCI and poor functional outcomes in male subjects.

Conclusions: Monocytosis was associated with DCI and poor functional outcomes after SAH. The association between neutrophils and NLR and infection may impact outcomes. Early elevation in monocytes had an improved ability to predict DCI and poor functional outcomes in males, which was independent of the occurrence of infection.

Keywords: monocytes, neutrophil-to-lymphocyte ratio, subarachnoid hemorrhage, neuroinflammation, delayed cerebral ischemia

OPEN ACCESS

Edited by:
Budbazar Enkhjargal, Boston University, United States

Reviewed by:
David Altschul, Montefiore Medical Center, United States
Michael Tso, Kelowna General Hospital, Canada

***Correspondence:**
Huimahn Alex Choi
huimahn.a.choi@uth.tmc.edu

Specialty section:
This article was submitted to Stroke, a section of the journal Frontiers in Neurology

Received: *14 April 2021*
Accepted: *24 June 2021*
Published: *26 July 2021*

Citation:
Gusdon AM, Savarraj JPJ, Shihabeddin E, Paz A, Assing A, Ko S-B, McCullough LD and Choi HA (2021) Time Course of Peripheral Leukocytosis and Clinical Outcomes After Aneurysmal Subarachnoid Hemorrhage. Front. Neurol. 12:694996. doi: 10.3389/fneur.2021.694996

INTRODUCTION

Aneurysmal subarachnoid hemorrhage (SAH) results in significant morbidity (1). Delayed cerebral ischemia (DCI) is a late complication occurring typically 4–14 days after onset in one-third of SAH caused by a combination of angiographic vasospasm, arterial constriction and thrombosis, and cortical spreading ischemia (2, 3) and is a major contributor to clinical outcomes (4, 5). Early brain injury (EBI) occurring within 72 h after aneurysmal rupture has been shown to be predictive of clinical outcomes (6). Global cerebral edema (GCE) quantifies the effacement of hemispheric sulci, and is a radiographic marker of early brain injury (7).

Uncontrolled inflammation occurs during EBI due to the reaction to extravascular blood (8), impaired cerebral autoregulation (9), release of products from injured brain tissue, and ischemia-reperfusion injury (7). Pro-inflammatory cytokines such as interleukin-1β (IL-1β) triggers the release of astrocyte derived extracellular vesicles that enter the peripheral circulation and promote the transmigration of leukocytes to the central nervous system (CNS) (10). The subsequent robust systemic inflammatory response occurring after SAH peaks at 24–48 h and contributes to delayed neurological deterioration (11, 12).

Peripheral leukocytes have been shown to migrate to the cerebrospinal fluid and brain after SAH (13) with activated neutrophils damaging brain micro-vessels (14). Preclinical models have shown that neutrophil and monocyte levels peaked by day 5 post SAH and that the leukocytes found in the brain originated from systemic blood circulation (5, 15). Early elevation in total peripheral leukocytes has been linked with the occurrence of DCI and poor functional outcomes (16, 17). However, leukocyte subtypes likely play distinct roles. After intracerebral hemorrhage (ICH), increased peripheral monocyte counts as well as neutrophil to lymphocyte ratios (NLR) are associated with worse outcomes (18–21). Similarly, after SAH, numerous studies have demonstrated that increased NLR is associated with worse outcomes (22–26). Peripheral monocytosis has also been linked to development of DCI (27). However, the biological mechanism underpinning the associations between leukocytes and outcomes and the link between inflammatory cells and EBI remain poorly understood.

The objective of this study is to investigate trends in leukocyte counts after SAH and the associations between leukocytes and outcomes. Total WBC count, monocytes, leukocytes, neutrophils, and basophils were collected at admission and each day for the next 8 days. We hypothesized that increased peripheral inflammatory cells will be associated with poor clinical outcomes and DCI.

MATERIALS AND METHODS

Study Population, Inclusion, and Exclusion Criteria

This is a retrospective, observational, single center study of SAH patients admitted between January 2009 and December 2016 to the Neuroscience Intensive Care Unit at Memorial Hermann Hospital, University of Texas (UT) Health Science center at Houston. Ethical approval was obtained from the UT Health Science Center institutional review board (17-0776). Inclusion criteria for the study were: presence of SAH on initial CT or presence of xanthochromia in cerebrospinal fluid, age above 18 years, and admission to hospital within 72 h of bleed ictus. Exclusion criteria for the study included: SAH associated with trauma, arteriovenous malformation, or mycotic aneurysms; presence of auto-immune diseases; and conditions that affect inflammation such as pregnancy or a history of malignancy. Subjects with perimesencephalic SAH were excluded due to the low likelihood of aneurysmal etiology and low risk of aneurysmal etiology and development of DCI (28).

Demographic, Clinical, and Radiographic Data

Subjects' demographics and clinical information were abstracted from the electronic medical record. The Hunt Hess Scale (HHS) score was used to quantify clinical severity on admission (29). Patients were dichotomized into good grade group (HH $\leq$3) and poor grade groups (HH $\geq$4). All patients were monitored for DCI. DCI is a dichotomous score (either 0 or 1) defined as "the occurrence of focal neurological impairment or a decrease of at least 2 points on the Glasgow Coma Scale that lasts for at least 1 h, is not apparent immediately after aneurysm occlusion, and cannot be attributed to other causes by means of clinical assessment, CT or MRI scanning of the brain, and appropriate laboratory studies" (30). The 0–6 modified Rankin score (mRS) was used to quantify functional outcome of patient at the time of discharge. Patients were dichotomized into good (mRS $\leq$3) and poor (mRS $\geq$4) clinical outcomes. Infection was defined as the presence of ventriculitis, urinary tract infection (UTI), or pneumonia.

Radiographic Markers of Injury

Initial computed tomography (CT) scans at the time of SAH diagnosis were graded for parameters including global cerebral edema (GCE), intraventricular hemorrhage (IVH), and modified Fisher Scale (mFS). GCE is an important radiographic marker of EBI which is also a risk factor for DCI (7). It is a qualitative and dichotomous score (either 0 or 1) based on the radiographic presence of [1] complete or near-complete effacement of hemispheric sulci and basal cisterns or [2] bilateral and extensive disruption of the hemispheric gray-white matter junction at the level of the central semi vale, which is due to either blurring or diffuse peripheral "fingerlike" extensions of the normal demarcation between gray and white matter (7). IVH is a qualitative and dichotomous radiographic score (either 0 or 1) defined as the presence or bleeding inside or around the ventricles in the brain that normally contain cerebral spinal fluid. GCE, IVH, and mRS were determined by at least two independent physicians, with at least one being an attending neurointensivist. All scores were adjudicated at a weekly research meeting.

Leukocytes Subtypes and Time Course

Complete blood counts (CBC) with differential were collected as a part of routine patient care and management. Differentials included total white blood cells (WBC), neutrophils, monocytes,

TABLE 1 | Demographics and clinical outcomes.

	Total	DCI (-)	DCI (+)	*P*	mRS (0-3)	mRS (4-6)	*P*
N	451	363	88		305	146	
Demographics							
Age	54 (45, 63)*	54 (44, 64)	54 (46, 62)	0.903	51 (42, 59)	61 (51, 71)	**<0.001**
Gender (*F*)	295 (65)	235	60	0.436	197 (65)	98 (67)	0.441
Hypertension	304 (67)†	248 (68)	56 (64)	0.461	197 (65)	107 (73)	**0.004**
HHS (4,5)	95 (21)	71 (20)	24 (27)	0.112	21 (6.9)	74 (51)	**<0.001**
mFS (3,4)	406 (90)	232 (64)	75 (85)	**<0.001**	186 (61)	121 (83)	**<0.001**
IVH	240 (53)	173 (48)	67 (76)	**<0.001**	133 (44)	107 (73)	**<0.001**
Aneurysm treatment:				**2.83×10^{-6}**			**8.00×10^{-9}**
Clipped	139 (31)	101 (28)	38 (43)	**0.041**	99 (32)	40 (27)	0.999
Coiled	222 (49)	172 (47)	50 (57)	0.898	146 (48)	76 (52)	0.999
No treatment	32 (7)	32 (9)	0 (0)	**0.031**	8 (3)	24 (16)	**1.00×10^{-6}**
No aneurysm	58 (13)	58 (16)	0 (0)	**0.0005**	52 (17)	6 (4)	**9.81×10^{-4}**
Outcomes							
DCI	88 (20)				39 (13)	49 (34)	**<0.001**
mRS (4-6)	146 (32)	97 (27)	49 (56)	**<0.001**			
Hospital LOS	13 (9, 18)	12 (9, 16)	19 (14, 24)	**<0.001**	12 (9,16)	16 (8, 23)	**0.001**

*Data are presented as either *median (interquartile range) or †N (percent). HHS, Hunt Hess Scale; mFS, modified Fisher Scale; IVH, intraventricular hemorrhage; DCI, delayed cerebral ischemia; mRS, modified Rankin Scale; LOS, length of stay. P-values that are statistically significant are in bold.*

lymphocytes, eosinophils, and basophils. Daily values for each cell type were abstracted from day of admission (day 0) to day 8. The early (within 48 h) period most likely corresponds with the occurrence of EBI after SAH (15–17). Days 3–5 reflect the time period immediately preceding the occurrence of DCI. The 6–8-day period represents the peak period of DCI. Given that leukocyte counts at different time points after injury may play distinct roles, we created a variety models using a variety of different time points. Models were created for cells counts on each individual day. Models were also created using median cell counts over days 1–5, as this timeframe was thought to precede development of DCI in most patients.

Statistical Analysis

Student's *t*-tests were performed on continuous variables while χ^2 tests were performed on categorical variables. $p < 0.05$ were considered to be significant. Univariate models were created to assess the association between each cell type over days 0–8. Given that 54 comparisons were made, a Bonferroni correction was used to set significance at a *P*-value of $< 9.3 \times 10^{-4}$ for univariate models. Multivariable logistic regression (MLR) models were used to determine independent associations after controlling for variables found to be significant in univariate models. Models presented herein reflect median cell counts over days 1–5, unless otherwise specified. Receiver operating characteristic (ROC) curves were calculated with an area under the curve (AUC) calculated for each. RStudio (v1.2.5033) was used for all statistical analysis.

RESULTS

Demographics and Outcomes

A total of 451 patients met the inclusion criteria and were included in this study. Demographic characteristics and clinical outcomes of subjects are shown in **Table 1**. The average age was 54 (IQR 45, 63), 295 (65%) were female, 304 (67%) had hypertension, 240 (53%) presented with IVH, and 95 (21%) had HH ≥4 at admission. Aneurysms were treated by surgical clipping in 139 (31%) and by coiling in 222 (49%). No surgical treatment for aneurysm was undertaken in 32 (7%), and no aneurysm was found in 58 (13%). Subjects who developed DCI had higher mFS scores [mFS ≥3: 232 (64%) vs. 75 (85%), $P < 0.001$], higher proportion of IVH [173 (48%) vs. 67 (76%), $P < 0.001$], higher frequency of aneurysm clipping [101 (28%) vs. 38 (43%), $P = 0.041$], worse outcomes [mRS ≥4: 97 (27%) vs. 49 (56%), $P < 0.001$], and longer hospital length of stay [12 days (IQR 9, 16) vs. 19 days (14, 24), $P < 0.001$]. Subjects with poor outcomes (mRS ≥4) were older [age 51 (IQR 42, 59) vs. 61 (31, 32), $P < 0.001$], had a higher proportion of hypertension [197 (65%) vs. 107 (73%), $P = 0.004$], had higher HH grade [HH 4,5: 21 (6.9%) vs. 74 (51%), $P < 0.001$], had higher mFS scores [mFS ≥3: 186 (61%) vs. 121 (83%), $P < 0.001$], had a higher proportion of IVH [133 (44%) vs. 107 (73%), $P < 0.001$], had a higher incidence of DCI [39 (13%) vs. 49 (34%), $P < 0.001$], and had a higher hospital length of stay [12 days (IQR 9, 16) vs. 16 days (IQR 8, 23), $P < 0.001$].

Leukocyte Trends

Overall trends in leukocytes are shown in **Supplementary Figure 1**. WBC count was highest on day 0 after SAH, decreased until day 5, and then increased again. This same trend occurred for neutrophils. Monocytes increased gradually after SAH, peaking at day 8. After an initial decrease from day 0 to day 1, basophil count increased gradually until peaking at day 7. Lymphocytes also decreased from day 0 to day 1, followed by an increase reaching a peak at day 7. NLR was highest at day 1 after SAH, and then decreased to

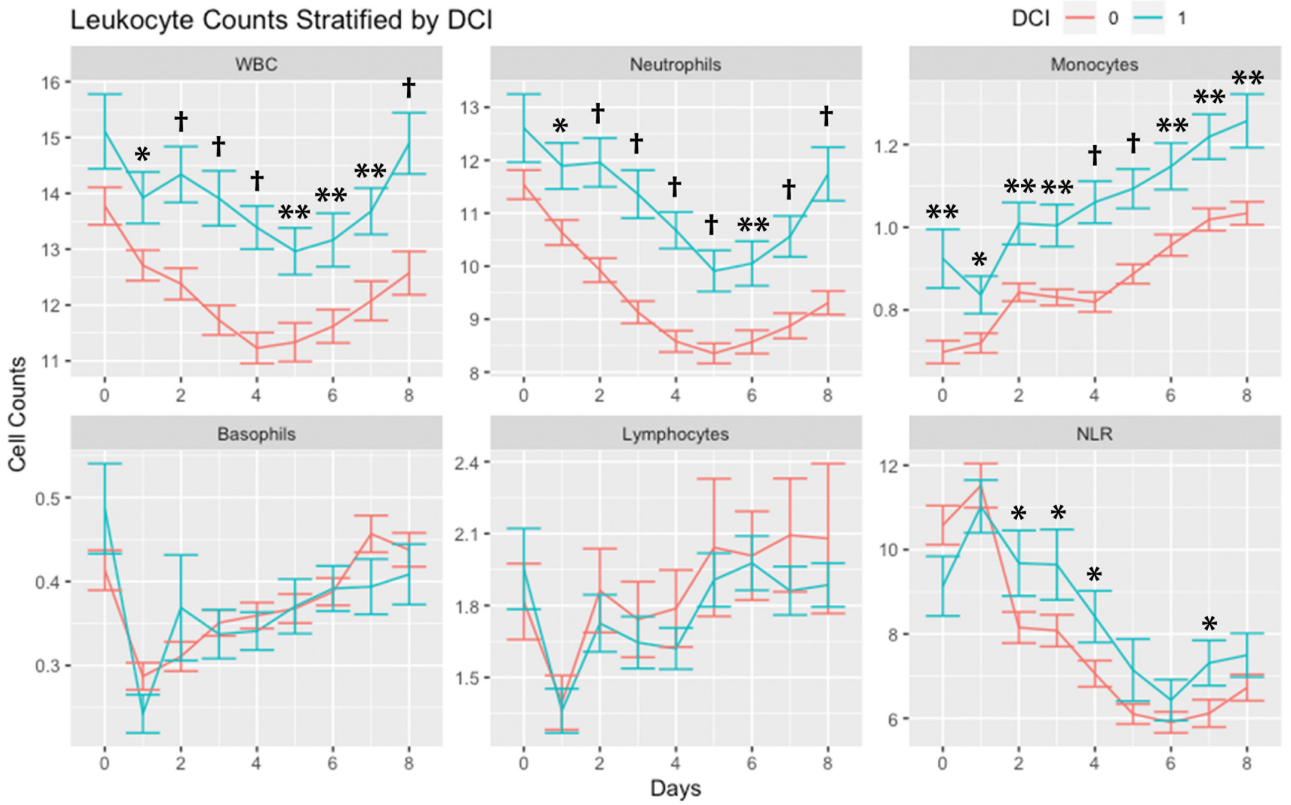

FIGURE 1 | Leukocyte counts stratified by occurrence of delayed cerebral ischemia (DCI). Leukocytes counts (mean and standard deviation) are shown from day of SAH (day 0) through day 8. Cells are in units of 1,000 per mm^3. *$P < 0.05$, **$P < 0.01$, †$P < 0.001$. Abbreviations: delayed cerebral ischemia (DCI), subarachnoid hemorrhage (SAH), white blood cells (WBC), neutrophil-to-lymphocyte ratio (NLR).

reach a minimum at day 6 after SAH, subsequently increasing again thereafter.

Associations With Disease Severity and Outcomes

Leukocytes stratified by HHS are shown in **Supplementary Figure 2**. In subjects with higher HHS (4, 5) on admission, WBC count was significantly higher on all days except day 5. Neutrophils were significantly higher in subjects with higher HHS across all days. Monocytes were higher in subjects with higher HHS on days 0, 1, and 2. There were no significant differences in basophils. Lymphocytes higher in subjects with higher HHS on day 0 and were lower on days 3, 4, 5, and 6. NLR was higher in subjects with higher HHS on all days except for day 0.

Leukocytes stratified by occurrence of DCI are shown in **Figure 1**. WBC and neutrophil counts were higher in subjects with DCI across all days with the exception of day 0. Monocytes were higher in subjects with DCI across all days. There were no differences in basophils and lymphocytes among subjects with and without DCI. NLR was higher in subjects with DCI on days 2, 3, 4, and 7.

Leukocytes stratified by outcomes (mRS 0-3 vs. 4-6) are shown in **Figure 2**. WBCs, neutrophils, and monocytes were higher in subjects with poor mRS outcomes across all days. Basophils were higher on day 0 in patients with poor mRS outcomes, while on days 4, 5, 6, and 7 basophils were higher in subjects with good mRS outcomes. Lymphocytes were higher on day 0 in patients with poor mRS outcomes. NLR was higher in subjects with poor mRS outcomes on all days except days 0 and 1.

Association With Infection

Leukocytes were stratified by the presence of any infection (**Figure 3**). WBCs and neutrophils were higher in subjects with any infection on day 2 through day 8. There were no significant differences in monocytes. Basophils were higher in subjects without infection on day 4. Lymphocytes were higher in subjects without infection on days 2, 3, 4, 5, 6, and 7. NLR was higher in subjects with infection on days 2 through day 8.

Sex Differences

Leukocytes were stratified according to sex (**Figure 4**). There were no significant differences in WBCs and neutrophils comparing males and females. Monocytes were higher in males on days 2 through day 8. There were no significant differences

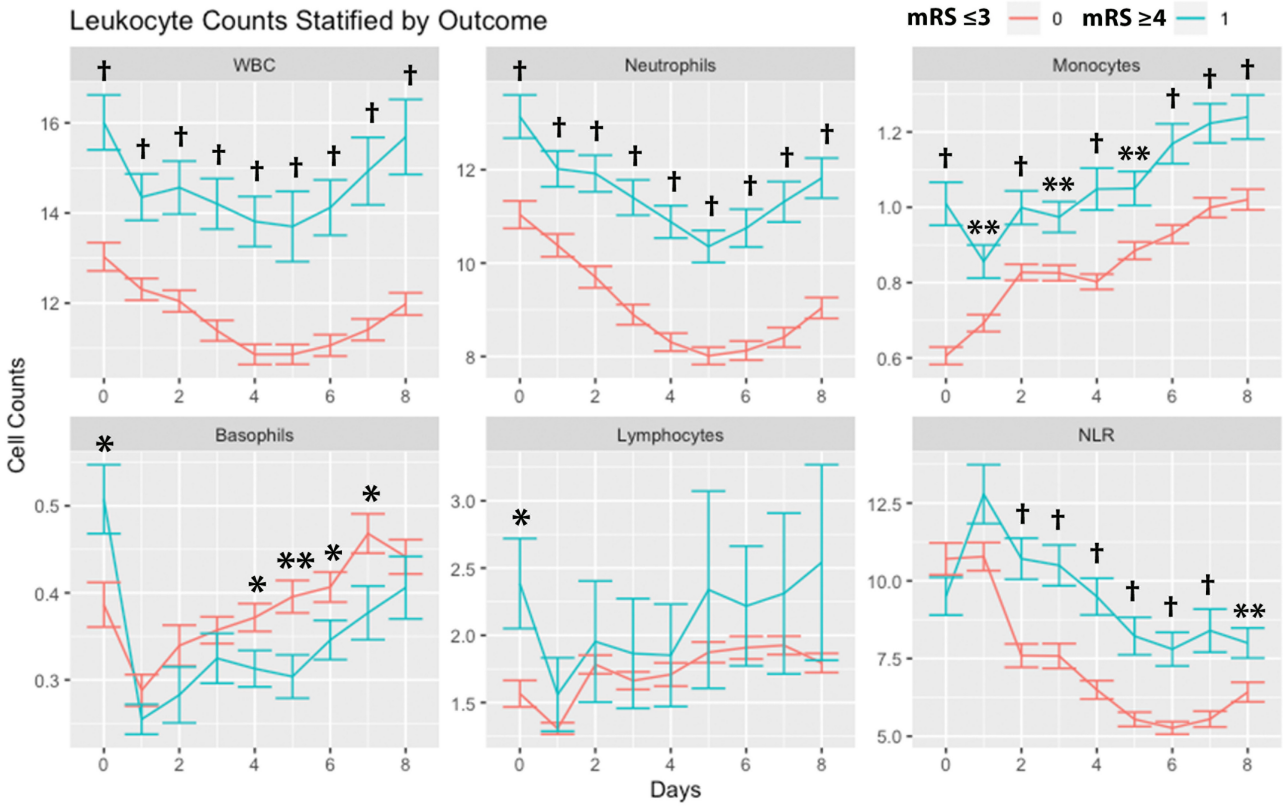

FIGURE 2 | Leukocyte counts stratified by outcomes. Leukocyte counts (mean and standard deviation) are shown from day of SAH (day 0) through day 8. Outcome is dichotomized according to mRS good (≤3) or poor (≥4). *$P < 0.05$, **$P < 0.01$, †$P < 0.001$. Cells are in units of 1,000 per mm^3. mRS, modified Rankin Scale; SAH, subarachnoid hemorrhage; WBC, white blood cells; NLR, neutrophil-to-lymphocyte ratio.

in basophils. Lymphocytes were higher in females on day 1. NLR was higher in females on day 8.

Outcome Models

Univariate models were created for each cell count on each day to assess associations with DCI (**Supplementary Table 1**) and mRS (**Supplementary Table 2**). Increased WBCs were associated with DCI on days 3 and 4 and neutrophils were associated with DCI on days 2, 3, 4, and 5. Increased monocytes were associated with DCI on all days except day 1. No associations were found for DCI among basophils, lymphocytes, or NLR on any day. Increased WBCs, neutrophils, and monocytes were associated with poor outcomes (mRS 4-6) on all days, while increased NLR was associated with poor outcomes on all days except days 0, 1, and 8. No associations with outcomes were found for basophils and lymphocytes.

MLR models were constructed to assess the associations between cell counts and outcomes. Models were created taking the median cell counts across days 1–5. After correction for covariates, neutrophils and monocytes were associated with DCI, while NLR was not (**Table 2**). IVH was associated with DCI in the model including monocytes and NLR. Occurrence of infection was associated with DCI only the NLR model. GCE was associated with DCI only in the model containing monocytes. Aneurysm treatment by surgical clipping was associated with DCI in the monocyte and NLR models. Neutrophils, monocytes, and NLR were associated with poor outcomes (mRS 4-6) (**Table 3**). Increased age, HHS, and presence of any infection were also associated with worse outcomes in each model. IVH was associated with poor outcomes in each model. GCE was associated with poor outcomes in the monocyte and NLR models. Aneurysmal clipping was not associated with function outcome in any model. No significant effect of sex was seen in models for DCI or functional outcomes (**Tables 2**, **3**).

MLR models were also created account for monocytes at day 0 (**Supplementary Table 3**). Increased day 0 monocyte count was strongly associated with DCI and poor functional outcomes in unadjusted models and after correction for covariates. IVH and infection were associated with DCI. Age, HHS, and infection were associated with worse functional outcomes.

MLR models were created to assess the association between cell count and infection (**Table 4**). Neutrophil count and NLR were associated with occurrence of infection after correction for covariates. In models adjusted for covariates, monocyte count was not associated with infection. Increased age and higher HHS were associated with infection across all models. Male sex was

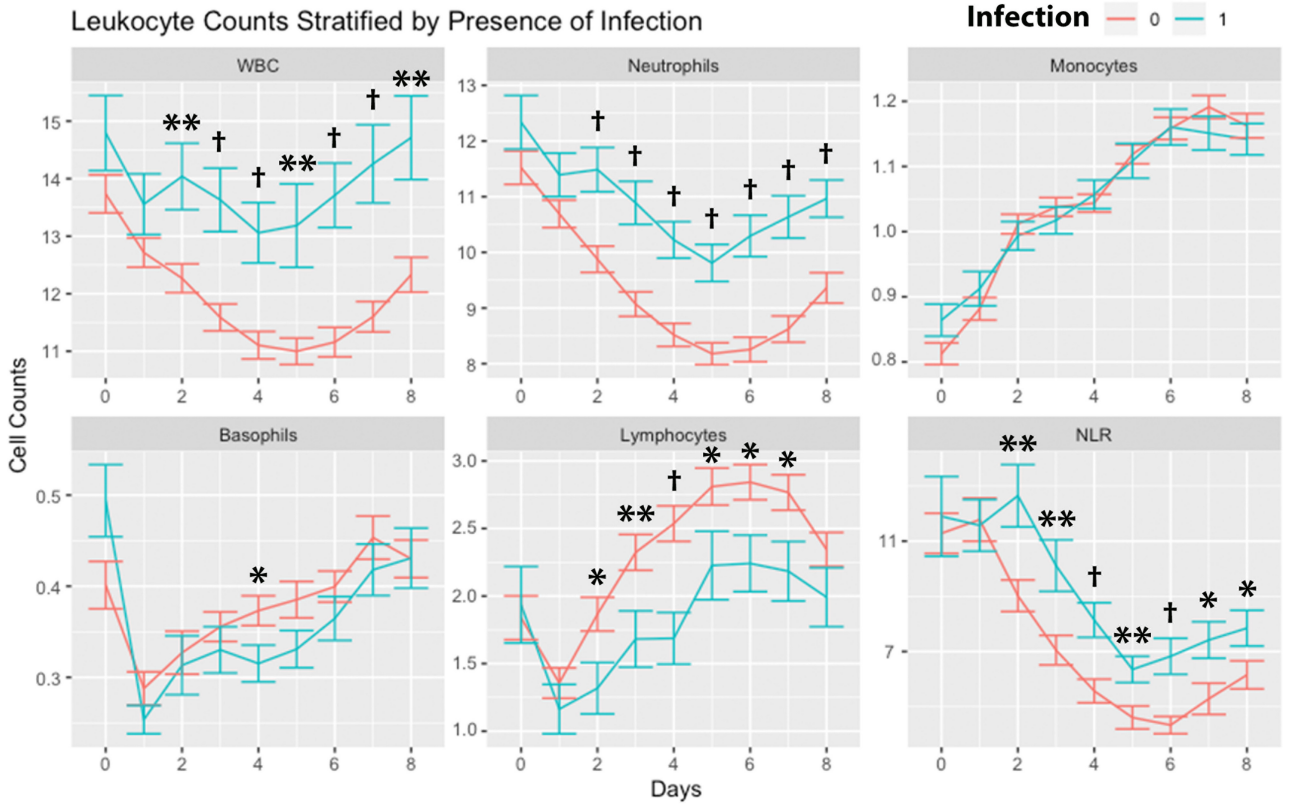

FIGURE 3 | Leukocyte counts stratified by infection. Leukocyte counts (mean and standard deviation) are shown from the day of SAH (day 0) through day 8. Counts are stratified by the occurrence of any infection within days 0–8. $^{*}P < 0.05$, $^{**}P < 0.01$, $^{\dagger}P < 0.001$. Cells are in units of 1,000 per mm^3. SAH, subarachnoid hemorrhage; WBC, white blood cells; NLR, neutrophil-to-lymphocyte ratio.

negatively associated with occurrence of infection in models containing monocytes. When only considering female subjects, monocytes were associated with infection ($\beta = 1.47$, 95%CI 0.99, 1.94) with correction for HHS, age, mFS, and IVH. When only considering male subjects, monocyte count was not associated with infection ($\beta = 0.19$, 95%CI −1.76, 2.12) with correction for HHS, age, mFS, and IVH.

Receiver Operating Characteristics (ROC) Curves

ROC curves were created considering monocyte count at day 0. For prediction of DCI, monocyte count had an area under the curve (AUC) of 0.640 (**Figure 5A**). For prediction of poor functional outcomes, monocyte count had an AUC of 0.719 (**Figure 5B**). Youden index for DCI yielded an optimal cutoff of 0.683 K/mm^3 (sensitivity 0.625, specificity 0.648). Youden index for mRS yield an optimal cutoff of 0.810 K/mm^3 (sensitivity 0.568, specificity 0.792). Baseline models were created including HHS, Age, mFS, infection, IVH, gender, and GCE. ROC curves were created for baseline models and baseline models plus day 0 monocyte count. AUC for the baseline model was 0.712 for DCI, which improved to 0.754 when including monocyte count (**Supplementary Figure 3A**). AUC for the baseline model was 0.858 for outcomes, which improved to 0.877 when including monocyte count (**Supplementary Figure 3B**).

In females, AUC of the ROC curve for DCI for day 0 monocytes was 0.611 (**Supplementary Figure 4A**). In males, AUC of the ROC curve for DCI was 0.703 (**Supplementary Figure 4B**). For females the optimal cutoff for DCI for day 0 monocytes was 0.683 K/mm^3 (sensitivity 0.571, specificity 0.667). For males, the optimal cutoff for DCI for day 0 monocytes was 0.760 K/mm^3 (sensitivity 0.760, specificity 0.739). In females, AUC of the ROC curve for mRS was 0.655 (**Supplementary Figure 5A**). In males, AUC of the ROC curve for mRS was 0.751 (**Supplementary Figure 5B**). For females, the optimal cutoff for mRS was 0.453 K/mm^3 (sensitivity 0.891, specificity 0.369). For males, the optimal cutoff for mRS was 0.796 K/mm^3 (sensitivity 0.595, specificity 0.837). These results are summarized in **Supplementary Table 4**.

DISCUSSION

This study demonstrates that peripheral leukocytes robustly distinguish outcomes after SAH, with persistently elevated WBCs, neutrophils, and NLR in those with DCI and poor outcomes. Although leukocytes were affected by clinical severity,

FIGURE 4 | Leukocyte counts stratified by sex. Leukocyte counts (mean and standard deviation) are shown from the day of SAH (day 0) through day 8. Subjects are divided into males and females. $^{*}P < 0.05$, $^{**}P < 0.01$, $^{\dagger}P < 0.001$. Cells are in units of 1,000 per mm^3. SAH, subarachnoid hemorrhage; WBC, white blood cells; NLR, neutrophil-to-lymphocyte ratio.

TABLE 2 | Associations between leukocytes and DCI.

	Neutrophils*	Monocytes	NLR
Unadjusted	0.19 [0.15, 0.24 (**6.05×10^{-6}**)]#	2.00 [1.52, 2.48 (**2.71×10^{-5}**)]	0.05 [0.03, 0.07 (**0.027**)]
Adjusted	0.18 [0.13, 0.23 (**3.45×10^{-4}**)]	1.50 [1.03, 1.97 (**0.0144**)]	0.03 [−0.003, 0.07 (0.358)]
Covariates			
Age	0.004 [−0.008, 0.01 (0.692)]	0.009 [−0.003, 0.02 (0.444)]	0.007 [−0.004, 0.02 (0.553)]
HHS	0.41 [0.05, 0.76 (0.553)]	−0.06 [−0.45, 0.32 (0.867)]	0.23 [−0.13, 0.50 (0.517)]
mFS	−0.44 [−0.92, 0.05 (0.303)]	0.26 [−0.24, 0.74 (0.406)]	0.36 [−0.03, 0.75 (0.274)]
IVH	0.95 [0.60, 1.30 (**0.008**)]	1.05 [0.66, 1.35 (**0.009**)]	1.04 [0.68, 1.35 (**0.002**)]
GCE	0.68 [0.29, 1.10 (0.094)]	0.88 [0.42, 1.23 (**0.047**)]	0.71 [0.32, 1.10 (0.061)]
Sex (Male)	0.05 [−0.29, 0.35 (0.866]	−0.04 [−0.36, 0.23 (0.913)]	0.008 [−0.30, 0.31 (0.979)]
Any infection	0.52 [0.21, 0.82 (0.092)]	0.31 [−0.10, 1.12 (0.088)]	0.61 [0.32, 0.91 (**0.036**)]
Aneurysm clipping	0.24 [−0.03, 0.51 (0.106)]	0.74 [0.47, 1.01 (**0.007**)]	0.64 [0.37, 0.90 (**0.061**)]

**Models based on median cell count for days 1–5.*

#Data are presented as β coefficient [95% confidence interval (P value)].

HHS, Hunt Hess Scale; mFS, modified Fisher Scale; IVH, intraventricular hemorrhage; GCE, global cerebral edema. P-values that are statistically significant are in bold.

there was an independent effect of cell counts on outcomes. Monocyte count (both on admission and medians from day 1–5) robustly predicted DCI and outcomes, in a sex dependent fashion. We found an association between infection and outcome and importantly demonstrated a link between neutrophils and NLR with the occurrence of infection after SAH.

Monocytes remained significantly elevated across all study days in subjects with DCI and poor functional outcomes.

TABLE 3 | Associations between leukocytes and outcomes (mRS 4-6).

	Neutrophil Count*	Monocyte Count	NLR
Unadjusted	0.23 [0.18, 0.27 (**4.31 × 10^{-7}**)]#	1.88 [1.42, 2.34 (**3.87 × 10^{-5}**)]	0.10 [0.07, 012 (**1.56 × 10^{-5}**)]
Adjusted	0.23 [0.17, 0.28 (**4.98 × 10^{-5}**)]	1.36 [0.83, 1.91 (**0.009**)]	0.07 [0.04, 0.08 (**0.033**)]
Covariates			
Age	0.06 [0.05, 0.08 (**2.35 × 10^{-6}**)]	0.06 [0.05, 0.07 (**1.76 × 10^{-6}**)]	0.05 [0.04, 0.07 (**1.01 × 10^{-5}**)]
HHS	1.62 [1.24, 2.00 (**2.09 × 10^{-5}**)]	1.47 [1.10, 1.84 (**8.31 × 10^{-5}**)]	1.52 [1.15, 1.88 (**3.58 × 10^{-5}**)]
mFS	−0.03 [−0.59, 0.53 (0.949)]	0.80 [0.13, 1.13 (0.112)]	0.09 [−0.31, 0.49 (0.883)]
IVH	0.86 [0.51, 1.22 (**0.014**)]	0.80 [0.45, 1.16 (**0.023**)]	0.99 [0.66, 1.33 (**0.003**)]
GCE	0.82 [0.35, 1.28 (0.081)]	0.90 [0.50, 1.39 (**0.043**)]	0.88 [0.44, 1.33 (**0.041**)]
Sex (Male)	−0.24 [−0.58, 0.07 (0.475)]	−0.37 [−0.71, 0.02 (0.282)]	−0.08 [−0.40, 0.24 (0.811)]
Any infection	0.75 [0.42, 1.08 (**0.021**)]	0.85 [0.47, 1.21 (**0.022**)]	0.80 [0.49, 1.11 (**0.011**)]
Aneurysm clipping	0.15 [−0.11, 0.41 (0.567)]	0.25 [−0.004, 0.52 (0.173)]	0.27 [−0.01, 0.55 (0.292)

**Models based on median cell count for days 1–5.*

#Data are presented as β coefficient [confidence interval (P-value)].

HHS, Hunt Hess Scale; mFS, modified Fisher Scale; IVH, intraventricular hemorrhage; GCE, global cerebral edema. P-values that are statistically significant are in bold.

TABLE 4 | Associations between leukocytes and presence of infection.

	Neutrophil count*	Monocyte count	NLR
Unadjusted	0.16 [0.12, 0.20 (**4.14 × 10^{-5}**)]#	0.44 [0.22, 0.66 (**0.043**)]	0.24 [0.16, 0.32 (**0.002**)]
Adjusted	0.10 [0.06, 0.15 (**0.02**)]	0.05 [−0.21, 0.30 (0.850)]	0.26 [0.17, 034 (**0.005**)]
Covariates			
Age	0.03 [0.02, 0.04 (**0.007**)]	0.03 [0.03, 0.04 (**0.0002**)]	0.03 [0.02, 0.04 (**0.0005**)]
HHS	0.92 [0.59, 12.6 (**0.006**)]	0.95 [0.63, 1.26 (**0.003**)]	0.87 [0.57, 1.18 (**0.004**)]
mFS	0.10 [−0.38, 0,58 (0.831)]	0.42 [−0.03, 0.88 (0.354)]	0.39 [−0.06, 0.84 (0.381)]
IVH	0.09 [−0.20, 0.39 (0.752)]	0.28 [-0.009, 1.27 (0.302)]	0.24 [−0.03, 0.51 (0.370)]
GCE	−0.57 [−1.42, −0.22 (0.170)]	−0.74 [−1.55, 0.02 (0.065)]	−0.49 [−1.15, 0.35 (0.204)]
Sex (Male)	−0.55 [−0.84, 0.25 (0.066)]	−0.75 [−1.04, −0.47 (**8.63 × 10^{-3}**)]	−0.50 [−1.04, 0.02 (0.064)]

**Models based on median cell count for days 1–5.*

#Data are presented as β coefficient [95% confidence interval (P-value)].

HHS, Hunt Hess Scale; mFS, modified Fisher Scale; IVH, intraventricular hemorrhage; GCE, global cerebral edema. P-values that are statistically significant are in bold.

Peripheral monocyte count has been shown to increase early after brain injury (33). Monocytes play a beneficial role by removing debris in the subarachnoid space (34), however increased monocyte counts have also been associated with worse outcome after ICH (18). The pathophysiology underlying this association is unclear. However, monocytes have been linked to hematoma expansion in patients with ICH (35). Monocytes are coated with physiological anticoagulants such as thrombomodulin and tissue factor pathway inhibitor 2 (36, 37). A mouse model also found decreased extent of bleeding in an ICH model with impaired CCL2-CCR2 chemoattractant system (38). Peripheral monocytes play an important role in cerebral inflammation after injury in stroke, ICH, Alzheimer's and status epilepticus (34, 35, 39–42). Mice deficient in Toll-like receptor 4 (TLR4) demonstrated decreased recruitment of monocytes after ICH associated with decreased perihematomal edema (39). Therefore, monocytes may play a role both in hemorrhage expansion and inflammation after SAH. Indeed, the innate immune system has been shown to be activated early after SAH, with cells trafficking to the brain from the periphery (43). $CD14^{+}CD16^{-}$ monocytes (22) as well as monocytes expressing programmed death-1 (PD-1) are thought to play a role in the development of vasospasm, as blocking their ingress to the CNS after SAH attenuated vasospasm (44).

The early (day 0 and 1) increase among subjects with DCI and poor functional outcomes distinguished monocytes and NLR. Indeed, increased monocytes were robustly associated with DCI and poor functional outcome both considering median cell counts over days 1–5 (**Tables 2**, **3**) and day 0 (**Supplementary Table 3**). The ability of monocytes to predict delayed cerebral infraction and poor outcomes after SAH has recently been demonstrated in a cohort of 204 patients (27). These authors found an optimal cutoff of 0.60 to discriminate development of cerebral infarction and poor outcomes after SAH, with AUC of 0.622. We found an improved AUCs for discrimination of DCI (0.640) and poor functional outcome (0.719). Our results also suggest a higher monocyte count may improve discrimination of DCI (0.683) and functional outcomes (0.810). When adding day 0 monocyte count to a baseline model including HHS, age, mFS, infection, IVH, and GCE, the AUCs

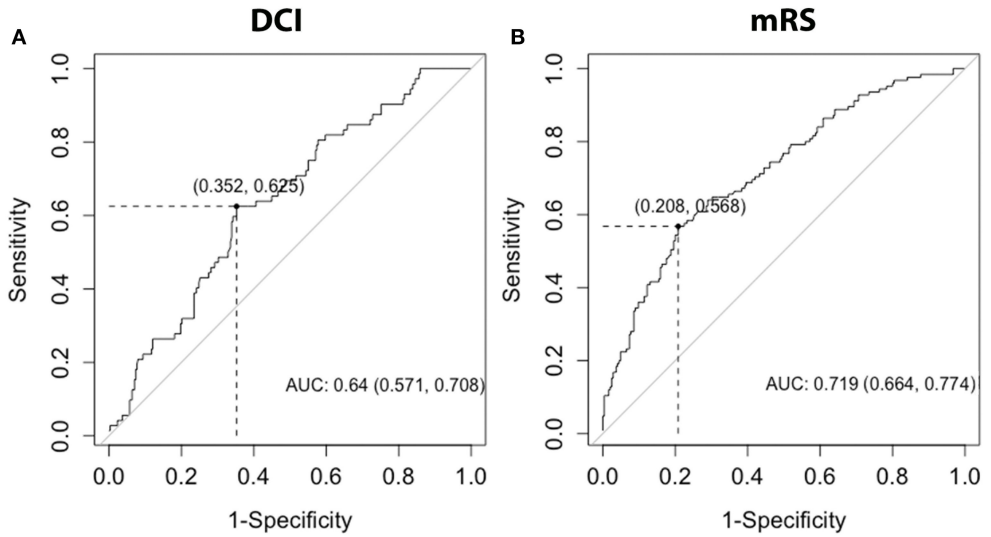

FIGURE 5 | ROC curves for DCI and mRS. ROC curves were generated for the discrimination of DCI or poor discharge mRS, with mRS dichotomized into good (0-3) and poor (4–6) outcomes, using day 0 monocytes. AUC and 95%CI interval were calculated for each ROC curve. DCI, delayed cerebral ischemia; mRS, modified Rankin Scale; AUC, area under the curve.

further improved to 0.754 to DCI and 0.877 for functional outcome (**Supplementary Figure 3**).

Monocyte counts were significantly higher in males (**Figure 4**). Of note, monocytes had a better ability to discriminate DCI (AUC 0.703 vs. 0.611) and outcomes (AUC 751 vs. 655) in males compared with females. Monocyte function is sex specific and absolute numbers of monocytes have been shown to be higher in males than females (45). Several studies have also reported more robust cytokine production in male compared with female monocytes (46–48). Sex hormones impact immune cell function. Estrogen has been found to promote M2 polarization, which was dependent on the function of estrogen receptor α (49). We theorize that male monocytes are more likely to undergo M1 polarization with increased pro-inflammatory cytokine production after SAH. Furthermore, unlike neutrophils and NLR, monocyte count was not significantly associated with occurrence of infection (**Table 4**). Interestingly, an association between infection and monocyte count was only found in women and not seen in males. To summarize, monocytes increased steadily in both sexes. Monocyte counts were predictive of the occurrence of DCI in men. Monocyte counts were predictive of the occurrence of infections in women. This suggests that there are sex-specific effects of monocytes after SAH. Further examination of the underlying pathophysiology of these differences should be pursued.

An elevated NLR likely represents dysregulation of the immune system reflecting an increased innate and attenuated adaptive immune response (8, 50). In addition to playing a role in ICH and stroke (26, 51) an elevated NLR has been linked to outcomes in patients with cancer, myocardial infarction, and sepsis (31, 52–56). Neutrophils infiltrate the cerebral vasculature within 10 min after SAH, and reduction of neutrophil levels or activity improves vascular integrity and outcomes in animal models (14, 57). In addition to producing pro-inflammatory cytokines, neutrophils generate substantial oxidative stress by releasing factors such as myeloperoxidase, which can generate hypochlorous acid and consume nitric oxide resulting in impaired vasodilation (58). Isoprostanes generated by neutrophil mediated oxidative stress can also result in vasoconstriction (59, 60). Indeed, neutrophils may also contribute to early cerebral hypoperfusion after SAH (61).

This study builds upon results from prior studies, which have demonstrated the role of peripheral leukocytes after SAH. While several important studies have shown that WBC count has an association with DCI (62, 63), herein we have provided a comprehensive assessment of the role of differential cell counts on DCI and functional outcomes. Our assessments of the role of sex differences and associations with infection have also not been addressed in prior studies. We also support findings from previous studies indicating an association between elevated NLR and DCI (23, 25) and outcomes (24, 26). Our study has key differences with these reports, with a main difference being that most studies have exclusively assessed the role of early leukocyte counts. The largest study to date, which evaluated 1067 SAH patients, found an admission NLR cutoff of 5.9 to be highly predictive of the development of DCI with no association between NLR and functional outcomes (25). Our results demonstrate that WBCs, neutrophils, and NLR remain elevated in patients with DCI and poor functional outcome for a week after the initial bleed and these differences increase after the first two post-bleed days (**Figure 1**). This is in line with granulocytes being persistently elevated in the brain for at least a week after SAH in a rat model (64). We did not find associations with outcomes using early (day 0) WBCs, neutrophils, and

NLR but found robust associations using median values over 5 days (**Tables 2**, **3**). We suggest that the earliest time point for WBCs and NLR may not be as tightly linked to ultimate clinical outcome.

There was an association between neutrophils and NLR and the occurrence of infection after SAH, while lymphocytes were associated with fewer infections (**Table 4**). Elevated NLR plays a role in post SAH immunosuppression (26) and contributes to the risk of pneumonia (65). Neutrophils may play a role in the suppression of the adaptive immune system (50). The immunosuppressive capacity of some neutrophils is due to the ability to inhibit T-cell activation, proliferation, and effector functions (66). However, it is unclear from our results whether neutrophilia precedes infection, or whether early infections drive persistently elevated neutrophils and NLR. The role of lymphocytes in the injured brain is complex and incompletely understood. T cells infiltrate 48–96 h after injury and peak around 5 days (67, 68) in mice but have been found in the CSF after ICH in humans after 6 h (69). T cells comprise a heterogenous population and have been shown to have both protective and deleterious roles (70). Both pro-inflammatory (γδT cells) and immunosuppressive regular T cells (Tregs) traffic to the area of hemorrhage (32). γδT cells have been shown to contribute to injury after ischemic stroke mainly due to the production of IL-17 (71). Tregs may provide benefits against the late tissue damage (72), while in the earlier time frame they have been shown to modulate the activity of invading pro-inflammatory cells (73). The role of γδT cells may be primarily in the periphery rather than brain parenchyma as they accumulate in the leptomeninges and control trafficking of other inflammatory cells (74). While our study is not able to distinguish between lymphocyte subtypes, it is possible that the serum lymphocytes and decreased NLR associated with good outcomes and decreased risk of infection outcomes are primarily Tregs. We suspect that increased neutrophils and decreased lymphocytes are key factor leading to risk of infection after SAH, with this serving as a major determinant of clinical outcomes.

A major caveat to the interpretation of the results presented herein is the prevalent use of corticosteroids. At our institution, patients with aneurysmal SAH are typically treated with a standard regimen of corticosteroids during the first week of hospitalization, affecting most subjects in this study. Corticosteroids have an important effect on circulating leukocytes. Corticosteroid treatment increases neutrophils due to increased entrance from bone marrow and decreased vascular removal. However, monocytes, lymphocytes, basophils, and eosinophils are decreased after steroid treatment. This effect is thought to be due to redistribution of these cells, although lymphocytes are known to undergo steroid induced apoptosis (75). In addition, corticosteroids have potent anti-inflammatory effects. Corticosteroids inhibit recruitment of neutrophils and monocytes (76) and inhibit neutrophil adherence to capillary endothelial cells by decreasing expression of adhesion molecules and the synthesis and release of prostaglandins (77, 78). It is therefore very likely that corticosteroid treatment has affected the cell counts used in this study. As nearly all patient received corticosteroid treatment, it is not possible to control for this effect in our multivariate regression models. Additional studies will be needed to confirm the findings described herein in SAH subjects not treated with corticosteroids.

In addition to the effect of corticosteroids, this study has several other important limitations. This is a single center study, which limits its generalizability. This study is also retrospective, and it is therefore prone to selection bias. Given that multiple comparisons among cell types and across different days were made, there is a risk of type I error. We have adjusted *P*-values considered to be significant in univariate analyses for cell counts for multiple comparisons using a Bonferroni correction to mitigate this risk. We attempt to explore the pathophysiological basis for the connection between leukocytes and outcomes, however our study is limited to clinically available differentials. Subtypes of each leukocyte may play distinct roles (e.g., lymphocyte subtypes may be beneficial or harmful). Future flow cytometry studies will be used to answer questions about specific cell types. Several variables of interest in the study require qualitative assessment such as GCE, mFS, and DCI. We attempt to control for any variability and subjectivity by having all variables adjudicated by multiple reviewers.

This study determined the time course of peripheral leukocyte responses after SAH. We found that monocytes were associated with DCI and poor functional outcome, in a sex dependent fashion. Monocytes were elevated in men compared to women. In men, monocyte counts predicted the occurrence of DCI, while in women monocyte counts were associated with infection. Both neutrophil count and NLR were associated with worse outcomes. We suspect increased NLR (reflective of increased neutrophils and decreased lymphocytes) results in an immunosuppressive environment that contributes to infection risk, and this plays a role in outcomes. We suggest that monocytes (especially in males) play a key role in driving systemic and central inflammation after SAH, while neutrophils and NLR affect outcomes by modulating infection risk. Monocyte count may help to predict DCI and outcomes after DCI and may serve as a target for therapeutic intervention.

DATA AVAILABILITY STATEMENT

The data supporting the conclusions of this article will be made available by the authors upon reasonable request.

ETHICS STATEMENT

The studies involving human participants were reviewed and approved by University of Texas McGovern School of Medicine Institutional Review Board. The patients/participants provided their written informed consent to participate in this study.

AUTHOR CONTRIBUTIONS

AG designed the study, acquired and analyzed data, and drafted the article. JS analyzed data and helped to draft the article. ES acquired and analyzed data and helped to draft the article. AP

acquired data and revised the article. AA acquired data and revised the article. S-BK contributed to study design and revised the article. LM contributed to study design and revised the article. HC contributed to study designed, analyzed data, and critically revised the article. All authors contributed to the article and approved the submitted version.

FUNDING

This study was supported by institutional startup funds from the Department of Neurosurgery at the University of Texas Health Science Center. Dr. McCullough is supported by funding from the National Institutes of Health and American Heart Association outside of the scope of this study.

ACKNOWLEDGMENTS

We are very grateful to all patients whose data were used in this study.

SUPPLEMENTARY MATERIAL

The Supplementary Material for this article can be found online at: https://www.frontiersin.org/articles/10.3389/fneur.2021.694996/full#supplementary-material

REFERENCES

1. Rinkel GJE, Algra A. Long-term outcomes of patients with aneurysmal subarachnoid haemorrhage. *Lancet Neurol.* (2011) 10:349–56. doi: 10.1016/S1474-4422(11)70017-5
2. Macdonald RL. Delayed neurological deterioration after subarachnoid hemorrhage. *Nat Rev Neurol.* (2014) 10:44–58. doi: 10.1038/nrneurol.2013.246
3. Eagles ME, Tso MK, Macdonald RL. Cognitive impairment, functional outcome, and delayed cerebral ischemia after aneurysmal subarachnoid hemorrhage. *World Neurosurg.* (2019) 124:e558–62. doi: 10.1016/j.wneu.2018.12.152
4. Qureshi AI, Mendelow AD, Hanley DF. Intracerebral haemorrhage. *Lancet*. (2009) 373:1632–44. doi: 10.1016/S0140-6736(09)60371-8
5. Lucke-Wold BP, Logsdon AF, Manoranjan B, Turner RC, McConnell E, Vates GE, et al. Aneurysmal subarachnoid hemorrhage and neuroinflammation: a comprehensive review. *Int J Mol Sci.* (2016) 17:1–17. doi: 10.3390/ijms17040497
6. Mocco J, Ransom ER, Komotar RJ, Schmidt JM, Sciacca RR, Mayer SA, et al. Preoperative prediction of long-term outcome in poor-grade aneurysmal subarachnoid hemorrhage. *Neurosurgery*. (2006) 59:529–38. doi: 10.1227/01.NEU.0000228680.22550.A2
7. Claassen J, Carhuapoma JR, Kreiter KT, Du EY, Connolly ES, Mayer SA. Global cerebral edema after subarachnoid hemorrhage: frequency, predictors, and impact on outcome. *Stroke*. (2002) 33:1225–32. doi: 10.1161/01.STR.0000015624.29071.1F
8. Provencio JJ. Inflammation in subarachnoid hemorrhage and delayed deterioration associated with vasospasm: a review. *Acta Neurochir Suppl.* (2013) 115:233–8. doi: 10.1007/978-3-7091-1192-5_42
9. Budohoski KP, Czosnyka M, Kirkpatrick PJ, Smielewski P, Steiner LA, Pickard JD. Clinical relevance of cerebral autoregulation following subarachnoid haemorrhage. *Nat Rev Neurol.* (2013) 9:152–63. doi: 10.1038/nrneurol.2013.11
10. Dickens AM, Tovar-y-Romo LB, Yoo S-W, Trout AL, Bae M, Kanmogne M, et al. Astrocyte-shed extracellular vesicles regulate the peripheral leukocyte response to inflammatory brain lesions. *Sci Signal*. (2017) 10:eaai7696. doi: 10.1126/scisignal.aai7696
11. Savarraj JPJ, Parsha K, Hergenroeder GW, Zhu L, Bajgur SS, Ahn S, et al. Systematic model of peripheral inflammation after subarachnoid hemorrhage. *Neurology*. (2017) 88:1535–45. doi: 10.1212/WNL.0000000000003842
12. Ahn SH, Savarraj JPJ, Parsha K, Hergenroeder GW, Chang TR, Kim DH, et al. Inflammation in delayed ischemia and functional outcomes after subarachnoid hemorrhage. *J Neuroinflammation.* (2019) 16:1–10. doi: 10.1186/s12974-019-1578-1
13. Schneider UC, Schiffler J, Hakiy N, Horn P, Vajkoczy P. Functional analysis of Pro-inflammatory properties within the cerebrospinal fluid after subarachnoid hemorrhage *in vivo* and *in vitro*. *J Neuroinflammation*. (2012) 9:28. doi: 10.1186/1742-2094-9-28
14. Friedrich V, Flores R, Muller A, Bi W, Peerschke EI, Sehba FA. Reduction of neutrophil activity decreases early microvascular injury after subarachnoid haemorrhage. *J Neuroinflammation.* (2011) 8:103. doi: 10.1186/1742-2094-8-103
15. Mracsko E, Veltkamp R. Neuroinflammation after intracerebral hemorrhage. *Front Neurosci.* (2014) 8:388. doi: 10.3389/fncel.2014.00388
16. Srinivasan A, Aggarwal A, Gaudihalli S, Mohanty M, Dhandapani M, Singh H, et al. Impact of early leukocytosis and elevated high-sensitivity C-reactive protein on delayed cerebral ischemia and neurologic outcome after subarachnoid hemorrhage. *World Neurosurg.* (2016) 90:91–5. doi: 10.1016/j.wneu.2016.02.049
17. Chamling B, Gross S, Stoffel-Wagner B, Schubert GA, Clusmann H, Coburn M, et al. Early Diagnosis of delayed cerebral ischemia: possible relevance for inflammatory biomarkers in routine clinical practice? *World Neurosurg.* (2017) 104:152–7. doi: 10.1016/j.wneu.2017.05.021
18. Walsh KB, Sekar P, Langefeld CD, Moomaw CJ, Elkind MSV, Boehme AK, et al. Monocyte count and 30-day case fatality in intracerebral hemorrhage. *Stroke*. (2015) STROKEAHA.115.009880. doi: 10.1161/STROKEAHA.115.009880
19. Zhang F, Ren Y, Fu W, Yang Z, Wen D, Hu X, et al. Predictive accuracy of neutrophil-to-lymphocyte ratio on long-term outcome in patients with spontaneous intracerebral hemorrhage. *World Neurosurg.* (2019) 125:e651–7. doi: 10.1016/j.wneu.2019.01.143
20. Lattanzi S, Cagnetti C, Provinciali L, Silvestrini M. Neutrophil-to-lymphocyte ratio and neurological deterioration following acute cerebral hemorrhage. *Oncotarget*. (2017) 8:57489–94. doi: 10.18632/oncotarget.15423
21. Wang F, Hu S, Ding Y, Ju X, Wang L, Lu Q, et al. Neutrophil-to-lymphocyte ratio and 30-day mortality in patients with acute intracerebral hemorrhage. *J Stroke Cerebrovasc Dis.* (2016) 25:182–7. doi: 10.1016/j.jstrokecerebrovasdis.2015.09.013
22. Bacigaluppi S, Ivaldi F, Bragazzi NL, Benvenuto F, Gallo F, D'Andrea A, et al. An early increase of blood leukocyte subsets in aneurysmal subarachnoid hemorrhage is predictive of vasospasm. *Front Neurol.* (2020) 11:587039. doi: 10.3389/fneur.2020.587039
23. Tao C, Wang J, Hu X, Ma J, Li H, You C. Clinical value of neutrophil to lymphocyte and platelet to lymphocyte ratio after aneurysmal subarachnoid hemorrhage. *Neurocrit Care*. (2017) 26:393–401. doi: 10.1007/s12028-016-0332-0
24. Jamali SA, Turnbull MT, Kanekiyo T, Vishnu P, Zubair AC, Raper CC, et al. Elevated neutrophil-lymphocyte ratio is predictive of poor outcomes following aneurysmal subarachnoid hemorrhage. *J Stroke Cerebrovasc Dis.* (2020) 29:104631. doi: 10.1016/j.jstrokecerebrovasdis.2019.104631
25. Al-Mufti F, Amuluru K, Damodara N, Dodson V, Roh D, Agarwal S, et al. Admission neutrophil-lymphocyte ratio predicts delayed cerebral ischemia following aneurysmal subarachnoid hemorrhage. *J Neurointerv Surg.* (2019) 11:1135–40. doi: 10.1136/neurintsurg-2019-014759
26. Giede-Jeppe A, Reichl J, Sprügel MI, Lücking H, Hoelter P, Eyüpoglu IY, et al. Neutrophil-to-lymphocyte ratio as an independent predictor for unfavorable functional outcome in aneurysmal subarachnoid hemorrhage. *J Neurosurg.* (2019) 132:400–7. doi: 10.3171/2018.9.JNS181975

27. Unda SR, Birnbaum J, Labagnara K, Wong M, Vaishnav DP, Altschul DJ. Peripheral monocytosis at admission to predict cerebral infarct and poor functional outcomes in subarachnoid hemorrhage patients. *World Neurosurg*. (2020) 138:e523–9. doi: 10.1016/j.wneu.2020.02.170
28. Mensing LA, Vergouwen MDI, Laban KG, Ruigrok YM, Velthuis BK, Algra A, et al. Perimesencephalic hemorrhage: a review of epidemiology, risk factors, presumed cause, clinical course, and outcome. *Stroke*. (2018) 49:1363–70. doi: 10.1161/STROKEAHA.117.019843
29. Hunt WE, Hess RM. Surgical risk as related to time of intervention in the repair of intracranial aneurysms. *J Neurosurg*. (1968) 28:14–20. doi: 10.3171/jns.1968.28.1.0014
30. Vergouwen MDI, Vermeulen M, van Gijn J, Rinkel GJE, Wijdicks EF, Muizelaar JP, et al. Definition of delayed cerebral ischemia after aneurysmal subarachnoid hemorrhage as an outcome event in clinical trials and observational studies: proposal of a multidisciplinary research group. *Stroke*. (2010) 41:2391–5. doi: 10.1161/STROKEAHA.110.589275
31. Kumar R, Geuna E, Michalarea V, Guardascione M, Naumann U, Lorente D, et al. The neutrophil-lymphocyte ratio and its utilisation for the management of cancer patients in early clinical trials. *Br J Cancer*. (2015) 112:1157–65. doi: 10.1038/bjc.2015.67
32. Gao L, Lu Q, Huang L-J, Ruan L-H, Yang J-J, Huang W-L, et al. Transplanted neural stem cells modulate regulatory T, γδ T cells and corresponding cytokines after intracerebral hemorrhage in rats. *Int J Mol Sci*. (2014) 15:4431–41. doi: 10.3390/ijms15034431
33. Askenase MH, Sansing LH. Stages of the inflammatory response in pathology and tissue repair after intracerebral hemorrhage. *Semin Neurol*. (2016) 36:288–97. doi: 10.1055/s-0036-1582132
34. Guo H, Zhao Z, Zhang R, Chen P, Zhang X, Cheng F, et al. Monocytes in the peripheral clearance of amyloid-β and alzheimer's disease. *J Alzheimers Dis*. (2019) 68:1391–400. doi: 10.3233/JAD-181177
35. Morotti A, Phuah C-L, Anderson CD, Jessel MJ, Schwab K, Ayres AM, et al. Leukocyte count and intracerebral hemorrhage expansion. *Stroke*. (2016) 47:1473–8. doi: 10.1161/STROKEAHA.116.013176
36. McCachren SS, Diggs J, Weinberg JB, Dittman WA. Thrombomodulin expression by human blood monocytes and by human synovial tissue lining macrophages. *Blood*. (1991) 78:3128–32. doi: 10.1182/blood.V78.12.3128.3128
37. Pou J, Rebollo A, Piera L, Merlos M, Roglans N, Laguna JC, et al. Tissue factor pathway inhibitor 2 is induced by thrombin in human macrophages. *Biochim Biophys Acta*. (2011) 1813:1254–60. doi: 10.1016/j.bbamcr.2011.03.020
38. Yao Y, Tsirka SE. The CCL2-CCR2 system affects the progression and clearance of intracerebral hemorrhage. *Glia*. (2012) 60:908–18. doi: 10.1002/glia.22323
39. Sansing LH, Harris TH, Welsh FA, Kasner SE, Hunter CA, Kariko K. Toll-like receptor 4 contributes to poor outcome after intracerebral hemorrhage. *Ann Neurol*. (2011) 70:646–56. doi: 10.1002/ana.22528
40. Jayaraj RL, Azimullah S, Beiram R, Jalal FY, Rosenberg GA. Neuroinflammation: friend and foe for ischemic stroke. *J Neuroinflammation*. (2019) 16:142. doi: 10.1186/s12974-019-1516-2
41. Varvel NH, Neher JJ, Bosch A, Wang W, Ransohoff RM, Miller RJ, et al. Infiltrating monocytes promote brain inflammation and exacerbate neuronal damage after status epilepticus. *Proc Natl Acad Sci USA*. (2016) 113:E5665–74. doi: 10.1073/pnas.1604263113
42. Fani Maleki A, Rivest S. Innate immune cells: monocytes, monocyte-derived macrophages and microglia as therapeutic targets for alzheimer's disease and multiple sclerosis. *Front Cell Neurosci*. (2019) 13:355. doi: 10.3389/fncel.2019.00355
43. Gris T, Laplante P, Thebault P, Cayrol R, Najjar A, Joannette-Pilon B, et al. Innate immunity activation in the early brain injury period following subarachnoid hemorrhage. *J Neuroinflammation*. (2019) 16:253. doi: 10.1186/s12974-019-1629-7
44. Jackson CM, Choi J, Routkevitch D, Pant A, Saleh L, Ye X, et al. PD-1+ monocytes mediate cerebral vasospasm following subarachnoid hemorrhage. *Neurosurgery*. (2020) 88:855–63. doi: 10.1093/neuros/nyaa495
45. Chen Y, Zhang Y, Zhao G, Chen C, Yang P, Ye S, et al. Difference in leukocyte composition between women before and after menopausal age, and distinct sexual dimorphism. *PLoS ONE*. 11:e0162953. doi: 10.1371/journal.pone.0162953
46. Lefèvre N, Corazza F, Duchateau J, Desir J, Casimir G. Sex differences in inflammatory cytokines and CD99 expression following *in vitro* lipopolysaccharide stimulation. *Shock*. (2012) 38:37–42. doi: 10.1097/SHK.0b013e3182571e46
47. Imahara SD, Jelacic S, Junker CE, O'Keefe GE. The influence of gender on human innate immunity. *Surgery*. (2005) 138:275–82. doi: 10.1016/j.surg.2005.03.020
48. Beenakker KGM, Westendorp RGJ, de Craen AJM, Chen S, Raz Y, Ballieux BEPB, et al. Men have a stronger monocyte-derived cytokine production response upon stimulation with the gram-negative stimulus lipopolysaccharide than women: a pooled analysis including 15 study populations. *J Innate Immun*. (2020) 12:142–53. doi: 10.1159/000499840
49. Keselman A, Fang X, White PB, Heller NM. Estrogen signaling contributes to sex differences in macrophage polarization during asthma. *J Immunol*. (2017) 199:1573–83. doi: 10.4049/jimmunol.1601975
50. el-Hag A, Clark RA. Immunosuppression by activated human neutrophils. Dependence on the myeloperoxidase system. *J Immunol*. (1987) 139:2406–13.
51. Tokgoz S, Kayrak M, Akpinar Z, Seyithanoglu A, Güney F, Yürüten B. Neutrophil lymphocyte ratio as a predictor of stroke. *J Stroke Cerebrovasc Dis*. (2013) 22:1169–74. doi: 10.1016/j.jstrokecerebrovasdis.2013.01.011
52. Núñez J, Núñez E, Bodí V, Sanchis J, Miñana G, Mainar L, et al. Usefulness of the neutrophil to lymphocyte ratio in predicting long-term mortality in ST segment elevation myocardial infarction. *Am J Cardiol*. (2008) 101:747–52. doi: 10.1016/j.amjcard.2007.11.004
53. Cho KH, Jeong MH, Ahmed K, Hachinohe D, Choi HS, Chang SY, et al. Value of early risk stratification using hemoglobin level and neutrophil-to-lymphocyte ratio in patients with ST-elevation myocardial infarction undergoing primary percutaneous coronary intervention. *Am J Cardiol*. (2011) 107:849–56. doi: 10.1016/j.amjcard.2010.10.067
54. Akpek M, Kaya MG, Lam YY, Sahin O, Elcik D, Celik T, et al. Relation of neutrophil/lymphocyte ratio to coronary flow to in-hospital major adverse cardiac events in patients with ST-elevated myocardial infarction undergoing primary coronary intervention. *Am J Cardiol*. (2012) 110:621–7. doi: 10.1016/j.amjcard.2012.04.041
55. Rehman FU, Khan A, Aziz A, Iqbal M, Mahmood SBZ, Ali N. Neutrophils to lymphocyte ratio: earliest and efficacious markers of sepsis. *Cureus*. (2020) 12:e10851. doi: 10.7759/cureus.10851
56. Marik PE, Stephenson E. The ability of procalcitonin, lactate, white blood cell count and neutrophil-lymphocyte count ratio to predict blood stream infection. Analysis of a large database. *J Crit Care*. (2020) 60:135–9. doi: 10.1016/j.jcrc.2020.07.026
57. Yang XM, Chen XH, Lu JF, Zhou CM, Han JY, Chen CH. *In vivo* observation of cerebral microcirculation after experimental subarachnoid hemorrhage in mice. *Neural Regen Res*. (2018) 13:456–62. doi: 10.4103/1673-5374.228728
58. Gaut JP, Yeh GC, Tran HD, Byun J, Henderson JP, Richter GM, et al. Neutrophils employ the myeloperoxidase system to generate antimicrobial brominating and chlorinating oxidants during sepsis. *Proc Natl Acad Sci USA*. (2001) 98:11961–6. doi: 10.1073/pnas.211190298
59. Bauer J, Ripperger A, Frantz S, Ergün S, Schwedhelm E, Benndorf RA. Pathophysiology of isoprostanes in the cardiovascular system: implications of isoprostane-mediated thromboxane A2 receptor activation. *Br J Pharmacol*. (2014) 171:3115–31. doi: 10.1111/bph.12677
60. Lahaie I, Hardy P, Hou X, Hasséssian H, Asselin P, Lachapelle P, et al. A novel mechanism for vasoconstrictor action of 8-isoprostaglandin F2 alpha on retinal vessels. *Am J Physiol*. (1998) 274:R1406–16. doi: 10.1152/ajpregu.1998.274.5.R1406
61. Neulen A, Pantel T, Kosterhon M, Kramer A, Kunath S, Petermeyer M, et al. Neutrophils mediate early cerebral cortical hypoperfusion in a murine model of subarachnoid haemorrhage. *Sci Rep*. (2019) 9:9460. doi: 10.1038/s41598-019-44906-9
62. Da Silva IRF, Gomes JA, Wachsman A, de Freitas GR, Provencio JJ. Hematologic counts as predictors of delayed cerebral ischemia after aneurysmal subarachnoid hemorrhage. *J Crit Care*. (2017) 37:126–9. doi: 10.1016/j.jcrc.2016.09.011
63. Al-Mufti F, Misiolek KA, Roh D, Alawi A, Bauerschmidt A, Park S, et al. White blood cell count improves prediction of delayed cerebral ischemia following aneurysmal subarachnoid hemorrhage. *Neurosurgery*. (2019) 84:397–403. doi: 10.1093/neuros/nyy045

64. Kubota T, Handa Y, Tsuchida A, Kaneko M, Kobayashi H, Kubota T. The kinetics of lymphocyte subsets and macrophages in subarachnoid space after subarachnoid hemorrhage in rats. *Stroke*. (1993) 24:1993–2000. doi: 10.1161/01.STR.24.12.1993
65. Chen Y, Lian B-Q, Peng L, Ding C-Y, Lin Y-X, Yu L-H, et al. Neutrophil to lymphocyte ratio is a prognosis factor for post-operative pneumonia in aneurysmal subarachnoid hemorrhage patients. *Chin Med J*. (2020) 9:8460. doi: 10.1097/CM9.0000000000001304
66. Zhao Y, Rahmy S, Liu Z, Zhang C, Lu X. Rational targeting of immunosuppressive neutrophils in cancer. *Pharmacol Ther*. (2020) 212:107556. doi: 10.1016/j.pharmthera.2020.107556
67. Loftspring MC, Mcdole J, Lu A, Clark JF, Johnson AJ. Intracerebral hemorrhage leads to infiltration of several leukocyte populations with concomitant pathophysiological changes. *J Cereb Blood Flow Metab*. (2009) 29:137–43. doi: 10.1038/jcbfm.2008.114
68. Mracsko E, Javidi E, Na SY, Kahn A, Liesz A, Veltkamp R. Leukocyte invasion of the brain after experimental intracerebral hemorrhage in mice. *Stroke*. (2014) 45:2107–14. doi: 10.1161/STROKEAHA.114.005801
69. Lee MC, Heaney LM, Jacobson RL, Klassen AC. Cerebrospinal fluid in cerebral hemorrhage and infarction. *Stroke*. (1975) 6:638–41. doi: 10.1161/01.STR.6.6.638
70. Iadecola C, Anrather J. The immunology of stroke: from mechanisms to translation. *Nat Med*. (2011) 17:796–808. doi: 10.1038/nm.2399
71. Shichita T, Sugiyama Y, Ooboshi H, Sugimori H, Nakagawa R, Takada I, et al. Pivotal role of cerebral interleukin-17-producing T cells in the delayed phase of ischemic brain injury. *Nat Med*. (2009) 15:946–50. doi: 10.1038/nm.1999
72. Chamorro Á, Meisel A, Planas AM, Urra X, van de Beek D, Veltkamp R. The immunology of acute stroke. *Nat Rev Neurol*. (2012) 8:401–10. doi: 10.1038/nrneurol.2012.98
73. Ooboshi H, Ibayashi S, Shichita T, Kumai Y, Takada J, Ago T, et al. Postischemic gene transfer of interleukin-10 protects against both focal and global brain ischemia. *Circulation*. (2005) 111:913–9. doi: 10.1161/01.CIR.0000155622.68580.DC
74. Benakis C, Brea D, Caballero S, Faraco G, Moore J, Murphy M, et al. Commensal microbiota affects ischemic stroke outcome by regulating intestinal γδ T cells. *Nat Med*. (2016) 22:516–23. doi: 10.1038/nm.4068
75. Schwartzman RA, Cidlowski JA. Glucocorticoid-induced apoptosis of lymphoid cells. *Int Arch Allergy Immunol*. (1994) 105:347–54. doi: 10.1159/000236781
76. Parrillo JE, Fauci AS. Mechanisms of glucocorticoid action on immune processes. *Annu Rev Pharmacol Toxicol*. (1979) 19:179–201. doi: 10.1146/annurev.pa.19.040179.001143
77. Balow JE, Rosenthal AS. Glucocorticoid suppression of macrophage migration inhibitory factor. *J Exp Med*. (1973) 137:1031–41. doi: 10.1084/jem.137.4.1031
78. Granelli-Piperno A, Vassalli JD, Reich E. Secretion of plasminogen activator by human polymorphonuclear leukocytes. Modulation by glucocorticoids and other effectors. *J Exp Med*. (1977) 146:1693–706. doi: 10.1084/jem.146.6.1693

Conflict of Interest: The authors declare that the research was conducted in the absence of any commercial or financial relationships that could be construed as a potential conflict of interest.

Publisher's Note: All claims expressed in this article are solely those of the authors and do not necessarily represent those of their affiliated organizations, or those of the publisher, the editors and the reviewers. Any product that may be evaluated in this article, or claim that may be made by its manufacturer, is not guaranteed or endorsed by the publisher.

frontiers in Neurology

STUDY PROTOCOL
published: 04 August 2021
doi: 10.3389/fneur.2021.693330

Rapid Intravenous Glyceryl Trinitrate in Ischemic Damage (RIGID) After Stroke: Rationale, Design and Protocol for a Prospective Randomized Controlled Trial

Lipeng Cai[1], Gary Rajah[2], Honglian Duan[1], Jie Gao[1], Zhe Cheng[1], Ruiqiang Xin[3], Shangqian Jiang[1,4], Peter Palmer[5], Xiaokun Geng[1,4,6] and Yuchuan Ding[6]**

[1] Department of Neurology, Beijing Luhe Hospital, Capital Medical University, Beijing, China, [2] Department of Neurosurgery, Munson Medical Center, Traverse City, MI, United States, [3] Department of Medical Imaging, Luhe Hospital, Capital Medical University, Beijing, China, [4] Department of China-America Institute of Neuroscience, Beijing Luhe Hospital, Capital Medical University, Beijing, China, [5] Department of Neurology, Northeast Ohio Medical University, Rootstown, OH, United States, [6] Department of Neurosurgery, Wayne State University School of Medicine, Detroit, MI, United States

OPEN ACCESS

Edited by:
Qin Hu,
Shanghai Jiao Tong University, China

Reviewed by:
Hailiang Tang,
Fudan University, China
Felix Ng,
University of Melbourne, Australia

***Correspondence:**
Xiaokun Geng
xgeng@ccmu.edu.cn
Yuchuan Ding
yding@med.wayne.edu

Specialty section:
This article was submitted to Stroke, a section of the journal Frontiers in Neurology

Received: 10 April 2021
Accepted: 29 June 2021
Published: 04 August 2021

Citation:
Cai L, Rajah G, Duan H, Gao J, Cheng Z, Xin R, Jiang S, Palmer P, Geng X and Ding Y (2021) Rapid Intravenous Glyceryl Trinitrate in Ischemic Damage (RIGID) After Stroke: Rationale, Design and Protocol for a Prospective Randomized Controlled Trial. Front. Neurol. 12:693330. doi: 10.3389/fneur.2021.693330

Background: Despite intravenous thrombolysis and endovascular therapy for acute ischemic stroke (AIS), many survivors still have varying degrees of disability. Glyceryl trinitrate (GTN), a nitric oxide (NO) donor, has been previously reported to induce neuroprotection after AIS. The use of GTN to reduce brain damage after stroke remains yet to be elucidated. This study was designed to explore the safety, feasibility, and preliminary efficacy of intravenous administration of GTN after AIS.

Methods: A prospective randomized controlled trial is proposed with AIS patients. Participants will be randomly allocated to GTN group and control group with a 1:1 ratio ($n = 40$). Both groups will be treated with standard therapies according to the current stroke guidelines. Participants allocated to the GTN group will receive intravenous administration of GTN (5 mg GTN in 50 ml saline at a rate of 0.4 mg/h that is continued for 12.5 h/day for 2 days) within 24 h of symptom onset. Participants allocated to the control group will receive intravenous administration at equal capacity of 0.9% normal saline (NS) (total 50 ml/day at 4 ml/h that is continued for 12.5 h/day for 2 days). The primary outcome is safety [systolic blood pressure (SBP) <110 mmHg, headache], while the secondary outcomes include changes in functional outcome and infarction volume.

Discussion: Rapid Intravenous Glyceryl Trinitrate in Ischemic Damage (RIGID) is a prospective randomized controlled trial that aims to ascertain the safety, feasibility, and preliminary efficacy of intravenous GTN as a neuroprotection strategy after AIS. These results will provide parameters for future studies as well as provide insights into treatment effects. Any possible neuroprotective qualities of GTN in AIS will also be elucidated.

Trial Registration: www.chictr.org.cn, identifier: ChiCTR2100046271.

Keywords: acute ischemic stroke, neuroprotection, nitric oxide, glyceryl trinitrate (GTN), intravenous thrombolysis

INTRODUCTION

Due to its high rate of mortality and morbidity, ischemic stroke is a devastating public health concern that also results in high socioeconomic burden (1–4). The effective treatments for acute ischemic stroke (AIS) are intravenous thrombolysis and mechanical thrombectomy. Due to the narrow time window for intravenous alteplase [tissue plasminogen activator (tPA)] of 4.5 h, the majority of patients are not eligible for this treatment. In addition, two-thirds of stroke patients still suffer from varying degrees of disability (5, 6) even after intravenous thrombolysis. Endovascular therapy (within 6 h of stroke and up to 24 h) has shown great benefit in improving functional outcomes in AIS patients with large vessel occluded (LVO) in the anterior circulation. However, only 46% of the patients achieve functional independence at 90 days with a 15.3% mortality rate (7). In the EXTEND trial (8), patients benefited from tPA between 4.5 and 9.0 h after the onset of stroke. This study suggested that the "tissue window" has advantages over the traditional "time window" in screening patients. Thus, exploring fast and effective neuroprotection strategies to save ischemic penumbra and to lengthen the "tissue window" may be the key in the treatment of AIS.

Ischemic stroke-induced brain damage results from the interaction of complex pathophysiological processes such as excitotoxicity, oxidative stress, inflammation, and apoptosis (9). NO has a central role in hypoxic signaling, and its physiologic and therapeutic levels exert potent cytoprotection after ischemia and reperfusion in various tissues including the brain (10). NO derived from endothelial nitric oxide synthase (eNOS) plays a critical role in the regulation of cerebral microvascular tone, the protection of the blood–brain barrier, the reduction of oxidative stress, and the alleviation of procoagulant stimulation (11–13). Various animal studies have reliably demonstrated a loss of cytoprotection when subjects were treated with NO scavengers or when NOS was inhibited or knocked out (14–16). NO donors are a heterogeneous group of drugs whose common feature is the ability to release NO or an NO-related species *in vitro* or *in vivo* independently of endogenous sources (17). NO donors have been implicated in improving cancer therapy, hypertension, and peripheral artery disease (17). Several preclinical studies suggest that NO donors could safely reduce infarct size, increase cerebral blood flow, and improve functional outcome in AIS in both transient and permanent stroke models (18). The neuroprotective effect of NO donors has been previously demonstrated to work at many different levels by several mechanisms including that of altering the cellular oxidative status, inhibiting monocyte activity, and diminishing primary hemostasis (19).

GTN, a Food and Drug Administration-approved vasodilator, is an example of a drug that functions as a NO donor. Transdermal GTN had been found to lower blood pressure (BP), have no deleterious effects on platelet function, and exert no changes in the middle cerebral artery blood flow velocity or regional cerebral blood flow in AIS patients (20–23). A recent larger sample size randomized controlled trial (RCT) to determine the efficacy of transdermal GTN for the management of high BP in AIS (ENOS) also revealed the potential to reduce BP without finding a functional improvement following AIS if administered within 48 h (24). However, this study indicated that administration of GTN within 6 h improved functional outcomes. The RIGHT-2 trial (25) focused on the safety and efficacy of transdermal GTN given within 4 h of onset of AIS assessed in the prehospital environment in the UK. This trial did not show that prehospital treatment with transdermal GTN improved functional outcomes in patients with presumed stroke. Importantly, the neuroprotective effect of NO donors after ischemia–reperfusion injury (IRI) has yet to be reported consistently with many factors contributing to this including dose, location, source, and environment (26). Further protocols have been proposed to evaluate the use of transdermal GTN in acute stroke treatment (26). In light of these parameters and owing to the short half-life of GTN, GTN administration as a patch on the arm or chest may not reach an effective concentration in the cerebrovascular system. As such, a continuous intravenous administration of GTN may be a rapid and effective way to maximize any benefit of this drug (26). Furthermore, 24-h continuous GTN administration can cause tolerance resulting in subtherapeutic levels. This knowledge hints that a better outcome may be possible if an "intermittent" therapy is used (27–29). At present, no study has been reported on the safety and efficacy of intravenous GTN as an adjuvant neuroprotective strategy for AIS. We have consequently designed this single-center, prospective RCT to evaluate the safety, feasibility, and preliminary efficacy of intravenous administration of GTN after AIS.

METHODS

Study Design

This study is a phase 1, single-center, prospective RCT. Participants will be patients with AIS within 24 h onset. Patients meeting the inclusion criteria but not the exclusion criteria will be randomly allocated to the GTN group or the control group. Both groups will be treated with the standard management according to the guidelines (30). GTN will be administered by continuous intravenous pump (5 mg GTN in 50 ml saline with a speed of GTN 0.4 mg/h continued for 12.5 h/day for 2 days) within 24 h of symptom onset in the GTN group. The control group will receive intravenous administration of equal capacity of 0.9% normal saline (NS) (total 50 ml/day at 4 ml/h continued for 12.5 h/day for 2 days). The clinical characteristics, medical history (diabetes, hypertension, hyperlipidemia, coronary heart disease, stroke, atrial fibrillation), smoking history, alcohol drinking history, and National Institutes of Health Stroke Scale (NIHSS) score at admission will be collected. Magnetic resonance imaging (MRI) will be performed at baseline and on day 7 ± 1. NIHSS and modified Rankin Scale (mRS) will be assessed at baseline and on days 1, 7, 14, 30, and 90.

All participants or proxies will be informed of potential risks and possible benefits and consent to this study. This consent will be provided to a legal representative if the patients do not have the capacity to consent. This study was approved by the ethics committee of Luhe Hospital, Capital Medical University,

Beijing, China, and has been registered at www.chictr.org.cn with ChiCTR2100046271. An independent physician will monitor the health and safety of the participants.

Patient Population: Inclusion and Exclusion Criteria

Participants will be recruited from the stroke center [the Stroke Intervention & Translational Center (SITC)] in Beijing Luhe Hospital (**Figure 1**). The inclusion criteria are (1) ≥18 and ≤80 years old, (2) clinical diagnosis of AIS, (3) systolic blood pressure (SBP) ≥120 mmHg, (4) NIHSS score ≥3 and ≤16, (5) patients with time from onset to treatment ≤24 h who did not receive endovascular treatment (EVT), (6) prestroke mRS ≤2, and (7) informed consent provided by participant or legally authorized representative.

Exclusion criteria are as follows: (1) severe anemia, hemoglobin (HGB) 60 g/L, (2) allergy to GTN, (3) glaucoma, (4) participant in another ongoing clinical trial, and (5) life expectancy of shorter than 1 year due to comorbidities.

Randomization and Blindness

During the recruitment period, participants will be allocated 1:1 to two groups ($n = 40$) by computer-generated randomization procedures using opaque envelopes. A research assistant not involved in the study will prepare the envelopes before the study. After recording baseline measures, participants will be randomly allocated to either the intervention or the control group by the treating physicians, who will open the sealed opaque envelopes. In order to minimize selection bias, patients and assessors involved in the trial will be masked to the treatment allocation. All outcome measurements will be assessed by two observers who will be blinded to the treatment plan. Any disagreement will be resolved by reaching a consensus between the two. If no consensus can be reached, a third observer blinded to the treatment assignment and not involved in the clinical treatment plan will have the final decision. Finally, an independent investigator blinded to the treatment assignment will collect the data of outcomes and information of the group and analyze them.

Interventions

Participants in both groups will be treated with the standard management according to the guidelines (30). In order to ensure the stability of administration speed and the stability of BP, patients allocated to the GTN group will undergo intravenous administration of GTN (5 mg GTN in 50 ml saline, with a speed of GTN 0.4 mg/h continued for 12.5 h/day, for 2 days) within 24 h of symptom onset. In the control group, 0.9% NS will be administered by continuous intravenous pumping with a speed of 4 ml/h continued for 12.5 h/day, for 2 days. Since no standard intravenous dose of GTN is available for AIS, the doses and administration of intravenous GTN are determined by following considerations. First, according to routine dosage of intravenous GTN, 0.3 mg/h (up to 20 mg/h) is applied. Second, because of the dose-dependent reductions in SBP (31) by GTN, we will use the similar low dose at 0.4 mg/h for 12.5 h/day to prevent excessive reduction of systemic BP for safety purposes. In addition, compared with intravenous administration, studies (20, 21, 25, 32) have shown that transdermal GTN patches (at a 0.4 mg/h rate for 12.5 h during a single application), in which there are about 75% of nitroglycerin systemically bioavailable after administration (33), reduce SBP by 5.8–13 mmHg after AIS that is within the range in the present study. Vital signs (i.e., BP, heart rate, body temperature, respiratory rate of the patients) and possible adverse drug reactions such as hypotension and headache, will be closely monitored during the whole treatment period. If the patients show a tendency to develop adverse reactions and complications, the trial shall be immediately stopped, and routine treatment shall be given.

Outcomes

Primary Outcomes (Safety Assessment)

The primary safety outcome is SBP <110 mmHg. The primary outcome SBP <110 mmHg was defined as average SBP <110 mmHg within 24 h after GTN has been started. BP will be measured every 15 min between 0 and 2 h after GTN is started, every 30 min between 2 and 12 h, every 120 min between 12 and 48 h, and twice a day after 48 h. The target levels of BP poststroke remain unclear within the available literature (34–37). The current AIS guidelines differentiate BP targets based on a variety of factors including whether the patient receives alteplase, undergoes mechanical embolectomy, and/or experiences a hemorrhagic conversion. Prior studies (34–37) found a U-shaped relation of BP with functional outcome: both low BP and high BP were associated with poor outcome. There is no clearly defined cutoff for low BP in patients with AIS. Previously identified nadirs such as the tipping point in the U-shaped association between BP and outcome also vary between 120 and 180 mmHg (34, 36). Because of this variability, according to prior studies, we will use the lowest 10th percentile as a cutoff, low SBP, namely, SBP <110 mmHg.

The secondary safety outcomes are headache. Headaches related to GTN were defined as follows: GTN responders are those who develop a mild to moderate headache (headache scores 3–6) within 5–15 min with a short-lasting duration (maximum of 30 min) and spontaneously recover within 1 h after administration of GTN without the need for any rescue medication (38). In addition, severe headaches (scores 7–10) or the use of analgesia for GTN-caused headaches will be accounted for as secondary safety outcomes. If patients experience severe headaches, vital signs (i.e., BP, heart rate, body temperature, respiratory rate of the patients) will be closely monitored, and a CT scan will be obtained to analyze the cause of the headache.

Secondary Outcomes (Efficacy Assessment)

The primary efficacy outcome is the mRS at 90 days (mRS scores of 0–2 indicate functional independence). Secondary efficacy outcomes include the rate of the 0–2 mRS at 90 days, the incidence of death at 90 days, blood nitrate index detection at 1 day [cyclic guanosine monophosphate (cGMP, second messenger to NO), L-arginine (substrate for NO), and L-citrulline (co-product with NO)], infarct volume, as well as NIHSS scores at days 1, 7, 14, 30, and 90. The mRS and NIHSS scores will

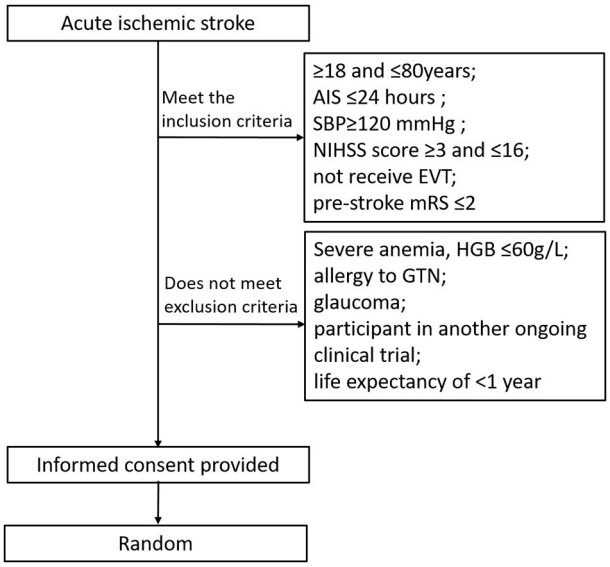

FIGURE 1 | Trial randomization flowchart. AIS, acute ischemic stroke; NIHSS, national institutes of health stroke scale; SBP, systolic blood pressure; mRS, modified rankin scale; GTN, glycerly trinitrate; HGB, hemoglobin.

be obtained by a blinded personnel to the research. Face-to-face encounters in the consultation room will be used in the study to calculate mRS and NIHSS. Brain infarct volume will be determined by MRI diffusion-weighted imaging technique. The lesion profile plotted at each individual level by an image tool [region of interest (ROI)] on the workstation will be used to calculate the area. The levels will be multiplied by the thickness of each level and summed to calculate the infarct volume. The calculations will be performed by personnel blinded to clinical data and randomization at baseline and at day 7 ± 1.

Patients diagnosed as AIS without corresponding lesions on MRI are rare (<2%) in our stroke center. Patients who are misdiagnosed with stroke through negative MRI will be reported, and subgroup analysis will be performed.

Estimation of Sample Size

There are no data available for reference because no completed clinical study of intravenous GTN in AIS patients currently exists. However, Hertzog (39) has suggested that 10–20 patients in each group are sufficient to assess the feasibility of a pilot study, while Dobkin (40) has shown that 15 patients in each group is usually enough to decide whether a larger multicenter trial should be conducted. In order to determine the sample size for each group, a power analysis was conducted based on the work of a prior study (20) that GTN can make a difference of 10 mmHg in SBP as compared to placebo groups. For the difference in BP at 10 mmHg, standard deviation at 10 mmHg, in order to have alpha exceed 95%, and beta = 0.8, a sample size of 16 patients per group has been calculated. As we expect to include around 20% for treatment dropouts and crossovers and for losses to follow-up, we will increase this sample size with 20% and aim to recruit 40 patients. The results of this study should be able to determine the initial safety and feasibility of intravenous infusion of GTN in AIS patients. The data will be used to estimate sample size and conduct a power calculation to plan a phase 2 trial for efficacy.

Statistical Analyses

All analyses are based on the intention-to-treat (ITT) principle, including all randomly enrolled subjects. Compared to the control group, if the GTN group did not have an increase in the incidence of adverse reactions and there was no difference in 90-day prognosis between the two groups, we would move forward with a phase 2 trial.

Categorical variables including the proportion of good functional outcomes and the frequency of adverse events will be presented as counts and percentages. χ^2 test, Fisher exact test, or continuity correction will be used where appropriate for comparison between the two groups. If the continuous variables including NIHSS score and infarct volume conform to the normal distribution, results shall be indicated by mean $\pm$ standard deviation and tested by *t*-test, and if they do not conform to the normal distribution, results shall be indicated by median and interquartile range and tested by Mann–Whitney *U*-test. $p < 0.05$ will be considered statistically significant. SPSS 22.0 software (IBM Inc., Armonk, NY) will be used for statistical analysis.

DISCUSSION

Over the past few decades, over 1,000 neuroprotective methods have been examined for adjunct neuroprotective administration in the setting of AIS (41). However, most neuroprotectants have only demonstrated benefit in animal stroke models without successful clinical transformation (42, 43). The cause of this failure was not immediately clear. One general conclusion would be that there is a low likelihood of success in targeting one pathway or one selective mechanism within a rather heterogeneous, nongenetically determined condition operative over many years (44). Ischemic stroke-induced brain injury results from the interaction of complex pathophysiological processes such as excitotoxicity, oxidative stress, inflammation, and apoptosis (9, 45–47). The post-ischemic cascade is a complex, multipathway, multifactorial process involving a variety of pathological mechanisms; therefore, multiple targets of neuroprotection drugs may be more effective.

NO is a ubiquitous molecule in the body, which plays a multitude of physiological actions such as a vasodilator, neurotransmitter, immunomodulator, and antagonist of platelets and leukocytes (48). In the brain, NO is mainly synthesized by various subtypes of NOSs: neuronal nitric oxide synthase (nNOS), eNOS, and inducible nitric oxide synthase (iNOS) (25). Previous studies demonstrate that organ injury can occur due to a reduction of NO, most commonly due to a reduction in eNOS activity during ischemia reperfusion injury (IRI) (49). In the setting of IRI, NO has been found to have various protective effects on inhibiting oxidative stress, leukocyte–endothelial adhesion, cytokine release, and apoptosis (50). NO can also reduce infarct size and inflammation after ischemic stroke and improve cerebral blood flow, cerebral metabolism, and nerve function in a preclinical study (51). A previous observational

study found that patients with ischemic stroke had significantly lower plasma NO levels than matched normal volunteers, and the low NO levels were associated with more severe stroke and worse outcome assessed at discharge disposition (52). A meta-analysis showed a significant association between different eNOS gene polymorphisms and risk of ischemic stroke in the Asian population (52).

NO plays a pivotal role in preventing inflammation and attenuating oxidative stress after IRI, and, therefore, NO supplementation using NO donor drugs is a reasonable approach to minimizing the cerebral damage after ischemia. GTN is one of the most widely used exogenous NO donors in the clinic. Three studies (20–22) on transdermal GTN in acute stroke showed that GTN lowered peripheral and central BP, 24-h BP, pulse pressure, and augmentation index. However, RCTs ENOS (53) and RIGHT-2 (25) on transdermal GTN patch (5 mg) showed that there was no significant change in functional or secondary outcomes measured at day 90. In a prespecified subgroup analysis of participants within 6 h of stroke presentation in the ENOS trial, those who received GTN had a favorable improvement in functional outcomes, less death and disability, and improved cognition (25). Transdermal GTN is a simple method to the delivery of GTN; however, not all of the drug released from the patch reaches the systemic circulation (54). Compared with intravenous administration, about 75% of nitroglycerin is systemically bioavailable after patch administration (55). The reason for lost drug is related to retention at the application site, tissue binding, and breakdown (33). The development of an intravenous form of nitroglycerin has further enhanced the role of nitrates in the therapy of cardiovascular disorders. Intravenous form of nitroglycerin permits prompt initiation of therapy and rapid attainment of high systemic levels (56). Although there is concern that lowering BP may worsen outcomes in the context of carotid stenosis, an analysis of the ENOS trial demonstrated that transdermal GTN appeared safe in both ipsilateral and bilateral stenoses (25). Considering that both GTN and NO (57) have a very short half-life in the body, an intravenous form of nitroglycerin with rapid dose titration is both feasible and safe. This may be the best method in a clinical trial for stroke patients to receive targeted cerebral NO donors. Prior clinical trials on the continuous application of nitroglycerin patches showed that 24-h continued use of GTN results in developing tolerance in the majority of patients with stable angina and suggested that "intermittent" therapy may provide a more rational approach to therapy. With removal of the patch for 10–12 h in each 24-h period, this will provide a patch-free period, which may allow the reestablishment of sensitivity (27–29). The daily dose at 5 mg/day [0.4 mg/h (54)] was recommended in the two important RCTs ENOS and RIGHT-2 on transdermal GTN patch (25, 58). In order to rescue the ischemic penumbra that infarct completed within 48 h after stroke onset (59), GTN at a speed of GTN 0.4 mg/h for 12.5 h/day, which makes 5 mg/day in total, was used in the present study, for 2 days. We will determine whether intravenous GTN is safe and has the potential to improve functional outcomes in patients with AIS.

There are limitations to this study. First, this is a single-center, small-sample experiment, which may affect the generalizability of the interventions. Second, although the target dosage has been shown to be safe and reliable in other small-cohort experiments, the dose used in the present study may still need optimization. In addition, there is a concern that an intravenous administration of an equal dosage of GTN might have more interactions given better bioavailability.

Rapid Intravenous Glyceryl Trinitrate in Ischemic Damage (RIGID) is designed to identify the safety, feasibility, and possible efficacy of intravenous administration of GTN in AIS patients. The preliminary results will provide clues for the design of future clinical trials. Based on past basic research and previous clinical studies, we predict that intravenous administration of GTN is safe for patients with AIS. The current proposed study may suggest a neuroprotective role for GTN in AIS and, thus, warrants an RCT.

ETHICS STATEMENT

The studies involving human participants were reviewed and approved by the Ethics Committee of Beijing Luhe Hospital, Capital Medical University, Beijing, China. The patients/participants provided their written informed consent to participate in this study.

AUTHOR CONTRIBUTIONS

YD and XG conceptualized the study and contributed to the study design and implementation. LC made substantial contributions to the design, implementation, and writing of the protocol. GR and PP contributed to the design of the trial from their area of expertise. HD, JG, ZC, RX, and SJ contributed to the implementation of specific procedures, conceptualized the study and contributed to the study design and implementation. All authors contributed to the article and approved the submitted version.

FUNDING

This work was supported by the National Nature Science Foundation of China (Nos. 21707095, 82072549, and 81871838).

REFERENCES

1. Wu S, Wu B, Liu M, Chen Z, Wang W, Anderson CS, et al. Stroke in china: advances and challenges in epidemiology, prevention, and management. *Lancet Neurol.* (2019) 18:394–405. doi: 10.1016/S1474-4422(18)30500-3
2. Stone CR, Geng X, Ding Y. From big data to battling disease: notes from the frontiers of cerebrovascular science. *Neurol Res.* (2019) 41:679–80. doi: 10.1080/01616412.2019.1603592
3. Stone C, Geng X, Ding Y. The pursuit of cures for cerebral disease persists, even through a pandemic. *Neurol Res.* (2020) 42:619–20. doi: 10.1080/01616412.2020.1778995

4. Zhao M, Guan L, Collet JP, Wang Y. Relationship between ischemic stroke locations, etiology subtypes, neurological outcomes, and autonomic cardiac function. *Neurol Res.* (2020) 42:630–9. doi: 10.1080/01616412.2020.1782103
5. Emberson J, Lees KR, Lyden P, Blackwell L, Albers G, Bluhmki E, et al. Effect of treatment delay, age, and stroke severity on the effects of intravenous thrombolysis with alteplase for acute ischaemic stroke: a meta-analysis of individual patient data from randomised trials. *Lancet.* (2014) 384:1929–35. doi: 10.1016/S0140-6736(14)60584-5
6. Leng T, Xiong ZG. Treatment for ischemic stroke: from thrombolysis to thrombectomy and remaining challenges. *Brain Circ.* (2019) 5:8–11. doi: 10.4103/bc.bc_36_18
7. Goyal M, Menon BK, van Zwam WH, Dippel DW, Mitchell PJ, Demchuk AM, et al. Endovascular thrombectomy after large-vessel ischaemic stroke: a meta-analysis of individual patient data from five randomised trials. *Lancet.* (2016) 387:1723–31. doi: 10.1016/S0140-6736(16)00163-X
8. Ma H, Parsons MW, Christensen S, Campbell BC, Churilov L, Connelly A, et al. A multicentre, randomized, double-blinded, placebo-controlled phase iii study to investigate extending the time for thrombolysis in emergency neurological deficits (extend). *Int J Stroke.* (2012) 7:74–80. doi: 10.1111/j.1747-4949.2011.00730.x
9. Khoshnam SE, Winlow W, Farzaneh M, Farbood Y, Moghaddam HF. Pathogenic mechanisms following ischemic stroke. *Neurol Sci.* (2017) 38:1167–86. doi: 10.1007/s10072-017-2938-1
10. Lundberg JO, Weitzberg E, Gladwin MT. The nitrate-nitrite-nitric oxide pathway in physiology and therapeutics. *Nat Rev Drug Discov.* (2008) 7:156–67. doi: 10.1038/nrd2466
11. Hossain M, Qadri SM, Liu L. Inhibition of nitric oxide synthesis enhances leukocyte rolling and adhesion in human microvasculature. *J Inflam.* (2012) 9:28. doi: 10.1186/1476-9255-9-28
12. Kuhlencordt PJ, Rosel E, Gerszten RE, Morales-Ruiz M, Dombkowski D, Atkinson WJ, et al. Role of endothelial nitric oxide synthase in endothelial activation: insights from enos knockout endothelial cells. *Am J Physiol Cell Physiol.* (2004) 286:C1195–1202. doi: 10.1152/ajpcell.00546.2002
13. Moore C, Sanz-Rosa D, Emerson M. Distinct role and location of the endothelial isoform of nitric oxide synthase in regulating platelet aggregation in males and females in vivo. *Eur J Pharmacol.* (2011) 651:152–8. doi: 10.1016/j.ejphar.2010.11.011
14. Jung KH, Chu K, Ko SY, Lee ST, Sinn DI, Park DK, et al. Early intravenous infusion of sodium nitrite protects brain against in vivo ischemia-reperfusion injury. *Stroke.* (2006) 37:2744–50. doi: 10.1161/01.STR.0000245116.40163.1c
15. Duranski MR, Greer JJ, Dejam A, Jaganmohan S, Hogg N, Langston W, et al. Cytoprotective effects of nitrite during in vivo ischemia-reperfusion of the heart and liver. *J Clin Invest.* (2005) 115:1232–40. doi: 10.1172/JCI22493
16. Webb A, Bond R, McLean P, Uppal R, Benjamin N, Ahluwalia A. Reduction of nitrite to nitric oxide during ischemia protects against myocardial ischemia-reperfusion damage. *Proc Natl Acad Sci USA.* (2004) 101:13683–8. doi: 10.1073/pnas.0402927101
17. Miller MR, Megson IL. Recent developments in nitric oxide donor drugs. *Br J Pharmacol.* (2007) 151:305–21. doi: 10.1038/sj.bjp.0707224
18. Willmot M, Gray L, Gibson C, Murphy S, Bath PM. A systematic review of nitric oxide donors and l-arginine in experimental stroke; effects on infarct size and cerebral blood flow. *Nitric Oxide Biol Chem.* (2005) 12:141–9. doi: 10.1016/j.niox.2005.01.003
19. Godinez-Rubi M, Rojas-Mayorquin AE, Ortuno-Sahagun D. Nitric oxide donors as neuroprotective agents after an ischemic stroke-related inflammatory reaction. *Oxid Med Cell Longev.* (2013) 2013:297357. doi: 10.1155/2013/297357
20. Bath PM, Pathansali R, Iddenden R, Bath FJ. The effect of transdermal glyceryl trinitrate, a nitric oxide donor, on blood pressure and platelet function in acute stroke. *Cerebrovasc Dis.* (2001) 11:265–72. doi: 10.1159/000047649
21. Rashid P, Weaver C, Leonardi-Bee J, Bath F, Fletcher S, Bath P. The effects of transdermal glyceryl trinitrate, a nitric oxide donor, on blood pressure, cerebral and cardiac hemodynamics, and plasma nitric oxide levels in acute stroke. *J Stroke Cerebrovasc Dis.* (2003) 12:143–51. doi: 10.1016/S1052-3057(03)00037-5
22. Willmot M, Ghadami A, Whysall B, Clarke W, Wardlaw J, Bath PM. Transdermal glyceryl trinitrate lowers blood pressure and maintains cerebral blood flow in recent stroke. *Hypertension.* (2006) 47:1209–15. doi: 10.1161/01.HYP.0000223024.02939.1e
23. Ankolekar S, Fuller M, Cross I, Renton C, Cox P, Sprigg N, et al. Feasibility of an ambulance-based stroke trial, and safety of glyceryl trinitrate in ultra-acute stroke: the rapid intervention with glyceryl trinitrate in hypertensive stroke trial (right, isrctn66434824). *Stroke.* (2013) 44:3120–8. doi: 10.1161/STROKEAHA.113.001301
24. Investigators ET. Efficacy of nitric oxide, with or without continuing antihypertensive treatment, for management of high blood pressure in acute stroke (enos): a partial-factorial randomised controlled trial. *Lancet.* (2015) 385:617–28. doi: 10.1016/S0140-6736(14)61121-1
25. Philip MB, Polly S, Craig SA, Jason PA, Evind B, Lesley C. Prehospital transdermal glyceryl trinitrate in patients with ultra-acute presumed stroke (right-2): An ambulance-based, randomised, sham-controlled, blinded, phase 3 trial. *Lancet.* (2019) 393:1009–20. doi: 10.1016/S0140-6736(19)30194-1
26. Maniskas ME, Roberts JM, Trueman R, Learoyd AE, Gorman A, Fraser JF, et al. Intra-arterial nitroglycerin as directed acute treatment in experimental ischemic stroke. *J Neurointervent Surg.* (2018) 10:29–33. doi: 10.1136/neurintsurg-2016-012793
27. Bergbauer M, Weber K. Haemodynamic studies with a phasic release nitroglycerin patch system. *Eur Heart J.* (1989) 10(Suppl. A):30–5. doi: 10.1093/eurheartj/10.suppl_A.30
28. Reiniger G, Menke G, Boertz A, Kraus F, Rudolph W. [interval therapy in effective treatment of angina pectoris using nitroglycerin patch systems. A controlled study with determination of nitroglycerin plasma levels]. *Herz.* (1987) 12:68–73.
29. Reiniger G, Rudolph W. [discontinuous drug release as an alternative to interval therapy in the treatment of coronary heart disease with nitroglycerin patches]. *Herz.* (1987) 12:348–53.
30. Powers WJ, Rabinstein AA, Ackerson T, Adeoye OM, Bambakidis NC, Becker K, et al. Guidelines for the early management of patients with acute ischemic stroke: 2019 update to the 2018 guidelines for the early management of acute ischemic stroke: a guideline for healthcare professionals from the american heart association/american stroke association. *Stroke.* (2019) 50:e344–418. doi: 10.1161/STR.0000000000000211
31. Persson MG, Agvald P, Gustafsson LE. Rapid tolerance to formation of authentic no from nitroglycerin in vivo. Agents and actions. *Supplements.* (1995) 45:213–7. doi: 10.1007/978-3-0348-7346-8_31
32. Gray LJ, Sprigg N, Rashid PA, Willmot MR, Bath PM. Effect of nitric oxide donors on blood pressure and pulse pressure in acute and subacute stroke. *J Stroke Cerebrovasc Dis.* (2006) 15:245–9. doi: 10.1016/j.jstrokecerebrovasdis.2006.06.002
33. Imhof PR, Vuillemin T, Gérardin A, Racine A, Müller P, Follath F. Studies of the bioavailability of nitroglycerin from a transdermal therapeutic system (nitroderm tts). *Eur J Clin Pharmacol.* (1984) 27:7–12. doi: 10.1007/BF02395198
34. Mulder M, Ergezen S, Lingsma HF, Berkhemer OA, Fransen PSS, Beumer D, et al. Baseline blood pressure effect on the benefit and safety of intra-arterial treatment in mr clean (multicenter randomized clinical trial of endovascular treatment of acute ischemic stroke in the netherlands). *Stroke.* (2017) 48:1869–76. doi: 10.1161/STROKEAHA.116.016225
35. Verschoof MA, Groot AE, Vermeij JD, Westendorp WF, van den Berg SA, Nederkoorn PJ, et al. Association between low blood pressure and clinical outcomes in patients with acute ischemic stroke. *Stroke.* (2020) 51:338–41. doi: 10.1161/STROKEAHA.119.027336
36. Castillo J, Leira R, García MM, Serena J, Blanco M, Dávalos A. Blood pressure decrease during the acute phase of ischemic stroke is associated with brain injury and poor stroke outcome. *Stroke.* (2004) 35:520–6. doi: 10.1161/01.STR.0000109769.22917.B0
37. Leonardi-Bee J, Bath PM, Phillips SJ, Sandercock PA. Blood pressure and clinical outcomes in the international stroke trial. *Stroke.* (2002) 33:1315–20. doi: 10.1161/01.STR.0000014509.11540.66
38. Gazerani P, Cairns BE, Yassin H, Yousefi JT, Sherzaman AR, Nedergaard BS, et al. Amplification of glyceryl trinitrate-induced headache features by noxious craniofacial stimuli in pain-free healthy humans. *Pain Manag.* (2019) 9:17–35. doi: 10.2217/pmt-2018-0035
39. Hertzog MA. Considerations in determining sample size for pilot studies. *Res Nurs health.* (2008) 31:180–91. doi: 10.1002/nur.20247

40. Dobkin BH. Progressive staging of pilot studies to improve phase iii trials for motor interventions. *Neurorehabil Neural Rep.* (2009) 23:197–206. doi: 10.1177/1545968309331863
41. Klomparens EA, Ding Y. The neuroprotective mechanisms and effects of sulforaphane. *Brain Circ.* (2019) 5:74–83. doi: 10.4103/bc.bc_7_19
42. Babadjouni RM, Walcott BP, Liu Q, Tenser MS, Amar AP, Mack WJ. Neuroprotective delivery platforms as an adjunct to mechanical thrombectomy. *Neuro Focus.* (2017) 42:E4. doi: 10.3171/2017.1.FOCUS16514
43. Savitz SI, Baron JC, Yenari MA, Sanossian N, Fisher M. Reconsidering neuroprotection in the reperfusion era. *Stroke.* (2017) 48:3413–9. doi: 10.1161/STROKEAHA.117.017283
44. Wiendl H, Elger C, Förstl H, Hartung HP, Oertel W, Reichmann H, et al. Gaps between aims and achievements in therapeutic modification of neuronal damage ("neuroprotection"). *Neurotherapeutics.* (2015) 12:449–54. doi: 10.1007/s13311-015-0348-8
45. Saber H, Somai M, Rajah GB, Scalzo F, Liebeskind DS. Predictive analytics and machine learning in stroke and neurovascular medicine. *Neurol Res.* (2019) 41:681–90. doi: 10.1080/01616412.2019.1609159
46. Zhao W, Wu C, Dornbos D III, Li S, Song H, Wang Y, et al. Multiphase adjuvant neuroprotection: a novel paradigm for improving acute ischemic stroke outcomes. *Brain Circ.* (2020) 6:11–8. doi: 10.4103/bc.bc_58_19
47. Yuan S, Liu KJ, Qi Z. Occludin regulation of blood-brain barrier and potential therapeutic target in ischemic stroke. *Brain Circ.* (2020) 6:152–62. doi: 10.4103/bc.bc_29_20
48. Snyder SH, Bredt DS. Biological roles of nitric oxide. *Scientif Am.* (1992) 266:68-71:74–67. doi: 10.1038/scientificamerican0592-68
49. Koken T, Inal M. The effect of nitric oxide on ischemia-reperfusion injury in rat liver. *Clin Chim Acta.* (1999) 288:55–62. doi: 10.1016/S0009-8981(99)00138-2
50. Phillips L, Toledo AH, Lopez-Neblina F, Anaya-Prado R, Toledo-Pereyra LH. Nitric oxide mechanism of protection in ischemia and reperfusion injury. *J Invest Surg.* (2009) 22:46–55. doi: 10.1080/08941930802709470
51. Fox-Robichaud A, Payne D, Hasan SU, Ostrovsky L, Fairhead T, Reinhardt P, et al. Inhaled no as a viable antiadhesive therapy for ischemia/reperfusion injury of distal microvascular beds. *J Clin Invest.* (1998) 101:2497–505. doi: 10.1172/JCI2736
52. Rashid PA, Whitehurst A, Lawson N, Bath PM. Plasma nitric oxide (nitrate/nitrite) levels in acute stroke and their relationship with severity and outcome. *J Stroke Cerebrovasc Dis.* (2003) 12:82–7. doi: 10.1053/jscd.2003.9
53. Woodhouse L, Scutt P, Krishnan K, Berge E, Gommans J, Ntaios G, et al. Effect of hyperacute administration (within 6 hours) of transdermal glyceryl trinitrate, a nitric oxide donor, on outcome after stroke: subgroup analysis of the efficacy of nitric oxide in stroke (enos) trial. *Stroke.* (2015) 46:3194–201. doi: 10.1161/STROKEAHA.115.009647
54. Todd PA, Goa KL, Langtry HD. Transdermal nitroglycerin (glyceryl trinitrate). A review of its pharmacology and therapeutic use. *Drugs.* (1990) 40:880–902. doi: 10.2165/00003495-199040060-00009
55. Isenschmid M, Müller M, Bührer M, Vorkauf H, Bircher J. Absolute bioavailability of glyceryl trinitrate from a transdermal system, assessed by digital plethysmography. *Int J Clin Pharmacol Ther Toxicol.* (1985) 23:345–51.
56. Jaffe AS, Roberts R. The use of intravenous nitroglycerin in cardiovascular disease. *Pharmacotherapy.* (1982) 2:273–80. doi: 10.1002/j.1875-9114.1982.tb03197.x
57. Chiesa JJ, Baidanoff FM, Golombek DA. Don't just say no: differential pathways and pharmacological responses to diverse nitric oxide donors. *Biochem Pharmacol.* (2018) 156:1–9. doi: 10.1016/j.bcp.2018.08.002
58. Krishnan K, Scutt P, Woodhouse L, Adami A, Becker JL, Berge E, et al. Glyceryl trinitrate for acute intracerebral hemorrhage: results from the efficacy of nitric oxide in stroke (enos) trial, a subgroup analysis. *Stroke.* (2016) 47:44–52. doi: 10.1161/STROKEAHA.115.010368
59. González RG. Imaging-guided acute ischemic stroke therapy: from "time is brain" to "physiology is brain". *Am J Neuroradiol.* (2006) 27:728–35.

Conflict of Interest: The authors declare that the research was conducted in the absence of any commercial or financial relationships that could be construed as a potential conflict of interest.

Publisher's Note: All claims expressed in this article are solely those of the authors and do not necessarily represent those of their affiliated organizations, or those of the publisher, the editors and the reviewers. Any product that may be evaluated in this article, or claim that may be made by its manufacturer, is not guaranteed or endorsed by the publisher.

frontiers in Neurology

ORIGINAL RESEARCH
published: 10 September 2021
doi: 10.3389/fneur.2021.726520

Association of Pericyte Loss With Microthrombosis After Subarachnoid Hemorrhage in ApoE-Deficient Mice

Jinwei Pang[1†], Yue Wu[2†], Jianhua Peng[1], Ping Yang[3], Ligang Chen[1,4] and Yong Jiang[1,4,5]*

[1] Department of Neurosurgery, The Affiliated Hospital of Southwest Medical University, Luzhou, China, [2] Department of Neurosurgery, The First Affiliated Hospital of Chongqing Medical University, Chongqing, China, [3] Department of Cardiology, The Affiliated Hospital of Southwest Medical University, Luzhou, China, [4] Sichuan Clinical Research Center for Neurosurgery, Luzhou, China, [5] Luzhou Key Laboratory of Neurological Diseases and Brain Function, Luzhou, China

OPEN ACCESS

Edited by:
Qin Hu,
Shanghai Jiao Tong University, China

Reviewed by:
Anatol Manaenko,
University Hospital Erlangen, Germany
Zongyi Xie,
Chongqing Medical University, China

***Correspondence:**
Yong Jiang
jiangyong@swmu.edu.cn

[†]These authors share first authorship

Specialty section:
This article was submitted to Stroke, a section of the journal Frontiers in Neurology

Received: 17 June 2021
Accepted: 19 August 2021
Published: 10 September 2021

Citation:
Pang J, Wu Y, Peng J, Yang P, Chen L and Jiang Y (2021) Association of Pericyte Loss With Microthrombosis After Subarachnoid Hemorrhage in ApoE-Deficient Mice. Front. Neurol. 12:726520. doi: 10.3389/fneur.2021.726520

Background: The occurrence of microthrombosis contributes to not only delayed cerebral ischemia (DCI), but also early brain injury (EBI) after SAH. However, the underlying mechanism is not completely investigated. In the current study, we explored the underlying mechanism of microthrombosis in EBI stage after SAH in ApoE-deficient mice.

Methods: Experimental SAH was established by endovascular perforation in apolipoprotein E (ApoE)-deficient mice and wild type (WT) mice. Neurobehavioral, molecular biological and histopathological methods were used to assess the relationship between pericytes loss, neurobehavioral performance, and microthrombosis.

Results: We found that the number of microthrombi was significantly increased and peaked 48 h after SAH in WT mice. The increased microthrombosis was related to the decreased effective microcirculation perfusion area and EBI severity. ApoE-deficient mice showed more extensive microthrombosis than that of WT mice 48 h after SAH, which was thereby associated with greater neurobehavioral deficits. Immunohistochemical staining showed that microthrombi were predominantly located in microvessels where pericytes coverage was absent. Mechanistically, ApoE deficiency caused more extensive CypA-NF-κB-MMP-9 pathway activation than that observed in WT mice, which thereby led to more degradation of N-cadherin, and subsequently more pericytes loss. Thereafter, the major adhesion molecule that promoting microthrombi formation in microvessels, P-selectin, was considerably increased in WT mice and increased to a greater extent in the ApoE-deficient mice.

Conclusion: Taken together, these data suggest that pericytes loss is associated with EBI after SAH through promoting microthrombosis. Therapies that target ApoE to reduce microthrombosis may be a promising strategy for SAH treatment.

Keywords: subarachnoid hemorrhage, early brain injury, apolipoprotein E, pericytes, microthrombosis

INTRODUCTION

Stroke is currently the second leading cause of death and disability worldwide (1). Despite accumulating knowledge of the disease pathology, treatments for stroke are limited (2). Although subarachnoid hemorrhage (SAH) represents approximately 5% of all strokes (3), it often affects people in a relatively young age with the mean age of time at SAH is around 50 years. It has a 35% mortality, and leaves many with lasting disabilities (4). The neurological outcomes of SAH patients are generally associated with the severity of initial bleeding, secondary brain injury, and/or medical complications (5). Early brain injury (EBI), which develops within the first 72 h after bleeding, in addition to cerebral vasospasm (CVS), is now believed to be the major predictor of early neurological deficits and long-term outcomes in SAH patients (6). However, the underlying mechanisms that contribute to EBI have not been fully identified. Therefore, therapeutics that completely cure EBI after SAH are still limited.

Microcirculatory dysfunction may contribute to delayed cerebral ischemia after SAH, but its role was largely ignored in the EBI stage after SAH. Microthrombosis was reported to induce cerebral ischemia, neurotoxic metabolic waste accumulation, cerebral edema, and neuronal apoptosis (7), which are all essential promoters of EBI and poor neurological outcomes after SAH. Clinically, the autopsies of SAH patients who died within 2 days after the initial bleeding event also showed a large number of microthrombi (8). Therefore, strategies that reduce microthrombosis in EBI after SAH may be beneficial for SAH treatment. Fortunately, the early administration of antiplatelet medications as well as anticoagulants has been suggested to be beneficial in improving neurological outcomes in some SAH patients (9, 10).

However, the mechanism by which microthrombi are induced after SAH remains incompletely understood. Previously, apolipoprotein E (ApoE: protein, APOE: gene) was shown to affect platelet activation (11), which is an important part of microthrombosis. Our recent study found that ApoE deficiency is associated with more significant EBI and neurological impairments after SAH (12). However, the underlying mechanisms have not been fully identified. In clinical studies, the lack of an association between the APOE epsilon4 allele and signs of visible angiography vasospasm but the presence of an association between the allele and an increased risk of delayed cerebral ischemia after SAH have linked ApoE to the cerebral microcirculation, probably through coagulation and fibrinolytic cascade impairment and microthrombosis (13).

In the current study, we evaluated behavioral, histological and molecular biological data to compare microthrombosis in WT and ApoE-deficient mice following SAH and explored the underlying mechanisms.

MATERIALS AND METHODS

Animals

All animal experiments were approved by the Ethics Committee of Southwest Medical University and carried out in accordance with Stroke Treatment and Academic Roundtable (STAIR) guidelines and the National Institutes of Health Guide for the Care and Use of Laboratory Animals. Healthy young adult male wild-type C57BL/6J mice (WT; 8–10 weeks; 20–25 g) and physiological condition-matched ApoE-deficient mice on a C57BL/6J background (KO; 8–10 weeks; 20–25 g) were used. The animals were housed and humanely cared for in the Laboratory Animal Resource Center (LARC) and allowed free access to food and water.

SAH Model Establishment

Experimental SAH was induced using the endovascular perforation technique as described previously (14). Briefly, the mice were anesthetized with 2% pentobarbital (50 mg/kg) by intraperitoneal injection. A 5-0 monofilament was inserted via the right external carotid artery to perforate the bifurcation of the middle and anterior cerebral artery. SAH was confirmed by an obvious Cushing response and autopsy after sacrifice at scheduled time points. In the sham-operated animals, all surgical procedures were repeated except SAH induction by vessel puncture. The mice were warmed by an electric blanket, and the rectal temperature was maintained at 37.5 $\pm$ 0.5°C during the surgery. The mice were administered 50 mg/kg ampicillin in 0.9% saline twice daily after surgery until sacrifice. The mice that died due to severe SAH were immediately replaced with condition-matched animals.

Brain Water Content Calculation

Brain water content was measured after neurological function evaluation as previously reported (15). The animals were euthanized with an overdose of pentobarbital sodium. The brains were harvested, and the left and right hemispheres were dissected for brain water content measurement. The wet weight was immediately recorded, and the dry weight was acquired after drying at 100°C for 72 h. The brain water content was calculated as (wet weight–dry weight)/wet weight $\times$ 100%.

Rota Rod Latency

To evaluate mouse neurological performance, Rota Rod latency was assessed in all animals ($n = 15$–22 for each experiment) using an automated Rota Rod device (ZB-200 Rota Rod Treadmill; Taimeng Software Co. LTD, Chengdu, China) by a blinded investigator, as previously reported (16). All animals completed a total of 9 training sessions over a period of 3 days before surgery. Baseline Rota Rod latency were assessed three times for each group before SAH induction using the accelerating mode (the rotating speed started at 0 rpm and was accelerated by 3 rpm every 10 s until it reached 30 rpm), and Rota Rod performance was assessed again after SAH. The Rota Rod latency was defined as the average latency of all three trials.

Effective Microcirculation Perfusion Area Analysis

Intravital lectin perfusion was used to identify the effective microcirculation perfusion area without microthrombi after SAH. Briefly, 1 mg/ml biotin-labeled Lycopersicon esculentum (Tomato) lectin (LEL) was dissolved in PBS, and the mice

received a 400 μl intravenous lectin injection 1 h before sacrifice. Brain samples were collected routinely, and 10-μm coronal frozen sections were made. The sections were rinsed three times in PBS and then incubated with AMCA-streptavidin (SA-5008, Vector Laboratories) for 1 h at room temperature. After rising and mounting, the sections were visualized under a fluorescence microscope (Olympus, Tokyo, Japan). Three nonadjacent coronary sections from each brain sample with a minimum distance of 100 μm from one another were used. Five randomly selected visual fields per section were observed and analyzed by a blinded observer using Image-Pro Plus (IPP) 6.0 software.

Western Blot Analyses

Protein from each right hemisphere sample was extracted, quantified, and denatured at 95°C in 5X loading buffer for 10 min. Western blot was performed as previously described (17). The following primary antibodies were used: Fibrin (ogen) (ab34269, Abcam), P-selectin (60322-1-Ig, Proteintech), PDGFRβ (ab69506, Abcam), CypA (ab41684, Abcam), N-cadherin (22018-1-AP, Proteintech), phospho-NF-κB p65 subunit (p-p65, ab86299, Abcam), MMP-9 (10375-2-AP, Proteintech), and β-actin (66009-1-Ig, Proteintech). The bands were visualized using a BeyoECL Plus kit (P0018; Beyotime) and photographed by a chemiluminescence imaging system (ChemiDoc XRS+; Bio-Rad, Hercules, CA, USA). Band densities were quantified by a blinded observer using ImageJ software.

Microthrombi Staining

Microthrombi were detected by immunohistochemical staining for fibrin (ogen) according to a previous study (18). Brain samples were routinely collected, and 10-μm coronal frozen sections were made. The sections were rinsed three times in PBS and then incubated with 3% hydrogen peroxide for 10 min at room temperature. Thereafter, the sections were washed again and blocked with 5% normal goat serum for 30 min at room temperature and then incubated with a fibrin (ogen) primary antibody (ab34269, Abcam) at 4°C overnight. After washing with PBS, the sections were incubated with a biotinylated goat anti-rabbit secondary antibody for 1 h at room temperature and then analyzed by an HRP/DAB IHC detection system. Three nonadjacent coronary sections from each brain sample with a minimum distance of 100 μm from one another were used. Five randomly selected visual fields per section were observed and analyzed using Image-pro plus (IPP) 6.0 software by a blinded observer.

Immunofluorescent Staining

For immunofluorescent staining, brain samples were routinely collected, and 10-μm coronal frozen sections were made. The immunofluorescent staining procedure was performed as previously reported (19). The following primary antibodies were used: PDGFR-β (ab32570, Abcam), biotinylated lectin (B-1175, Vector Laboratories), fibrin (ogen) (ab34269, Abcam) and P-selectin (60322-1-Ig, Proteintech). Secondary antibodies, including AMCA-streptavidin (SA-5008, Vector Laboratories), DyLight 488 goat anti-rabbit IgG (A23220, Abbkine), and DyLight 594 goat anti-mouse IgG (A23410, Abbkine) were used. Three nonadjacent coronary sections from each brain sample with a minimum distance of 100 μm from one another were used. Five randomly selected visual fields per section were observed and analyzed by a blinded observer using Image-pro plus (IPP) 6.0 software by a blinded observer.

Statistical Analysis

The normally distributed quantitative data are expressed as the mean ± SD. For normally distributed data, one-way analysis of variance (ANOVA) with Tukey's *post-hoc* test was used to compare the means of the different groups. A $p < 0.05$ was considered statistically significant. Mortality analysis was performed by Fisher's exact test. Correlation analysis between two parameters was tested by the Pearson correlation test. All statistical values were analyzed using SPSS 20.0 software (SPSS, Inc. Chicago, IL, USA).

RESULTS

SAH Severity and Animal Mortality

The SAH grade of the WT mice from each time course subgroup and the ApoE-deficient mice were not significantly different. No animal from the WT-Sham or KO-Sham groups died. The overall mortality rate was 14.7% (13 of 88) in the WT group and 21.05% (8 of 38) in the KO group. Although the mortality in the KO group was higher than that in the WT group, there was no significant difference in mortality between these groups.

The Number of Microthrombi Was Increased in EBI Stage After SAH

The expression of the microthrombi marker fibrinogen was significantly increased and peaked 48 h after SAH compared to the sham group. Even at 72 h, the expression of fibrinogen was still higher than that in the sham group (**Figures 1A,B**). Immunochemical staining of fibrinogen also showed a similar trend in the number of microthrombi (**Figures 1C,E**). Conversely, intravital lectin perfusion showed that the effective microcirculatory perfusion area gradually decreased until 48 h after SAH and then increased toward baseline levels 72 h after SAH (**Figures 1D,F,G**). The Pearson correlation test showed that the number of microthrombi was closely correlated with neurological performance in the mice (Rota Rod latency) ($R^2 = 0.19$, $p = 0.028$) and the effective microcirculatory area ($R^2 = 0.77$, $p < 0.001$; **Figures 1H,I**).

Effective Microcirculation Area Was Reduced in ApoE Deficient Mice After SAH

In both the WT-Sham and KO-Sham mice, the effective microcirculation perfusion areas observed in the intravital lectin perfusion study were not significantly different. However, 48 h after SAH, the effective microcirculation perfusion area was significantly reduced in both the WT-SAH group and KO-SAH group. The reduction in the effective microcirculation perfusion area was dramatically higher in the ApoE-deficient mice 48 h after SAH (**Figures 2A–C**). The greater reduction in microcirculation perfusion was associated with more severe brain

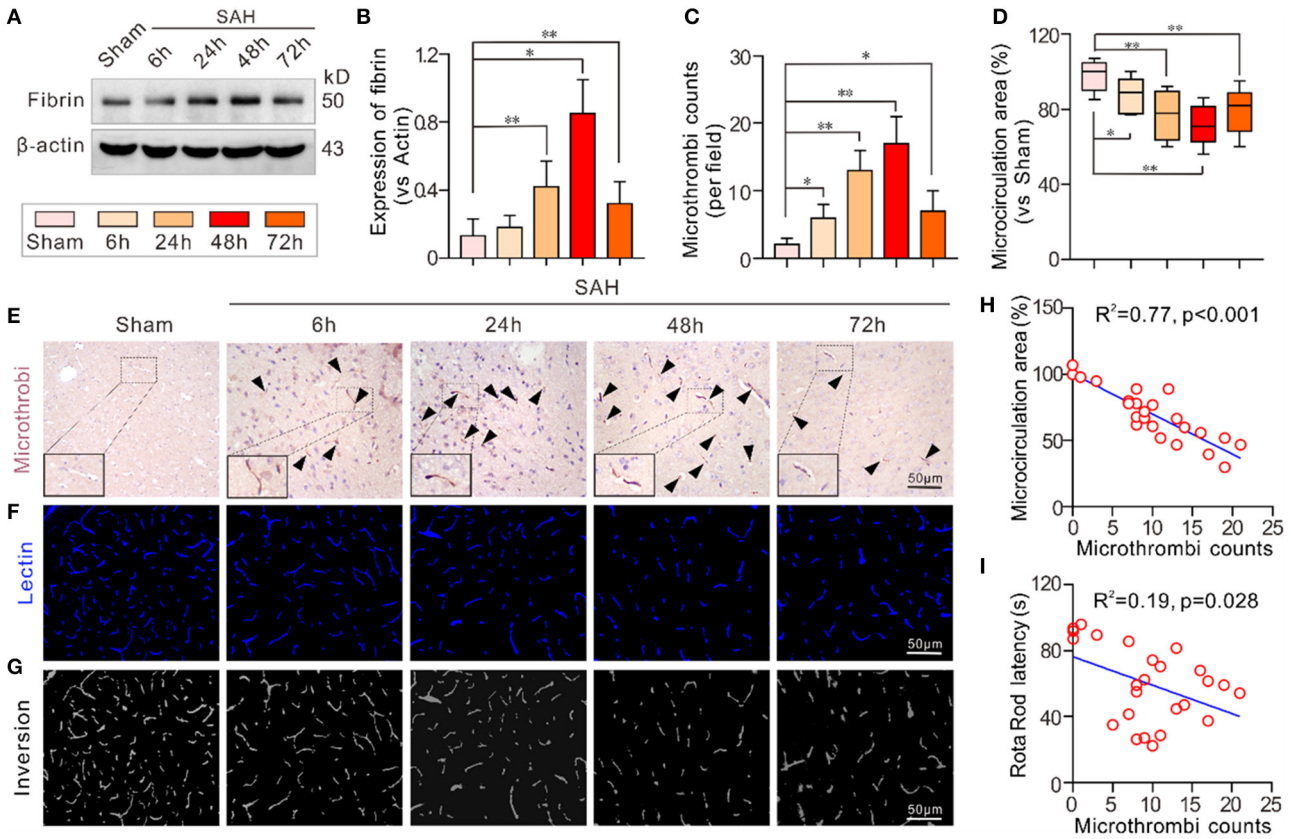

FIGURE 1 | Microthrombosis was increased in EBI after SAH. **(A,B)** The expression of the microthrombi marker fibrinogen gradually increased at different time points and peaked 48 h after SAH. **(C,D)** The quantification of the number of microthrombi and effective microcirculation perfusion area. **(E)** Representative pictures of the fibrinogen-positive microthrombi at each time point. **(F)** Representative pictures of the intravital lectin perfusion study for evaluating the effective microcirculation area. **(G)** Grayscale inversion images corresponding to the pictures shown in **(E)**. **(H,I)** The Pearson correlation test between the number of microthrombi, and effective microcirculation area and neurobehavioral performance. Except for Pearson correlation analysis, the data are expressed as the mean ± SD, one-way ANOVA with Tukey's *post hoc*, $^{*}p < 0.05$, $^{**}p < 0.01$, vs. Sham group; $n = 5$ per group; Fibrin, fibrinogen; scale bar = 50 mm.

edema and lower Rota rod latency in the ApoE-deficient mice than in the WT mice (**Figures 2D,E**).

Pericytes Loss Associated With Microthrombosis in ApoE-Deficient Mice After SAH

Prior to SAH, no significant difference was observed in the expression of PDGFRβ and fibrinogen between the WT-Sham group and the KO-Sham group. However, 48 h after SAH, the mice in the WT-SAH group showed a significant decrease in PDGFRβ expression, which was accompanied by a significant increase in fibrinogen expression. These changes were increased to an even greater extent in the ApoE-deficient mice (**Figures 3A–C**). Immunofluorescent staining showed that no obvious microthrombi were observed in either the WT-Sham group or the KO-Sham group, but abundant microthrombi was observed in WT-SAH, and the number of microthrombi was increased to an even greater extent in the ApoE-deficient mice. Notably, the microthrombi were mainly located in sites where PDGFRβ-positive pericytes were absent, especially in the ApoE-deficient mice (**Figures 3D,F**). The Pearson correlation test showed that the number of microthrombi was closely correlated with pericytes coverage ($R^2 = 0.49$, $p = 0.002$; **Figure 3E**).

N-Cadherin Degradation Promoted Pericytes Loss and P-Selectin Elevation in EBI Stage After SAH

Prior to SAH, no significant difference was observed in the expression of N-cadherin, the major tight junction molecule between endothelial cells and pericytes, between the WT-Sham group and the KO-Sham group. Additionally, the expression of the major promoter of microthrombosis, P-selectin, was also not obviously different between the WT-Sham group and the KO-Sham group. However, 48 h after SAH, N-cadherin expression was significantly decreased in the WT mice, which resulted in a significant loss of pericytes coverage and an increase in P-selectin expression. These changes were more severe in the ApoE-deficient mice (**Figures 4A–C**). Further analysis by

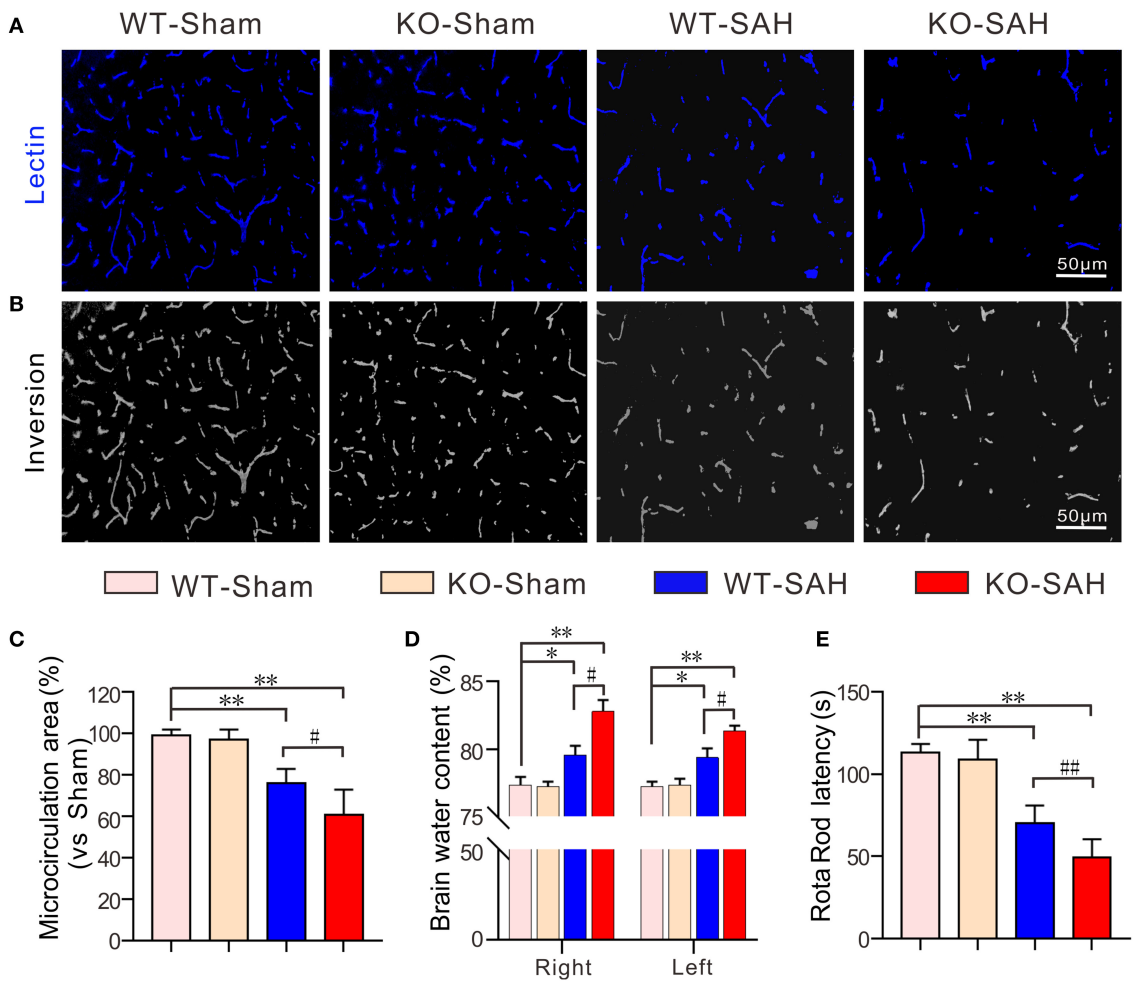

FIGURE 2 | ApoE deficiency promotes effective microcirculation perfusion area reduction after SAH. **(A)** Representative pictures of the intravital lectin perfusion study for evaluating the effective microcirculation area in WT mice and ApoE-deficient mice 48 h after SAH. **(B)** Corresponding grayscale inversion images of the pictures shown in **(A)**. **(C)** The quantification of the effective microcirculation perfusion area in each group. **(D)** The quantification of brain water content in each group. **(E)** The quantification of the rotarod latency in each group. Data are expressed as the mean ± SD, one-way ANOVA with Tukey's *post hoc*, $^{*}p < 0.05$, $^{**}p < 0.01$, vs. the WT-Sham group; $^{\#}p < 0.05$, vs. the WT-SAH group; $n = 5$ per group; Right, right hemisphere; Left, left hemisphere; scale bar = 50 mm.

immunofluorescent staining showed that pericytes coverage was significantly reduced after SAH, and P-selectin was mainly expressed by endothelial cells in areas where pericytes were absent, and co-localized with microthrombi marker fibrinogen (**Figures 4D–F**). The Pearson correlation test showed that P-selectin expression was closely correlated with pericytes coverage ($R^2 = 0.59$, $p < 0.001$; **Figure 4G**).

The CypA-NF-κB-MMP-9 Pathway Was Activated in EBI Stage After SAH

A previous study showed that the CypA-NF-κB-MMP-9 pathway can regulate the integrity of the BBB via affecting the interactions between endothelial cells and pericytes (20). In line with our previous work (12), our results showed that the expression of CypA and phosphorylated NF-κB p65 subunit (p-p65) was slightly higher in the sham-operated ApoE-deficient mice, but there was no significant difference when this group was compared to the WT-Sham mice. However, CypA, p-p65, and MMP-9 were dramatically upregulated 48 h after SAH, with larger increases of these proteins in the ApoE-deficient mice (**Figure 5**).

DISCUSSION

The microcirculation plays a pivotal role in the maintenance of cerebral homeostasis and neuronal metabolite exchange (21, 22). However, after SAH, the microcirculation can be destroyed due to increased BBB disruption and microthrombosis, which result in cerebral ischemia, neuronal nutrient deprivation and severe brain edema, which subsequently induces neuronal death (23–25). Hence, cerebral microcirculation dysfunction has been

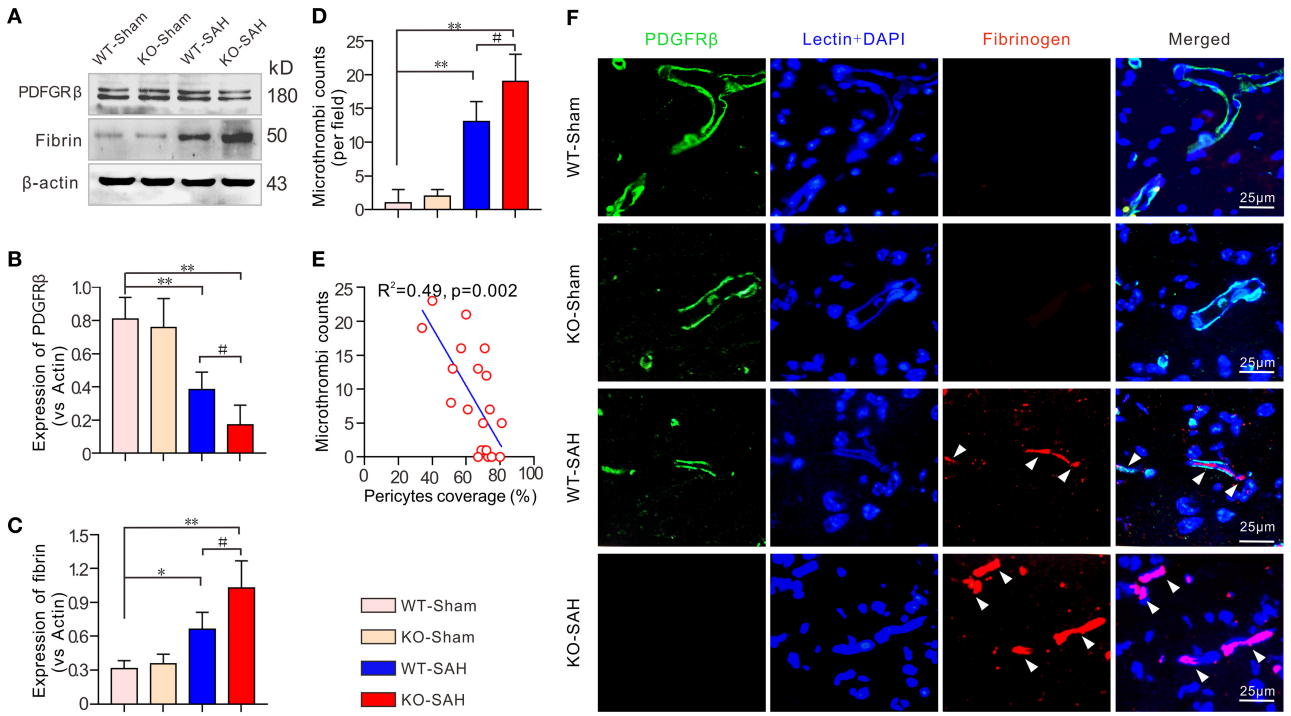

FIGURE 3 | Pericytes loss promoted icrothrombosis in ApoE-deficient mice after SAH. **(A)** Immunoblotting analysis of the expression of the pericytes marker PDGFRβ and the microthrombi marker fibrinogen in each group. **(B,C)** The quantification of PDGFRβ and fibrinogen. **(D)** Quantification of the microthrombi in each group 48 h after SAH. **(E)** Pearson correlation test between pericytes coverage and microthrombi number in each group. **(F)** Immunofluorescent triple staining with lectin + PDGFRβ+ fibrinogen showed that microthrombi were primarily located where PDGFRβ-positive pericytes were missing. Except for Pearson correlation analysis, data are expressed as the mean ± SD, one-way ANOVA with Tukey's *post hoc*, $^{*}p < 0.05$, $^{**}p < 0.01$, vs. the WT-Sham group; $^{\#}p < 0.05$, vs. the WT-SAH group; $n = 5$ per group; Fibrin, fibrinogen; scale bar = 25 mm.

demonstrated to be an important part of secondary pathogenic changes after SAH. However, despite microcirculatory thrombosis has been reported to affect secondary brain injury after SAH, little is known about how and why it forms. Therefore, a better understanding of the underlying mechanism involved in cerebral microcirculatory thrombosis is warranted for improving SAH treatment.

The current study explored microthrombosis and the associated underlying mechanism in the EBI stage after experimental SAH using ApoE-deficient mouse. First, to further identify the importance of microthrombosis in EBI, we analyzed the formation of microthrombi and the correlation of microthrombi with neurobehavioral performance and the effective microcirculatory perfusion area. The fact that microthrombi increase in our study were similar with the fact that microthrombi was also increased in brain autopsies of SAH patients (26). Our results showed that the number of microthrombi was significantly increased after SAH, while the intravital lectin perfusion study showed that the effective microcirculatory perfusion area was greatly decreased after SAH. The Pearson correlation test showed that number of microthrombi was closely correlated with neurological performance in the mice (Rota Rod latency) ($R^2 = 0.19$, $p = 0.028$) and the effective microcirculatory area ($R^2 = 0.77$, $p < 0.001$).

Furthermore, when compared with the WT mice, there was no microthrombi in the sham-operated ApoE-deficient mice, but the expression of the microthrombi marker fibrinogen and the number of microthrombi were more significantly increased in the ApoE-deficient mice at 48 h after SAH. Brain edema, the effective microcirculatory perfusion area and neurobehavioral performance were also changed more markedly in the ApoE-deficient mice at this time point. Thus, ApoE gene knockout is associated with increased microthrombosis in EBI after SAH. These findings are consistent with our previous data showing that EBI is more severe in ApoE-deficient mice after SAH (12).

Although the number of microthrombi was increased in EBI after SAH and was further increased in ApoE-deficient mice, the mechanisms by which microthrombosis is affected after SAH remain elusive. P-selectin belongs to the adhesion glycoprotein family, which mediates leukocyte-endothelial cell and leukocyte-platelet adhesive interactions (27). It can be significantly upregulated and translocated to the surface of platelets and endothelial cells to promote vascular changes in many microcirculatory disturbance events. It has been reported that the increased expression of P-selectin in endothelial

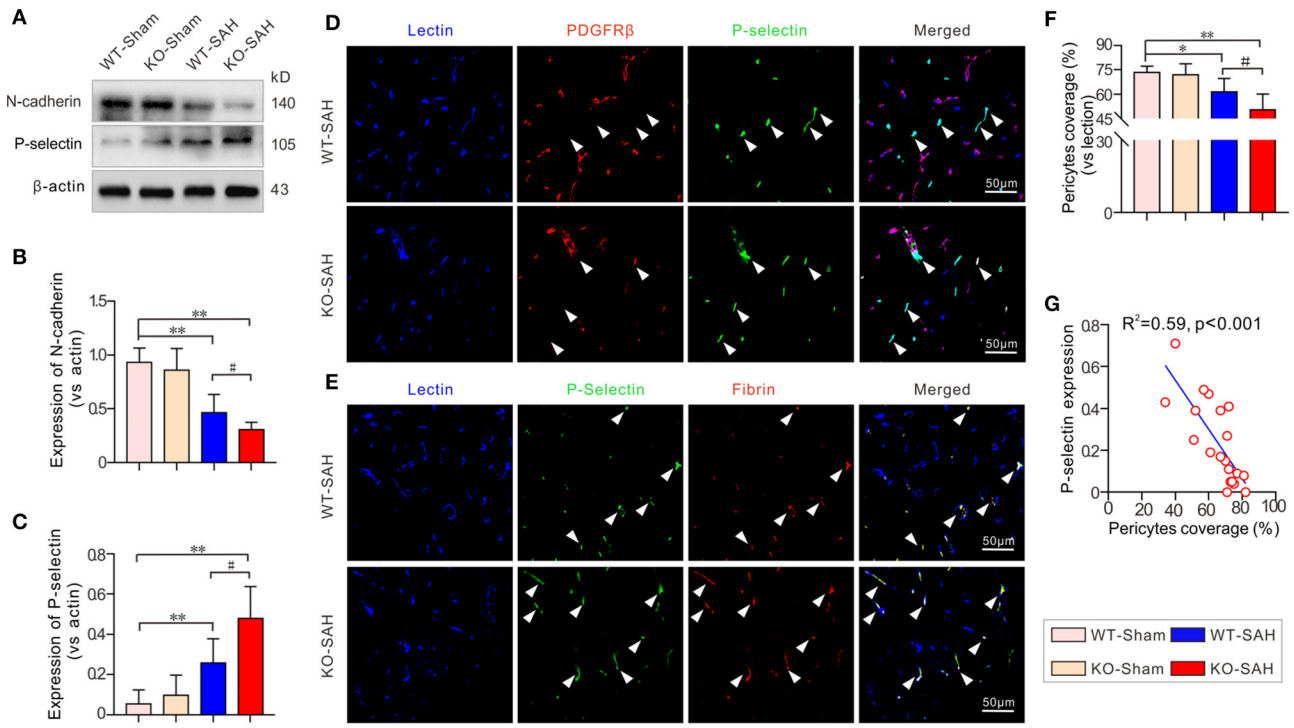

FIGURE 4 | N-cadherin degradation promoted pericyte loss and P-selectin elevation in EBI stage after SAH. **(A)** Immunoblotting analysis of the expression of N-cadherin and P-selectin. **(B,C)** The quantification of N-cadherin and P-selectin. **(D)** Representative pictures of immunofluorescent triple-staining with lectin + PDGFRβ + P-selectin. **(E)** Representative pictures of immunofluorescent triple-staining with lectin + P-selectin + fibrinogen. The results showed that P-selectin was primarily localized to fibrinogen-positive microthrombi and was mainly located in locations where PDGFRβ-positive pericytes were absent. **(F)** The quantification of the pericytes coverage change in each group 48 h after SAH. **(G)** The Pearson correlation test between pericytes coverage and P-selectin expression. Except for Pearson correlation analysis, the data are expressed as the mean ± SD, one-way ANOVA with Tukey's *post hoc*, $^{*}p < 0.05$, $^{**}p < 0.01$, vs. the WT-Sham group; $^{\#}p < 0.05$, vs. the WT-SAH group; $n = 5$ per group; Fibrin, fibrinogen; scale bar = 50 mm.

cells, which facilitates platelet adhesion, is the main cause of microthrombosis after traumatic brain injury (28).

In SAH studies, the increased expression of P-selectin in endothelial cells, which subsequently facilitates platelet adhesion, has also been reported to be the main cause of microthrombosis (29). ApoE deficiency has been reported to increase P-selectin expression in various situations. Therefore, the ApoE deficiency-induced increase in microthrombosis after SAH may be related to an increase in P-selectin expression. We then checked the expression of P-selectin after SAH in WT mice and ApoE-deficient mice. In the current study, P-selectin expression was significantly upregulated after SAH in WT mice and upregulated to a greater extent in ApoE-deficient mice. Moreover, as observed by immunofluorescent staining, P-selectin was mainly expressed by endothelial cells in the presence of abundant microthrombi. Thus, understanding how P-selectin expression is regulated may contribute to understanding the mechanism of microthrombosis after SAH.

Pericytes, as an important cellular component of the microvasculature, are necessary for neuronal homeostasis and the maintenance of the cerebral microcirculation. Traditionally, pericyte, served as capillary contraction handler, is recently considered as the main participant of microcirculation regulation in SAH pathophysiology (30). Although cerebral pericytes loss was involved in the dysfunction of microcirculation in EBI after SAH (31), this role has been largely overlooked.

In the current study, most of the microvessels were covered with pericytes in both the WT-Sham mice and KO-Sham mice. However, 48 h after SAH, the pericytes coverage was significantly reduced in the WT-SAH group and further decreased in the ApoE-deficient mice. Immunofluorescent staining showed that P-selectin was primarily colocalized with fibrinogen-positive microthrombi and was mainly located in areas where PDGFRβ-positive pericytes were absent, both in the WT mice and the ApoE-deficient mice. In addition, P-selectin and microthrombi were more frequently observed due to lower microvessel pericytes coverage 48 h after SAH in the ApoE-deficient mice. These data suggest that SAH-induced pericytes loss can lead to the upregulation of P-selectin expression and thereby facilitate microthrombosis. ApoE deficiency can further promote pericytes loss and subsequently induce more microthrombosis in EBI after SAH Thus, knowing how pericytes loss occurs after SAH and ApoE deficiency can help determine the mechanism of microthrombosis after SAH.

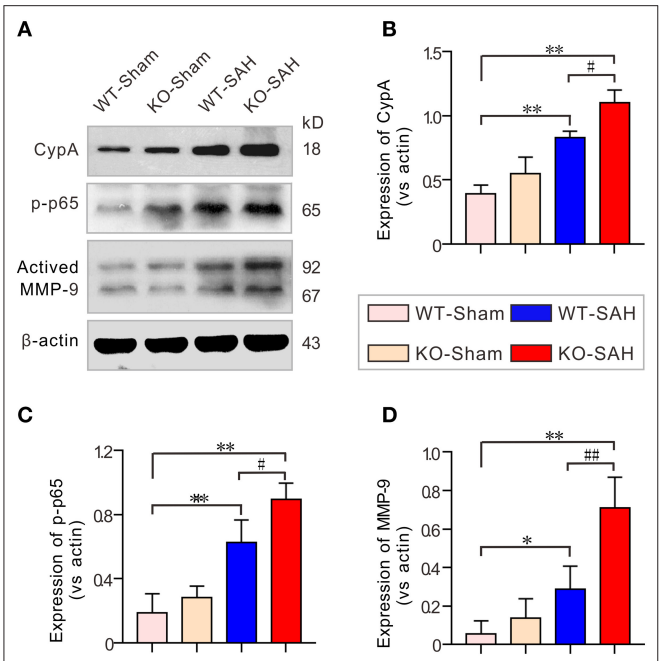

FIGURE 5 | The CypA-NF-κB-MMP-9 pathway was activated in EBI after SAH. **(A)** Immunoblotting analysis of CypA, p-p65 and MMP-9 expression in each group 48 h after SAH. **(B–D)** The quantification of CypA, p-p65, and MMP-9. The data are expressed as the mean ± SD, one-way ANOVA with Tukey's *post hoc*, $^{*}p < 0.05$, $^{**}p < 0.01$, vs. the WT-Sham group; $^{\#}p < 0.05$, $^{\#\#}p < 0.01$, vs. the WT-SAH group; $n = 5$ per group.

Given that pericytes-endothelial cell interactions are mainly controlled by the N-cadherin complex (32), we then measured the expression of N-cadherin and its upstream regulators to further identify the mechanism that promotes pericytes loss and microthrombosis after SAH. The results showed that the N-cadherin protein level was significantly reduced after SAH and decreased to a greater extent in the ApoE-deficient mice. It has been reported that MMP-9 activation can lead to N-cadherin degradation and thereby promote pericytes and endothelial cell decoupling (33, 34). Our previous study reported that CypA-NF-κB pathway-induced MMP-9 activation is associated with BBB tight junction protein degradation and EBI formation (35). We then measured the protein levels of CypA, NF-κB, and MMP-9. The results showed that both CypA, phosphorylated NF-κB subunit p65 (p-p65) and MMP-9 were dramatically upregulated 48 h after SAH, with greater increases in these proteins being observed in ApoE-deficient mice, whereas the expression of N-cadherin showed the opposite trend. Therefore, N-cadherin protein degradation is likely mediated by the activation of the CypA-NF-κB- MMP-9 pathway.

Taken together, the present findings support the hypothesis that pericytes loss is associated with EBI after SAH through promoting microthrombosis. ApoE deficiency can lead to a greater loss of pericytes and subsequently lead to more microthrombi and a more severe EBI. This phenomenon is mediated at least partly by the activation of CypA-NF-κB-MMP-9 signaling pathway-dependent N-cadherin degradation. Therapies that targeting ApoE to reduce microthrombosis may be a promising strategy for SAH treatment.

Although our findings are informative for future studies of SAH, several limitations of this study should be noted. First, it was reported that women have a 1.6 times higher risk of SAH than men (36), and estrogen has an impact on coagulation and fibrinolytic systems (37). The current study used only young male mice. Whether gender difference affect the effects of ApoE on pericytes loss and microthrombosis after SAH is not clear. In addition, although we found that pericytes loss is associated with an increase in P-selectin and microthrombosis in ApoE-deficient mice after SAH, the direct mechanism that upregulates P-selectin after SAH is still not clear. Furthermore, this study focused on the effect of ApoE on microthrombosis in the EBI stage after SAH, but no long-term outcomes were evaluated. Whether ApoE deficiency-related microthrombosis is associated with long-term outcomes remains unclear. Therefore, further investigation is still needed to completely clarify the effect of ApoE on SAH induced secondary brain injuries.

DATA AVAILABILITY STATEMENT

The original contributions presented in the study are included in the article/supplementary material, further inquiries can be directed to the corresponding author/s.

ETHICS STATEMENT

The animal study was reviewed and approved by Ethics Committee of Southwest Medical University.

AUTHOR CONTRIBUTIONS

JPa and YW conceived and designed the study, performed the experiments, and wrote the manuscript. JPe contributed to the acquisition and/or interpretation of data. JPe and PY contributed to manuscript writing. LC and YJ made substantial contributions to fund the study. All authors contributed to the article and approved the submitted version.

FUNDING

This work was supported by the National Natural Science Foundation of China (81801176, 81771278, and 81971132) and the Sichuan Science and Technology Program (2019JDRC0062 and 2019JDTD0004).

REFERENCES

1. Wang SN, Wang Z, Xu TY, Cheng MH, Li WL, Miao CY. Cerebral organoids repair ischemic stroke brain injury. *Transl Stroke Res.* (2020) 11:983–1000. doi: 10.1007/s12975-019-00773-0
2. Chen W, Huang J, Hu Y, Khoshnam SE, Sarkaki A. Mitochondrial transfer as a therapeutic strategy against ischemic stroke. *Transl Stroke Res.* (2020) 11:1214–28. doi: 10.1007/s12975-020-00828-7
3. He W, Liu Y, Feng J, Huang Q, Xu J, Liu X, et al. The epidemiological characteristics of stroke in hunan province, China. *Front Neurol.* (2018) 9:583. doi: 10.3389/fneur.2018.00583
4. Neifert SN, Chapman EK, Martini ML, Shuman WH, Schupper AJ, Oermann EK, et al. Aneurysmal subarachnoid hemorrhage: the last decade. *Transl Stroke Res.* (2021) 12:428–46. doi: 10.1007/s12975-020-00867-0
5. Barry C, Turner RJ, Corrigan F, Vink R. New therapeutic approaches to subarachnoid hemorrhage. *Expert Opin Investig Drugs.* (2012) 21:845–59. doi: 10.1517/13543784.2012.683113
6. Suzuki H. What is early brain injury? *Transl Stroke Res.* (2015) 6:1–3. doi: 10.1007/s12975-014-0380-8
7. Boluijt J, Meijers JC, Rinkel GJ, Vergouwen MD. Hemostasis and fibrinolysis in delayed cerebral ischemia after aneurysmal subarachnoid hemorrhage: a systematic review. *J Cereb Blood Flow Metab.* (2015) 35:724–33. doi: 10.1038/jcbfm.2015.13
8. Vergouwen MD, Vermeulen M, Coert BA, Stroes ES, Roos YB. Microthrombosis after aneurysmal subarachnoid hemorrhage: an additional explanation for delayed cerebral ischemia. *J Cereb Blood Flow Metab.* (2008) 28:1761–70. doi: 10.1038/jcbfm.2008.74
9. Nagahama Y, Allan L, Nakagawa D, Zanaty M, Starke RM, Chalouhi N, et al. Dual antiplatelet therapy in aneurysmal subarachnoid hemorrhage: association with reduced risk of clinical vasospasm and delayed cerebral ischemia. *J Neurosurg.* (2018) 129:702–10. doi: 10.3171/2017.5.JNS17831
10. Schuss P, Hadjiathanasiou A, Brandecker S, Guresir A, Borger V, Wispel C, et al. Anticoagulation therapy in patients suffering from aneurysmal subarachnoid hemorrhage: influence on functional outcome-a single-center series and multivariate analysis. *World Neurosurg.* (2017) 99:348–52. doi: 10.1016/j.wneu.2016.12.036
11. Pfennig O, Zhao B, Dierichs R. Influence of purified apoprotein E on platelet activation induced by serotonin. *Am J Hematol.* (1996) 52:319–21. doi: 10.1002/(SICI)1096-8652(199608)52:4<319::AID-AJH14>3.0.CO;2-8
12. Pang J, Wu Y, Peng J, Yang P, Kuai L, Qin X, et al. Potential implications of Apolipoprotein E in early brain injury after experimental subarachnoid hemorrhage: involvement in the modulation of blood-brain barrier integrity. *Oncotarget.* (2016) 7:56030–044. doi: 10.18632/oncotarget.10821
13. Rowland MJ, Hadjipavlou G, Kelly M, Westbrook J, Pattinson KT. Delayed cerebral ischaemia after subarachnoid haemorrhage: looking beyond vasospasm. *Br J Anaesth.* (2012) 109:315–29. doi: 10.1093/bja/aes264
14. Xu P, Hong Y, Xie Y, Yuan K, Li J, Sun R, et al. TREM-1 exacerbates neuroinflammatory injury via NLRP3 inflammasome-mediated pyroptosis in experimental subarachnoid hemorrhage. *Transl Stroke Res.* (2020) 12:643–59. doi: 10.1007/s12975-020-00840-x
15. Shen J, Xin W, Li Q, Gao Y, Yuan L, Zhang J. Methylene blue reduces neuronal apoptosis and improves blood-brain barrier integrity after traumatic brain injury. *Front Neurol.* (2019) 10:1133. doi: 10.3389/fneur.2019.01133
16. Cao F, Jiang Y, Wu Y, Zhong J, Liu J, Qin X, et al. Apolipoprotein E-mimetic COG1410 reduces acute vasogenic edema following traumatic brain injury. *J Neurotrauma.* (2016) 33:175–82. doi: 10.1089/neu.2015.3887
17. Wu M, Gao R, Dang B, Chen G. The blood component iron causes neuronal apoptosis following intracerebral hemorrhage via the PERK pathway. *Front Neurol.* (2020) 11:588548. doi: 10.3389/fneur.2020.588548
18. Sabri M, Ai J, Lakovic K, Macdonald RL. Mechanisms of microthrombosis and microcirculatory constriction after experimental subarachnoid hemorrhage. *Acta Neurochirurgica Suppl.* (2013) 115:185–92. doi: 10.1007/978-3-7091-1192-5_35
19. Huang T, Wan X, Alvarez AA, James CD, Song X, Yang Y, et al. MIR93 (microRNA−93) regulates tumorigenicity and therapy response of glioblastoma by targeting autophagy. *Autophagy.* (2019) 15:1100–11. doi: 10.1080/15548627.2019.1569947
20. Bell RD, Winkler EA, Singh I, Sagare AP, Deane R, Wu Z, et al. Apolipoprotein E controls cerebrovascular integrity via cyclophilin A. *Nature.* (2012) 485:512–6. doi: 10.1038/nature11087
21. Haeren RHL, Rijkers K, Schijns O, Dings J, Hoogland G, van Zandvoort M H, et al. In vivo assessment of the human cerebral microcirculation and its glycocalyx: a technical report. *J Neurosci Methods.* (2018) 303:114–25. doi: 10.1016/j.jneumeth.2018.03.009
22. Joutel A, Monet-Lepretre M, Gosele C, Baron-Menguy C, Hammes A, Schmidt S, et al. Cerebrovascular dysfunction and microcirculation rarefaction precede white matter lesions in a mouse genetic model of cerebral ischemic small vessel disease. *J Clin Invest.* (2010) 120:433–45. doi: 10.1172/JCI39733
23. Lei Q, Li S, Zheng R, Xu K, Li S. Endothelin-1 expression and alterations of cerebral microcirculation after experimental subarachnoid hemorrhage. *Neuroradiology.* (2015) 57:63–70. doi: 10.1007/s00234-014-1435-y
24. Ostergaard L, Aamand R, Karabegovic S, Tietze A, Blicher JU, Mikkelsen IK, et al. The role of the microcirculation in delayed cerebral ischemia and chronic degenerative changes after subarachnoid hemorrhage. *J Cereb Blood Flow Metab.* (2013) 33:1825–37. doi: 10.1038/jcbfm.2013.173
25. Song JN, Chen H, Zhang M, Zhao YL, Ma XD. Dynamic change in cerebral microcirculation and focal cerebral metabolism in experimental subarachnoid hemorrhage in rabbits. *Metab Brain Dis.* (2013) 28:33–43. doi: 10.1007/s11011-012-9369-8
26. Suzuki S, Kimura M, Souma M, Ohkima H, Shimizu T, Iwabuchi T. Cerebral microthrombosis in symptomatic cerebral vasospasm–a quantitative histological study in autopsy cases. *Neurol Med Chir (Tokyo).* (1990) 30:309–16. doi: 10.2176/nmc.30.309
27. Schutzman LM, Rigor RR, Khosravi N, Galante JM, Brown IE. P-selectin is critical for de novo pulmonary arterial thrombosis following blunt thoracic trauma. *J Trauma Acute Care Surg.* (2018) 86:583–91. doi: 10.1097/TA.0000000000002166
28. Martin GE, Xia B, Kim Y, Johnson MD, Veile R, Friend LA, et al. Platelet function changes in a time-dependent manner following traumatic brain injury in a murine model. *Shock.* (2018) 50:551–6. doi: 10.1097/SHK.0000000000001056
29. Sabri M, Ai J, Lakovic K, D'Abbondanza J, Ilodigwe D, Macdonald RL. Mechanisms of microthrombi formation after experimental subarachnoid hemorrhage. *Neuroscience.* (2012) 224:26–37. doi: 10.1016/j.neuroscience.2012.08.002
30. Chen Y, Li Q, Tang J, Feng H, Zhang JH. The evolving roles of pericyte in early brain injury after subarachnoid hemorrhage. *Brain Res.* (2015) 1623:110–22. doi: 10.1016/j.brainres.2015.05.004
31. Fumoto T, Naraoka M, Katagai T, Li Y, Shimamura N, Ohkuma H. The role of oxidative stress in microvascular disturbances after experimental subarachnoid hemorrhage. *Transl Stroke Res.* (2019) 10:684–94. doi: 10.1007/s12975-018-0685-0
32. Zechariah A, ElAli A, Doeppner TR, Jin F, Hasan MR, Helfrich I, et al. Vascular endothelial growth factor promotes pericyte coverage of brain capillaries, improves cerebral blood flow during subsequent focal cerebral ischemia, and preserves the metabolic penumbra. *Stroke.* (2013) 44:1690–7. doi: 10.1161/STROKEAHA.111.000240
33. Halliday MR, Rege SV, Ma Q, Zhao Z, Miller CA, Winkler EA, et al. Accelerated pericyte degeneration and blood-brain barrier breakdown in apolipoprotein E4 carriers with Alzheimer's disease. *J Cereb Blood Flow Metab.* (2016) 36:216–27. doi: 10.1038/jcbfm.2015.44
34. Cui J, Chen S, Zhang C, Meng F, Wu W, Hu R, et al. Inhibition of MMP-9 by a selective gelatinase inhibitor protects neurovasculature from embolic focal cerebral ischemia. *Mol Neurodegener.* (2012) 7:21. doi: 10.1186/1750-1326-7-21
35. Pang J, Chen Y, Kuai L, Yang P, Peng J, Wu Y, et al. Inhibition of blood-brain barrier disruption by an apolipoprotein E-Mimetic peptide ameliorates early brain injury in experimental subarachnoid hemorrhage. *Transl Stroke Res.* (2017) 8:257–72. doi: 10.1007/s12975-016-0507-1

36. Grasso G, Alafaci C, Macdonald RL. Management of aneurysmal subarachnoid hemorrhage: state of the art and future perspectives. *Surg Neurol Int.* (2017) 8:11. doi: 10.4103/2152-7806.198738
37. Huang Y, Zhao Y, Yan L, Chuai YH, Liu LL, Chen Y, et al. Changes in coagulation and fibrinolytic indices in women with polycystic ovarian syndrome undergoing controlled ovarian hyperstimulation. *Int J Endocrinol.* (2014) 2014:731498. doi: 10.1155/2014/731498

Conflict of Interest: The authors declare that the research was conducted in the absence of any commercial or financial relationships that could be construed as a potential conflict of interest.

The reviewer ZX declared a shared affiliation, with no collaboration, with one of the authors YW to the handling Editor.

Publisher's Note: All claims expressed in this article are solely those of the authors and do not necessarily represent those of their affiliated organizations, or those of the publisher, the editors and the reviewers. Any product that may be evaluated in this article, or claim that may be made by its manufacturer, is not guaranteed or endorsed by the publisher.

frontiers in Neurology

REVIEW
published: 23 September 2021
doi: 10.3389/fneur.2021.697779

Imaging Acute Stroke: From One-Size-Fit-All to Biomarkers

Jianfei Lu[1†], Qiyong Mei[2†], Xianhua Hou[3†], Anatol Manaenko[4], Lili Zhou[5], David S. Liebeskind[6], John H. Zhang[7], Yao Li[8] and Qin Hu[1*]*

[1] Central Laboratory, Renji Hospital, Shanghai Jiao Tong University School of Medicine, Shanghai, China, [2] Department of Neurosurgery, Changzheng Hospital, Navy Medical University, Shanghai, China, [3] Department of Neurology, Southwest Hospital, Army Medical University, Chongqing, China, [4] National Health Commission Key Laboratory of Diagnosis and Treatment on Brain Functional Diseases, The First Affiliated Hospital of Chongqing Medical University, Chongqing, China, [5] Department of Neurology, Chinese People's Liberation Army General Hospital, Beijing, China, [6] Neurovascular Imaging Research Core and University of California Los Angeles Stroke Center, University of California, Los Angeles, Los Angeles, CA, United States, [7] Department of Anesthesiology, Loma Linda University School of Medicine, Loma Linda, CA, United States, [8] School of Biomedical Engineering, Shanghai Jiao Tong University, Shanghai, China

In acute stroke management, time window has been rigidly used as a guide for decades and the reperfusion treatment is only available in the first few limited hours. Recently, imaging-based selection of patients has successfully expanded the treatment window out to 16 and even 24 h in the DEFUSE 3 and DAWN trials, respectively. Recent guidelines recommend the use of imaging techniques to guide therapeutic decision-making and expanded eligibility in acute ischemic stroke. A tissue window is proposed to replace the time window and serve as the surrogate marker for potentially salvageable tissue. This article reviews the evolution of time window, addresses the advantage of a tissue window in precision medicine for ischemic stroke, and discusses both the established and emerging techniques of neuroimaging and their roles in defining a tissue window. We also emphasize the metabolic imaging and molecular imaging of brain pathophysiology, and highlight its potential in patient selection and treatment response prediction in ischemic stroke.

Keywords: ischemic stroke, tissue window, metabolic imaging, molecular imaging, reperfusion therapy

OPEN ACCESS

Edited by:
Eduardo Candelario-Jalil, University of Florida, United States

Reviewed by:
Saurav Das, Washington University in St. Louis, United States
Chengcheng Zhu, University of Washington, United States

****Correspondence:***
Yao Li
yaoli118@gmail.com
Qin Hu
huqinle20010709@126.com

† These authors have contributed equally to this work

Specialty section:
This article was submitted to Stroke, a section of the journal Frontiers in Neurology

Received: *20 April 2021*
Accepted: *30 June 2021*
Published: *23 September 2021*

Citation:
Lu J, Mei Q, Hou X, Manaenko A, Zhou L, Liebeskind DS, Zhang JH, Li Y and Hu Q (2021) Imaging Acute Stroke: From One-Size-Fit-All to Biomarkers. Front. Neurol. 12:697779. doi: 10.3389/fneur.2021.697779

INTRODUCTION

Stroke is the worldwide leading cause of death and adult disability. More than 80% of all strokes are caused by brain ischemia, which results from obstruction of one or more cerebral arteries. Rapid and safe restoration of the blood flow through thrombolysis or/and thrombectomy is the only approved therapy for ischemic stroke. Such treatment is strictly limited by a narrow time window and need to be performed within the first few hours after the onset of symptoms (1, 2). The "time is brain" mantra has been the golden principle for acute management of ischemic stroke for decades. Due to the narrow therapeutic window and strict indications, recanalization therapy is restricted to only a small fraction (≤10%) of stroke patients[1]. In the past decade, accumulating clinical trials have shown that with the patients selecting by neuroimaging, the time window for reperfusion has been iteratively extended (**Table 1**) (3–6). The results of these studies revolutionize the field and suggested that "tissue window" might be more personalized than a "time window" to guide precision medicine for ischemic stroke (7, 8). With the rapid development of imaging technology, the ischemic penumbral tissue is now discernible and quantifiable, which provides the possibility to detect salvageable tissue and select the eligible patients for reperfusion therapies (9, 10). A tissue

[1]https://seekingalpha.com/article/4263610-athersys-stem-cell-therapy-for-ischemic-stroke

window defined by neuroimaging can serve as surrogate marker for brain physiology in ischemic stroke and facilitate therapeutic decision-making. Here we review the evolution of the time window, address the advantage of tissue window for clinic manage of ischemic stroke, and discuss the roles of neuroimaging in defining a tissue window. We also emphasize metabolic imaging and molecular imaging of brain pathophysiology, and highlight its potential in patient selection and treatment response prediction in ischemic stroke.

THE EVOLUTION OF TIME WINDOW FOR REPERFUSION THERAPY

The main aim of existing therapies in ischemic stroke is to restore the blood flow quickly and rescue the potentially salvageable brain tissue. After ischemic stroke, the injured brain is characterized by two major zones: the penumbra and the infarct core. The penumbra is the region around the core that neuronal function is partially preserved (11). The fate of penumbral cells critically relies on regional cerebral blood flow (CBF) and it worsens into infarct core in a time-dependent manner. If reperfusion is established during the early hours, cells in penumbra are salvageable (12). On the contrary, the blood flow in the infarct core declines below to 15–20% of the baseline, this would cause irreversibly damage within the first few minutes of the stroke onset (13). Unfortunately, methods of ischemic core imaging, which is currently in clinical use, are unable to discriminate between incomplete infarction and pan-necrosis. In order to overcome it and revise the clinically relevant parameters more accurately, Goyal et al. suggested replacing the "infarct core" with "ischemic tissue with severity of uncertain viability (SIT-uv)" (14). SIT-uv is considered as tissue that is potentially salvageable by timely reperfusion. Therefore, "time is brain" is still the most important principle guiding reperfusion therapy since the 1990's (15).

Two primary reperfusion strategies have been demonstrated effectiveness: intravenous thrombolysis with tissue plasminogen activator (tPA) and endovascular thrombectomy with stent retrievers (16). However, the benefits of both tPA and endovascular thrombectomy are strongly time-dependent and restricted to only a fraction of stroke patients due to the narrow time window and strict indications (17, 18). In 1995, tPA was originally recommended to treat ischemic stroke within 3 h of the onset (19). Until 2008, Hacke et al. suggested that administration of tPA could be extended to 4.5 h with computed tomographic scan to exclude the patients with hemorrhage or major infarction (20). Because of the narrow time window and strict contraindications, only 2–5% of patients present with ischemic stroke received tPA (21). Recently, guided by perfusion imaging, the window for thrombolysis with alteplase was extended up to 9 h after onset of stroke (EXTEND trial) (22, 23).

TABLE 1 | Imaging modalities used in the key clinical trials to expand the therapeutic window of ischemic stroke.

Study	Sample size	Time window	Imaging modalities	Treatment	Implications
EPITHET	101	3–6 h after onset	PWI/ DWI	Alteplase or placebo	Alteplase increased Reperfusion and neurological outcome at 90 days
ECASS III	821	3–4.5 h after onset	CT or MRI	Alteplase or placebo	Alteplase improved neurological outcome at 90 days
MR CLEAN	500	6 h after onset	CTA or MRA	Intraarterial treatment or standard care alone	Intraarterial treatment improved neurological outcome at day 90
EXTEND-IA	70	6 h after onset	CTP	Alteplase with thrombectomy or alteplase alone	Thrombectomy improved reperfusion, early neurologic recovery, and functional outcome
SWIFT PRIME	833	6 h after onset	CTP, or PWI/DWI	tPA, or tPA with endovascular thrombectomy	Thrombectomy showed more effective recanalization than tPA alone
REVASCAT	206	8 h after onset	CT, DWI	Thrombectomy or standard care alone	Thrombectomy reduced the severity of disability
ESCAPE	316	12 h after onset	CT, CTA	Thrombectomy plus standard care or standard care alone	Endovascular thrombectomy benefited the patients with moderate-to-severe ischemic stroke.
DEFUSE-3	182	6–16 h after onset	CTP, PWI/DWI	Thrombectomy plus standard care or standard care alone	Thrombectomy resulted in better functional outcomes than standard medical therapy alone
DOWN	206	6–24 h after onset	DWI, CTP	Thrombectomy plus standard care or standard care alone	Thrombectomy improved the outcomes at 90 days
WAKE UP	503	4.5 h to unknown time of onset	DWI, FLAIR	Alteplase or placebo	Alteplase improved functional outcome at 90 days

CT, computed tomography; CTP, computed tomography perfusion; CTA, computed tomography angiography; MRI, magnetic resonance imaging; MRA, magnetic resonance angiography; DWI, diffusion-weighted imaging; PWI, perfusion-weighted imaging; FLAIR, fluid-attenuated inversion recovery; tPA, tissue plasminogen activator.

However, the authors had certain doubts that positive results of the WAKE-up trail nullified the equipoise and terminated the trail early for this reason (3). Furthermore, due to the small number of patients (225 patients from 27 hospitals over 8 years) and because 80% of the patients had large vessel occlusions, the conclusion of EXTEND trail was not reflected in the current guidelines of American Heart Association (AHA). Still AHA recommended taking into account the conclusion of WAKE-UP trail, which stated that patients, who awoke with stroke or had an unclear time of onset which might be more than 4.5 h of the past (>4.5 h from the last known well) could be treated with IV alteplase (24). The eligibility is magnetic resonance imaging (MRI) mismatch between abnormal signal on diffusion-weighted magnetic resonance imaging (DW-MR) and no visible signal change on FLAIR. Present guidelines also endorsed the usage of tenecteplase in patients eligible to mechanical thrombectomy who do not have contraindications for IV fibrinolysis. There is emerging evidence for the non-inferiority of tenecteplase compared to alteplase, although it has not been widely accepted in clinical practice yet (25).

In 2015, it was proven that mechanic thrombectomy with/without intravenous thrombolysis can improve functional outcomes within 6 h after stroke onset (26–28). In patients who have proximal arterial occlusion and small infarct core, mechanical thrombectomy can extend the therapeutic window to 8 h (REVASCAT Trial) even to 12 h (ESCAPE Trial) (29–31). Based on two other recent trials DEFUSE 3 and DAWN, the therapeutic time window can be extended to 24 h since stroke onset (5, 6). Case studies even reported that delayed thrombectomy days or weeks after onset achieved good clinical outcome (32, 33). Recent animal studies proved that delayed recanalization at 3, 7, or 14 days after permanent middle cerebral artery occlusion (MCAO) led to better functional and histological recovery (34). These researches represent a new milestone in acute stroke therapy (**Figure 1**). Imaging-based patient selection plays a crucial role in the success of these clinical trials and inspires us to rethink the principle "time is brain."

The salvageability of the affected brain tissue depends primarily on both the duration and the severity of ischemia. The onset-to-treatment time is not the inflexible determinant of reperfusion therapy when takes the collateral flow into accounts. The more extensive the collateral flow, the longer the brain tissue is tolerant to ischemia. However, the collateral flow is highly variable among individuals, which results in variation in tissue susceptibility and therapeutic window. The current "one-size-fit-all" therapeutic time window does not consider the collateral circulation and varied tissue susceptibility, and how to evaluate the viability of the ischemic tissue quickly and accurately is a challenge for the individualized reperfusion therapy.

DETECTION OF THE PENUMBRA

The penumbra was first experimentally delineated by Astrup in a baboon MCAO model in 1977. Using somatosensory-evoked potentials, he defined the penumbra as an area surrounding the ischemic core in which neurons are affected but have the

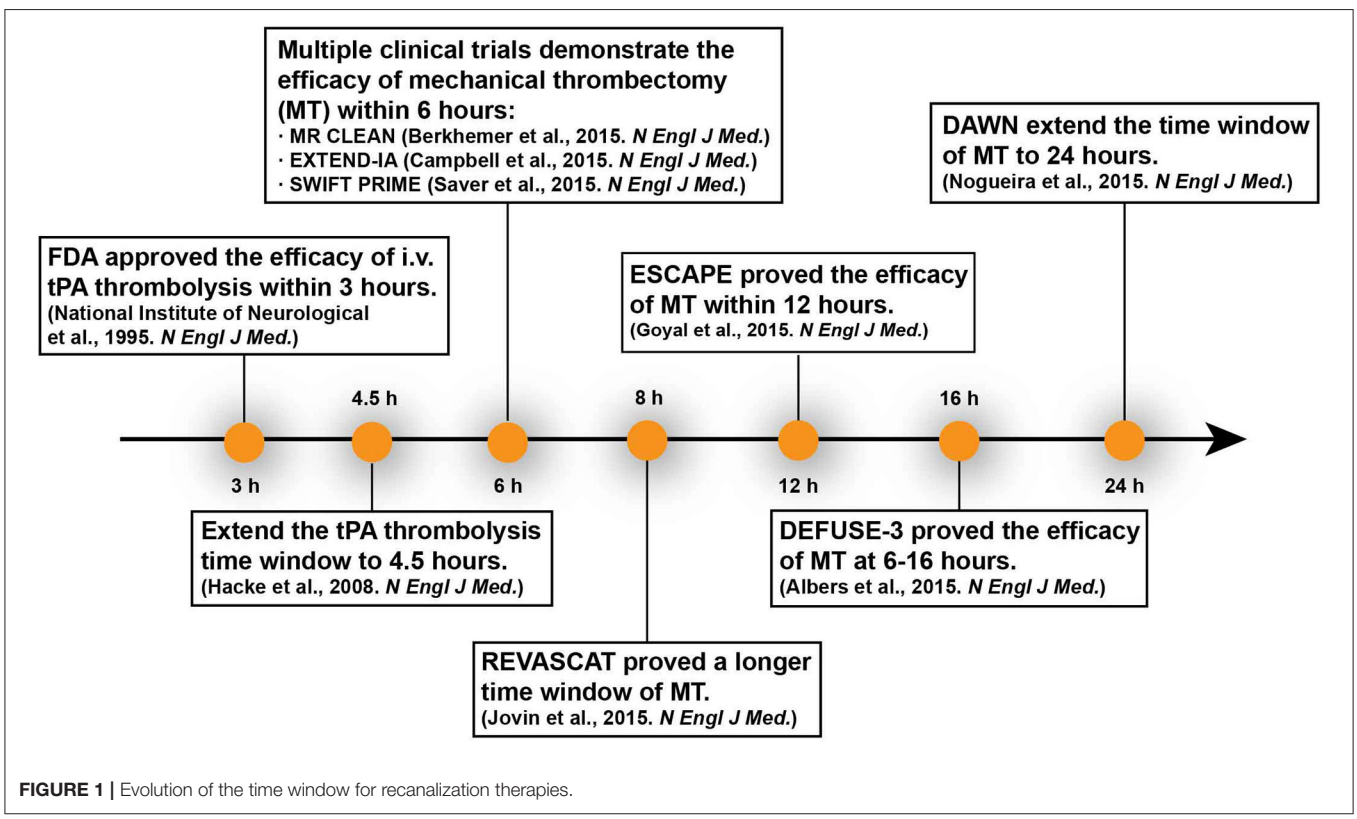

FIGURE 1 | Evolution of the time window for recanalization therapies.

potential for recovery. Neurons in this area are characterized by low electric activity but sustained energy metabolism, and they do not have noticeable morphological damage (35). Because of the invasive method, it was difficult to translate this experimental concept to clinic and improve stroke diagnosis and treatment. Modern imaging techniques such as positron emission tomography (PET), MRI, and computerized tomography (CT) can distinguish salvageable tissue invasively by measuring hemodynamics and energy metabolism. PET is considered as the "gold standard" for penumbra imaging, however, MRI is more favorable in practice. In addition, CT perfusion is being increasingly used for its low cost and wide availability. The strengths and weaknesses of these imaging modalities on penumbra identification are summarized in **Table 2**.

PET

The existence of penumbra in stroke patients was demonstrated for the first time by PET. In 1981, Baron et al. observed decreased CBF and increased oxygen extraction fraction (OEF) in an ischemic stroke patient by PET and coined this modality as "misery perfusion" which indicated potential viable tissue (36). This area with increased OEF was the original definition of penumbra. Labeling arterial blood sample with ^{15}O allows PET to assess the regional CBF, OEF and cerebral metabolic rate of oxygen ($CMRO_2$) ($CMRO_2$ = CBF × OEF × arterial oxygen content) and determine the penumbra. Early PET studies classified the ischemic tissue into 3 regions depending on CBF rate: the infarct core with CBF <12 ml/100 g·min, the penumbra with CBF of 12–22 ml/100 g·min and the oligemia with CBF >22 ml/100 g·min (37–40). In practical applications, the extent of penumbra is dynamic and time dependent process, which varies with the severity and duration of ischemia. CBF value only reflects the reperfusion status at the time of imaging. An initial severe ischemia may show a normal appearing CBF value because of partial restoration of blood flow, but the ischemic tissue has already irreversibly damaged (37, 41). The advanced ^{15}O-O_2 PET can detect OEF and distinguish viable tissue from core infarction. Thus, the mismatch between CBF and oxygen metabolism is usually considered as the *in vivo* hallmark of penumbra region, which maintains transient oxygen supply while suffering severe hypoperfusion (40, 42). Recently, some advanced approaches have been used to identify the penumbra. ^{11}C-flumazenil (^{11}C FMZ), a marker of cortical neuron integrity, combine with ^{15}O-H_2O PET can detect early neuronal death irrespective of time elapse and without arterial blood sampling. Based on the specific metabolic parameters, it is well-accepted that PET is the gold standard for determining the penumbra (43, 44).

However, detection of penumbra by PET has several limitations, such as technical difficulty, invasive procedures, exposure to radioactivity and high cost, which prevent PET from broad acceptance in clinical routine (44). Therefore, both improvement of current methods and the development of other imaging modalities are needed.

TABLE 2 | Comparison of strengths and weaknesses of different imaging modalities for penumbra identification.

	Parameters	Strengths	Weaknesses
PET	^{15}O-OEF ^{15}O-rCBF ^{15}O-$CMRO_2$	Gold standard	Technical difficulty Invasive procedure Radiation High cost
MRI	DWI/PWI $^{23}Na/^{1}H$ MRI Sodium MRI DWI/SWI T2* OC/PWI	Easy-to-use Good spatial resolution High sensitivity Non-invasive No radiation	Time-consuming High cost Inaccuracy
CT	CBF CBV MTT TTP Tmax	Widely accessible Easy-to-use	Radiation Contrast agent required Hard to standardization

PET, positron emission tomography; MRI, magnetic resonance imaging; CT, computed tomography; OEF, oxygen extraction fraction; rCBF, regional cerebral blood flow; $CMRO_2$, cerebral metabolic rate of oxygen; DWI, diffusion weighted imaging; PWI, perfusion weighted imaging; SWI, susceptibility-weighted imaging; OC, oxygen challenge; CBF, cerebral blood flow; CBV, cerebral blood volume; MTT, mean transit time; TTP, time to peak; Tmax, time to maximum.

MRI

Compare to PET, MRI has better spatial and temporal resolution, and no risk of radiation exposure of patients. MRI has largely replaced PET in acute stroke imaging in clinic (45). The MRI-based perfusion-diffusion mismatch (PDM) is a surrogate of PET-based penumbra evaluation (**Figure 2**). Diffusion weighted imaging (DWI) refers to the visualization of random Brownian movement of water molecules in brain tissue. Lower diffusion coefficients generally resulted from energy failure and subsequent cytotoxic edema, and it is suggested to delineate infarct core tissue that irreversibly damaged (**Figure 3**) (46). Perfusion weighted imaging (PWI) measures brain perfusion dynamically with such parameters as CBF, cerebral blood volume (CBV), mean transit time (MTT) and time to peak (TTP) (**Figure 3**) (47). PWI abnormality provides the information on both infarct core and the surrounding hypoperfused tissue. Volumetric-based PDM is usually defined as a mismatch ratio of PWI/DWI ≥1.2, which is postulated to represent the penumbra that locates outside the infarct core but is at risk of infarction (48). The concept of PDM has been proved practically in both experimental and clinical studies (49–51). Early clinic studies have shown that salvage of brain tissue delineated by the PDM improved neurological functions (52, 53), and selection of patients with PDM increased the rate of reperfusion and achieved favorable clinical response when treated within 6 h (54, 55). However, this surrogate marker of penumbra is challenged by several limitations (44). Comparative PET/MRI studies confirmed the mismatch area imprecisely depicts elevated OEF and overestimated the penumbra from benign oligemia defined by PET. Because of the wide variation in thresholds, DWI also overestimates the infarct core by including part of the penumbra (56–58). And as the viability and metabolic state of brain tissue strongly depends on the duration of ischemia, for those "wake-up" patients who didn't know stroke onset time

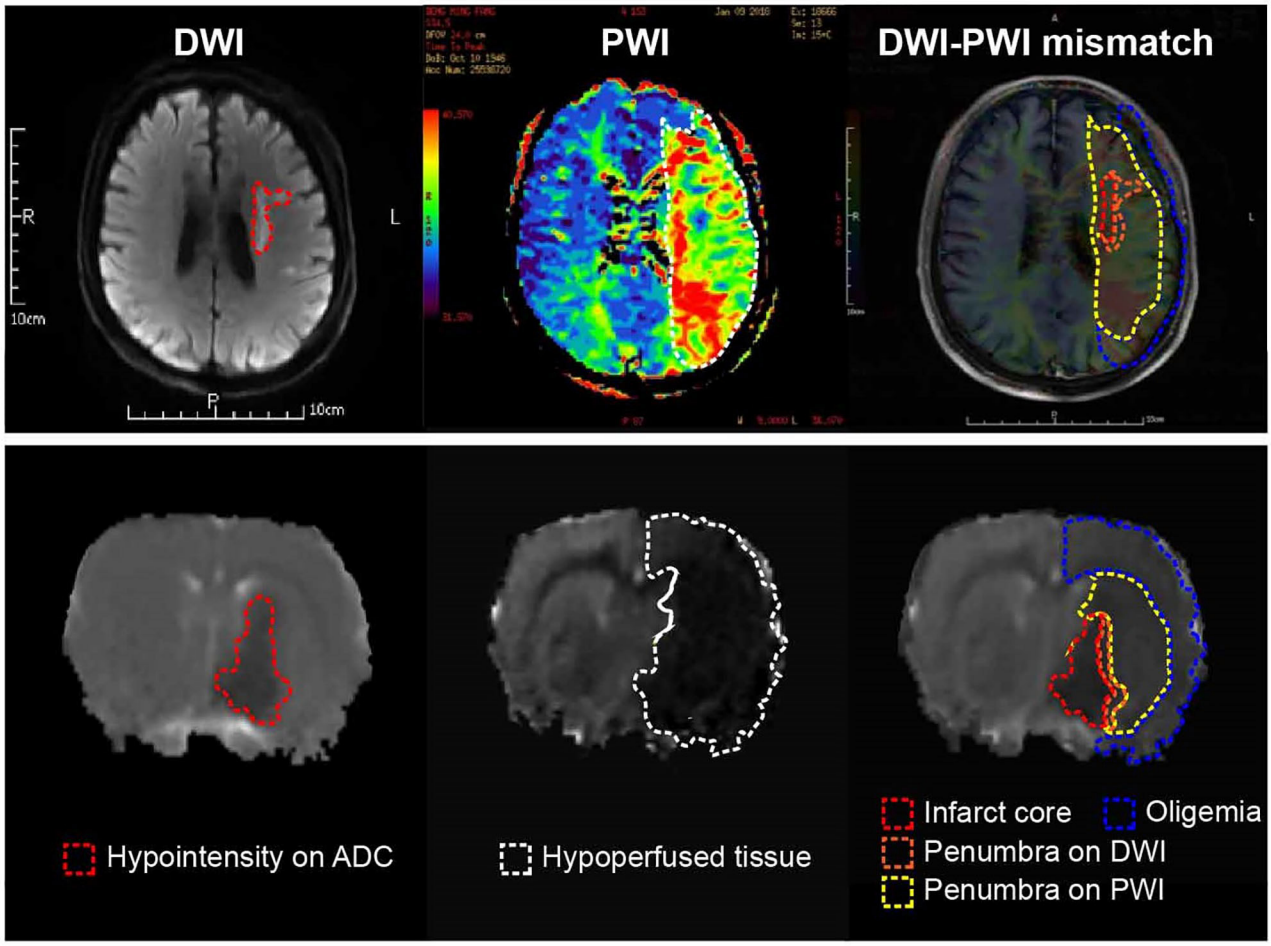

FIGURE 2 | Current concept of the ischemic penumbra. Both clinical (Upper) and experimental (Below) MRI data showed early abnormality on DWI equals the infarct core plus a part of tissue at risk (penumbra), and the perfusion deficiency on PWI includes part of the region of benign oligemia. MRI, magnetic resonance imaging; PWI, perfusion-weighted imaging.

(SOT), it is hard to set threshold of the parameters [such as TTP and time to maximum (Tmax)] (57).

Accumulating evidence has shown that there was no clear association between PDM and penumbra (59–62), and the inaccuracy of PDM in defining penumbra may be responsible for the failure of some reperfusion and neuroprotection therapies in clinic (63, 64). It is urgent to develop novel imaging paradigms that can serve as a clinical marker of penumbra. Several attempts have been made to improve the accuracy of PDM in penumbra predicting. Combined ^{23}Na-MRI to ^{1}H-MRI was developed to complement PDM and serve as a viability marker for penumbra detection in several animal models. Tissue sodium concentration increased in the core and decreased in the penumbra so that the viable penumbra could be differentiated from the core in transient MCAO rats (65, 66). In addition, it has been proposed that sodium MRI may help determine the SOT by calculating this retrospectively (67, 68). Susceptibility-weighted imaging (SWI) is also used to identify the penumbra in stroke patients. SWI detects the paramagnetic susceptibility difference between deoxygenated and oxygenated hemoglobin, which reflects the OEF of brain tissue (69). DWI-SWI mismatch is shown to be a promising marker for evaluating penumbra (70). In addition, by mapping the ratio changes of deoxyhemoglobin/oxyhemoglobin, T_2^* oxygen challenge combined PWI assessed the viability of penumbra serially and showed advantages over PDM for penumbra detection (71).

Computed Tomography Perfusion (CTP)

CTP is an imaging technique that is increasingly used for determination of infarct core and penumbra in acute ischemic stroke patients. The clear advantages of this technique are its easily accessibility and fast acquisition (72). Similar to PWI MRI, raw data of CTP is also displayed in parameter maps, including CBF, CBV, MMT, TTP, and Tmax. Regions with dramatically reduced CBF or CBV correspond to the core infarction, while regions with prolonged MTT, TTP, or Tmax delineate the penumbra (**Figure 4**) (73). However, there is significant

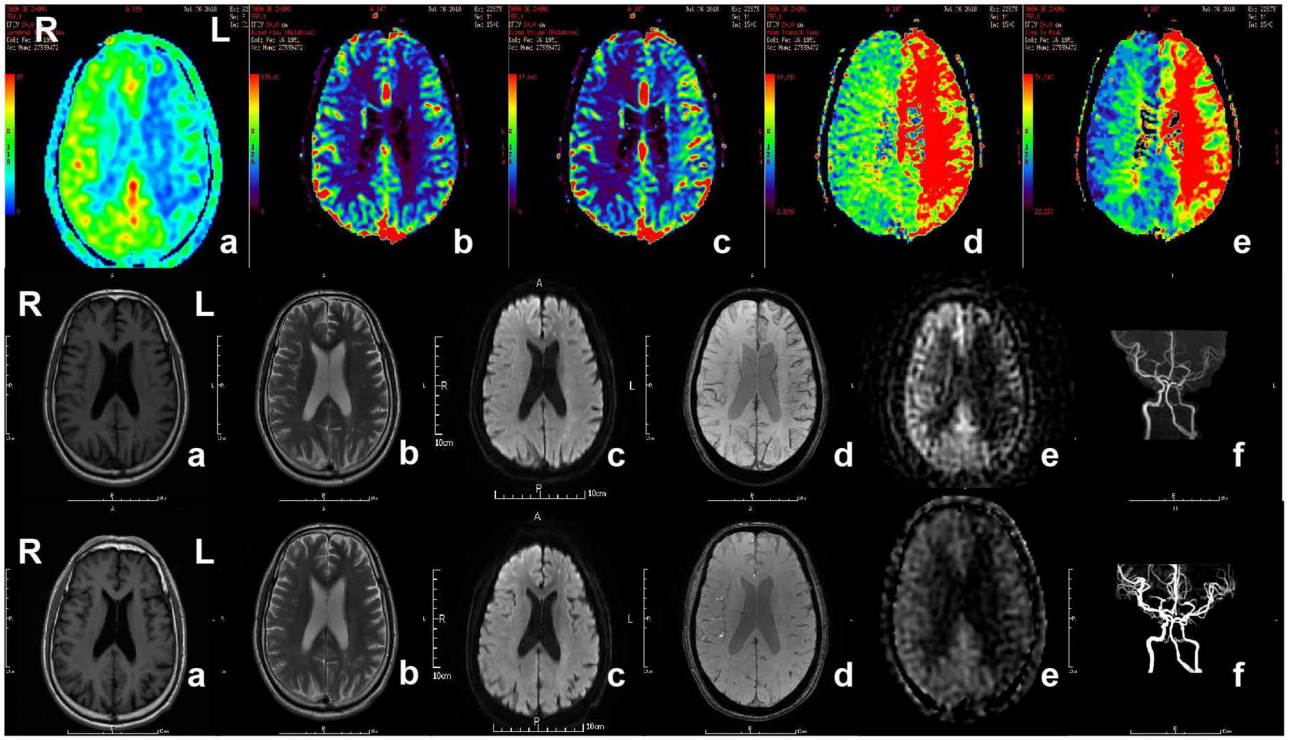

FIGURE 3 | MR imaging of the patient with acute ischemic stroke. The patient, 71-year-old male, suffered from weakness of right limbs, alalia and was unable to walk 3 h prior to the imaging. Medical history included hypertension, diabetes and varicosity of both lower extremities. Physical examination showed right facial paralysis, the muscle strength of right limbs was grade I, right Babinski sign (+), Chaddock sigh (+), and NIHSS score was 13. The diagnosis of the patient is acute ischemic stroke. The patient was given multimodal MRI and MRA before and after recanalization. The first row showed perfusion-weighted imaging. a and b, Lower CBF in left cerebral hemisphere. c, Higher CBV in left cerebral hemisphere. d, Longer MTT in left cerebral hemisphere. e, Longer TTP in left cerebral hemisphere. The second row and third row showed MRI and MRA before recanalization and after recanalization, respectively. a, b, and c, In the left frontal lobe and lateral ventricle had sporadic dots with slightly longer T1 signal, longer T2 signal higher signal, respectively, in T1WI, T2WI, DWI. d, No cerebral microbleeds in SWI. e, Original ASL. f, MRA showed the intracranial segment of the left internal carotid artery and the left middle cerebral artery were significantly narrow in the second row, while recanalization got in left internal carotid artery and middle cerebral artery. MR, magnetic resonance; MRA, magnetic resonance angiography; SWI, susceptibility weighted imaging; ASL, arterial spin labeling; CBV, cerebral blood volume; CBF, cerebral blood flow; TTP, time to peak; MTT, mean transit time.

variability in CTP technique between different CT scanners, processing software and prior institutional optimization, and this results in controversy about the accurate measurement of penumbra (74). Moreover, due to the delay of the arrival of contrast to brain, CBV calculation always results in an overestimation of the core lesion that leads to an underestimation of penumbra (75). CTP still has the risk of radiation exposure and toxicity of the contrast agent.

METABOLIC IMAGING OF ISCHMEIC STROKE

For patients excluded from reperfusion therapy due to exit of the therapeutic time window established by imaging strategy mentioned above, there is another opportunity to expand the treatable population: selecting of the patients by advanced physiologic imaging. Both MRI-based PDM and CTP depend on selecting threshold values of blood flow to differentiate the penumbra from infarct core and benign oligemic brain tissue. And these thresholds change with the evolution of stroke. So far, there are no validated thresholds that accepted for routine penumbra imaging in the clinical setting. Parameters which display the physiology of brain immediately and independently of the onset-time are in urgent need to delineate penumbra accurately and guide the precision therapy in stroke. When the blood flow is compromised, energy metabolism disturbance occurs within seconds as brain has very limited supply of energy producing substances and relies on oxidative metabolism to meet its tremendous energy requirements (76, 77). The metabolic stress induces ionic perturbations and oxidative stress which trigger the cascade of pathophysiological events ultimately resulting in neuronal death (78). Accumulating evidence has suggested that energy status is associated with cell survival and determines the fate of ischemic tissue (79–81). Direct measurement of the metabolic status provides more accurate information to delineate the viable tissue. Therefore, energy metabolism can serve as a direct indicator of the salvageable tissue in the penumbra zone. Quantification of cerebral oxygen metabolism has shown great promise in revealing the viability of ischemic tissue during stroke. Several imaging modalities, such

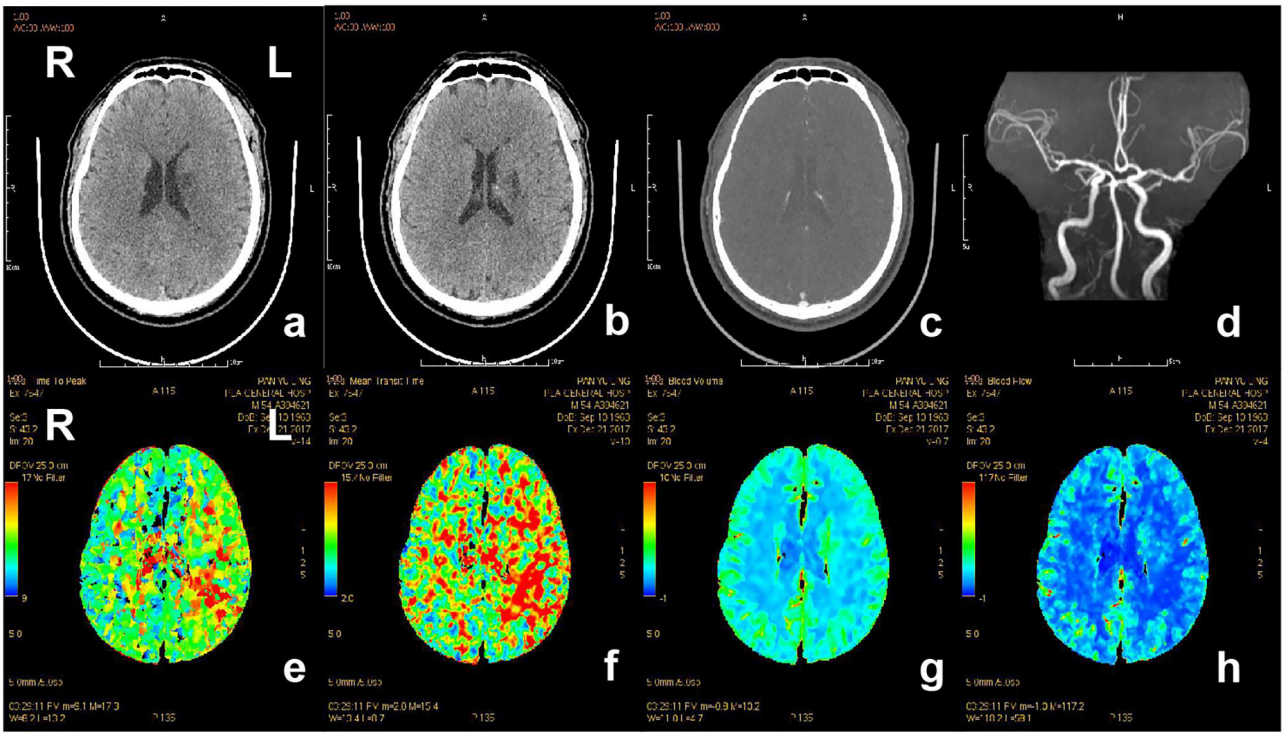

FIGURE 4 | CT and CTP imaging of the patient with acute ischemic stroke. The patient, 80-year-old-female, suffered from weakness of right limbs, alalia and was unable to walk 3.5 h prior to the imaging. Medical history included hypertension, atrial fibrillation and gout. Physical examination showed right facial paralysis, the muscle strength of right limbs was grade I, right Babinski sign (+), and NIHSS score was 10. The diagnosis of the patient is acute ischemic stroke. The patient was given multimodal CT and MRA before recanalization. a and b, The left bilateral basal ganglia and bilateral frontal lobe showed sporadic dots and patches with low-density shadow on non-contrast CT scan. c, Contrast-enhanced CT showed no abnormal enhanced shadow. d, MRA showed the lumen of bilateral middle cerebral artery was not smooth, the left cerebral artery M1 segment had multiple stenosis, and distal branch vessels were disappeared. e and f, Prolonged TTP and MTT in the area of left middle cerebral artery. g and h, CBF and CBV showed no significant abnormal area. CT, computed tomography; CTP, computed tomography perfusion; CBV, cerebral blood volume; CBF, cerebral blood flow; TTP, time to peak; MTT, mean transit time.

as PET and MRI, have been applied to image cerebral oxygen metabolism in both experimental research as well as clinical practice (82). These imaging methods and parameters they can detect are summarized in **Table 3**. Furthermore, we review the most recently advances in metabolic imaging, which may greatly facilitate routine clinical applications to guide optimal therapy decision for acute ischemic stroke as well as subacute or chronic stroke with permanent large vessel occlusion.

PET Metabolic Imaging

As mentioned above, ^{15}O multi-tracer PET can provide the tomographic distributed imaging of brain oxygen extraction and metabolism. More importantly, it is the reference standard for quantitative evaluations of OEF, $CMRO_2$, CBV, and CBF. In the late 1970's, scientists successfully measured the regional brain CBV and CBF, and oxygen metabolism in stroke patients with ^{15}O-labeled PET, and distinguished the severely hypoperfused but potentially salvageable tissue from the irreversibly damaged (83–85). Using ^{15}O-H_2O PET, Heiss et al. found that the misery perfused tissue was salvaged by early intravenous thrombolysis (86). This study is a millstone in stroke research. It revolutionized the management of acute stroke patients by demonstrating the positive result of rt-PA. However, due to the technical complexity, ^{15}O PET is not widely performed in clinical settings, with issues involving requirement of on-site cyclotron and radiochemistry facility because of the short half-life of ^{15}O (2 min), real-time artery blood sampling and analyzing to obtain the regional CBF (rCBF), as well as complex post processing (87). Efforts have been made to streamline the ^{15}O-PET examination for routine clinical practice, including: (i) quantitative voxel-by-voxel maps of rCBF without a direct arterial input function (88); (ii) shortening the clinical examination period by dual-tracer ($H_2^{15}O$ and $^{15}O_2$) autoradiography approach (89); and (iii) developing non-invasive techniques to assess CBF, OEF, and $CMRO_2$ (90). Attempts were also made in animal stroke studies. Methodological inventions, such as intravenous administration of injectable $^{15}O_2$ and inhalation of $^{15}O_2$ gas, had been tried to facilitate the evaluation of $CMRO_2$ and OEF in small animals (91–93). These developments potentiate the possibility of using PET in clinical routine to expand the treatable stroke patients in early stage.

The improvement of the radiotracers has revolutionized the use of PET in measuring OEF and $CMRO_2$ and mapping the cerebrovascular reserve and the penumbra. The newly

TABLE 3 | The three major imaging methods for acute stroke and physiological parameters they can detect.

	Parameters	PET	MRI	CT
Metabolism	Oxygen metabolism	^{15}O-OEF ^{15}O-CMRO$_2$	OCI	
	Neuronal death	^{11}C-FMZ		
	Hypoxia	^{18}F-MISO Cu-ATSM		
	pH		APT-MRI ^{13}P MRS	
	Lactate		^{1}H MRS ^{13}C MRS	
	NAA		^{1}H MRS	
	PCr/Pi		^{13}P MRS	
	ATP		^{13}P MRS	
Pathophysiology	Excitotoxicity		^{1}H MRS GluCEST	
	Apoptosis		^{1}H MRS	
	Inflammation	Cu-ATSM TSPO	SPIO/USPIO	
			MNP-PBP MPIO	
	BBB leakage		DCE-MRI	DCE-CT Micro-CT

FMZ, flumazenil; MISO, misonidazole; Cu-ATSM, Copper-based Radiopharmaceuticals; APT, amide proton transfer; MRS, MR spectroscopy; NAA, N-acetylaspartate;PCr, phosphocreatine; Pi, inorganic phosphate; ATP, adenosine triphosphate; CEST, chemical exchange saturation transfer;S PIO/USPIO, small and ultrasmall superparamagnetic iron oxide particles; MNP-PBP, magnetic nanoparticle-P-selectin binding peptide; MPIO, microparticles of iron-oxide; TSPO, translocator protein; DCE, dynamic contrast-enhanced.

developed PET ligands, including radio-labeled FMZ, radio-labeled fluoromisonidazole (FMISO), and copper-based radiopharmaceuticals (Cu-ATSM) have been explored to delineate the disease in preclinical and clinical research. In 1997, ^{11}C-FMZ PET was used to indicate the development of infarction in cat stroke model and showed the potential to select eligible patients for early therapeutic intervention (94). In 2000, a clinical trial proved that 11C-FMZ PET was able to differentiate the viable tissue from the irreversibly damaged at the early stage of acute stroke (95). In this study, the areas with reduced perfusion but preserved ^{11}C-FMZ binding could benefit from reperfusion therapy, while the areas with ^{11}C-FMZ uptake defects were permanent lesions. Thiel et al. reported that ^{11}C-FMZ PET could be used to estimate rCBF in ischemia without arterial input function (96). However, the application of ^{11}C-FMZ PET in clinical practice is limited by several issues: the requirement of cyclotron to produce ^{11}C, the regional expression of benzodiazepine receptors in cerebral cortex, and the low affinity of ^{11}C-FMZ to bind with its receptor at the acute phase of ischemia/reperfusion (97). New PET tracers are still in urgent need to meet the clinical requirements.

Compared with^{11}C-FMZ PET, ^{18}F-FMISO PET is more broadly used (98). In a preclinical study, ^{18}F-FMISO microPET was used to map the brain hypoxia in the acute stage of permanent distal MCAO rats, and supported that ^{18}F-FMISO might be a marker of core area as well as of penumbra (99). Besides, ^{18}F-FMISO uptake was also used to predict the tissue fate. The patients without ^{18}F-FMISO uptake had no infarct growth on the follow-up DWI, while those with abnormally increased ^{18}F-FMISO uptake showed grown infarct (100). And white matter was reported to take up more ^{18}F-FMISO than gray matter, indicating stronger resistance to ischemia than gray matter (101). However, the penumbra outlined with ^{18}F-FMISO may be overestimated. When using ^{18}F-FMISO in ischemic stroke patients, large regions of hypoxic tissue was found surrounding the ischemic core, which spontaneously reverted back to normal (102). The major drawback of ^{18}F-FMISO PET is the slow kinetics of ^{18}F-FMISO, which requires 2–3 h to clear it from the hypoxic tissue. A faster kinetic and metabolic rate tracer is needed for metabolic imaging. Compared with nitroimidazole, Cu-ATSM is rapidly washed out, and the imaging can be finished with 20–30 min after injection (103). Cu-ATSM has also been proved to modulate inflammation and has therapeutic potential in experimental stroke (104).

MRI Metabolic Imaging

Studies have investigated MR-based PWI and DWI, and suggested the PWI-DWI mismatch regions as potentially salvageable tissue (51). This clinical routine protocol does not define metabolic activity directly; however, PWI and DWI clearly indicate different metabolic regions. The following sections will carefully discuss related major MRI metabolic imaging techniques, which have been summarized in **Table 2**.

Magnetic Resonance Spectroscopy

MRS acquires the signal arising from brain metabolites by analyzing molecules such as hydrogen ions or protons. Because of high spatial and temporal resolution, proton MRS (^{1}H MRS) is the more commonly used. The most assessed metabolites with potential value for clinical stroke evaluation are lactate (1.30 ppm) and tNAA (2.02 ppm) (105–107). Preclinical studies have shown that levels of total N-acetylaspartate (tNAA) decrease to 50% in the first 6 h after ischemic stroke, followed by a milder decrease to 20% for the subsequent 24 h, and gradually returned to 30% until 7 day (107). Clinically, the concentration of tNAA in penumbra and in core infarction may even decrease below the level of detection (108, 109). Severely decreased tNAA is related to serious clinical syndrome and extensive infarction, which means poor clinical outcome (110). Lactate is the end product of anaerobic glycolysis and rises within minutes after ischemic stroke. Elevated lactate in the core of ischemic tissue is positively related to the final infarct size and neurological deficits (111). The increase of lactate accompanied with reduction of tNAA was observed in patients with large infarction and poor outcome (110). Therefore, the level of lactate and tNAA is important for evaluating the severity of stroke and predicting the recurrence of ischemic events (112). Interestingly, a recent MRS stroke animal study suggested that ML3 (bis-alyllic protons of polyunsaturated fatty acids, 2.80 ppm), which was detected of a significant increase at 7 days after stroke, may be a non-invasive surrogate biomarker

of cumulative apoptosis in stroke, which could be used as a clinical predictive marker (107).

^{13}P MRS is also used to evaluate brain energy metabolism in ischemic stroke by assessing the high energy phosphate metabolism, particularly adenosine triphosphate (ATP) and creatine phosphate (PCr) (113). A gradual decrease in ATP was only exhibited in severe stroke, not mild stroke (114). The ratio of PCr to inorganic phosphate (Pi) (PCr/Pi) showed a precipitous decrease during ischemia as well as reperfusion (114). Cerebral intracellular pH can also be measured by ^{13}P MRS. It was calculated by the chemical shift (δ) of the Pi resonance peak relative to the PCr resonance peak (115).

Though MRS is of great value in assessing the severity of ischemia and predicting the risk for recurrence, low signal-noise ratio, long sequence duration and the risk of lipid contamination make MRS not suitable for routine assessment of acute ischemic stroke patients.

Oxygen Challenge Imaging

Oxygen challenge imaging (OCI) is based on blood oxygen level-dependent (BOLD) contrast MRI that reflects the changes in blood oxygen saturation. OCI uses transient hyperoxia during T_2^*-weighted MRI to present dynamic changes in deoxyhemoglobin concentration. Therefore, tissues in the penumbra exhibit an increase in T_2^* signal intensity, with diminished or absent T_2^* signal intensity in the infarct core. Time to peak value from OCI offers additional information to facilitate the identification of at-risk tissue in ischemic stroke rats (116). The region of OCI response was reported to be larger than the PWI-DWI mismatch region (117). The T_2^* OCI was developed using 100% normobaric hyperoxia and has showed clinical translational potential for stroke diagnosis. However, inhaled 100% oxygen induces sinus artifacts in the front lobe. Decreasing the concentration of inhaled oxygen can decrease these artifacts, but makes more difficult to distinguish the penumbra from surrounding tissues (117). Recently, the combination of 40% oxygen and perfluorocarbons and fluorinated hydrocarbons with respiratory gas significantly enhanced T_2^* response to 40% oxygen in T_2^* defined penumbra (118). The same group also developed the GOLD (Glasgow Oxygen Level Dependent) diagnostic imaging method by using T_2^*oxygen challenge (T_2^*OC, 100% inhaled oxygen) combined with lactate change MRS technique (119). This method worked concurrently to identify the salvageable tissue in penumbra based on the glucose metabolic status in MCAO rats. However, the disadvantages of OCI are, as mentioned above, the poor signal-to-noise due to the limited oxygen that delivered to the tissues and the artifacts caused by the paramagnetic effect of 100% O_2 within the paranasal sinuses (120).

pH-Weighted Imaging

Zhou et al. developed a new MRI approach which was predominantly sensitive to the intracellular pH changes (121). This method benefited from the chemical exchange processes, which amide protons transfer between cellular peptides and proteins in a pH-dependent manner. Because amide proton transfer (APT) is pH dependent, measures of APT may be used to measure pH value (122). Acute ischemic stroke causes an accumulation of lactic acid and results in the decrease of pH, which could be the earliest sign for the tissue at risk. Accordingly, there were research data which suggested that pH imaging could be used to define the ischemic penumbra. The hypoperfused tissue with normal ADC and low pH may represent ischemic penumbra (121, 123, 124). A further study suggested that an additional pH-weighted imaging with PWI-DWI was superior to PWI-DWI alone to predict the tissue outcome in ischemic stroke rats (125).

Although most early studies, which investigated pH-weighted imaging technique, were performed in rodents, there is increasing translation of this technique to human studies. Tietze et al., for the first time, demonstrated that clinical application of pH-weighted imaging in acute stroke patients was possible and could be quantified, which carried potential for providing additional information on metabolic changes in acute ischemia (126). Subsequently, scientists from Oxford successfully identified the ischemic penumbra using pH-weighted magnetic resonance imaging (127).

Although studies related to pH-weighted imaging have provided important insights in the pathology of acute stroke, they currently cannot be applied in clinical routine due to their technical limitations, such as hardware constraints of human MRI scanner (short repetition time and strong radio-frequency saturation power), acquisition protocols selection (single-slice or volumetric APT imaging) and analyzing techniques (128). Consequently, pH-weighted imaging studies have paid more attention to develop better quantifying approaches and improve the APT MRI sensitivity to pH, thus, the acidosis in ischemic penumbra can be more reliably delineated (128–130).

Other Mmetabolic Imaging Techniques

There are many other imaging modalities that are at early stage of ischemic metabolic imaging, such as sodium imaging, PET ^{17}O imaging, and MR-derived cerebral metabolic oxygen index (MR COMI) (131). While metabolic imaging is promising, emerging imaging technologies require considerable validation to consider how they fit into the current imaging protocols and what information they accurately provide to guide the recanalization therapy. Many of these techniques will require technical refinement before they can be used in clinical acute ischemic stroke.

MOLECULAR IMAGING OF PATHOPHYSIOLOGY

Ischemia causes the shortage of glucose and oxygen and subsequently depletion of ATP, which result in the dysfunction of sodium-potassium pump and membrane depolarization (132). That induces multiple pathophysiological cascades, including excitotoxicity, apoptosis, acidosis, blood-brain barrier (BBB) leakage, and immune response, which lead to ischemic neuronal loss (133).

Several imaging techniques have been used in the visualization of ischemic stroke pathophysiology (134). For example, ischemia

results in marked reduction of tissue pH that triggers neuronal death (135). As mentioned above, pH-weighted MRI can detect the changes of tissue pH value that reflect the progress of acidotoxicity. MRS can evaluate tissue levels of lactate and ML3 that on this way estimate the status of acidosis and apoptosis. Current developments of pathophysiology imaging facilitate the *in vivo* assessment of pathophysiological markers and therapeutic targets after stroke, and provide the opportunities for the translation of multimodal imaging strategies in stroke diagnosis and treatment. The pathophysiological parameters that can be detected are summarized in **Table 2**.

Visualization of Excitotoxicity

Excitotoxicity caused by excessive release of glutamate is one of the major culprits that responsible for the neuronal death and neurological deficits after stroke. The levels of glutamate can be detected by ^{1}H MRS. In MCAO model in rats, Ramos-Cabrer et al. demonstrated that the levels of glutamate increase in center of the infarction core and then spread to the peri-infarction. Within 24 h after stroke, glutamate levels decreased significantly in the infarct core area, whereas regular levels were detected in the periphery of the core lesion (136). A clinical research found the differences of glutamate levels between infarct core and reperfused ischemic penumbra. In the ischemic stroke patients who received intravenous tPA within 4.5 h, high glutamate concentrations in peri-infarct were observed in the hyperperfused patients, while glutamate concentrations were low in the non-hyperperfused patients (137). The evaluation of glutamate depends on the magnetic field strengths. At low magnetic field scanner, the peak of glutamate and glutamine are consecutive that cannot distinguish glutamate from glutamine. At field strengths of 3.0 T or higher, the separation of glutamate and glutamine is feasible. Besides, ^{1}H MRS technique requires long acquisition times and has low spatial resolution.

Recently, a new MRI technique for imaging glutamate has been developed based on chemical exchange saturation transfer (CEST) effect. The CEST effects of amide and hydroxyl protons have also been used to measure pH value changes after ischemic stroke. It has been demonstrated that middle cerebral artery occlusion (MCAO) induced about 100% elevation of glutamate CEST (GluCEST) in the ischemic tissue compared with the contralateral side in rats. This method images the relative changes of glutamate and has the advantages of high spatial and temporal resolution. However, GluCEST imaging is only achievable in the human brain in ultrahigh field (7.0 T) and is not currently accessible in the clinic (138).

Monitoring the Neuroinflammation and Immune System

The immune system plays a pivotal role in the response to ischemia and the eventual recovery of function (139). The complex cascade of immune cells and inflammatory factors contribute to the breakdown of BBB. After stroke, microglia immediately respond to the ischemic insult, followed by the proliferation of macrophages, dendritic cells, and lymphocytes. With the occurrence of BBB breakdown, neutrophilic cells permeate the infarct and peri-infarct region. The immune cells release excessive pro-inflammatory cytokines (i.e., TNF-α and IL-1β) and produce large amounts of free radicals, which contribute to the upregulation of cell adhesion molecule and further propagate the inflammatory response (133). Additionally, inflammation elevates production of matrix metalloproteins (MMPs) and myeloperoxidase, both of which are major factors leading to BBB breakdown.

After ischemic stroke, the spatiotemporal profile of neuroinflammation with cellular and molecular MRI has been increasingly explored. In cellular and molecular MRI, paramagnetic contrast agents such as gadolinium chelates and small particles of iron oxide were used to detect specific leukocyte populations or molecular inflammatory markers after stroke. Several pre-clinical and clinical studies have demonstrated the application of contrast agents to image the monocyte infiltration after ischemic stroke. The most common strategy for labeling circulating monocytes is the administration of iron oxide nanoparticles. For the labeling, two kinds of particles can be used: small and ultrasmall superparamagnetic iron oxide particles (SPIO and USPIO, respectively) (140–144). SPIO and USPIO shorten the transverse relaxation times T_2 andT_2^*, and the cells taken up SPIO or USPIO present hypointense on T_2 or T_2^*-weighted images. Rausch et al. found that USPIOs distributed in patches within the lesion and surrounding area on the first 2 days. On day 4, USPIOs expanded within the lesion core. On day 7 they were found predominantly within the boundary area. This strategy has been used in some human studies to detect macrophage activity in stroke patients (140, 141). With the target-specific contrast agents, molecular MRI have shown the potential to examine inflammation markers *in vivo* in experimental stroke. Jin et al. designed a magnetic nanoparticle-P-selectin binding peptide (MNP-PBP) to image endothelial P-selectin and E-selectin. MNP-PBP showed a notably greater T_2 effect in the infarction and had a tighter binding affinity with selectin (145, 146). Vascular cell adhesion molecule (VCAM-1) and MMPs are other targets for neuroinflammation imaging. In a pre-clinical study, researchers developed microparticles of iron-oxide (MPIO), an MRI contrast agent that could bind with VCAM-1 on the cerebral vascular endothelium and visualize the expression of VCAM-1 (147). The result showed the spatial extent of VCAM-1 was considerably larger than the lesion core area measured by DWI MRI. The authors thought that this molecular MRI imaging of VCAM-1 might include both ischemic core and potentially salvageable penumbral regions.

Microglial activation can be monitored by PET imaging with related molecular biomarkers. The 18 kDa translocator protein (TSPO) system is the most commonly used target system for neuroinflammatory imaging. Due to the activation of microglia, the TSPO density is elevated after ischemic stroke. Furthermore, it has been demonstrated that using [^{11}C] vinpocetine, a prospective radio ligand of TSPO, the regional changes of TSPO can be measured in the brain of ischemic stroke patients (148). The elevated level of TSPO which indicated the activated microglia was found both in the ischemic core and peri-infarct area.

As far as imaging modalities concern there are only a few options, which allow do discriminate different cell types in

the infarcted tissue of patients. Molecular MRI has shown promising futures regarding monitoring of inflammatory cells such as neutrophils, leukocytes and microglia, but it is unable to provide the information in regards of cell viability. Futhermore, the molecular MRI is currently not highly specific and the interpretation of obtained results is sometimes challenging. The toxicity of contrast agents is another concern. All these shortcomings complicate the clinical implementation of this imaging technique.

Imaging Blood-Brain Barrier Leakage

Restoration of blood flow can induce reperfusion injury, reperfusion injury is one of the events that compromises the BBB. The leakage of BBB, which has been reported have a biphasic pattern, can cause severe brain edema and hemorrhagic transformation (149, 150). MRI and CT are the most widely used clinical imaging tools to evaluate BBB disruption by detecting the extravasation of the intravenously administered small molecular weight contrast agents (151).

Dynamic contrast-enhanced MRI (DCE-MRI) is considered as the gold standard MRI approach to evaluate BBB permeability (152). Gadolinium-diethylenetriamine penta-acetic acid and its variant gadolinium-diethylenetriamine penta-acetic acid-bis (methylamide) are the most used contrast agents that are given as intravenous bolus injection. The accumulation of contrast agents in the extracellular matrix of ischemic tissues results in increased longitudinal relaxation rate and hyperintensity in T_1-weighted MRI. DCE-MRI exploits this T_1 enhancement to extract quantitative or semi-quantitative information regarding BBB integrity (153). Several pre-clinical studies using DCE-MRI assessed BBB integrity after ischemic stroke. The results consistently have shown a biphasic pattern of BBB permeability after ischemic stroke. Compared to sham-operated animals, the BBB permeability on ipsilateral striatum increased at 4 h after the onset of ischemic stroke. Compared to the 4 h value, a significant decline of stroke-induced BBB disruption was observed at 24 h. Another rise of BBB permeability followed at 48 h. At this time point, the BBB disruption was more prominent than at both 4

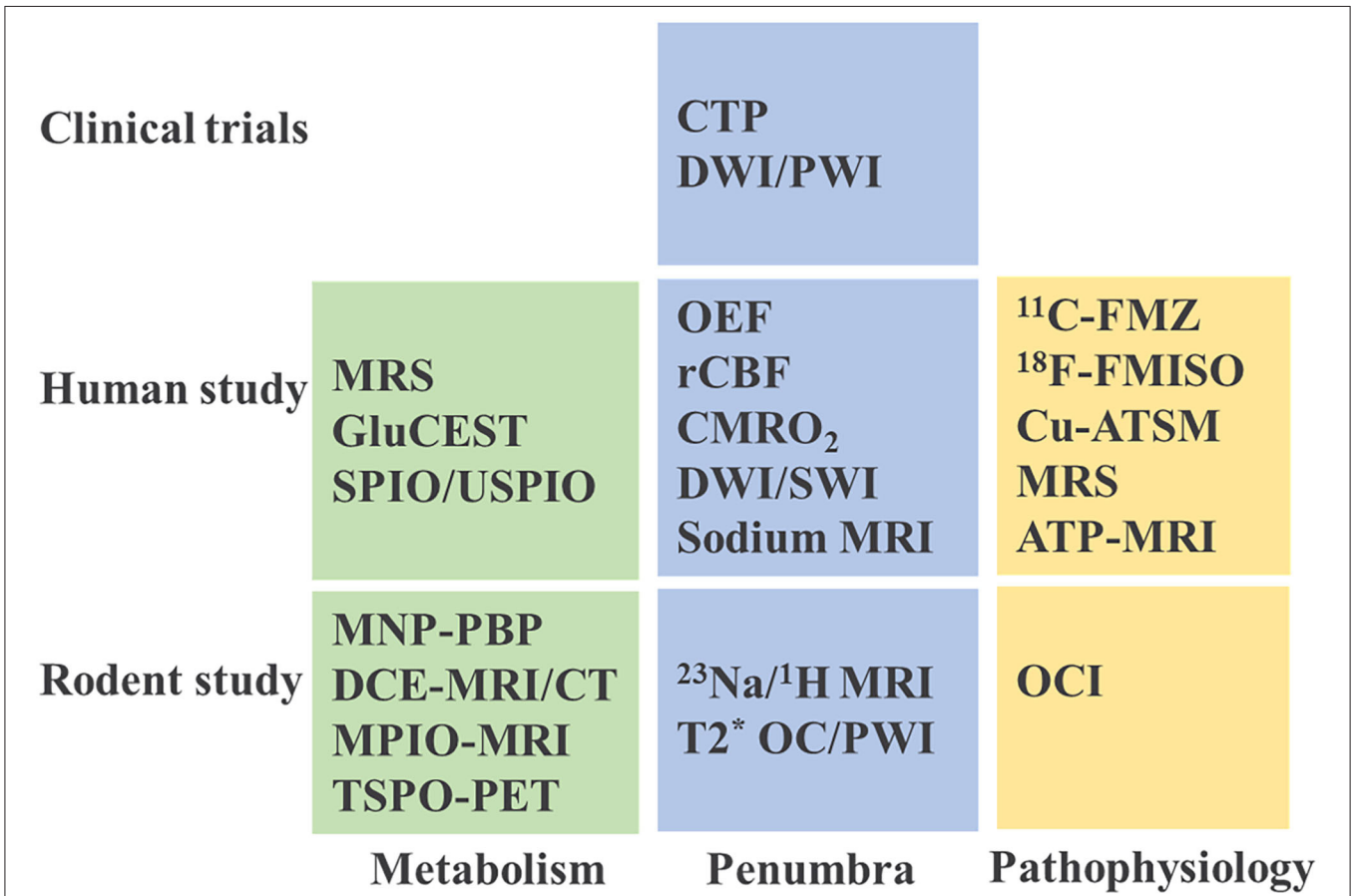

FIGURE 5 | Current imaging practice in stroke studies. MRS, magnetic resonance spectroscopy; GluCEST, glutamate weighted chemical exchange saturation transfer; SPIO, superparamagnetic iron oxide; USPIO, ultrasmall superparamagnetic iron oxide; MNP-PBP, magnetic nanoparticle-P-selectin binding peptide; MRI, magnetic resonance imaging; DCE, dynamic contrast enhanced; CT, computed tomography; MPIO, microparticles of iron oxide; TSPO-PET, translocator protein-positron emission tomography; OEF, oxygen extraction fraction; rCBF, regional cerebral blood flow; $CMRO_2$, cerebral metabolic rate of oxygen; DWI/SWI, diffusion weighted imaging/ susceptibility weighted imaging; T_2^*OC/PWI, T_2^* oxygen challenge/perfusion-weighted imaging; ^{11}C-FMZ, ^{11}C-flumazenil; ^{18}F-FMISO, ^{18}F-Fluoromisonidazole; Cu-ATSM, copper-diacetyl-bis(N_4-methylthiosemicarbazone); ATP, adenosine triphosphate; OCI, oxygen challenge imaging.

and at 24 h after stroke induction (154). The mechanisms of this partial recovery in BBB function are not completely understood. Besides, biphasic pattern of BBB permeability has not been categorically confirmed in stroke patients.

CT can also be used to evaluate BBB integrity. Similar with DCE-MRI, DCE-CT involves intravenous injection of an iodinated contrast agent and voxel-wise measurement of attenuation coefficient as a function of time (155). In the clinical setting, the accessibility and the fast scanning speed of CT makes it the first choice for making treatment decisions for ischemic stroke. BBB disruption can potentially be assessed by incorporating a DCE-CT protocol into the initial CT imaging of a patient. Recently, Park et al. developed a new *in vivo* micro-CT which uses iopromide to visualize the leakage of BBB. The new micro-CT BBB imaging technique has a high resolution and sensitivity (156).

Although some other imaging techniques (such as PET and optical imaging) have been also used to evaluate BBB permeability, their limitations, such as low resolution and inter-rater reliability, restrict their application in the clinic setting (157, 158).

CONCLUSIONS AND PERSPECTIVE

Reperfusion therapies are critically time dependent. The earlier treatment within time windows leads to more benefits. For the patients reached beyond the time windows, "tissue window" should be considered. Emerging evidence from recent clinical trials have recognized that tissue viability defined by the imaging modalities might be a more precise and reliable surrogate marker than time window (159). The newly issued guidelines have recommended evaluation of the penumbra or infarction by DWI, PWI, and CTP to expand eligibility for mechanical thrombectomy in the 6–24 h window after stroke onset. Compared to PDM, the novel imaging features on metabolism and pathophysiology, are more specific and sensitive to examine the salvageable tissue after stroke, and show great potential to define the therapeutic window. However, there are still challenges and controversies. Nonetheless, it needs to be said, that there is no reliable setting to determine the viability of brain tissue in the acute stage of stroke. Although visibility of such imaging setting as oxygen challenge MRI and DCE-MRI/CT for the detection of BBB leakage were tested in rodent studies, their usefulness for clinic have not been evaluated yet. Others, such as pH-weighted imaging and glutamate imaging, have only been validated in human studies, but all the same the utility of the concepts have not been evaluated in clinical trials yet (**Figure 5**). Though PDM tempts us to differentiate the potential salvageable tissue from infarction, unfortunately, the ideal imaging parameters and their accuracy remain elusive. Definitive validation is necessary in the future research and clinical trials. And because of a lack of standardization, the incorporation of the imaging modalities in clinical practice will be consequently limited. Future investigations on standardization of the imaging sequences and parameters to define tissue window are expected. Besides, the restricted attainability and long time needed for examination are burdens that limit PDM application for stroke patients. For instance, in Europe on average only 4% of the decision in regards of possible treatment will be based on MR perfusion and this number varied greatly from country to country (160). The time needed for an MRI perfusion scan is ∼16 min. That is longer than 10 min, which are needed for CTP. However, it is possible to standardized stroke MRI protocols and reduce time in this way down to 10 min or even to 6 min by using echo planar imaging at 3 T (161). It is clear that with increased availability and standardization of the parameters, PDM could become the prime imaging technique able to precisely define the tissue window and identify patients eligible for endovascular thrombectomy.

AUTHOR CONTRIBUTIONS

JL, QH, YL, and XH wrote the manuscript. DL and JZ made suggestions for improvement. QM and LZ created the figures. AM edited the language. All authors read, revised, and approved the final manuscript.

FUNDING

This research was supported by the National Natural Science Foundation of China No. 82071283 to QH, China Postdoctoral Science Foundation Grant No. 2018M632130 to JL, and the National Institutes of Health P01 NS082124 to JZ.

REFERENCES

1. Yang SH, Liu R. Four decades of ischemic penumbra and its implication for ischemic stroke. *Transl Stroke Res.* (2021). doi: 10.1007/s12975-021-00916-2. [Epub ahead of print].
2. Lapchak PA. Critical early thrombolytic and endovascular reperfusion therapy for acute ischemic stroke victims: a call for adjunct neuroprotection. *Transl Stroke Res.* (2015) 6:345–54. doi: 10.1007/s12975-015-0419-5
3. Thomalla G, Simonsen CZ, Boutitie F, Andersen G, Berthezene Y, Cheng B, et al. Wake up-mri-guided thrombolysis for stroke with unknown time of onset. *N Engl J Med.* (2018) 379:611–22. doi: 10.1056/NEJMoa1804355
4. Amiri H, Bluhmki E, Bendszus M, Eschenfelder CC, Donnan GA, Leys D, et al. European cooperative acute stroke study-4: extending the time for thrombolysis in emergency neurological deficits ecass-4: extend. *Int J Stroke.* (2016) 11:260–7. doi: 10.1177/1747493015620805
5. Nogueira RG, Jadhav AP, Haussen DC, Bonafe A, Budzik RF, Bhuva P, et al. Thrombectomy 6 to 24 hours after stroke with a mismatch between deficit and infarct. *N Engl J Med.* (2018) 378:11–21. doi: 10.1056/NEJMoa1706442
6. Albers GW, Marks MP, Lansberg MG. DEFUSE 3-Thrombectomy for stroke with selection by perfusion imaging. *N Engl J Med.* (2018) 378:708–18. doi: 10.1056/NEJMoa1713973
7. Yang SH, Lou M, Luo B, Jiang WJ, Liu R. Precision medicine for ischemic stroke, let us move beyond time is brain. *Transl Stroke Res.* (2018) 9:93–5. doi: 10.1007/s12975-017-0566-y
8. Hacke W. A new dawn for imaging-based selection in the treatment of acute stroke. *N Engl J Med.* (2018) 378:81–3. doi: 10.1056/NEJMe1713367
9. Dehkharghani S, Andre J. Imaging approaches to stroke and neurovascular disease. *Neurosurgery.* (2017) 80:681–700. doi: 10.1093/neuros/nyw108

10. Scheldeman L, Wouters A, Boutitie F, Dupont P, Christensen S, Cheng B, et al. Different mismatch concepts for magnetic resonance imaging-guided thrombolysis in unknown onset stroke. *Ann Neurol.* (2020) 87:931–8. doi: 10.1002/ana.25730
11. Astrup J, Siesjo BK, Symon L. Thresholds in cerebral ischemia - the ischemic penumbra. *Stroke.* (1981) 12:723–5. doi: 10.1161/01.STR.12.6.723
12. Iglesias-Rey R, Rodriguez-Yanez M, Rodriguez-Castro E, Pumar JM, Arias S, Santamaria M, et al. Worse outcome in stroke patients treated with rt-pa without early reperfusion: associated factors. *Transl Stroke Res.* (2018) 9:347–55. doi: 10.1007/s12975-017-0584-9
13. Ahnstedt H, Sweet J, Cruden P, Bishop N, Cipolla MJ. Effects of early post-ischemic reperfusion and tpa on cerebrovascular function and nitrosative stress in female rats. *Transl Stroke Res.* (2016) 7:228–38. doi: 10.1007/s12975-016-0468-4
14. Goyal M, Ospel JM, Menon B, Almekhlafi M, Jayaraman M, Fiehler J, et al. Challenging the ischemic core concept in acute ischemic stroke imaging. *Stroke.* (2020) 51:3147–55. doi: 10.1161/STROKEAHA.120.030620
15. Gomez CR. Editorial: time is brain! *J Stroke Cerebrovasc Dis.* (1993) 3:1–2. doi: 10.1016/S1052-3057(10)80125-9
16. Mikulik R, Wahlgren N. Treatment of acute stroke: an update. *J Intern Med.* (2015) 278:145–65. doi: 10.1111/joim.12387
17. Wadiwala MF, Kamal AK. Extending the window for thrombolysis in acute stroke. *J Pak Med Assoc.* (2012) 62:858–9.
18. Desilles JP, Consoli A, Redjem H, Coskun O, Ciccio G, Smajda S, et al. Successful reperfusion with mechanical thrombectomy is associated with reduced disability and mortality in patients with pretreatment diffusion-weighted imaging-alberta stroke program early computed tomography score </=6. *Stroke.* (2017) 48:963–9. doi: 10.1161/STROKEAHA.116.015202
19. National Institute of Neurological Disorders, Stroke rt-PA Stroke Study Group. Tissue plasminogen activator for acute ischemic stroke. *N Engl J Med.* (1995) 333:1581–7. doi: 10.1056/NEJM199512143332401
20. Hacke W, Kaste M, Bluhmki E, Brozman M, Davalos A, Guidetti D, et al. Thrombolysis with alteplase 3 to 45 hours after acute ischemic stroke. *N Engl J Med.* (2008) 359:1317–29. doi: 10.1056/NEJMoa0804656
21. Miller DJ, Simpson JR, Silver B. Safety of thrombolysis in acute ischemic stroke: a review of complications, risk factors, and newer technologies. *Neurohospitalist.* (2011) 1:138–47. doi: 10.1177/1941875211408731
22. Ma H, Campbell BCV, Parsons MW, Churilov L, Levi CR, Hsu C, et al. Thrombolysis guided by perfusion imaging up to 9 hours after onset of stroke. *N Engl J Med.* (2019) 380:1795–803. doi: 10.1056/NEJMoa1813046
23. Sykora M, Kellert L, Michel P, Eskandari A, Feil K, Remi J, et al. Thrombolysis in stroke with unknown onset based on non-contrast computerized tomography (trust ct). *J Am Heart Assoc.* (2020) 9:e014265. doi: 10.1161/JAHA.119.014265
24. Powers WJ, Rabinstein AA, Ackerson T, Adeoye OM, Bambakidis NC, Becker K, et al. Guidelines for the early management of patients with acute ischemic stroke: 2019 update to the 2018 guidelines for the early management of acute ischemic stroke: a guideline for healthcare professionals from the american heart association/american stroke association. *Stroke.* (2019) 50:e344–418. doi: 10.1161/STR.0000000000000211
25. Katsanos AH, Safouris A, Sarraj A, Magoufis G, Leker RR, Khatri P, et al. Intravenous thrombolysis with tenecteplase in patients with large vessel occlusions: systematic review and meta-analysis. *Stroke.* (2021) 52:308–12. doi: 10.1161/STROKEAHA.120.030220
26. Saver JL, Goyal M, Bonafe A, Diener HC, Levy EI, Pereira VM, et al. Stent-retriever thrombectomy after intravenous t-pa vs. T-pa alone in stroke. *N Engl J Med.* (2015) 372:2285–95. doi: 10.1056/NEJMoa1415061
27. Campbell BC, Mitchell PJ, Kleinig TJ, Dewey HM, Churilov L, Yassi N, et al. (Extend-ia) endovascular therapy for ischemic stroke with perfusion-imaging selection. *N Engl J Med.* (2015) 372:1009–18. doi: 10.1056/NEJMoa1414792
28. Berkhemer OA, Fransen PS, Beumer D, van den Berg LA, Lingsma HF, Yoo AJ, et al. Mr clean-a randomized trial of intraarterial treatment for acute ischemic stroke. *N Engl J Med.* (2015) 372:11–20. doi: 10.1056/NEJMoa1411587
29. Jovin TG, Chamorro A, Cobo E, de Miquel MA, Molina CA, Rovira A, et al. Revascat-thrombectomy within 8 hours after symptom onset in ischemic stroke. *N Engl J Med.* (2015) 372:2296–306. doi: 10.1056/NEJMoa1503780
30. Goyal M, Demchuk AM, Menon BK, Eesa M, Rempel JL, Thornton J, et al. Randomized assessment of rapid endovascular treatment of ischemic stroke. *N Engl J Med.* (2015) 372:1019–30. doi: 10.1056/NEJMoa1414905
31. Motyer R, Thornton J, Power S, Brennan P, O'Hare A, Looby S, et al. Endovascular thrombectomy beyond 12 hours of stroke onset: a stroke network's experience of late intervention. *J Neurointerv Surg.* (2018) 10:1043–6. doi: 10.1136/neurintsurg-2017-013575
32. Gunawardena R, Cheung A, Spira P, He J, Wenderoth J, Chiu AHY. Successful endovascular thrombectomy 90h after stroke onset. *J Clin Neurosci.* (2017) 46:69–71. doi: 10.1016/j.jocn.2017.08.047
33. Janjua N, Farkas J. Thrombectomy for delayed basilar stent occlusion with good outcome. *J Vasc Interv Neurol.* (2013) 6:19–24.
34. McBride DW, Wu G, Nowrangi D, Flores JJ, Hui L, Krafft PR, et al. Delayed recanalization promotes functional recovery in rats following permanent middle cerebral artery occlusion. *Transl Stroke Res.* (2018) 9:185–98. doi: 10.1007/s12975-018-0610-6
35. Astrup J, Symon L, Branston NM, Lassen NA. Cortical evoked potential and extracellular k+ and h+ at critical levels of brain ischemia. *Stroke.* (1977) 8:51–7. doi: 10.1161/01.STR.8.1.51
36. Baron JC, Bousser MG, Rey A, Guillard A, Comar D, Castaigne P. Reversal of focal "misery-perfusion syndrome" by extra-intracranial arterial bypass in hemodynamic cerebral ischemia. A case study with 15o positron emission tomography. *Stroke.* (1981) 12:454–9. doi: 10.1161/01.STR.12.4.454
37. Heiss WD. Ischemic penumbra: evidence from functional imaging in man. *J Cereb Blood Flow Metab.* (2000) 20:1276–93. doi: 10.1097/00004647-200009000-00002
38. Powers WJ, Grubb RL Jr, Darriet D, Raichle ME. Cerebral blood flow and cerebral metabolic rate of oxygen requirements for cerebral function and viability in humans. *J Cereb Blood Flow Metab.* (1985) 5:600–8. doi: 10.1038/jcbfm.1985.89
39. Heiss WD, Graf R, Wienhard K, Lottgen J, Saito R, Fujita T, et al. Dynamic penumbra demonstrated by sequential multitracer pet after middle cerebral artery occlusion in cats. *J Cereb Blood Flow Metab.* (1994) 14:892–902. doi: 10.1038/jcbfm.1994.120
40. Baron JC. Mapping the ischaemic penumbra with pet: Implications for acute stroke treatment. *Cerebrovasc Dis.* (1999) 9:193–201. doi: 10.1159/000015955
41. Marchal G, Benali K, Iglesias S, Viader F, Derlon JM, Baron JC. Voxel-based mapping of irreversible ischaemic damage with pet in acute stroke. *Brain.* (1999) 122:2387–400. doi: 10.1093/brain/122.12.2387
42. Baron JC. Perfusion thresholds in human cerebral ischemia: historical perspective and therapeutic implications. *Cerebrovasc Dis.* (2001) 11 Suppl 1:2–8. doi: 10.1159/000049119
43. Zaro-Weber O, Fleischer H, Reiblich L, Schuster A, Moeller-Hartmann W, Heiss WD. Penumbra detection in acute stroke with perfusion magnetic resonance imaging: validation with (15) o-positron emission tomography. *Ann Neurol.* (2019) 85:875–86. doi: 10.1002/ana.25479
44. Sobesky J. Refining the mismatch concept in acute stroke: lessons learned from pet and mri. *J Cereb Blood Flow Metab.* (2012) 32:1416–25. doi: 10.1038/jcbfm.2012.54
45. Rother J, Schellinger PD, Gass A, Siebler M, Villringer A, Fiebach JB, et al. Effect of intravenous thrombolysis on mri parameters and functional outcome in acute stroke <6 hours. *Stroke.* (2002) 33:2438–45. doi: 10.1161/01.STR.0000030109.12281.23
46. Duong TQ, Fisher M. Applications of diffusion/perfusion magnetic resonance imaging in experimental and clinical aspects of stroke. *Curr Atheroscler Rep.* (2004) 6:267–73. doi: 10.1007/s11883-004-0057-y
47. Ford AL, An H, Kong L, Zhu H, Vo KD, Powers WJ, et al. Clinically relevant reperfusion in acute ischemic stroke: Mtt performs better than tmax and ttp. *Transl Stroke Res.* (2014) 5:415–21. doi: 10.1007/s12975-014-0325-2
48. Schellinger PD, Fiebach JB, Jansen O, Ringleb PA, Mohr A, Steiner T, et al. Stroke magnetic resonance imaging within 6 hours after onset of hyperacute cerebral ischemia. *Ann Neurol.* (2001) 49:460–9. doi: 10.1002/ana.95
49. Muller TB, Haraldseth O, Jones RA, Sebastiani G, Godtliebsen F, Lindboe CF, et al. Combined perfusion and diffusion-weighted magnetic resonance

imaging in a rat model of reversible middle cerebral artery occlusion. *Stroke.* (1995) 26:451–7. doi: 10.1161/01.STR.26.3.451
50. Kohno K, Hoehn-Berlage M, Mies G, Back T, Hossmann KA. Relationship between diffusion-weighted mr images, cerebral blood flow, and energy state in experimental brain infarction. *Magn Reson Imaging.* (1995) 13:73–80. doi: 10.1016/0730-725X(94)00080-M
51. Schlaug G, Benfield A, Baird AE, Siewert B, Lovblad KO, Parker RA, et al. The ischemic penumbra: operationally defined by diffusion and perfusion mri. *Neurology.* (1999) 53:1528–37. doi: 10.1212/WNL.53.7.1528
52. Singer OC, Du Mesnil De Rochemont R, Foerch C, Stengel A, Sitzer M, Lanfermann H, et al. Early functional recovery and the fate of the diffusion/perfusion mismatch in patients with proximal middle cerebral artery occlusion. *Cerebrovasc Dis.* (2004) 17:13–20. doi: 10.1159/000073893
53. Baird AE, Lovblad KO, Dashe JF, Connor A, Burzynski C, Schlaug G, et al. Clinical correlations of diffusion and perfusion lesion volumes in acute ischemic stroke. *Cerebrovasc Dis.* (2000) 10:441–8. doi: 10.1159/000016105
54. Albers GW, Thijs VN, Wechsler L, Kemp S, Schlaug G, Skalabrin E, et al. Magnetic resonance imaging profiles predict clinical response to early reperfusion: the diffusion and perfusion imaging evaluation for understanding stroke evolution (defuse) study. *Ann Neurol.* (2006) 60:508–17. doi: 10.1002/ana.20976
55. Davis SM, Donnan GA, Parsons MW, Levi C, Butcher KS, Peeters A, et al. Effects of alteplase beyond 3 h after stroke in the echoplanar imaging thrombolytic evaluation trial (epithet): a placebo-controlled randomised trial. *Lancet Neurol.* (2008) 7:299–309. doi: 10.1016/S1474-4422(08)70044-9
56. Sobesky J, Zaro Weber O, Lehnhardt FG, Hesselmann V, Neveling M, Jacobs A, et al. Does the mismatch match the penumbra? Magnetic resonance imaging and positron emission tomography in early ischemic stroke. *Stroke.* (2005) 36:980–5. doi: 10.1161/01.STR.0000160751.79241.a3
57. Heiss WD, Sobesky J, Hesselmann V. Identifying thresholds for penumbra and irreversible tissue damage. *Stroke.* (2004) 35:2671–4. doi: 10.1161/01.STR.0000143329.81997.8a
58. Dani KA, Thomas RG, Chappell FM, Shuler K, MacLeod MJ, Muir KW, et al. Computed tomography and magnetic resonance perfusion imaging in ischemic stroke: definitions and thresholds. *Ann Neurol.* (2011) 70:384–401. doi: 10.1002/ana.22500
59. Hussain MS, Bhagat YA, Liu S, Scozzafava J, Khan KA, Dillon WP, et al. Dwi lesion volume reduction following acute stroke treatment with transient partial aortic obstruction. *J Neuroimaging.* (2010) 20:379–81. doi: 10.1111/j.1552-6569.2009.00407.x
60. Kidwell CS, Alger JR, Saver JL. Beyond mismatch: evolving paradigms in imaging the ischemic penumbra with multimodal magnetic resonance imaging. *Stroke.* (2003) 34:2729–35. doi: 10.1161/01.STR.0000097608.38779.CC
61. Rivers CS, Wardlaw JM, Armitage PA, Bastin ME, Carpenter TK, Cvoro V, et al. Do acute diffusion- and perfusion-weighted mri lesions identify final infarct volume in ischemic stroke? *Stroke.* (2006) 37:98–104. doi: 10.1161/01.STR.0000195197.66606.bb
62. Powers WJ. Perfusion-diffusion mismatch: does it identify who will benefit from reperfusion therapy? *Transl Stroke Res.* (2012) 3:182–7. doi: 10.1007/s12975-012-0160-2
63. Davis SM, Donnan GA. Mr mismatch and thrombolysis: appealing but validation required. *Stroke.* (2009) 40:2910. doi: 10.1161/STROKEAHA.109.552893
64. Wardlaw JM. Surrogate outcomes: a cautionary note. *Stroke.* (2009) 40:1029–31. doi: 10.1161/STROKEAHA.108.540641
65. Wetterling F, Gallagher L, Mullin J, Holmes WM, McCabe C, Macrae IM, et al. Sodium-23 magnetic resonance imaging has potential for improving penumbra detection but not for estimating stroke onset time. *J Cereb Blood Flow Metab.* (2015) 35:103–10. doi: 10.1038/jcbfm.2014.174
66. Wetterling F, Chatzikonstantinou E, Tritschler L, Meairs S, Fatar M, Schad LR, et al. Investigating potentially salvageable penumbra tissue in an in vivo model of transient ischemic stroke using sodium, diffusion, and perfusion magnetic resonance imaging. *BMC Neurosci.* (2016) 17:82. doi: 10.1186/s12868-016-0316-1
67. Boada FE, Qian Y, Nemoto E, Jovin T, Jungreis C, Jones SC, et al. Sodium mri and the assessment of irreversible tissue damage during hyper-acute stroke. *Transl Stroke Res.* (2012) 3:236–45. doi: 10.1007/s12975-012-0168-7
68. Wang Y, Hu W, Perez-Trepichio AD, Ng TC, Furlan AJ, Majors AW, et al. Brain tissue sodium is a ticking clock telling time after arterial occlusion in rat focal cerebral ischemia. *Stroke.* (2000) 31:1386–91. doi: 10.1161/01.STR.31.6.1386
69. Chalian M, Tekes A, Meoded A, Poretti A, Huisman TA. Susceptibility-weighted imaging (swi): a potential non-invasive imaging tool for characterizing ischemic brain injury? *J Neuroradiol.* (2011) 38:187–90. doi: 10.1016/j.neurad.2010.12.006
70. Luo S, Yang L, Wang L. Comparison of susceptibility-weighted and perfusion-weighted magnetic resonance imaging in the detection of penumbra in acute ischemic stroke. *J Neuroradiol.* (2015) 42:255–60. doi: 10.1016/j.neurad.2014.07.002
71. Robertson CA, McCabe C, Lopez-Gonzalez MR, Deuchar GA, Dani K, Holmes WM, et al. Detection of ischemic penumbra using combined perfusion and t2* oxygen challenge imaging. *Int J Stroke.* (2015) 10:42–50. doi: 10.1111/ijs.12327
72. Zhu G, Michel P, Zhang W, Wintermark M. Standardization of stroke perfusion ct for reperfusion therapy. *Transl Stroke Res.* (2012) 3:221–7. doi: 10.1007/s12975-012-0156-y
73. Wintermark M, Albers GW, Alexandrov AV, Alger JR, Bammer R, Baron JC, et al. Acute stroke imaging research roadmap. *Stroke.* (2008) 39:1621–8. doi: 10.1161/STROKEAHA.107.512319
74. Zhu G, Jovin T, Aghaebrahim A, Michel P, Zhang W, Wintermark M. Does perfusion imaging add value compared with plain parenchymal and vascular imaging? *J Neurointerv Surg.* (2012) 4:246–50. doi: 10.1136/neurintsurg-2012-010416
75. Alves JE, Carneiro A, Xavier J. Reliability of ct perfusion in the evaluation of the ischaemic penumbra. *Neuroradiol J.* (2014) 27:91–5. doi: 10.15274/NRJ-2014-10010
76. Hossmann KA. Viability thresholds and the penumbra of focal ischemia. *Ann Neurol.* (1994) 36:557–65. doi: 10.1002/ana.410360404
77. Kiewert C, Mdzinarishvili A, Hartmann J, Bickel U, Klein J. Metabolic and transmitter changes in core and penumbra after middle cerebral artery occlusion in mice. *Brain Res.* (2010) 1312:101–7. doi: 10.1016/j.brainres.2009.11.068
78. Galeffi F, Sinnar S, Schwartz-Bloom RD. Diazepam promotes atp recovery and prevents cytochrome c release in hippocampal slices after in vitro ischemia. *J Neurochem.* (2000) 75:1242–9. doi: 10.1046/j.1471-4159.2000.0751242.x
79. Kuroiwa T, Mies G, Hermann D, Hakamata Y, Hanyu S, Ito U. Regional differences in the rate of energy impairment after threshold level ischemia for induction of cerebral infarction in gerbils. *Acta Neuropathol.* (2000) 100:587–94. doi: 10.1007/s004010000235
80. Hata R, Maeda K, Hermann D, Mies G, Hossmann KA. Evolution of brain infarction after transient focal cerebral ischemia in mice. *J Cereb Blood Flow Metab.* (2000) 20:937–46. doi: 10.1097/00004647-200006000-00006
81. Welsh FA, Marcy VR, Sims RE. Nadh fluorescence and regional energy metabolites during focal ischemia and reperfusion of rat brain. *J Cereb Blood Flow Metab.* (1991) 11:459–65. doi: 10.1038/jcbfm.1991.88
82. Wang Z, Mascarenhas C, Jia X. Positron emission tomography after ischemic brain injury: current challenges and future developments. *Transl Stroke Res.* (2020) 11:628–42. doi: 10.1007/s12975-019-00765-0
83. Baron JC, Jones T. Oxygen metabolism, oxygen extraction and positron emission tomography: historical perspective and impact on basic and clinical neuroscience. *Neuroimage.* (2012) 61:492–504. doi: 10.1016/j.neuroimage.2011.12.036
84. Heiss WD. The ischemic penumbra: correlates in imaging and implications for treatment of ischemic stroke. The johann jacob wepfer award 2011. *Cerebrovasc Dis.* (2011) 32:307–20. doi: 10.1159/000330462
85. Jones T, Chesler DA, Ter-Pogossian MM. The continuous inhalation of oxygen-15 for assessing regional oxygen extraction in the brain of man. *Br J Radiol.* (1976) 49:339–43. doi: 10.1259/0007-1285-49-580-339
86. Heiss WD, Grond M, Thiel A, von Stockhausen HM, Rudolf J, Ghaemi M, et al. Tissue at risk of infarction rescued by early reperfusion: a positron emission tomography study in systemic recombinant tissue plasminogen activator thrombolysis of acute stroke. *J Cereb Blood Flow Metab.* (1998) 18:1298–307. doi: 10.1097/00004647-199812000-00004

87. Lin W, Powers WJ. Oxygen metabolism in acute ischemic stroke. *J Cereb Blood Flow Metab.* (2018) 38:1481–99. doi: 10.1177/0271678X17722095
88. Treyer V, Jobin M, Burger C, Teneggi V, Buck A. Quantitative cerebral h2(15)o perfusion pet without arterial blood sampling, a method based on washout rate. *Eur J Nucl Med Mol Imaging.* (2003) 30:572–80. doi: 10.1007/s00259-002-1105-x
89. Kudomi N, Hirano Y, Koshino K, Hayashi T, Watabe H, Fukushima K, et al. Rapid quantitative cbf and cmro(2) measurements from a single pet scan with sequential administration of dual (15)o-labeled tracers. *J Cereb Blood Flow Metab.* (2013) 33:440–8. doi: 10.1038/jcbfm.2012.188
90. Kudomi N, Maeda Y, Yamamoto H, Yamamoto Y, Hatakeyama T, Nishiyama Y. Reconstruction of input functions from a dynamic pet image with sequential administration of (15)o2 and [formula: See text] for noninvasive and ultra-rapid measurement of cbf, oef, and cmro2. *J Cereb Blood Flow Metab.* (2018) 38:780–92. doi: 10.1177/0271678X17713574
91. Magata Y, Temma T, Iida H, Ogawa M, Mukai T, Iida Y, et al. Development of injectable o-15 oxygen and estimation of rat oef. *J Cereb Blood Flow Metab.* (2003) 23:671–6. doi: 10.1097/01.WCB.0000066792.97069.B3
92. Temma T, Koshino K, Moriguchi T, Enmi J, Iida H. Pet quantification of cerebral oxygen metabolism in small animals. *ScientificWorldJournal.* (2014) 2014:159103. doi: 10.1155/2014/159103
93. Tiwari VN, Kiyono Y, Kobayashi M, Mori T, Kudo T, Okazawa H, et al. Automatic labeling method for injectable 15o-oxygen using hemoglobin-containing liposome vesicles and its application for measurement of brain oxygen consumption by pet. *Nucl Med Biol.* (2010) 37:77–83. doi: 10.1016/j.nucmedbio.2009.08.004
94. Heiss WD, Graf R, Fujita T, Ohta K, Bauer B, Lottgen J, et al. Early detection of irreversibly damaged ischemic tissue by flumazenil positron emission tomography in cats. *Stroke.* (1997) 28:2045–51. doi: 10.1161/01.STR.28.10.2045
95. Heiss WD, Kracht L, Grond M, Rudolf J, Bauer B, Wienhard K, et al. Early [(11)c]flumazenil/h(2)o positron emission tomography predicts irreversible ischemic cortical damage in stroke patients receiving acute thrombolytic therapy. *Stroke.* (2000) 31:366–9. doi: 10.1161/01.STR.31.2.366
96. Thiel A, Lottgen J, Grond M, Pietrzyk U, Heiss WD. Estimation of regional cerebral blood flow levels in ischemia using [(15)o]water of [(11)c]flumazenil pet without arterial input function. *J Comput Assist Tomogr.* (2001) 25:446–51. doi: 10.1097/00004728-200105000-00019
97. Rojas S, Martin A, Pareto D, Herance JR, Abad S, Ruiz A, et al. Positron emission tomography with 11c-flumazenil in the rat shows preservation of binding sites during the acute phase after 2 h-transient focal ischemia. *Neuroscience.* (2011) 182:208–16. doi: 10.1016/j.neuroscience.2011.03.013
98. Takasawa M, Moustafa RR, Baron JC. Applications of nitroimidazole *in vivo* hypoxia imaging in ischemic stroke. *Stroke.* (2008) 39:1629–37. doi: 10.1161/STROKEAHA.107.485938
99. Takasawa M, Beech JS, Fryer TD, Jones PS, Ahmed T, Smith R, et al. Single-subject statistical mapping of acute brain hypoxia in the rat following middle cerebral artery occlusion: a micropet study. *Exp Neurol.* (2011) 229:251–8. doi: 10.1016/j.expneurol.2011.02.005
100. Lee GH, Kim JS, Oh SJ, Kang DW, Kim JS, Kwon SU. (18)f-fluoromisonidazole (fmiso) positron emission tomography (pet) predicts early infarct growth in patients with acute ischemic stroke. *J Neuroimaging.* (2015) 25:652–5. doi: 10.1111/jon.12180
101. Falcao AL, Reutens DC, Markus R, Koga M, Read SJ, Tochon-Danguy H, et al. The resistance to ischemia of white and gray matter after stroke. *Ann Neurol.* (2004) 56:695–701. doi: 10.1002/ana.20265
102. Markus R, Reutens DC, Kazui S, Read S, Wright P, Pearce DC, et al. Hypoxic tissue in ischaemic stroke: persistence and clinical consequences of spontaneous survival. *Brain.* (2004) 127:1427–36. doi: 10.1093/brain/awh162
103. Lewis JS, Herrero P, Sharp TL, Engelbach JA, Fujibayashi Y, Laforest R, et al. Delineation of hypoxia in canine myocardium using pet and copper(ii)-diacetyl-bis(n(4)-methylthiosemicarbazone). *J Nucl Med.* (2002) 43:1557–69.
104. Huuskonen MT, Tuo QZ, Loppi S, Dhungana H, Korhonen P, McInnes LE, et al. The copper bis(thiosemicarbazone) complex cu(ii)(atsm) is protective against cerebral ischemia through modulation of the inflammatory milieu. *Neurotherapeutics.* (2017) 14:519–32. doi: 10.1007/s13311-016-0504-9
105. van der Toorn A, Verheul HB, Berkelbach van der Sprenkel JW, Tulleken CA, Nicolay K. Changes in metabolites and tissue water status after focal ischemia in cat brain assessed with localized proton mr spectroscopy. *Magn Reson Med.* (1994) 32:685–91. doi: 10.1002/mrm.1910320602
106. Sager TN, Laursen H, Hansen AJ. Changes in n-acetyl-aspartate content during focal and global brain ischemia of the rat. *J Cereb Blood Flow Metab.* (1995) 15:639–46. doi: 10.1038/jcbfm.1995.79
107. Jimenez-Xarrie E, Davila M, Gil-Perotin S, Jurado-Rodriguez A, Candiota AP, Delgado-Mederos R, et al. *In vivo* and *ex vivo* magnetic resonance spectroscopy of the infarct and the subventricular zone in experimental stroke. *J Cereb Blood Flow Metab.* (2015) 35:828–34. doi: 10.1038/jcbfm.2014.257
108. Saunders DE. Mr spectroscopy in stroke. *Br Med Bull.* (2000) 56:334–45. doi: 10.1258/0007142001903256
109. Bruhn H, Frahm J, Gyngell ML, Merboldt KD, Hanicke W, Sauter R. Cerebral metabolism in man after acute stroke: new observations using localized proton nmr spectroscopy. *Magn Reson Med.* (1989) 9:126–31. doi: 10.1002/mrm.1910090115
110. Wardlaw JM, Marshall I, Wild J, Dennis MS, Cannon J, Lewis SC. Studies of acute ischemic stroke with proton magnetic resonance spectroscopy: relation between time from onset, neurological deficit, metabolite abnormalities in the infarct, blood flow, and clinical outcome. *Stroke.* (1998) 29:1618–24. doi: 10.1161/01.STR.29.8.1618
111. Parsons MW Li T, Barber PA, Yang Q, Darby DG, Desmond PM, et al. Combined (1)h mr spectroscopy and diffusion-weighted mri improves the prediction of stroke outcome. *Neurology.* (2000) 55:498–505. doi: 10.1212/WNL.55.4.498
112. Klijn CJ, Kappelle LJ, van der Grond J, Algra A, Tulleken CA, van Gijn J. Magnetic resonance techniques for the identification of patients with symptomatic carotid artery occlusion at high risk of cerebral ischemic events. *Stroke.* (2000) 31:3001–7. doi: 10.1161/01.STR.31.12.3001
113. Cheung JS, Wang X, Zhe Sun P. Magnetic resonance characterization of ischemic tissue metabolism. *Open Neuroimag J.* (2011) 5:66–73. doi: 10.2174/1874440001105010066
114. Komatsumoto S, Nioka S, Greenberg JH, Yoshizaki K, Subramanian VH, Chance B, et al. Cerebral energy metabolism measured *in vivo* by 31p-nmr in middle cerebral artery occlusion in the cat–relation to severity of stroke. *J Cereb Blood Flow Metab.* (1987) 7:557–62. doi: 10.1038/jcbfm.1987.105
115. Germano IM, Pitts LH, Berry I, De Armond SJ. High energy phosphate metabolism in experimental permanent focal cerebral ischemia: an *in vivo* 31p magnetic resonance spectroscopy study. *J Cereb Blood Flow Metab.* (1988) 8:24–31. doi: 10.1038/jcbfm.1988.4
116. Shen Q, Huang S, Duong TQ. T2*-weighted fmri time-to-peak of oxygen challenge in ischemic stroke. *J Cereb Blood Flow Metab.* (2016) 36:283–91. doi: 10.1177/0271678X15606461
117. Shen Q, Huang S, Du F, Duong TQ. Probing ischemic tissue fate with bold fmri of brief oxygen challenge. *Brain Res.* (2011) 1425:132–41. doi: 10.1016/j.brainres.2011.09.052
118. Deuchar GA, Brennan D, Griffiths H, Macrae IM, Santosh C. Perfluorocarbons enhance a t2*-based mri technique for identifying the penumbra in a rat model of acute ischemic stroke. *J Cereb Blood Flow Metab.* (2013) 33:1422–8. doi: 10.1038/jcbfm.2013.86
119. Deuchar GA, Brennan D, Holmes WM, Shaw M, Macrae IM, Santosh C. Perfluorocarbon enhanced glasgow oxygen level dependent (gold) magnetic resonance metabolic imaging identifies the penumbra following acute ischemic stroke. *Theranostics.* (2018) 8:1706–22. doi: 10.7150/thno.21685
120. Deuchar GA, van Kralingen JC, Work LM, Santosh C, Muir KW, McCabe C, et al. Preclinical validation of the therapeutic potential of glasgow oxygen level dependent (gold) technology: a theranostic for acute stroke. *Transl Stroke Res.* (2019) 10:583–95. doi: 10.1007/s12975-018-0679-y
121. Zhou J, Payen JF, Wilson DA, Traystman RJ, van Zijl PC. Using the amide proton signals of intracellular proteins and peptides to detect ph effects in mri. *Nat Med.* (2003) 9:1085–90. doi: 10.1038/nm907
122. Cheung J, Doerr M, Hu R, Sun PZ. Refined ischemic penumbra imaging with tissue ph and diffusion kurtosis magnetic resonance imaging. *Transl Stroke Res.* (2020). doi: 10.1007/s12975-020-00868-z. [Epub ahead of print].
123. Sun PZ, Cheung JS, Wang E, Lo EH. Association between ph-weighted endogenous amide proton chemical exchange saturation transfer mri and

tissue lactic acidosis during acute ischemic stroke. *J Cereb Blood Flow Metab.* (2011) 31:1743–50. doi: 10.1038/jcbfm.2011.23
124. Sun PZ, Zhou J, Sun W, Huang J, van Zijl PC. Detection of the ischemic penumbra using ph-weighted mri. *J Cereb Blood Flow Metab.* (2007) 27:1129–36. doi: 10.1038/sj.jcbfm.9600424
125. Jokivarsi KT, Hiltunen Y, Tuunanen PI, Kauppinen RA, Grohn OH. Correlating tissue outcome with quantitative multiparametric mri of acute cerebral ischemia in rats. *J Cereb Blood Flow Metab.* (2010) 30:415–27. doi: 10.1038/jcbfm.2009.236
126. Tietze A, Blicher J, Mikkelsen IK, Ostergaard L, Strother MK, Smith SA, et al. Assessment of ischemic penumbra in patients with hyperacute stroke using amide proton transfer (apt) chemical exchange saturation transfer (cest) mri. *NMR Biomed.* (2014) 27:163–74. doi: 10.1002/nbm.3048
127. Harston GW, Tee YK, Blockley N, Okell TW, Thandeswaran S, Shaya G, et al. Identifying the ischaemic penumbra using ph-weighted magnetic resonance imaging. *Brain.* (2015) 138:36–42. doi: 10.1093/brain/awu374
128. Heo HY, Zhang Y, Burton TM, Jiang S, Zhao Y, van Zijl PCM, et al. Improving the detection sensitivity of ph-weighted amide proton transfer mri in acute stroke patients using extrapolated semisolid magnetization transfer reference signals. *Magn Reson Med.* (2017) 78:871–80. doi: 10.1002/mrm.26799
129. Tee YK, Harston GW, Blockley N, Okell TW, Levman J, Sheerin F, et al. Comparing different analysis methods for quantifying the mri amide proton transfer (apt) effect in hyperacute stroke patients. *NMR Biomed.* (2014) 27:1019–29. doi: 10.1002/nbm.3147
130. Jin T, Wang P, Hitchens TK, Kim SG. Enhancing sensitivity of ph-weighted mri with combination of amide and guanidyl cest. *Neuroimage.* (2017) 157:341–50. doi: 10.1016/j.neuroimage.2017.06.007
131. Dani KA, Warach S. Metabolic imaging of ischemic stroke: the present and future. *Am J Neuroradiol.* (2014) 35:S37–43. doi: 10.3174/ajnr.A3789
132. Dong S, Maniar S, Manole MD, Sun D. Cerebral hypoperfusion and other shared brain pathologies in ischemic stroke and alzheimer's disease. *Transl Stroke Res.* (2018) 9:238–50. doi: 10.1007/s12975-017-0570-2
133. Pennypacker KR. Peripheral immune response to cns injury. *Transl Stroke Res.* (2012) 3:305. doi: 10.1007/s12975-012-0204-7
134. Chen B, Ng G, Gao Y, Low SW, Sandanaraj E, Ramasamy B, et al. Non-invasive multimodality imaging directly shows trpm4 inhibition ameliorates stroke reperfusion injury. *Transl Stroke Res.* (2019) 10:91–103. doi: 10.1007/s12975-018-0621-3
135. Ren Y, Li C, Chang J, Wang R, Wang Y, Chu XP. Hi1a as a novel neuroprotective agent for ischemic stroke by inhibition of acid-sensing ion channel 1a. *Transl Stroke Res.* (2018) 9:96–8. doi: 10.1007/s12975-017-0575-x
136. Ramos-Cabrer P, Campos F, Sobrino T, Castillo J. Targeting the ischemic penumbra. *Stroke.* (2011) 42:S7–11. doi: 10.1161/STROKEAHA.110.596684
137. Bivard A, Krishnamurthy V, Stanwell P, Yassi N, Spratt NJ, Nilsson M, et al. Spectroscopy of reperfused tissue after stroke reveals heightened metabolism in patients with good clinical outcomes. *J Cereb Blood Flow Metab.* (2014) 34:1944–50. doi: 10.1038/jcbfm.2014.166
138. Cai K, Haris M, Singh A, Kogan F, Greenberg JH, Hariharan H, et al. Magnetic resonance imaging of glutamate. *Nat Med.* (2012) 18:302–6. doi: 10.1038/nm.2615
139. Drieu A, Buendia I, Levard D, Helie P, Brodin C, Vivien D, et al. Immune responses and anti-inflammatory strategies in a clinically relevant model of thromboembolic ischemic stroke with reperfusion. *Transl Stroke Res.* (2020) 11:481–95. doi: 10.1007/s12975-019-00733-8
140. Saleh A, Schroeter M, Jonkmanns C, Hartung HP, Modder U, Jander S. *In vivo* mri of brain inflammation in human ischaemic stroke. *Brain.* (2004) 127:1670–7. doi: 10.1093/brain/awh191
141. Saleh A, Schroeter M, Ringelstein A, Hartung HP, Siebler M, Modder U, et al. Iron oxide particle-enhanced mri suggests variability of brain inflammation at early stages after ischemic stroke. *Stroke.* (2007) 38:2733–7. doi: 10.1161/STROKEAHA.107.481788
142. Rausch M, Sauter A, Frohlich J, Neubacher U, Radu EW, Rudin M. Dynamic patterns of uspio enhancement can be observed in macrophages after ischemic brain damage. *Magn Reson Med.* (2001) 46:1018–22. doi: 10.1002/mrm.1290
143. Oude Engberink RD, Blezer EL, Hoff EI, van der Pol SM, van der Toorn A, Dijkhuizen RM, et al. Mri of monocyte infiltration in an animal model of neuroinflammation using spio-labeled monocytes or free uspio. *J Cereb Blood Flow Metab.* (2008) 28:841–51. doi: 10.1038/sj.jcbfm.9600580
144. Shichinohe H, Kuroda S, Kudo K, Ito M, Kawabori M, Miyamoto M, et al. Visualization of the superparamagnetic iron oxide (spio)-labeled bone marrow stromal cells using a 30-t mri-a pilot study for clinical testing of neurotransplantation. *Transl Stroke Res.* (2012) 3:99–106. doi: 10.1007/s12975-011-0138-5
145. Jin AY, Tuor UI, Rushforth D, Filfil R, Kaur J, Ni F, et al. Magnetic resonance molecular imaging of post-stroke neuroinflammation with a p-selectin targeted iron oxide nanoparticle. *Contrast Media Mol Imaging.* (2009) 4:305–11. doi: 10.1002/cmmi.292
146. Barber PA, Foniok T, Kirk D, Buchan AM, Laurent S, Boutry S, et al. Mr molecular imaging of early endothelial activation in focal ischemia. *Ann Neurol.* (2004) 56:116–20. doi: 10.1002/ana.20162
147. Hoyte LC, Brooks KJ, Nagel S, Akhtar A, Chen R, Mardiguian S, et al. Molecular magnetic resonance imaging of acute vascular cell adhesion molecule-1 expression in a mouse model of cerebral ischemia. *J Cereb Blood Flow Metab.* (2010) 30:1178–87. doi: 10.1038/jcbfm.2009.287
148. Gulyas B, Toth M, Schain M, Airaksinen A, Vas A, Kostulas K, et al. Evolution of microglial activation in ischaemic core and peri-infarct regions after stroke: a pet study with the tspo molecular imaging biomarker [((11))c]vinpocetine. *J Neurol Sci.* (2012) 320:110–7. doi: 10.1016/j.jns.2012.06.026
149. Bernardo-Castro S, Sousa JA, Bras A, Cecilia C, Rodrigues B, Almendra L, et al. Pathophysiology of blood-brain barrier permeability throughout the different stages of ischemic stroke and its implication on hemorrhagic transformation and recovery. *Front Neurol.* (2020) 11:594672. doi: 10.3389/fneur.2020.594672
150. Zeynalov E, Jones SM, Elliott JP. Therapeutic time window for conivaptan treatment against stroke-evoked brain edema and blood-brain barrier disruption in mice. *PLoS ONE.* (2017) 12:e0183985. doi: 10.1371/journal.pone.0183985
151. Jiang Q, Ewing JR, Chopp M. Mri of blood-brain barrier permeability in cerebral ischemia. *Transl Stroke Res.* (2012) 3:56–64. doi: 10.1007/s12975-011-0133-x
152. Villringer K, Sanz Cuesta BE, Ostwaldt AC, Grittner U, Brunecker P, Khalil AA, et al. Dce-mri blood-brain barrier assessment in acute ischemic stroke. *Neurology.* (2017) 88:433–40. doi: 10.1212/WNL.0000000000003566
153. Heye AK, Culling RD, Valdes Hernandez Mdel C, Thrippleton MJ, Wardlaw JM. Assessment of blood-brain barrier disruption using dynamic contrast-enhanced mri. A systematic review. *Neuroimage Clin.* (2014) 6:262–74. doi: 10.1016/j.nicl.2014.09.002
154. Pillai DR, Dittmar MS, Baldaranov D, Heidemann RM, Henning EC, Schuierer G, et al. Cerebral ischemia-reperfusion injury in rats–a 3 t mri study on biphasic blood-brain barrier opening and the dynamics of edema formation. *J Cereb Blood Flow Metab.* (2009) 29:1846–55. doi: 10.1038/jcbfm.2009.106
155. Merali Z, Wong T, Leung J, Gao MM, Mikulis D, Kassner A. Dynamic contrast-enhanced mri and ct provide comparable measurement of blood-brain barrier permeability in a rodent stroke model. *Magn Reson Imaging.* (2015) 33:1007–12. doi: 10.1016/j.mri.2015.06.021
156. Park JY, Lee SK, Kim JY, Je KH, Schellingerhout D, Kim DE, et al. New micro-computed tomography-based high-resolution blood-brain barrier imaging technique to study ischemic stroke. *Stroke.* (2014) 45:2480–4. doi: 10.1161/STROKEAHA.114.006297
157. Okada M, Kikuchi T, Okamura T, Ikoma Y, Tsuji AB, Wakizaka H, et al. *In-vivo* imaging of blood-brain barrier permeability using positron emission tomography with 2-amino-[3-11c]isobutyric acid. *Nucl Med Commun.* (2015) 36:1239–48. doi: 10.1097/MNM.0000000000000385
158. Jaffer H, Adjei IM, Labhasetwar V. Optical imaging to map blood-brain barrier leakage. *Sci Rep.* (2013) 3:3117. doi: 10.1038/srep03117
159. Demeestere J, Wouters A, Christensen S, Lemmens R, Lansberg MG. Review of perfusion imaging in acute ischemic stroke: from time to tissue. *Stroke.* (2020) 51:1017–24. doi: 10.1161/STROKEAHA.119.028337

160. Peultier A-C, Redekop WK, Dippel DWJ, Bereczki D, Si-Mohamed S, Douek PC, et al. What stroke image do we want? European survey on acute stroke imaging and revascularisation treatment. *Health Pol Technol.* (2019) 8:261–7. doi: 10.1016/j.hlpt.2019.08.005
161. Provost C, Soudant M, Legrand L, Ben Hassen W, Xie Y, Soize S, et al. Magnetic resonance imaging or computed tomography before treatment in acute ischemic stroke. *Stroke.* (2019) 50:659–64. doi: 10.1161/STROKEAHA.118.023882

Conflict of Interest: The authors declare that the research was conducted in the absence of any commercial or financial relationships that could be construed as a potential conflict of interest.

Publisher's Note: All claims expressed in this article are solely those of the authors and do not necessarily represent those of their affiliated organizations, or those of the publisher, the editors and the reviewers. Any product that may be evaluated in this article, or claim that may be made by its manufacturer, is not guaranteed or endorsed by the publisher.

frontiers in Neurology

ORIGINAL RESEARCH
published: 21 October 2021
doi: 10.3389/fneur.2021.728984

Transcriptomic Profiling Reveals the Antiapoptosis and Antioxidant Stress Effects of *Fos* in Ischemic Stroke

Qiancheng Mu[1,2†], *Yuxuan Zhang*[1,2†], *Long Gu*[2], *Stefan T. Gerner*[3], *Xiancheng Qiu*[1,2], *Qianke Tao*[1,2], *Jinwei Pang*[1,2,4,5], *Ghosh Dipritu*[1,2], *Lifang Zhang*[2,6], *Shigang Yin*[2,4,5], *Yong Jiang*[1,2,4,5*] *and Jianhua Peng*[1,2,5,6*]

[1] *Department of Neurosurgery, The Affiliated Hospital of Southwest Medical University, Luzhou, China,* [2] *Luzhou Key Laboratory of Neurological Diseases and Brain Function, The Affiliated Hospital of Southwest Medical University, Luzhou, China,* [3] *Department of Neurology, University Hospital Erlangen-Nuremberg, Erlangen, Germany,* [4] *Academician (Expert) Workstation of Sichuan Province, The Affiliated Hospital of Southwest Medical University, Luzhou, China,* [5] *Institute of Epigenetics and Brain Science, Southwest Medical University, Luzhou, China,* [6] *Sichuan Clinical Research Center for Neurosurgery, The Affiliated Hospital of Southwest Medical University, Luzhou, China*

OPEN ACCESS

Edited by:
Qin Hu,
Shanghai Jiao Tong University, China

Reviewed by:
Guofang Shen,
Loma Linda University, United States
Yingyu Chen,
Fujian Medical University, China

****Correspondence:***
Jianhua Peng
pengjianhua@swmu.edu.cn
Yong Jiang
jiangyong@swmu.edu.cn

[†] These authors have contributed equally to this work

Specialty section:
This article was submitted to Stroke, a section of the journal Frontiers in Neurology

Received: *22 June 2021*
Accepted: *09 September 2021*
Published: *21 October 2021*

Citation:
Mu Q, Zhang Y, Gu L, Gerner ST, Qiu X, Tao Q, Pang J, Dipritu G, Zhang L, Yin S, Jiang Y and Peng J (2021) Transcriptomic Profiling Reveals the Antiapoptosis and Antioxidant Stress Effects of Fos in Ischemic Stroke. Front. Neurol. 12:728984. doi: 10.3389/fneur.2021.728984

Arterial hypertension is considered the most prevalent risk factor for stroke. Both pathophysiologic and clinical data previously acquired suggest a strong correlation between the hemodynamic nature of arterial hypertension and an increase in the risk of ischemic insult to tissues. However, the knowledge of specific molecular interactions between hypertension and ischemic stroke (IS) is limited. In this study, we performed systematic bioinformatics analysis of stroke-prone spontaneous hypertensive brain tissue samples of rats (GSE41452), middle cerebral artery occlusion of brain tissue samples of rats (GSE97537), and peripheral blood array data of IS patients (GSE22255). We identified that *Fos*, an immediate-early gene (IEG) that responds to alterations in arterial blood pressure, has a strong correlation with the occurrence and prognosis of IS. To further evaluate the potential function of *Fos*, the oxygen–glucose deprivation model and RNA sequencing of HT22 neuronal cells were performed. Consistent with the sequencing results, real-time quantitative PCR and Western blot indicate that *Fos* was elevated at 3 h and returned to normal levels at 6 h after oxygen–glucose deprivation. Knock-down of *Fos* by lentivirus significantly increased the oxidative stress level, neuronal apoptosis, and inhibited the mitochondrial function. In conclusion, *Fos* acts as an important link between hypertension and IS. Furthermore, *Fos* can be used as a potential biomarker for target therapy in the prevention of stroke among hypertensive patients and also potential treatment targeting apoptosis and oxidative stress after its onset.

Keywords: hypertension, ischemic stroke, *Fos*, oxygen-glucose deprivation, apoptosis, oxidative stress, mitochondria

INTRODUCTION

Ischemic stroke (IS) is still a leading cause of death and disability worldwide, despite a decline in stroke mortality due to improved recognition and management of cardiovascular risk factors (1, 2). Arterial hypertension is a major robust non-modifiable risk factor for cardiovascular disease (CVD), particularly cerebrovascular events (3). The cross-linking of stroke and hemodynamics makes the blood pressure management of stroke patients challenging, requiring accurate diagnosis

and precise definition of treatment goals. There are many studies about the genomic regions associated with hypertension, and some genetic characteristics of IS susceptibility among different ethnic groups have been reported (4–6). However, there are no effective biomarkers for screening individuals with high stroke risk.

Based on high-throughput sequencing technology, clinical and basic stroke studies have provided resource data of stroke and revealed the transcriptional regulation mechanisms and potential therapeutic targets of a series of key stroke-related genes (7). In addition, a large number of genes and transcription factors related to hypertension have been revealed in previous studies. Therefore, we questioned whether there may be some common pathophysiological processes and specific key regulator molecules between hypertension and stroke.

In this study, we systematically analyzed the array data of stroke-prone spontaneous hypertensive brain tissue of rats, middle cerebral artery occlusion (MCAO) of brain tissue of rats, and peripheral blood of IS patients. Bioinformatics analysis revealed that *Fos* is an important link between hypertension and IS, which provides a new perspective of hypertension and its participation in the development and prognosis of cerebral stroke (For simplification purposes, throughout this paper, *Fos* denotes gene names in rats and cells, *FOS* denotes gene names in humans, and c-Fos denotes proteins in rats and cells). We further demonstrated that *Fos* exerts antiapoptosis and antioxidant stress effects in the HT22 cell oxygen–glucose deprivation (OGD) model and serves as a promising therapeutic target for the prevention and treatment of stroke.

MATERIALS AND METHODS

Data Collection and Processing

The gene expression matrix of the microarray data numbered GSE41452, GSE22255, and GSE97537 were downloaded from the Gene Expression Omnibus (GEO) database (https://www.ncbi.nlm.nih.gov/geo/). The sequencing platform of GSE41452 was Agilent-028282, corresponding to the GEO platform number GPL14745 (8). The microarray samples of GSE41452 included the Kyoto Wistar–Kyoto rats (WKY) control group, spontaneously hypertensive rats, and hypertension stroke-prone rats at two time points (3 and 6 weeks old; each group has three biological repeats). The platform annotation file of GPL14745 was downloaded by the R software package, which id named GEOquery (version 2.58.0). The GSE41452 expression matrix was normalized by microarray probe transformation, gene name transformation, and log transformation. The maximum expression value taken from different probes of the same gene was used for further analysis. Limma package (version 3.46.0) in *R* software was used to screen out IS-related genes after probe and gene name transformation in GSE97537 brain tissue gene expression data. GSE22255 is the HG-U133_Plus_2 chip platform sample, GPL number GPL570, which contains 40 peripheral blood samples including 20 IS patients and 20 sex- and age-matched controls. The detailed information of the controls and patients is shown in **Supplementary Table 2** (9). GSE97537 was generated on GPL1355 (Rat230_2) Affymetrix Rat Genome 230 2.0 Array platform. A total of seven brain samples from MCAO rats and five brain samples from sham-operated rats were included in the GSE97537 dataset.

Construction of the Weighted Gene Coexpression Network and Screening the Key Module

The order is based on the median value of each gene expressed, and the top 5,000 genes in the GSE41452 expression matrix were selected using the R language for cluster analysis to identify outlier samples and to calculate the Pearson coefficient between any two genes. The pickSoftThreshold function of the *Constructing of the Weighted Gene Co-expression Network* package was applied for the expression matrix. By calculating the scale-free topological fit index of several different soft threshold β ($R^2 = 0.9$), the appropriate soft threshold β was provided for the construction of the adjacency matrix representing the connection strength among genes (10). A new relation matrix was obtained by transforming the adjacency matrix into a topological overlap matrix (TOM), and the transformation was used to reduce noise and false correlation by calculation of the dissimilarity degree of genes. Genes were hierarchically clustered based on the dissimilarity degree obtained by topological overlap, and dynamic sharing algorithm to cluster the dissimilarity degree to get different gene modules. The Pearson coefficients of genes and sample characteristics in different modules were calculated, and the correlation between modules and sample traits was defined as the average correlation of the containing genes, finally to obtain the module, which is the most related to the sample traits.

Screening of Key Nodes in the Protein Interaction Network in Key Modules

All the genes in the key modules were inputted into the STRING protein interaction database (https://string-db.org/) to construct the protein–protein interaction (PPI) network with the Cytoscape software (https://cytoscape.org/; version 3.6.1) (11). The cytoHubba plug-in in Cytoscape was used to screen the key nodes of the protein interaction network, and the top 10 nodes were selected as key nodes (genes) according to the degree ranking score (12).

Cell Culture

HT22 cells were maintained in Dulbecco's modified Eagle's medium (DMEM) basic (Gbico, USA) supplemented with 10% fetal bovine serum (Biological Industries) and a 1% penicillin and streptomycin combination under the condition of 37°C and 5% CO_2. Cells were harvested by trypsin-EDTA treatment and then seeded in the appropriate dish at a density of 1×10^5 cells/cm^2 for 24 h (24H) before the assay.

Oxygen–Glucose Deprivation

HT22 cells were subjected to an OGD state for 3 and 6 h to mimic transient focal ischemic stroke *in vitro*. Serum-free DMEM without glucose (Solarbio, China) was used for OGD. Briefly, cells were cultured in the normal incubator for 24H, then the DMEM basic medium was removed and washed using PBS three times. The serum-free DMEM without glucose was added,

and cells were cultured in a hypoxia incubator (Eppendorf, Germany) for 3 and 6 h. Cells obtained were then used for further experiments.

Total RNA-seq Library Generation and Sequencing

Total RNA was extracted from OGD-treated cells and control cells by using the RNeasy kit (TIANGEN, China). Library preparation was performed by using VAHTS® Universal V6 RNA-seq Library Prep Kit for Illumina (Vazyme, NR604-01/02, China) according to the instructions of the manufacturer. All libraries were sequenced using the Illumina HiSeq X 10 with 150PE reads according to the instructions of the manufacturer. Differentially expressed mRNAs were selected for Gene Ontology (GO) and Kyoto Encyclopedia of Genes and Genomes (KEGG) pathway analysis as previously described (13). GO analysis covers three domains: cellular component (CC), molecular function (MF), and biological process (BP) (http://www.geneontology.org). The significance of the KEGG pathways (http://www.genome.jp/kegg) among differentially expressed genes was denoted by the *p*-value. A value of $p < 0.05$ is recommended.

Real-Time Quantitative PCR

HT22 cells were removed from a Petri dish and were collected for total RNA extraction using an RNeasy kit (TIANGEN, China). Eight hundred nanograms of RNA was used for cDNA synthesis. The RT-qPCR assay was performed according to the detailed procedure described by Ratchford et al. (14). Each reaction was run in triplicate and consisted of 10 ng of cDNA, 16 μl of Power SYBR Green PCR System (Vazyme, China), and 4 mM forward/reverse primers. The fold change in gene expression was calculated using the $^{\Delta\Delta}$Ct method (15) with the housekeeping gene, glyceraldehyde-3-phosphate dehydrogenase (GAPDH), as the internal control. The primer sequences are listed below:

Fos-forward: GGGAATGGTGAAGACCGTGTCA;
Fos-reverse: GCAGCCATCTTATTCCGTTCCC;
GAPDH-forward: ATTGTCAGCAATGCATCCTG;
GAPDH-reverse: ATGGACTGTGGTCATGAGCC.

Cell Viability Assay

Cell viability was quantified by using an MTT assay kit (Beyotime, China). HT22 cells were seeded onto 96-well plates (1×10^4/well) and cultured in a 5% CO_2 incubator for 24H. The OGD-treated cells and control cells were added at 10 μl/well of MTT (5 mg/ml) [3-(4,5-dimethyl-2-thiazolyl)-2,5-diphenyl-2H-tetrazolium bromide (MTT)], and subsequently incubated in a 37°C incubator for 4H to form MTT formazan. MTT formazan was solubilized by the addition of formazan solvent (100 μl/well) in a 37°C incubator for 4H. The yield of the MTT formazan product was determined by measuring the absorbance at 570 nm on a microplate reader (OMEGA, Switzerland). By setting the wells with only medium but no cells as the blank control group, data were represented as the percentage of viable cells compared with vehicle-treated control cells, which were arbitrarily assigned a viability value of 100%.

Western Blot

Cells were homogenized in a RIPA Lysis Buffer (Beyotime, China) containing 20 μl/ml of protease and phosphatase inhibitor cocktail (Beyotime, China). Protein samples were boiled in SDS-polyacrylamide gradient gels (PAGE) loading buffer and subjected to SDS-PAGE. Equal concentrations of solubilized proteins were separated in 12% PAGE and transferred onto polyvinylidene difluoride (PVDF) membranes. Non-specific binding to the membranes was prevented by the incubation with 5% Blotto (5% non-fat dry milk and 1% Tween-20 in TBS) for at least 1 h at room temperature (RT). Membranes were then incubated with various primary antibodies overnight at 4°C. On the following day, membranes were washed and further incubated for 1 h in the presence of horseradish peroxidase (HRP)-conjugated goat anti-rabbit or goat anti-mouse secondary antibodies at room temperature. Clarity Western ECL Substrate A and Peroxide Solution B (Vazyme, China) were used for protein band visualization, and Western blot (WB) exposures were captured using the ChemiDoc XRS + imaging system (VLBER, France). Protein loading was normalized with β-actin (1:8,000, 20536-1-AP, Proteintech, China). Primary antibodies included c-Fos (1:1,000, 2250S, Cell Signaling Technology, USA), SOD2 (1:2,000, 24127-1-AP, Proteintech, China), Pgc-1α (1:800, 2178S, Cell Signaling Technology, USA), Tfam (1:2,000, 22586-1-AP, Proteintech, China), Bcl-2 (1:600, 12789-1-AP, Proteintech, China), and Bax (1:2,000, ab32503, Abcam, UK).

MDA/GPx/ATP Content

The MDA content was determined using a Lipid Peroxidation MDA Assay Kit (S0131S, Beyotime, China). The GPx content was detected using the Total Glutathione Peroxidase Assay Kit with NADPH (S0058, Beyotime, China), and ATP content was detected using the ATP Assay Kit (S0026, Beyotime, China). All operational processes followed the instructions of the manufacturer.

Cell Immunofluorescence

HT22 cells, 1×10^5, were seeded onto a polylysine-coated cell climbing slice and cultured for 24H, then treated with OGD insult for 0, 3, and 6 h. Next, the cells were then incubated with a Mito Tracker Red solution (1:5,000, M7512, Invitrogen, USA) for 30 min at 37°C, replaced with 500 μl of 4% paraformaldehyde after 30 min, and further incubated at RT for 20 min with gentle shaking. Termination was carried out using 0.1 M glycine/PBS for 15 min at RT and then permeabilized with 0.1% Triton X-100/PBS for 10 min at RT. After blocking with 10% goat serum/PBS, the cells were incubated overnight at 4°C with cytochrome c antibody (1:200,10993-1-AP, Proteintech, China). Then cells were washed three times with PBS and incubated for 1 h at RT with secondary antibodies (1:200, SA00013-2, Proteintch, China), and finally stained with Mounting Medium with DAPI (4′,6- diamidino-2-phenylindole) (ab104139, Abcam, UK). Cell images were subsequently acquired with a microscope (Nikon, Japan).

Fos shRNA Transfection

Lentiviral particles expressing shRNA against *Fos* and the corresponding control sequence were constructed by Genechem (Shanghai Genechem Co., Ltd.). Knocked-down cells (KD) and negative control cells (NC) were generated by transfecting HT22 cells with pre-synthesized *Fos* (or control) shRNA lentiviral particles as per the standard protocol of the manufacturer. At 72-h post-infection, transfected cells emitted a green fluorescence signal, and puromycin (2 μg/ml) was added to the culture medium for selection and further characterization. The target sequences of shRNA of *Fos* were as follows: KD shRNA: ccGT CTCTAGTGCCAACTTTA. NC shRNA: TTCTCCGAACGTGT CACGT.

TUNEL Assay

The TUNEL assay was done using the TUNEL assay kit obtained from Beyotime (China, C1089). HT22 cells were seeded onto polylysine-coated cell climbing slice and treated with OGD by the same way with cell immunofluorescence. The next operational processes followed the instructions of the manufacturer.

Statistical Analyses

Data are presented as the mean ± SEM from at least three independent experiments. Statistical analysis and graph presentation were carried out using GraphPad Prism software version 8.0 (GraphPad Software, La Jolla, CA, USA). The significance of differences between groups was assessed by two-tailed unpaired Student's *t*-test or one-way ANOVA. A value of $p < 0.05$ was considered as a significant difference.

RESULTS

Construction of WGCNA Network and Identification of Key Modules

Through the gene clustering analysis of the first 5,000 of the average expression amounts of GSE41452 gene expression matrix, we found that the clusters consisted of the experimental design grouping and internal correlation, indicating that this part of the gene can represent the overall gene expression characteristics, and there were no outlier samples (**Supplementary Figure 1**).

The selection of soft threshold power is an important step in the construction of WGCNA. The network topologies with soft thresholds from 1 to 20 were screened to determine the best soft threshold β for balancing scale independence and mean connectivity. When the scale-free topology fitting index was closest to 0.9, the lowest β value was 8 and was taken as the best soft threshold (**Figure 1A**). The modules whose dissimilarity degree was <0.25 were set up to merge the other modules (**Supplementary Figure 2B**), and the dynamic shearing branching algorithm was used to analyze the dissimilarity among the modules, and a total of 26 modules were obtained. Among them, the genes that cannot be included in any screening module were included in the gray module (**Figure 1B**).

This study also explored the relationship between modules, and the results exhibited a high degree of independence between each module and the phase independence of gene expression in the top 400 genes (**Supplementary Figure 2C**). To investigate the coexpression similarity of all modules, the eigengene matrix was calculated and clustered according to their correlation (**Supplementary Figure 2A**). After defining the independence of each module, this study further calculated the relationship between the modules and the sample character. To get the correlation coefficient and probability between the modules and the sample character, we calculated the average Pearson correlation coefficient between the eigengene and the character of the modules. We found that the blue module was highly negatively correlated with WKY traits ($r = -0.87$, $p = 2 \times 10^{-6}$) and positively correlated with hypertension-related phenotypes with SHRSP traits as the main component (**Figure 1D**). In addition, we also evaluate not only the correlation between a single gene and the whole module but also the correlation between modules and characters in the blue module (**Figure 1C**) and found that there was a linear correlation between a single gene and the whole module and also between the module and character (Pearson's correlation coefficient was 0.72, $p = 4.4 \times 10^{-73}$). The genes of the blue module can represent the correlation between modules and traits. Therefore, the blue module was selected as the key module, and its genes may play an important role in the process of hypertension and stroke.

Construction of Protein–Protein Interaction in Key Modules and Selection of Key Genes Related to Stroke Process

All the 450 genes in the key modules were entered into the STRING database for protein interaction analysis. The genes that could not connect any node were removed (**Figure 2A**). Next, we used the cytoHubba (ver 0.1 version) plug-in to obtain the top 10 key genes in the degree scores; the top 10 genes are *Il6*, *Fos*, *Ccl5*, *C1qc*, *C3*, *Il21*, *Ptgs2*, *C1qa*, *Atf3*, and *Emr1* (**Figure 2B**).

Despite the 450 genes that are closely related to the development of hypertension to stroke-prone in rats, whether these genes have expression changes during the stroke and continue to have an impact from stroke-prone to stroke needs further research. Therefore, brain tissue microarray data of rats with IS were selected to make further analysis to determine whether there is a relationship between the stroke-prone genes and established stroke genes.

GSE97537 was obtained from Affymetrix Rat Genome 2302.0 Array sequencing platform, including 12 brain tissues derived from 7 middle cerebral artery occlusion models (MCAO) and 5 sham-operated SD rats. The limma package (version 3.46.0) was used to analyze the differential expression genes (DEGs) of the annotated expression matrix. Two hundred and seventeen upregulated DEGs and nine downregulated DEGs were obtained according to the screening criteria of $|\log FC| > 1$ and $p < 0.05$. *Il6*, *Fos*, *Atf3*, *Ptgs*2, and *C1qc* are the top part of the DEGs (**Figure 2D**).

Through further analysis of these five genes, we found that there were close interactions among the four genes

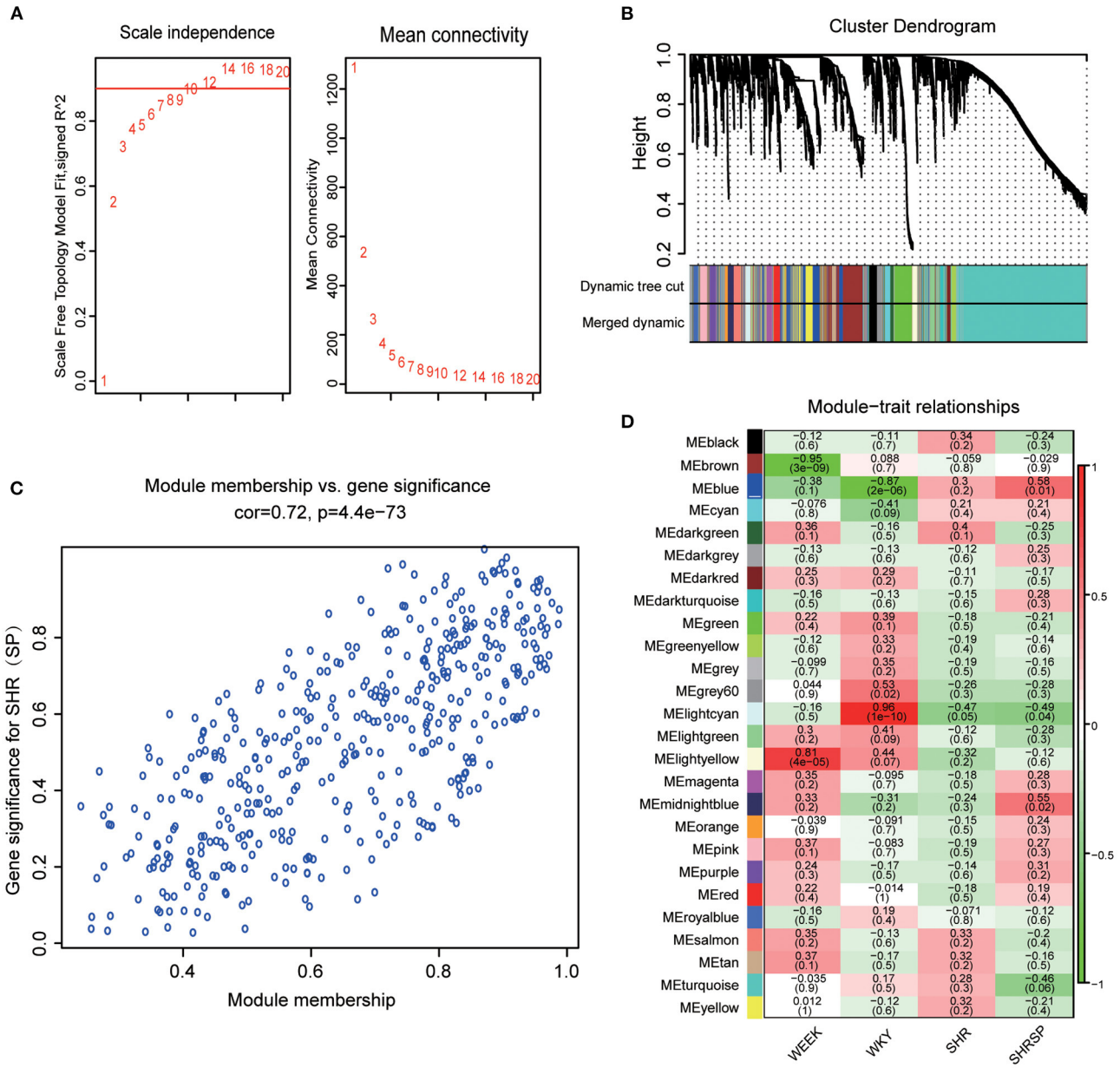

FIGURE 1 | Determination of the best soft threshold and module selection. **(A)** Through the scale independence and mean connectivity to choose the best soft threshold. The red words represent the soft threshold. **(B)** The tree clustering of genes and module form the cluster dendrogram; each color of the module represents a collection of genes with a similar expression. **(C)** Module membership and gene significance were analyzed. **(D)** The ordinate colors represent different modules, the abscissa represents different sample characters, the corresponding heat map shows its Pearson coefficient and probability, and the heat map color represents the correlation (the highest in red and the lowest in blue).

except *C1qc* in PPI. We also found that the total combined score of *Fos* was higher than the other three genes through seven evaluation methods, such as Neighborhood in the Genome, Gene Fusion, Co-Occurrence Across Genomes, Co-Expression, Experimental/Biochemical Data, Association in Curated Databases, and Co-Mentioned in PubMed Abstracts (**Figure 2C**). Therefore, we chose *Fos* as the key gene for further evaluation.

Expression of *FOS* in the Peripheral Blood of Ischemic Stroke Patients

There were also significant differences in the expression of *FOS* in the peripheral blood of stroke patients. Previously, through the analysis of brain tissue sample data of stroke rats, we found five key genes including *Fos*. Next, we used peripheral blood samples from patients with IS from the open database for verification. Using the IS samples from the gene expression

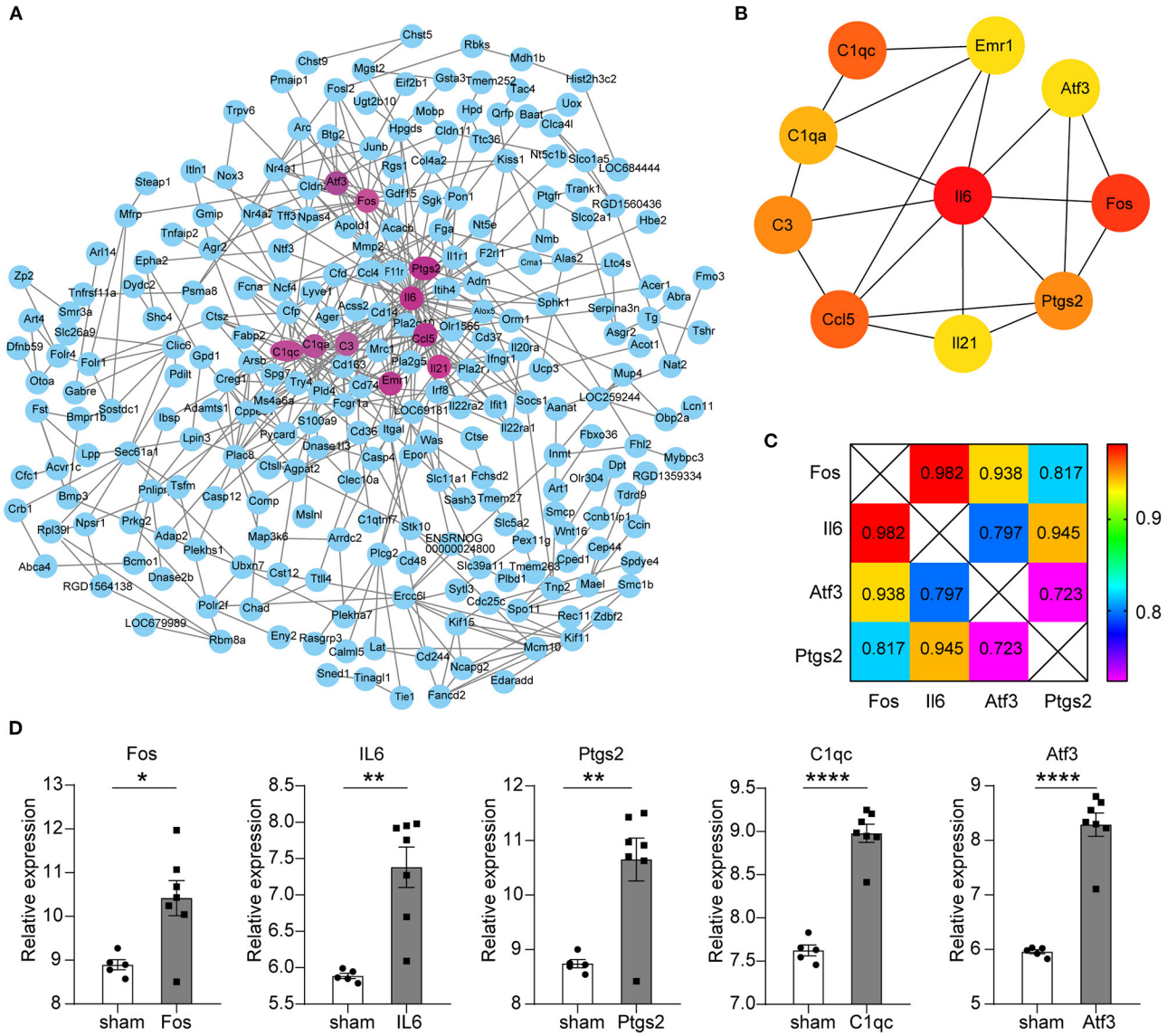

FIGURE 2 | Protein–protein interaction (PPI) network construction for key modules and screening of key genes. **(A)** The circle represents the protein corresponding to the gene, and the wiring represents the interaction. The circles with mauve represent the top 10 key genes in the degree scores. **(B)** Circles represent genes, lines represent interactions, and color represents degree scores, of which red was the highest score. **(C)** The number is the PPI interaction score of differential genes; the different colors indicate different scores. Total score: *Fos* = 2.737, *Il6* = 2.724, *Atf3* = 2.458, *Ptgs2* = 2.485. **(D)** Five differential gene expression levels in GSE97537. The abscissa represents different groups; the ordinate shows the relative gene expression levels, and the error bar is the mean ± SEM, $^{*}p < 0.05$, $^{**}p < 0.01$, $^{****}p < 0.0001$.

matrix, which had been treated by probe conversion, the *FOS* expression was divided into two groups according to the median of DNA expression, and the DEGs between the two groups were analyzed. The results showed that compared with the control group, many genes were differentially expressed in peripheral blood of IS patients, including 27 genes upregulated and 3 genes downregulated, including *FOS* (**Supplementary Table S1**).

In our previous analysis, *Fos*/*FOS* was validated in the brain tissues of hypertensive stroke-prone rats, MCAO rats, and peripheral blood of patients with IS. Therefore, *Fos*/*FOS* may play an important role in the transformation of hypertension to stroke and the regulation of gene expression in IS and may be further used as a biomarker and potential therapeutic target for pre-stroke prevention and stroke prognosis.

RNA-Sequencing Analysis of Oxygen–Glucose Deprivation-Treated HT22 Cells

The samples used in the previous databases were all animal or human organs or tissues; here we used an OGD model of

cells. After the OGD state was established for different time points, RNA sequencing was performed. The results showed that *Fos* was significantly upregulated in 3 h compared with 0 h (**Figure 3A**). In addition, the heatmap of the *p*-value of DEGs among 3 vs. 0 h showed that the *p*-value of *Fos* was the smallest among the DEGs (**Figure 3B**). By GO analysis of the upregulated DEGs among 3 vs. 0 h, we found that response to inorganic substance was the most significant process, followed by cellular response to metal ion and response to reactive oxygen species (**Figure 3C**). Therefore, we can conclude that *Fos* may be involved in oxidative stress regulation (16, 17). In the cellular component category, the upregulated DEGs in 3 vs. 0 h were enriched for traits associated with the RNA polymerase II transcription regulator complex, ubiquitin ligase complex, intrinsic component of organelle membrane, and endosome membrane. RNA polymerase II cis-regulatory reign sequence-specific DNA binding was the most abundant in the molecular function category. The results of the GO enrichment revealed

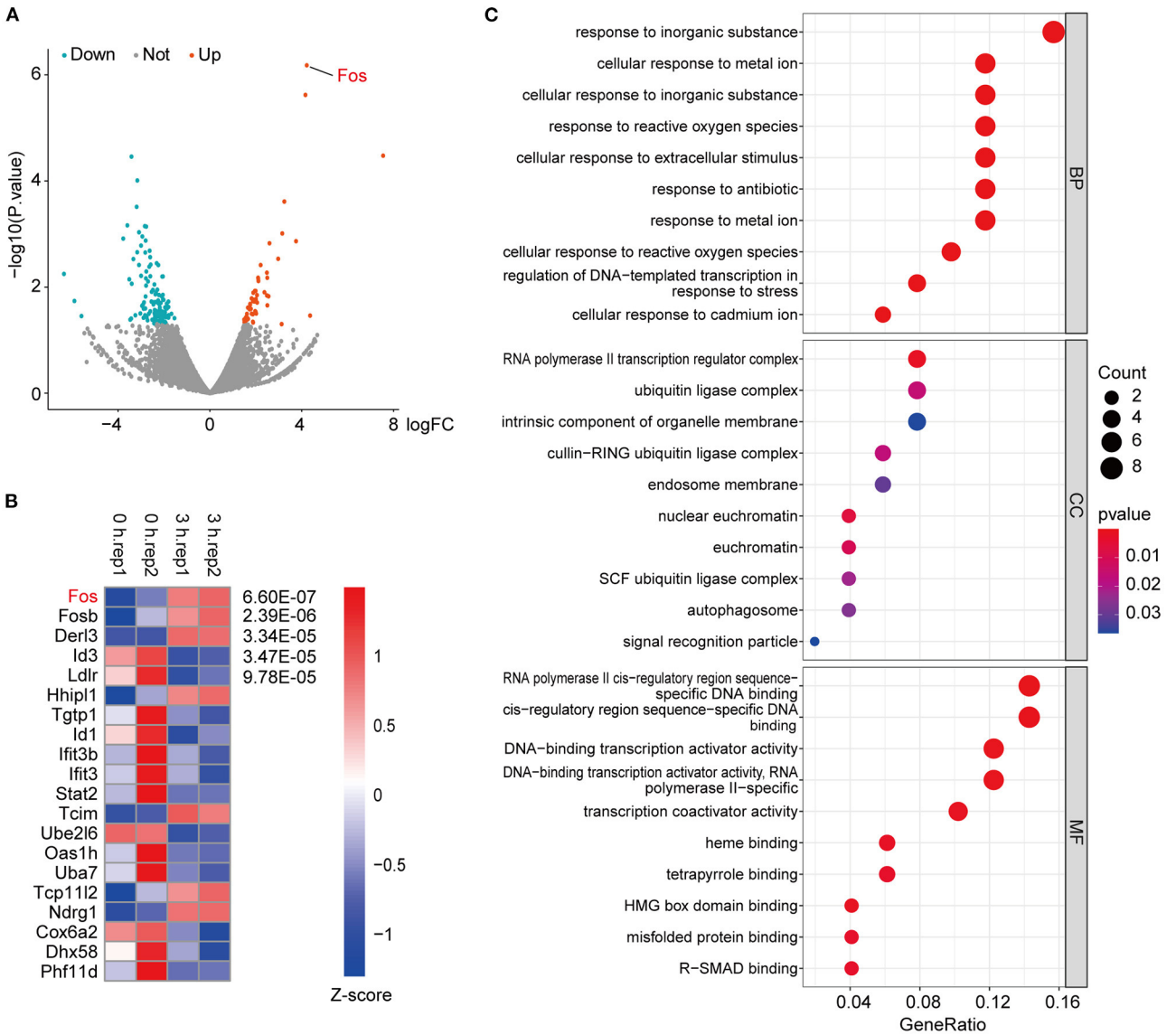

FIGURE 3 | RNA-sequencing of oxygen–glucose deprivation (OGD)-treated HT22 cells. **(A)** These criteria identified 51 upregulated and 119 downregulated genes in 3 vs. 0 h, as shown in the volcano plot, in which the red and green spots represent upregulated and downregulated differentially expressed genes (DEGs), respectively. **(B)** The top 20 genes with the smallest *p*-value among the DEGs were extracted, through normalizing the log2-based TPM + 1 value and the expression matrix by *Z*-score and using the *R* package pheatmap to make a map. **(C)** Gene ontology (GO) enrichment analysis of the upregulated DEGs in RNA-seq data. Gene ratio indicates the number of genes enriched in one pathway compared with the total genes changed in all pathways. Count indicates the number of genes. The colors represent *p*-value, and red is the highest. BP, biological process; CC, cellular component; MF, molecular function.

that the proteins of DEGs were predominantly binding DNA and have transcriptional regulatory functions, located in the regulator complex.

There were also many DEGs in 6 vs. 3 h and 6 vs. 0 h (**Supplementary Figures 3A,B**). The upregulated DEGs in both 6 vs. 3 h and 6 vs. 0 h were used for GO analysis and was found that the generation of precursor metabolites and energy is the top process (**Supplementary Figures 3C,D**). In the cellular component category, the upregulated DEGs in 6 vs. 3 h and 6 vs. 0 h were enriched for traits associated with ribosome, ribosomal subunit, and mitochondrial inner membrane. Structural molecule activity was the most abundant molecular function category. The results of the GO enrichment revealed that the proteins of DEGs in 6 vs. 3 h and 6 vs. 0 h were predominantly binding ribosomes, have structural molecule activity, and are involved in regulating energy generation.

Through KEGG analysis of the RNA-seq data, we found that (1) The KEGG pathway enrichment results of the DEGs in 3 vs. 0 h were mainly enriched for osteoclast differentiation, amphetamine addiction, FoxO signaling pathway, B-cell receptor signaling pathway, and other related signaling pathways, which are mainly involved in regulating cell growth and differentiation, addiction, OGD, and inflammatory immunity pathways (**Supplementary Figure 4A**); (2) The KEGG pathway enrichment results of the DEGs in 6 vs. 3 h were mainly enriched for ribosome, biosynthesis of amino acids, glycolysis/gluconeogenesis, and hypoxia-inducible factor-1 signaling pathway (HIF-1). These pathways are mainly involved in the synthesis of amino acids and proteins and the cellular response to OGD (**Supplementary Figure 4B**); (3) The KEGG pathway enrichment results of the DEGs in 6 vs. 0 h and 6 vs. 3 h were generally consistent (**Supplementary Figure 4C**).

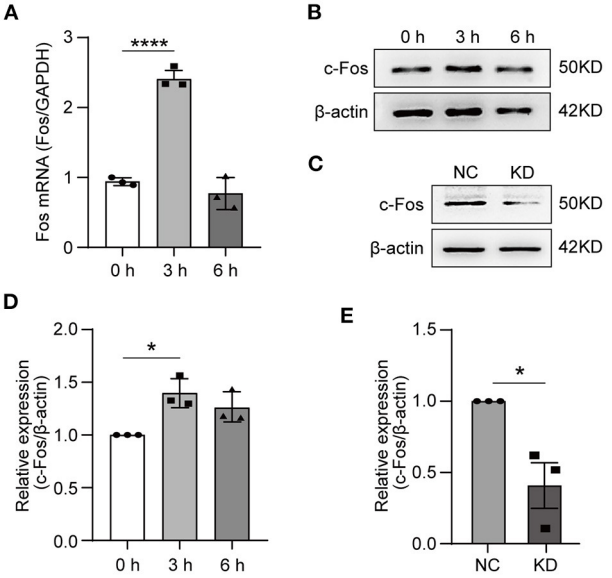

FIGURE 4 | Expression of *Fos* in HT22 cells. HT22 cells were treated by OGD for 0, 3, and 6 h. The total RNA and protein were collected for analysis. **(A)** The *Fos* gene expression level in OGD cells was measured by quantitative real-time PCR. Glyceraldehyde-3-phosphate dehydrogenase (GAPDH) served as the control. **(B)** The c-Fos protein level in OGD cells was detected by Western blot (WB). **(C)** The knockdown efficiency was determined by WB. **(D)** Relative expression levels of c-Fos at each time point after OGD. **(E)** Relative expression levels of c-Fos in the NC group and KD. Each result is expressed as the mean of three independent experiments ± SEM. The statistical analysis of A were performed using one-way ANOVA, and the unpaired *t*-tests were used in **(C)**. $^{*}p < 0.05$, $^{****}p < 0.0001$. NC, negative control cells; KD, knock-down cells.

RT-qPCR and Western Blot Validation

To validate the RNA-seq data, the HT22 cells were treated with OGD for 3 or 6 h. We used RT-qPCR to measure the *Fos* gene expression level after OGD treatment, the results indicated that the expressing level of *Fos* was the highest at 3 h and was not statistically significant at 6 h compared with 0 h (**Figure 4A**). The WB technique was further used to measure the *Fos* protein level after OGD (**Figure 4B**). Analysis of WB bands reveals similar results and trends with the RT-qPCR results (**Figure 4D**). To conclude, we found that *Fos* expression level increased at 3 h and decreased near the normal level at 6 h.

To further solidify our findings, we knocked down *Fos* by lentiviral transfection in HT22 cells. The knocked-down efficiency of *Fos* was confirmed by WB (**Figures 4C,E**). Ultimately, NC and KD were used for subsequent studies.

Knockdown of *Fos* Aggravated Neuronal Oxidative Stress After Oxygen–Glucose Deprivation

One of the mitochondrial biogenesis regulation pathways is the Pgc-1α/Tfam pathway. In our research, we detected the expression of Pcg-1α and Tfam by WB (**Figure 5A**). Through analysis of the WB results, we found Pgc-1α (**Figure 5B**) and Tfam (**Figure 5C**) expression reduced in KD at 3 and 6 h after OGD compared with NC. The MDA, GPx, and SOD2 content can be used to measure antioxidative stress ability. We found that knockdown of *Fos* increased MDA expression and reduced GPx expression at 3 and 6 h after OGD, but MDA and GPx expression was increased in NC at 0 h compared with the KD (**Figures 5E,F**). SOD2 expression levels were also measured by WB, and the expression level of SOD2 was also reduced in the KD at 3 and 6 h after OGD compared with NC (**Figures 5A,D**). Through immunofluorescence, we further found that cytochrome c in the cytoplasm of KD was significantly higher than that in NC at 3 and 6 h after OGD, while there was no significant difference in 0 h (**Figure 5G**). This indirectly implies that *Fos* can attenuate the mitochondrial function of HT22 cells at 3 and 6 h after OGD.

Knockdown of *Fos* Aggravated Neuronal Apoptosis After Oxygen–Glucose Deprivation

To assess the effect on apoptosis, different methods were used in our study. First, WB was used to validate the knockdown of *Fos* at different time points after OGD, and the results showed that

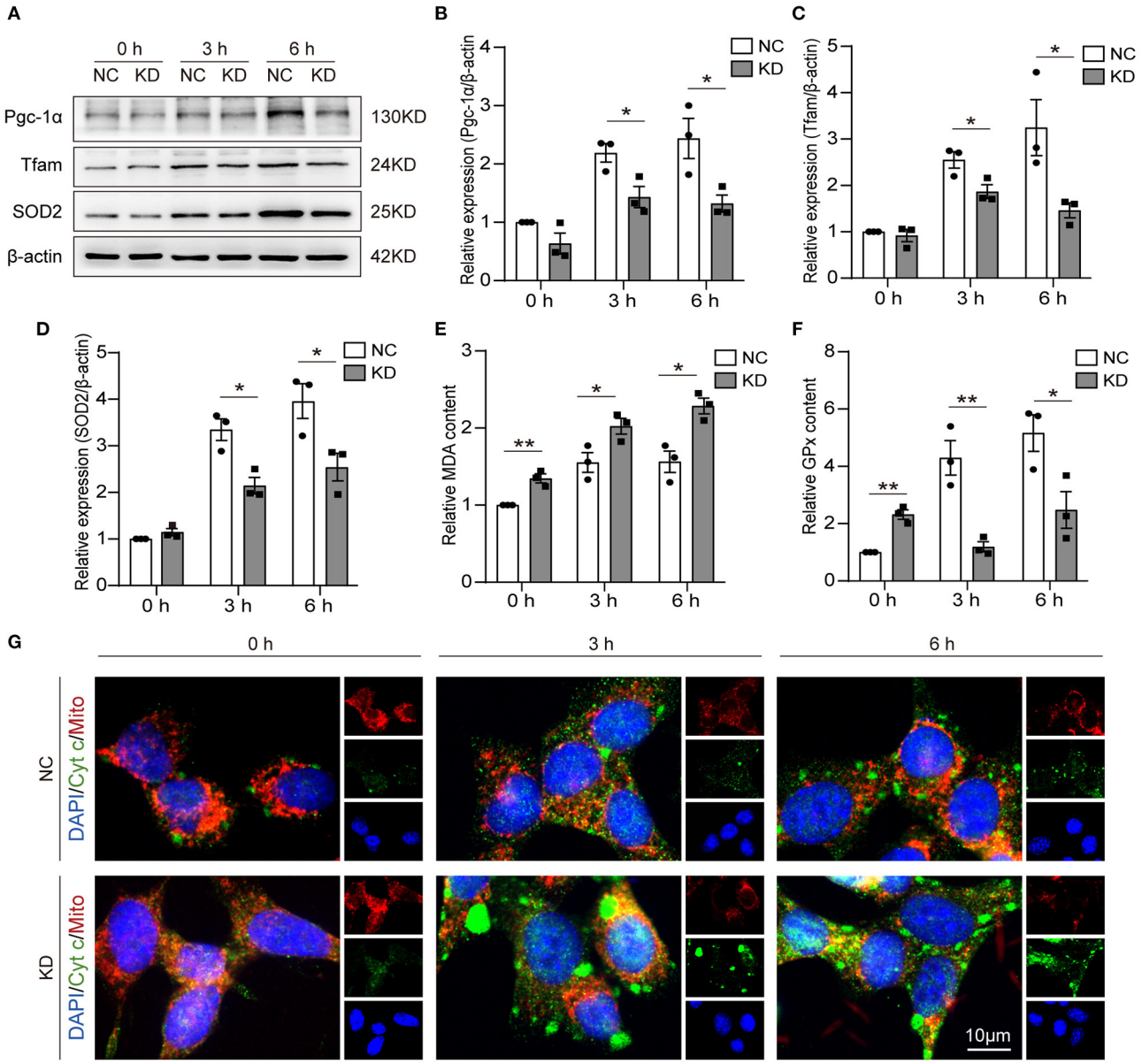

FIGURE 5 | Knockdown of *Fos* aggravated oxidative stress and impaired mitochondrial function. **(A–D)** Representative bands and quantification of SOD2, Pgc-1α, and Tfam from WB. **(E)** MDA levels were assessed in *Fos* knockdown cells after OGD. **(F)** GPx levels were assessed in *Fos* knockdown cells after OGD. **(G)** Representative immunofluorescence microphotographs of the NC and KD groups at each time point after OGD. Mitochondria (Mito) and Cytochrome c (Cyt c) were labeled by red and green puncta, respectively; the nuclear (DAPI) was labeled by blue. Scale bar = 10 μm. Each result is expressed as the mean of three independent experiments ± SEM. *$p < 0.05$, **$p < 0.01$. NC, negative control cells; KD, knock-down cells.

the knockdown of *Fos* was significant at 0 and 3 h. Knockdown of *Fos* could exacerbate HT22 cell apoptosis by increasing the Bax/Bcl-2 ratio (**Figures 6A–C**). The number of survived cells of KD was reduced, and cytoplasmic contraction of KD was more apparent at 0, 3, and 6 h after OGD compared with NC. MTT results indicated that the cell survival rate of KD decreased at 0, 3, and 6 h after OGD compared with NC (**Figures 6D,E**). On the other hand, it also proved that intracellular ATP concentration is an important determinant of cell death. Since mitochondrial structure and function determine ATP production, necrosis is associated with ATP deficiency, while apoptosis required ATP (18). We evaluated the ATP content of our models and found that *Fos* knockdown increased ATP content at 0, 3, and 6 h after OGD (**Figure 6F**). In addition, the results of TUNEL assay suggested that the number of apoptotic cells was significantly increased in the KD group at 0 and 3 h in HT22 cells with knockdown of *Fos* (**Figure 6G**), indicating that knockdown of *Fos* in HT22 cells aggravated apoptosis after OGD.

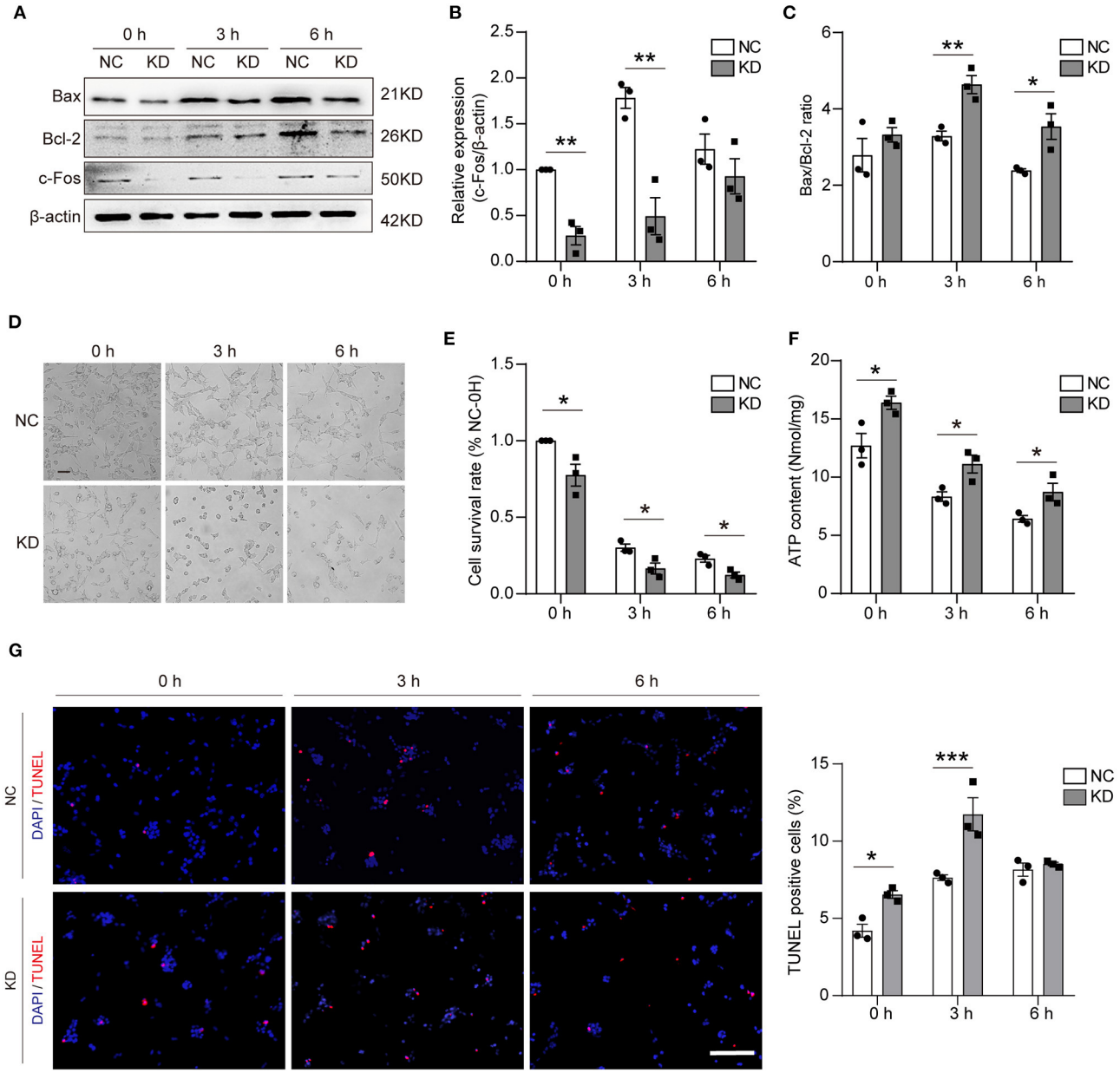

FIGURE 6 | Apoptosis was aggravated in the KD group after OGD. **(A–C)** Representative WB bands and quantification of c-Fos, Bax, and Bcl-2 expression levels. **(D,E)** Cell morphology and cell survival rate at 0, 3, and 6 h. Scale bar = 50 μm. **(F)** ATP content (nmol/mg) was detected by an ATP Assay Kit. **(G)** The TUNEL-positive cells were labed by red, and the nuclear (DAPI) was labeled by blue. Scale bar = 100 μm. Each result is expressed as the mean of three independent experiments ± SEM. $^{*}p < 0.05$, $^{**}p < 0.01$, $^{***}p < 0.001$. NC, negative control cells; KD, knock-down cells.

DISCUSSION

The present study, for the first time, systematically evaluated the transcriptomic profiling interaction between hypertension and IS. Several novel findings were made in the present study: (1) By analyzing microarrays from a variety of stroke samples, we found that *Fos* can act as a key gene between hypertension and stroke. (2) Our high-throughput sequencing data suggest that upregulated genes after stroke are mainly involved in inflammatory and reactive oxygen species (ROS)-related pathways including oxidative stress. (3) *Fos* was increased in neurons at 3 h after OGD, then returned to normal levels at 6 h. (4) Knockdown of *Fos* increased oxidative stress and apoptosis in OGD-treated cells and exacerbated the functional impairment of the mitochondria.

Hypertension has been identified as a key factor associated with the development and prognosis of cerebrovascular disease in patients (especially in older patients) with either ischemic or

hemorrhagic strokes. There are several ways in which clinicians can control arterial blood pressure to reduce stroke incidence and manage stroke patients. However, new strategies to identify and reduce stroke risk and improve management of acute stroke are necessary (19).

Notably, pre-stroke hypertension has a substantial impact on the prognostic outcome of IS (20). Pathophysiological processes such as oxidative stress, inflammatory immune response, and structural changes in the vasculature are all involved in the development of stroke or hypertension (21–23). However, exploration of hypertension-related gene expression and their alterations associated with IS has not been reported previously. Therefore, our study on exploring the molecular factors associated with hypertension in pre-stroke and stroke patients might further clarify the impact of hypertension on stroke and, thus, provide theoretical guidance for stroke prevention interventions during the hypertensive phase and pharmacological interventions after stroke.

In this study, gene expression microarray data were extracted from public databases, which included samples of spontaneously hypertensive stroke-prone rats, MCAO rats, peripheral blood of IS patients, and their respective control groups. We identified five hypertension-prone stroke genes and screened for *Fos* with the highest PPI score. Consistent with our findings, Yoshida et al. previously reported that *Fos* is one of the hypertension-prone stroke genes (24). The other four genes are involved in oxidative stress, immune response, and transcriptional regulation, which is consistent with the pathophysiological processes involved in stroke (25–29). For example, ROS can induce the expression of ATF3, which in turn inhibits the activity of the PINK1 promoter and causes accumulation of depolarized mitochondria, increased production of mitochondrial ROS, and loss of cell viability (30, 31). *Fos* is one of the immediate-early genes that are activated transiently and rapidly in response to a wide variety of cellular stimuli. Recent studies revealed that *Fos* plays important roles in cell proliferation, neuron activation, inflammatory, apoptosis, tumor, and oxidative stress (32–35). In addition, our RNA-seq data indicated that (a) *Fos* was increased at 3 h and returned to normal levels at 6 h after OGD compared with control, and (b) the upregulated genes are widely involved in pathophysiological processes such as cellular energy metabolism and oxidative stress.

Hypoxia and oxidative stress have been reported to be closely linked in previous studies. Hypoxia can cause excessive ROS production and, thus, alter redox homeostasis, while both short-term and long-term hypoxic exposure can induce oxidative stress (36, 37). Mitochondria and stroke have become a major topic of research nowadays (38). In our study, by knocking down *Fos*, we found that the GPx and SOD2 levels were significantly reduced, while MDA was significantly increased in OGD-treated neurons. The Pgc-1α/Tfam pathway is downregulated in the KD compared with the NC. Immunofluorescence shows that cytochrome c in the cytoplasm was also significantly increased after *Fos* knockdown. The evidence further suggests that *Fos* may function in regulating oxidative stress and mitochondrial homeostasis during IS. Under oxidative stress, ROS including free radicals such as superoxide, hydroxyl radical, and hydrogen peroxide are generated at high levels inducing cellular damage and cell death. Interestingly, the role of *Fos* in apoptosis appears to be diverse. Some studies suggested that *Fos* can reduce apoptosis, while others suggest that *Fos* can increase apoptosis (34, 39–41). Our study found that knockdown of *Fos* can reduce cell survival rate, increase Bax/Bcl-2 ratio, and increase ATP content, which means knockdown of *Fos* increases neuron apoptosis after OGD. Mitochondria is also one of the new therapeutic targets in stroke, and *Fos* is involved in the regulation of mitochondrial function and oxidative stress, so *Fos* may be a potential new target for stroke therapy (42, 43).

We acknowledge that our results should be interpreted cautiously due to some limitations. The neuronal OGD model is a single-cell model of stroke, a model that helps to control variables and reduce the interference of factors other than neurons. However, the brain has many other types of cells in addition to neurons, and there are multiple cells in the peripheral blood, and stroke is a complex pathophysiological process that can involve many cells. Therefore, the combination of multiple models of cells and animals with each other helps our results to be closer to the reality of the human condition. Further validation in animals or humans in future studies will be necessary to apply our results to clinical practice. Despite many novel findings, we did not provide specific evidence on how *Fos* affects mitochondria and ROS. Further studies are needed to fully establish the underlying mechanism of immediate-early oxidative stress after ischemic injury and the specific role of *Fos* in this process.

CONCLUSIONS

In conclusion, *Fos*, a hypertensive stroke-prone gene, may be involved in the regulation of oxidative stress and neuronal apoptosis after stroke and may represent a new therapeutic target and clinical indicator for stroke.

DATA AVAILABILITY STATEMENT

The datasets presented in this study can be found in online repositories. The names of the repository/repositories and accession number(s) can be found here: GEO database with the following Accession Number: GSE178997.

AUTHOR CONTRIBUTIONS

QM wrote the manuscript and generated the figures. YZ and LG helped to generate and design the figures. SG, XQ, QT, SY, JPa, GD, and LZ proposed suggestions for revisions. JPe revised the manuscript. YJ, JPe, and SY designed the content. All authors have read and approved the final manuscript.

FUNDING

This work was supported by grants from the Young Elite Scientist Sponsorship Program by the China Association for Science and

Technology and the National Natural Science Foundation of China (81771278, 81801176 and 81971132); the Sichuan Science and Technology Program (2019JDTD0004 and 2019JDRC0062); the doctoral Research Initiation Fund of Affiliated Hospital of Southwest Medical University.

SUPPLEMENTARY MATERIAL

The Supplementary Material for this article can be found online at: https://www.frontiersin.org/articles/10.3389/fneur.2021.728984/full#supplementary-material

REFERENCES

1. Muse ED, Wineinger NE, Spencer EG, Peters M, Henderson R, Zhang Y, et al. Validation of a genetic risk score for atrial fibrillation: a prospective multicenter cohort study. *PLoS Med.* (2018) 15:e1002525. doi: 10.1371/journal.pmed.1002525
2. Zhao BQ, Chauhan AK, Canault M, Patten IS, Yang JJ, Dockal M, et al. von Willebrand factor-cleaving protease ADAMTS13 reduces ischemic brain injury in experimental stroke. *Blood*. (2009) 114:3329–34. doi: 10.1182/blood-2009-03-213264
3. Prenissl J, Manne-Goehler J, Jaacks LM, Prabhakaran D, Awasthi A, Bischops AC, et al. Hypertension screening, awareness, treatment, and control in India: a nationally representative cross-sectional study among individuals aged 15 to 49 years. *PLoS Med.* (2019) 16:e1002801. doi: 10.1371/journal.pmed.1002801
4. Fukunaga Y, Itoh H, Hosoda K, Doi K, Matsuda J, Son C, et al. Altered gene expression of uncoupling protein-2 and−3 in stroke-prone spontaneously hypertensive rats. *J Hypertens.* (2000) 18:1233–8. doi: 10.1097/00004872-200018090-00009
5. Hoffman GE, Smith MS, Verbalis JG. c-Fos and related immediate early gene products as markers of activity in neuroendocrine systems. *Front Neuroendocrinol.* (1993) 14:173–213. doi: 10.1006/frne.1993.1006
6. Sun Y, Lin Z, Liu CH, Gong Y, Liegl R, Fredrick TW, et al. Inflammatory signals from photoreceptor modulate pathological retinal angiogenesis *via* c-Fos. *J Exp Med.* (2017) 214:1753–67. doi: 10.1084/jem.20161645
7. Simpkins AN, Janowski M, Oz HS, Roberts J, Bix G, Doré S, et al. Biomarker application for precision medicine in stroke. *Transl Stroke Res.* (2020) 11:615–27. doi: 10.1007/s12975-019-00762-3
8. Watanabe Y, Yoshida M, Yamanishi K, Yamamoto H, Okuzaki D, Nojima H, et al. Genetic analysis of genes causing hypertension and stroke in spontaneously hypertensive rats: gene expression profiles in the kidneys. *Int J Mol Med.* (2015) 36:712–24. doi: 10.3892/ijmm.2015.2281
9. Krug T, Gabriel JP, Taipa R, Fonseca BV, Domingues-Montanari S, FernandezCadenas I, et al. TTC7B emerges as a novel risk factor for ischemic stroke through the convergence of several genome-wide approaches. *J Cereb Blood Flow Metab*. (2012) 32:1061–72. doi: 10.1038/jcbfm.2012.24
10. Li J, Yu H, Wang W, Fu C, Zhang W, Han F, et al. Genomic and transcriptomic insights into molecular basis of sexually dimorphic nuptial spines in Leptobrachium leishanense. *Nat Commun.* (2019) 10:5551. doi: 10.1038/s41467-019-13531-5
11. Kohl M, Wiese S, Warscheid B. Cytoscape: software for visualization and analysis of biological networks. *Methods Mol Biol.* (2011) 696:291–303. doi: 10.1007/978-1-60761-987-1_18
12. Chin CH, Chen SH, Wu HH, Ho CW, Ko MT, Lin CY. cytoHubba: identifying hub objects and sub-networks from complex interactome. *BMC Syst Biol.* (2014) 8(Suppl. 4):S11. doi: 10.1186/1752-0509-8-S4-S11
13. Peng J, Wu Y, Tian X, Pang J, Kuai L, Cao F, et al. High-throughput sequencing and co-expression network analysis of lncRNAs and mRNAs in early brain injury following experimental subarachnoid haemorrhage. *Sci Rep*. (2017) 7:46577. doi: 10.1038/srep46577
14. Ratchford AM, Esguerra CR, Moley KH. Decreased oocyte-granulosa cell gap junction communication and connexin expression in a type 1 diabetic mouse model. *Mol Endocrinol.* (2008) 22:2643–54. doi: 10.1210/me.2007-0495
15. Frolova A, Flessner L, Chi M, Kim ST, Foyouzi-Yousefi N, Moley KH. Facilitative glucose transporter type 1 is differentially regulated by progesterone and estrogen in murine and human endometrial stromal cells. *Endocrinology.* (2009) 150:1512–20. doi: 10.1210/en.2008-1081
16. Helmig S, Walter D, Putzier J, Maxeiner H, Wenzel S, Schneider J. Oxidative and cytotoxic stress induced by inorganic granular and fibrous particles. *Mol Med Rep.* (2018) 17:8518–29. doi: 10.3892/mmr.2018.8923
17. Luo T, Gao J, Lin N, Wang J. Effects of two kinds of iron nanoparticles as reactive oxygen species inducer and scavenger on the transcriptomic profiles of two human leukemia cells with different stemness. *Nanomaterials (Basel)*. (2020) 10:951. doi: 10.3390/nano10101951
18. Leist M, Single B, Castoldi AF, Kühnle S, Nicotera P. Intracellular adenosine triphosphate (ATP) concentration: a switch in the decision between apoptosis and necrosis. *J Exp Med.* (1997) 185:1481–6. doi: 10.1084/jem.185.8.1481
19. Wajngarten M, Silva GS. Hypertension and stroke: update on treatment. *Eur Cardiol.* (2019) 14:111–5. doi: 10.15420/ecr.2019.11.1
20. Cao Q, Zhou S, Cai B, Wang Q, Zhang J, Shi R, et al. The impacts of premorbid hypertension treatment on functional outcomes of ischemic stroke. *J Neurol Sci.* (2016) 363:1–4. doi: 10.1016/j.jns.2016.02.020
21. Guzik TJ, Touyz RM. Oxidative stress, inflammation, and vascular aging in hypertension. *Hypertension.* (2017) 70:660–7. doi: 10.1161/HYPERTENSIONAHA.117.07802
22. Pistoia F, Sacco S, Degan D, Tiseo C, Ornello R, Carolei A. Hypertension and stroke: epidemiological aspects and clinical evaluation. *High Blood Press Cardiovasc Prev.* (2016) 23:9–18. doi: 10.1007/s40292-015-0115-2
23. Sun W, Ding Z, Xu S, Su Z, Li H. Crosstalk between TLR2 and Sphk1 in microglia in the cerebral ischemia/reperfusion-induced inflammatory response. *Int J Mol Med.* (2017) 40:1750–8. doi: 10.3892/ijmm.2017.3165
24. Yoshida M, Watanabe Y, Yamanishi K, Yamashita A, Yamamoto H, Okuzaki D, et al. Analysis of genes causing hypertension and stroke in spontaneously hypertensive rats: gene expression profiles in the brain. *Int J Mol Med.* (2014) 33:887–96. doi: 10.3892/ijmm.2014.1631
25. Onodera Y, Teramura T, Takehara T, Shigi K, Fukuda K. Reactive oxygen species induce Cox-2 expression *via* TAK1 activation in synovial fibroblast cells. *FEBS Open Bio*. (2015) 5:492–501. doi: 10.1016/j.fob.2015.06.001
26. Sontheimer RD, Racila E, Racila DM. C1q: its functions within the innate and adaptive immune responses and its role in lupus autoimmunity. *J Invest Dermatol.* (2005) 125:14–23. doi: 10.1111/j.0022-202X.2005.23673.x
27. Tanaka T, Narazaki M, Kishimoto T. IL-6 in inflammation, immunity, and disease. *Cold Spring Harb Perspect Biol.* (2014) 6:a016295. doi: 10.1101/cshperspect.a016295
28. Woodruff TM, Thundyil J, Tang SC, Sobey CG, Taylor SM, Arumugam TV. Pathophysiology, treatment, and animal and cellular models of human ischemic stroke. *Mol Neurodegener*. (2011) 6:11. doi: 10.1186/1750-1326-6-11
29. Zhao J, Li X, Guo M, Yu J, Yan C. The common stress responsive transcription factor ATF3 binds genomic sites enriched with p300 and H3K27ac for transcriptional regulation. *BMC Genomics.* (2016) 17:335. doi: 10.1186/s12864-016-2664-8
30. Bueno M, Brands J, Voltz L, Fiedler K, Mays B, St Croix C, et al. ATF3 represses PINK1 gene transcription in lung epithelial cells to control mitochondrial homeostasis. *Aging Cell*. (2018) 17:720. doi: 10.1111/acel.12720
31. Hoetzenecker W, Echtenacher B, Guenova E, Hoetzenecker K, Woelbing F, Brück J, et al. ROS-induced ATF3 causes susceptibility to secondary infections during sepsis-associated immunosuppression. *Nat Med 18(1).* (2011) 128–34. doi: 10.1038/nm.2557
32. Hsieh HL, Wang HH, Wu CY, Yang CM. Reactive oxygen species-dependent c-Fos/activator protein 1 induction upregulates heme oxygenase-1 expression by bradykinin in brain astrocytes. *Antioxid Redox Signal.* (2010) 13:1829–44. doi: 10.1089/ars.2009.2957
33. Motrich RD, Castro GM, Caputto BL. Old players with a newly defined function: Fra-1 and c-Fos support growth of human malignant breast tumors by activating membrane biogenesis at the cytoplasm. *PLoS ONE.* (2013) 8:e53211. doi: 10.1371/journal.pone.0053211
34. Preston GA, Lyon TT, Yin Y, Lang JE, Solomon G, Annab L, et al. Induction of apoptosis by c-Fos protein. *Mol Cell Biol.* (1996) 16:211–8. doi: 10.1128/MCB.16.1.211

35. Wagner EF, Eferl R. Fos/AP-1 proteins in bone and the immune system. *Immunol Rev.* (2005) 208:126–40. doi: 10.1111/j.0105-2896.2005.00332.x
36. Dosek A, Ohno H, Acs Z, Taylor AW, Radak Z. High altitude and oxidative stress. *Respir Physiol Neurobiol.* (2007) 158:128–31. doi: 10.1016/j.resp.2007.03.013
37. Joanny P, Steinberg J, Robach P, Richalet JP, Gortan C, Gardette B, et al. Operation Everest III (Comex'97): the effect of simulated sever hypobaric hypoxia on lipid peroxidation and antioxidant defence systems in human blood at rest and after maximal exercise. *Resuscitation.* (2001) 49:307–14. doi: 10.1016/S0300-9572(00)00373-7
38. Hayakawa K, Esposito E, Wang X, Terasaki Y, Liu Y, Xing C, et al. Transfer of mitochondria from astrocytes to neurons after stroke. *Nature.* (2016) 535:551–5. doi: 10.1038/nature18928
39. Pirzad Jahromi G. P Shabanzadeh A, Mokhtari Hashtjini M, Sadr SS, Rasouli Vani J, Raouf Sarshoori J, et al. Bone marrow-derived mesenchymal stem cell and simvastatin treatment leads to improved functional recovery and modified c-Fos expression levels in the brain following ischemic stroke Iran. *J Basic Med Sci.* (2018) 21:1004–12. doi: 10.22038/IJBMS.2018.29382.7100
40. Yuan Z, Gong S, Luo J, Zheng Z, Song B, Ma S, et al. Opposing roles for ATF2 and c-Fos in c-Jun-mediated neuronal apoptosis. *Mol Cell Biol.* (2009) 29:2431–42. doi: 10.1128/MCB.01344-08
41. LZ, Man QW, Liu JY, Zhong WQ, Zheng YY, Zhao YF, et al. Overexpression of Fra-1, c-Jun and c-Fos in odontogenic keratocysts: potential correlation with proliferative and anti-apoptotic activity. *Histopathology*. (2018) 73:933–42. doi: 10.1111/his.13705
42. Chen W, Huang J, Hu Y, Khoshnam SE, Sarkaki A. Mitochondrial transfer as a therapeutic strategy against ischemic stroke. *Transl Stroke Res.* (2020) 11:1214–28. doi: 10.1007/s12975-020-00828-7
43. Park JH, Lo EH, Hayakawa K. Endoplasmic reticulum interaction supports energy production and redox homeostasis in mitochondria released from astrocytes. *Transl Stroke Res*. (2021). doi: 10.1007/s12975-021-00892-7

Conflict of Interest: The authors declare that the research was conducted in the absence of any commercial or financial relationships that could be construed as a potential conflict of interest.

Publisher's Note: All claims expressed in this article are solely those of the authors and do not necessarily represent those of their affiliated organizations, or those of the publisher, the editors and the reviewers. Any product that may be evaluated in this article, or claim that may be made by its manufacturer, is not guaranteed or endorsed by the publisher.

frontiers in Neurology

REVIEW
published: 29 October 2021
doi: 10.3389/fneur.2021.727569

Contribution of Various Types of Transfusion to Acute and Delayed Intracerebral Hemorrhage Injury

Siddharth Kumar[1], *Matthew Andoniadis*[1], *Ali Solhpour*[1], *Salman Asghar*[1], *Madison Fangman*[1], *Rani Ashouri*[1] *and Sylvain Doré*[1,2]*

[1] *Department of Anesthesiology, University of Florida College of Medicine, Gainesville, FL, United States,* [2] *Departments of Psychiatry, Pharmaceutics, Psychology, and Neuroscience, Center for Translational Research in Neurodegenerative Disease, McKnight Brain Institute, University of Florida College of Medicine, Gainesville, FL, United States*

Intracerebral hemorrhage (ICH) is the second most prevalent type of stroke, after ischemic stroke, and has exceptionally high morbidity and mortality rates. After spontaneous ICH, one primary goal is to restrict hematoma expansion, and the second is to limit brain edema and secondary injury. Various types of transfusion therapies have been studied as treatment options to alleviate the adverse effects of ICH etiopathology. The objective of this work is to review transfusions with platelets, fresh frozen plasma (FFP), prothrombin complex concentrate (PCC), and red blood cells (RBCs) in patients with ICH. Furthermore, tranexamic acid infusion studies have been included due to its connection to ICH and hematoma expansion. As stated, the first line of therapy is limiting bleeding in the brain and hematoma expansion. Platelet transfusion is used to promote recovery and mitigate brain damage, notably in patients with severe thrombocytopenia. Additionally, tranexamic acid infusion, FFP, and PCC transfusion have been shown to affect hematoma expansion rate and volume. Although there is limited available research, RBC transfusions have been shown to cause higher tissue oxygenation and lower mortality, notably after brain edema, increases in intracranial pressure, and hypoxia. However, these types of transfusion have varied results depending on the patient, hemostasis status/blood thinner, hemolysis, anemia, and complications, among other variables. Inconsistencies in published results on various transfusion therapies led us to review the data and discuss issues that need to be considered when establishing future guidelines for patients with ICH.

Keywords: edema, acute and delayed injury, intracerebral hemorrhage, transfusion, secondary injury, hematoma expansion

OPEN ACCESS

Edited by:
Devin William McBride, University of Texas Health Science Center at Houston, United States

Reviewed by:
Joao Rodrigues Gomes, Universidade do Porto, Portugal
Nikoloz Tsiskaridze, Pineo Medical Ecosystem, Georgia

***Correspondence:**
Sylvain Doré
SDore@ufl.edu

Specialty section:
This article was submitted to Stroke, a section of the journal Frontiers in Neurology

Received: *18 June 2021*
Accepted: *28 September 2021*
Published: *29 October 2021*

Citation:
Kumar S, Andoniadis M, Solhpour A, Asghar S, Fangman M, Ashouri R and Doré S (2021) Contribution of Various Types of Transfusion to Acute and Delayed Intracerebral Hemorrhage Injury. Front. Neurol. 12:727569. doi: 10.3389/fneur.2021.727569

INTRODUCTION

Intracerebral hemorrhage (ICH) is the second most prevalent type of stroke, behind ischemic stroke, and has exceptionally high morbidity and mortality rates, with 5.3 million cases and 3 million reported deaths worldwide in 2010. Case fatality rates reach nearly 60% at 1 year after stroke, and only 20% of patients who survive become independent within 6 months of injury (1). ICH is the most common form of hemorrhagic stroke, resulting from bleeding in the brain tissue and ventricles and caused by hypertension, arteriovenous malformations, or head trauma. Pathophysiological considerations of ICH involve inflammation, edema, iron toxicity, oxidative

stress, and thrombin formation. The primary injury leading to compression of the brain is the development of the hematoma, a collection of blood outside of blood vessels. Accordingly, the hematoma would increase the intracranial pressure (ICP), leading to brain hernias caused by a lack of blood flow (2).

Pathophysiology

ICH hematoma expansion is a frequent phenomenon that occurs in 70% of cases, and the majority (26%) of relevant growth occurs within 4 h of symptom onset; therefore, a repeat early computed tomography (CT) scan is needed to detect it (3). Hematoma expansion can be prevented, and urgent identification of patients with a high risk of active bleeding is crucial (4). In patients with ICH, intraventricular hemorrhage imaging is frequently present upon admission and is associated with poor long-term outcomes. Delayed intraventricular hemorrhage on subsequent scans is far less common and appears to be associated with a better outcome (5). The pathophysiology of early hematoma expansion remains unclear; however, it could result from leakage, rebleeding, or structural damage to the immediate surrounding environment. The primary reason is supportive and protective tissue disruption, but other factors such as elevated ICP and reduced oxygen supply might act on vessels and the blood-brain barrier (BBB) (3). According to Naidech et al. and others, coagulopathies or anticoagulants can also account for repeated or continuous bleeding, disturbing autoregulation (6–8). In addition, hypertension initiates uncontrolled perfusion pressure, which causes further bleeding. Death and physiological dysfunction will often result from the secondary expansion of hematoma after spontaneous intracerebral hemorrhage. Hematoma expansion includes all forms of the extended three-dimensional distribution of the initial hemorrhage, including intraparenchymal or intraventricular volume enlargement or transition, invasion, or rebleeding into compartments, to the side of the original bleeding but excluding perihematomal edema (9). Furthermore, a hematoma expansion is considered early when it occurs within the first 24 h of ICH onset (3). A late hematoma expansion occurs from days 2–14 and days 14–28 (10).

ICH and other patients in the neuro-intensive care unit (ICU) require treatment that is different than that for most regular ICU patients. They often require more invasive hemodynamic and intracranial monitoring systems along with tracheostomy but with fewer intravenous sedations than regular ICU patients (11). The surgical evacuation of the hematoma can be performed via stereotactic aspiration, endoscopic surgery and craniotomy, and the comparison of safety and efficacy of these methods have been investigated before (12). Furthermore, to help with the increase in ICP and brain swelling, decompressive craniectomy may be indicated, but it also has many caveats (13).

Risk Factors for Hematoma Expansion

Naidech et al. in 2009 investigated patient and treatment characteristics such as hematoma volume, intraventricular invasion, early neurological deterioration, treatment with recombinant coagulation factor VIIa, and blood pressure treatment. Ederies et al. in 2009 studied radiological characteristics such as shorter time between onset and first CT, hematoma density heterogeneity on admission CT, and occurrence of a "spot sign" in CT angiography. Delgado et al. studied laboratory characteristics such as reduced platelet activity and elevated IL-6, cellular fibronectin, and D-dimers (14).

Three groups and their respective studies have described prior use of platelets (6, 15, 16). The authors described platelets as a risk factor for hematoma growth in patients with ICH treated with tranexamic acid and antihypertensives within 24 h; however, one limitation in this study is the uncertainty in the timing of CT scans performed. Goldstein is credited with contrast extravasation on admission CT angiography ("spot sign") as a predictor of hematoma expansion, leading to Delgado et al. proposing a "spot sign score" in 2006. Independent predictors of poor outcomes were presenting hematoma volume, expansion of hematoma volume, and the development of intraventricular hemorrhage, shown in the landmark studies by the Davis and Tuhrim groups (17, 18). A landmark paper by Ohwaki et al. proved conclusively that maximum systolic blood pressure of 150 mmHg was independently associated with hematoma expansion in 76 patients with spontaneous ICH (19). Another large trial addressed the effect of lowering blood pressure in ICH (20). The INTEnsive blood pressure Reduction in Acute Cerebral hemorrhage Trial (INTERACT) studied rapid blood pressure reduction within the first 6 h, which was shown to be safe and feasible and to reduce hematoma expansion. A limitation of the study was that there was no difference in outcome when compared with similar studies. Another prospective trial investigating this issue is the Antihypertensive Treatment of Acute Cerebral Hemorrhage (ATACH) trial. The authors reported in this Phase I dose-finding trial that the treatment was safe and feasible (21).

Brain edema and herniation can cause secondary injuries, leading to increased mortality rates and poorer outcomes in patients with ICH (2). ICH can also result from severe complications of oral anticoagulant therapy, with mortality levels reaching over 50%. The medications used to prevent blood clottings, such as vitamin K antagonists and newer oral anticoagulant drugs, increase the likelihood of ICH and account for more than 15% of all cases (1). ICH is life-threatening due to continuous bleeding, which can cause massive pressure buildup in the brain, leading to a midline shift of the brain and compressing vital structures. Other etiological factors of ICH include arteriovenous malformation or hypertension. ICH has been thoroughly reviewed in research, as seen in **Table 1**, with numerous proposed treatment plans that have had a limited impact on recovery. Over the years, treatment options for ICH have examined platelet transfusion and red blood cell (RBC) transfusion. Platelet transfusion allows for platelet activation and, thus, potentially reduces hemorrhage size (22). In contrast, RBC transfusion restores hemoglobin (Hgb) levels and can ameliorate anemia in these patients, although additional research is needed to elucidate its effectiveness fully. Various transfusion treatment options may be available to limit hematoma expansion, as well as delayed brain injury associated with ICH. Overall, current data are limited and ambiguous regarding the relationship between transfusion therapies and their benefit in treating patients with ICH. However, what is known is that it is essential to first mitigate

the hematoma size and expansion rate and then limit brain edema and secondary injury. This review discusses the current state of research, the purpose of transfusion therapy, problems related to this course of treatment, and putative considerations for future research in this field.

LITERATURE SEARCH

Through extensive searching in four significant databases, PubMed, Google Scholar, OneSearch, and Dimensions, relevant articles from all possible years were searched with studies from 1982 to 2020 used to uncover the foundation of transfusion therapy research and build on our current understanding. We limited our search to articles written in English, as well as only those relating to humans. The following search terms were used in all databases: "blood transfusion and ICH," "blood transfusion and intracerebral hemorrhage," "transfusion and ICH," "packed red blood cell (PRBC) and ICH," "whole blood cell and ICH," "platelet transfusion and ICH," "tranexamic acid and ICH," "PCC transfusion and ICH," and "FFP transfusion and ICH." We also expanded our search with different wording, for example, using the phrase "effects of PRBC transfusion on ICH patients." Abbreviations were also incorporated if more articles could be found.

USE OF BLOOD PRODUCT TRANSFUSION AND TRANEXAMIC ACID INFUSION THERAPIES

The primary reason for using transfusion therapy in patients with ICH is to minimize hemorrhage volume and expansion. Additional reasons for using transfusion therapy include increasing blood perfusion and oxygen to promote adequate oxygen and nutrient delivery and slow hematoma expansion while mitigating delayed brain injuries. Due to sufficient blood loss, Hgb deficiency can cause improper oxygen delivery to muscles and tissues throughout the body. Using transfusion therapies makes it possible to restore Hgb levels and reestablish adequate oxygen delivery (38). Current indications for transfusion include blood replacement for surgical blood loss in certain circumstances with a significant Hgb level drop and ongoing bleeding or for patients with symptomatic anemia. Other indications include anemia, sickle cell disease (SCD), cancer, Hgb H disease, beta-thalassemia intermedia, beta-thalassemia major, and hemophilia, among other blood disorders (39). SCD, although not the focus of this paper, remains heavily reliant on transfusion therapy, but future SCD stroke treatments may focus on alternatives to blood transfusion therapy, such as hydroxyurea (40). There are multiple transfusion therapy types, including plasma transfusion, RBC transfusion, clotting factor transfusion, and platelet transfusion. Within these transfusion modalities, RBC and platelet transfusion are the most commonly used (41). Additionally, prothrombin complex concentrate (PCC) transfusion and tranexamic acid infusion have been studied. Tranexamic acid is a lysine-derived clotting promoter that has been shown to mitigate hematoma size and expansion compared to control groups (36). RBC transfusion can be further subdivided and categorized as either packed RBC (PRBC) transfusion, which contains only erythrocytes without the surrounding plasma content, or whole blood transfusion. RBC transfusion may help improve oxygen transport and delivery and restore original blood volume after ICH. On the other hand, in certain patients platelet therapy is used to stop bleeding during a hemorrhage to prevent further hematoma expansion. Platelets may help certain patients with ICH achieve better outcomes, as mentioned in the discussion section. For the prevention and treatment of bleeding in general medical cases, FFP, platelets, and cryoprecipitate are used (42). RBC transfusions are intended to improve tissue oxygenation in cases of anemia or acute blood loss due to trauma or surgery.

More than 90% of critically ill patients are anemic by the third day in the ICU (43). The multitude of factors implicated in anemia in critical illness includes decreased production of erythropoietin (EPO), inadequate EPO-induced bone marrow response, and diminished red cell survival, as well as treatment-associated traumatic blood loss (44). Almost half of all patients admitted to an ICU receive a blood transfusion, even though blood transfusions have been shown not to improve the outcome of patients in the ICU (44). Most patients with ICH are hospitalized in the ICU, many of whom have concomitant diseases. Thus, anemia may be common among this patient population, and they may be considered for blood transfusion.

The standard oxygen delivery equation (DO_2) shows increasing oxygen delivery efficiency when increasing Hgb concentration. Blood transfusion increases oxygen use mostly in patients with Hgb below 4 g/dL (45, 46). Marik, Conrad, and Creteur and their colleagues studied oxygen consumption in critically ill patients, measuring it before and up to 6 h after a blood transfusion, but they failed to conclusively prove an increase in oxygen use and tissue oxygen tension after such transfusions (47–49). There are other significant but less-recognized risks of RBC transfusion related to the effects of blood storage and the immunomodulating effects of such transfusions, which occur in almost all recipients (50, 51). Non-infectious complications, which were shown in the 2009 study by Marik, should also be considered (52). A study conducted in healthy volunteers reported the presence of higher extravascular hemolysis after older RBC transfusion (storage of 40–42 days) than fresh blood (storage of 3–7 days) (53). As for when to start transfusion, patients who required transfusion have been administered it at certain trigger values throughout the years. The Canadian Critical Care Trials Group Study (TRICC) randomized 838 adult patients in the ICU to a transfusion trigger Hgb value of <7 or 10 g/dL (54). The TRIPICU study randomized 889 pediatric patients in the ICU to a transfusion trigger Hgb of <7 or <9.5 g/dL (55). Villanueva and colleagues randomized 921 patients with severe acute upper gastrointestinal bleeding to a transfusion trigger Hgb value of <7 or <9 g/dL (56). These studies indicate that the common transfusion trigger Hgb value is between 7 and 10 g/dL.

The Scientific Subcommittee on Disseminated Intravascular Coagulation (DIC) of the International Society on Thrombosis and Haemostasis (ISTH) has suggested that DIC be considered

TABLE 1 | Summary of studies that have used blood product transfusion and tranexamic acid infusion therapy in patients with ICH.

Transfusion/ Infusion Type	References	Study type/Years of study/Sample size (Sex %)/Age	Variables	Transfusion measurements	Transfusion amount added or end goal	Clinical endpoints	Outcomes
Platelet	Guerrero et al. (23) Variability in the use of platelet transfusion in patients with intracerebral hemorrhage: observations from the ethnic/racial variations of intracerebral hemorrhage study.	• Prospective • Date Range N/A • Total Sample: 2,572 • (60.0% M) • Platelet Transfused: 302 • (60.3% M) • Transfused Mean Age: 64.2 yr • Non-transfused Mean Age: 60.4 yr	Platelet count, external ventricular drain, hematoma evacuation, intracranial pressure monitoring	Platelet count for transfused: <50,000 8, 51,000–1,000:39, 101,000–150,000:32, 150,000–200,000: 545, >200,000: 161 Not transfused: <50,000:10, 51,000–100,000:33, 101,000–150,000: 222, 150,000–200,000: 545, >200,000: 1,409	N/D	ICH, mortality, worse outcomes (mRS>4), volume of hematoma	Platelet therapy was associated with antiplatelet use before onset (OR: 5.02, 95% CI: 3.81 to 6.61, $p < 0.0001$), thrombocytopenia (OR: 13.53, 95% CI: 8.43–21.72, $p < 0.0001$), and ventriculostomy placement (OR: 1.85, 95% CI: 1.36–2.52, $p < 0.0001$). At 3 mo, there was no difference in mortality or poor outcome in platelet therapy groups and groups that did not receive platelets.
Platelet	Baschin et al. (24) Platelet transfusion to reverse antiplatelet therapy before decompressive surgery in patients with intracranial hemorrhage.	• Retrospective • 2012–2014 • Total Sample: 72 • (69.4% M) • Received acetylsalicylic acid and P2Y12 inhibitor: 14 • Received acetylsalicylic acid: 53 • Received clopidogrel: 5 • Median Age: 75 yr	Sex, age, prior anticoagulation, antiplatelet therapy, cause of bleeding, onset of bleeding, location of bleeding, surgical procedure	N/D	19 patients received at least 2 units of RBC concentrates	Frequency of new arterial thrombotic complications and frequency of recurrent ICH	Low risk for cardio-cerebral thrombotic complications was shown by platelet transfusion before cranial decompressive surgery in patients with ICH complicating antiplatelet therapy. Patients with chronic ICH and patients treated with clopidogrel had a higher risk of rebleeding.
Platelet	Ducruet et al. (25) Impact of platelet transfusion on hematoma expansion in patients receiving antiplatelet agents before intracerebral hemorrhage.	• Retrospective • 06-2003-07-2008 • Total Sample: 66 • Platelet Transfused: 35 (58.9% M) • Non-transfused: 31 • (58.1% M) • Platelet Group Age: 73.2 ± 10.1 yr • No platelet Group Age: 71.7 ± 13.5 yr	Clopidogrel, hypertension, GCS score, myocardial infarction, deep venous thrombosis, cerebrovascular accident, kidney failure, pneumonia, urinary tract infection, bacteremia, initial hematoma volume, final hematoma volume, absolute change in volume, days in NICU, days in hospital, mortality	N/D	N/D	Rate of significant hematoma expansion in transfused vs. non-transfused patients. Discharged mRS and rates of systemic complications	The study suggests that platelet administration does not reduce the frequency of hematoma expansion in patients with ICH receiving antiplatelet therapy. Transfusion timing may play a role in this because hematoma expansion typically occurs during the first 6 h after a stroke.
Platelet	Chen et al. (26) Effects of platelet infusion, anticoagulant, and other risk factors on the rehemorrhagia after surgery of hypertensive cerebral hemorrhage.	• Selective trial • 04-2007-06-2012 • Total sample: 269 • (58% M) • Platelet Received: 186 • Age: 67.1 ± 12.1 yr	GCS score at admission, symptoms including headache, nausea, vomiting, complications including hemiplegia, meningeal intracranial infection, multiple organ failure, acute renal failure, urinary	N/D	N/D	Re-hemorrhage after surgery for HCH	A decreased risk of hemorrhage recurrence was associated with platelet transfusion. Out of 186 patients who received platelet infusions, 18 had hemorrhage recurrences, whereas 16 had recurrences among the other 83 patients who did not receive platelet infusions. Analysis indicated a significant difference between these two groups ($p < 0.05$).

(Continued)

TABLE 1 | Continued

Transfusion/ Infusion Type	References	Study type/Years of study/Sample size (Sex %)/Age	Variables	Transfusion measurements	Transfusion amount added or end goal	Clinical endpoints	Outcomes
			system infection, dysphoria, Glasgow outcome scale score, and coagulation function data				
Platelet	Naidech et al. (22) Early platelet transfusion improves platelet activity and may improve outcomes after intracerebral hemorrhage.	• Prospective • Date Range: N/A • Total Sample: 45 • (58% M) • Age: 67.3 ± 14.0	ICH score, age, aspirin use, clopidogrel use, intraventricular hemorrhage, craniotomy, blood pressure, initial and follow-up hematoma size, mRS<4 at 3 mo, minutes from symptom onset to diagnostic CT	N/D	N/D	Hemorrhage size, platelet activity, patient outcome	Platelet transfusion was shown to significantly change platelet activity assays in ICH patients. In patients identified as being at high risk for poor outcome and hemorrhage growth, administration of platelets within 6 or 12 h of symptom onset was associated with a smaller final hemorrhage size as well as improved odds of independence at 3 months.
FFP & PCC	Steiner et al. (27) Fresh frozen plasma vs. prothrombin complex concentrate in patients with intracranial hemorrhage related to vitamin K antagonists (INCH): a randomized trial.	• Randomized trial • 08-2009-01-2015 • Total sample: 54 • (62% M) • Mean Age:75.6 yr	Sex, INR, mean systolic, and diastolic blood pressure, median hematoma volume, mean body mass index, diabetes, hypertension, mRS, GCS score	N/D	N/D	INR 1–2 or lower, anticoagulation reversal, death, hematoma expansion by day 90 after treatment, mRS, NIHSS, quality of life at day 90	When studying FFP vs. PCC, patients with ICH related to vitamin K antagonists (VKA-ICH) showed more promising results regarding hematoma expansion rates when using PCC. Eight of the FFP patients died 48 h after symptom onset, 5 from hematoma expansion. PCC patients only had 5 deaths, but none were related to hematoma expansion.
FFP & PCC	Huttner et al. (28) Hematoma growth and outcome in treated neurocritical care patients with intracerebral hemorrhage related to oral anticoagulant therapy: comparison of acute treatment strategies using vitamin K, fresh frozen plasma, and prothrombin complex concentrates	• Retrospective • 01-1999-12-2003 • Total sample: 55 • PCC alone or in combination with FFP and VAK: 31 (58% M) • FFP alone or in combination with VAK: 18 • (61% M) • VAK only: 6 • (66% M) • PCC Group Mean Age: 68 yr • FFP Group Mean Age: 70 yr • VAK only Mean Age: 71 yr	Gender, age, GCS score, glucose, cholesterol, mean arterial pressure, treatment regimens	N/D	N/D	Hematoma volume, INR, hematoma expansion	Oral anticoagulant therapy patients with ICH who had undergone PCC transfusion had a more significant reduction in the hematoma expansion rate than patients who received FFP transfusion. The INR reversal was quicker in PCC patients than in FFP patients.
PRBC	Roh et al. (29) Red blood cell transfusions and outcomes after intracerebral hemorrhage.	• Retrospective • 2002-2011 • Total sample: 587,046 • PRBC transfused: 3.8% (47.3% M) • No PRBC transfused: 96.2% • (47.5% M) • Age range: • 65–79 yr	In-hospital mortality, home discharge, unfavorable discharge, favorable discharge, modified Charlson Comorbidity Index, cases with anemia	N/D	N/D	ICH, Charlson Comorbidity Index, comorbidities, hospitalization length	The effects of PRBC transfusion on patients with ICH were mixed. When looking at patients requiring mechanical ventilation, transfusion was related to poor outcomes (OR: 1.33, 95% CI: 1.27–1.39). However, there was no significant association in cases without mechanical ventilation (OR: 0.88, 95% CI: 0.83–1.13). In addition, patients with ICH requiring external ventriculostomy and PRBC treatment (16.1%) did not have poor ICH outcomes (OR: 1.05, 95% CI: 0.97–1.10), whereas patients not

(Continued)

TABLE 1 | Continued

Transfusion/ Infusion Type	References	Study type/Years of study/Sample size (Sex %)/Age	Variables	Transfusion measurements	Transfusion amount added or end goal	Clinical endpoints	Outcomes
							requiring ventriculostomy had poor ICH outcomes (OR: 1.51, 95% CI: 1.46–1.57).
PRBC	Ibrahim (30) Blood transfusion does not improve outcomes in patients with spontaneous intracerebral hemorrhage.	• Retrospective • Date Range: N/A • Total Sample: 163 (51.5% M) • PRBC transfused: 25 • Median age: 59 yr	Mortality, Hgb level, morbidity, length of stay (LOS), poor outcome	Patients with Hgb<8 g/dL received a transfusion	N/D	ICH, length of stay, mortality, morbidity	Based on a univariate analysis, patients receiving PRBC therapy were shown to have significantly increased 30 d mortality. PRBC patients had a 30 d mortality of 48%, in contrast to patients without PRBC with 30 d mortality of 25.4% ($p = 0.03$). PRBC patients also had higher morbidity of 84 vs. 50.7% at $p = 0.004$. The length of stay in the hospital also increased to 11.7 ± 12.3 d from 7.5 ± 6.7 d ($p = 0.01$). However, multivariate logistical regression analysis did not show a significant effect caused by PRBC transfusion.
PRBC	Martin-Schild (31) Packed red blood cell transfusion is associated with adverse outcomes in ICH patients.	• Prospective • 2008–2010 • Total Sample: 111 • PRBC Transfused:19 • Age: N/D	Age, Hgb level, admission ICH score, intubation time, mRS score	N/D	N/D	ICH, NIHSS score, ICH score, mRS score	The study indicated that upon receiving PRBC transfusion, the NIHSS score was 17, compared to 15 for a patient not receiving PRBC ($p = 0.021$). The ICH score in PRBC patients was 2, compared to 1 in those not receiving PRBC ($p = 0.013$). Hgb levels were also lower at 9.3 vs. 14.0 g/dL in patients not undergoing transfusion ($p = 0.001$). Transfused patients also had a higher likelihood of needing intubation, at 84 vs. 39% ($p = 0.0003$). Transfused patients also had more significant poor functional outcomes, at 78.9 vs. 29.4%, with an mRS of 5–6 ($p = 0.0002$). Most importantly, transfused patients were 3 times more likely to die (OR: 2.99, 95% CI: 1.01–8.85, $p = 0.047$). However, when the data were adjusted for age, intubation, Hgb level, and admission ICH score, the data were not significant.
PRBC	Moman et al. (32) Red blood cell transfusion in acute brain injury subtypes: An observational cohort study.	• Retrospective • 2008–2015 • Total Sample: 2,638 • PRBC Transfused: 225 • (48% M) • Transfused median Age: 62 yr • Non-transfused Median Age: 68 yr	Use of RBC transfusion, age, gender, body mass index, comorbidities, Charlson Comorbidity Index score, GCS score, sequential organ failure assessment (SOFA) score albumin, creatinine, Hgb	8.0 g/dL	Between 7 and 10 g/dL	Length of stay, ICU length of stay, mortality, change in SOFA score 24 h after RBC transfusion	PRBC transfusion was related to increased hospital and ICU length of stay in patients with ICH with acute brain injury. However, mortality rates seemed to be lower. With these results, it is evident that further research is required. Using a restrictive transfusion protocol would be beneficial in allowing for PRBC transfusion to provide valuable results.
PRBC	Sheth et al. (33) Packed red blood cell transfusion and decreased mortality in intracerebral hemorrhage.	• Prospective and Retrospective • 1999–2005 • Total Sample: 546 • PRBC Transfused: 100 (55% M) • Transfused Median Age: 74 yr	Age, ICH volume, GCS score, location of hemorrhage	Mean baseline Hgb level: 13.0 g/dL	N/D	30 d mortality rate, ICH, GCS score, hemorrhage volume	The study indicates that anemia is a problem that can cause increased mortality in patients with ICH. Therefore, the use of PRBC transfusion may help mitigate the adverse effects of ICH. However, more research is necessary to determine this. A multivariate analysis controlled for admission GCS score, hematoma volume and location, anemia, warfarin use, and do not resuscitate status and found

(Continued)

TABLE 1 | Continued

Transfusion/ Infusion Type	References	Study type/Years of study/Sample size (Sex %)/Age	Variables	Transfusion measurements	Transfusion amount added or end goal	Clinical endpoints	Outcomes
		Non-transfused Median Age: 73 yr					that transfusion was related with a lower 30 d mortality (OR: 0.40, 95% CI: 0.19–0.69, $p = 0.02$).
PRBC	Chang et al. (34) Nadir hemoglobin is associated with poor outcome from intracerebral hemorrhage.	• Retrospective • 2008–2010 • Total Sample: 109 • Low Hgb: 30 (60.0% M) • Normal Hgb: 79 (51.9% M) • Low Hgb Median Age: 56.5 yr • Normal Hgb Median Age: 61.0 yr	Admit ICH score, systolic blood pressure, diastolic blood pressure, GCS score, nadir Hgb level	Low: 8.7 g/dL Normal: 12 g/dL	N/D	Length of stay, discharge NIHSS, discharge mRS	Patients who received PRBC transfusion, in an unadjusted model, showed that they had 9 times greater odds of having a discharge mRS of 5–6. However, the results were no longer significant when the data were adjusted for admission ICH score, nadir Hgb, age, and intubation, although they still showed a positive relation (OR: 4.01, 95% CI 0.64–25.32, $p = 0.0473$).
Tranexamic acid	Arumugam et al. (35) Tranexamic acid as antifibrinolytic agent in non-traumatic intracerebral hemorrhages.	• Randomized trial • 09-2012-10-2013 • Total Sample: 30 • (60% M) • Mean Age: • 52.93 yr	Age, sex, ethnicity, co-morbidities, hypertension, hypertension/diabetes mellitus, time of onset to first CT brain scan, time from first CT brain scan to treatment administration, admission GCS score, symptoms of presentation	N/D	N/D	Hematoma volume, hematoma expansion	The use of tranexamic acid was associated with the maintenance of hematoma volume. The treatment group's hematoma volume was initially measured at an average of 10.00 cm^3 and the after-treatment value was 10.08 cm^3 indicating no statistical difference in the size ($p = 0.313$). However, the control group had a significant hematoma volume growth of 3.07 cm^3 ($p = 0.001$).
Tranexamic acid	Gao et al. (36) Tranexamic acid inhibits hematoma expansion in intracerebral hemorrhage and traumatic brain injury. Does blood pressure play a potential role? A meta-analysis from randomized controlled trials.	• Meta-analysis • 01-2001-05-2020 • Total sample: 1,553 • Age: N/D	Hematoma type, sample size, GCS score, treatment admission time, systolic blood pressure, ethnic origin, hematoma volume, hematoma expansion rate	N/D	N/D	GCS score, hematoma expansion rate, hematoma volume	In patients with ICH with moderate to severe hypertension (>160 mmHg), the tranexamic acid levels were associated with a lower rate of hematoma expansion ($p = 0.02$) and a decrease in hematoma volume ($p = 0.04$).
Tranexamic acid	Hu et al. (37) Tranexamic acid in cerebral hemorrhage: a meta-analysis and systematic review.	• Systematic review and meta-analysis • Studies until 09-2018 • Total Sample: 4,703 • Age: N/D	Sex, diagnosis, age, sample size, examination method	N/D	N/D	Mortality, GCS score >3, mRS>4, hydrocephalus, convulsions, seizures, hematoma expansion rate, hematoma volume	Patients with ICH undergoing tranexamic acid treatment showed improved 90-day mortality (OR: 0.99, 95% CI: 0.84–1.18; $p = 95$). The reduction in hematoma expansion (OR: 0.54, 95% CI: 0.37–0.80; $p = 0.002$) and volume (95% CI: −3.00 to −0.97, $p = 0.0001$) had a mean difference of −1.98 from the baseline value.

an acquired syndrome that is represented as an intravascular coagulation activation with a loss of localization originating from different causes. This is when blood clots form inside the blood vessels, using up much of the available clotting factors and leading to bleeding in other areas. This can cause damage to the microvasculature of the brain. If it is severe enough, it can lead to organ dysfunction (57).

ISSUES SURROUNDING TRANSFUSION THERAPY

Although transfusion therapy produces rapid results, adverse effects might be a concern (58). It is essential to ensure blood or platelet therapy compatibility to limit side effects and promote proper acquisition. Another important consideration is that RBC storage affects the physical characteristics of RBCs. Changes in surface-to-volume ratio, cell shape, and osmotic rigidity are among the reported adverse effects of stored RBCs. These morphological changes are a limitation of using transfusion therapies because they have been associated with lower effectiveness in patients and adverse or worsened outcomes. One example of the detrimental effects of storing blood is the decrease in the post-transfusion 24-h RBC survival rate due to the change in the cell's surface-to-volume ratio. These unfavorable alterations are associated with impaired oxygen delivery and ATP depletion, lowering microvascular perfusion (38). Furthermore, stored cells release cytokines that can have an undesirable effect on the patient and may be associated with numerous adverse effects such as changing the sensitivity and expression of IL-6, IL-8, T cells, and TNFα (58). Future in-depth studies on the storage and time point of the delivery of blood and its effects, specifically on patients with ICH, remain an important consideration.

The lack of response from transfused blood to correct tissue perfusion might be due to biochemical and biomechanical changes termed the storage lesion. Decreased oxygen delivery to tissues results from storage lesions. After storage for 7 days, blood is depleted of 2,3-diphosphoglycerate, a compound that increases oxygen release from Hgb to tissues (59, 60). This shifts the oxygen dissociation curve to the left, reducing the available oxygen for tissue consumption. Increased storage time leads to acidemia and hyperkalemia, culminating in RBC lysis and release of free Hgb. Free Hgb scavenges nitric oxide and, therefore, may result in vasoconstriction and exacerbation of organ dysfunction (61–63). Structural changes due to RBC storage compromise microvascular circulation (64). The deformation of the biconcave structure of the 8-μm erythrocyte makes it difficult to navigate smaller capillaries and may result in vessel occlusion. The microvesiculation and loss of surface-to-volume ratio result in sphero-echinocytes. The formation of microvesicles denotes high osmotic fragility and diminished RBC survival (65, 66). Corpuscular changes occur because of ATP depletion (67). Vasoconstriction due to lysophosphatidylcholine species released from the cellular membrane of senescent RBCs is the cause of storage longer than 42 days (68). Increased RBC aggregability and adhesion compromises microvascular circulation (69, 70). Leukocyte changes due to the storage lesion also result in clinical side effects and transmitted infections due to contaminated leukocytes (71).

Effect on Intracerebral Hemorrhage

Kumar et al. demonstrated a dose-dependent relationship between anemia and ICH volume (72). Sheth et al. reported that RBC transfusion was associated with improved survival at 30 days (OR: 2.76, 95% CI: 1.45–5.26, $p = 0.002$) and decreased mortality at 30 days (OR: 0.40, 95% CI: 0.19–0.69, $p = 0.02$). Despite transfusion, there was no significant increase in Hgb concentration (33). Hence, the protective mechanism remains unknown. Whether increased Hgb is required in the post-ICH period requires more research.

DISCUSSION

Platelet Transfusion

A platelet count below 175,000/μL has been noted to be a significant predictor of ICH progression. Furthermore, patients with ICH with a platelet count below 100,000/μL have been associated with a 9 times greater risk of death (OR: 9.5, 95% CI: 1.3–71.4, adjusted $p = 0.029$) (73). There is significantly more research on platelet transfusion in patients with ICH than on RBC transfusions in acute and delayed ICH injuries, although published data reveal conflicting results. One study includes results that show patients who were considered high risk for hemorrhage growth had a decrease in modified Rankin Scale (mRS) scores upon early platelet transfusion (22). Groups that received platelet treatment <12 h after symptom onset had a better mRS (score <4) than groups who received it after 12 h, 3 months after treatment (11/20 patients compared to 0/7 patients, $p = 0.01$). However, this study has limitations because the patients were not randomly chosen for treatment and the sample size was too small for multivariate analysis.

The use of platelet transfusion has also been shown to be beneficial in patients undergoing tissue plasminogen activator (tPA) therapy. The tPA thrombolysis induces an increased risk in ICH formation, which is fatal in patients with ischemic stroke after tPA treatment (74). One study with mice highlighted that platelets could safeguard BBB integrity, suggesting that resting platelet transfusion can be a viable treatment option for improving tPA thrombolysis safety in ischemic stroke and patients with ICH (75). This report showed that platelet transfusion could significantly block the tPA-associated loss of cerebrovascular integrity and protect BBB permeability (75). Another study conducted by Baschin et al. reported that platelet concentrate transfusion given before cranial decompressive surgery in patients with ICH correlated with a low risk for cardio-cerebral thrombotic complications (24). Furthermore, when platelet transfusion coincided with surgical treatment in patients with ICH, it was administered with no reported issues, indicating that surgery can be performed safely after platelet transfusion (76). Additionally, clinical studies have shown that platelet transfusion can lead to a lower mRS score in patients with ICH. This finding indicates that platelet transfusion may be

a viable ICH treatment option, although more support is needed in addition to a lower mRS score to solidify this claim (22).

A radiographic analysis by Ducruet et al. found no significant decrease in hematoma volume in either the ICH group treated with platelets or the ICH group without platelet treatment, with initial values of 27.7 ± 25.4 compared to 30.9 ± 28.3 ($p = 0.63$) and final values of 33.1 ± 30.8 compared to 33.9 ± 32.6 ($p = 0.92$) (25). However, after surgery for hypertensive cerebral hemorrhage, platelet use has been noted to prevent hemorrhage recurrence. A 2015 study by Chen et al. showed that after surgery, out of the 186 patients receiving platelet therapy, 18 patients had rebleeding, whereas 16 out of the 83 non-transfused patients rebled. The difference was shown to be statistically significant with a χ^2-value of 4.790 ($p = 0.045$) (26). The use of platelet transfusion in patients with ICH undergoing antiplatelet therapy is an area of controversy. The American Association of Blood Banks' platelet guidelines in 2015 reported a lack of data on this topic and did not recommend transfusion in these particular cases (77). Another study showed that among patients with acute leukemia, the risk of ICH was higher among patients with low platelet counts and after receiving more platelet transfusions. However, the latter is potentially due to clinical factors leading to increased transfusion needs (78). On the other hand, prophylactic platelet transfusion for medical procedures has been associated with thrombosis and poor outcomes, including death. Most deaths were due to infection, sepsis, or organ failure, and none were due to bleeding or thrombosis (79).

It should be noted that in standard ICU settings, platelet use is reasonable for patients using antiplatelet agents (80). However, it is still important to evaluate the degree of hematoma growth because it is an independent indicator of mortality (17). This is because the mass effect of the primary bleeding can lead to an increase in ICP caused by the migration of lesions into the ventricles. Hematoma can also cause local edema and neurological damage in the parenchyma (81). Patients with a Glasgow Coma Scale (GCS) score of 8 or less and parenchymal hemorrhage volume ≥60 mL from their first CT have a predicted 30-day mortality rate of 91% (82). The perihematomal edema is promoted by thrombin within the hematoma. This can be dangerous because heme, iron, and Hgb can lead to cell death because they are strong mitochondrial toxins.

It has also been reported that patients on antiplatelet therapy with isolated ICH had worse mRS (OR: 3.6) after platelet transfusion than when first admitted to a treatment facility (83). Additionally, patients with isolated ICH had trauma-induced platelet dysfunction, whereas patients using aspirin had drug-induced abnormalities related to platelets in response to arachidonic acid. These results indicate that platelet transfusion does not improve trauma-induced platelet dysfunction but does improve aspirin-induced platelet dysfunction, further emphasizing the conflicting results published around transfusion therapy (84). However, ICH occurs in a closed space of the head; thus, the bleeding will cease in this space, resulting in the patient not losing a high volume of blood. Furthermore, a deficiency of platelet and coagulation factors is not significant enough on its own to instigate platelet transfusion. But the problems occur when patients have underlying diseases with platelet dysfunction or are using antiplatelet medications. In this scenario, the pressure effect of the expanded hematoma increases ICP due to the surrounding edema or hydrocephalus and may contribute to brain injury and neurologic deterioration. In this situation, the need for transfusion is highlighted for patients with severe thrombocytopenia and platelet dysfunction. Donor screening procedures and pathogen inactivation do not eliminate the risk of bacterial and other blood-borne infections, and infection by bacterially contaminated platelets represents a potentially serious problem with platelet transfusion (85). This is because platelets are stored at room temperature where bacteria can proliferate rapidly. The incidence of bacterial contamination is higher for platelets (∼1 in 2,000) than it is for RBCs (∼1 in 30,000) (86).

Overall, patients with severe thrombocytopenia may benefit from platelet transfusion. The threshold for transfusion varies case by case based on hematoma expansion, underlying disease, and history of antiplatelet or anticoagulant use. For patients on antiplatelet therapy, the available data suggest that platelet transfusions may be hazardous and should be avoided. However, further studies are warranted to compare different antiplatelet medications because some may lead to more bleeding than others. Moreover, it seems in a small number of patients that there is a likelihood for rebleeding and hematoma expansion in the first several hours of hemorrhage. This finding highlights the potential for platelet transfusion in the first hours of hemorrhage to lead to severe thrombocytopenia or platelet dysfunctions with expanding hematoma.

A 2017 study by Guerrero et al. showed that various factors such as prior use of antiplatelets (OR: 5.02, 95% CI: 3.81–6.61, $p < 0.00001$), thrombocytopenia (OR: 13.53, 95% CI: 8.43–21.72, $p < 0.00001$), and ventriculostomy placement (OR: 1.85, 95% CI: 1.36–2.52, $p < 0.00001$) were significantly associated with platelet therapy use in ICH patients. In addition, an interesting field of research might be the association of race and transfusion therapy in ICH patients, as the study showed that Black individuals were less likely to receive platelet transfusion therapy in this case (OR: 0.57, 95% CI: 0.41–0.80) (23). Furthermore, the ambiguity of the effectiveness of transfusion in patients with ICH is evident in anticoagulation treatment. ICH patients taking oral anticoagulants may not be sufficiently treated with platelet transfusion alone. This is because emergency treatment of anticoagulant-ICH requires rapid restoration of coagulation, which uses hemostatic factors such as PCC and recombinant factor VIIa, in addition to vitamin K, factor IX concentrates, and FFP. Emergency management of ICH is more difficult when the patient is also being treated with oral anticoagulants (39).

Fresh Frozen Plasma (FFP) vs. Prothrombin Complex Concentrate (PCC) Transfusion

Few studies have drawn comparisons between the effects of FFP on patients with ICH and the use of PCC on these patients. A randomized trial by Steiner studied the two treatment options (FFP and PCC) for patients with ICH related to vitamin K antagonists (VKA-ICH). After administering FFP to 23 patients and PCC to 27 patients, it was discovered that the PCC was

more effective regarding smaller hematoma expansion (27). The results showed that 8 of the patients administered FFP died, 5 from hematoma expansion within 48 h of symptom onset. The remaining 3 patients died from the initial ICH. In contrast, 5 of the patients administered PCC died, although it was reported that none of these deaths were from hematoma expansion. In this group, the first death occurred 5 days after the start of the PCC treatment and was due to cardiac arrest. Limitations of this study include a small sample size and early stoppage of the trial due to the significant differences in hematoma expansion between FFP and PCC. The study acknowledged the premature ending of the treatment as a reason for possible bias away from their null hypothesis (27). Further research involving a more extended study time is required to fully understand the differences between PCC and FFP on hematoma expansion. However, the data provided can still be used as a decent marker for the possible effects of PCC and FFP on hematoma expansion within the first 90 days of treatment.

In a retrospective study by Huttner et al., PCC was associated with a reduced incidence and hematoma expansion than FFP in patients who had ICH related to oral anticoagulant therapy (28). Hematoma growth was defined as a >33% increase in hemorrhage size compared to baseline measurements. The study emphasized that this result appeared to be related to the international normalized ratio (INR) reversal being more rapid in patients administered PCC. However, since this was a cumulative review, causality could not be determined. The study acknowledged the need for more randomized controlled trials to determine the best acute treatment to maintain INR reversal, given that higher INR levels were associated with hematoma expansion (28). From these studies, there appears to be an association between more effective maintenance of hematoma size and PCC use. When compared to PCC use, FFP treatment groups reported notably few patients who benefitted from treatment. Despite these results, each study had limitations that needed to be addressed, such as sample size, testing duration, and the nature of the study (retrospective). Although PCC may be a better option than FFP, more research is required with larger and more robust samples.

However, in situations involving warfarin, the results of using PCC vs. FFP become more ambiguous. Warfarin leads to hematoma expansion, as well as a higher incidence of ICH in 27–54% of cases, which partially explains an increase in mortality of up to 70% (87–90). The logical option is to rapidly reverse anticoagulation by substituting vitamin K for oral vitamin K antagonists to rapidly normalize coagulation (91).

RBC Transfusion

Reviewing RBC transfusion therapy for ICH treatment reveals many conflicting results. Along with the general steps taken in the treatment of ICH, as shown in **Figure 1**, PRBC has also been used during the treatment of ICH. One study with positive results used PRBC transfusion to evaluate whether the therapy could mitigate ICH damage and anemia. Study outcomes showed improved survival rates at 30 days in 100 patients after receiving PRBC therapy (OR: 2.76, 95% CI: 1.45–5.26, $p = 0.002$) (33). Although this study expressed improved patient outcomes, it did not specify the change in hematoma expansion and volume and focused solely on anemia.

According to the WHO, anemia is defined as Hgb <12 g/dL for women and Hgb <13 g/dL for men. The volume of bleeding into the brain determines ICH outcome. Anemia is common in many critically ill patients. The presence of anemia in patients with ICH has been associated with larger ICH volumes. To date, two studies have evaluated anemia status in acute ICH, reporting that on admission, anemia was associated with larger hematoma volume and lower Hgb levels during a hospital stay, which was related to poorer outcomes. Anemia appears to be a predictor of unfavorable functional outcomes with independent factors beyond its association with a larger hematoma size. Recognizing anemia and the respective treatment may help influence the outcomes after ICH (92).

Critically ill patients commonly suffer from a lack of Hgb; 95% are anemic by day 3, and RBC transfusion is given to up to 50% of patients during their stay (93). Only three ICH studies are available that analyzed anemia and ICH in the context of oral anticoagulants. Diedler et al. in 2010 showed a direct relationship of nadir Hgb level during the hospital stay with functional outcomes in ICH (94). The study by Kumar et al. showed that anemia on admission was independently associated with greater hemorrhage volume increases, indicating through multivariate analysis that it may be possible for anemia to have effects on the outcomes that were not simply related to ICH size (72). Sheth et al. in 2011 reported improved survival rates 30 days after RBC transfusions during acute ICH treatment. Whether anemia is a marker for critical patients or whether it directly leads to increased hemorrhage volumes impacting outcomes remains to be proved (92). Mayer et al. and Anderson et al. in 2008 sought to answer this question by investigating the effect of anemia on outcomes in patients with minor-volume ICH (i.e., <30 cm^3) (20, 95). This study showed that patients with anemia had larger baseline volumes and poorer neurological status.

Anemia had a positive but poorer association with larger hemorrhage volumes (AUC = 0.67), whereas the association with functional outcome was positive and more accurate for all patients with spontaneous ICH in another study by Kuramatsu in 2013 (AUC = 0.75; 95% CI: 0.70–0.80, $p < 0.01$). The study by Kuramatsu also showed worse outcomes in patients with minor-volume ICH with anemia. Despite similar characteristics, patients with anemia appeared to have a tendency for an increased rate of hemorrhage growth ($p = 0.07$). The relevance of anemia is even more striking in patients with minor-volume ICH. The only meaningful explanation for the observed outcome difference is anemia itself (92). Focusing on anemia upon admission facilitates in identifying high-risk patients with comorbidities and increased risk for hematoma expansion.

In a PRBC transfusion study by Chang et al., the unadjusted cumulative logit model reported that the odds of being discharged with an mRS of 5–6 were 9 times greater in transfused patients than in those who were not transfused (OR: 9.37, 95% CI: 2.84–30.88, $p = 0.0002$). When these data were adjusted for age, nadir Hgb, intubation time, and admitted ICH score, the data were no longer statistically significant, although there was still a positive association between PRBC transfusion and discharge

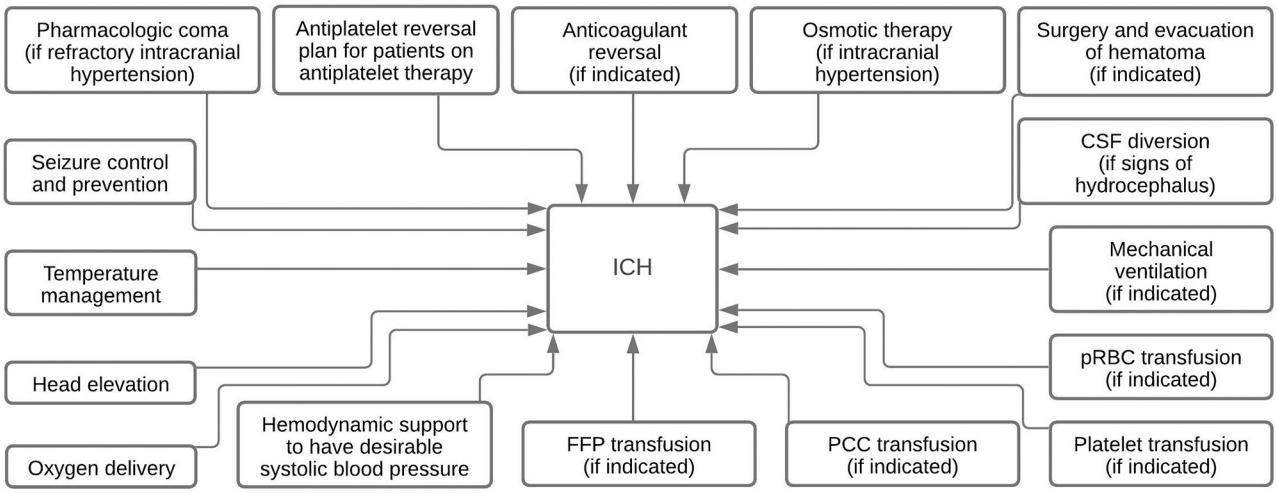

FIGURE 1 | Summary diagram depicting various ICH treatment modalities.

with an mRS of 5–6 (OR: 4.01, 95% CI: 0.64–25.32, $p = 0.1392$) (31, 34). Overall, the results indicated that neither transfusion nor nadir Hgb could be used as independent predictors for in-hospital mortality (34). One consideration is the existence of confounding medical conditions that may have led to poorer outcomes in patients. Additionally, this study was limited by the small sample size and its retrospective nature. One factor that was not standardized was patient anemia levels upon admission; as other studies have noted, anemia at admission has been associated with larger hematoma volume, making it an essential consideration for standardization of this data (72).

Other studies indicate that RBC transfusion is associated with adverse effects in patients with ICH. In a study conducted by Ibrahim et al., patients who received PRBC treatment had an increased length of stay in health facilities and had similar morbidity and mortality rates as patients with ICH who did not receive the transfusion therapy. This study also implied that PRBC transfusion might cause worse outcomes, although it proposed that a larger sample size was needed to solidify this claim (30). Additionally, a retrospective study conducted by Roh et al. revealed that when using a large sample size of 597,046 patients with ICH, including 22,904 RBC transfusion patients, RBC transfusion was associated with increased odds of in-hospital mortality (adjusted OR: 1.22, 95% CI: 1.10–1.35, $p < 0.001$). Furthermore, after a sensitivity analysis, RBC transfusion correlated with worsened outcomes regardless of accounting for comorbidities and disease severity (adjusted OR: 1.43, 95% CI: 1.34–1.51, $p < 0.001$). Although the study incorporated a considerable sample size in its analysis from various databases, it was still a retrospective study and could not determine causality between RBC transfusion and outcomes in patients with ICH. The study acknowledged limitations, including a lack of granularity in the data and unavailable Hgb levels. This prevented the study from examining the direct connection of RBC transfusion and patient outcomes because other underlying diseases may have confounded the data for patients with ICH (29). Similar results were noted in a cohort study by Moman et al. that showed RBC transfusions resulted in longer hospital and intensive care unit stays for patients with ICH (32). Despite varied results, limited research exists on RBC transfusion and its effects on acute and delayed ICH injury, indicating that more in-depth research is required to further understand the effectiveness of RBC transfusion therapy after ICH.

Tranexamic Acid

Studies have shown a link between the use of tranexamic acid and the mitigation of hematoma volume in patients with ICH. Tranexamic acid, a pharmaceutical agent, is a lysine-derived clotting promoter. In a randomized controlled trial of patients with non-traumatic ICH by Arumugam et al., tranexamic acid was linked to hematoma size maintenance after 24 h of administering the treatment compared to the placebo group (35). The control group's baseline median hematoma size was 14.53 cm^3 compared to the post-24 h size of 17.59 cm^3. The median difference of 3.07 cm^3 was statistically significant ($p = 0.001$). On the other hand, the treatment group had a baseline value of 10.06 cm^3 and a post-24 h size of 10.08 cm^3, indicating no statistical difference ($p = 0.313$). Limitations of this study were that the patients received the treatment within 8 h of symptom onset. Although administering treatment at hour 8 can be helpful because hematoma expansion peaks from 4.5 to 12 h after symptom onset, the effectiveness of the treatment might not be the same for all time ranges. Some patients who might have had peak hematoma expansion at hour 12 may not have experienced the same effects of the treatment as patients who had a peak hematoma expansion at hour 5. Furthermore, the study was conducted with strict control of systolic blood pressure maintained at 140–160 mmHg, which led to the removal of two patients in the control group because of uncontrollable hypertension (35). To further elucidate the

usefulness of tranexamic acid as a treatment option for acute and delayed ICH injury, studies that include a greater blood pressure range to assess the optimal time point of administration are needed.

Regarding the effects of blood pressure on tranexamic acid infusion for patients with ICH, a study by Gao et al. found that in spontaneous and traumatic ICH, patients who had moderate and severe hypertension (>160 mmHg) might be the more appropriate candidates for tranexamic acid treatment. Tranexamic acid was associated with a reduction in hematoma expansion ($p = 0.002$) and a decrease in hematoma volume ($p = 0.03$) compared to a placebo group. Patients with moderate to severe hypertension had an increased reduction in hematoma expansion rate ($p = 0.02$) and hematoma volume ($p = 0.04$) (36). Although this meta-analysis presented valid statistical interpretations of various trials, and although there appeared to be an association with tranexamic acid infusion and lower hematoma expansion, the study had several limitations. For example, the randomized controlled trial had significant gaps in sample sizes, and the results did not show whether tranexamic acid had different effects on hematoma expansion across genders. However, this meta-analysis has validity because it included data from 3,102 patients from multiple randomized controlled trials. In a systematic review by Hu et al., tranexamic acid led to an improvement in 90-day mortality (OR: 0.99, 95% CI: 0.84–1.18, $p = 0.95$). Additionally, reduction in hematoma expansion (OR: 0.54, 95% CI: 0.37–0.80, $p = 0.002$) and volume were noted (95% CI: −3.00 to −0.97, $p = 0.0001$) with a mean difference of −1.98 from the baseline value (37). The occurrence of single ischemic events and reported functional outcomes remained at statistically similar levels as the baseline; however, the use of tranexamic acid was associated with an increased risk of combined ischemic events such as myocardial infarction, deep vein thrombosis, ischemic stroke, transient ischemic attack, pulmonary embolism, or acute coronary syndrome (OR: 1.47, 95% CI: 1.07–2.01, $p = 0.02$) (37). Although the use of tranexamic acid may be associated with a reduced hematoma expansion rate and volume, these data indicate the potential risk of combined ischemic events associated with tranexamic acid treatment in patients with ICH. This finding limits the possible uses of tranexamic acid in patients with ICH and is a barrier for many patients who require an effective solution to hematoma expansion and volume and other factors such as edema. The study also reported that poor functional outcomes did not change, potentially because the degree of reduction in hematoma expansion and volume was not enough to do so or because the increase in combined ischemic risk counteracted these reductions (37). Furthermore, a limitation of this study is that it used data from only 14 studies. A larger sample size might be required to better understand the factors involved in using tranexamic acid in patients with ICH.

GENERAL CONSIDERATIONS

Proper education and training are essential considerations regarding correctly transfusing patients, including adequate hospital blood product management and health quality improvement programs. Currently, our healthcare protocols would benefit from improved standards and regulations for transfusion therapy, given the inconsistencies in proposed research data. The lack of clinical transfusion guidelines for patients with ICH has led to unclear outcomes and an extensive knowledge gap in research. It would be helpful to incorporate a specific hospital-wide oversight program to provide an evidence-based approach for patients with ICH. Healthcare neuro-ICU professionals should evaluate specific patients with ICH who would potentially benefit from rigorous blood transfusion therapies. A multidisciplinary approach with contributions from critical care, vascular neurosurgery, vascular neurology, and rehabilitation medicine may help explain the efficacy of transfusion therapies (96). Adverse effects, such as hemolysis and iron overload, can be mitigated by creating standard protocols, for example, restricting the number of transfusions given to a patient and carefully transfusing only the amount necessary to achieve the clinical goal. A restrictive approach to blood transfusion may help to lower the overall cost of treatment. Financial considerations of blood transfusions are important because at least 50% of high-frequency transfusions are improperly administered to patients and, therefore, may place a financial strain on patients (97). A reduction in the frequency of blood transfusions may be possible if the effects of blood withdrawals, surgery, and other anemia-provoking procedures on the patient are considered. Protocols that properly screen for anemia and insufficient iron levels are associated with reduced blood transfusion frequency, length of stay, and overall cost (98).

It would be beneficial to provide alternative blood transfusion methods in patients when time is critical. The COVID-19 pandemic has increasingly strained health facilities, so much so that they may not be able to provide transfusion therapy to patients in a limited time frame. Methods to mitigate the spread of COVID-19, such as social distancing and stay-at-home orders, have contributed to the massive decrease in the amount of blood and platelet donations received. Furthermore, the influx of patients to hospitals worldwide has also contributed to low amounts of blood storage. We recommend efforts to research blood and platelet alternatives. Further research is also required to understand whether blood transfusion is safe during pandemic situations and how the viral spread may affect blood donation distribution. It would be helpful to consider optimizing the methods for properly storing and transporting packaged blood that emphasizes maintaining the contents' integrity.

Based on the mechanisms of ICH neurologic injury, several possible steps can be taken to alleviate ICH central and systemic symptoms. For example, the first step would be to reduce hematoma size through surgery. Another step would be to limit hematoma expansion. This can be possible by reversal of coagulopathy, hemostatic agents, or hypotensive therapy. Another step is modify molecular events, such as inflammation caused by Hgb degradation products, heme, and iron-mediated toxicity, or by quickening hematoma resolution (99).

CONCLUSION

Currently, data are mixed regarding transfusions in patients with ICH. Various transfusion types appear to have different effects on hematoma size and expansion rates, as well as on edema and related secondary injuries. Some studies indicate that platelet transfusion is useful in promoting better patient outcomes; however, one study showed that it did not decrease in hematoma size. However, a mix of studies provides ambiguous conclusions, with some indicating better patient outcomes, some indicating worsened patient outcomes, and some showing no significant benefit from platelet transfusions. Furthermore, platelet transfusion in patients with ICH undergoing antiplatelet therapy has been controversial. RBC transfusion should theoretically provide better oxygen perfusion through tissues and allow for better patient outcomes, but this does not always appear to be the case. Many cases indicate that RBC transfusion may not be the best way to treat patients with ICH because it has not been shown to affect hematoma size and edema. However, patients with ICH who already have anemia could potentially use RBC transfusion, but these results appear to be controversial as well. It is vital to consider the reported adverse effects of transfusion therapies and critically evaluate their usefulness in every patient because simply increasing oxygen and Hgb levels may be detrimental. It may also be helpful to understand the effects of storage on transfusion products and how they relate to treating hematoma, as well as edema. Studies that observe and experiment with tranexamic acid, FFP, and PCC have had more promising results. Notably, tranexamic acid or PCC have been shown to control, or at least maintain, hematoma expansion rates more effectively than other transfusable compounds. However, these studies have limitations that need to be addressed to provide a complete understanding of when and how to use these therapies. Furthermore, it is important to consider the ischemic complications such as deep vein thrombosis that may be associated with tranexamic acid use. Such complications may counteract the benefits of this drug on patient outcomes. Anticoagulation reversal is also an important point to understand when treating patients with ICH with transfusion, as outlined in the discussion. Future research considerations include accounting for ICH severity, patient comorbidities, proper packaging of transfusable content, and RBC fragility. Further research is also required to fully understand the effects of each transfusion type on hematoma expansion rate and edema, as well as the associated secondary injuries.

AUTHOR CONTRIBUTIONS

SD: conceptualization and funding acquisition. SK and SD: methodology and analysis and writing—original draft preparation. SK, MA, AS, SA, MF, RA, and SD: writing—review and editing. All authors have read and agreed to the published version of the manuscript.

FUNDING

Funding to support this work was provided by grants from the NIH (R21NS110008, R21NS103036, R21NS095166, and R56NS116076), Brain Aneurysm Foundation, DOD (AZ180127), and American Heart Association, and the Department of Anesthesiology (University of Florida College of Medicine, Gainesville, FL).

ACKNOWLEDGMENTS

The authors wish to thank members of the NeuroICU Doré Lab, the University of Florida College of Medicine Department of Anesthesiology, and the Center for Translational Research in Neurodegenerative Disease.

REFERENCES

1. de Oliveira Manoel AL, Goffi A, Zampieri FG, Turkel-Parrella D, Duggal A, Marotta TR, et al. The critical care management of spontaneous intracranial hemorrhage: a contemporary review. *Crit Care.* (2016) 20:272. doi: 10.1186/s13054-016-1432-0
2. Shao Z, Tu S, Shao A. Pathophysiological mechanisms and potential therapeutic targets in intracerebral hemorrhage. *Front Pharmacol.* (2019) 10:1079. doi: 10.3389/fphar.2019.01079
3. Steiner T, Bösel J. Options to restrict hematoma expansion after spontaneous intracerebral hemorrhage. *Stroke.* (2010) 41:402–9. doi: 10.1161/STROKEAHA.109.552919
4. Morotti A, Dowlatshahi D, Boulouis G, Al-Ajlan F, Demchuk AM, Aviv RI, et al. Predicting intracerebral hemorrhage expansion with noncontrast computed tomography: the BAT score. *Stroke.* (2018) 49:1163–9. doi: 10.1161/STROKEAHA.117.020138
5. Witsch J, Bruce E, Meyers E, Velazquez A, Schmidt JM, Suwatcharangkoon S, et al. Intraventricular hemorrhage expansion in patients with spontaneous intracerebral hemorrhage. *Neurology.* (2015) 84:989–94. doi: 10.1212/WNL.0000000000001344
6. Naidech AM, Jovanovic B, Liebling S, Garg RK, Bassin SL, Bendok BR, et al. Reduced platelet activity is associated with early clot growth and worse 3-month outcome after intracerebral hemorrhage. *Stroke.* (2009) 40:2398–401. doi: 10.1161/STROKEAHA.109.550939
7. Aguilar MI, Hart RG, Kase CS, Freeman WD, Hoeben BJ, García RC, et al. Treatment of warfarin-associated intracerebral hemorrhage: literature review and expert opinion. *Mayo Clin Proc.* (2007) 82:82–92. doi: 10.1016/S0025-6196(11)60970-1
8. Rosand J, Hylek EM, O'Donnell HC, Greenberg SM. Warfarin-associated hemorrhage and cerebral amyloid angiopathy: a genetic and pathologic study. *Neurology.* (2000) 55:947–51. doi: 10.1212/WNL.55.7.947
9. Chen S, Zhao B, Wang W, Shi L, Reis C, Zhang J. Predictors of hematoma expansion predictors after intracerebral hemorrhage. *Oncotarget.* (2017) 8:89348–63. doi: 10.18632/oncotarget.19366
10. Sangha NS, Ajani Z, Dhanji R, McCartney D, Zhang X, Cai C, et al. Abstract WP321: strokes in your own backyard: a hospital wide quality improvement initiative to create and improve inpatient code stroke metrics which lead to quicker interventions. *Stroke.* (2018) 49(Suppl. 1):49. doi: 10.1161/str.49.suppl_1.WP321
11. Kurtz P, Fitts V, Sumer Z, Jalon H, Cooke J, Kvetan V, et al. How does care differ for neurological patients admitted to a neurocritical care unit versus a general ICU? *Neurocrit Care.* (2011) 15:477–80. doi: 10.1007/s12028-011-9539-2
12. Li Y, Yang R, Li Z, Yang Y, Tian B, Zhang X, et al. Surgical evacuation of spontaneous supratentorial lobar intracerebral hemorrhage: comparison of safety and efficacy of stereotactic aspiration,

endoscopic surgery, and craniotomy. *World Neurosurg.* (2017) 105:332–40. doi: 10.1016/j.wneu.2017.05.134
13. Kuramatsu JB, Biffi A, Gerner ST, Sembill JA, Sprügel MI, Leasure A, et al. Association of surgical hematoma evacuation vs conservative treatment with functional outcome in patients with cerebellar intracerebral hemorrhage. *JAMA*. (2019) 322:1392–403. doi: 10.1001/jama.2019.13014
14. Delgado P, Alvarez-Sabín J, Abilleira S, Santamarina E, Purroy F, Arenillas JF, et al. Plasma d-dimer predicts poor outcome after acute intracerebral hemorrhage. *Neurology.* (2006) 67:94–8. doi: 10.1212/01.wnl.0000223349.97278.e0
15. Goldstein JN, Fazen LE, Snider R, Schwab K, Greenberg SM, Smith EE, et al. Contrast extravasation on CT angiography predicts hematoma expansion in intracerebral hemorrhage. *Neurology.* (2007) 68:889–94. doi: 10.1212/01.wnl.0000257087.22852.21
16. Sansing LH, Kaznatcheeva EA, Perkins CJ, Komaroff E, Gutman FB, Newman GC. Edema after intracerebral hemorrhage: correlations with coagulation parameters and treatment. *J Neurosurg.* (2003) 98:985–92. doi: 10.3171/jns.2003.98.5.0985
17. Davis SM, Broderick J, Hennerici M, Brun NC, Diringer MN, Mayer SA, et al. Hematoma growth is a determinant of mortality and poor outcome after intracerebral hemorrhage. *Neurology.* (2006) 66:1175–81. doi: 10.1212/01.wnl.0000208408.98482.99
18. Tuhrim S, Horowitz DR, Sacher M, Godbold JH. Volume of ventricular blood is an important determinant of outcome in supratentorial intracerebral hemorrhage. *Crit Care Med.* (1999) 27:617–21. doi: 10.1097/00003246-199903000-00045
19. Ohwaki K, Yano E, Nagashima H, Hirata M, Nakagomi T, Tamura A. Blood pressure management in acute intracerebral hemorrhage: relationship between elevated blood pressure and hematoma enlargement. *Stroke.* (2004) 35:1364–7. doi: 10.1161/01.STR.0000128795.38283.4b
20. Anderson CS, Huang Y, Wang JG, Arima H, Neal B, Peng B, et al. Intensive blood pressure reduction in acute cerebral haemorrhage trial (INTERACT): a randomised pilot trial. *Lancet Neurol.* (2008) 7:391–9. doi: 10.1016/S1474-4422(08)70069-3
21. Qureshi AI. Antihypertensive Treatment of Acute Cerebral Hemorrhage (ATACH): rationale and design. *Neurocrit Care.* (2007) 6:56–66. doi: 10.1385/NCC:6:1:56
22. Naidech AM, Liebling SM, Rosenberg NF, Lindholm PF, Bernstein RA, Batjer HH, et al. Early platelet transfusion improves platelet activity and may improve outcomes after intracerebral hemorrhage. *Neurocrit Care.* (2012) 16:82–7. doi: 10.1007/s12028-011-9619-3
23. Guerrero WR, Gonzales NR, Sekar P, Kawano-Castillo J, Moomaw CJ, Worrall BB, et al. Variability in the use of platelet transfusion in patients with intracerebral hemorrhage: observations from the ethnic/racial variations of intracerebral hemorrhage study. *J Stroke Cerebrovasc Dis.* (2017) 26:1974–80. doi: 10.1016/j.jstrokecerebrovasdis.2017.06.014
24. Baschin M, Selleng S, Zeden JP, Westphal A, Kohlmann T, Schroeder HW, et al. Platelet transfusion to reverse antiplatelet therapy before decompressive surgery in patients with intracranial haemorrhage. *Vox Sang.* (2017) 112:535–41. doi: 10.1111/vox.12542
25. Ducruet AF, Hickman ZL, Zacharia BE, Grobelny BT, DeRosa PA, Landes E, et al. Impact of platelet transfusion on hematoma expansion in patients receiving antiplatelet agents before intracerebral hemorrhage. *Neurol Res.* (2010) 32:706–10. doi: 10.1179/174313209X459129
26. Chen T, Xu G, Tan D, Wu C. Effects of platelet infusion, anticoagulant and other risk factors on the rehaemorrhagia after surgery of hypertensive cerebral hemorrhage. *Eur Rev Med Pharmacol Sci.* (2015) 19:795–9.
27. Steiner T, Poli S, Griebe M, Hüsing J, Hajda J, Freiberger A, et al. Fresh frozen plasma versus prothrombin complex concentrate in patients with intracranial haemorrhage related to vitamin K antagonists (INCH): a randomised trial. *Lancet Neurol.* (2016) 15:566–73. doi: 10.1016/S1474-4422(16)00110-1
28. Huttner HB, Schellinger PD, Hartmann M, Köhrmann M, Juettler E, Wikner J, et al. Hematoma growth and outcome in treated neurocritical care patients with intracerebral hemorrhage related to oral anticoagulant therapy: comparison of acute treatment strategies using vitamin K, fresh frozen plasma, and prothrombin complex concentrates. *Stroke.* (2006) 37:1465–70. doi: 10.1161/01.STR.0000221786.81354.d6
29. Roh DJ, Carvalho Poyraz F, Magid-Bernstein J, Elkind MSV, Agarwal S, Park S, et al. Red blood cell transfusions and outcomes after intracerebral hemorrhage. *J Stroke Cerebrovasc Dis.* (2020) 29:105317. doi: 10.1016/j.jstrokecerebrovasdis.2020.105317
30. Ibrahim M. Blood transfusion does not improve outcomes in patients with spontaneous intracerebral hemorrhage (P7.143). *Neurology.* (2014) 82(10 Suppl):147.
31. Martin-Schild S. Packed red blood cell transfusion is associated with adverse outcomes in ICH patients (P04.072). *Neurology.* (2012) 78(1 Suppl.):P04.072. doi: 10.1212/WNL.78.1_MeetingAbstracts.P04.072
32. Moman RN, Kor DJ, Chandran A, Hanson AC, Schroeder DR, Rabinstein AA, et al. Red blood cell transfusion in acute brain injury subtypes: an observational cohort study. *J Crit Care.* (2019) 50:44–9. doi: 10.1016/j.jcrc.2018.11.006
33. Sheth KN, Gilson AJ, Chang Y, Kumar MA, Rahman RM, Rost NS, et al. Packed red blood cell transfusion and decreased mortality in intracerebral hemorrhage. *Neurosurgery.* (2011) 68:1286–92. doi: 10.1227/NEU.0b013e31820cccb2
34. Chang TR, Boehme AK, Aysenne A, Albright KC, Burns C, Beasley TM, et al. Nadir hemoglobin is associated with poor outcome from intracerebral hemorrhage. *Springerplus.* (2013) 2:379. doi: 10.1186/2193-1801-2-379
35. Arumugam A, A Rahman NA, Theophilus SC, Shariffudin A, Abdullah JM. Tranexamic acid as antifibrinolytic agent in non traumatic intracerebral hemorrhages. *Malays J Med Sci.* (2015) 22(Spec Issue):62–71.
36. Gao B, Xue T, Rong X, Yang Y, Wang Z, Chen Z, et al. Tranexamic acid inhibits hematoma expansion in intracerebral hemorrhage and traumatic brain injury. does blood pressure play a potential role? A meta-analysis from randmized controlled trials. *J Stroke Cerebrovasc Dis.* (2021) 30:105436. doi: 10.1016/j.jstrokecerebrovasdis.2020.105436
37. Hu W, Xin Y, Chen X, Song Z, He Z, Zhao Y. Tranexamic acid in cerebral hemorrhage: a meta-analysis and systematic review. *CNS Drugs.* (2019) 33:327–36. doi: 10.1007/s40263-019-00608-4
38. Tsai AG, Hofmann A, Cabrales P, Intaglietta M. Perfusion vs. oxygen delivery in transfusion with "fresh" and "old" red blood cells: the experimental evidence. *Transfus Apher Sci.* (2010) 43:69–78. doi: 10.1016/j.transci.2010.05.011
39. Veltkamp R, Rizos T, Horstmann S. Intracerebral bleeding in patients on antithrombotic agents. *Semin Thromb Hemost.* (2013) 39:963–71. doi: 10.1055/s-0033-1357506
40. Verduzco LA, Nathan DG. Sickle cell disease and stroke. *Blood.* (2009) 114:5117–25. doi: 10.1182/blood-2009-05-220921
41. National Heart, Lung, and Blood Institute. *Blood Transfusion - Types of Blood Transfusions | National Heart, Lung, and Blood Institute (NHLBI).* Available online at: https://www.nhlbi.nih.gov/node/3576 (accessed May 17, 2018)
42. Marik PE. *Transfusion of Blood and Blood Products. Evidence-Based Critical Care*. Cham: Springer International Publishing (2015). p. 585–619. doi: 10.1007/978-3-319-11020-2_38
43. Corwin HL, Gettinger A, Pearl RG, Fink MP, Levy MM, Abraham E, et al. The CRIT study: anemia and blood transfusion in the critically ill–current clinical practice in the United States. *Crit Care Med.* (2004) 32:39–52. doi: 10.1097/01.CCM.0000104112.34142.79
44. Vincent JL, Baron J-F, Reinhart K, Gattinoni L, Thijs L, Webb A, et al. Anemia and blood transfusion in critically ill patients. *JAMA*. (2002) 288:1499–507. doi: 10.1001/jama.288.12.1499
45. Ronco JJ, Fenwick JC, Tweeddale MG, Wiggs BR, Phang PT, Cooper DJ, et al. Identification of the critical oxygen delivery for anaerobic metabolism in critically ill septic and nonseptic humans. *JAMA*. (1993) 270:1724–30. doi: 10.1001/jama.270.14.1724
46. van Woerkens EC, Trouwborst A, van Lanschot JJ. Profound hemodilution: what is the critical level of hemodilution at which oxygen delivery-dependent oxygen consumption starts in an anesthetized human? *Anesth Analg.* (1992) 75:818–21. doi: 10.1213/00000539-199211000-00029
47. Creteur J, Neves AP, Vincent J-L. Near-infrared spectroscopy technique to evaluate the effects of red blood cell transfusion on tissue oxygenation. *Crit Care.* (2009) 13(Suppl. 5):S11. doi: 10.1186/cc8009
48. Marik PE. Effect of stored-blood transfusion on oxygen delivery in patients with sepsis. *JAMA*. (1993) 269:3024. doi: 10.1001/jama.1993.03500230106037

49. Conrad SA, Dietrich KA, Hebert CA, Romero MD. Effect of red cell transfusion on oxygen consumption following fluid resuscitation in septic shock. *Circ Shock.* (1990) 31:419–29.
50. Marik PE, Corwin HL. Efficacy of red blood cell transfusion in the critically ill: a systematic review of the literature. *Crit Care Med.* (2008) 36:2667–74. doi: 10.1097/CCM.0b013e3181844677
51. Raghavan M, Marik PE. Anemia, allogenic blood transfusion, and immunomodulation in the critically ill. *Chest.* (2005) 127:295–307. doi: 10.1378/chest.127.1.295
52. Marik PE. The hazards of blood transfusion. *Br J Hosp Med.* (2009) 70:12–5. doi: 10.12968/hmed.2009.70.1.37688
53. Hod EA, Brittenham GM, Billote GB, Francis RO, Ginzburg YZ, Hendrickson JE, et al. Transfusion of human volunteers with older, stored red blood cells produces extravascular hemolysis and circulating non-transferrin-bound iron. *Blood.* (2011) 118:6675–82. doi: 10.1182/blood-2011-08-371849
54. Hébert PC, Wells G, Blajchman MA, Marshall J, Martin C, Pagliarello G, et al. A multicenter, randomized, controlled clinical trial of transfusion requirements in critical care. transfusion requirements in critical care investigators, Canadian Critical Care Trials Group. *N Engl J Med.* (1999) 340:409–17. doi: 10.1056/NEJM199902113400601
55. Lacroix J, Hébert PC, Hutchison JS, Hume HA, Tucci M, Ducruet T, et al. Transfusion strategies for patients in pediatric intensive care units. *N Engl J Med.* (2007) 356:1609–19. doi: 10.1056/NEJMoa066240
56. Villanueva C, Colomo A, Bosch A, Concepción M, Hernandez-Gea V, Aracil C, et al. Transfusion strategies for acute upper gastrointestinal bleeding. *N Engl J Med.* (2013) 368:11–21. doi: 10.1056/NEJMoa1211801
57. Taylor FB, Toh CH, Hoots WK, Wada H, Levi M, Scientific Subcommittee on Disseminated Intravascular Coagulation (DIC) of the International Society on Thrombosis and Haemostasis (ISTH). Towards definition, clinical and laboratory criteria, and a scoring system for disseminated intravascular coagulation. *Thromb Haemost*. (2001) 86:1327–30. doi: 10.1055/s-0037-1616068
58. Shukla R, Patel T, Gupte S. Release of cytokines in stored whole blood and red cell concentrate: effect of leukoreduction. *Asian J Transfus Sci.* (2015) 9:145–9. doi: 10.4103/0973-6247.162708
59. Apstein CS, Dennis RC, Briggs L, Vogel WM, Frazer J, Valeri CR. Effect of erythrocyte storage and oxyhemoglobin affinity changes on cardiac function. *Am J Physiol.* (1985) 248:H508–15. doi: 10.1152/ajpheart.1985.248.4.H508
60. Kramer AH, Zygun DA. Anemia and red blood cell transfusion in neurocritical care. *Crit Care.* (2009) 13:R89. doi: 10.1186/cc7916
61. Zallen G, Moore EE, Ciesla DJ, Brown M, Biffl WL, Silliman CC. Stored red blood cells selectively activate human neutrophils to release IL-8 and secretory PLA2. *Shock.* (2000) 13:29–33. doi: 10.1097/00024382-200013010-00006
62. Nishiyama T, Hanaoka K. Hemolysis in stored red blood cell concentrates: modulation by haptoglobin or ulinastatin, a protease inhibitor. *Crit Care Med.* (2001) 29:1979–82. doi: 10.1097/00003246-200110000-00021
63. Scott AV, Nagababu E, Johnson DJ, Kebaish KM, Lipsitz JA, Dwyer IM, et al. 2,3-Diphosphoglycerate concentrations in autologous salvaged versus stored red blood cells and in surgical patients after transfusion. *Anesth Analg.* (2016) 122:616–23. doi: 10.1213/ANE.0000000000001071
64. Card RT, Mohandas N, Perkins HA, Shohet SB. Deformability of stored red blood cells. relationship to degree of packing. *Transfusion.* (1982) 22:96–101. doi: 10.1046/j.1537-2995.1982.22282177134.x
65. Beutler E, Kuhl W, West C. The osmotic fragility of erythrocytes after prolonged liquid storage and after reinfusion. *Blood.* (1982) 59:1141–7. doi: 10.1182/blood.V59.6.1141.bloodjournal5961141
66. Card RT, Mohandas N, Mollison PL. Relationship of post-transfusion viability to deformability of stored red cells. *Br J Haematol.* (1983) 53:237–40. doi: 10.1111/j.1365-2141.1983.tb02016.x
67. Tinmouth A, Fergusson D, Yee IC, Hébert PC, ABLE Investigators, Canadian Critical Care Trials Group. Clinical consequences of red cell storage in the critically ill. *Transfusion*. (2006) 46:2014–27. doi: 10.1111/j.1537-2995.2006.01026.x
68. Knight JA, Voorhees RP, Martin L, Anstall H. Lipid peroxidation in stored red cells. *Transfusion.* (1992) 32:354–7. doi: 10.1046/j.1537-2995.1992.32492263451.x
69. Berezina TL, Zaets SB, Morgan C, Spillert CR, Kamiyama M, Spolarics Z, et al. Influence of storage on red blood cell rheological properties. *J Surg Res.* (2002) 102:6–12. doi: 10.1006/jsre.2001.6306
70. Hovav T, Yedgar S, Manny N, Barshtein G. Alteration of red cell aggregability and shape during blood storage. *Transfusion.* (1999) 39:277–81. doi: 10.1046/j.1537-2995.1999.39399219284.x
71. Chu RW. Leukocytes in blood transfusion: adverse effects and their prevention. *Hong Kong Med J.* (1999) 5:280–4.
72. Kumar MA, Rost NS, Snider RW, Chanderraj R, Greenberg SM, Smith EE, et al. Anemia and hematoma volume in acute intracerebral hemorrhage. *Crit Care Med.* (2009) 37:1442–7. doi: 10.1097/CCM.0b013e31819ced3a
73. Schnüriger B, Inaba K, Abdelsayed GA, Lustenberger T, Eberle BM, Barmparas G, et al. The impact of platelets on the progression of traumatic intracranial hemorrhage. *J Trauma.* (2010) 68:881–5. doi: 10.1097/TA.0b013e3181d3cc58
74. Whiteley WN, Slot KB, Fernandes P, Sandercock P, Wardlaw J. Risk factors for intracranial hemorrhage in acute ischemic stroke patients treated with recombinant tissue plasminogen activator: a systematic review and meta-analysis of 55 studies. *Stroke.* (2012) 43:2904–9. doi: 10.1161/STROKEAHA.112.665331
75. Luo H, Wei L, Lu L, Kang L, Cao Y, Yang X, et al. Transfusion of resting platelets reduces brain hemorrhage after intracerebral hemorrhage and tpa-induced hemorrhage after cerebral ischemia. *Front Neurosci.* (2019) 13:338. doi: 10.3389/fnins.2019.00338
76. Sugimoto K, Ishihara H, Shinoyama M, Sadahiro H, Suzuki M. [Effect of platelet concentrate transfusion on prognosis of patients with intracerebral hemorrhage treated with anti-platelet agents]. *No Shinkei Geka.* (2017) 45:965–70. doi: 10.11477/mf.1436203629
77. Gehrie EA, Tobian AAR. PATCHing platelet data to improve transfusion. *Blood.* (2020) 135:1309–10. doi: 10.1182/blood.2020005384
78. Cornelissen LL, Kreuger AL, Caram-Deelder C, Middelburg RA, Kerkhoffs JLH, von dem Borne PA, et al. Thrombocytopenia and the effect of platelet transfusions on the occurrence of intracranial hemorrhage in patients with acute leukemia - a nested case-control study. *Ann Hematol.* (2021) 100:261–71. doi: 10.1007/s00277-020-04298-7
79. Schmidt AE, Henrichs KF, Kirkley SA, Refaai MA, Blumberg N. Prophylactic preprocedure platelet transfusion is associated with increased risk of thrombosis and mortality. *Am J Clin Pathol.* (2017) 149:87–94. doi: 10.1093/ajcp/aqx151
80. Hobbs K. *Management of ICH in the ICU*. Stanford University (2015). Available online at: https://www.smchealth.org/sites/main/files/file-attachments/2015_stroke_conf_hobbs_management_of_ich_in_the_icu.pdf (accessed January 16, 2021)
81. Rymer MM. Hemorrhagic stroke: intracerebral hemorrhage. *Mo Med.* (2011) 108:50–4.
82. Broderick JP, Brott TG, Duldner JE, Tomsick T, Huster G. Volume of intracerebral hemorrhage. a powerful and easy-to-use predictor of 30-day mortality. *Stroke.* (1993) 24:987–93. doi: 10.1161/01.STR.24.7.987
83. Arnone GD, Kumar P, Wonais MC, Esfahani DR, Campbell-Lee SA, Charbel FT, et al. Impact of platelet transfusion on intracerebral hemorrhage in patients on antiplatelet therapy-an analysis based on intracerebral hemorrhage score. *World Neurosurg.* (2018) 111:e895–904. doi: 10.1016/j.wneu.2018.01.006
84. Briggs A, Gates JD, Kaufman RM, Calahan C, Gormley WB, Havens JM. Platelet dysfunction and platelet transfusion in traumatic brain injury. *J Surg Res.* (2015) 193:802–6. doi: 10.1016/j.jss.2014.08.016
85. Kuehn B. Fatal sepsis linked to platelets. *JAMA.* (2018) 320:540. doi: 10.1001/jama.2018.10994
86. Jacobs MR, Smith D, Heaton WA, Zantek ND, Good CE, PGD Study Group. Detection of bacterial contamination in prestorage culture-negative apheresis platelets on day of issue with the Pan Genera Detection test. *Transfusion.* (2011) 51:2573–82. doi: 10.1111/j.1537-2995.2011.03308.x
87. Flibotte JJ, Hagan N, O'Donnell J, Greenberg SM, Rosand J. Warfarin, hematoma expansion, and outcome of intracerebral hemorrhage. *Neurology.* (2004) 63:1059–64. doi: 10.1212/01.WNL.0000138428.40673.83
88. Flaherty ML, Kissela B, Woo D, Kleindorfer D, Alwell K, Sekar P, et al. The increasing incidence of anticoagulant-associated intracerebral hemorrhage. *Neurology.* (2007) 68:116–21. doi: 10.1212/01.wnl.0000250340.05202.8b

89. Rosand J, Eckman MH, Knudsen KA, Singer DE, Greenberg SM. The effect of warfarin and intensity of anticoagulation on outcome of intracerebral hemorrhage. *Arch Intern Med.* (2004) 164:880–4. doi: 10.1001/archinte.164.8.880
90. Hart RG, Boop BS, Anderson DC. Oral anticoagulants and intracranial hemorrhage. *Stroke.* (1995) 26:1471–7. doi: 10.1161/01.STR.26.8.1471
91. Yasaka M, Sakata T, Minematsu K, Naritomi H. Correction of INR by prothrombin complex concentrate and vitamin K in patients with warfarin related hemorrhagic complication. *Thromb Res.* (2002) 108:25–30. doi: 10.1016/S0049-3848(02)00402-4
92. Kuramatsu JB, Gerner ST, Lücking H, Kloska SP, Schellinger PD, Köhrmann M, et al. Anemia is an independent prognostic factor in intracerebral hemorrhage: an observational cohort study. *Crit Care.* (2013) 17:R148. doi: 10.1186/cc12827
93. Corwin HL, Carson JL. Blood transfusion–when is more really less? *N Engl J Med.* (2007) 356:1667–9. doi: 10.1056/NEJMe078019
94. Diedler J, Sykora M, Hahn P, Heerlein K, Schölzke MN, Kellert L, et al. Low hemoglobin is associated with poor functional outcome after non-traumatic, supratentorial intracerebral hemorrhage. *Crit Care.* (2010) 14:R63. doi: 10.1186/cc8961
95. Mayer SA, Brun NC, Begtrup K, Broderick J, Davis S, Diringer MN, et al. Efficacy and safety of recombinant activated factor VII for acute intracerebral hemorrhage. *N Engl J Med.* (2008) 358:2127–37. doi: 10.1056/NEJMoa0707534
96. Aguilar MI, Brott TG. Update in intracerebral hemorrhage. *Neurohospitalist.* (2011) 1:148–59. doi: 10.1177/1941875211409050
97. Shander A. *Mechanism of Transfusion Overuse*. Department of Cardiovascular Surgery Grand Rounds (2016). Available online at: https://www.slideserve.com/ehren/mechanism-of-transfusion-overuse (accessed February 13, 2020)
98. Trentino KM, Mace H, Symons K, Sanfilippo FM, Leahy MF, Farmer SL, et al. Associations of a preoperative anemia and suboptimal iron stores screening and management clinic in colorectal surgery with hospital cost, reimbursement, and length of stay: a net cost analysis. *Anesth Analg.* (2021) 132:344–52. doi: 10.1213/ANE.0000000000005241
99. Sonni S, Lioutas V-A, Selim MH. New avenues for treatment of intracranial hemorrhage. *Curr Treat Options Cardiovasc Med.* (2014) 16:277. doi: 10.1007/s11936-013-0277-y

Conflict of Interest: The authors declare that the research was conducted in the absence of any commercial or financial relationships that could be construed as a potential conflict of interest.

Publisher's Note: All claims expressed in this article are solely those of the authors and do not necessarily represent those of their affiliated organizations, or those of the publisher, the editors and the reviewers. Any product that may be evaluated in this article, or claim that may be made by its manufacturer, is not guaranteed or endorsed by the publisher.

frontiers in Neurology

ORIGINAL RESEARCH
published: 30 November 2021
doi: 10.3389/fneur.2021.764718

Longitudinal, Quantitative, Multimodal MRI Evaluation of Patients With Intracerebral Hemorrhage Over the First Year

Muhammad E. Haque[1], Seth B. Boren[1], Octavio D. Arevalo[2], Reshmi Gupta[3], Sarah George[1], Maria A. Parekh[1], Xiurong Zhao[1], Jaraslow Aronowski[1] and Sean I. Savitz[1]*

[1] Institute for Stroke and Cerebrovascular Diseases and Department of Neurology, Louisiana State University, Shreveport, LA, United States, [2] Biostatistics, Epidemiology, and Research Design Component, Center for Clinical and Translational Sciences, Louisiana State University, Shreveport, LA, United States, [3] Department of Radiology, McGovern Medical School, The University of Texas Health Science Center at Houston, Louisiana State University, Shreveport, LA, United States

OPEN ACCESS

Edited by:
Budbazar Enkhjargal, Boston University, United States

Reviewed by:
Sangeetha Sukumari Ramesh, Augusta University, United States
Mangmang Xu, Sichuan University, China
Xiao Wei, Chongqing Medical and Pharmaceutical College, China

***Correspondence:**
Muhammad E. Haque
muhammad.e.haque@uth.tmc.edu

Specialty section:
This article was submitted to Stroke, a section of the journal Frontiers in Neurology

Received: *25 August 2021*
Accepted: *01 November 2021*
Published: *30 November 2021*

Citation:
Haque ME, Boren SB, Arevalo OD, Gupta R, George S, Parekh MA, Zhao X, Aronowski J and Savitz SI (2021) Longitudinal, Quantitative, Multimodal MRI Evaluation of Patients With Intracerebral Hemorrhage Over the First Year. Front. Neurol. 12:764718. doi: 10.3389/fneur.2021.764718

In most patients with intracerebral hemorrhage (ICH), the hematoma and perihematomal area decrease over the subsequent months but patients continue to exhibit neurological impairments. In this serial imaging study, we characterized microstructural and neurophysiological changes in the ICH-affected brain tissues and collected the National Institute of Health Stroke Scale (NIHSS) and modified Rankin Score (mRS), two clinical stroke scale scores. Twelve ICH patients were serially imaged on a 3T MRI at 1, 3, and 12 months (M) after injury. The hematoma and perihematomal volume masks were created and segmented using FLAIR imaging at 1 month which were applied to compute the susceptibilities (χ), fractional anisotropy (FA), mean diffusivity (MD), and cerebral blood flow (CBF) in the same tissues over time and in the matching contralesional tissues. At 3 M, there was a significant ($p < 0.001$) reduction in hematoma and perihematomal volumes. At 1 M, the χ, FA, and CBF were decreased in the perihematomal tissues as compared to the contralateral side, whereas MD increased. In the hematomal tissues, the χ increased whereas FA, MD, and CBF decreased as compared to the contralesional area at 1 M. Temporally, CBF in the hematoma and perihematomal tissues remained significantly ($p < 0.05$) lower compared with the contralesional areas whereas MD in the hematoma and χ in the perihematomal area increased. The NIHSS and mRS significantly correlated with hematoma and perihematomal volume but not with microstructural integrity. Our serial imaging studies provide new information on the long-term changes within the brain after ICH and our findings may have clinical significance that warrants future studies.

Keywords: intracerebral hemorrhage stroke, quantitative susceptibility mapping (QSM), arterial spin labeling, diffusion tensor imaging, serial magnetic resonance imaging

INTRODUCTION

Intracerebral hemorrhage (ICH) accounts for about 10–15% of all strokes and is associated with high mortality (1, 2). ICH-induced death may occur within hours to days of the ictus (3, 4). ICH is characterized by two primary modes of injury: (1) mechanical stress due to rupture of brain blood vessels, physical compression of brain tissues, an increase in intracranial pressure, and midline shift; (2) high levels of iron concentration from hemoglobin and its breakdown products causing cytotoxic and vasogenic edema, iron toxicity, oxidative stress, protein, and DNA damage (5–11). ICH also causes neuroinflammation, which has been characterized by the presence of neutrophils, and macrophages/monocytes as well as microglial activation around the hemorrhagic foci (12–14). In the acute phase of ICH, hematoma and perihematomal volume is routinely monitored using computed tomography (CT) in the hospitalized setting but the long-term effects on tissue physiology such as cerebral blood flow (CBF) and microstructural integrity have received little attention (15, 16). While hematomas are absorbed over time and tissue is restored to partial or full normal-appearing (17), patients continue to exhibit hemiparesis and other neurological impairments. Recent advancements in non-invasive quantitative magnetic resonance imaging enable us to serially probe the integrity and physiological status of the hematomal and perihematomal tissues over the long term. In this pilot study, we aimed to longitudinally monitor changes in the iron concentration, microstructural integrity, and cerebral perfusion within the perihematomal and hematomal tissues using quantitative susceptibility mapping (QSM), diffusion tensor imaging (DTI), and arterial spin labeling (ASL), respectively. We selected QSM to measure iron induced susceptibilities over gold standard gradient echo (GRE) to eliminate acquisition parameter dependency and hematoma volume overestimation, well-documented phenomena (17). We selected DTI to evaluate the microstructural integrity of the tissues after hematoma resolution and ASL as a marker of tissue functional status. We hypothesize localized change in blood flow over time will only occur if tissues are viable and functional after hematoma and edema re-absorption. Our study provides detailed findings on the dynamic changes in a number of novel endpoints as an initial approach to understanding and characterizing the long-term evolution of ICH within the first year after injury.

METHODS AND PROCEDURES

Patient Enrollment and Human Protection

Twelve patients with ICH admitted to the Memorial Hermann Hospital-Texas Medical Center between 2016 and 2020 participated in a longitudinal MR imaging study. The study was approved by the institutional review board of the University of Texas Health Sciences Center at Houston and by the Memorial Hermann Hospital Office of Research. Written informed consent was obtained after a thorough discussion with patients and family members. The inclusion criteria were all patients diagnosed with parenchymal ICH age 18–80 years, hematoma volume <100 cc, NIHSS 0–20. Patients with a brain tumor, traumatic brain injury, brain aneurysm, claustrophobia, and metal implantation were excluded.

Neurological and Radiological Assessments

All participants underwent baseline and serial assessment of neurological deficits via the NIHSS (18) and mRS, a disability severity score (19, 20). The neurological assessments were correlated with the hematoma volume, perihematomal volume, and imaging matrices (χ, FA, MD, and CBF) within the hematoma and perihematomal ROI. Baseline images (CT or MRI) were obtained within 6–24 h of onset as part of the standard of care protocols without quantitative MRI. Follow-up imaging was obtained at 1 month (M), 3, and 12 M. The qualitative radiological assessment included serial changes in hematoma and perihematomal volume, acute presence of mass effect or midline shift, and development of Wallerian Degeneration (WD).

Imaging Sequences

Complete detail of these imaging methods can be found elsewhere, but are briefly summarized below.

Quantitative susceptibility mapping (QSM), an emerging advanced image-processing algorithm of gradient echo (GRE) imaging, is highly sensitive and specific to magnetic susceptibility sources. Unlike GRE, QSM not only measures hematoma volume accurately, but also creates a clear delineation between paramagnetic substances (such as iron, ferritin, and hemosiderin) from diamagnetic substances (such as calcium, water, brain tissues) by positive and negative susceptibilities, respectively. The voxel intensity in QSM is linearly proportional to the source of susceptibilities (χ) and using an external calibration curve, these maps can be applied to compute iron concentrations within the hematoma and surrounding perihematomal area (21–23).

Diffusion Tensor Imaging (DTI) exploits both the magnitude and direction of water molecules diffusion as a tracer to probe tissue integrity. It can provide quantitative information *via* measuring scalar matrices known as fractional anisotropy (FA) and mean diffusivity (MD). On the FA scale between 0 (unrestricted or isotropic diffusion) and 1 (restricted or anisotropic diffusion), a decrease in FA indicates microstructural damage. The mean diffusivity can tag the magnitude of the water molecule diffusion coefficient, which changes in damaged tissues (24, 25).

Arterial Spin Labeling (ASL) measures cerebral perfusion by employing arterial blood as an endogenous tracer labeled with a radio frequency pulse. These labeled water molecules in the blood are allowed to enter the brain parenchyma and images are obtained at 1–2 s delay. Subsequently, images are also obtained without labeling, and perfusion contrast is calculated by subtracting the labeled and non-labeled images depicting the exchange of magnetization (26, 27).

Image Acquisition

Serial images were obtained on a full body 3.0 T Philips Intera system that was later upgraded to Ingenia (Philips Medical Systems, Best, Netherland). Anatomical imaging included: 3D T1-weighted (TR/TE = 8.11/3.74 ms, imaging matrix = 256 × 256 × 180 mm^3, slice thickness = 1 mm), and 3D fluid attenuated

inversion recovery (FLAIR, TR/TE = 4800/129 ms, imaging matrix = 256 × 256 × 180 mm^3, slice thickness = 1 mm). Quantitative imaging included: 3D quantitative susceptibility mapping (multiecho GRE, number of echo = 8, echo spacing = 6.93 ms, TR = 57.7 ms, first TE = 4.52 ms, voxel size = 0.75 x 0.75 x 1.0 mm^3), diffusion-tensor imaging (TR/TE = 9.5 s/66 ms, b-value = 0, 1000 s/mm^2, number of gradient direction = 21, matrix = 128 128, slice thickness = 3 mm), arterial spin label (PCASL, labeling duration/delay = 1.9 /2.0 sec, number of dynamics = 70, TR/TE = 4.8 s/15.8 ms, slice thickness/no slice = 5 mm, martix = 88 x 88 mm^2).

Image Processing

The DTI and ASL data were pre-processed using FSL (http://www.fmrib.ox.ac.uk/fsl). The QSM maps were computed using Susceptibility Tensor Imaging (STI) software (https://people.eecs.berkeley.edu/$\sim$chunlei.liu/software.html) to compute susceptibilities (χ). T1-weighted and FLAIR images were registered to FA, MD, CBF, and QSM quantitative maps.

Lesion Volume Measurements and Region of Interest

A semi-automated seed growing algorithm using Analyze 12.0 (Analyze Direct Inc., KS, USA) software was used to delineate and compute hematoma and perihematomal volume on FLAIR images at all three-time points as shown in **Figure 1**. Briefly, a seed point was selected within the hematoma and signal intensity was threshold so neighboring pixels with similar signal intensity were added to the seed region to create a hematoma mask. The process was iterated several times and the hematoma mask was manually edited whenever necessary by including or removing pixels. The same process was repeated to delineate perihematomal mask. The hematoma and perihematomal masks that were delineated at 1 month were saved as ROI and registered to the QSM, FA, MD, and CBF maps to compute temporal imaging matrices in the same regions. The same ROI was also used for contralesional healthy tissues. We equated the perihematomal area with cerebral edema.

Statistical Analysis

Standard descriptive statistics summarized participant characteristics at baseline. Categorical variables were calculated as frequencies and percentages. A quantile-quantile plot was used to determine whether response variables (hematoma and perihematomal volumes, magnetic susceptibility, fractional anisotropy, mean diffusivity, and CBF) were normally distributed and amenable to analysis with traditional parametric techniques. Linear mixed models with random intercept and unstructured covariance were used to determine the changes over time in the above-mentioned variables from baseline. The statistical significance level was set at $\alpha = 0.05$ (i.e., the probability of rejecting the null hypothesis when it is true is set at 0.05) with 95% confidence intervals for all the model parameters. Bonferroni adjustment for multiple testing was used for all *post hoc* comparisons. All analyses were conducted with SAS statistical software version 9.4 (SAS Institute Inc., Cary, NC).

RESULTS

Demographics and Clinical Information

Imaging data from a total of 12 ICH patients (35 scans) were used in this analysis. All participants completed all the visits except one patient who missed the last visit. There were eight men and four women with an average age of 54.4 ± 16.6 years with no previous stroke. All patients had unilateral hemorrhage with six patients in the left and the other six in the right hemisphere. The median NIHSS on admission was four (IQR 2–9.5) and decreased to 0 (IQR 0–2) over 1 year. The median mRS was 2.5 (IQR 1–3.25) at 1 M and 1.5(IQR 0.5–2) at 12 M. Only one patient underwent acute hemicraniectomy due to expansion of edema. All participants had hypertensive bleeding except P12 who had a venous vascular malformation and P09 who had a cerebral venous thrombosis. P11 might have had bleeding due to anticoagulation. None of the patients had bleeding due to cerebral amyloid angiopathy or metastasis. All patients exhibited variable degrees of mass effects and four patients had midline shifts in the acute phase. Four patients showed signs of Wallerian Degeneration by the end of the study. The demographics and qualitative radiological assessment, and clinical scores are summarized in **Table 1**.

Hematoma and Perihematoma Volume

Figure 1 delineates serial hematoma and perihematomal regions used to calculate the hematoma and perihematomal volume. Both hematoma and perihematomal volumes were significantly ($p < 0.05$) decreased within 3 M of onset. As compared with 1 M, the average hematoma volume (1 M, 16.59 ± 21.03; 3 M, 5.66 ± 8.64 cm^3) and perihematomal volume (1 M, 18.7 ± 21.8; 3 M, 1.59 ± 2.34 cm^3) were decreased by 66 and 91.4%, at 3 M, respectively. Between 3 and 12 M, only 16% of the hematoma volume (3 M, 5.66 ± 8.84; 12 M, 4.71 ± 7.70 cm^3) and 96.2% of perihematomal volume (3 M, 1.59 ± 2.34; 12 M, 0.06 ± 0.12 cm^3) had resolved. The temporal hematoma and perihematomal volume changes are summarized in **Figure 4A**. **Figures 2**, **3** (top row) show the typical hematoma and perihematomal region at each time point which was used to calculate changes in the imaging matrices.

Magnetic Susceptibility

The average hematoma susceptibilities at 1 and 3 M (1 M, 0.274 ± 0.3; 3 M, 0.089 ± 0.03 ppm) were significantly higher ($p < 0.01$) than matching contralesional ones (1 M, 0.021 ± 0.01; 3 M, 0.01 ± 0.01 ppm) whereas no significant difference in susceptibilities was found at 12 M. As compared to 1 M, the hematoma susceptibilities were significantly decreased ($p < 0.01$) at 3 and 12 M. The perihematoma susceptibility at 1 M (−0.029 ± 0.03 ppm) was decreased as compared to the contralesional tissues (−0.008 ± 0.01 ppm). Temporally, perihematomal susceptibilities increased to 0.002 ± 0.03 ppm at 12 M. There was no significant difference in susceptibility between the perihematomal area and the corresponding contralesional tissues. Temporally, perihematomal susceptibility was not significantly changed (**Figures 2**, **3**, row 2; **Figures 4B,C**).

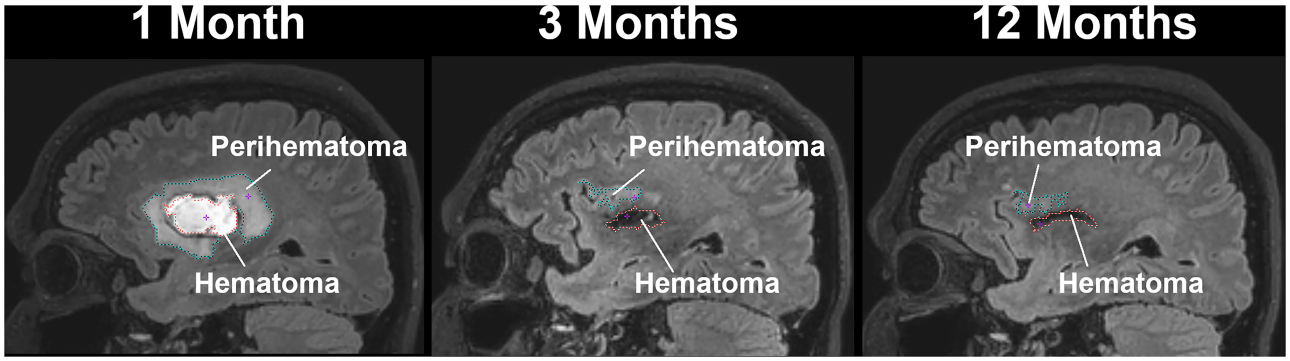

FIGURE 1 | A sagittal view of a patient with intracerebral hemorrhage displaying temporal changes in a hematoma (red-dotted line) and perihematomal (cyan dotted line) volume.

TABLE 1 | Patient demographics and clinical assessment.

PID	Age/ Gender	Lesion side	Lesion location	NIHSS acute/12 M	mRS 1 M/12 M	Edema 1 M/12 M	Hematoma 1M/12M	Midline shift (acute)	WD (01 M)	WD (12 M)
						Volume (cc)				
P01	60/M	R	Insula, CST, BG	5/NA	0/NA	20.7/NA	0.54/NA	N	N	N
P02	69/M	L	Precuneus	0/0	1/0	28.6/4.45	21.2/0.37	N	N	N
P03	64/M	L	BG, CST	4/3	3/2	2.0/2.14	5.8/0	N	N	Y
P04	67/F	L	BG, CST	13/2	4/3	2.3/1.85	5.1/0	N	N	N
P05	54/M	R	Thalamus, BG	3/0	1/1	7.2/1.01	6.6/0.15	N	N	N
P06	52/M	L	CR, putamen, Insula	4/1	3/2	17.3/1.44	6.6/0	Y	N	Y
P07	33/M	R	Fronto-parietal, BG, Internal Capsule	14/3	4/2	12.7/27.1	55.5/0	Y	N	Y
P08	35/M	R	Insula, CST, BG	15/2	4/2	49.9/6.71	62.4/0.16	Y	N	Y
P09	29/F	L	Temporal lobe	2/0	2/0	71.4/4.35	27.9/0	Y	N	N
P10	72/F	R	BG, CR, Thalamus	2/0	0/1	4.2/0.59	1.3/0	N	N	N
P11	78/F	L	Temporo-occipital	6/0	1/2	5.6/1.34	4.8/0	N	N	N
P12	40/M	R	Vermian Cavernoma	0/0	2/0	2.1/0.66	0.86/0	N	N	N

NIHSS, National Institute of Stroke Scale; WD, Wallerian Degeneration; CST, Corticospinal Tracts; CR, Corona Radiata; BG, Basal Ganglia.

Fractional Anisotropy and Mean Diffusivity

FA at 1 M in both the hematoma (0.23 ± 0.03) and perihematomal (0.28 ± 0.02) tissues was significantly decreased ($p < 0.05$) as compared to the contralesional tissues (0.35 ± 0.02 and 0.32 ± 0.02, respectively). Between 1 and 3 M, FA in the hematoma and perihematomal increased to 0.28 ± 0.03 and 0.34 ± 0.02, respectively, but the increase was not statistically significant. Between 3 and 12 M, there was no temporal change in FA in either hematoma or perihematoma. The contralesional FA remained constant throughout the study (**Figures 2**, **3**, row 4; **Figures 4D,E**). The MD in the hematoma (756 ± 73 x 10^{-6} mm^2/s) was significantly ($p < 0.01$) decreased as compared to the contralesional area (925 ± 67 x 10^{-6} mm^2/s) at 1 M. Moreover, the hematomal MD was significantly ($p < 0.01$) higher at 3 and 12 M as compared to 1 Mmonths. Matching contralesional tissue remained constant throughout the study. The average perihematomal MD was slightly higher than the contralesional one and remained elevated throughout the study, but without being statistically different. There was no temporal difference in perihematomal MD (**Figures 2**, **3**, row 4; **Figures 4F,G**).

Cerebral Blood Flow

The CBF in both the hematoma and perihematomal regions was significantly decreased ($p < 0.01$) as compared to the matching contralesional tissues at all-time points. Temporally, CBF in both the hematoma (1 M, 45.7 ± 6.9; 12 M, 64.3 ± 6.8 ml/100 g of tissue/min) and perihematomal space (1 M, 46.6 ± 6.9; 12 M, 71.8 ± 6.8 ml/100 g of tissue/min) significantly increased ($p < 0.05$) between 1 and 12 M. There was no change at the contralesional side (**Figures 2**, **3**, row 5; **Figures 4H,I**).

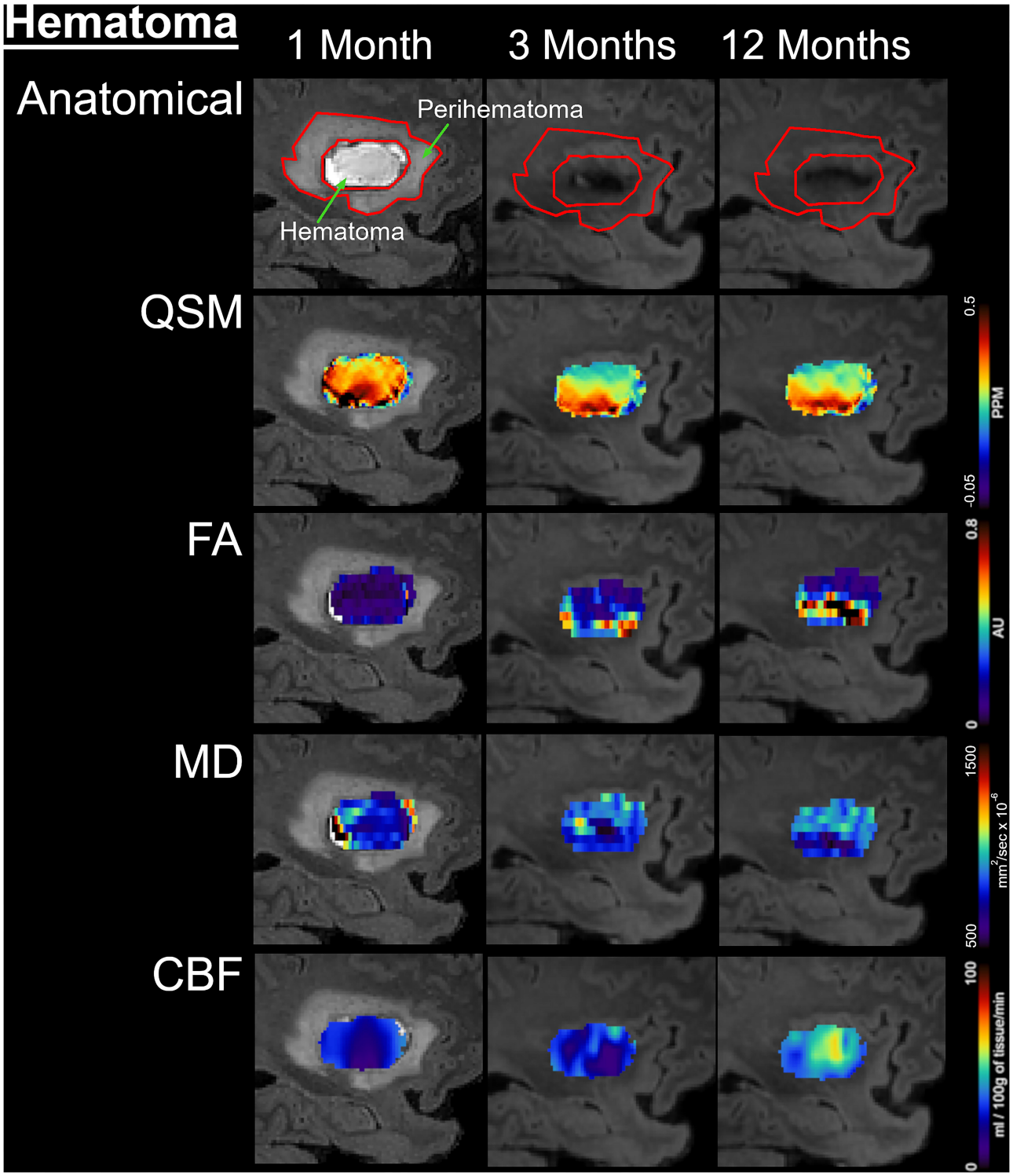

FIGURE 2 | Temporal changes in the hematomal tissues are shown on a fluid-attenuated inversion recovery (FLAIR) by color-coded voxel by voxel quantitative maps in a patient. The rows are illustrating the imaging measurements whereas columns are showing changes at 1, 3, and 12 M after onset. In the top row, the first image outlines the perihematomal and hematoma regions that were used as an ROI to measure imaging matrices over time. The other two images on the same row are showing the decrease in hematoma volume with a hypo-intense hemosiderin region at 3 and 12 M. The rows 2–5 display QSM maps, FA, MD, and CBF in the hematomal tissues over time, respectively.

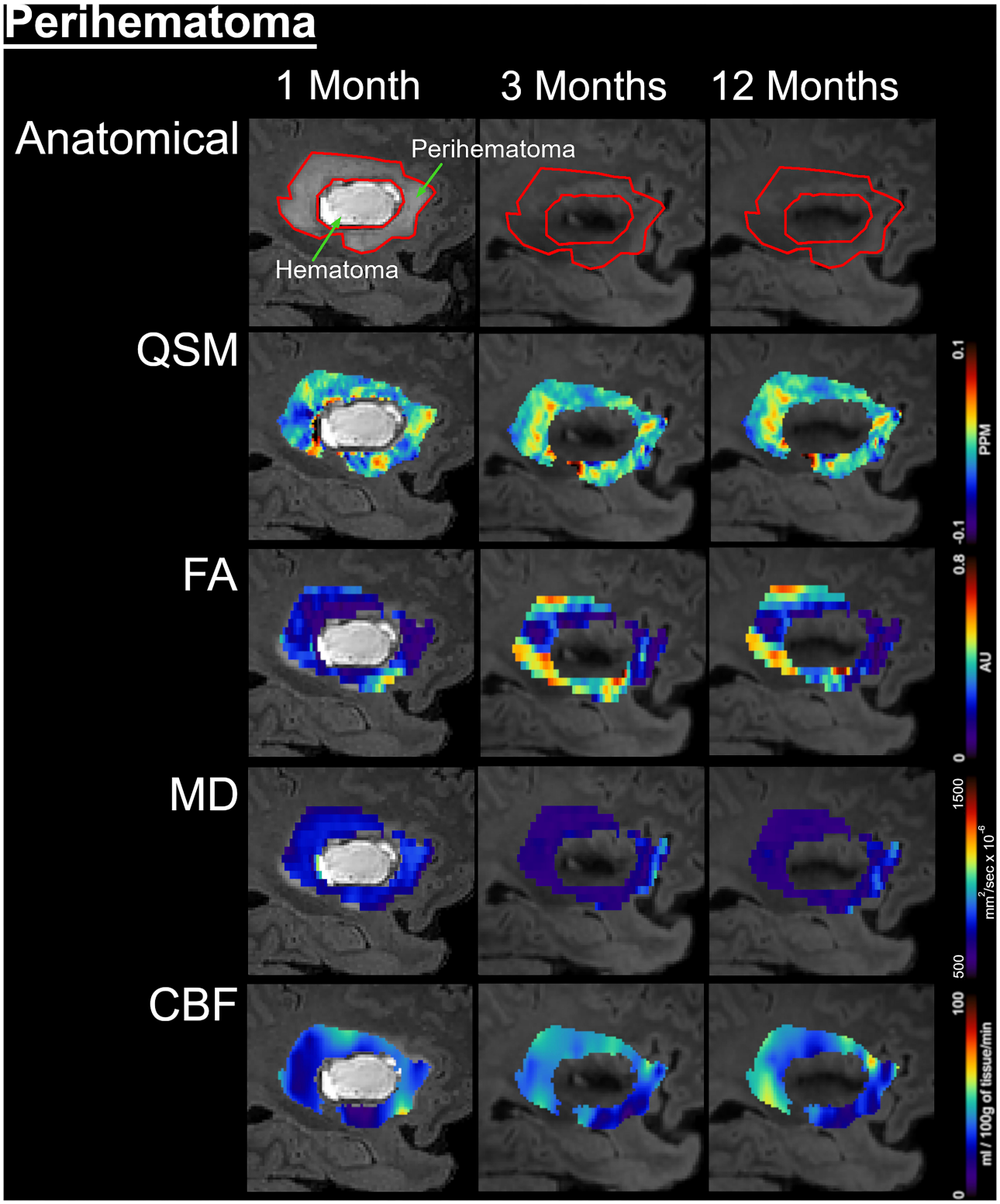

FIGURE 3 | Temporal changes in the perihematomal tissues are shown on a fluid-attenuated inversion recovery (FLAIR) by color-coded voxel by voxel quantitative maps in a represented patient. The rows are illustrating the imaging measurements whereas columns are showing changes at 1, 3, and 12 months of onset. In the top row, the first image outlined the perihematomal and hematoma regions that were used as regions-of-interest (ROI) to measure imaging matrices over time. The rows 2–5 are displaying quantitative susceptibilities maps (QSM), fractional anisotropy (FA), mean diffusivity (MD), and cerebral blood flow (CBF) in the perihematomal tissues overtime, respectively.

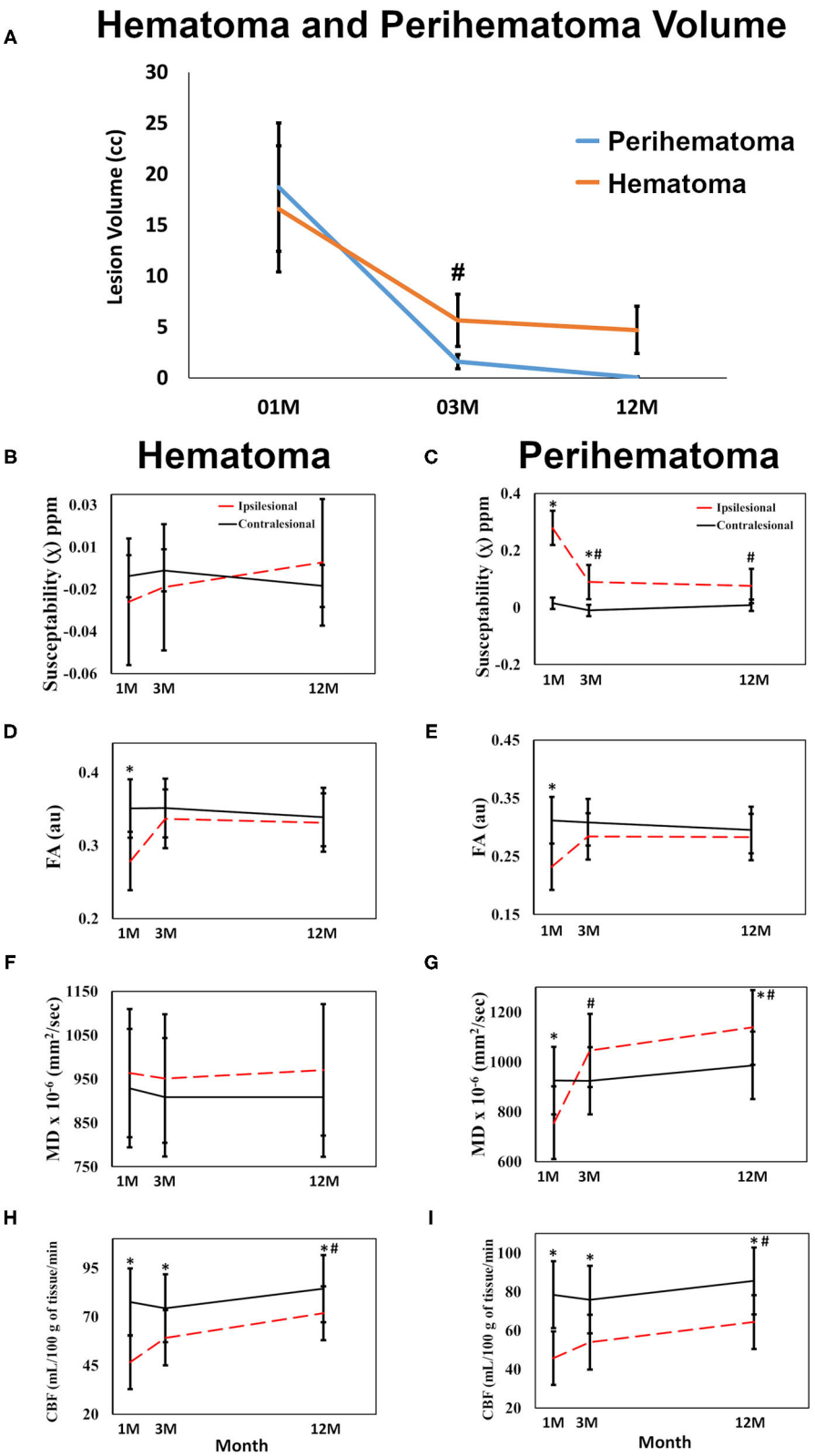

FIGURE 4 | Quantitative changes in imaging matrices are shown over time in the hematomal and perihematomal ROIs compared to the matching contralesional one. **(A)** Significant reduction in both the perihematoma and hematoma volume between 1 and 3 M with no significant reduction thereafter. Plots **(B,C)** changes in susceptibilities; **(D,E)** FA; **(F,G)** MD changes over time in the hematoma and perihematomal ROIs compared to the contralesional side. **(H,I)** temporal changes CBF in the hematoma and perihematoma ROIs as compared to the contralesional side. $^{*}p < 0.05$ as compared with the contralesional tissues, $^{\#}p < 0.05$ ipsilesional changes over time as compared with the 1 M, error bar are STD err.

TABLE 2 | Summarized association between imaging measurements within hematoma and perihematomal volumes and clinical scores.

	Perihematoma volume		Hematoma volume		NIHSS		mRS	
	β(SE)	*p*-value	β(SE)	*p*-value	β(SE)	*p*-value	β(SE)	*p*-value
Perihematoma								
χ	−0.001(<0.001)	0.089	–	–	−0.011(0.003)	0.004[a]	0.003(0.006)	0.612
FA	−0.002(0.001)	0.002[a]	–	–	0.000(0.006)	0.981	0.002(0.012)	0.880
MD	4.890(2.470)	0.057	–	–	−4.692(21.353)	0.828	−16.370(39.931)	0.685
CBF	−0.383(0.236)	0.116	–	–	−2.441(2.014)	0.236	−5.954(4.011)	0.149
Hematoma								
χ	–	–	0.004(0.003)	0.206	−0.006(0.020)	0.778	−0.006(0.032)	0.852
FA	–	–	−0.002(0.001)	0.083	−0.003(0.008)	0.697	0.011(0.015)	0.462
MD	–	–	−7.231(5.920)	0.236	−16.449(35.142)	0.645	19.608(65.352)	0.767
CBF	–	–	−0.885(0.350)	0.021[a]	1.734(2.212)	0.443	−3.869(3.978)	0.344

NIHSS, National Institute of Health Stroke Scale; mRS, Modified ranking scale; β(SE), Estimated coefficient from mixed-effects model (Standard Error); χ, Iron induced susceptibilities; FA, Fractional Anisotropy; MD, Mean Diffusivity; CBF, Cerebral Blood Flow.

[a]*statistically significant at 0.05 level.*

Correlation Between Imaging Matrices and Clinical Assessment

Both hematoma and perihematomal volume was significantly associated ($p < 0.01$) with initial but not later mRS scores. A negative association between perihematomal volume and FA ($p < 0.01$) and hematoma volume with CBF ($p < 0.05$) was found in that particular ROI. The susceptibilities in the perihematoma were significantly ($p < 0.01$) correlated with the NIHSS. There was no significant association between clinical assessments and imaging matrices over time. All the correlations between the imaging matrices and clinical scores are summarized in **Table 2**.

DISCUSSION

In this multimodal, serial quantitative MRI pilot study, we assessed long-term microstructural and physiological changes in the perihematomal and hematomal tissues of ICH patients. Hematoma and perihematomal volumes are a strong prognostic tool for patients with acute ICH; however, we have a poor understanding of the long-term changes in the brain after the initial injury. In addition, neurological impairments persist months to years afterward, despite a significant reduction in hematoma and perihematomal volume.

Acute evaluation of the pathological changes in intracerebral hematomas is challenging with MRI. The red blood cell lysis changes the heme iron oxidation state resulting in oxyhemoglobin changing to deoxyhemoglobin, which further converts to methemoglobin, which then leads to hemosiderin. These molecular changes affect MR contrast, making it very challenging to accurately measure hematoma volume in the acute to subacute phase (28). In this study, we add pilot quantitative information on localized changes within the hematoma and perihematomal tissue between the sub-acute to the chronic phase. The GRE MR imaging sequence is considered the gold standard for ICH diagnosis and hematoma volume measurements, but it is known for overestimating the hematoma volume due to blooming artifacts. In addition, it relies on image acquisition protocol making it difficult to reliably estimate the hematoma volume. Susceptibility-weighted imaging (SWI) maximizes the susceptibility sensitivity by using a high-pass filter of phase image, creating a mask to the magnitude image, long echo time, and 3D flow compensated gradient to overcome the artifact. However, both GRE and SWI rely on echo time, SWI is qualitative and encounters artifact due to dipole effect of phase signal. QSM computes susceptibility distribution in the phase component of MR signal. The variation in susceptibility leads to a change in phase signal which can be calculated (23). The serial hematoma volume measurements showed that the hematoma did not fully resolve at 12 M, given the detection of positive susceptibility due to the presence of aggregated paramagnetic iron molecules in the form of hemosiderin. Previously, in a serial study, Sun et al. showed a direct correlation between CT and QSM hematoma volume measurements (29). Concordant with the previous report, our data also show a decrease in hematoma susceptibility between the subacute (1 M) to the chronic stage (3 M) (29, 30). In the perihematomal region, the decrease in negative susceptibility at 1 M suggests an increase in diamagnetic substances, such as water, protein, cerebrospinal fluid (CSF) etc., as compared to the contralesional side. Several animal studies reported diffused iron toxicity to the neighboring perihematomal tissues (31). Contrary to the literature, our data show a decrease in susceptibilities, suggesting either there was no diffused iron in the surrounding tissues or our methods lacked the required sensitivity. Another possible explanation is an increase in diamagnetic water molecules, which could be diluting the iron content in the perihematomal area. The minimal reduction in hematoma volume and susceptibilities between 3 and 12 M suggest that iron remains localized and no significant reduction in volume occurred beyond 3 M. Analogous to animal studies (32), QSM data also showed signal intensity heterogeneity within the hematoma, suggesting the non-uniform distribution of aggregated free iron. This signal heterogeneity could be due to the restricted movement of iron molecules accumulating in

certain regions of the hematoma, suggesting the presence of intact tissue (33). This heterogeneity within hematoma volume creates variation in the MRI signal; therefore, very high standard deviations in the χ measurement were found.

As compared to the contralesional tissues, both the hematoma and perihematomal regions exhibited a reduction in FA at 1 M, indicating an increase in isotropic diffusion, indicative of changes in microstructural tissue architecture. The decrease in perihematomal FA is in line with previously published reports in acute and subacute stages (34). However, both regions showed a FA regain at 12 M, suggesting reversible changes. We postulate that the FA changes in the hematoma and perihematomal ROIs could be the results of two different molecular phenomena which can be supported by the mean diffusivity changes. Mathematically, FA and MD are inversely related as shown in the perihematomal regions where ipsilesional FA is relatively lower, and MD is higher than at the contralesional side. However, this is not the case in the hematoma region where both FA and MD decreased at 1 M as compared to the contralesional side. We speculate the MD decrease in the hematoma at 1 M is due to the presence of cellular debris in the region which restricts the movement of water molecules in the area. Over time, the debris is cleared resulting in an increase in MD in the hematomal region. Furthermore, a continual increase in MD in the hematomal region suggests possible tissue loss, and increasing regional extracellular fluid or possibly CSF, which will be verified by measuring longitudinal relaxation time in future studies. A serial study by Knight et al. reported a similar pattern of change in MD within hematoma over 3 months (35). An increase of FA in both the perihematomal and hematoma regions between the first two imaging time points suggests an increase in restricted diffusion, which could be due to microstructural restoration or an increase in regional cellular debris. However, a negative association between perihematomal ($p < 0.01$) and hematoma ($p = 0.083$) volume with FA is most likely due to improvement in microstructural integrity. No change in FA between 3 and 12 months suggests there is no microstructural repair beyond 3 M.

Previously, both human and animal studies have linked mechanical tissue compression by the hematoma and perihematoma to compromise capillary blood flow and possibly the creation of ischemic environments in the acute setting of ICH (36–38). As compared to the contralesional ROI, our data showed a significant decrease in CBF in both regions. Several previous studies reported post-ICH perihematomal CBF declines between acute to sub-chronic stages (39–42). The temporal reduction in CBF probably occurred before our first measurement, suggesting the decrease in CBF occurred in the acute phase or it may vary with ICH location, size, and amount of tissue pressure by the expansion or it could be a result of aggressive hypertension management in the acute phase (43). However, our data also showed a gradual increase in CBF in both regions starting at 1 M after injury, suggesting a change in supply and demand which could be due to cellular function. The non-uniform increase in the CBF maps in each region suggests that not all tissues within the perihematoma or hematoma were damaged. The rise in CBF may also reflect tissue repair or capillary sprouting by reorganization over time.

We identified imaging characteristics that correlated with clinical scores in this study. However, the NIHSS and mRS may not be appropriate to detect clinical changes over 1 year. Using domain-specific endpoints may be more appropriate in further studies. Another interesting observation was that three out of four patients with acute midline-shift developed Wallerian degeneration. The MRI findings of WD depend on the stage of the axonal injury process. In the first few weeks after the brain insult, no appreciable imaging abnormalities can be seen; however, as early as 5 weeks after the injury, the white matter (WM) tracts arising from the injured brain tissue demonstrate a slightly increased T1w signal and low T2w signal due to accelerated axonal breakdown with relative sparing of the lipid-containing structures. The imaging findings of WD become more evident after 3 months after the insult when the T1w signal intensity drops, and the T2w-based sequences show a significant increase in signal intensity as a reflection of myelin lipid breakdown and settling gliosis. These findings ultimately progress into volume loss, which is easily picked up visually by comparing symmetry.

Our study has a number of limitations. As a pilot study, the sample size was small with wide variability in hematoma size and location. On the other hand, this study provides detailed and repeated assessments on a number of imaging endpoints over 1 year, not been reported previously. We found important, dynamic, structural, and physiological changes occur over time within the hematoma and perihematomal areas. The changes may have important clinical implications to better understand the chronic and persistent neurological impairments of patients with ICH. A lack of repair in the chronic setting may underlie persistent impairments. The findings help to build new hypotheses and thus merit larger studies to identify extended treatment time windows or specific therapies that could modify these changes in the subacute to chronic phase to ultimately promote better recovery of specific clinical impairments in ICH patients. Finally, since most of our patient population had a hypertensive etiology, we will also need to study the generalizability of our findings and assess differential long-term changes based on ICH etiology.

In conclusion, we present novel data on the longitudinal changes that occur within the hematoma and perihematomal areas in the brain over 1 year in patients with ICH. We find active, persistent, and long-term microstructural and physiological changes that require further research in larger observational studies.

DATA AVAILABILITY STATEMENT

The raw data supporting the conclusions of this article will be made available by the authors, without undue reservation.

ETHICS STATEMENT

The studies involving human participants were reviewed and approved by Institutional Review Board of the University of Texas Health Sciences Center at Houston and by the Memorial

Hermann Hospital Office of Research. The patients/participants provided their written informed consent to participate in this study.

AUTHOR CONTRIBUTIONS

MH: concept and design, data analysis and interpretation, and writing manuscript. SB: data analysis and created figures. OA: radiological assessment and data analysis. RG: statistical analyses. SG and MP: clinical and neurological assessment. XZ and JA: manuscript writing. SS: financial support, data interpretation, writing, and final approval of the manuscript. All authors contributed to the article and approved the submitted version.

ACKNOWLEDGMENTS

The authors thank Mr. Vipulkumar Patel for his help with MRI experiments.

REFERENCES

1. Poon MT, Fonville AF, Al-Shahi Salman R. Long-term prognosis after intracerebral hemorrhage: systematic review and meta-analysis. *J Neurol Neurosurg Psychiatry*. (2014) 85:660–7. doi: 10.1136/jnnp-2013-306476
2. Feigin VL, Krishnamurthi RV, Parmar P, Norrving B, Mensah GA, Bennett DA, et al. Update on the Global Burden of Ischemic and Hemorrhagic Stroke in 1990-2013: The GBD 2013 Study. *Neuroepidemiology*. (2015) 45:161–76. doi: 10.1159/000441085
3. Truelsen T, Krarup LH, Iversen HK, Mensah GA, Feigin VL, Sposato LA, et al. Causes of death data in the global burden of disease estimates for ischemic and hemorrhagic stroke. *Neuroepidemiology*. (2015) 45:152–60. doi: 10.1159/000441084
4. Thrift AG, Thayabaranathan T, Howard G, Howard VJ, Rothwell PM, Feigin VL, et al. Global stroke statistics. *Int J Stroke*. (2017) 12:13–32. doi: 10.1177/1747493016676285
5. Wagner KR, Sharp FR, Ardizzone TD, Lu A, Clark JF. Heme and iron metabolism: role in cerebral hemorrhage. *J Cereb Blood Flow Metab*. (2003) 23:629–52. doi: 10.1097/01.WCB.0000073905.87928.6D
6. Aronowski J, Hall CE. New horizons for primary intracerebral hemorrhage treatment: experience from preclinical studies. *Neurol Res*. (2005) 27:268–79. doi: 10.1179/016164105X25225
7. Cherubini A, Ruggiero C, Polidori MC, Mecocci P. Potential markers of oxidative stress in stroke. *Free Radic Biol Med*. (2005) 39:841–52. doi: 10.1016/j.freeradbiomed.2005.06.025
8. Seo JW, Jones SM, Hostetter TA, Iliff JJ, West GA. Methamphetamine induces the release of endothelin. *J Neurosci Res*. (2016) 94:170–8. doi: 10.1002/jnr.23697
9. Zille M, Karuppagounder SS, Chen Y, Gough PJ, Bertin J, Finger J, et al. Neuronal death after hemorrhagic stroke *in vitro* and *in vivo* shares features of ferroptosis and necroptosis. *Stroke*. (2017) 48:1033–43. doi: 10.1161/STROKEAHA.116.015609
10. Bernstein JE, Savla P, Dong F, Zampella B, Wiginton JGT, Miulli DE, et al. Inflammatory markers and severity of intracerebral hemorrhage. *Cureus*. (2018) 10:e3529. doi: 10.7759/cureus.3529
11. Wilkinson DA, Pandey AS, Thompson BG, Keep RF, Hua Y, Xi G. Injury mechanisms in acute intracerebral hemorrhage. *Neuropharmacology*. (2018) 134:240–8. doi: 10.1016/j.neuropharm.2017.09.033
12. Zhao X, Sun G, Zhang J, Strong R, Song W, Gonzales N, et al. Hematoma resolution as a target for intracerebral hemorrhage treatment: role for peroxisome proliferator-activated receptor gamma in microglia/macrophages. *Ann Neurol*. (2007) 61:352–62. doi: 10.1002/ana.21097
13. Wu H, Zhang Z, Hu X, Zhao R, Song Y, Ban X, et al. Dynamic changes of inflammatory markers in brain after hemorrhagic stroke in humans: a postmortem study. *Brain Res*. (2010) 1342:111–7. doi: 10.1016/j.brainres.2010.04.033
14. Yang C, Hawkins KE, Dor,é S, Candelario-Jalil E. Neuroinflammatory mechanisms of blood-brain barrier damage in ischemic stroke. *Am J Physiol Cell Physiol*. (2019) 316:C135–53. doi: 10.1152/ajpcell.00136.2018
15. Hakimi R, Garg A. Imaging of hemorrhagic stroke. *Continuum*. (2016) 22:1424–50. doi: 10.1212/CON.0000000000000377
16. Cordonnier C, Demchuk A, Ziai W, Anderson CS. Intracerebral hemorrhage: current approaches to acute management. *Lancet*. (2018) 392:1257–68. doi: 10.1016/S0140-6736(18)31878-6
17. Morales H. Pitfalls in the imaging interpretation of intracranial hemorrhage. *Semin Ultrasound CT MR*. (2018) 39:457–68. doi: 10.1053/j.sult.2018.07.001
18. Brott T, Adams HP Jr, Olinger CP, Marler JR, Barsan WG, Biller J, et al. Measurements of acute cerebral infarction: a clinical examination scale. *Stroke*. (1989) 20:864–70. doi: 10.1161/01.STR.20.7.864
19. Van Swieten JC, Koudstaal PJ, Visser MC, Schouten HJ, Van Gijn J. Interobserver agreement for the assessment of handicap in stroke patients. *Stroke*. (1988) 19:604–7. doi: 10.1161/01.STR.19.5.604
20. Wilson JT, Hareendran A, Hendry A, Potter J, Bone I, Muir KW. Reliability of the modified Rankin Scale across multiple raters: benefits of a structured interview. *Stroke*. (2005) 36:777–81. doi: 10.1161/01.STR.0000157596.13234.95
21. Liu C, Li W, Tong KA, Yeom KW, Kuzminski S. Susceptibility-weighted imaging and quantitative susceptibility mapping in the brain. *J Magn Reson Imaging*. (2015) 42:23–41. doi: 10.1002/jmri.24768
22. Schweser F, Deistung A, Reichenbach JR. Foundations of MRI phase imaging and processing for quantitative susceptibility mapping (QSM). *Z Med Phys*. (2016) 26:6–34. doi: 10.1016/j.zemedi.2015.10.002
23. Ruetten PPR, Gillard JH, Graves MJ. Introduction to quantitative susceptibility mapping and susceptibility weighted imaging. *Br J Radiol*. (2019) 92:20181016. doi: 10.1259/bjr.20181016
24. Basser PJ, Mattiello J, Lebihan D. Estimation of the effective self-diffusion tensor from the NMR spin echo. *J Magn Reson B*. (1994) 103:247–54. doi: 10.1006/jmrb.1994.1037
25. Le Bihan D, Mangin JF, Poupon C, Clark CA, Pappata S, Molko N, et al. Diffusion tensor imaging: concepts and applications. *J Magn Reson Imaging*. (2001) 13:534–46. doi: 10.1002/jmri.1076
26. Detre JA, Zhang W, Roberts DA, Silva AC, Williams DS, Grandis DJ, et al. Tissue specific perfusion imaging using arterial spin labeling. *NMR Biomed*. (1994) 7:75–82. doi: 10.1002/nbm.1940070112
27. Williams DS. Quantitative perfusion imaging using arterial spin labeling. *Methods Mol Med*. (2006) 124:151–73. doi: 10.1385/1-59745-010-3:151
28. Parizel PM, Makkat S, Van Miert E, Van Goethem JW, Van Den Hauwe L, Schepper D, et al. Intracranial hemorrhage: principles of CT and MRI interpretation. *Eur Radiol*. (2001) 11:1770–83. doi: 10.1007/s003300000800
29. Sun H, Klahr AC, Kate M, Gioia LC, Emery DJ, Butcher KS, et al. Quantitative susceptibility mapping for following intracranial hemorrhage. *Radiology*. (2018) 288:830–9. doi: 10.1148/radiol.2018171918
30. Chang S, Zhang J, Liu T, Tsiouris AJ, Shou J, Nguyen T, et al. Quantitative susceptibility mapping of intracerebral hemorrhages at various stages. *J Magn Reson Imaging*. (2016) 44:420–5. doi: 10.1002/jmri.25143
31. Perez De La O. Iron-related brain damage in patients with intracerebral hemorrhage. *Stroke*. (2010) 41:810–3. doi: 10.1161/STROKEAHA.109.570168
32. Haque ME, Gabr RE, Zhao X, Hasan KM, Valenzuela A, Narayana PA, et al. Serial quantitative neuroimaging of iron in the intracerebral hemorrhage pig model. *J Cereb Blood Flow Metab*. (2018) 38:375–81. doi: 10.1177/0271678X17751548
33. Zhang D, Chen J, Guo J, Jiang Y, Dong Y, Ping-Chi Chen B, et al. Hematoma heterogeneity on noncontrast computed tomography predicts intracerebral hematoma expansion: a meta-analysis. *World Neurosurg*. (2018) 114:e663–76. doi: 10.1016/j.wneu.2018.03.048
34. Mccourt R, Misaghi E, Tu W, Kate M, Gioia L, Treit S, et al. Peri-hematoma corticospinal tract integrity in intracerebral hemorrhage

patients: a diffusion-tensor imaging study. *J Neurol Sci.* (2021) 421:117317. doi: 10.1016/j.jns.2021.117317
35. Knight RA, Nagaraja TN, Li L, Jiang Q, Tundo K, Chopp M, et al. A prospective safety trial of atorvastatin treatment to assess rebleeding after spontaneous intracerebral hemorrhage: a serial MRI investigation. *Austin J Cerebrovasc Dis Stroke.* (2016) 3:1043.
36. Zhao X, Wang Y, Wang C, Li S, Yang Z. Quantitative evaluation for secondary injury to perihematoma of hypertensive cerebral hemorrhage by functional MR and correlation analysis with ischemic factors. *Neurol Res.* (2006) 28:66–70. doi: 10.1179/016164106X91898
37. Chieregato A, Tanfani A, Noto A, Fronza S, Cocciolo F, Fainardi E. Cerebral blood flow thresholds predicting new hypoattenuation areas due to macrovascular ischemia during the acute phase of severe and complicated aneurysmal subarachnoid hemorrhage. *A preliminary study Acta Neurochir Suppl.* (2008) 102:311–6. doi: 10.1007/978-3-211-85578-2_59
38. Fainardi E, Borrelli M, Saletti A, Schivalocchi R, Azzini C, Cavallo M, et al. CT perfusion mapping of hemodynamic disturbances associated to acute spontaneous intracerebral hemorrhage. *Neuroradiology.* (2008) 50:729–40. doi: 10.1007/s00234-008-0402-x
39. Zazulia AR, Diringer MN, Videen TO, Adams RE, Yundt K. Aiyagari Jr, et al. Hypoperfusion without ischemia surrounding acute intracerebral hemorrhage. *J Cereb Blood Flow Metab.* (2001) 21:804–10. doi: 10.1097/00004647-200107000-00005
40. Tiebosch IA, Van Den Bergh WM, Bouts MJ, Zwartbol R, Van Der Toorn A, Dijkhuizen RM. Progression of brain lesions in relation to hyperperfusion from subacute to chronic stages after experimental subarachnoid hemorrhage: a multiparametric MRI study. *Cerebrovasc Dis.* (2013) 36:167–72. doi: 10.1159/000352048
41. Yin L, Cheng S, Xiao J, Zhu Y, Bu S, Zhang X, et al. (2018) 3D. pseudocontinuous arterial spin-labeling perfusion imaging detected crossed cerebellar diaschisis in acute, subacute and chronic intracerebral hemorrhage. *Clin Imaging* 50, 37–42. doi: 10.1016/j.clinimag.2017.12.007
42. Morotti A, Busto G, Bernardoni A, Leuci E, Casetta I, Fainardi E. Comparison of perihematomal perfusion in deep and lobar intracerebral hemorrhage. *Neuroradiology.* (2020) 62:257–61. doi: 10.1007/s00234-019-02331-9
43. Shah QA, Ezzeddine MA, Qureshi AI. Acute hypertension in intracerebral hemorrhage: pathophysiology and treatment. *J Neurol Sci.* (2007) 261:74–9. doi: 10.1016/j.jns.2007.04.036

Conflict of Interest: The authors declare that the research was conducted in the absence of any commercial or financial relationships that could be construed as a potential conflict of interest.

Publisher's Note: All claims expressed in this article are solely those of the authors and do not necessarily represent those of their affiliated organizations, or those of the publisher, the editors and the reviewers. Any product that may be evaluated in this article, or claim that may be made by its manufacturer, is not guaranteed or endorsed by the publisher.

frontiers in Neurology

ORIGINAL RESEARCH
published: 06 December 2021
doi: 10.3389/fneur.2021.735771

Higher Cerebral Blood Flow Predicts Early Hematoma Expansion in Patients With Intracerebral Hemorrhage: A Clinical Study

Weijing Wang [1,2,3†], Weitao Jin [4†], Hao Feng [1,5,6], Guoliang Wu [7], Wenjuan Wang [1,5,6], Jiaokun Jia [1,5,6], Ruijun Ji [1,5,6], Anxin Wang [1] and Xingquan Zhao [1,5,6]*

[1] Department of Neurology, Beijing Tiantan Hospital, Capital Medical University, Beijing, China, [2] Department of Neurology, Beijing Haidian Hospital, Beijing, China, [3] Department of Neurology, Haidian Section of Peking University Third Hospital, Beijing, China, [4] Department of Neurosurgery, Peking University International Hospital, Beijing, China, [5] China National Clinical Research Center for Neurological Diseases, Beijing, China, [6] Research Unit of Artificial Intelligence in Cerebrovascular Disease, Chinese Academy of Medical Sciences, Beijing, China, [7] Department of Radiology, Beijing Tiantan Hospital, Capital Medical University, Beijing, China

The early hematoma expansion of intracerebral hemorrhage (ICH) indicates a poor prognosis. This paper studies the relationship between cerebral blood flow (CBF) around the hematoma and hematoma expansion (HE) in the acute stage of intracerebral hemorrhage. A total of 50 patients with supratentorial cerebral hemorrhage were enrolled in this study. They underwent baseline whole-brain CTP within 6 h after intracerebral hemorrhage, and non-contrast CT within 24 h. Absolute hematoma growth and relative hematoma growth were calculated, respectively. A relative growth of Hematoma volume >33% was considered to be hematoma expansion. The Ipsilateral peri-edema CBF and Ipsilateral edema CBF were calculated by CTP maps in patients with and without hematoma expansion, respectively. In this study the incidence of hematoma expansion in the early stage of supratentorial cerebral hemorrhage was 32%; The CBF of the hematoma expansion group was higher than that of the patients without hematoma expansion (23.5 ± 12.5 vs. 15.1 ± 7.4, $P = 0.004$). After adjusting for age, gender, Symptom onset to NCCT and Baseline hematoma volume, ipsilateral peri-edema CBF was still an independent risk factor for early HE (or = 1.095, 95% CI = 1.01–1.19, $P = 0.024$). Here, we concluded that higher cerebral blood flow predicts early hematoma expansion in patients with intracerebral hemorrhage.

Keywords: intracerebral hemorrhage, hematoma expansion, cerebral blood flow (CBF), CT perfusion (CTP), prognosis

OPEN ACCESS

Edited by:
Devin William McBride, University of Texas Health Science Center at Houston, United States

Reviewed by:
Mehmet Akif Topçuoglu, Hacettepe University, Turkey
Xin-Ni Lv, First Affiliated Hospital of Chongqing Medical University, China

****Correspondence:***
Xingquan Zhao
zxq@vip.163.com

†These authors share first authorship

Specialty section:
This article was submitted to Stroke, a section of the journal Frontiers in Neurology

Received: *03 July 2021*
Accepted: *03 November 2021*
Published: *06 December 2021*

Citation:
Wang W, Jin W, Feng H, Wu G, Wang W, Jia J, Ji R, Wang A and Zhao X (2021) Higher Cerebral Blood Flow Predicts Early Hematoma Expansion in Patients With Intracerebral Hemorrhage: A Clinical Study. Front. Neurol. 12:735771. doi: 10.3389/fneur.2021.735771

INTRODUCTION

Acute spontaneous (non-traumatic) intracerebral hemorrhage is the most common type of spontaneous intracerebral hemorrhage. It affects about 2 million people around the world every year and exhibits the worst prognosis of all stroke types (1). The burden of hemorrhagic stroke is increasing rapidly worldwide between 1990 and 2010, with an increase of 47% in the absolute number of people with incident hemorrhagic stroke, 20% in deaths, and 14% in DALYs (1).

Intracerebral hemorrhage (ICH) expansion occurs in about one-third of ICH patients and is strongly associated with a poor outcome (2, 3).

Several imaging signs on non-contrast CT may be related to the hematoma expansion and poor prognosis after intracerebral hemorrhage (4–8). The spot sign on CT angiography also received attention as an indicator of the hematoma expansion (9). However, the interpretation of those signs in the CT relies on the clinical experience of neuroradiologists, and the standard of that interpretation is not objective and cannot be evaluated quantitatively.

In our study, CBF was used as a quantitative method to calculate the cerebral blood flow of edematous tissue around a hematoma and its surrounding tissue after early hemorrhage, so as to study the correlation between the cerebral blood flow and the hematoma expansion.

METHODS

Study Design and Population Eligibility

This study was a prospective, observational cohort study. From December 2014 to September 2016 patients who presented with an acute symptomatic and CT confirmed ICH were recruited to the study. Patients aged 18 years or older were eligible for entry. NCCT was performed in 215 patients who had acute symptoms (severe headache, paralysis, aphasia etc.). 184 patients were confirmed supratentorial intracerebral hemorrhage. 50 of them finished CTP within 6 hours and NCCT review within 24 hours after the symptoms attack. Therefore, 50 patients are included in this study (**Figure 1**).

Inclusion criteria: (1) age > 18 years, (2) within 6 h of onset, (3) NCCT + CTA + CTP at baseline, (4) NCCT reexamination within 24 h of onset, (5) informed consent. Exclusion criteria: (1) failure to cooperate with the completion of imaging examination (refusal of examination or sensitization of imaging agent), (2) planned or completed surgical craniotomy or hematoma aspiration, (3) refusal to join the study.

Sources of Funding

This study was sponsored by Capital health research and development of special (grant number: Capital 2011–2004-03; institute: Beijing Municipal Commission of Health and Family Planning; the author who received the funding: XZ) and the Beijing Municipal Science & Technology Commission, PR China (grant number: Z131107002213009).

Image Acquisition

All participants were scanned on a 16-slice multidetector CT (Somatom volume zoom; Siemens, Erlangen, Germany). Whole-brain NCCT was performed first with a slice thickness of 9 mm for the supratentorial area and 4.5 mm for the infratentorial area to confirm primary ICH. Acquisition parameters were: 120 kVp; 310 mA; and field of view (FOV) = 24 cm (10).

CTP covering two continuous sections at the level across the maximum transverse section of the hematoma lesion was performed. The scanning parameters were: tube current = 80 kVp; 209 mA; rotation time¼ 1.0 s/rotation; total scan time 40 s; section thickness = 12 mm; and 40 images per section. CTP was started 4 s after injection of a bolus of 40 ml of iobitridol (300 mg/mL, Xenetix; Guerbet, Aulnay-sous-Bois, France) at a rate of 8 mL/s into the antecubital vein (with a 20-gauge intravenous

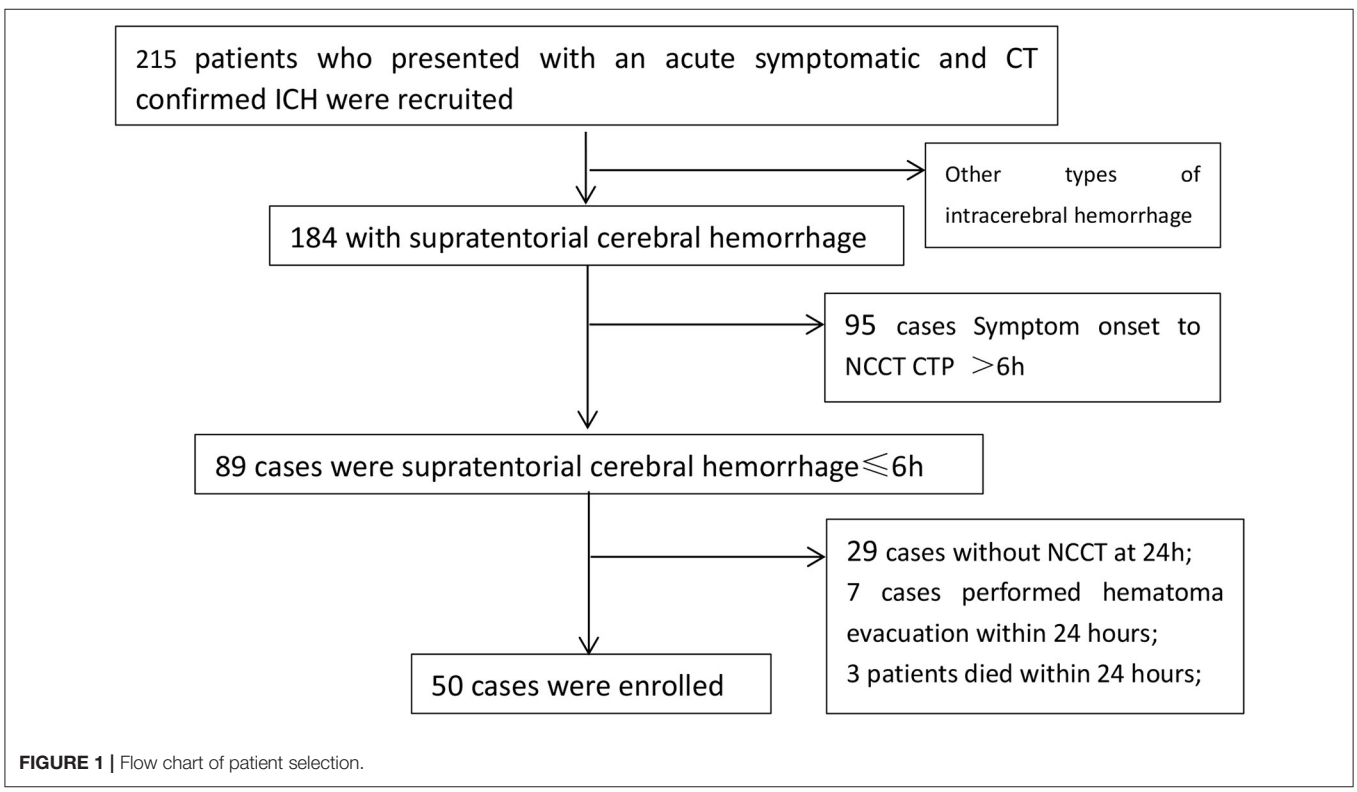

FIGURE 1 | Flow chart of patient selection.

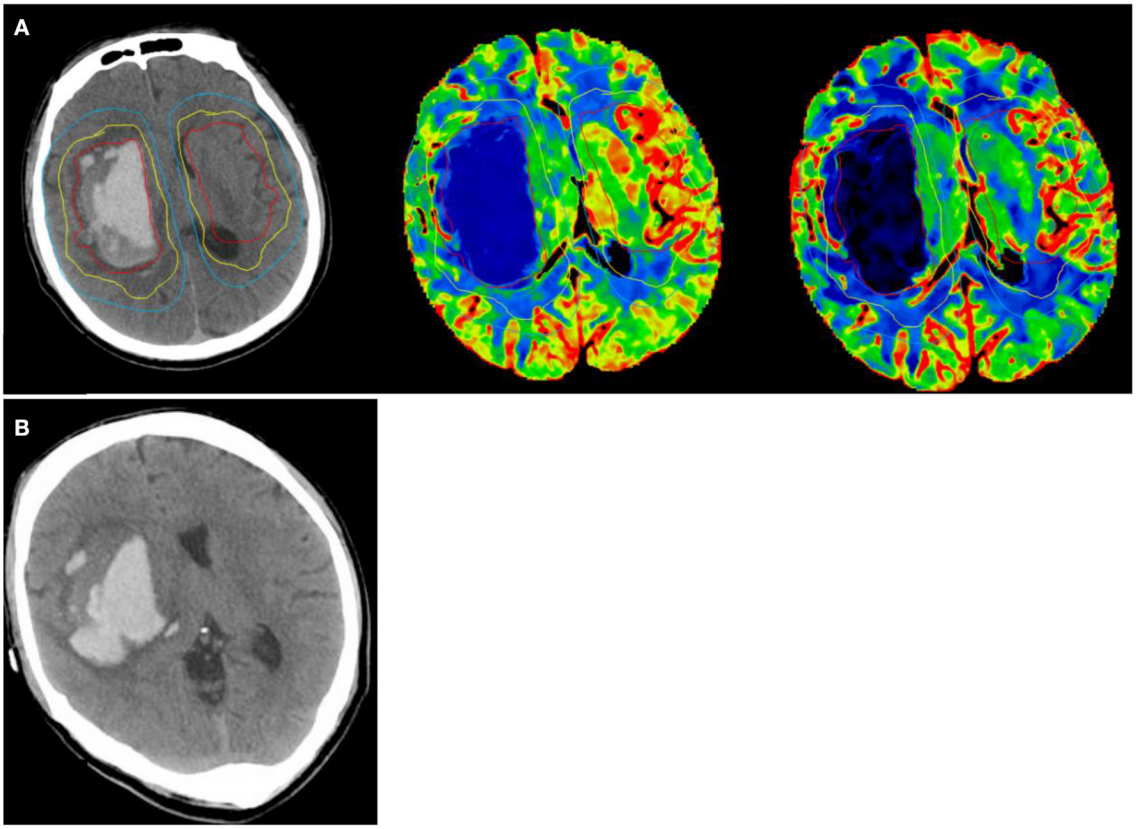

FIGURE 2 | A 42 year old man with a sudden headache and loss of consciousness, NCCT shows hematoma volume 49.5 ml at randomization. Ipsilateral peri-edema CBF was 30.48 ml/100 g/min at randomization. **(A)** (1) perihematomal low-density area in the yellow circle as Ipsilateral edema area; (2) an area mirroring the Ipsilateral edema area located in the contralateral hemisphere as Contralateral edema area; (3) 1 cm rim of normal-appearing brain tissue surrounding the perilesional low-density area in the blue circle as Ipsilateral peri-edema area; (4) an area mirroring the Ipsilateral peri-edema area located in the contralateral hemisphere as Contralateral peri-edema area. **(B)** NCCT at 24 h after symptom onset shows hematoma volume was 69.14 ml.

cannula) using a power injector. The effective radiation dose was 3.51 mSv for one-time scanning (10).

All patients were followed up with NCCT using the same CT system and parameters 24 h after the onset of the disease to evaluate whether the hematoma expanded.

Image Analysis

Hematoma volumes were calculated at baseline and at follow-up NCCT images using the method as follows: Hematoma volumes were defined using semiautomated Hounsfield Unit thresholding. Edema volumes were measured using a threshold of 5 to 23 Hounsfield Units, which has been demonstrated to be the most reliable CT Hounsfield Unit threshold for edema (11, 12).

Absolute ICH growth (follow-up volume–baseline volume) and relative ICH growth ([follow-up volume–baseline volume]/baseline volume) were calculated, respectively. A relative hematoma increase growth >33% was considered to indicate significant hematoma expansion (13). Post-processing of raw CTP source images was completed centrally on a GE aw workstation. CTP maps were derived from the tissue time–density curve and contrast bolus delay and dispersion were corrected for using a singular value deconvolution algorithm. Region of interest (ROI) analyses were completed using the Analyze 11.0 software package (13). As previously reported (14), ROIs were drawn using planimetric techniques on CTP base images and then transferred to the corresponding CBF, CBV, MTT maps. ROIs included the edema, a 1-cm region surrounding the edema, contralateral mirror regions (**Figure 2**). Image post-processing was completed by an experienced neuroradiologist and then reviewed by a chief radiologist independently.

Statistical Analysis

Statistical analysis was performed using SPSS 21.0 (SPSS Inc, Chicago, IL). Comparison of baseline mean characteristics between the 2 groups was made using independent *t*-tests, Mann–Whitney tests, or Pearson χ^2-tests. The relationships between hematoma expansion and CBF were assessed using Logistic regression. Paired *t*-tests were used to assess CBF differences between different parts. The influence of different

TABLE 1 | Baseline characteristics.

	Total $N = 50$	Without hematoma expansion, $N = 34$	With hematoma expansion*, $N = 16$	p
Age, mean ± SD	50.8 ± 13.4	51.9 ± 2.3	48.6 ± 3.50	0.42
Gender, Male, *n* (%)	34 (68.0)	22 (64.7)	12 (75.0)	0.47
Time from symptom onset to randomization, h, mean ± SD	3.3 ± 1.6	3.2 ± 1.6	3.4 ± 1.6	0.72
Time from symptom onset to NCCT, h, mean ± SD	3.6 ± 1.5	3.5 ± 0.3	3.9 ± 0.4	0.48
Medical history				
Hypertension, *n* (%)	29 (58.0)	1 (55.9)	10 (62.5)	0.66
Diabetes, *n* (%)	9 (18.0)	6 (17.7)	3 (18.8)	0.93
Ischemic stroke, *n* (%)	5 (10.0)	3 (8.8)	2 (12.5)	0.69
Previous ICH, *n* (%)	3 (6.0)	2 (5.9)	1 (6.3)	0.96
Clinical characteristics				
mRS score before onset, ≤1, *n* (%)	49 (98.0)	34 (100.0)	15 (93.8)	0.18
BMI, median (IQR)	24.6 (22.7–26.8)	25.3 (22.8–27.6)	24.2 (22.3–26.1)	0.35
Systolic BP, mmHg, mean ± SD	169.8 ± 23.8	166.1 ± 4.3	177.5 ± 5.2	0.12
Diastolic BP, mmHg, mean ± SD	99.7 ± 16.6	97.2 ± 2.8	104.7 ± 4.1	0.14
Heart rate, bpm, mean ± SD	77.8 ± 11.2	76.1 ± 11.8	81.1 ± 9.3	0.16
NIHSS score, mean ± SD	9.1 ± 6.3	9.1 ± 1.1	9.2 ± 1.5	0.96
GCS score, median (IQR)	14.0 (13.0–15.0)	14.0 (12.8–15.0)	14.0 (14.0–15.0)	0.33
Hematoma				
Lobar, *n* (%)	12 (24.0)	8 (23.5)	4 (25.0)	0.91
Deep, *n* (%)	38 (76.0)	26 (76.5)	12 (75.0)	0.91
Baseline hematoma volume, ml, mean ± SD	24.7 ± 22.0	26.3 ± 22.6	21.5 ± 21.2	0.48
24 h-Hematoma volume, ml, median (IQR)	24.6 (9.1–45.7)	21.1 (8.5–41.9)	29.81 (10.4–52.8)	0.28
Edema				
Baseline edema volume, ml, median (IQR)	15.2 (9.3–23.9)	14.0 (7.4–23.9)	16.8 (10.0–24.9)	0.51
24 h-Edema volume, ml, median (IQR)	20.2 (10.6–31.3)	19.9 (11.8–31.3)	20.2 (10.0–32.1)	0.97
Cerebral blood flow				
Ipsilateral edema CBF, ml/100 g/min, mean ± SD	11.8 ± 6.6	12.3 ± 6.8	10.7 ± 6.3	0.42
Ipsilateral peri-edema CBF, ml/100 g/min, mean ± SD	17.8 ± 10.0	15.1 ± 7.4	23.5 ± 12.5	0.004
Cerebral blood volume				
Ipsilateral edema CBV, ml/100 g, mean ± SD	1.5 ± 0.7	1.5 ± 0.7	1.4 ± 0.7	0.60
Ipsilateral peri-edema CBV, ml/100 g, mean ± SD	1.9 ± 0.9	1.8 ± 0.9	2.1 ± 0.8	0.17
Mean transit time				
Ipsilateral edema MTT, s, mean ± SD	10.4 ± 3.4	10.3 ± 3.5	10.6 ± 3.5	0.80
Ipsilateral peri-edema MTT, s, mean ± SD	8.6 ± 2.8	9.1 ± 2.8	7.6 ± 2.7	0.095
Laboratory				
WBC, 10 ^ 9/L, mean ± SD	9.4 ± 3.8	9.6 ± 3.7	9.1 ± 3.9	0.67
PLT, 10 ^ 9/L, mean ± SD	218.1 ± 56.6	223.9 ± 10.6	205.6 ± 10.7	0.29
INR, mean ± SD	0.9 ± 0.1	0.9 ± 0.0	0.9 ± 0.0	0.68
Fbg, ug/ml, mean ± SD	2.5 ± 0.6	2.6 ± 0.5	2.5 ± 0.8	0.47
APTT, sec, mean ± SD	26.2 ± 3.9	25.8 ± 3.4	26.9 ± 4.9	0.39
Glu, mmol/L, mean ± SD	7.5 ± 2.6	7.6 ± 0.5	7.3 ± 0.6	0.68
Crea, umol/L, mean ± SD	61.2 ± 10.9	62.1 ± 2.0	59.7 ± 2.6	0.52
Bun, mmol/L, mean ± SD	5.1 ± 1.4	5.2 ± 1.2	4.9 ± 1.7	0.58
Total cholesterol, mmol/L, mean ± SD	4.7 ± 1.0	4.5 ± 1.0	4.9 ± 1.0	0.34
Triglyceride, mmol/L, mean ± SD	1.5 ± 1.3	1.5 ± 1.5	1.6 ± 0.4	0.84
HDL, mmol/L, mean ± SD	1.3 ± 0.4	1.3 ± 0.5	1.3 ± 0.4	0.97
LDL, mmol/L, mean ± SD	2.8 ± 0.9	2.8 ± 0.9	2.9 ± 0.9	0.63
Clinical outcomes				
NIHSS 24, mean ± SD	8.5 ± 6.1	8.6 ± 1.0	8.2 ± 1.5	0.83
GCS 24, median (IQR)	14.0 (14.0–15.0)	14.0 (12.8–15.0)	14.5 (14.0–15.0)	0.44

*****Hematoma expansion defined as an absolute increase in hematoma >12.5 ml or relative growth >33%.*

TABLE 2 | CBF in different location.

	Ipsilateral edema CBF, ml/100 g/min	Ipsilateral peri-edema CBF, ml/100 g/min	*p*
Total, $n = 50$	11.80 ± 6.64	17.83 ± 10.01	0.001
Without hematoma expansion, $n = 34$	12.33 ± 6.81	15.14 ± 7.40	0.099
With hematoma expansion*, $n = 16$	10.67 ± 6.33	23.54 ± 12.48	0.002

**Hematoma expansion defined as an relative increase in hematoma >33%.*

sites and CBF on hematoma expansion was evaluated by the method of interaction analysis.

RESULTS

Baseline Characteristics

A total of 50 patients were included in the study (Baseline characteristics shown in **Table 1**). The study population included 34 (68.0%) males and 16 (32.0%) females with an average age of 50.8 years. The baseline demographic and clinical cohort characteristics are described in **Table 1**. The median time from symptom onset to baseline CT scan was 3.6 ± 1.5 h, The median baseline hematoma volume was 24.7 ± 22.0 ml. 16 patients (32%) showed early hematoma expansion. All patients completed CT Perfusion at baseline. There was a difference between the two groups in the CBF of the peri-edema area. (CBF on the peri-edema area of patients with hematoma expansion was 23.5 ml/100 g/min; CBF on the peri-edema area of patients without hematoma expansion was 15.1 ml/100 g/min; *p*-value 0.004).

CBF in Different Locations

The mean Ipsilateral edema CBF was 11.8 ± 6.6 ml/100 g/min. The mean Ipsilateral peri-edema CBF was 17.8 ± 10.0 ml/100 g/min. The Ipsilateral peri-edema CBF was higher than Ipsilateral edema CBF (17.8 ± 10.0 ml/100 g/min vs. 11.8 ± 6.6 ml/100 g/min, $p = 0.001$) in all groups, the Ipsilateral peri-edema CBF was higher than Ipsilateral edema CBF (15.1 ± 7.4 ml/100 g/min vs. 12.3 ± 6.8 ml/100 g/min, $p = 0.099$) in patients without hematoma expansion group, and the Ipsilateral peri-edema CBF was higher than Ipsilateral edema CBF (23.5 ± 12.5 ml/100 g/min vs. 10.7 ± 6.3 ml/100 g/min, $p = 0.099$) in patients with hematoma expansion group (**Table 2**).

Multivariate Analysis of Hematoma Expansion

Univariate analysis showed that Ipsilateral peri-edema CBF was a risk factor for early hematoma expansion (OR = 1.10, 95% CI 1.02–1.19, $P = 0.014$). Model 1 included covariates with $p < 0.20$ in univariable analysis. Model 2 adjusted for age and sex. Model 3 adjusted for age, sex, and predictors of hemorrhage growth identified from the literature such as time from onset to NCCT and ICH volume. Multivariate analysis showed that Ipsilateral peri-edema CBF was an independent risk factor for hematoma expansion (**Table 3**).

TABLE 3 | Multivariate analysis of hematoma expansion.

		OR	OR (95% CI)	*p*
Model 1	SBP	1.009	0.971–1.048	0.655
	DBP	1.031	0.973–1.092	0.303
	Ipsilateral peri-edema CBF	1.101	1.022–1.185	0.011
Model 2	SBP	1.013	0.973–1.054	0.541
	DBP	1.030	0.971–1.092	0.330
	Ipsilateral peri-edema CBF	1.260	1.022–1.544	0.031
	Ipsilateral peri-edema CBV	0.288	0.050–1.661	0.164
	Ipsilateral peri-edema MTT	1.336	0.859–2.079	0.199
Model 3	Age	1.010	0.953–1.070	0.749
	Gender (male)	2.569	0.446–14.799	0.291
	SBP	1.011	0.970–1.054	0.595
	DBP	1.033	0.972–1.099	0.296
	Ipsilateral peri-edema CBF	1.091	1.011–1.178	0.025
Model 4	Age	1.010	0.949–1.075	0.754
	Gender (male)	4.447	0.556–35.543	0.159
	SBP	1.017	0.974–1.061	0.452
	DBP	1.032	0.970–1.098	0.315
	Ipsilateral peri-edema CBF	1.095	1.012–1.185	0.024
	Contralateral peri-edema CBF	1.031	0.949–1.120	0.476
	Symptom onset to NCCT (h)	1.293	0.754–2.216	0.350
	Baseline hematoma volume (ml)	0.983	0.945–1.021	0.370

Model 1: unadjusted.
Model 2: Adjusted CBV and MTT.
Model 3: Adjusted age and gender.
Model 4: Adjusted age, gender, Symptom onset to NCCT, and Baseline hematoma volume.

DISCUSSION

The incidence of hematoma expansion in the early stage of supratentorial intracerebral hemorrhage is 32% in this study. Hematoma expansion was defined as a 33% increase in hematoma volume compared with baseline (13), which is consistent with the results Brott et al. (15) reported in the previous literature of about 38%. However, due to the disunity of the definitional standard of hematoma expansion, the incidence of hematoma expansion reported in the relevant studies is quite different. The longer the difference between the first CT and the reexamination CT is, the closer the first CT is to the onset time, and the incidence of hematoma expansion is correspondingly increased. In 1990, Fujitsu et al. (16) studied 107 patients with intracerebral hemorrhage within 6 h of onset, rescanned NCCT within 24 h, and found that the incidence of hematoma expansion was about 20.3%; Mayer et al. (17) observed 46 patients with intracerebral hemorrhage within 11 h of onset, and the hematoma expansion rate was only 9%.

In recent years, some clinical studies have focused on the relationship between hematoma expansion and prognosis. Some results have revealed the relationship between hematoma expansion and poor prognosis. Davis et al. (18) in a 2006 meta-analysis showed that hematoma volume increased by 10%, mortality increased by 5%.

However, the pathophysiological mechanism of hematoma expansion is still unclear. Further study on the pathophysiological mechanism of hematoma expansion and the cerebral blood flow around the hematoma is helpful to clarify the causes of hematoma expansion, so as to provide targeted prevention and treatment and improve the prognosis.

This study showed the CBF of ipsilateral peri-edema was higher than that of edema CBF, suggesting that after cerebral hemorrhage, the edema was hypoperfusion, and there was an area of hyperperfusion around the edema. Using single-photon emission computed tomography (SPECT), Mayer et al. (19) demonstrated depressed perfusion surrounding the hemorrhage and concluded that the restoration of perilesional blood flow in the early stage of ICH resulted from perihematoma cerebral edema formation. Zhou et al. (20) found that a gradient of hypoperfusion surrounding the hematoma, which showed a thin rim of reduced perfusion in the perilesional zone in rCBF maps. In addition to perilesional hyperperfusion, the local hyperemia can also be observed in the regions distant from the hematoma, even in the cortical regions of the uninvolved hemisphere. The hyperemia often results from the vasodilation of pia arteries and arterioles in the periphery of the injury zone (19), as efforts are made to restore blood flow in the regions of reduced perfusion after ICH onset. The unstable blood flow perfusion occurring in perilesional tissue and remote brain may, on the one hand, reflect the exhaustion of autoregulation of CBF correlated with ICH, and on the other hand, predict that the secondary brain injury will occur in the related cerebral tissue.

Intracerebral hemorrhage is a dynamic, complex, and continuous process. Hematoma expansion occurs in the early stage of intracerebral hemorrhage. The hematoma expansion comes from blood pressure. The higher the blood pressure is, the more likely the hematoma to expand. There are two reasons why the hematoma is no longer enlarged. One is the spontaneous hemostasis mechanism after vascular rupture; the other is that the pressure inside and outside the ruptured blood vessel wall is reduced due to the pressure increase in the hematoma cavity caused by edema compression. Therefore, the study of edema area and surrounding tissue is helpful to understand the pathophysiological mechanism of hematoma expansion.

On the other hand, some imaging signs can also indicate the occurrence of hematoma expansion. The most classic is the "spot sign" (9). A spot sign is defined as one or more 1- to 2-mm foci of enhancement within the hematoma on CTA source images, which is the exudation point of contrast inside the hematoma. The occurrence of spot signs indicates an increased risk of hematoma expansion. The spot signs indicated that the enlargement of the hematoma was caused by the internal part of the hematoma.

However, some researchers have found that island sign can also indicate the risk of hematoma expansion (8). Island sign is the irregular edge of hematoma, suggesting the occurrence of hematoma expansion, which is caused by the fact that some relatively normal tissues outside the hematoma also become hemorrhagic brain tissue.

This study showed that there were blood flow changes in the peripheral tissue of hematoma. The higher the CBF of the tissue at the far side of the edema, the more likely the hematoma to expand, suggesting that the hematoma expansion may start from the outside.

However, the exact pathophysiological mechanism of hematoma expansion remains to be confirmed, for patients with ICH who have completed CTP examination in the early stage of admission, the measurement of ipsilateral peri edema CBF can be used as a supplementary prediction tool.

STUDY LIMITATION

In our study, due to the strict limitations of timing and sequence of imaging examination, only 50 patients met the inclusion criteria, and more than 150 patients were excluded, which may have resulted in a selective bias. On the other hand, the patients who underwent NCCT and CTP at baseline and reviewed NCCT 24 h usually need to be in a relatively stable condition, and so for the patients with a large or deadly hemorrhage, whether the conclusion is still applicable is not clear. This study found that the relative increased rCBF between the peri-hematoma region and the contralateral region related with the hemorrhage expansion, but the increase of the CBF in peri-hematoma region did not show a similar result. This could be due to an interference caused by the treatments such as lowering the blood pressure or use of mannitol. These treatments could reduce the CBF of both sides, but the different vascular reactivity between the tissues surrounding the hematoma and the contralateral side made the range of decrease different, and then impacted on the result. However, this assumption still requires further study to be confirmed.

CONCLUSION

Higher cerebral blood flow predicts early hematoma expansion in patients with intracerebral hemorrhage.

DATA AVAILABILITY STATEMENT

The original contributions presented in the study are included in the article/supplementary material, further inquiries can be directed to the corresponding author/s.

ETHICS STATEMENT

The studies involving human participants were reviewed and approved by Ethics Committee of Tiantan Hospital. The patients/participants provided their written informed consent to participate in this study.

AUTHOR CONTRIBUTIONS

WeiW and XZ contributed to the conception and design of the study. WenW and JJ organized the database. HF and GW performed the statistical analysis. WeiW and WJ wrote the first draft of the manuscript. RJ and AW revised the manuscript. All authors contributed to manuscript revision, read, and approved the submitted version.

FUNDING

This study was sponsored by Capital Health Research and Development of Special (Grant No. Capital 2011-2004-03; Institute: Beijing Municipal Commission of Health and Family Planning; the author who received the funding: XZ) and the Beijing Municipal Science & Technology Commission, PR China (Grant No. Z131107002213009).

REFERENCES

1. Krishnamurthi RV, Feigin VL, Forouzanfar MH, Mensah GA, Connor M, Bennett DA, et al. Global and regional burden of first-ever ischaemic and haemorrhagic stroke during 1990-2010: findings from the global burden of disease study 2010. *Lancet Glob Health.* (2013) 1:e259–81. doi: 10.1016/S2214-109X(13)70089-5
2. Dowlatshahi D, Demchuk AM, Flaherty ML, Ali M, Lyden PL, Smith EE. Defining hematoma expansion in intracerebral hemorrhage: relationship with patient outcomes. *Neurology.* (2011) 76:1238–44. doi: 10.1212/WNL.0b013e3182143317
3. Steiner T, Bösel J. Options to restrict hematoma expansion after spontaneous intracerebral hemorrhage. *Stroke.* (2010) 4::402–9. doi: 10.1161/STROKEAHA.109.552919
4. Barras CD, Tress BM, Christensen S, MacGregor L, Collins M, Desmond PM, et al. Density and shape as CT predictors of intracerebral hemorrhage growth. *Stroke.* (2009) 40:1325–31. doi: 10.1161/STROKEAHA.108.536888
5. Blacquiere D, Demchuk AM, Al-Hazzaa M, Deshpande A, Petrcich W, Aviv RI, et al. Intracerebral hematoma morphologic appearance on noncontrast computed tomography predicts significant hematoma expansion. *Stroke.* (2015) 46:3111–6. doi: 10.1161/STROKEAHA.115.010566
6. Li Q, Zhang G, Huang YJ, Dong MX, Lv FJ, Wei X, et al. Blend sign on computed tomography: novel and reliable predictor for early hematoma growth in patients with intracerebral hemorrhage. *Stroke.* (2015) 46:2119–23. doi: 10.1161/STROKEAHA.115.009185
7. Li Q, Zhang G, Huang YJ, Dong MX, Lv FJ, Wei X, et al. Black hole sign: novel imaging marker that predicts hematoma growth in patients with intracerebral hemorrhage. *Stroke.* (2016) 47:1777–81. doi: 10.1161/STROKEAHA.116.013186
8. Li Q, Zhang G, Huang YJ, Dong MX, Lv FJ, Wei X, et al. Island sign: an imaging predictor for early hematoma expansion and poor outcome in patients with intracerebral hemorrhage. *Stroke.* (2017) 48:3019–25. doi: 10.1161/STROKEAHA.117.017985
9. Wada R, Aviv RI, Fox AJ, Sahlas DJ, Gladstone DJ, Tomlinson G, et al. CT angiography "spot sign" predicts hematoma expansion in acute intracerebral hemorrhage. *Stroke.* (2007) 38:1257–62. doi: 10.1161/01.STR.0000259633.59404.f3
10. Fu F, Sui B, Liu L, Su Y, Sun S, Li Y. Quantitative assessment of local perfusion change in acute intracerebral hemorrhage areas with and without "dynamic spot sign" using CT perfusion imaging. *Acta Radiol.* (2019) 60:367–73. doi: 10.1177/0284185118780893
11. McCourt R, Gould B, Gioia L, Kate M, Coutts SB, Dowlatshahi D, et al. Cerebral perfusion and blood pressure do not affect perihematoma edema growth in acute intracerebral hemorrhage. *Stroke.* (2014) 45:1292–8. doi: 10.1161/STROKEAHA.113.003194
12. Clasen RA, Huckman MS, Von Roenn KA, Pandolfi S, Laing I, Lobick JJ. A correlative study of computed tomography and histology in human and experimental vasogenic cerebral edema. *J Comput Assist Tomogr.* (1981) 5:313–27. doi: 10.1097/00004728-198106000-00001
13. Kazui S, Naritomi H, Yamamoto H, Sawada T, Yamaguchi T. Enlargement of spontaneous intracerebral hemorrhage. Incidence and time course. *Stroke.* (1996) 27:1783–7. doi: 10.1161/01.STR.27.10.1783
14. Fainardi E, Borrelli M, Saletti A, Schivalocchi R, Azzini C, Cavallo M, et al. CT perfusion mapping of hemodynamic disturbances associated to acute spontaneous intracerebral hemorrhage. *Neuroradiology.* (2008) 50:729–40. doi: 10.1007/s00234-008-0402-x
15. Brott T, Broderick J, Kothari R, Barsan W, Tomsick T, Sauerbeck L, et al. Early hemorrhage growth in patients with intracerebral hemorrhage. *Stroke.* (1997) 28:1–5. doi: 10.1161/01.STR.28.1.1
16. Egila AA, Khodair RM, Faheem MK, Kasem SM. Hematoma expansion in spontaneous intracerebral hemorrhage. *J neurosurg.* (1994) 80:51–7. doi: 10.3171/jns.1994.80.1.0051
17. Fujitsu K, Muramoto M, Ikeda Y, Inada Y, Kim I, Kuwabara T. Indications for surgical treatment of putaminal hemorrhage. *Journal of Neurosurgery.* (2009) 73:518–25. doi: 10.3171/jns.1990.73.4.0518
18. Davis SM, Broderick J, Hennerici M, Brun NC, Diringer MN, Mayer SA, et al. Hematoma growth is a determinant of mortality and poor outcome after intracerebral hemorrhage. *Neurology.* (2006) 66:1175–81. doi: 10.1212/01.wnl.0000208408.98482.99
19. Mayer SA, Lignelli A, Fink ME, Kessler DB, Thomas CE, Swarup R, et al. Perilesional blood flow and edema formation in acute intracerebral hemorrhage: a SPECT study. *Stroke.* (1998) 29:1791–8. doi: 10.1161/01.STR.29.9.1791
20. Zhou J, Zhang H, Gao P, Lin Y, Li X. Assessment of perihematomal hypoperfusion injury in subacute and chronic intracerebral hemorrhage by CT perfusion imaging. *Neurol Res.* (2010) 32:642–9. doi: 10.1179/016164109X12445616596328

Conflict of Interest: The authors declare that the research was conducted in the absence of any commercial or financial relationships that could be construed as a potential conflict of interest.

Publisher's Note: All claims expressed in this article are solely those of the authors and do not necessarily represent those of their affiliated organizations, or those of the publisher, the editors and the reviewers. Any product that may be evaluated in this article, or claim that may be made by its manufacturer, is not guaranteed or endorsed by the publisher.

frontiers in Neurology

ORIGINAL RESEARCH
published: 03 January 2022
doi: 10.3389/fneur.2021.763471

Lower Body Temperature Independently Predicts Delayed Cerebral Infarction in the Elderly With Ruptured Intracranial Aneurysm

Hui Lin[1†], *Haojie Wang*[2†], *Yawen Xu*[2†], *Zhangya Lin*[2†], *Dezhi Kang*[2,3,4†], *Shufa Zheng*[2*] and *Peisen Yao*[2*]

[1] Department of Emergency, The First Affiliated Hospital, Fujian Medical University, Fuzhou, China, [2] Department of Neurosurgery, Neurosurgery Research Institute, The First Affiliated Hospital, Fujian Medical University, Fuzhou, China, [3] Fujian Key Laboratory of Precision Medicine for Cancer, The First Affiliated Hospital, Fujian Medical University, Fuzhou, China, [4] Key Laboratory of Radiation Biology of Fujian Higher Education Institutions, The First Affiliated Hospital, Fujian Medical University, Fuzhou, China

OPEN ACCESS

Edited by:
Qin Hu,
Shanghai Jiao Tong University, China

Reviewed by:
Zhen-Ni Guo,
First Affiliated Hospital of Jilin University, China
Jinwei Pang,
The Affiliated Hospital of Southwest Medical University, China

***Correspondence:**
Shufa Zheng
zsf2002110@163.com
Peisen Yao
peisen.yao@163.com

[†] These authors have contributed equally to this work and share first authorship

Specialty section:
This article was submitted to Stroke, a section of the journal Frontiers in Neurology

Received: 24 August 2021
Accepted: 03 December 2021
Published: 03 January 2022

Citation:
Lin H, Wang H, Xu Y, Lin Z, Kang D, Zheng S and Yao P (2022) Lower Body Temperature Independently Predicts Delayed Cerebral Infarction in the Elderly With Ruptured Intracranial Aneurysm. Front. Neurol. 12:763471. doi: 10.3389/fneur.2021.763471

Purpose: To assess the correlation between admission body temperature and delayed cerebral infarction in elderly patients with ruptured intracranial aneurysm (IA).

Methods: Patients with ruptured IA diagnosed between 2012 and 2020 were retrospectively analyzed. Patients were divided into a non-infarction and an infarction group based on the presence of cerebral infarction after treatment. The demographic and clinical information of the patients was gathered. Outcomes at the 3-month follow-up were assessed using the modified Rankin Scale. Correlation between admission body temperature and cerebral infarction was assessed using Spearman's rank correlation coefficient. A receiver operating characteristic (ROC) curve was used to assess the specificity and sensitivity of admission body temperature to predict cerebral infarction.

Results: A total of 426 patients (142 men and 284 women) with ruptured IA were enrolled. Elderly patients with cerebral infarction (12.4%) had a lower body temperature at admission ($p < 0.001$), higher prevalence of hypertension and diabetes ($p = 0.051$ and $p = 0.092$, respectively), and higher rate of poor outcomes ($p < 0.001$). Admission body temperature was independently associated with cerebral infarction (odds ratio [OR] = 5.469, $p < 0.001$); however, hypertension (OR = 0.542, $p = 0.056$), diabetes (OR = 0.750, $p = 0.465$), and aneurysm size (OR = 0.959, $p = 0.060$) showed no association. An inverse correlation between admission body temperature and the incidence of cerebral infarction was observed (Spearman's $r = -0.195$, $p < 0.001$). An admission body temperature of 36.6°C was able to distinguish infarction and non-infarction patients. The area under the ROC curve was 0.669 (specificity, 64.15%; sensitivity, 81.50%; $p < 0.001$).

Conclusions: Lower body temperature at admission (≤36.6°C) is an independent predictor of delayed cerebral infarction in elderly patients who have undergone treatment for ruptured IA. Therefore, it could be a risk factor for adverse outcomes of IA.

Keywords: cerebral infarction, intracranial aneurysm, risk factor, diabetes, hypertension, body temperature

INTRODUCTION

Cerebral infarction following intracranial aneurysm (IA) rupture is a significant cause of unfavorable clinical outcomes (1). Several studies have shown that cerebral infarction is worsened by hyperthermia and alleviated by hypothermia (2–4). Particularly, it has been shown that hyperthermia is a predictor of in-hospital mortality and negatively affects 1-year survival probability for ischemic stroke but not 1-year mortality for hemorrhagic stroke (5, 6). Although it has been suggested that low body temperature is therapeutic, as it slows down the cerebral artery flow velocity leading to low perfusion pressure (7), this, in turn, may increase blood viscosity, promote erythrocyte aggregation and platelet microemboli, activate leukocytes, and reduce microcirculatory blood flow (8), ultimately resulting in arterial infarction. This notion is supported by several reports, including that of Naess et al., who have reported that low body temperature is associated with neurological worsening in patients with lacunar infarction (9). Similarly, Kvistad et al. reported that hypothermia within 6 h of symptom onset is associated with more severe neurological damage in the early phase of stroke (10).

Therefore, whether hypothermia aggravates the neurological function of stroke patients or reduces the risk of cerebral infarction following aneurysmal subarachnoid hemorrhage (SAH) still remains unclear (11, 12). The relationship between body temperature and stroke is controversial, specifically in elderly patients with IA who have undergone clipping or coiling. In fact, no reports have examined this topic. Therefore, this study aimed to investigate the relationship between body temperature at admission and cerebral infarction in elderly patients with ruptured IA. To elucidate this, we retrospectively analyzed the different clinical outcomes of elderly patients with or without cerebral infarction following IA treatment.

MATERIALS AND METHODS

Patients

The Ethics Committee of the First Affiliated Hospital of Fujian Medical University approved the study and waived the requirement for written informed consent (approval number: MRCTA, ECFAH of FMU [2017] 079).

A total of 426 elderly patients with ruptured IA who underwent treatment between 2012 and 2020 were enrolled. The inclusion criteria were the following: (1) ruptured IA diagnosed by computed tomography angiography (CTA) and/or digital subtraction angiography (DSA) and (2) age ≥ 60 years. The exclusion criteria were the following: (1) prior

TABLE 1 | Characteristics of infarction and non-infarction groups.

Characteristics	Infarction group (Group I, $n = 53$)	Non-infarction group (Group II, $n = 373$)	*p*-value
Age(years)	66.64 ± 3.89	65.99 ± 5.19	0.377
Gender			0.177
Female	31 (58.5%)	253 (67.8%)	
Male	22 (41.5%)	120 (32.2%)	
Pulse	79.74 ± 14.14	77.23 ± 16.94	0.305
Body temperature (°C)	36.67 ± 0.38	36.89 ± 0.37	0.000
SBP, mmHg	144.08 ± 25.92	143.44 ± 24.87	0.862
DBP, mmHg	84.75 ± 11.73	82.07 ± 13.78	0.178
Hypertension			0.051
No	35 (66.1%)	193 (51.7%)	
Yes	18 (33.9%)	180 (48.3%)	
Diabetes			0.092
No	42 (79.2%)	327 (87.7%)	
Yes	11 (20.8%)	46 (12.3%)	
Hunt-Hess grade			0.228
Grade I	8 (15.1%)	64 (17.2%)	
Grade II	20 (37.7%)	137 (36.7%)	
Grade III	12 (22.6%)	118 (31.6%)	
Grade IV	10 (18.9%)	34 (9.1%)	
Grade V	3 (5.7%)	20 (5.4%)	
Fisher grade			0.646
Grade 0	10 (18.8%)	62 (16.6%)	
Grade 1	4 (7.5%)	49 (13.1%)	
Grade 2	14 (26.4%)	115 (30.8%)	
Grade 3	12 (22.6%)	64 (17.2%)	
Grade 4	13 (24.5%)	83 (22.3%)	
Aneurysm location			0.722
ACA	1 (1.9%)	19 (5.1%)	
ACoA	12 (22.6%)	91 (24.4%)	
ICA	11 (20.8%)	68 (18.2%)	
MCA	14 (26.4%)	71 (19.0%)	
PCoA	12 (22.6%)	98 (26.3%)	
others	3 (5.7%)	26 (7.0%)	
Aneurysm size	7.67 ± 6.93	6.12 ± 5.44	0.061
Treatment methods			0.591
Microsurgical clipping	41 (77.3%)	301 (80.7%)	

(Continued)

TABLE 1 | Continued

Characteristics	Infarction group (Group I, $n = 53$)	Non-infarction group (Group II, $n = 373$)	*p*-value
Endovascular coiling	5 (9.4%)	39 (10.5%)	
Conservative treatment	7 (13.2%)	33 (8.8%)	
Duration of temporary clip			0.847
0 min	8 (19.5%)	48 (15.9%)	
0–5 min	21 (51.2%)	174 (57.8%)	
5–10 min	8 (19.5%)	61 (20.3%)	
10–15 min	3 (7.3%)	14 (4.7%)	
>15 min	1 (2.4%)	4 (1.3%)	
Surgical time			0.972
<3days	28 (52.8%)	198 (53.1%)	
>3days	25 (47.2%)	175 (46.9%)	
Serum leukocyte count (*109/L)	9.81 ± 3.88	9.30 ± 3.99	0.380
Neutrophil	7.62 ± 3.79	8.76 ± 10.11	0.317
Lymphocyte	1.36 ± 0.64	1.43 ± 1.89	0.791
Hemoglobin, g/L	127.09 ± 14.24	124.66 ± 17.63	0.337
Coagulation parameters			
Prothrombin time(s)	11.86 ± 1.11	11.91 ± 0.75	0.686
Activated partial prothrombin time(s)	29.71 ± 6.06	29.46 ± 6.38	0.793
INR	0.98 ± 0.12	1.01 ± 0.10	0.162
Fib fibrinogen(g/l)	2.98 ± 0.96	3.17 ± 1.64	0.416
D-dimer (ug/mL)	2.48 ± 1.98	1.99 ± 2.15	0.201
Seasons			0.348
Spring (March–May)	13 (24.5%)	96 (25.7%)	
Summer (June–August)	9 (17.0%)	93 (24.9%)	
Autumn (September–November)	14 (26.4%)	102 (27.3%)	
Winter (December–February)	17 (32.1%)	82 (22.0%)	
mRS			0.000
0–2	36 (67.9%)	328 (87.9%)	
3–6	17 (32.1%)	45 (12.1%)	

history or presence of intracranial arteriovenous malformations, arteriovenous fistula, or moyamoya disease; (2) prior history of ischemic stroke; (3) presence of ongoing infections, such as pneumonia and sepsis; and (4) age < 60 years. Patients who developed delayed cerebral infarction during hospitalization were also enrolled.

Data Collection

The following demographic and clinical characteristics of patients with ruptured IA were gathered: age, sex, pulse rate, body temperature at admission (measured at the armpit), systolic blood pressure (SBP), diastolic blood pressure (DBP), medical history of hypertension and diabetes, Hunt-Hess (H-H) grade, Fisher grade, aneurysm location and size, treatment method, duration of temporary clipping (0, 0–5, 5–10, 10–15, >15 min), surgical time (duration between morbidity and surgery), laboratory data on admission (white blood cells, neutrophils, and lymphocytes), hemoglobin levels, coagulation parameters (prothrombin time, activated partial prothrombin time, international normalized ratio [INR], fibrinogen, D-dimer), season of admission (spring: March–May; summer: June–August; autumn: September–November; winter: December–February), and outcomes at the 3-month follow-up.

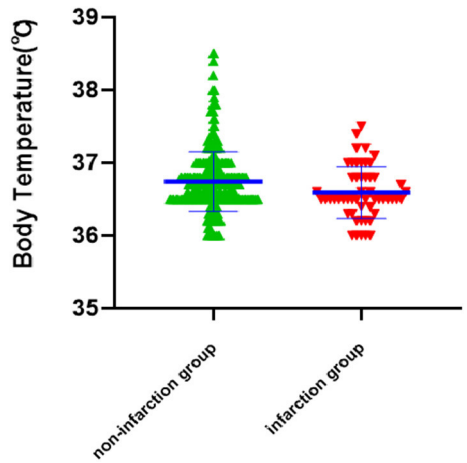

FIGURE 1 | The scatterplot graph for the correlation analysis of body temperature and cerebral infarction ($P < 0.001$).

Patient Treatment

Delayed cerebral infarction was diagnosed in the cases where new or worsening focal neurological deficits, such as hemiparesis, aphasia, or neglect, and decreased levels of consciousness were present. A decreased level of consciousness without focal neurological deficits was considered as a global or non-localized change. In the cases in which these critically ill patients were stable, computed tomography (CT) or magnetic resonance imaging (MRI) were performed. Specifically, in the cases in which CT scans could not detect delayed cerebral infarction, MRI was performed. The clinical symptom patterns of delayed cerebral infarction were also recorded, and the location of cerebral infarction was determined as previously described (13).

Treatment methods for IA included microsurgical clipping, endovascular coiling, or other conservative methods. Perioperative treatment was performed according to the Chinese guidelines for the management of aneurysmal SAH. All patients underwent CTA or DSA examination within 7 postoperative days to determine whether cerebral vasospasm or residual neck

TABLE 2 | Independent risk factors associated with cerebral infarction.

	Unadjusted			Adjusted		
Parameter	**OR**	**OR (95%CI)**	***P*-value**	**OR**	**OR (95%CI)**	***P*-value**
Body Temperature	5.561	2.272–13.611	0.000	5.469	2.202–13.581	0.000
Hypertension	0.551	0.302–1.008	0.053	0.542	0.289–1.015	0.056
Diabetes	0.537	0.258–1.117	0.096	0.750	0.347–1.623	0.465
Aneurysm size	0.961	0.921–1.003	0.066	0.959	0.917–1.002	0.060

aneurysm had occurred. The 3-month outcome was assessed using the modified Rankin Scale (mRS). Scores of 0–2 were considered as good outcomes, whereas scores of 3–6 indicated poor outcomes.

Data Analysis

Statistical analyses were performed using SPSS version 26.0 (IBM, Chicago, IL, USA). The homogeneity of variance was evaluated. Student's *t*-test or a one-way analysis of variance (ANOVA) was employed to compare continuous variables, while the chi-squared test (χ^2 test) or Fisher's exact test was utilized to evaluate qualitative variables. Variables that achieved a significance of $p < 0.10$ in the univariate analysis were employed in the multivariable analysis. The correlation between body temperature and cerebral infarction was assessed using Spearman's rank correlation coefficient. The difference in body temperature between the positive outcome group (mRS scores 0–2) and poor outcome group (mRS scores 3–6) was computed with the Mann–Whitney U test. Statistical significance was set at $p < 0.05$. A receiver operating characteristic (ROC) curve was used to assess the specificity and sensitivity of admission body temperature for predicting cerebral infarction in elderly patients with ruptured IA.

RESULTS

Demographic and Clinical Characteristics

The medical records of 426 patients (142 men and 284 women) with ruptured IA were retrospectively analyzed. Patients were divided into an infarction group ($n = 53$) or a non-infarction group ($n = 373$) based on the presence of cerebral infarction following IA treatment. **Table 1** summarizes the demographic and clinical data of the patients. The infarction group had a lower body temperature at admission (infarction vs. non-infarction: 36.67 ± 0.38°C vs. 36.89 ± 0.37; $p < 0.001$) (**Figure 1**), a lower prevalence of hypertension (33.9% vs. 48.3%; $p = 0.051$), a higher prevalence of diabetes (20.8% vs. 12.3%; $p = 0.092$), and a higher rate of poor outcomes (32.1% vs. 12.1%; $p < 0.001$). No other statistical differences in the analyzed variables were detected between the two groups ($p > 0.05$).

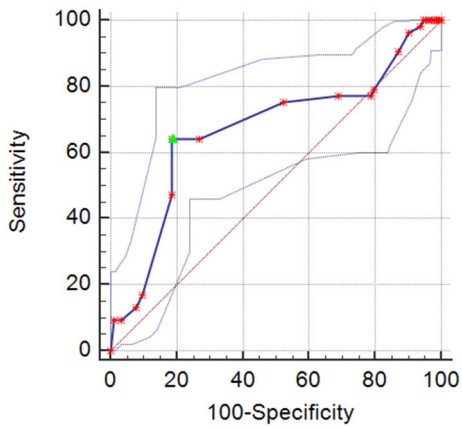

FIGURE 2 | The receiver operating characteristic (ROC) curve for the correlation between body temperature and the occurrence of cerebral infarction in elderly IA patients (the upper and lower dotted curves are the 95% confidence intervals), area under curve 0.669(95% confidence interval [CI], 0.622–0.714; $p < 0.001$). The cutoff = 36.6°C (sensitivity = 64.15%, specificity = 81.50%).

Correlation Between Admission Body Temperature and Cerebral Infarction

The results of the multivariable logistic regression analysis showed that admission body temperature was independently associated with cerebral infarction in elderly patients with IA (odds ratio [OR] = 5.469; 95% confidence interval [CI] = 2.202–13.581; $p < 0.001$). However, hypertension (OR = 0.542, 95% CI = 0.289–1.015; $p = 0.056$), diabetes (OR = 0.750, 95% CI: 0.347–1.623; $p = 0.465$), and aneurysm size (OR = 0.959, 95% CI = 0.917–1.002; $p = 0.060$) showed no correlation with cerebral infarction (**Table 2**). There was an inverse correlation between admission body temperature and the incidence of cerebral infarction (Spearman's $r = -0.195$, $p < 0.001$). **Figure 2** shows the ROC curve for the specificity and sensitivity of admission body temperature in predicting cerebral infarction. An admission body temperature of 36.6°C was able to distinguish infarction and non-infarction patients. The area under the ROC curve was 0.669 (specificity: 64.15%; sensitivity: 81.50%; $p < 0.001$) (**Figure 2**).

TABLE 3 | Clinical manifestations of delayed cerebral infarction according to the pattern in the infarction group.

Pattern of delayed cerebral infarction	Clinical manifestation			Total (*n*%)
	Asymptomatic (*n*%)	Focal neurological deficits (*n*%)	Global or non-localizing (*n*%)	
Single cortical	2 (3.8%)	12 (22.6%)	2 (3.8%)	16 (30.2%)
Single deep	6 (11.3%)	6 (11.3%)	5 (9.4%)	17 (32.1%)
Multiple cortical	1 (1.9%)	4 (7.5%)	5 (9.4%)	10 (18.9%)
Multiple deep	0 (0%)	1 (1.9%)	1 (1.9%)	2 (3.8%)
Multiple combined cortical and deep	0 (0%)	3 (5.7%)	5 (9.4%)	8 (15.1%)
Total	9 (17.0%)	26 (49.1%)	18 (33.9%)	53 (100.0%)

Hemiparesis, aphasia, or neglect was considered as focal neurological deficits. Decreased level of consciousness without focal neurological deficits was considered as global or non-localizing.

Relationship Between Clinical Manifestation and Imaging Findings

The relationship between the symptoms and imaging findings of patients with cerebral infarction is shown in **Table 3**. Clinical manifestations included symptomatic cerebral infarction ($n = 43$, 81.1%), focal neurological deficits ($n = 26$, 49.1%), and global or non-localized changes ($n = 17$, 32.1%). Cerebral infarctions involved single cortical ($n = 16$, 30.2%), single deep ($n = 16$, 30.2%), multiple cortical ($n = 10$, 18.9%), multiple deep ($n = 2$, 3.8%), and multiple combined cortical and deep territories ($n = 8$, 15.1%). Asymptomatic cerebral infarction frequently occurred in patients with single deep infarction. In addition, cerebral infarction more frequently involved a single cortical or a single deep territory.

DISCUSSION

In this study, we explored the association between admission body temperature and cerebral infarction in elderly patients with ruptured IA. Our results demonstrated that patients with cerebral infarction had a lower body temperature at admission, higher prevalence of hypertension and diabetes, and a higher rate of poor outcomes than patients without infarction. In addition, multivariate logistic regression analysis revealed that body temperature is independently associated with cerebral infarction, and a body temperature of 36.6°C is the optimal cutoff value to distinguish infarction and non-infarction patients.

Rupture of IAs is one of the most common causes of stroke and results in high mortality and increased risk of disability. Disturbances in normal brain metabolism are known to play a role in the prognosis of SAH (14), and several cerebral metabolites, including lactate (15) and pyruvate (16), are considered predictive biomarkers of aneurysmal SAH outcomes. Several reports showed that hypothermia is therapeutic, as it reduces intracranial pressure and improves functional recovery (7, 17), while hypometabolism could prevent or reduce secondary brain injury following SAH (18). It is possible that hypothermia suppresses brain metabolism and protects the brain tissue from potentially injurious conditions in which brain metabolism is disturbed. However, the detailed mechanism by which hypothermia exerts its protective effects on brain tissues remains unclear. Conversely, recent studies showed that moderate hypothermia might not be beneficial for stroke patients (19), as it did not reduce the likelihood of death or disability in patients with neonatal encephalopathy, but rather, it significantly increased the risk of death (20). Rahmig et al. (19) found that, in surgically treated patients with middle carotid artery (MCA) infarction, the risk of death was lower for individuals with high body temperature than for those with low body temperature. The discrepancies observed in the abovementioned findings may be explained by the fact that low body temperature and therapeutic hypothermia may be different conditions. In fact, the former is due to reduced heat production by the body, which can arise from any number of circumstances, while therapeutic or iatrogenic hypothermia is an externally controlled reduction in body temperature. Therefore, in cerebral ischemic conditions, the mechanisms underlying the response to therapeutic hypothermia and low body temperature might be different. However, such mechanisms remain unclear.

Evidence suggests that therapeutic hypothermia decreases cerebral artery flow velocity (7). Low body temperature could operate through this same mechanism. Low perfusion pressure may promote the ability of blood viscosity, red cell aggregation, platelet microemboli, and activated leucocytes to reduce microcirculatory blood flow (8), ultimately leading to artery infarction. This hypothesis is supported by the findings of Starnoni et al., who showed that delayed cerebral ischemia is associated with reduced cerebral blood flow (21). More importantly, the temporary blocking of the parent artery during cerebral aneurysm clipping is likely to aggravate the ischemic cerebral injury induced by decreased cerebral artery flow. In older adults, the observed low basal metabolic rate is also caused by low body temperature. Studies suggest that glucose hypometabolism might be an early risk factor for cerebral infarction (8), indicating that low temperature-induced hypometabolism could predict cerebral infarction in elderly patients with IA. However, the role of glucose hypometabolism needs to be further studied.

Our research has several limitations. This was a retrospective study with a small sample size, and relevant metabolic factors, such as the basal metabolic rate, were not included. In addition, our study solely focuses on patients with ruptured IA; thus, our results cannot be generalized to cases of unruptured IA. Further research with a larger sample size is needed to conducted subgroup analyses and understand the specific mechanisms of action of hypothermia and low body temperature. In conclusion, lower admission body temperature ($\leq$36.6°C) is an independent predictor of delayed cerebral infarction and therefore could be a risk factor for adverse outcomes in elderly patients with ruptured IA.

DATA AVAILABILITY STATEMENT

The original contributions presented in the study are included in the article/supplementary material, further inquiries can be directed to the corresponding author/s.

ETHICS STATEMENT

The studies involving human participants were reviewed and approved by the Ethics Committee of the First Affiliated Hospital of Fujian Medical University. Written informed consent for participation was not required for this study in accordance with the national legislation and the institutional requirements.

AUTHOR CONTRIBUTIONS

HL, HW, YX, and ZL: acquisition of data and critical revision of manuscript for intellectual content. DK, SZ, and PY: study concept and design. SZ and PY: analysis and interpretation of data and study supervision. All authors contributed to the article and approved the submitted version.

FUNDING

This work was supported by key Clinical Specialty Discipline Construction Program of Fujian, P.R.C, major project of Fujian Provincial Department of Science and Technology (No. 2014YZ0003 and No. 2014YZ01 to DK), the Young and Middle-aged Backbone Key Research Project of National Health and Family Planning Commission of Fujian Province (No. 2017-ZQN-46 to PY), Natural Science Funding of Fujian Province (No. 2018J01175 to PY and No. 2018J01176 to SZ) and Natural Science Funding of China (No. 81802492 to PY).

REFERENCES

1. Ayling OG, Ibrahim GM, Alotaibi NM, Gooderham PA. Macdonald RL.Dissociation of early and delayed cerebral infarction after aneurysmal subarachnoid hemorrhage. *Stroke.* (2016) 47:2945–51. doi: 10.1161/STROKEAHA.116.014794
2. Reith J, Jorgensen HS, Pedersen PM, Nakayama H, Raaschou HO, Jeppesen LL, et al.Body temperature in acute stroke:relation to stroke severity, infarct size, mortality, and outcome. *Lancet.* (1996) 347:422–5. doi: 10.1016/S0140-6736(96)90008-2
3. Jorgensen HS, Reith J, Pedersen PM, Nakayama H. Olsen TS. Body temperature and outcome in stroke patients. *Lancet.* (1996) 348:193. doi: 10.1016/S0140-6736(05)66135-1
4. Naess H, Idicula T, Lagallo N, Brogger J, Waje-Andreassen U. Thomassen L. Inverse relationship of baseline body temperature and outcome between ischemic stroke patients treated and not treated with thrombolysis: the Bergen stroke study. *Acta Neurol Scand.* (2010) 122:414–7. doi: 10.1111/j.1600-0404.2010.01331.x
5. Wang Y, Lim LL, Levi C, Heller RF. Fisher J. Influence of admission body temperature on stroke mortality. *Stroke.* (2000) 31:404–9. doi: 10.1161/01.STR.31.2.404
6. Kammersgaard LP, Jorgensen HS, Rungby JA, Reith J, Nakayama H, Weber UJ, et al. Admission body temperature predicts long-term mortality after acute stroke: the copenhagen stroke study. *Stroke.* (2002) 33:1759–62. doi: 10.1161/01.STR.0000019910.90280.F1
7. Seule M, Muroi C, Sikorski C, Hugelshofer M, Winkler K. Keller E. Therapeutic hypothermia reduces middle cerebral artery flow velocity in patients with severe aneurysmal subarachnoid hemorrhage. *Neurocrit Care.* (2014) 20:255–62. doi: 10.1007/s12028-013-9927-x
8. Martin A, Rojas S, Pareto D, Santalucia T, Millan O, Abasolo I, et al. Depressed glucose consumption at reperfusion following brain ischemia does not correlate with mitochondrial dysfunction and development of infarction: an *in vivo* positron emission tomography study. *Curr Neurovasc Res.* (2009) 6:82–8. doi: 10.2174/156720209788185650
9. Naess H, Thomassen L, Waje-Andreassen U, Glad S. Kvistad CE. High risk of early neurological worsening of lacunar infarction. *Acta Neurol Scand.* (2019) 139:143–49. doi: 10.1111/ane.13029
10. Kvistad CE, Thomassen L, Waje-Andreassen U. Naess H. Low body temperature associated with severe ischemic stroke within 6 hours of onset: the bergen norstroke study. *Vasc Health Risk Manag.* (2012) 8:333–8.
11. Todd MM, Hindman BJ, Clarke WR, Torner JC, Weeks JB, Bayman EO, et al. Perioperative fever and outcome in surgical patients with aneurysmal subarachnoid hemorrhage. *Neurosurgery.* (2009) 64:897–908. doi: 10.1227/01.NEU.0000341903.11527.2F
12. D'Souza S.Aneurysmal subarachnoid hemorrhage. *J Neurosurg Anesthesiol.* (2015) 27:222–40. doi: 10.1097/ANA.0000000000000130
13. Rabinstein AA, Weigand S, Atkinson JL. Wijdicks EF.Patterns of cerebral infarction in aneurysmal subarachnoid hemorrhage. *Stroke.* (2005) 36:992–7. doi: 10.1161/01.STR.0000163090.59350.5a
14. Zahra K, Gopal N, Freeman WD, Turnbull MT.Using Cerebral metabolites to guide precision medicine for subarachnoid hemorrhage:lactate and pyruvate. *Metabolites.* (2019) 9:10.3390/metabo9110245. doi: 10.3390/metabo9110245
15. Poblete RA, Cen SY, Zheng L, Emanuel BA. Serum lactic acid following aneurysmal subarachnoid hemorrhage is a marker of disease severity but is not associated with hospital outcomes. *Front Neurol.* (2018) 9:593. doi: 10.3389/fneur.2018.00593
16. Patet C, Quintard H, Zerlauth JB, Maibach T, Carteron L, Suys T, et al. Bedside cerebral microdialysis monitoring of delayed cerebral hypoperfusion in comatose patients with poor grade aneurysmal subarachnoid haemorrhage. *J Neurol Neurosurg Psychiatry.* (2017) 88:332–38. doi: 10.1136/jnnp-2016-313766
17. Torok E, Klopotowski M, Trabold R, Thal SC, Plesnila N, Scholler K. Mild hypothermia (33 degrees C) reduces intracranial hypertension and improves functional outcome after subarachnoid hemorrhage in rats. *Neurosurgery.* (2009) 65:352–9. doi: 10.1227/01.NEU.0000345632.09882.FF

18. Dearden NM.Mechanisms and prevention of secondary brain damage during intensive care. *Clin Neuropathol*. (1998) 17:221-8.
19. Rahmig J, Kuhn M, Neugebauer H, Juttler E, Reichmann H. Schneider H. Normothermia after decompressive surgery for space-occupying middle cerebral artery infarction:a protocol-based approach. *BMC Neurol.* (2017) 17:205. doi: 10.1186/s12883-017-0988-x
20. Thayyil S, Pant S, Montaldo P, Shukla D, Oliveira V, Ivain P, et al. Hypothermia for moderate or severe neonatal encephalopathy in low-income and middle-income countries (helix):a randomised controlled trial in India, Sri Lanka, and Bangladesh. *Lancet Glob Health*. (2021) 9:e1273–85. doi: 10.1016/S2214-109X(21)00264-3
21. Starnoni D, Maduri R, Hajdu SD, Pierzchala K, Giammattei L, Rocca A, et al. Early perfusion computed tomography scan for prediction of vasospasm and delayed cerebral ischemia after aneurysmal subarachnoid hemorrhage. *World Neurosurg.* (2019) 130:e743–52. doi: 10.1016/j.wneu.2019.06.213

Conflict of Interest: The authors declare that the research was conducted in the absence of any commercial or financial relationships that could be construed as a potential conflict of interest.

frontiers in Neurology

ORIGINAL RESEARCH
published: 13 January 2022
doi: 10.3389/fneur.2021.785428

Association of Stress Hyperglycemia Ratio With Acute Ischemic Stroke Outcomes Post-thrombolysis

Chuan-Li Shen[1], *Nian-Ge Xia*[2], *Hong Wang*[2] *and Wan-Li Zhang*[2]*

[1] Department of Ultrasonography, The First Affiliated Hospital of Wenzhou Medical University, Wenzhou, China, [2] Department of Neurology, The First Affiliated Hospital of Wenzhou Medical University, Wenzhou, China

Background and Purpose: The association between stress hyperglycemia and clinical outcomes in patients with acute ischemic stroke treated with intravenous thrombolysis (IVT) is uncertain. We sought to analyze the association between the stress hyperglycemia ratio (SHR) using different definitions and clinical outcomes in acute patients with ischemic stroke undergoing IVT.

Methods: A total of 341 patients with ischemic stroke receiving IVT were prospectively enrolled in this study. The SHR was evaluated using different equations: SHR1, fasting glucose (mmol/L)/glycated hemoglobin (HbA1c) (%); SHR2, fasting glucose (mmol/L)/[(1.59 × HbA1c)−2.59]; SHR3, admission blood glucose (mmol/L)/[(1.59 × HbA1c)−2.59]. A poor functional outcome was defined as a modified Rankin scale score of 3–6 at 3 months. Multivariate logistic regression analysis was used to identify the relationship between different SHRs and clinical outcomes after IVT.

Results: A total of 127 (37.2%) patients presented with poor functional outcomes at 3 months. The predictive value of SHR1 for poor functional outcomes was better than that of SHR2 and SHR3 in receiver operating characteristic analyses. On multivariate analysis, SHR1 [odds ratio (OR) 14.639, 95% CI, 4.075–52.589; $P = 0.000$] and SHR2 (OR, 19.700; 95% CI; 4.475–86.722; $P = 0.000$) were independently associated with an increased risk of poor functional outcome but not SHR3.

Conclusions: Our study confirmed that the SHR, as measured by SHR1 and SHR2, is independently associated with worse clinical outcomes in patients with ischemic stroke after intravenous thrombolysis. Furthermore, SHR1 has a better predictive performance for outcomes than other SHR definitions.

Keywords: ischemic stroke, stress hyperglycemia, thrombolysis, outcomes, stress hyperglycemia ratio

OPEN ACCESS

Edited by:
Qin Hu,
Shanghai Jiao Tong University, China

Reviewed by:
Wen-Jun Tu,
Chinese Academy of Medical Sciences and Peking Union Medical College, China
Andrea Zini,
IRCCS Institute of Neurological Sciences of Bologna (ISNB), Italy

***Correspondence:**
Wan-Li Zhang
zhangwanli36@126.com

Specialty section:
This article was submitted to Stroke, a section of the journal Frontiers in Neurology

Received: *29 September 2021*
Accepted: *06 December 2021*
Published: *13 January 2022*

Citation:
Shen C-L, Xia N-G, Wang H and Zhang W-L (2022) Association of Stress Hyperglycemia Ratio With Acute Ischemic Stroke Outcomes Post-thrombolysis. Front. Neurol. 12:785428. doi: 10.3389/fneur.2021.785428

INTRODUCTION

Acute ischemic stroke is associated with high mortality and disability rates (1, 2). Intravenous thrombolysis with alteplase within 4.5 h of the onset of acute ischemic stroke is the safest and most effective treatment recommended by the guidelines (3, 4). Several studies have investigated the prognostic factors of intravenous thrombolytic therapy for ischemic stroke (5–8), among which the serum glucose level has attracted the attention of many researchers (9).

Several studies have demonstrated that hyperglycemia is independently associated with poor outcomes and symptomatic intracerebral hemorrhage (SICH) in patients with thrombolyzed AIS (7, 10, 11). However, a potential disparity exists in the association between hyperglycemia and poor outcomes when stratified by the history of diabetes mellitus (12, 13). Hyperglycemia was independently associated with mortality and SICH following intravenous thrombolysis in patients without diabetes but not in patients with diabetes (13). Known diabetes can affect the association between hyperglycemia and clinical outcomes. None of the clinical trials that target serum glucose levels have been proved to improve the prognosis of ischemic stroke (14, 15). We may need to find new indicators to replace serum glucose as a treatment target to obtain better clinical trial results.

Recently, the stress hyperglycemia ratio, which is defined as the ratio of blood glucose to glycated hemoglobin (HbA1c), has been considered a novel marker of worse outcomes in patients with ischemic stroke after intravenous thrombolysis (16, 17). However, the definitions of SHR using other equations also predicted poor outcomes in patients with ischemic stroke or critical illness (18, 19). Moreover, the potential mechanism of these phenomena is not fully understood. No studies have explored the effect of different kinds of SHR on the prognosis of patients with acute ischemic stroke. Therefore, the objective of the present study was to determine whether SHR using different definitions was associated with the clinical outcomes of patients with acute ischemic stroke undergoing intravenous thrombolysis.

MATERIALS AND METHODS

Study Population

We performed a prospective, observational study from March 2013 to May 2019 in which we collected data from consecutive patients with AIS undergoing intravenous thrombolysis at the First Affiliated Hospital of Wenzhou Medical University. Each patient was assessed by an experienced neurologist, and the eligible ones received intravenous alteplase within 4.5 h of the stroke onset. The inclusion criteria for enrollment were as follows: 1. Age ≥18 years, 2. The diagnosis of acute ischemic stroke met the World Health Organization's criteria (20), 3. An onset-to-treatment time within 4.5 h after the stroke onset. The exclusion criteria were in accordance with the 2013 AHA/ASA Guidelines (21). In addition, 73 normal healthy subjects were included in the control group. The study protocol was approved by the ethics committee of the First Affiliated Hospital of Wenzhou Medical University (No. KY2021-R077). All the patients or their representatives provided written informed consent.

Clinical Protocol and Laboratory Tests

On admission and at the time point of 24 h after treatment, the severity of neurological deficits using the National Institutes of

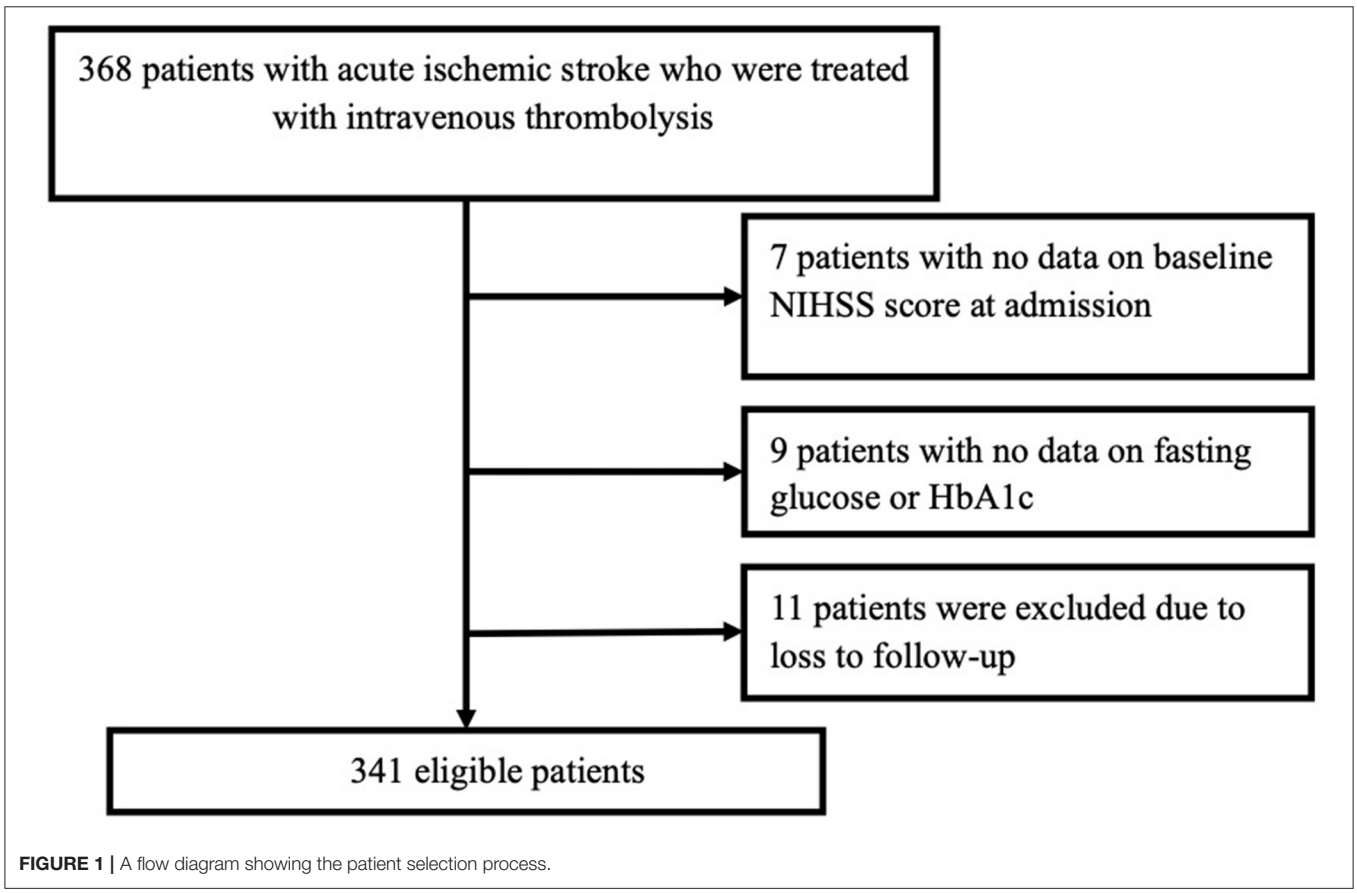

FIGURE 1 | A flow diagram showing the patient selection process.

Health Stroke Scale (NIHSS) scores was assessed by certified neurologists. We also collected baseline data on age, sex, clinical laboratory findings, onset-to-treatment time, admission blood pressure, medical history, including potential risk factors in stroke, and 12-lead electrocardiography during hospitalization. The blood glucose level on admission had been rapidly measured before the treatment. A medical history of diabetes mellitus was determined based on previous physicians' diagnoses and the use of antidiabetic drugs. All the participants routinely underwent computed tomographic scans at admission and repeated imaging 24 h after thrombolysis, or any other time when the patient experienced neurological deterioration.

Fasting glucose and 2-h postprandial blood glucose were collected during the morning hours (range: 06:00 AM−10:00 AM) after overnight fasting within 24 h after intravenous thrombolysis. HbA1c levels were routinely measured within 48 h after hospitalization. SHR was evaluated using the following equations: SHR1, fasting glucose (mmol/L)/HbA1c (%) (16); SHR2, fasting glucose (mmol/L)/[(1.59 × HbA1c)−2.59] (18); SHR3, admission blood glucose (mmol/L)/[(1.59 × HbA1c)−2.59] (19). The attending physicians and follow-up staff were blinded to the SHR, which was calculated only after all the information had been acquired.

Outcome Measures

Our primary endpoint of all patients was a poor functional outcome, which was defined as a modified Rankin Scale (mRS) score of 3–6 at the 3-month follow-up appointment. The mRS score was obtained *via* the outpatient department or by a telephone follow-up interview. The secondary outcomes included early neurological improvement (ENI), death within 3 months of follow-up, and intracerebral hemorrhage. ENI was defined as an NIHSS score improvement of ≥ 8 from the baseline or decreased to 0 or 1 at 24 h after treatment (22). The definition of **symptomatic intracerebral hemorrhage (SICH)** was based on the Safe Implementation of Thrombolysis in Stroke-Monitoring Study protocol (23): Type 2 parenchymal hemorrhage that occurred within 24 h after treatment, combined with an increase of ≥ 4 points in the NIHSS score.

Statistical Analyses

All analyses were conducted using SPSS Statistics (version 24.0; SPSS Inc., Chicago, IL, USA). The threshold for statistical significance was set at $p < 0.05$. Continuous variables were expressed as means with standard deviations or medians with interquartile ranges. Categorical variables are presented as frequencies and percentages. Statistical analyses were performed using Student's *t*-tests, one-way ANOVA test, and the Kruskal-Wallis test for continuous variables, and the chi-square test or Fisher's exact test for categorical variables. Receiver operating characteristic (ROC) curves were constructed to determine the predictive value of admission blood glucose, fasting plasma glucose, HbA1c, SHR1, SHR2, and SHR3 for a poor functional outcome at 3 months. The established optimal cutoff was used to transform SHR1 into a categorical variable. According to the optimal cutoff, we divided all the patients into two groups and compared their baseline characteristics. We employed different multivariate logistic regression models to identify the associations between SHR1, SHR2, SHR3, and outcome measures at 3 months.

TABLE 1 | Comparison of the baseline characteristics between patients with poor and good functional outcomes.

Characteristics	Total ($n = 341$)	Good outcome ($n = 214$)	Poor outcome ($n = 127$)	*P*
Age (y), mean ± SD	66.4 ± 12.6	63.3 ± 11.8	71.6 ± 12.1	0.000
Gender, male, *n* (%)	241 (70.7)	157 (73.4)	84 (66.1)	0.157
Baseline NIHSS score, median (IQR)	7 (4, 11)	6 (3, 9)	11 (7, 15)	0.000
24 h NIHSS score, median (IQR)	5 (2, 11)	3 (2, 6)	11 (7,16)	0.000
History of smoking, *n* (%)	139 (40.8)	98 (45.8)	41 (32.3)	0.014
Coronary artery disease, *n* (%)	36 (10.6)	21 (9.8)	15 (11.8)	0.562
Hypertension, *n* (%)	229 (67.2)	134 (62.6)	95 (74.8)	0.021
Diabetes, *n* (%)	77 (22.6)	49 (22.9)	28 (22.0)	0.856
Hyperlipidemia, *n* (%)	119 (34.9)	69 (32.2)	50 (39.4)	0.182
Previous stroke/TIA, *n* (%)	41 (12.0)	23 (10.7)	18 (14.2)	0.347
Atrial fibrillation, *n* (%)	85 (24.9)	38 (17.8)	47 (37.0)	0.000
Systolic BP (mmHg), mean ± SD	155.3 ± 23.3	153.7 ± 22.4	158.1 ± 24.5	0.088
Diastolic BP (mmHg), mean ± SD	86.1 ± 15.2	86.2 ± 14.9	85.9 ± 15.7	0.855
Admission blood glucose (mmol/L), mean ± SD	8.0 ± 3.2	7.7 ± 3.1	8.3 ± 3.2	0.098
Fasting plasma glucose (mmol/L), mean ± SD	6.2 ± 2.5	5.8 ± 2.1	6.9 ± 3.0	0.000
2-h postprandial blood glucose	8.3 ± 3.4	8.3 ± 3.5	8.5 ± 3.2	0.666
HbA1c (%), mean ± SD	6.4 ± 1.5	6.3 ± 1.4	6.5 ± 1.6	0.169
SHR1, mean ± SD	0.96 ± 0.24	0.91 ± 0.19	1.05 ± 0.29	0.000
SHR2, mean ± SD	0.83 ± 0.20	0.78 ± 0.16	0.90 ± 0.23	0.000
SHR3, mean ± SD	1.07 ± 0.26	1.05 ± 0.25	1.09 ± 0.28	0.154
Onset to treatment time, min, mean ± SD	203.8 ± 63.0	202.4 ± 63.0	206.3 ± 63.1	0.583
Cell count at admission				
WBC, x10∧9/L, mean ± SD	8.2 ± 2.8	8.1 ± 2.8	8.1 ± 2.7	0.784
RBC, x10∧12/L, mean ± SD	4.6 ± 0.6	4.6 ± 0.5	4.5 ± 0.6	0.016
PLT, x10∧9/L, mean ± SD	210.3 ± 67.2	214.4 ± 68.1	203.4 ± 65.4	0.152

*NIHSS, National Institute of Health Stroke Scale; TIA, transient ischemic attack; BP, blood pressure; HbA1c, glycated hemoglobin; SHR, **s**tress hyperglycemia ratio; WBC, white blood cell; RBC, red blood cell; PLT, platelet; SD, standard deviation; IQR, interquartile range.*

RESULTS

Baseline Characteristics

After excluding patients with missing data for fasting glucose or HbA1c, those with no data on the NIHSS score at

TABLE 2 | Receiver operating characteristic curves, identifying the predictive value of admission blood glucose, fasting plasma glucose, HbA1c, and SHR for poor outcomes at 3 months.

	AUC (95% CI)	*p*-value
Admission blood glucose	0.574 (0.511–0.637)	0.023
Fasting plasma glucose	0.654 (0.593–0.714)	0.000
HbA1c	0.544 (0.481–0.606)	0.178
SHR1	0.671 (0.611–0.731)	0.000
SHR2	0.663 (0.602–0.724)	0.000
SHR3	0.549 (0.485–0.612)	0.138

HbA1c, glycated hemoglobin; SHR, stress hyperglycemia ratio; AUC, area under the curve; CI, confidence interval.

admission, and those lost to follow-up at 3 months, we identified 341 eligible patients in the present study (**Figure 1**). The general clinical characteristics of the subjects are presented in **Table 1**. The mean age of the included patients was 66.4 ± 12.6 years, and 70.7% of them were males. Among the 341 patients, 26 (7.6%) died during the 3 months, 10 (2.9%) presented with SICH, 69 (20.2%) experienced ENI, and 127 (37.2%) experienced poor functional outcomes. The baseline and clinical characteristics of the patients stratified according to the primary outcomes are summarized in **Table 1**. The patients with poor functional outcomes had higher NIHSS scores on admission, SHR1, and SHR2 than the patients with good functional outcomes.

Supplementary Table S1 also shows the comparison of baseline characteristics between the normal, good outcome, and poor outcome groups. The good outcome group and the poor outcome group showed higher levels of SHR1 and SHR2 than the normal group.

ROC Curve Evaluating the Predictive Value of SHR for Outcomes

Receiver operating characteristic curve analysis was used to evaluate the predictive values of admission blood glucose, fasting plasma glucose, HbA1c, SHR1, SHR2, and SHR3 for 3-month poor functional outcomes (**Table 2**). The predictive value of SHR1 for clinical outcomes was better than that of admission blood glucose, HbA1c, fasting plasma glucose, SHR2, and SHR3. The area under the curve (AUC) of SHR1 was 0.671 (95% CI,0.611–0.731; $P = 0.000$), and the optimized cut-off of SHR1 value was 0.98.

Association Between SHR and Clinical Outcomes

As presented in **Table 3**, the patients with an SHR1 of ≥0.98 had higher NIHSS scores on admission and at 24 h after intravenous thrombolysis. This group also had a smaller number of smokers and higher prevalence of diabetes mellitus and hypertension compared to the group of patients with an SHR1 of <0.98. Systolic blood pressure, diastolic blood pressure, and admission blood glucose were significantly higher in patients in the SHR1 ≥0.98 group than in the SHR1 <0.98 group. The distribution of the mRS score at 3 months stratified by the SHR1 cutoff value is presented in **Figure 2**. A poor functional outcome and hemorrhagic transformation were more frequent in the higher SHR1 group but less likely to have ENI (**Table 3**). **Table 4** shows the results of the binary logistic regression analysis of the different SHRs and outcome measures. Regardless of whether Model 1 or Model 2 was used, we observed that SHR1 and SHR2 were independently associated with all the outcomes but not SHR3.

TABLE 3 | Comparison of the baseline characteristics and outcomes between subgroups stratified according to the SHR1 cutoff.

Characteristics	SHR1≥0.98 (*n* =119)	SHR1<0.98 (*n* =222)	*P*
Age (y), mean ± SD	67.3 ± 12.6	65.9 ± 12.6	0.323
Gender, male, *n* (%)	78 (65.5)	163 (73.4)	0.128
Baseline NIHSS score, median (IQR)	10 (5, 14)	7 (4, 10)	0.000
24 h NIHSS score, median (IQR)	9 (4, 13)	4 (2, 9)	0.000
History of smoking, *n* (%)	35 (29.4)	104 (46.8)	0.002
Coronary artery disease, *n* (%)	11 (9.2)	25 (11.3)	0.563
Hypertension, *n* (%)	88 (73.9)	141 (63.5)	0.050
Diabetes, *n* (%)	39 (32.8)	38 (17.1)	0.001
Hyperlipidemia, *n* (%)	44 (37.0)	75 (33.8)	0.556
Previous stroke/TIA, *n* (%)	18 (15.1)	23 (10.4)	0.197
Atrial fibrillation, *n* (%)	36 (30.3)	49 (22.1)	0.096
Systolic BP (mmHg), mean ± SD	158.9 ± 24.5	153.4 ± 22.5	0.041
Diastolic BP (mmHg), mean ± SD	89.8 ± 15.9	84.0 ± 14.4	0.001
Admission blood glucose (mmol/L), mean ± SD	9.0 ± 3.4	7.4 ± 2.9	0.000
Fasting plasma glucose (mmol/L), mean ± SD	8.2 ± 3.1	5.1 ± 1.3	0.000
HbA1c (%), mean ± SD	6.7 ± 1.7	6.2 ± 1.3	0.001
Onset to treatment time, min, mean ± SD	205.4 ± 64.2	203.0 ± 62.5	0.733
Cell count at admission			
WBC, x10∧9/L, mean ± SD	8.3 ± 2.7	8.1 ± 2.8	0.424
RBC, x10∧12/L, mean ± SD	4.5 ± 0.6	4.6 ± 0.5	0.510
PLT, x10∧9/L, mean ± SD	215.8 ± 78.1	207.4 ± 60.7	0.274
Outcomes			
ENI, *n* (%)	13 (10.9)	56 (25.2)	0.002
mRS score, median (IQR)	3 (1, 4)	1 (0, 3)	0.000
mRS score of 3–6, *n* (%)	66 (55.5)	61 (27.5)	0.000
Hemorrhagic transformation, *n* (%)	33 (27.7)	22 (9.9)	0.000
SICH, *n* (%)	6 (5.0)	4 (1.8)	0.176
Death, *n* (%)	16 (13.4)	10 (4.5)	0.003

SHR, stress hyperglycemia ratio; NIHSS, National Institute of Health Stroke Scale; TIA, transient ischemic attack; BP, blood pressure; HbA1c, glycated hemoglobin; WBC, white blood cell; RBC, red blood cell; PLT, platelet; ENI, early neurological improvement; mRS, modified Rankin Scale; SICH, symptomatic intracerebral hemorrhage; SD, standard deviation; IQR, interquartile range.

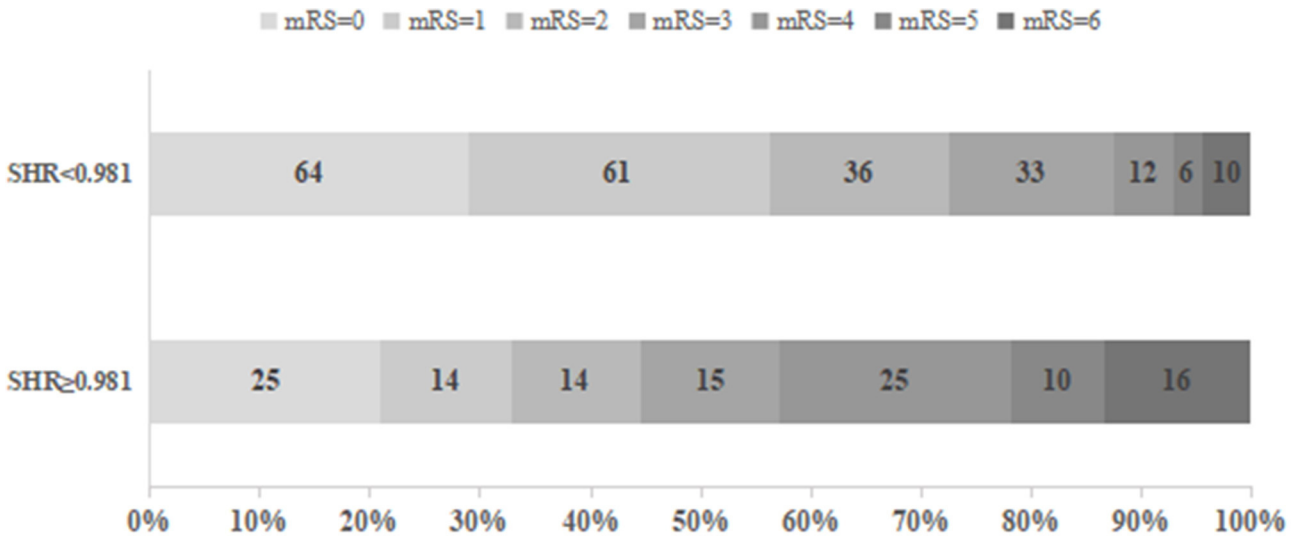

FIGURE 2 | Functional outcomes at 3 months in groups stratified according to the cutoff value of SHR1.

DISCUSSION

Our study showed that the stress hyperglycemia ratio, as defined by SHR1 and SHR2, was associated with an elevated risk of worse outcomes in patients with ischemic stroke after intravenous thrombolysis. For the first time, we compared all definitions of SHRs from previous studies in our study (16, 18, 19, 24, 25). The present study found that SHR1 calculated by fasting glucose-to-HbA1c ratio has a better predictive performance for worse outcomes than other SHR definitions. Furthermore, multivariate logistic regression analysis showed that SHR1 and SHR2 were independently associated with ENI, death during the 3-month follow-up, and intracerebral hemorrhage but not SHR3.

HbA1c was considered as the average glycemia level over the past 8–12 weeks, representing the mean level of baseline blood glucose before stroke (26). Several studies have suggested that HbA1c and fasting glucose predicted a higher risk of worse clinical outcomes in patients with ischemic stroke undergoing intravenous thrombolysis (27, 28). In the present study, SHR was evaluated using different equations (16, 18, 19), which involved the extent of the acute elevation in plasma glucose based on the baseline glucose level prior to stroke. Our study showed that SHR1, which is defined as the ratio of fasting glucose to HbA1c, proved to have a better predictive ability for poor outcomes than HbA1c and fasting glucose alone in ROC analyses, as well as other SHR definitions.

Hyperglycemia is an independent predictor of unfavorable clinical outcomes in patients with ischemic stroke treated with intravenous thrombolysis (9, 12). However, the relationship between hyperglycemia and poor outcomes after ischemic stroke in patients receiving intravenous thrombolysis is controversial. A study carried out in Greece revealed that NIHSS at admission attenuates the risk of poor outcomes associated with hyperglycemia (29). In our study, the severity of stress hyperglycemia was associated with increasing stroke severity based on the NIHSS score. We adjusted for stroke severity at admission in the multivariate regression models, which did not weaken the risk of poor outcomes associated with SHR. Our study indicated that SHR was not only associated with the activation of the stress response but was also independently associated with an increased risk of poor functional outcomes. We speculate that SHR may synthetically reflect the degree of acute and chronic hyperglycemia, suggesting that the association between acute hyperglycemia and poor outcome risk may be a result of the long-term vascular destruction attributed to chronic hyperglycemia rather than acute hyperglycemia alone (27).

The results of our study were partly in line with the findings of previous studies (16, 17, and 24), confirming that SHR1 is a marker of increased risk of worse outcomes in patients with ischemic stroke receiving intravenous thrombolysis. We performed SHR2 as the stress hyperglycemia ratio and was predictive of worse outcomes, which was also presented in another study on mechanical thrombectomy for ischemic stroke (18). However, many studies carried out in both ICU and non-ICU patients indicate that SHR3 increased the likelihood of adverse outcomes (19, 30), which is contrary to the findings of our study. Tatiana et al. found that ENI could accurately predict vascular recanalization and prognosis after thrombolytic therapy (22). We found that SHR1 and SHR2 were inversely associated with ENI, indicating that higher SHR may be associated with lower vascular recanalization. To our knowledge, this is the first study to report a comparison of different definitions of SHRs associated with poor outcomes in patients with ischemic stroke after intravenous

TABLE 4 | Multivariate logistic regression analysis of the associations between SHR and outcomes.

	Multivariate adjusted model (Model 1)		*P*	Multivariate adjusted model (Model 2)		*P*
	OR	95% CI		OR	95% CI	
Poor outcome						
SHR1	10.903	3.401–34.954	0.000	14.639	4.075–52.589	0.000
SHR1≥0.98	2.792	1.647–4.731	0.000	2.842	1.595–5.065	0.000
SHR2	8.054	2.790–30.789	0.000	19.700	4.475–86.722	0.000
SHR3	1.864	0.729–4.763	0.194	2.111	0.781–5.705	0.141
ENI						
SHR1	0.133	0.028–0.621	0.010	0.086	0.014–0.510	0.007
SHR1≥0.98	0.413	0.212–0.804	0.009	0.332	0.155–0.710	0.004
SHR2	0.155	0.028–0.869	0.034	0.082	0.011–0.600	0.014
SHR3	1.014	0.354–2.901	0.979	0.931	0.288–3.007	0.905
Death						
SHR1	12.208	2.450–60.838	0.002	32.317	4.542–229.915	0.001
SHR1≥0.98	2.063	0.818–5.205	0.125	3.387	1.093–10.497	0.035
SHR2	11.790	2.333–49.488	0.003	88.767	7.087–1111.859	0.001
SHR3	1.765	0.329–9.460	0.507	2.992	0.372–24.049	0.303
Presence of hemorrhagic transformation						
SHR1	9.988	3.205–31.129	0.000	9.521	2.564–35.350	0.001
SHR1≥0.98	3.038	1.635–5.645	0.000	3.074	1.504–6.283	0.002
SHR2	10.342	3.885–60.013	0.000	16.622	3.310–83.464	0.001
SHR3	2.673	0.910–7.848	0.074	2.219	0.693–7.103	0.179
Presence of SICH						
SHR1	12.237	2.128–70.359	0.005	15.187	1.936–119.150	0.010
SHR1≥0.98	2.897	0.754–11.133	0.121	4.323	0.941–19.859	0.060
SHR2	18.703	2.118–212.356	0.010	28.418	1.966–410.681	0.014
SHR3	1.246	0.113–13.737	0.857	1.306	0.093–18.292	0.843

Model 1 ***was*** *adjusted for age, sex, and NIHSS.*

Model 2 ***was*** *adjusted for the variables included in Model 1 plus the following variables: hypertension, smoking, previous stroke/TIA, atrial fibrillation, diabetes, hyperlipidemia, systolic BP, diastolic BP, RBC, and PLT, which were identified as having P-values of <0.2 in* ***Tables 1***, ***3****.*

*SHR****, s****tress hyperglycemia ratio; NIHSS, National Institute of Health Stroke Scale; SICH, symptomatic intracerebral hemorrhage; TIA, transient ischemic attack; BP, blood pressure; RBC, red blood cell; PLT, platelet; OR, odds ratio; CI, confidence interval.*

thrombolysis. Thus, our study contributes greatly to the available literature on stroke by consolidating the current concepts in public knowledge.

According to a previous study, SHR1 predicted hemorrhagic transformation in patients with non-thrombolysis ischemic stroke (25). However, few studies have investigated the relationship between SHRs and all-cause mortality. Our study showed that stress hyperglycemia, as measured by SHR1 and SHR2, was independently associated with **an increased risk of** death during the 3-month follow-up and SICH. Stress hyperglycemia represents an intense inflammatory response resulting from critical events such as acute stroke (31–33), which may exacerbate endothelial dysfunction and oxidative stress (34, 35). Hyperglycemia following ischemic stroke may increase free radical production and matrix metalloproteinase-9 activity, contributing to blood-brain barrier dysfunction (36).

This study had several limitations. First, the NIHSS score at admission, follow-up data, and SHR were not available in the 27 patients included in the study. However, no significant differences in baseline demography and disease characteristics were observed between the excluded and included participants. Second, only 29.3% of the patients were females, which may not be generalizable to other clinical centers. Third, this was a retrospective, single-center observational study with its inherent limitations, which indicates that multicenter clinical studies are necessary. Fourth, serum glucose was only collected at three time points in this study. Future prospective studies should focus on stress hyperglycemia fluctuations during follow-up.

CONCLUSIONS

In conclusion, our study demonstrated that the stress hyperglycemia ratio, as measured by SHR1 and SHR2, was independently associated with worse clinical outcomes in patients with ischemic stroke after intravenous thrombolysis. Furthermore, SHR1 has a better predictive performance for outcomes than other SHR definitions. None of the randomized controlled clinical trials demonstrated that intensive glucose control enhances functional outcomes in patients with ischemic stroke and hyperglycemia. Then, we provide SHR instead of the

absolute plasma glucose to become a potential treatment target for clinical trials.

DATA AVAILABILITY STATEMENT

The raw data supporting the conclusions of this article will be made available by the authors, without undue reservation.

ETHICS STATEMENT

The studies involving human participants were reviewed and approved by the Ethics Committee of the First Affiliated Hospital of Wenzhou Medical University. The patients/participants provided their written informed consent to participate in this study.

AUTHOR CONTRIBUTIONS

C-LS and W-LZ conceived, designed the study, and wrote the manuscript. C-LS and HW organized the database. N-GX performed the statistical analysis. C-LS, N-GX, and HW reviewed and edited the manuscript. All authors read and approved the manuscript.

FUNDING

This study was supported by the Wenzhou Science and Technology Bureau (No. Y20210913 and Y20180632) and Natural Science Foundation of Zhejiang Province (No. LQ21H090018).

ACKNOWLEDGMENTS

We would like to thank Editage (www.editage.cn) for English language editing.

SUPPLEMENTARY MATERIAL

The Supplementary Material for this article can be found online at: https://www.frontiersin.org/articles/10.3389/fneur.2021.785428/full#supplementary-material

REFERENCES

1. Chao BH, Yan F, Hua Y, Liu JM, Yang Y, Ji XM, et al. Stroke prevention and control system in china: Csppc-stroke program. *Int J Stroke.* (2021) 16:265–72. doi: 10.1177/1747493020913557
2. Tu WJ, Qiu HC, Liu YK, Liu Q, Zeng X, Zhao J. Elevated levels of adiponectin associated with major adverse cardiovascular and cerebrovascular events and mortality risk in ischemic stroke. *Cardiovasc Diabetol.* (2020) 19:125. doi: 10.1186/s12933-020-01096-3
3. Powers WJ, Rabinstein AA, Ackerson T, Adeoye OM, Bambakidis NC, Becker K, et al. 2018 guidelines for the early management of patients with acute ischemic stroke: A guideline for healthcare professionals from the american heart association/american stroke association. *Stroke.* (2018) 49:e46–e110. doi: 10.1161/STR.0000000000000158
4. Hacke W, Kaste M, Bluhmki E, Brozman M, Davalos A, Guidetti D. et al. Thrombolysis with alteplase 3 to 45 hours after acute ischemic stroke. *N Engl J Med.* (2008) 359:1317–29. doi: 10.1056/NEJMoa0804656
5. Chen SY, Lin YS, Cheng YF, Wang H, Niu XT, Zhang WL. Mean platelet volume-to-lymphocyte ratio predicts poor functional outcomes among ischemic stroke patients treated with intravenous thrombolysis. *Front Neurol.* (2019) 10:1274. doi: 10.3389/fneur.2019.01274
6. Frank B, Fulton R, Weimar C, Shuaib A, Lees KR, Collaborators V. Impact of atrial fibrillation on outcome in thrombolyzed patients with stroke: evidence from the virtual international stroke trials archive (vista). *Stroke.* (2012) 43:1872–7. doi: 10.1161/STROKEAHA.112.650838
7. Masrur S, Cox M, Bhatt DL, Smith EE, Ellrodt G, Fonarow GC, et al. Association of acute and chronic hyperglycemia with acute ischemic stroke outcomes post-thrombolysis: Findings from get with the guidelines-stroke. *J Am Heart Assoc.* (2015) 4:e002193. doi: 10.1161/JAHA.115.002193
8. Tsivgoulis G, Katsanos AH, Mandava P, Kohrmann M, Soinne L, Barreto AD, et al. Blood pressure excursions in acute ischemic stroke patients treated with intravenous thrombolysis. *J Hypertens.* (2021) 39:266–72. doi: 10.1097/HJH.0000000000002628
9. Tsivgoulis G, Katsanos AH, Mavridis D, Lambadiari V, Roffe C, Macleod MJ, et al. Association of baseline hyperglycemia with outcomes of patients with and without diabetes with acute ischemic stroke treated with intravenous thrombolysis: a propensity score-matched analysis from the sits-istr registry. *Diabetes.* (2019) 68:1861–9. doi: 10.2337/db19-0440
10. Mundiyanapurath S, Hees K, Ahmed N, Wahlgren N, Uhlmann L, Kieser M, et al. Predictors of symptomatic intracranial haemorrhage in off-label thrombolysis: an analysis of the safe implementation of treatments in stroke registry. *Eur J Neurol.* (2018) 25:340–e11. doi: 10.1111/ene.13507
11. Lin SF, Chao AC, Hu HH, Lin RT, Chen CH, Chan L, et al. Hyperglycemia predicts unfavorable outcomes in acute ischemic stroke patients treated with intravenous thrombolysis among a chinese population: a prospective cohort study. *J Neurol Sci.* (2018) 388:195–202. doi: 10.1016/j.jns.2018.03.022
12. Poppe AY, Majumdar SR, Jeerakathil T, Ghali W, Buchan AM, Hill MD, et al. Admission hyperglycemia predicts a worse outcome in stroke patients treated with intravenous thrombolysis. *Diabetes Care.* (2009) 32:617–22. doi: 10.2337/dc08-1754
13. Ahmed N, Davalos A, Eriksson N, Ford GA, Glahn J, Hennerici M, et al. Association of admission blood glucose and outcome in patients treated with intravenous thrombolysis: Results from the safe implementation of treatments in stroke international stroke thrombolysis register (sits-istr). *Arch Neurol.* (2010) 67:1123–30. doi: 10.1001/archneurol.2010.210
14. Litke R, Moulin S, Cordonnier C, Fontaine P, Leys D. Influence of glycaemic control on the outcomes of patients treated by intravenous thrombolysis for cerebral ischaemia. *J Neurol.* (2015) 262:2504–12. doi: 10.1007/s00415-015-7874-5
15. Gray CS, Hildreth AJ, Sandercock PA, O'Connell JE, Johnston DE, Cartlidge NE, et al. Glucose-potassium-insulin infusions in the management of post-stroke hyperglycaemia: the uk glucose insulin in stroke trial (gist-uk). *Lancet Neurol.* (2007) 6:397–406. doi: 10.1016/S1474-4422(07)70080-7
16. Ngiam JN, Cheong CWS, Leow AST, Wei YT, Thet JKX, Lee IYS, et al. Stress hyperglycaemia is associated with poor functional outcomes in patients with acute ischaemic stroke after intravenous thrombolysis. *QJM.* (2020) doi: 10.1093/qjmed/hcaa253. [Epub ahead of print].
17. Merlino G, Smeralda C, Gigli GL, Lorenzut S, Pez S, Surcinelli A, et al. Stress hyperglycemia is predictive of worse outcome in patients with acute ischemic stroke undergoing intravenous thrombolysis. *J Thromb Thrombolysis.* (2021) 51:789–97. doi: 10.1007/s11239-020-02252-y
18. Chen X, Liu Z, Miao J, Zheng W, Yang Q, Ye X, et al. High stress hyperglycemia ratio predicts poor outcome after mechanical thrombectomy for ischemic stroke. *J Stroke Cerebrovasc Dis.* (2019) 28:1668–73. doi: 10.1016/j.jstrokecerebrovasdis.2019.02.022
19. Lee TF, Drake SM, Roberts GW, Bersten A, Stranks SN, Heilbronn LK, et al. Relative hyperglycemia is an independent determinant of in-hospital

mortality in patients with critical illness. *Crit Care Med.* (2020) 48:e115–e22. doi: 10.1097/CCM.0000000000004133
20. Stroke—1989. Recommendations on stroke prevention, diagnosis, and therapy. Report of the who task force on stroke and other cerebrovascular disorders. *Stroke.* (1989) 20:1407–31. doi: 10.1161/01.STR.20.10.1407
21. Jauch EC, Saver JL, Adams HP Jr, Bruno A, Connors JJ, Demaerschalk BM, et al. Guidelines for the early management of patients with acute ischemic stroke: A guideline for healthcare professionals from the american heart association/american stroke association. *Stroke.* (2013) 44:870–947. doi: 10.1161/STR.0b013e318284056a
22. Kharitonova T, Mikulik R, Roine RO, Soinne L, Ahmed N, Wahlgren N, et al. Association of early national institutes of health stroke scale improvement with vessel recanalization and functional outcome after intravenous thrombolysis in ischemic stroke. *Stroke.* (2011) 42:1638–43. doi: 10.1161/STROKEAHA.110.606194
23. Mazya M, Egido JA, Ford GA, Lees KR, Mikulik R, Toni D, et al. Predicting the risk of symptomatic intracerebral hemorrhage in ischemic stroke treated with intravenous alteplase: Safe implementation of treatments in stroke (sits) symptomatic intracerebral hemorrhage risk score. *Stroke.* (2012) 43:1524–31. doi: 10.1161/STROKEAHA.111.644815
24. Zhu B, Pan Y, Jing J, Meng X, Zhao X, Liu L, et al. Stress hyperglycemia and outcome of non-diabetic patients after acute ischemic stroke. *Front Neurol.* (2019) 10:1003. doi: 10.3389/fneur.2019.01003
25. Yuan C, Chen S, Ruan Y, Liu Y, Cheng H, Zeng Y, et al. The stress hyperglycemia ratio is associated with hemorrhagic transformation in patients with acute ischemic stroke. *Clin Interv Aging.* (2021) 16:431–42. doi: 10.2147/CIA.S280808
26. American Diabetes A. Standards of medical care in diabetes—2014. *Diabetes Care.* (2014) 37 (Suppl 1):S14–80. doi: 10.2337/dc14-S014
27. Rocco A, Heuschmann PU, Schellinger PD, Kohrmann M, Diedler J, Sykora M, et al. Glycosylated hemoglobin a1 predicts risk for symptomatic hemorrhage after thrombolysis for acute stroke. *Stroke.* (2013) 44:2134–8. doi: 10.1161/STROKEAHA.111.675918
28. Cao W, Ling Y, Wu F, Yang L, Cheng X, Dong Q. Higher fasting glucose next day after intravenous thrombolysis is independently associated with poor outcome in acute ischemic stroke. *J Stroke Cerebrovasc Dis.* (2015) 24:100–3. doi: 10.1016/j.jstrokecerebrovasdis.2014.07.029
29. Tziomalos K, Dimitriou P, Bouziana SD, Spanou M, Kostaki S, Angelopoulou SM, et al. Stress hyperglycemia and acute ischemic stroke in-hospital outcome. *Metabolism.* (2017) 67:99–105. doi: 10.1016/j.metabol.2016.11.011
30. Roberts GW, Quinn SJ, Valentine N, Alhawassi T, O'Dea H, Stranks SN, et al. Relative hyperglycemia, a marker of critical illness: introducing the stress hyperglycemia ratio. *J Clin Endocrinol Metab.* (2015) 100:4490–7. doi: 10.1210/jc.2015-2660
31. Capes SE, Hunt D, Malmberg K, Pathak P, Gerstein HC. Stress hyperglycemia and prognosis of stroke in nondiabetic and diabetic patients: a systematic overview. *Stroke.* (2001) 32:2426–32. doi: 10.1161/hs1001.096194
32. Marik PE. Bellomo R. Stress hyperglycemia: An essential survival response! *Crit Care.* (2013) 17:305. doi: 10.1186/cc12514
33. Dungan KM, Braithwaite SS, Preiser JC. Stress hyperglycaemia. *Lancet.* (2009) 373:1798–807. doi: 10.1016/S0140-6736(09)60553-5
34. Robbins NM, Swanson RA. Opposing effects of glucose on stroke and reperfusion injury: Acidosis, oxidative stress, and energy metabolism. *Stroke.* (2014) 45:1881–6. doi: 10.1161/STROKEAHA.114.004889
35. Ceriello A, Esposito K, Piconi L, Ihnat MA, Thorpe JE, Testa R, et al. Oscillating glucose is more deleterious to endothelial function and oxidative stress than mean glucose in normal and type 2 diabetic patients. *Diabetes.* (2008) 57:1349–54. doi: 10.2337/db08-0063
36. Kamada H, Yu F, Nito C, Chan PH. Influence of hyperglycemia on oxidative stress and matrix metalloproteinase-9 activation after focal cerebral ischemia/reperfusion in rats: Relation to blood-brain barrier dysfunction. *Stroke.* (2007) 38:1044–9. doi: 10.1161/01.STR.0000258041.75739.cb

Conflict of Interest: The authors declare that the research was conducted in the absence of any commercial or financial relationships that could be construed as a potential conflict of interest.

Publisher's Note: All claims expressed in this article are solely those of the authors and do not necessarily represent those of their affiliated organizations, or those of the publisher, the editors and the reviewers. Any product that may be evaluated in this article, or claim that may be made by its manufacturer, is not guaranteed or endorsed by the publisher.

frontiers in Neurology

ORIGINAL RESEARCH
published: 02 March 2022
doi: 10.3389/fneur.2022.774720

Basic Surveillance Parameters Improve the Prediction of Delayed Cerebral Infarction After Aneurysmal Subarachnoid Hemorrhage

*István Csók[1], Jürgen Grauvogel[1], Christian Scheiwe[1], Jürgen Bardutzky[2], Thomas Wehrum[2], Jürgen Beck[1], Peter C. Reinacher[3,4] and Roland Roelz[1]**

[1] Department of Neurosurgery, Medical Center – University of Freiburg, Faculty of Medicine, University of Freiburg, Freiburg, Germany, [2] Department of Neurology, Medical Center – University of Freiburg, Faculty of Medicine, University of Freiburg, Freiburg, Germany, [3] Department of Stereotactic and Functional Neurosurgery, Medical Center – University of Freiburg, Faculty of Medicine, University of Freiburg, Freiburg, Germany, [4] Fraunhofer Institute for Laser Technology, Aachen, Germany

Background: To establish a practical risk chart for prediction of delayed cerebral infarction (DCI) after aneurysmal subarachnoid hemorrhage (aSAH) by using information that is available until day 5 after ictus.

Methods: We assessed all consecutive patients with aSAH admitted to our service between September 2008 and September 2015 ($n = 417$). The data set was randomly split into thirds. Two-thirds were used for model development and one-third was used for validation. Characteristics that were present between the bleeding event and day 5 (i.e., prior to >95% of DCI diagnoses) were assessed to predict DCI by using logistic regression models. A simple risk chart was established and validated.

Results: The amount of cisternal and ventricular blood on admission CT (**Hijdra sum score**), early **sonographic vasospasm** (i.e., mean flow velocity of either intracranial artery >160 cm/s until day 5), and a simplified binary **level of consciousness** score until day 5 were the strongest predictors of DCI. A model combining these predictors delivered a high predictive accuracy [the area under the receiver operating characteristic (AUC) curve of 0.82, Nagelkerke's R^2 0.34 in the development cohort]. Validation of the model demonstrated a high discriminative capacity with the AUC of 0.82, Nagelkerke's R^2 0.30 in the validation cohort.

Conclusion: Adding level of consciousness and sonographic vasospasm between admission and postbleed day 5 to the initial blood amount allows for simple and precise prediction of DCI. The suggested risk chart may prove useful for selection of appropriate candidates for interventions to prevent DCI.

Keywords: subarachnoid hemorrhage, cerebral vasospasm (CVS), delayed cerebral infarction, prediction, risk chart

OPEN ACCESS

Edited by:
Prativa Sherchan,
Loma Linda University, United States

Reviewed by:
Ya Su,
Fudan University, China
Neha Dangayach,
Icahn School of Medicine at Mount Sinai, United States
Basil Erwin Grüter,
Aarau Cantonal Hospital, Switzerland

****Correspondence:***
Roland Roelz
roland.roelz@uniklinik-freiburg.de

Specialty section:
This article was submitted to Stroke, a section of the journal Frontiers in Neurology

Received: *12 September 2021*
Accepted: *19 January 2022*
Published: *02 March 2022*

Citation:
Csók I, Grauvogel J, Scheiwe C, Bardutzky J, Wehrum T, Beck J, Reinacher PC and Roelz R (2022) Basic Surveillance Parameters Improve the Prediction of Delayed Cerebral Infarction After Aneurysmal Subarachnoid Hemorrhage. Front. Neurol. 13:774720. doi: 10.3389/fneur.2022.774720

INTRODUCTION

Delayed cerebral infarction (DCI) affects ∼20–30% of patients with aneurysmal subarachnoid hemorrhage (aSAH) and contributes considerably to the high morbidity and mortality of this condition (1). The amount of extravasated blood during aneurysm rupture is a central risk factor for DCI (2). Furthermore, poor clinical condition on admission, age, race, smoking,

hypertension, and many other factors may be linked to the risk of patients for DCI (3). Yet, at the individual level, DCI prediction remains difficult. This interferes with optimal allocation of preventive, diagnostic, and therapeutic measures to counteract DCI.

Delayed cerebral infarction risk prediction models that are currently available commonly rely on parameters that are available on hospital admission (4–6). However, existing scores attain only moderate predictive accuracy.

Since DCI does not occur during the first days after an aSAH, observation characteristics during the pre-DCI period may be used to increase predictive accuracy (7, 8). Transcranial Doppler (TCD) ultrasonography represents the most commonly applied routine diagnostic for cerebral vasospasm (CVS) in neurocritical care (9). Pathological increase in arterial flow velocity in TCD is associated with an increased risk for DCI (10) and timing of TCD changes seem to be crucial (11–14). In addition, the level of consciousness potentially represents an important lead to DCI risk stratification (3).

Therefore, we set out to establish a simple-to-use risk prediction model based on classical admission characteristics as well as TCD and level of consciousness surveillance during the first days after an aSAH.

METHODS

Study data are available upon reasonable request and in accordance with European data protection rules.

Study Population

This retrospective study took place in the neurosurgical department of a tertiary referral center. This study was approved by the independent ethics committee of our medical center (reference number: 575/16) and informed consent was waived.

The study adheres to the Strengthening the Reporting of Observational Studies in Epidemiology (STROBE) guidelines for reporting of observational studies (15).

We included all consecutive patients with an aSAH, confirmed by CT or MRI, who were admitted to our neurosurgical service over a 7-year period (September 2008 to September 2015). Patients with admission delay (admission $\geq$4 days after the aSAH) and early mortality ($\leq$4 days after the aSAH) were excluded. This period was chosen because electronic documentation of daily TCD and level of consciousness were available from September 2008. The period ends when methods of intracranial blood clearance were implemented in our department (16).

Intensive care was provided in accordance with current guidelines and without changes throughout the treatment period (17). In particular, preventive and therapeutic interventions for DCI were not modified.

Data Collection

Baseline Data

Age, sex, the Charlson Comorbidity Index (18), history of hypertension, clinical condition on admission [World Federation of Neurosurgical Societies (WFNS) grade], location and size of the ruptured aneurysm, aneurysm treatment method, and intracerebral hemorrhage were recorded as baseline data.

TABLE 1 | Patient, aSAH, and treatment characteristics in a consecutive aSAH population randomly distributed into the prediction development (two-thirds) and validation (one-third) cohorts.

	Development cohort	Validation cohort	*p*-value
Number of patients	283	134	
Delayed cerebral infaction (DCI), *n* (%)	55 (19.4)	29 (21.6)	0.60
Latency of DCI, days after ictus, mean (SD)	12.4 (8.6)	13.1 (6.1)	0.23
DCI prior day 5 after aSAH, *n* (% of DCI cases)	3 (5)	0 (0)	0.55
Patient characteristics			
Female, *n* (%)	193 (68)	87 (65)	0.51
Age at diagnosis, years, mean (IQR)	55.2 (46–64)	56.6 (48–64)	0.28
Charlson Comorbidity Index, median (IQR)	1 (0–2)	0 (0–2)	0.21
Arterial hypertension, *n* (%)	105 (37)	51 (38)	0.85
aSAH characteristics			
Admission WFNS-Grade, *n* (%)			0.37
1	85 (30)	39 (29)	
2	51 (18)	20 (15)	
3	14 (5)	7 (5)	
4	37 (13)	11 (8)	
5	96 (34)	57 (43)	
Modified fisher scale, *n* (%)			
0	3 (1)	3 (2)	0.89
1	29 (10)	12 (9)	
2	22 (8)	11 (8)	
3	67 (24)	33 (25)	
4	161 (57)	75 (56)	
Hijdra score, median (IQR)			
Total	16 (9–24)	15 (8–23)	0.75
Ventricles	2 (0–4)	2 (0–4)	0.96
Cisterns	13 (6–20)	12 (5–21)	0.84
Intracerebral hemorrhage, *n* (%)	76 (27)	43 (32)	0.30
Location of ruptured aneurysms, *n* (%)			
ICA	53 (19)	19 (14)	0.48
MCA	61 (22)	36 (27)	
ACA	123 (43)	60 (45)	
PCA	46 (16)	19 (14)	
Aneurysm size (mm) median (IQR)	6.0 (4.0–8.4)	6.8 (4.5–9.2)	0.15
Aneurysm treatment, *n* (%)			
Clip	139 (49)	61 (46)	0.49
Coil	144 (51)	73 (54)	

ACA, anterior cerebral artery; aSAH, aneurysmal subarachnoid hemorrhage; DCI, delayed cerebral infarction; ICA, internal carotid artery; IQR, interquartile range; MCA, middle cerebral artery; PCA, posterior circulation artery; WFNS, World Federation of Neurosurgical Societies.

Delayed Cerebral Infarction

The primary endpoint was DCI, which refers exclusively to DCI visualized by cranial imaging. We did not apply a

compound endpoint (commonly termed as delayed cerebral ischemia), consisting of both the delayed infarction and delayed neurological deterioration. Available imaging studies were assessed for DCI according to the imaging criteria suggested by Vergouwen et al. (19). Imaging studies and clinical data were reviewed by an interdisciplinary board of aSAH specialists consisting of a neurologist (JBa), a neurosurgeon (CS), and a neuroradiologist. Board rating adjudicated cerebral infarcts to DCI or early cerebral infarcts (e.g., due to aneurysm rupture or medical procedures or other causes). New cerebral infarction on CT or MRI within 6 weeks after aSAH or on the latest CT or MRI before death within 6 weeks, not present on the CT or MRI scan between 24 and 48 h after early aneurysm occlusion and not attributable to other causes such as surgical clipping or endovascular treatment, was classed as DCI. Hypodensities on CT resulting from hydrocephalus, ventricular catheters, or intraparenchymal hematomas were not regarded as DCI (19). The time between aSAH onset and an imaging diagnosis of DCI as defined above was recorded (DCI latency).

Blood Amount

The amount of subarachnoid blood on the admission CT scan was classified by using the semiquantitative Hijdra sum score, ranging from 0 to 30 for blood amount in the basal cisterns and from 0 to 12 for the blood amount within the four brain ventricles (20). The modified Fisher scale was also recorded (21).

Transcranial Doppler Ultrasonography

Daily TCD assessment and documentation were performed by the treating physicians at the time of aSAH therapy. Documentation of the maximum mean flow velocity (MFV) of either intracranial artery was retrieved. According to our clinical practice and cutoffs proposed in the pertinent literature, sonographic CVS (sCVS) was defined as MFV of $\geq$160 cm/s of either intracranial artery (22).

Level of Consciousness

Daily routine clinical documentation of the level of consciousness was reviewed by two physicians (IC + RR). To obtain a simple, clinically oriented, and dichotomous grading of the level of consciousness, we followed the proposal of Kupas et al. (23) and used the following binary transformation of the Glasgow Coma Scale (GCS): judgment was made for each day whether a patient "follows commands" or "does not follow commands". In patients with aphasia, "follows commands" was rated, if the patient was at least able to make contact with the treating physician. Patients with deep sedation were rated "does not follow commands". To maintain simplicity and clinical applicability, we avoided consciousness scores of higher complexity (e.g., GCS) that feature poor interrater reliability (24) and are particularly difficult to apply in intubated patients (25, 26).

Development and Validation Cohort

Patients were randomly (using the random numbers function, Microsoft Excel) allocated to the three groups: groups 1 and 2 were merged and used for development of a DCI prediction model. Group 3 was used for the model validation. For calibration of the model (i.e., accordance of predicted and observed DCI rates), the validation cohort was randomly split into three blocks. For each block, predicted and observed DCI rates were statistically compared.

Statistical Analysis

Baseline characteristics are presented as means $\pm$ SD, medians with interquartile range (IQR), or frequencies (%), as appropriate. Differences in baseline characteristics between patients from the development and validation cohorts were assessed by using the Mann–Whitney *U* test, the Fisher's exact test, or the Pearson's chi-squared test, as appropriate.

Delayed cerebral infarction was the primary endpoint of all the statistical analyses.

By using the development cohort only, the univariate regression analyses of available variables were calculated to identify potential risk factors for DCI.

Variables reaching a significance level of $p < 0.2$ were then included in the multivariate logistic regression model. Backward stepwise variable elimination was performed to identify independent predictors of DCI.

The discriminative capacity of the predictive model was described by the area under the receiver operating characteristic (AUC) curve. The coefficients of the multivariate regression analysis were used to calculate predicted DCI risks for every point increase in the Hijdra sum score and either value of sCVS and "follows commands" to establish the DCI risk chart. Jamovi version 1.2.27 (www.jamovi.org) statistical software was applied for statistical analyses.

RESULTS

Baseline Data

Table 1 summarizes the baseline data of the development and validation cohorts. Two hundred and eighty-three patients were included in the development cohort and 134 patients were included in the validation cohort. DCI occurred in 55 patients (19.4%) of the development cohort and DCI occurred in 29 patients (21.6%) of the validation cohort. Both the cohorts were similar for all the clinical characteristics.

Variable Derivation

The development cohort was interrogated for associations between: (a) the **number of days with sCVS** and the DCI rate and (b) the **number of days with "follows commands"** and the DCI rate (**Figures 1A,B**). Thirty percent of patients featured sCVS on at least one of the first 5 days after aSAH. Patients with sCVS had a higher rate of DCI compared to patients without sCVS (28.2 vs. 15.2%, $p = 0.013$). However, no correlation between the number of days with sCVS and an increasing DCI rate was observed. Thirty-one percent of patients "followed commands" on all the 5 days after aSAH and a low DCI rate of 5.6% occurred in these patients. The DCI rate was higher in patients who did not "follow commands" on at least one of the first 5 days postbleed (30.7 vs. 13.9%, $p < 0.001$). Variable rates of DCI were observed with an increasing number of days with "follows commands".

Given the lack of a correlation between the observed number of days with both the sCVS and "follows commands"

A Number of days with sonographic vasospasm and corresponding DCI rates

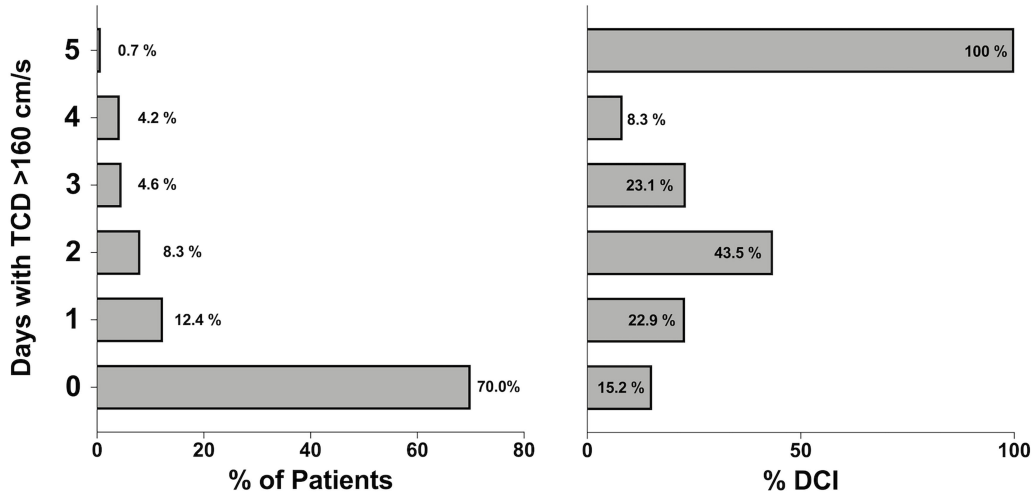

B Number of days with "follows commands" and corresponding DCI rates

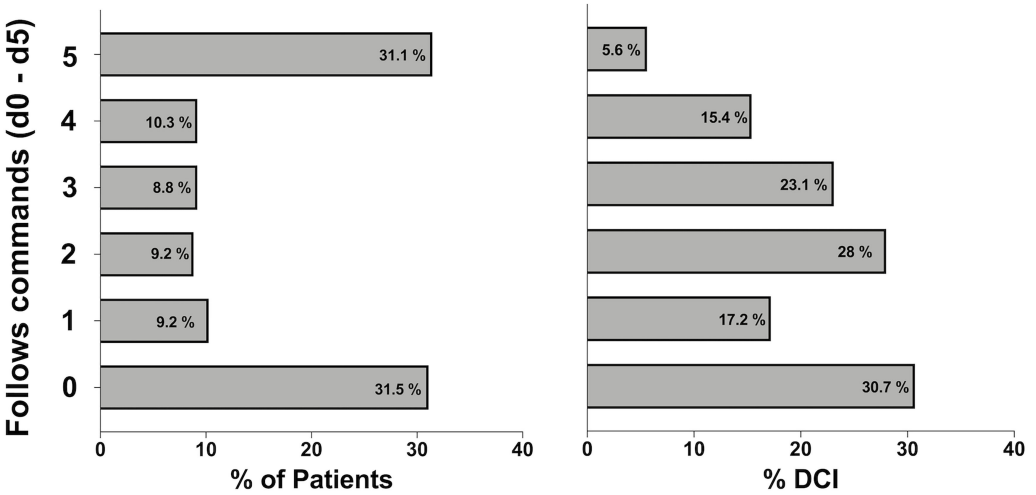

C Frequencies of dichotomized variables and corresponding DCI rates

DCI rate (patient number)		Follows commands (d0 - d5) +	Follows commands (d0 - d5) -
Sonographic Vasospasm d0 - d5	-	**10.5%** n = 143 (50,5%)	**27.3%** n = 55 (19.4%)
	+	**23.1%** n = 52 (18.4%)	**36.4%** n = 33 (11.7%)

FIGURE 1 | (A) Number of days with sonographic cerebral vasospasm (sCVS) until postbleed day 5 and corresponding delayed cerebral infarction (DCI) rates. **(B)** Number of days with "follows commands" until postbleed day 5 and corresponding DCI rates. **(C)** Summary of DCI rates observed when sCVS and "follows commands" were applied as dichotomous variables.

A **Univariate Associations with DCI**

Age	0.603
Sex	0.704
Charlson Comorbidity Index	0.842
Hypertension	0.747
WFNS	**< .001**
Intracerebral hemorrhage	0.866
modified Fisher Scale	**< .001**
Hijdra Sum Score	**< .001**
Aneurysm location	***0.061***
Aneurysm size	0.210
Clip/Coil	0.875
Sonographic Vasospasm day 0-5	**0.010**
"Follows commands" day 0-5	**< .001**

C **ROC Curve, DEVELOPMENT Model**

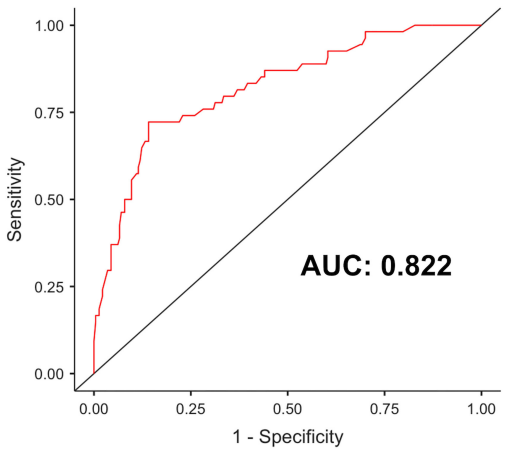

B **Multivariable Predictors of DCI**

Predictor	p	Odds Ratio	95% Confidence Interval	
Hijdra Sum Score	< .001	1.1442	1.09596	1.1946
Sonographic Vasospasm day 0-5	0.016	2.4105	1.18140	4.9184
"Follows commands" day 0-5	0.092	0.5500	0.27424	1.1029

FIGURE 2 | (A) The univariate analysis of predictors of DCI in the development cohort. **(B)** The multivariate logistic regression analysis of independent predictors of DCI. **(C)** The receiver operating characteristic (ROC) curve of the predictive model including the Hijdra sum score, sCVS, and "follows commands" showed the area under the curve (AUC) of 0.822.

and the DCI rate, both the variables were dichotomized for further analyses: "any number of days with sCVS" vs. "no sCVS" and "any number of days with follows commands" vs. "no day with follows commands." **Figure 1C** summarizes observed the DCI rates corresponding to these dichotomized variables.

Uni- and Multivariable Predictors of DCI: Development of a Predictive Model

The univariate logistic regression analysis showed statistically significant associations between DCI and the following variables: WFNS grade, modified Fisher scale, the Hijdra sum score, sCVS, and "follows commands" (**Figure 2A**). The multivariate logistic regression analysis identified the Hijdra sum score and sCVS as independent predictors of DCI ($p < 0.05$). "Follows commands" featured a near-significant association [odds ratio (OR) 0.55, 95% CI 0.27–1.10, $p = 0.092$]. "Follows commands" was kept in the model, since it substantially improved the model fit (Nagelkerke's R^2 from 0.32 to 0.34) (**Figure 2B**). Predictive accuracy of the model was the AUC of 0.82 (**Figure 2C**).

Model Validation

The model was applied to the validation cohort and an excellent accordance with the development data was observed. The OR and 95% CIs of the Hijdra sum score, sCVS, and "follows commands" were highly congruent (**Figure 3A**). The validation cohort was randomly split into three blocks. In each block, statistical agreement of predicted and observed DCI rates was maintained (**Figure 3B**). The discriminatory performance for DCI was high (AUC 0.82) and the model fit (Nagelkerke's R^2: 0.30) was good (**Figure 3C**).

Delayed Cerebral Infarction Risk Chart

A DCI risk chart was created on the basis of the development model. The x-axis of the chart is represented by the Hijdra sum score. For every point increase in the Hijdra sum score, DCI risks were calculated for all the four possible categories of the binary variables sCVS and "follows commands." We included the "Hijdra sum score only" predictive model (pink line) to demonstrate the impact of both the observation variables for DCI risk estimates (**Figure 4**). A strong upward shift of the DCI risk curve resulted, if both the observation variables were unfavorable (occurrence of sCVS on either day 0–5 and lack of

A **Multivariable Predictors of DCI in the VALIDATION Cohort**

Predictor	p	Odds ratio	95% Confidence Interval	
Hijdra Sum Score	< .001	1.0985	1.03885	1.162
Sonographic Vasospasm day 0-5	0.032	2.8961	1.09710	7.645
"Follows commands" day 0-5	0.105	0.4393	0.16263	1.187

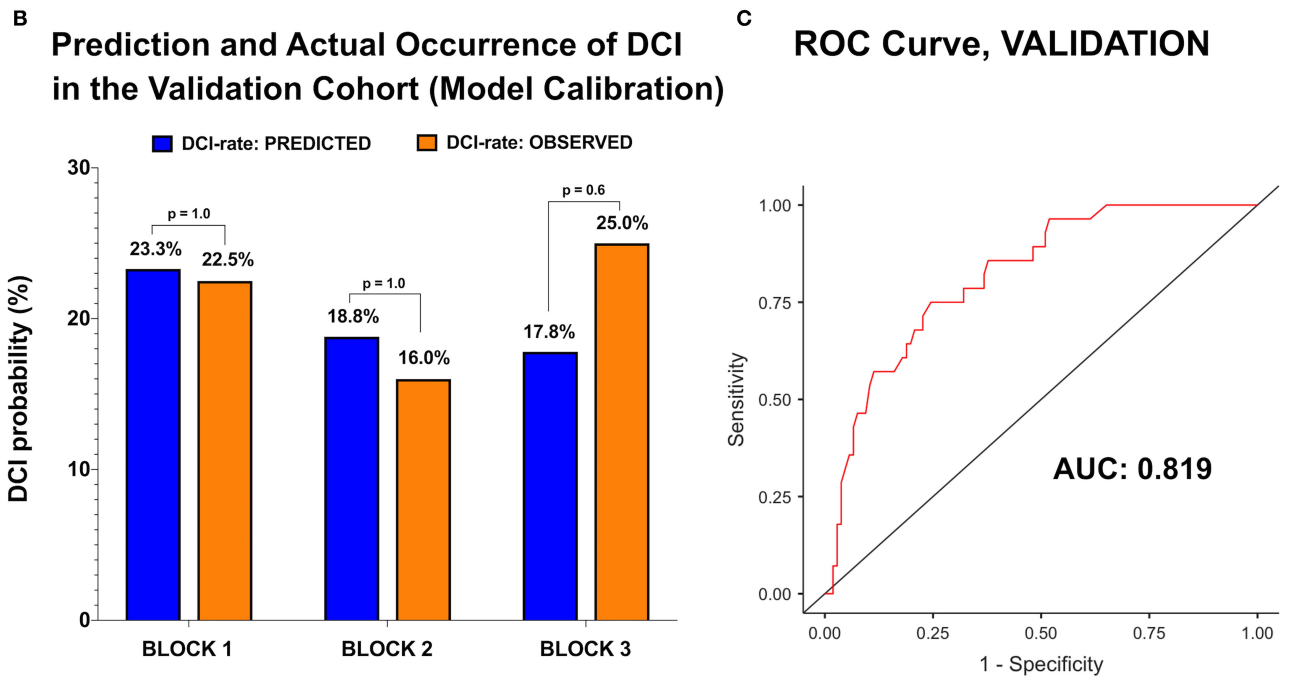

FIGURE 3 | (A) The multivariate logistic regression analysis of independent predictors of DCI in the validation cohort. **(B)** The validation cohort was split in three blocks. Predicted and observed DCI rates were congruent in all the three blocks. **(C)** The ROC curve of the development model showed the AUC of 0.819.

"follows commands" on every day 0–5) (red line). Conversely, the DCI risk dropped drastically below the baseline "Hijdra sum score only" risk, if both the variables were favorable (green line). Opposing values for sCVS and "follows commands" neutralized the impact of each other and led to DCI risks near the "Hijdra sum score only" baseline (yellow and blue lines).

DISCUSSION

We created a simple-to-use risk chart to accurately predict DCI in patients with aSAH. The only information needed is the baseline amount of extravasated blood (recorded by the semiquantitative Hijdra sum score) and daily information on sCVS and a simplified level of consciousness assessment ("follows commands: yes/no") until postbleed day 5. Validation of the risk chart confirmed a high predictive accuracy (AUC 0.82).

Currently, available DCI prediction approaches mainly rely on baseline data and achieve only moderate predictive accuracy (4–6, 8). DeRooij et al. suggested a score based on cisternal and ventricular blood amount, the WFNS grade, and age that yielded the AUC of 0.63 (4). The predictive accuracy of a score based on the WFNS and the modified Fisher grade equally yielded the AUC of 0.63 (5). We hypothesized that taking surveillance parameters into account until the onset of the critical phase of DCI (prior to postbleed day 6) could improve DCI prognostication and, thereby, assist clinical decisions to guide aSAH therapy. Our focus was to improve DCI prognostication by using *simple means*. We believe that incorporating complex or technically demanding parameters into prognostic models considerably limits their clinical utility. Accordingly, only parameters that are collected in clinical routine were eligible for the creation of the model.

The amount of blood on the initial cranial CT is an undisputed risk factor for DCI (27). The Hijdra sum score is a simple and quick semiquantitative classification of the blood amount that features high interrater reliability (28). It has repeatedly been

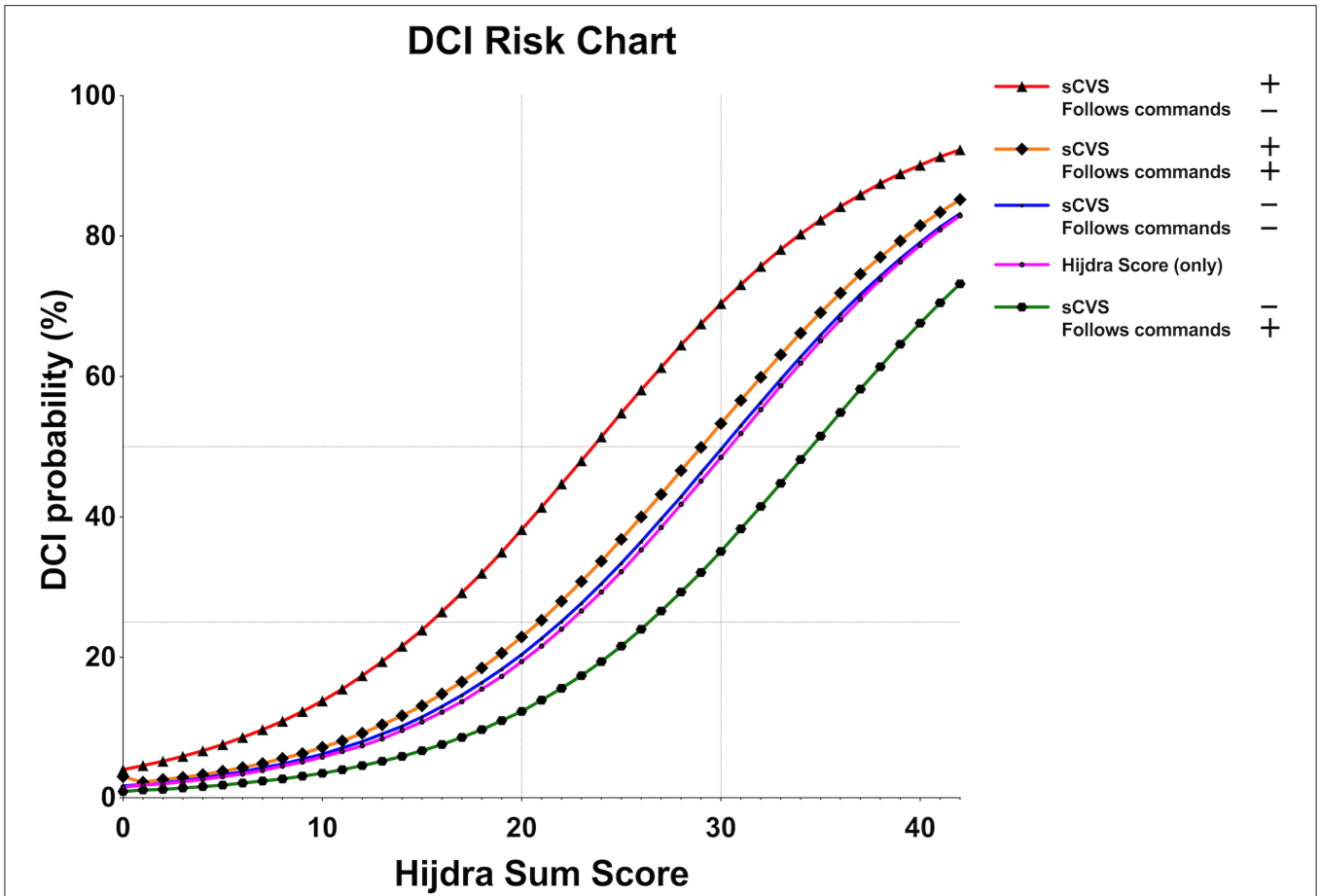

FIGURE 4 | Predicted DCI risk relative to the baseline Hijdra sum score. sCVS and the level of consciousness—simplified to a binary parameter: "follows commands/does not follow commands" —represent important modifiers to the individual DCI risk profile. A sharp increase in DCI risk applies to patients who feature sCVS and "does not follow commands" on the first 5 days after aneurysmal subarachnoid hemorrhage (aSAH) (red line). In contrast, the baseline DCI risk according to the blood amount (the Hijdra sum score, pink line) is considerably reduced in patients who follows commands and lack sCVS (green line). If one modifier is favorable and the other is unfavorable, the DCI risk is neutralized to the baseline risk according to the Hijdra sum score.

found to deliver a relatively accurate DCI prognostication that outweighs categorical blood amount classifications (e.g., Fisher scale/modified Fisher scale) (29). These findings are confirmed in this study.

We chose sCVS as an observation variable, since TCD represents the only non-invasive method for vasospasm surveillance recommended by current guidelines (30). Despite all the technical limitations (poor sensitivity, low interrater reliability, and inadequate insonation in 10% of patients), occurrence of sCVS is clearly associated with DCI. (10, 31) This study confirms the prognostic relevance of sCVS for DCI prognostication. We observed that a binary grading "sCVS on either of the first 5 days postbleed: yes/no" represented a strong modifier of the baseline DCI risk. Considering the number of days with sCVS did not further improve DCI prognostication. We believe that specific training of physicians and technicians could further increase the value of vasospasm surveillance by TCD.

Poor clinical status has been linked to an increased DCI risk in numerous previous investigations. Commonly, the level of consciousness on admission (typically in the form of the WFNS or Hunt and Hess grade) is considered (4–6). Our analysis shows that the observation of the level of consciousness during the first days after an aSAH outweighs the admission status for DCI prognostication. We argue that the true severity of the bleeding event is better represented by the level of consciousness throughout the first days compared to hospital admission. Epilepsy, hydrocephalus, sedation, and many other factors may skew the initial judgment of the neurological condition of patients with aSAH. To comply with clinical routine and maintain simplicity of DCI prognostication, we avoided the use of complex neurological grading scales. The GCS features a relatively poor interrater reliability and is of limited use in intubated patients (25, 26). Accordingly, we adopted a simplified and validated version of the GCS that dichotomizes the neurological status into "follows commands: yes/no" (23).

The derived DCI risk chart is extremely simple to apply in all the patients with an aSAH. It is intended to improve the identification of patients at risk for DCI and, accordingly,

assist clinical decisions to implement DCI diagnostics and treatments.

Study Limitations

This study is subjected to the general constraints of retrospective analyses. In particular, measurement bias for DCI due to lack of standardization of imaging across patients cannot be ruled out. Further retrospective analyses may always be subjected to researcher bias. We tried to exclude any potential bias on the study endpoints by independent and external assessments. The primary endpoint, DCI, was assessed by an independent and blinded rating board consisting of experienced physicians who were not involved in the treatment of patients.

CONCLUSION

Initial blood amount and surveillance of sonographic vasospasm and "follows commands/does not follow commands" until postbleed day 5 allow accurate DCI prediction in patients with aSAH. On this basis, we created a simple risk chart to improve DCI prognostication.

DATA AVAILABILITY STATEMENT

The raw data supporting the conclusions of this article will be made available by the authors upon reasonable request and in accordance with European data protection rules.

ETHICS STATEMENT

The studies involving human participants were reviewed and approved by Ethics Committee, Medical Center – University of Freiburg, Germany. Written informed consent for participation was not required for this study in accordance with the national legislation and the institutional requirements.

AUTHOR CONTRIBUTIONS

IC and RR contributed to the study conceptualization, data collection, analysis and interpretation, statistical analyses, visualization, and drafting of the manuscript. JG contributed to the data curation, data collection and interpretation, and reviewed the manuscript for important intellectual content. CS contributed to the data curation, study supervision, interpretation of data, and reviewed the manuscript for important intellectual content. JBa and TW contributed to the interpretation of data and reviewed the manuscript for important intellectual content. JBe contributed to the study conceptualization, data curation, project administration, and reviewed the manuscript for important intellectual content. PR contributed to the study conceptualization, collection and interpretation of data, and drafting of the manuscript. All authors contributed to the article and approved the submitted version.

FUNDING

RR was funded by the Berta-Ottenstein-Programme for Advanced Clinician Scientists, Faculty of Medicine, University of Freiburg, Germany. The article processing charge was funded by the Baden-Wuerttemberg Ministry of Science, Research and Art and the University of Freiburg in the funding programme Open Access Publishing.

REFERENCES

1. Macdonald RL. Delayed neurological deterioration after subarachnoid haemorrhage. *Nat Rev Neurol.* (2014) 10:44–58. doi: 10.1038/nrneurol.2013.246
2. Duan W, Pan Y, Wang C, Wang Y, Zhao X, Wang Y, et al. Risk factors and clinical impact of delayed cerebral ischemia after aneurysmal subarachnoid hemorrhage: analysis from the China national stroke registry. *Neuroepidemiology*. (2018) 50:128–36. doi: 10.1159/000487325
3. Adams HP, Kassell NF, Torner JC, Haley EC. Predicting cerebral ischemia after aneurysmal subarachnoid hemorrhage: influences of clinical condition, CT results, and antifibrinolytic therapy. A report of the cooperative aneurysm study. *Neurology*. (1987) 37:1586–91. doi: 10.1212/WNL.37.10.1586
4. de Rooij NK, Greving JP, Rinkel GJE, Frijns CJM. Early prediction of delayed cerebral ischemia after subarachnoid hemorrhage: development and validation of a practical risk chart. *Stroke J Cereb Circ.* (2013) 44:1288–94. doi: 10.1161/STROKEAHA.113.001125
5. de Oliveira Manoel AL, Jaja BN, Germans MR, Yan H, Qian W, Kouzmina E, et al. The VASOGRADE: a simple grading scale for prediction of delayed cerebral ischemia after subarachnoid hemorrhage. *Stroke J Cereb Circ.* (2015) 46:1826–31. doi: 10.1161/STROKEAHA.115.008728
6. Crobeddu E, Mittal MK, Dupont S, Wijdicks EFM, Lanzino G, Rabinstein AA. Predicting the lack of development of delayed cerebral ischemia after aneurysmal subarachnoid hemorrhage. *Stroke.* (2012) 43:697–701. doi: 10.1161/STROKEAHA.111.638403
7. Megjhani M, Terilli K, Weiss M, Savarraj J, Chen LH, Alkhachroum A, et al. Dynamic detection of delayed cerebral ischemia: a study in 3 centers. *Stroke*. (2021) 52:1370–9. doi: 10.1161/STROKEAHA.120.032546
8. Qureshi AI, Sung GY, Razumovsky AY, Lane K, Straw RN, Ulatowski JA. Early identification of patients at risk for symptomatic vasospasm after aneurysmal subarachnoid hemorrhage. *Crit Care Med.* (2000) 28:984–90. doi: 10.1097/00003246-200004000-00012
9. Francoeur CL, Mayer SA. Management of delayed cerebral ischemia after subarachnoid hemorrhage. *Crit Care Lond Engl.* (2016) 20:277. doi: 10.1186/s13054-016-1447-6
10. Kumar G, Shahripour RB, Harrigan MR. Vasospasm on transcranial doppler is predictive of delayed cerebral ischemia in aneurysmal subarachnoid hemorrhage: a systematic review and meta-analysis. *J Neurosurg.* (2016) 124:1257–64. doi: 10.3171/2015.4.JNS15428
11. Marshall SA, Nyquist P, Ziai WC. The role of transcranial doppler ultrasonography in the diagnosis and management of vasospasm after aneurysmal subarachnoid hemorrhage. *Neurosurg Clin N Am.* (2010) 21:291–303. doi: 10.1016/j.nec.2009.10.010
12. Washington CW, Zipfel GJ. Participants in the international multidisciplinary consensus conference on the critical care management of subarachnoid hemorrhage. Detection and monitoring of vasospasm and delayed cerebral ischemia: a review and assessment of the literature. *Neurocrit Care.* (2011) 15:312–7. doi: 10.1007/s12028-011-9594-8
13. Westermaier T, Pham M, Stetter C, Willner N, Solymosi L, Ernestus R-I, et al. Value of transcranial doppler, perfusion-CT and neurological evaluation to forecast secondary ischemia after aneurysmal SAH. *Neurocrit Care.* (2014) 20:406–12. doi: 10.1007/s12028-013-9896-0
14. Lee H, Perry JJ, English SW, Alkherayf F, Joseph J, Nobile S, et al. Clinical prediction of delayed cerebral ischemia in aneurysmal subarachnoid hemorrhage. *J Neurosurg.* (2018) 1:1–8. doi: 10.3171/2018.1.JNS172715

15. von Elm E, Altman DG, Egger M, Pocock SJ, Gøtzsche PC, Vandenbroucke JP, et al. The strengthening the reporting of observational studies in epidemiology (STROBE) statement: guidelines for reporting observational studies. *Lancet Lond Engl.* (2007) 370:1453–7. doi: 10.1016/S0140-6736(07)61602-X
16. Roelz R, Schaefer JH, Scheiwe C, Sajonz B, Csok I, Steiert C, et al. Impact of stereotactic ventriculocisternostomy on delayed cerebral infarction and outcome after subarachnoid hemorrhage. *Stroke.* (2020) 51:431–9. doi: 10.1161/STROKEAHA.119.027424
17. Steiner T, Juvela S, Unterberg A, Jung C, Forsting M, Rinkel G, et al. European stroke organization guidelines for the management of intracranial aneurysms and subarachnoid haemorrhage. *Cerebrovasc Dis Basel Switz.* (2013) 35:93–112. doi: 10.1159/000346087
18. Charlson ME, Pompei P, Ales KL, MacKenzie CR, A new method of classifying prognostic comorbidity in longitudinal studies: development and validation. *J Chronic Dis.* (1987) 40:373–83. doi: 10.1016/0021-9681(87)90171-8
19. Vergouwen MDI, Vermeulen M, van Gijn J, Rinkel GJE, Wijdicks EF, Muizelaar JP, et al. Definition of delayed cerebral ischemia after aneurysmal subarachnoid hemorrhage as an outcome event in clinical trials and observational studies proposal of a multidisciplinary research group. *Stroke.* (2010) 41:2391–5. doi: 10.1161/STROKEAHA.110.589275
20. Hijdra A, Brouwers PJ, Vermeulen M, van Gijn J. Grading the amount of blood on computed tomograms after subarachnoid hemorrhage. *Stroke J Cereb Circ.* (1990) 21:1156–61. doi: 10.1161/01.STR.21.8.1156
21. Claassen J, Bernardini GL, Kreiter K, Bates J, Du YE, Copeland D, et al. Effect of cisternal and ventricular blood on risk of delayed cerebral ischemia after subarachnoid hemorrhage: the fisher scale revisited. *Stroke.* (2001) 32:2012–20. doi: 10.1161/hs0901.095677
22. Vora YY, Suarez-Almazor M, Steinke DE, Martin ML, Findlay JM. Role of transcranial doppler monitoring in the diagnosis of cerebral vasospasm after subarachnoid hemorrhage. *Neurosurgery*. (1999) 44:1237–47. doi: 10.1227/00006123-199906000-00039
23. Kupas DF, Melnychuk EM, Young AJ. Glasgow coma scale motor component ("Patient Does Not Follow Commands") performs similarly to total glasgow coma scale in predicting severe injury in trauma patients. *Ann Emerg Med*. (2016) 68:744–750.e3. doi: 10.1016/j.annemergmed.2016.06.017
24. Gill MR, Reiley DG, Green SM. Interrater reliability of glasgow coma scale scores in the emergency department. *Ann Emerg Med.* (2004) 43:215–23. doi: 10.1016/S0196-0644(03)00814-X
25. Segatore M, Way C. The glasgow coma scale: time for change. *Heart Lung J Crit Care.* (1992) 21:548–57.
26. Green SM. Cheerio, laddie! Bidding farewell to the glasgow coma scale. *Ann Emerg Med.* (2011) 58:427–30. doi: 10.1016/j.annemergmed.2011.06.009
27. Lawton MT, Vates GE. Subarachnoid hemorrhage. *N Engl J Med.* (2017) 377:257–66. doi: 10.1056/NEJMcp1605827
28. Jiménez-Roldán L, Alén JF, Gómez PA, Lobato RD, Ramos A, Munarriz PM, et al. Volumetric analysis of subarachnoid hemorrhage: assessment of the reliability of two computerized methods and their comparison with other radiographic scales. *J Neurosurg.* (2013) 118:84–93. doi: 10.3171/2012.8.JNS12100
29. van der Steen WE, Leemans EL, van den Berg R, Roos YBWEM, Marquering HA, Verbaan D, et al. Radiological scales predicting delayed cerebral ischemia in subarachnoid hemorrhage: systematic review and meta-analysis. *Neuroradiology.* (2019) 61:247–56. doi: 10.1007/s00234-019-02161-9
30. Connolly ES, Rabinstein AA, Carhuapoma JR, Derdeyn CP, Dion J, Higashida RT, et al. Guidelines for the management of aneurysmal subarachnoid hemorrhage: a guideline for healthcare professionals from the american heart association/american stroke association. *Stroke.* (2012) 43:1711–37. doi: 10.1161/STR.0b013e3182587839
31. Carrera E, Schmidt JM, Oddo M, Fernandez L, Claassen J, Seder D, et al. Transcranial doppler for predicting delayed cerebral ischemia after subarachnoid hemorrhage. *Neurosurgery.* (2009) 65:316–23. doi: 10.1227/01.NEU.0000349209.69973.88

Conflict of Interest: PR received personal fees and non-financial support from Boston Scientific (Marlborough, USA), personal fees and travel support and honoraria for lectures from Brainlab (Munich, Germany), and a research grant from the Fraunhofer Society (Munich, Germany).

The remaining authors declare that the research was conducted in the absence of any commercial or financial relationships that could be construed as a potential conflict of interest.

Advantages of publishing in Frontiers

OPEN ACCESS
Articles are free to read for greatest visibility and readership

FAST PUBLICATION
Around 90 days from submission to decision

HIGH QUALITY PEER-REVIEW
Rigorous, collaborative, and constructive peer-review

TRANSPARENT PEER-REVIEW
Editors and reviewers acknowledged by name on published articles

Frontiers
Avenue du Tribunal-Fédéral 34
1005 Lausanne | Switzerland

Visit us: www.frontiersin.org
Contact us: frontiersin.org/about/contact

REPRODUCIBILITY OF RESEARCH
Support open data and methods to enhance research reproducibility

DIGITAL PUBLISHING
Articles designed for optimal readership across devices

FOLLOW US
@frontiersin

IMPACT METRICS
Advanced article metrics track visibility across digital media

EXTENSIVE PROMOTION
Marketing and promotion of impactful research

LOOP RESEARCH NETWORK
Our network increases your article's readership